

HIGH RESOLUTION SEQUENCE STRATIGRAPHY AND
RESERVOIR CHARACTERIZATION OF
THE "MISSISSIPPIAN LIMESTONE" IN
NORTH-CENTRAL OKLAHOMA

By

STEPHANIE LEIGH LEBLANC

Bachelor of Science in Geology

Baylor University

Waco, TX

2012

Submitted to the Faculty of the
Graduate College of the
Oklahoma State University
in partial fulfillment of
the requirements for
the Degree of
MASTER OF SCIENCE
December, 2014

HIGH RESOLUTION SEQUENCE STRATIGRAPHY AND
RESERVOIR CHARACTERIZATION OF
THE “MISSISSIPPIAN LIMESTONE” IN
NORTH-CENTRAL OKLAHOMA

Thesis Approved:

Dr. G. Michael Grammer

Thesis Advisor

Dr. James Puckette

Dr. Darwin Boardman II

ACKNOWLEDGEMENTS

I would first like to thank Dr. Michael Grammer for his insight, assistance, and constant encouragement throughout my research. I have learned so much from him in my two years at Oklahoma State University and I would not be the geologist I am today without his guidance. I am honored to call him a mentor and a friend. I would also like to thank my committee members, Dr. Jim Puckette and Dr. Darwin Boardman for their assistance as well. Their knowledge of the Mississippian of the Mid-Continent was invaluable when beginning this research.

I would like to say a huge thank you to my colleagues Buddy Price, Miranda Childress, Beth Vanden Berg, and Taylor Thompson. Their assistance and insight in regards to my study were greatly appreciated. They have made my time here at Oklahoma State University very enjoyable and I am thankful I had the opportunity to work alongside such intelligent and kind people. I would also like to thank some of the newest additions to our group, Ahmed El Belasy, Ibukun Bode, and Yulun Wang, for their encouragement while finishing my degree. I would also like to thank Sahar Mohammadi, Preston Doll, and Johnny Bertalott for their assistance with this research as well.

Furthermore, I would like to thank Dr. Matt Pranter and Dr. Mohammed Abdel Salam. Although neither professor had direct connections to my research, each of them went above and beyond to assist me with different aspects of my work. Their experience and insight helped me to greatly improve the quality of my research and I am thankful for their help.

Lastly, I would like to express my love and gratitude to my family. My deepest gratitude is due to my husband, Alex Dale, for his unwavering understanding, support, encouragement, and love throughout the duration of graduate studies. I would also like to sincerely thank my biggest cheerleaders, my parents, AJ and Myra LeBlanc, for believing in me and always supporting, encouraging, and loving me. This work was done in hopes to make all them proud to call me a wife or daughter.

Name: STEPHANIE LEBLANC

Date of Degree: DECEMBER, 2014

Title of Study: HIGH RESOLUTION SEQUENCE STRATIGRAPHY AND RESERVOIR
CHARACTERIZATION OF THE "MISSISSIPPIAN LIMESTONE" IN NORTH-
CENTRAL OKLAHOMA

Major Field: GEOLOGY

Abstract:

Mississippian limestone reservoirs are significant unconventional hydrocarbon reservoirs in central and northern Oklahoma and southern Kansas that are found at relatively shallow depths (3,000-6,000ft; 915-1,825m). Over 14,000 vertical wells have been drilled in the "Mississippian Lime" reservoirs, but recent activity has focused on developing the reservoir using horizontal drilling methods. Despite historic and recent drilling activity, little is understood about the properties and distribution of many of the productive Mississippian reservoirs.

Detailed facies analysis suggests deposition on a regionally extensive, carbonate ramp to distally steepened carbonate ramp. Facies stack into shoaling upwards packages consisting of glauconitic sandstones and weakly calcareous mudstones to wackestones at the base, followed by progressively higher energy, traction-dominated grainstone facies. The sequence stratigraphic hierarchy of the "Mississippian Limestone" can be defined as an overall 3rd order sequence (100's of meters thick) containing 4th order high frequency sequences (10's of meters thick) and 5th order cycles (few meters thick), which form due to variations in eustatic and relative sea level.

The stratigraphic hierarchy plays a major role in controlling the overall quality and vertical heterogeneity of the reservoir units. Core and thin section analyses demonstrate that the "Mississippian Limestone" is characterized mostly by fracture, moldic and vug porosity, and that the highest reservoir quality units exist in the higher energy, traction current facies. Reservoir quality appears to be mainly controlled by the 4th order high frequency sequences. Impermeable mudstones and cemented grainstones associated with these high frequency sequences likely cause vertical compartmentalization of the reservoir. Incorporating a detailed sequence stratigraphic framework into the reservoir characterization of the "Mississippian Limestone" provides an enhanced understanding of the complex lateral and vertical variability of the subsurface reservoir facies, and leads to better reservoir prediction at the exploration and production scales.

TABLE OF CONTENTS

Chapter	Page
I. INTRODUCTION	1
“Mississippian Limestone” Play History.....	1
Summary of the Problem.....	2
Overarching Questions and Hypothesis	5
Study Objectives	6
GEOLOGIC BACKGROUND	8
Structural and Tectonic History	8
Paleogeography and Climate	13
Sea Level	16
High Frequency Cyclicity.....	16
Mississippian Sea Level	18
Potential Problems in Delineating High Frequency Cyclicity	20
Regional Stratigraphy.....	21
Northeast Oklahoma	22
Northwest Arkansas	23
Southwest Missouri.....	24
Proposed Modifications to Mid-Continent Mississippian Stratigraphy	24
DEPOSITIONAL FABRICS/ARCHITECTURE AND INTERPRETATIONS	26
Kinderhookian	28
Bachelor Formation	29
Compton Formation.....	29
Northview Formation.....	30
Osagean	31
Pierson Formation.....	31
Reeds Spring Formation.....	32
Bentonville Formation (Burlington-Keokuk Formation)	35
Short Creek Member	36
Meramecian	36
Chesterian.....	38
Hindsville Formation	38
Batesville Formation	39
DATA AND METHODS.....	39

Chapter	Page
Sequence Stratigraphic Analysis	39
Core Descriptions	40
Petrographic Analysis.....	43
X-Ray Diffraction	44
Wireline Logs.....	44
Dataset Limitations	46
II. HIGH RESOLUTION SEQUENCE STRATIGRAPHY AND RESERVOIR CHARACTERIZATION OF THE “MISSISSIPPIAN LIMESTONE” IN NORTH-CENTRAL OKLAHOMA	48
INTRODUCTION	48
Geologic Setting.....	49
Stratigraphy	52
Sea Level	53
DATA AND METHODS.....	55
Core Descriptions	55
Petrographic Analysis.....	56
X-Ray Diffraction.....	59
Wireline Logs	59
FACIES ASSOCIATIONS	60
Facies 1: Glauconitic Sandstone.....	62
Facies 2: Burrowed Calcareous Mudstone-Wackestone	65
Facies 3: Bioturbated Wackestone-Packstone.....	69
Facies 4: Peloidal Packstone-Grainstone.....	72
Facies 5: Skeletal Packstone-Grainstone.....	74
SEQUENCE STRATIGRAPHIC FRAMEWORK	77
Idealized Facies Succession	77
Sequence Stratigraphic Hierarchy	78
Third-Order Sequences	78
Fourth-Order High Frequency Sequences	78
Fifth-Order High Frequency Cycles	79
Wireline Log Correlation	82
Whole Rock Mineralogy/XRD	82
Gamma-Ray.....	85
Density and Neutron Porosity.....	86

Chapter	Page
DEPOSITIONAL ANALOGS.....	88
Ancient (Outcrop) Analog: San Andres Formation.....	88
Modern Analog: Persian (Arabian) Gulf	91
3-D SEQUENCE MODELING	95
Dataset	95
Surface Modeling	96
Stratigraphic and Structural Modeling Framework.....	100
Results	101
Limitations	104
III. DISCUSSION.....	106
Reservoir Considerations.....	106
Nemaha Uplift/Ridge and Structurally Controlled Accommodation.....	113
Fair Weather Wave Base Fluctuations.....	119
IV. SUMMARY AND CONCLUSIONS	121
REFERENCES.....	125
APPENDICES	137
Appendix A	137
Appendix B	161
Appendix C	172
Appendix D	246

LIST OF TABLES

Table	Page
1. List of Wells/Cores Used in This Investigation.....	41
2. List of Wells/Cores Used in This Investigation.....	56
3. Facies Summary and Diagnostic Attributes.....	60
4. Rock-Color Chart.....	138
5. Bioturbation Index.....	139
6. Fracture Density.....	140

LIST OF FIGURES

Figure	Page
1. “Mississippian Limestone” Play Map.....	2
2. Mississippian Outcrop Map of the Tri-State Region.....	4
3. Study Area and Core Locations.....	7
4. Map of Oklahoma Structural Features	8
5. Generalized Paleo-Depositional Model of the Mid-Continent during the Early Mississippian.....	10
6. Faulting Associated with the Nemaha Uplift/Ridge	12
7. Paleogeographic Map of the Early Mississippian (345 Ma).....	14
8. Paleogeographic Map of the Late Mississippian (325 Ma).....	15
9. Variations in Greenhouse and Icehouse Conditions throughout Geologic Time	19
10. Global Sea Level and Onlap Curves for the Carboniferous Period	20
11. Stratigraphic Nomenclature for Oklahoma, Arkansas, and Missouri.....	22
12. Paleodepositional Model of the Mid-Continent during the Early Mississippian (Tournasian) Time	28
13. Dunham Classification of Carbonate Rocks	42
14. Choquette and Pray Classification of Porosity Types	42
15. Study Area and Core Locations.....	50

Figure	Page
16. Generalized Paleo-Depositional Model of the Mid-Continent during the Early Mississippian	51
17. Global Sea Level and Onlap Curves for the Carboniferous Period	54
18. Core Measured Sections and Sample Locations.....	58
19. Sub-Environments within a Carbonate Ramp Setting	59
20. Core Photographs and Thin Section Photomicrographs of Facies 1.....	63-64
21. Core Photograph and Thin Section Photomicrographs of Facies 2	67
22. Core Photographs and Thin Section Photomicrographs of Facies 3.....	70
23. Core Photograph and Thin Section Photomicrographs of Facies 4	73
24. Core Photographs and Thin Section Photomicrograph of Facies 5	75
25. Idealized Facies Succession.....	77
26. Sequence Stratigraphic Hierarchy	81
27. Sequence Stratigraphic Hierarchy and Whole Rock Mineralogy/XRD and Spectral Gamma-Ray.....	84
28. Sequence Stratigraphic Hierarchy and Borehole Measured Gamma-Ray and Density-Neutron Porosity	87
29. Facies Distribution Observed in the Permian-Aged San Andres Formation.....	89
30. Comparison of Vertical Facies Stacking Patterns Observed in the Permian-Aged San Andres Formation and the “Mississippian Limestone” in North-Central Oklahoma.....	90
31. Facies Distribution Observed in the Persian (Arabian) Gulf	94
32. Dataset Used for 3-D Sequence Modeling.....	96
33. Surfaces Used for 3-D Sequence Modeling	99
34. 3-D Model of the Mississippian Section across the Study Area	102

Figure	Page
35. Strike-Oriented (W-E) Slice through the 3-D Model.....	103
36. Dip-Oriented (N-S) Slices through the 3-D Model	104
37. Cross-Plot of Whole Core Porosity and Permeability by Depositional Facies .	107
38. Cross-Plots of Whole Core Porosity and Permeability for Each Depositional Facies.....	109
39. Core Photographs and Thin Section Photomicrographs of Reservoir-Quality Facies 5.....	110
40. Cross-Plot of Whole Core Porosity and Permeability by High Frequency Sequence Number	112
41. Cross-Plot of Whole Core Porosity and Permeability by Transgressive/Regressive Phase.....	113
42. Faulting Associated with the Nemaha Uplift/Ridge	116
43. Schematic Block Diagram of Structures within and Around the Study Area.....	11

CHAPTER I

INTRODUCTION

“MISSISSIPPIAN LIMESTONE” PLAY HISTORY

Mississippian reservoirs are significant unconventional hydrocarbon reservoirs (i.e. - reservoirs characterized by low porosities and/or low permeabilities) in central and northern Oklahoma and southern Kansas that have traditionally been developed using vertical wells (Figure 1). Fairly recent developments and advancements in horizontal drilling and completion techniques have allowed for economic production of hydrocarbons from these types of largely uneconomic unconventional reservoirs. The “Mississippian Limestone” plays represent a group of plays that have once been considered depleted, but have reemerged as a result of lateral drilling and completion techniques.

Shallow drilling depths (3,000-6,000ft/915-1,825m) and low well costs (approx. \$3.5 million) makes the “Mississippian Limestone” an appealing unconventional prospect. Smaller, independent companies comprise the majority of the “Mississippian Limestone” operators in the Mid-Continent. However, the “Mississippian Limestone”

has also attracted the attention of a few larger international companies. High water-oil ratios that can potentially shorten the economic life of a well are problematic in the “Mississippian Limestone” and emphasize the need to establish a sequence stratigraphic framework in order to better characterize and predict low water reservoir facies.

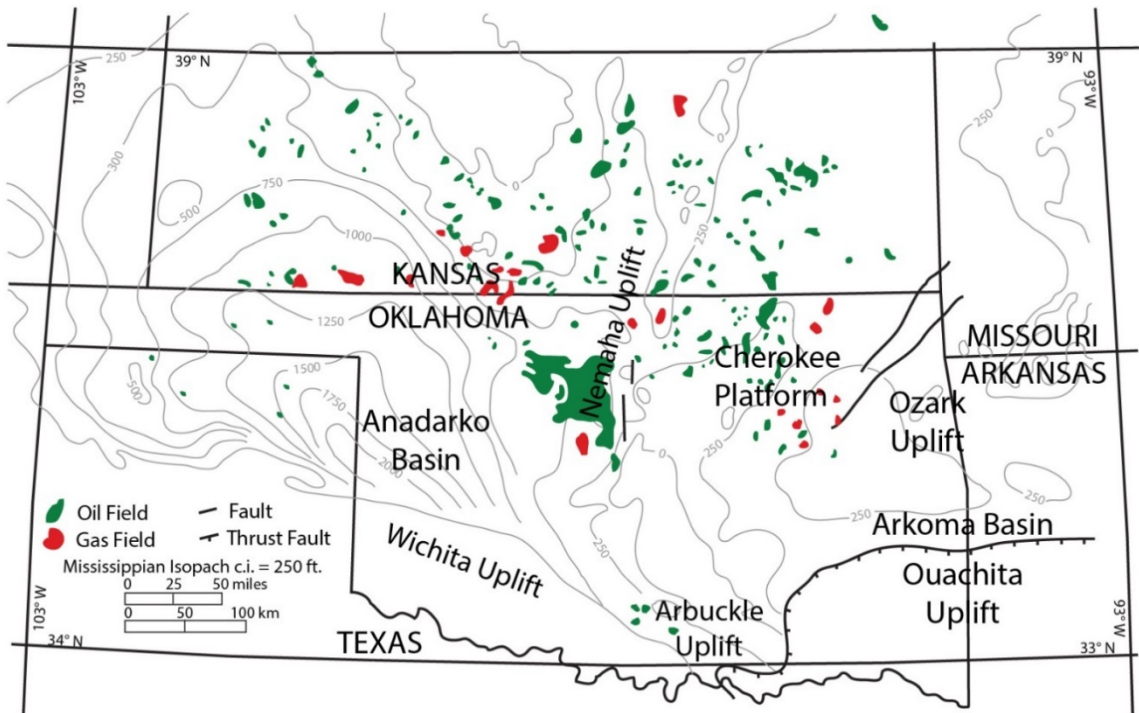


Figure 1. “Mississippian Limestone” play map showing the distribution of oil (green) and gas (red) fields across Oklahoma and Kansas. Thickness of the Mississippian section is shown in gray and is contoured in 250ft (76.2m) intervals. The largest Mississippian oil field is located in north central Oklahoma, with most of the smaller oil fields occurring to the northwest and northeast. Thickness of the Mississippian section reaches a maximum of 2000ft (610m) in western Oklahoma and is not present in southern Oklahoma on the Wichita or Ouachita Uplifts. Modified from Harris, 1987.

SUMMARY OF THE PROBLEM

The “Mississippian Limestone” is a regionally extensive mixed siliciclastic/carbonate unconventional play extending from northern Oklahoma to

southern Kansas. Unconventional plays such as the “Mississippian Limestone” are aurally extensive reservoirs characterized by low porosity and/or permeabilities that inhibit buoyancy-driven hydrocarbon migration and therefore require stimulation for economic exploitation (Roundtree et al., 2010). The “Mississippian Limestone” contains several different reservoir types including spiculite, tripolite, chert (“chat”), dolomite, mound/build-up, and grainstone facies. Recent advancements in horizontal drilling and completion methods have caused industry and academia to reconsider the reservoir potential within “Mississippian Limestone”. Historic production for over 50 years from vertical wells has shown that the “Mississippian Limestone” is a viable hydrocarbon reservoir, but horizontal drilling has revealed that reservoir units are laterally discontinuous and highly unpredictable in the subsurface.

Due to the large aerial extent of the “Mississippian Limestone” reservoirs, a wide range of carbonate environments and sub-environments are represented within the system. Previous studies have mapped the “Mississippian Limestone” across northern Oklahoma and southern Kansas using wire-line log datasets, as well as outcrop investigations in southwestern Missouri and northwestern Arkansas (Figure 2). Although attempts have been made, correlating outcrop observations to the subsurface has proven to be difficult. However, previous studies have focused on macro-scale variations in lithofacies within the Mississippian and have not clearly defined a sequence stratigraphic hierarchy within the Mississippian. Previous work on the Mississippian system in the Mid-Continent can be related to sea level fluctuations on the order of one to ten million years, but no studies have addressed the effects of higher frequency

(Milankovitch-band) sea level changes (on the scale of 20,000-400,000 years), which control facies, and therefore reservoir, distribution. Incorporating a detailed stratigraphic framework into the reservoir characterization will provide an enhanced understanding of the complex lateral and vertical variability of subsurface facies and allow for better prediction of reservoir-quality facies in the subsurface.

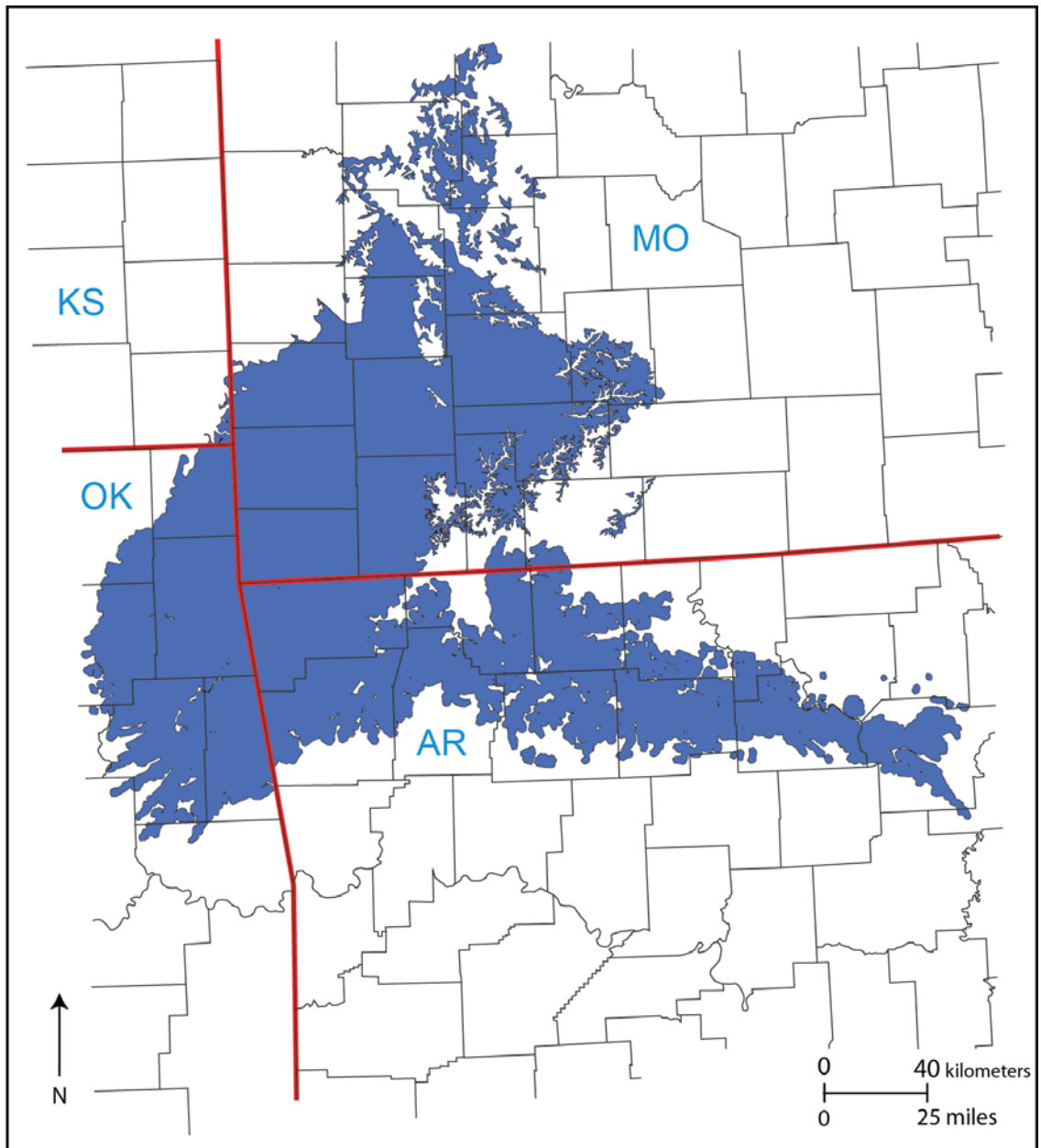


Figure 2. Map of the Tri-State region (Oklahoma, Arkansas, and Missouri) showing the aerial extent of Mississippian outcrops (blue). Deposits become younger to the west and south as the Mississippian units dip into the subsurface. Modified from Mazzullo et al., 2011a.

Building upon previous studies, this investigation established a sequence stratigraphic framework for a portion of the Mississippian in the Mid-Continent to provide an enhanced understanding of the internal 3-D architecture, fabrics, textures, and compositions associated with subsurface reservoir, and non-reservoir, facies using three representative wells from within the current play area in north-central Oklahoma.

OVERARCHING QUESTIONS AND HYPOTHESIS

The fundamental hypothesis of this investigation is that the sequence stratigraphic hierarchy demonstrated within the “Mississippian Lime” consists of regular and predictable sequences and cycles that control the development of reservoir facies at various scales. Previous outcrop and subsurface studies do not discuss how meter-scale variations in internal architecture and composition effect conventional wire-line log responses or reservoir development.

The overarching questions to be addressed in this investigation are related to Mississippian deposits in Logan and Payne Counties in northern Oklahoma (Figure 3).

The fundamental questions are as follows:

1. What attributes (i.e. - sedimentary structures, textural fabric, mineralogy, and biological constituents) characterize the internal architecture of reservoir, and non-reservoir, facies?
2. How does the sequence stratigraphic hierarchy control the development of reservoir facies?
3. Can these units be defined using commonly accepted carbonate depositional models?

STUDY OBJECTIVES

The objective of this investigation is to characterize reservoir-scale architectural attributes of the “Mississippian Lime” in northern Oklahoma. The primary goals of this investigation are to: 1) define the high-resolution sequence stratigraphic framework by identifying facies types and examining the vertical stacking patterns of facies using core and thin section data from Logan and Payne Counties; and 2) characterize variations in reservoir facies (textures, pore systems, porosity, and permeability) in order to establish controls on reservoir development. Facies data and identification of key stratigraphic surfaces in subsurface cores will allow for an enhanced understanding of the lateral and vertical variability of subsurface units. Incorporation of a detailed sequence stratigraphic framework into the reservoir characterization of the “Mississippian Lime” will increase the predictability of reservoir-quality units in the subsurface and allow for enhanced hydrocarbon production.

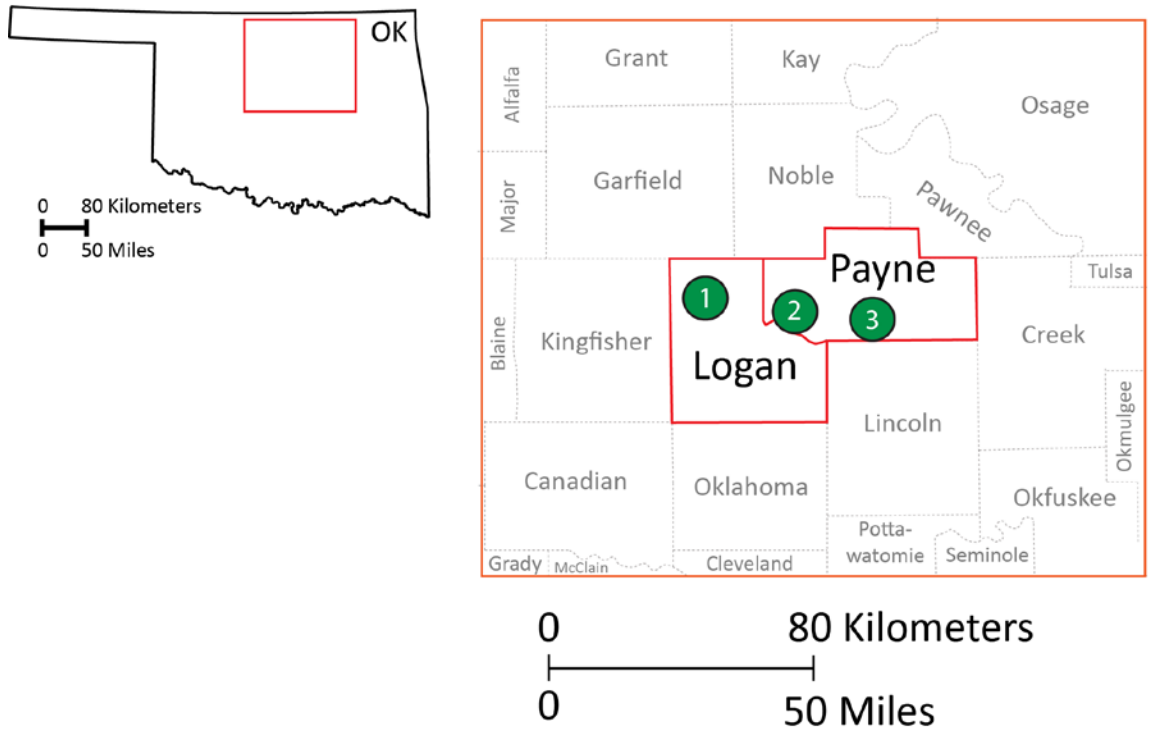


Figure 3. Map of Oklahoma showing the location of the study area and the three wells included in this study (green circles). Individual wells are, from west to east, the Adkisson #1-33, Winney #1-8, and Elinore #1-18.

GEOLOGIC BACKGROUND

STRUCTURAL AND TECTONIC HISTORY

The study area is located in north central/northeast Oklahoma on the Cherokee Platform in Logan and Payne Counties. Structural features bordering the study area are the Ozark Uplift and Arkoma Basin to the east and southeast, the Arbuckle Uplift to the south, the Anadarko Basin to the southwest and west, and the Nemaha Uplift to the west and northwest. Figure 4 illustrates the approximate size and orientation of these structural elements in relation to Logan and Payne Counties.

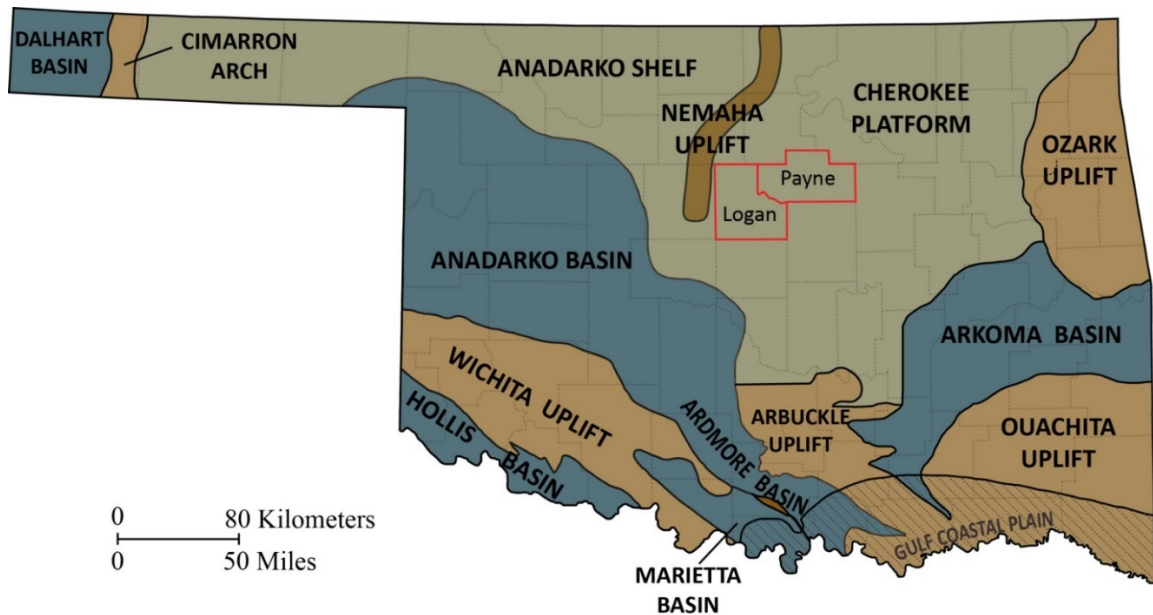


Figure 4. Map of Oklahoma showing the size and orientation of structural features relative to the study area (outlined in red). Note the location of the study region on the Cherokee Platform, east of the Nemaha Uplift. Blue regions represent depression features relative to uplifted regions (brown). Shelf and platform regions are shown in green. Modified from Northcutt and Campbell, 1996.

During the Early (~359Ma) and Middle Mississippian (~345Ma), the Mid-Continent was relatively inactive in terms of structural deformation and tectonic activity. Mississippian carbonates were deposited across hundreds of square miles across portions of Colorado, Nebraska, Kansas, Oklahoma, Arkansas, Missouri, Iowa, and Illinois across the ancient Burlington Shelf (Figure 5; Gutschick and Sandberg, 1983; Lane, 1978). The depositional strike of the system was roughly east-west, with shallower water settings occurring to the north and deeper water settings to the south. The entire ramp/shelf system was bounded to the north and northwest by the Transcontinental Arch, to the east by the Ozark Uplift in eastern Oklahoma and western Missouri and Arkansas, and to the south by the deep water settings of the Anadarko and Arkoma Basins in southern Oklahoma (Figures 4 and 5). However, outcrop relationships in eastern Oklahoma, southern Missouri, and Northern Arkansas suggest the presence of a fore-bulge in this region that created a local back-bulge basin and shelf in central and northern Missouri that prevented deposition of early Mississippian sediments to the south (Wilhite et al., 2011).

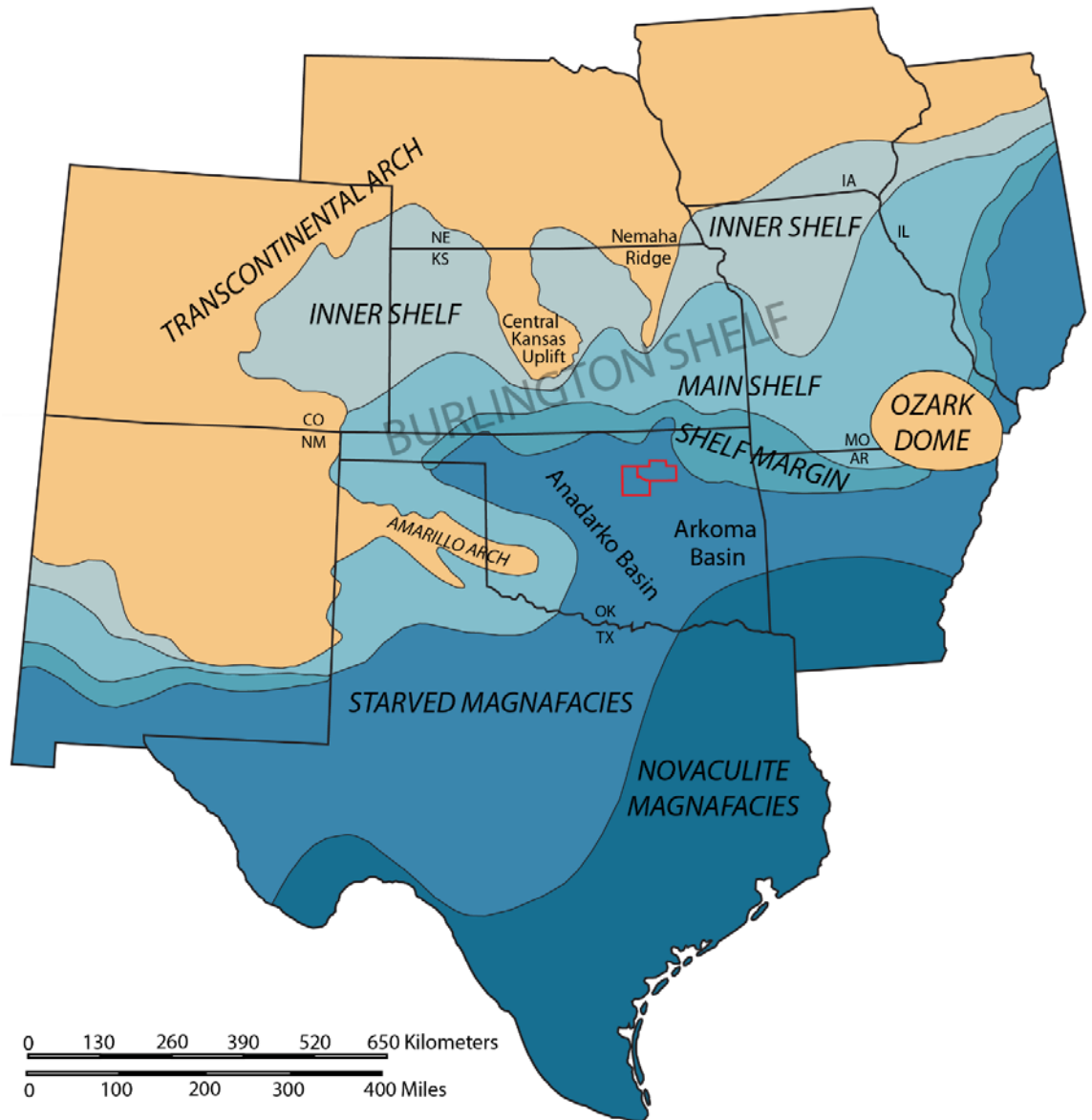


Figure 5. Generalized paleo-depositional model of the Mid-Continent representative of Early Mississippian time with the study area outlined in red. Mississippian carbonates were deposited across hundreds of square miles across portions of Colorado, Nebraska, Kansas, Oklahoma, Arkansas, Missouri, Iowa, and Illinois on the ancient Burlington Shelf. The system was bounded to the west and north by the Transcontinental Arch, to the east by the Ozark Dome, and to the south by the ancestral Anadarko and Arkoma Basins. Modified from Lane and DeKyser, 1980.

Although there was little tectonic activity during the Early and Middle Mississippian, Late Mississippian (~328Ma) and Early Pennsylvanian (~318Ma) tectonism associated with the Ouachita Orogeny led to the development of structural and geologic features in and around the study area that directly affected the deposition and spatial distribution of Late Mississippian carbonates, and the preservation of Early and Middle Mississippian carbonates. These structural features include the Wichita Uplift, Arbuckle Uplift, and the Ouachita Fold and Thrust Belt, all of which are still currently present.

The Nemaha Uplift, or Nemaha Ridge, is a north-south trending structural high that extends from Kansas into Oklahoma. It is believed to have been active during Late Mississippian or Early Pennsylvanian time (Gay, 2003; Gay, 1999). The Nemaha Uplift was formed by thrusting that occurred during a regional compressional event, resulting in widespread reverse faulting in Nebraska, Kansas, and Oklahoma (Gay, 2003; Gay, 1999). Faulting associated with the Nemaha Uplift is believed to have affected Late Mississippian deposition and likely results in complex distribution of reservoir units laterally and vertically (Figure 6).

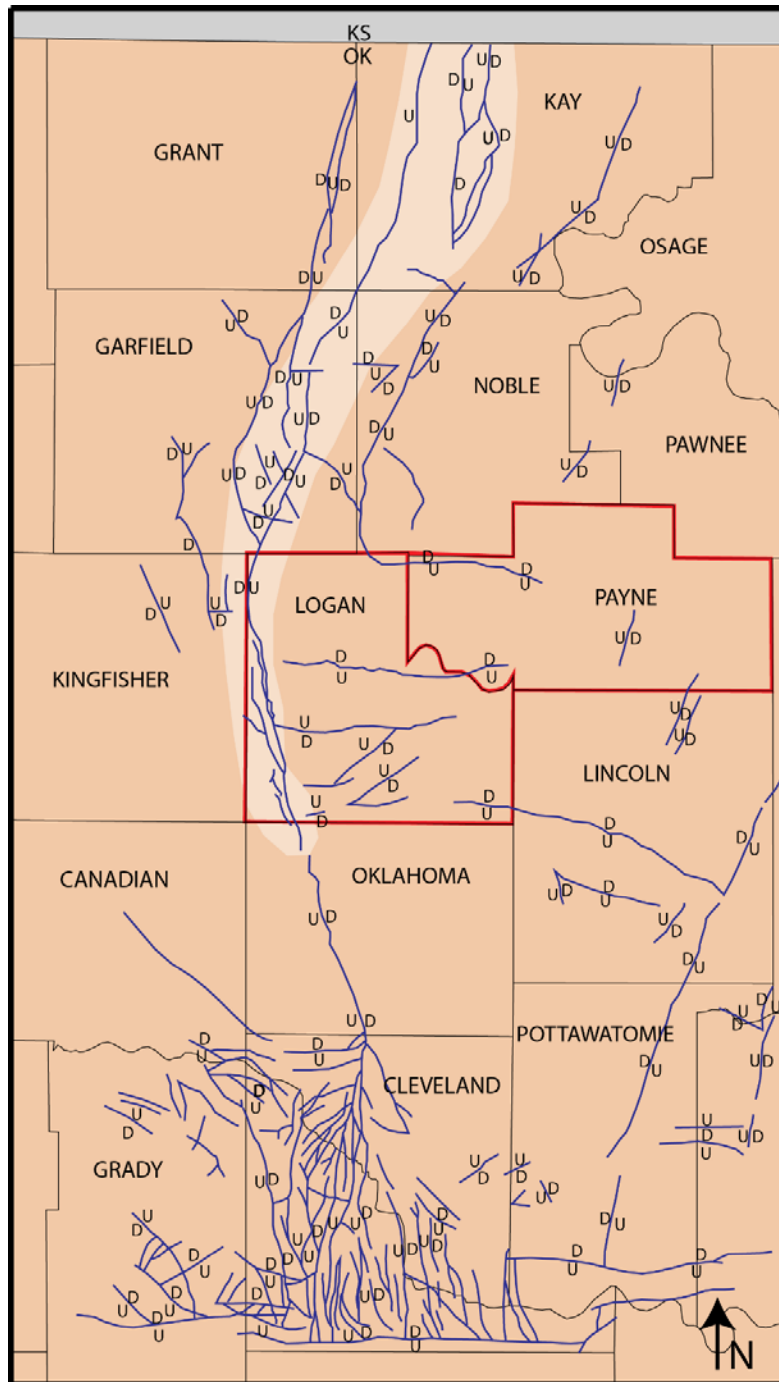


Figure 6. Map showing faulting (blue) associated with the Nemaha Uplift (off-white) in central Oklahoma. The study area is outlined in red. Faulting associated with the Nemaha Uplift is believed to have affected Late Mississippian deposition and likely results in complex distribution of reservoir units laterally and vertically. Modified from Gay, 2003.

PALEOGEOGRAPHY AND CLIMATE

During Mississippian time, much of the southern United States was covered by shallow seas and warm-temperate to subtropical, equatorial climatic conditions existed (Curtis and Champlin, 1959; Gutschick and Sandberg, 1983). Northern Oklahoma was located approximately 20-30° south of the paleoequator (Figures 7 and 8) (Mazzullo et al., 2009a). Paleo-reconstructions of the region during this time indicate that paleo-winds blew from present day northeast (Mazzullo et al., 2009a).

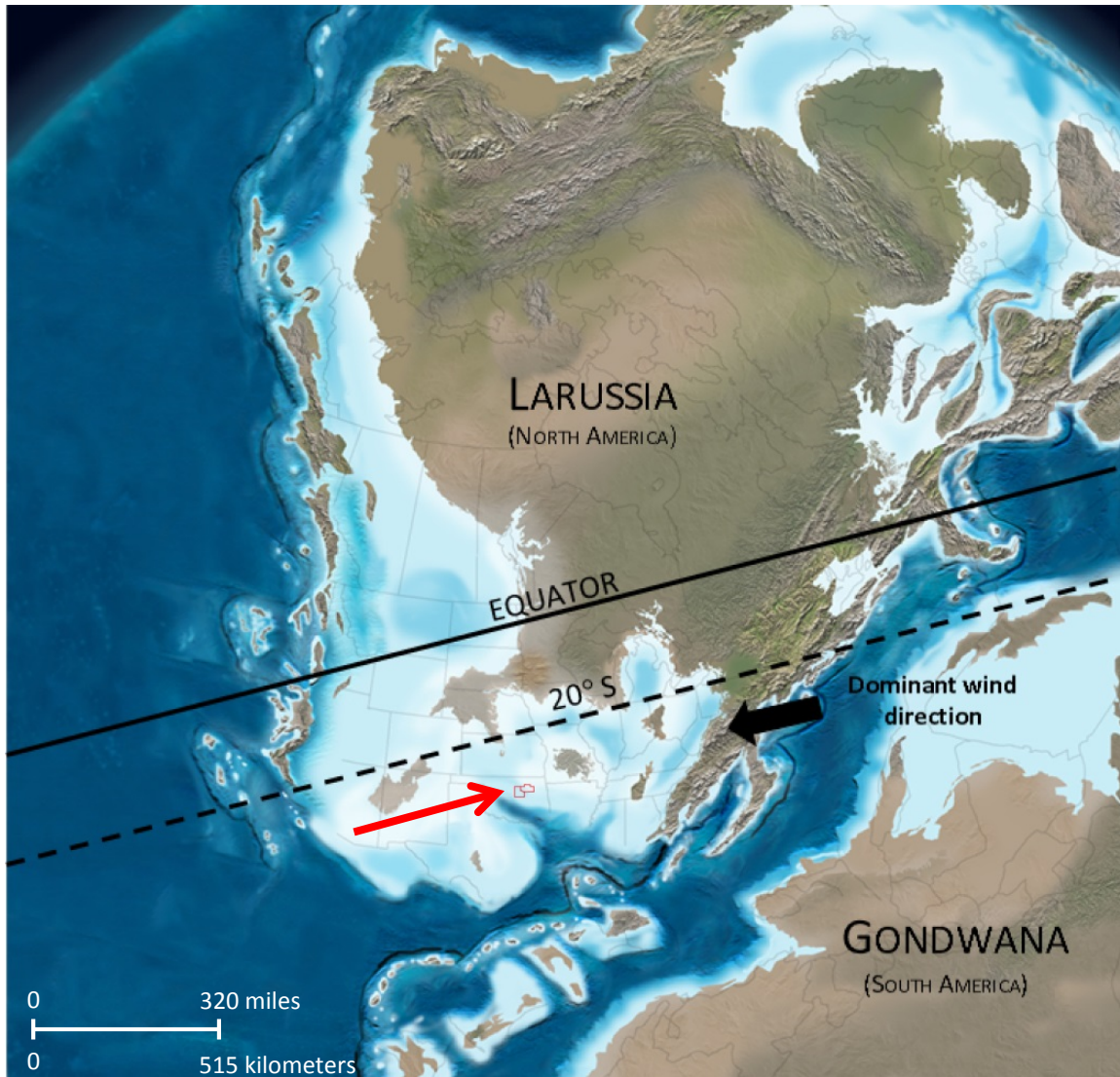


Figure 7. Early Mississippian (345 Ma) paleogeography. The study area (outlined in red and denoted by red arrow) is located between 20-30°S of the paleoequator. Water depth is indicated by color contrast with light blue indicating shallow water and darker blue indicating deeper water. During the Early Mississippian, the study area was characterized by shallow-water marine conditions that extended to the northwest, north, and northeast, with deeper waters existing to the south-southeast. Paleo-wind direction is interpreted to have come from the east-northeast. A number of uplift features (illustrated in brown and green) are shown to the northeast of the study area. Geography and wind direction at the time of deposition could potentially affect facies distribution across the study area. Modified from Blakey (2013).

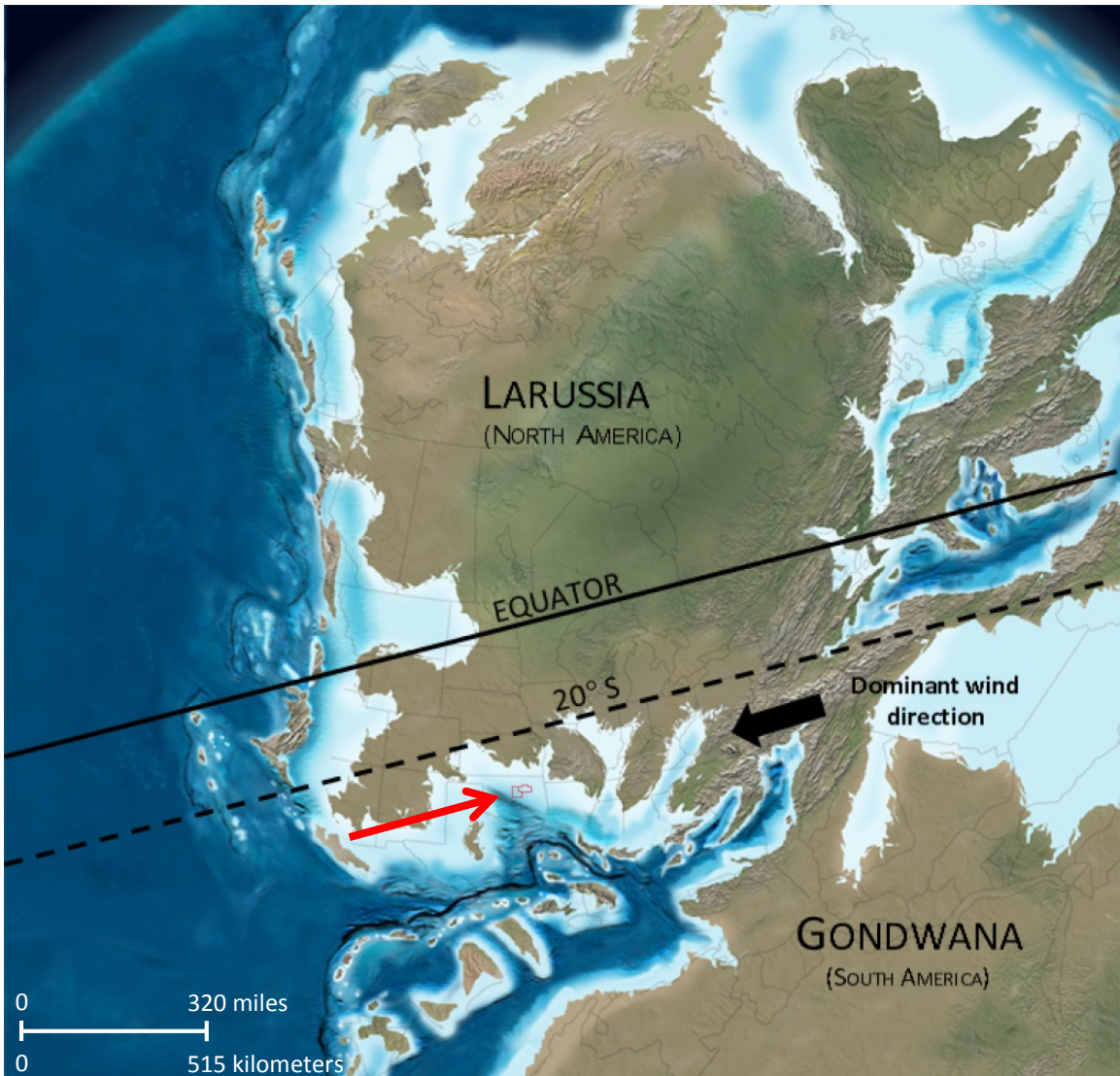


Figure 8. Late Mississippian (325 Ma) paleogeography. The study area (outlined in red and indicated by red arrow) is located between 20-30°S of the paleoequator. Water depth is indicated by color contrast with light blue indicating shallow water and darker blue indicating deeper water. During the Late Mississippian, the study area was characterized by shallow-water marine conditions while deeper waters existed to the south-southeast. Paleo-wind direction is interpreted to have come from the east-northeast. During the Late Mississippian, as opposed to the Early Mississippian, significantly more exposed land existed across the Mid-Continent and the extent of shallow-water marine conditions to the northwest, north, and northeast of the study area is greatly reduced. Geography and wind direction present at the time of deposition could potentially affect facies distribution across the study area. Modified from Blakey (2013).

The Mississippian was a transitional period between greenhouse climactic conditions that existed during the Devonian and icehouse climactic conditions that existed during the Pennsylvanian (Buggisch et al., 2008; Read, 1995). Isotope ratios measured on conodont apatite demonstrate that ocean surface temperatures cooled throughout Mississippian time, dropping from approximately 30°C during the Early Mississippian (Tournasian) to about 15°C during the Late Mississippian (Serpukhovian) (Buggisch et al., 2008; Haq and Schutter, 2008). This isotope data also suggests that the first major Mississippian glaciation event occurred in the Tournasian and persisted throughout the Visean (Middle Mississippian), and that a second glaciation event occurred in the Serpukhovian (Buggisch et al., 2008).

SEA LEVEL

Shallow-water marine carbonate systems are fundamentally influenced by water depth, therefore the character of the system is in part dependent upon sea level. Eustatic and relative sea level changes are controlled by both autogenic (internally derived) and allogenic (externally derived) factors including sedimentation rates, climate, tectonic activity, and variability in continental ice volumes due to variations in the Earth's orbit (Read, 1995). Glacial cycles are characterized by gradual regressions during glaciation and relatively rapid transgressions during de-glaciation (Read, 1995). The magnitude of sea level fluctuation is directly related to the volume of continental ice. During times characterized by icehouse conditions (i.e. – high volumes of

continental ice), sea level fluctuations can be as much as 100m (Read, 1995). However, during greenhouse conditions (i.e. – low volumes of continental ice), sea level fluctuations are generally less than 10m (Read, 1995).

HIGH FREQUENCY CYCLICITY (FOURTH- AND FIFTH-ORDER)

This study focuses on the fourth- and fifth-order, or high-frequency cyclicality in sea level change related to variability in the Earth's orbit and axial orientation with respect to the sun (Read, 1995). Fourth- and fifth-order high frequency variations in eustatic sea level are controlled primarily by Milankovitch Cyclicality. Milankovitch Cycles bring about variations in intensity and distribution of solar radiation in the higher latitudes, which in turn influences climate and glaciation. Glacio-eustatic changes in sea level related to Milankovitch Cycles are caused by: 1) eccentricity, or changes in the Earth's orbital path about the sun (100-400ky cycle) resulting in fourth-order cycles; 2) obliquity, or changes in the Earth's axial tilt in reference to the orbital plane (~40ky cycle) resulting in fifth-order cyclicality; and 3) precession, or "wobble" of the Earth's axial orientation (~21ky cycle) resulting in fifth-order cycles (Read, 1995). According to Read (1995), obliquity cycles of ~40ky are more important during icehouse times and transitional periods from greenhouse to icehouse conditions.

MISSISSIPPIAN SEA LEVEL

The Mississippian comprises the upper portion of the Kaskaskia Sequence as defined by Sloss (1963), and represents a transitional period from greenhouse conditions that existed during the Devonian to icehouse conditions that existed during the Pennsylvanian and Permian (Read, 1995) (Figure 9). Long term (first-order) eustatic sea level was positioned between 50-100m above present day sea level (Haq and Schutter, 2008). The Kinderhookian through Osagean aged strata correspond to the Tournasian through Middle Visean Stages representing approximately twenty million years (Figure 10). Six to seven 3rd order cycles were identified within this period ranging from one to six million years in length (Haq and Schutter, 2008; Ross and Ross, 1988). Ross and Ross (1988) identify 14-15 transgressive-regressive cycles throughout the entire Mississippian on the order of 1-3 million years. Haq and Schutter (2008) recognize 21 cycles of similar length within the same time frame and also note anomalously long third-order sequences (6 million years) during the Tournasian and Visean Stages (Figure 10).

Outcrop studies of the Mississippian across the Mid-Continent region have identified key exposure surfaces and sequences of strata indicative of cycles, but have not explored their significance in terms of high frequency cyclicity or determined their position within the overall sequence stratigraphic hierarchy – both of which play a major role in controlling the quality, aerial distribution, and vertical heterogeneity of reservoir units.

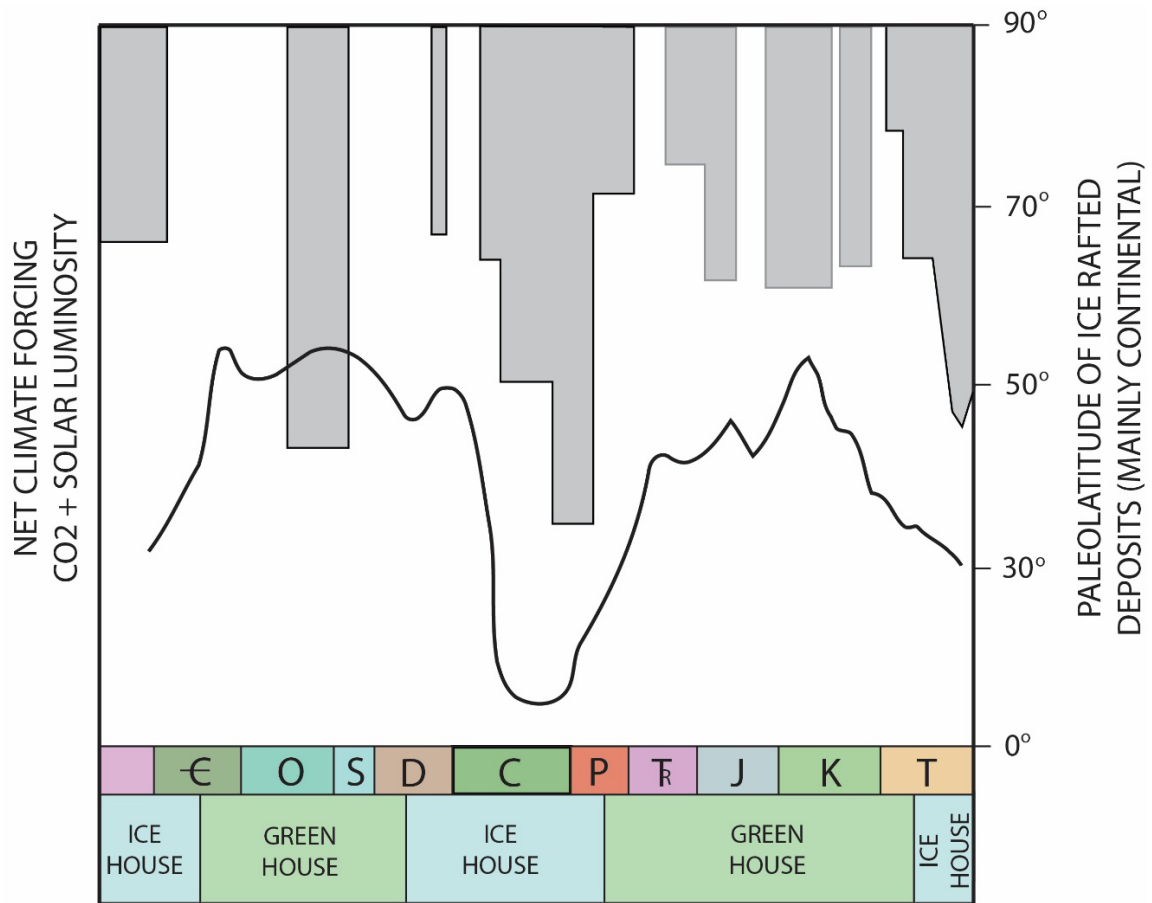


Figure 9. Diagram illustrating icehouse and greenhouse conditions that existed throughout the Phanerozoic. Paleo-latitudes of ice-rafted glacial deposits data (gray boxes with black outline) and marine ice-rafted deposits data (gray boxes with no outline) coupled with climatic change due to variation in CO₂ and solar intensity data (solid line) indicate that the Mississippian (Lower Carboniferous) represents a transitional period from greenhouse conditions that existed during the Devonian to icehouse conditions that existed during the Pennsylvanian and Early Permian. Modified from Read, 1995.

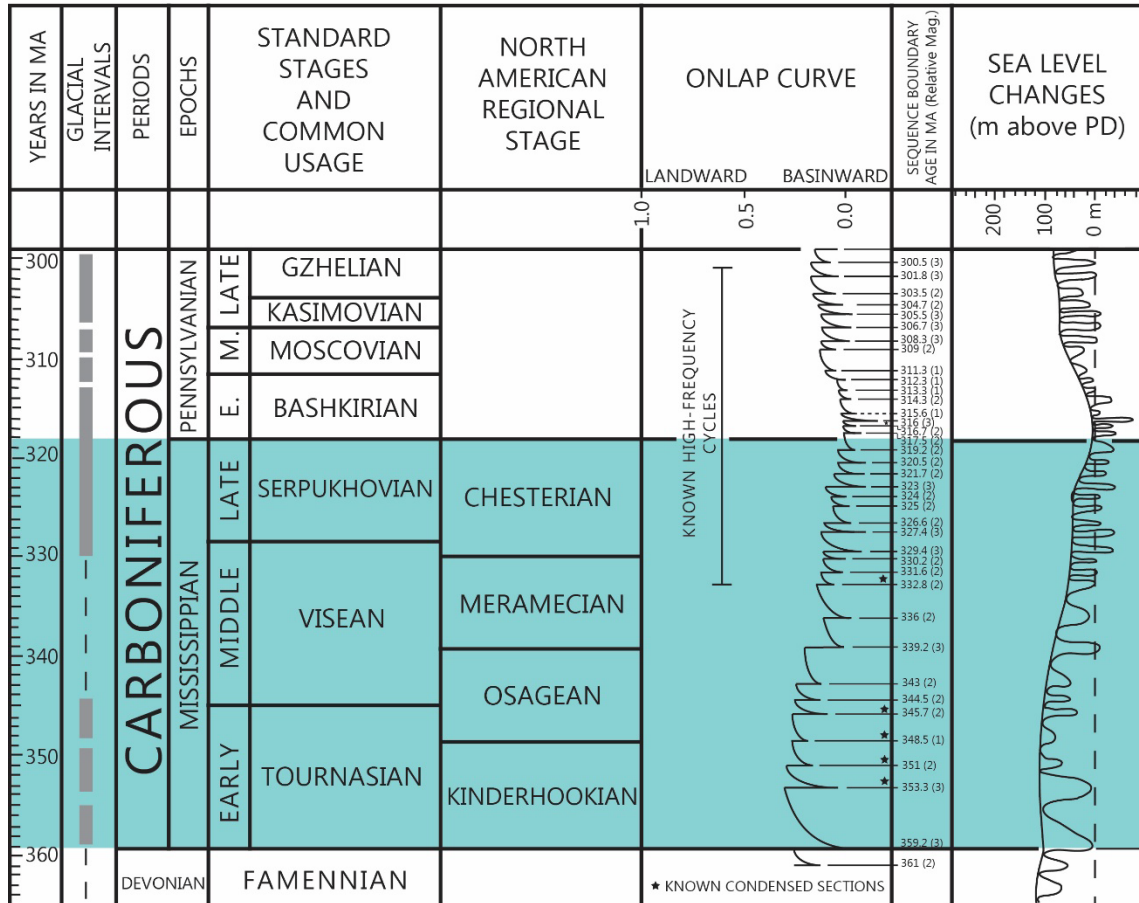


Figure 10. Diagram displaying global sea level and onlap curve for the Carboniferous Period. The Mississippian Epoch is highlighted in blue. North American regional stage names are usually used in literature when describing the age of Mississippian deposits. Length of high-frequency cycles decreases during Middle and Late Mississippian times and is possibly related to dominance of icehouse conditions. Modified from Haq and Schutter, 2008.

POTENTIAL PROBLEMS IN DELINEATING HIGH FREQUENCY CYCLICITY

Although there is a direct relationship between sea level fluctuation and the response of carbonate sedimentary systems, a number of variables can complicate the identification of high frequency cycles. Subsidence, rate of sedimentation, and sediment body migration can produce meter-scale packages of rocks similar to those attributed to high frequency (fourth- and fifth-order) cycles that are unrelated to changes in eustatic

sea level (Cowan and James, 1996; Drummond and Wilkinson, 1993; Rankey, 2002).

Without understanding the mechanism responsible for the formation of high frequency cycles, the hierarchy of cycles can easily be misinterpreted. While both autocyclic and allocyclic processes can cloud the signal of sea level fluctuation, an understanding of how facies are distributed, how facies migrate within the system, and how tectonic activity and subsidence rates affected the system, can aid in the identification of high frequency cycles related to sea level change (Drummond and Wilkinson, 1993; Rankey, 2002).

REGIONAL STRATIGRAPHY

The term “Mississippian Limestone” is an informal term that refers to all Mississippian-aged strata across the Mid-Continent. Although Mississippian strata across the Mid-Continent are dominated by carbonate deposits, they can be more accurately described as being composed of a mixture of carbonate and siliciclastic rocks. Stratigraphy of the Mississippian-aged deposits is not well-defined and is further complicated by changes in nomenclature across short distances, and between outcrop and subsurface units. Generalized lithostratigraphic columns were designed for each state and are used to characterize local outcrop and subsurface strata (Figure 11). Modifications to the Mississippian nomenclature have been recently suggested by Mazzullo et al. (2013) on the premise that the revised lithostratigraphic nomenclature is more useful in correlating strata observed in outcrop to that in the subsurface. A brief

description of each state’s generalized lithostratigraphic column is given below as these are most commonly used in literature.

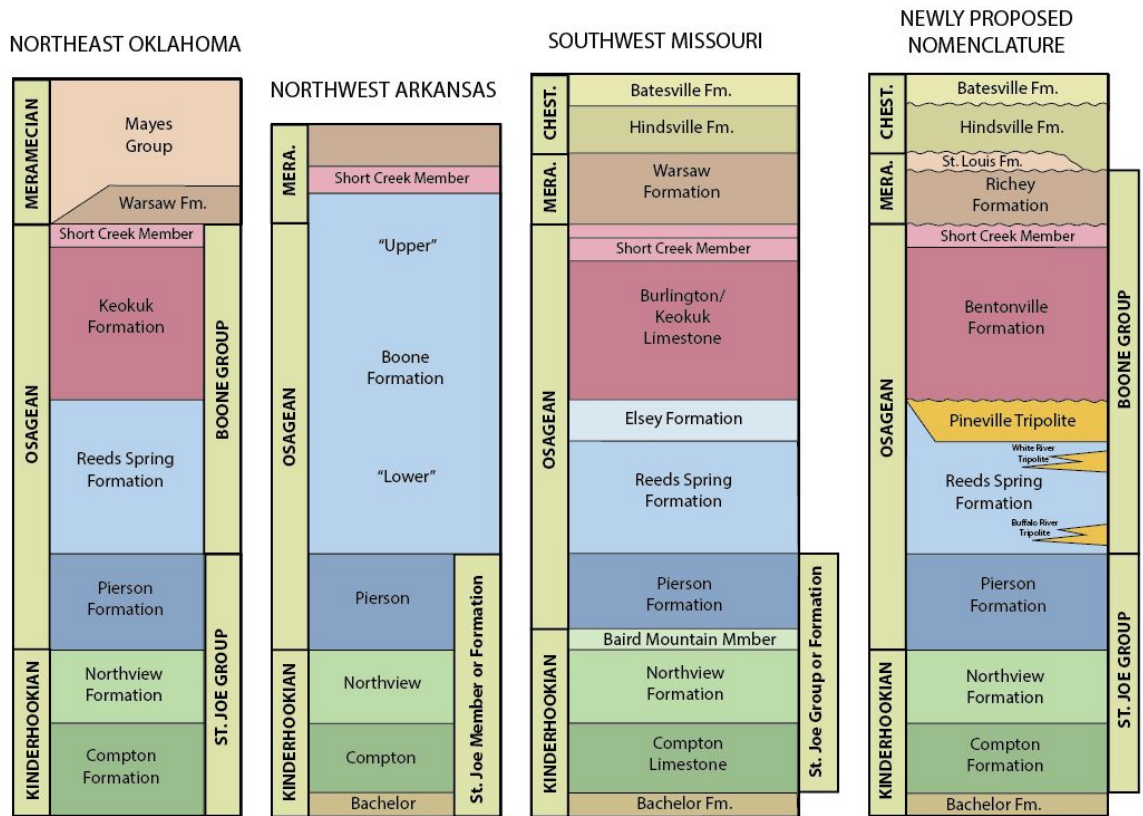


Figure 11. Stratigraphic columns and associated nomenclature for the Mississippian section in northeast Oklahoma, northwest Arkansas, and southwest Missouri. Mazzullo et al., 2013 have recently suggested modifications to nomenclature in order to standardize group, formation, and member names. Modifications to the nomenclature has been suggested on the premise that the revised lithostratigraphic nomenclature is more useful in correlating the outcrop to the subsurface. Modified from Mazzullo et al., 2013.

NORTHEAST OKLAHOMA

The Mississippian section in northeastern Oklahoma is characterized by Kinderhookian- through Meramecian-aged strata (Figure 11). Although not all sources

agree, some state that at the base of the Kinderhookian-aged strata there is a thin, shaley, siliciclastic-dominated bed present that is correlative to the Bachelor Formation (Mazzullo et al., 2013). The Bachelor Formation is often correlated to the Sycamore Sandstone (Upper Devonian) due to the presence of reworked Devonian-aged clasts, but conodont biostratigraphy indicates that deposition occurred entirely during Mississippian time (Manger and Shanks, 1976; Mehl, 1961). Kinderhookian-aged strata are composed of, in ascending order, the Compton (also referred to as the St. Joe Limestone) and Northview Formations. The base of the overlying Osagean strata is represented by the Pierson Formation. The Compton, Northview, and Pierson formations comprise what is collectively referred to as the St. Joe Group (Mazzullo et al., 2013). The remainder of the Osagean strata is composed of the Reeds Spring Formation, Keokuk Formation, and, locally, Short Creek Member, which are collectively described as the Boone Group (Mazzullo et al., 2013). Meramecian-aged strata in northeast Oklahoma is composed of the Warsaw Formation and the Mayes Group (Mazzullo et al., 2013).

NORTHWEST ARKANSAS

The Mississippian strata in northwest Arkansas are similar to those in northeastern Oklahoma, but does not include the upper units of the Meramecian (Figure 11) (Mazzullo et al., 2013). The Kinderhookian-aged strata are defined by the Bachelor, Compton, and Northview. The base of the Osagean is represented by the Pierson, and the Bachelor, Compton, Northview, and Pierson are collectively referred to

as the St. Joe Member or Formation. The rest of the Osagean and the base of the Meramecian is referred to as the Lower and Upper Boone Formations respectively. The Boone Formation is overlain by the Meramecian-aged Short Creek Member.

SOUTHWEST MISSOURI

The Mississippian section in southwest Missouri is the most complete, consisting of Kinderhookian- through Chesterian-aged strata (Figure 11) (Mazzullo et al., 2013). Here, the Bachelor Formation is not considered part of the St. Joe Group/Formation, rather it is a separate formation that exists below the St. Joe. The St. Joe Group/Formation consists of the Kinderhookian-aged Compton Limestone, Northview Formation, and Baird Mountain Member, and the Osagean-aged Pierson Limestone. The rest of the Osagean-aged strata is made up of the Reeds Spring Limestone, Elsey Formation, Burlington-Keokuk Limestone, and Short Creek Member. The terms “Boone Group” and “Boone Formation” are not recognized in southwest Missouri. Meramecian-aged strata is represented by the Warsaw Formation, and the Chesterian-aged strata consists of the Hindsville and Batesville Formations.

PROPOSED MODIFICATIONS TO MID-CONTINENT MISSISSIPPIAN STRATIGRAPHY

Mazzullo et al. (2013) propose a new stratigraphic nomenclature in an attempt to resolve current discrepancies (Figure 11). The nomenclature resembles that used in each state, but also suggests a few additional names. At the base of the stratigraphic

column is the Bachelor Formation, which is not considered to be part of the St. Joe Group. The overlying St. Joe Group is composed of the Compton Formation, Northview Formation, and the Pierson Formation. The basal unit of the Boone Group is the Osagean-aged Reeds Spring Formation. Mazzullo et al. (2013) suggest the names Buffalo River tripolite and White River tripolite for two separate tripolite facies present in the lower and upper portion of the Reeds Spring Formation respectively. Mazzullo et al. (2013) also suggest the name Pineville for the tripolite facies in the uppermost portion of the Reeds Spring Formation. Unconformably overlying the Pineville tripolite facies is the Bentonville Formation, a newly suggested name for the section that is equivalent to the Keokuk Formation, Upper Boone Formation, and Burlington-Keokuk Limestone. The top of the Osagean section is capped by the Short Creek Member. Each of the overlying formations that make up the Meramecian- and Chesterian-aged portion of the stratigraphic column are separated by unconformities, beginning with the Ritchey (top of the Boone Group) and St. Louis Formations in the Meramecian, and ending with the Chesterian-aged Hindsville and Batesville Formations.

DEPOSITIONAL FABRICS/ARCHITECTURE AND INTERPRETATIONS

Deposition of the Mississippian carbonates occurred across large portions of the United States, including Colorado, Nebraska, Kansas, Oklahoma, Arkansas, Missouri, Iowa, and Illinois, as part of a regionally extensive carbonate platform referred to as the Burlington Shelf (Figure 12; Gutschick and Sandberg, 1983; Lane, 1978; Lane and De Keyser, 1980). The Burlington Shelf transitioned abruptly into the deep, starved Illinois Basin to the north, but demonstrated a gradual transition across Missouri, Arkansas, and Oklahoma into the Anadarko Basin and the Ouachita Trough to the south (Gutschick and Sandberg, 1983).

The overall depositional system for the Mississippian is still highly debated. Lane (1978) describes the Mississippian sediments as being deposited on a carbonate shelf referred to as the Burlington Shelf (Figure 12). Although Gutschick and Sandberg (1983) also use shelf terminology to describe Mississippian carbonate deposits across the Mid-Continent, they state that there is no true definition of a shelf edge. Presently, the Mississippian carbonates are believed to have been deposited across Missouri, Arkansas, and Oklahoma on a ramp to distally steepened ramp environment, and demonstrating aggradational (Early Mississippian/ Kinderhookian) followed by progradational (Middle to Late Mississippian/Osagean) geometries (Wilhite et al., 2011). This architecture is typically recognized in the subsurface in north-central Oklahoma and southern Kansas where the focus of the “Mississippian Limestone” play exists (Wilhite et al., 2011). However, based on field observations further east in the outcrop belt, Wilhite et al. (2011) have suggested the presence of a fore-bulge region extending from eastern

Oklahoma across northern Arkansas and southern Missouri that existed during the Early Mississippian and likely affected 1) the extent to which Early to Middle Mississippian carbonates were deposited, and 2) the architecture of Middle to Late Mississippian deposits in easternmost Oklahoma, southern Missouri, and northern Arkansas. Effects of this Early Mississippian fore-bulge region are recognized in the subsurface and can cause difficulty when correlating (Wilhite et al., 2011).

Because the specific time range captured by the cores used in this study is not known, a brief summary of all described units within the “Mississippian Limestone” is given.

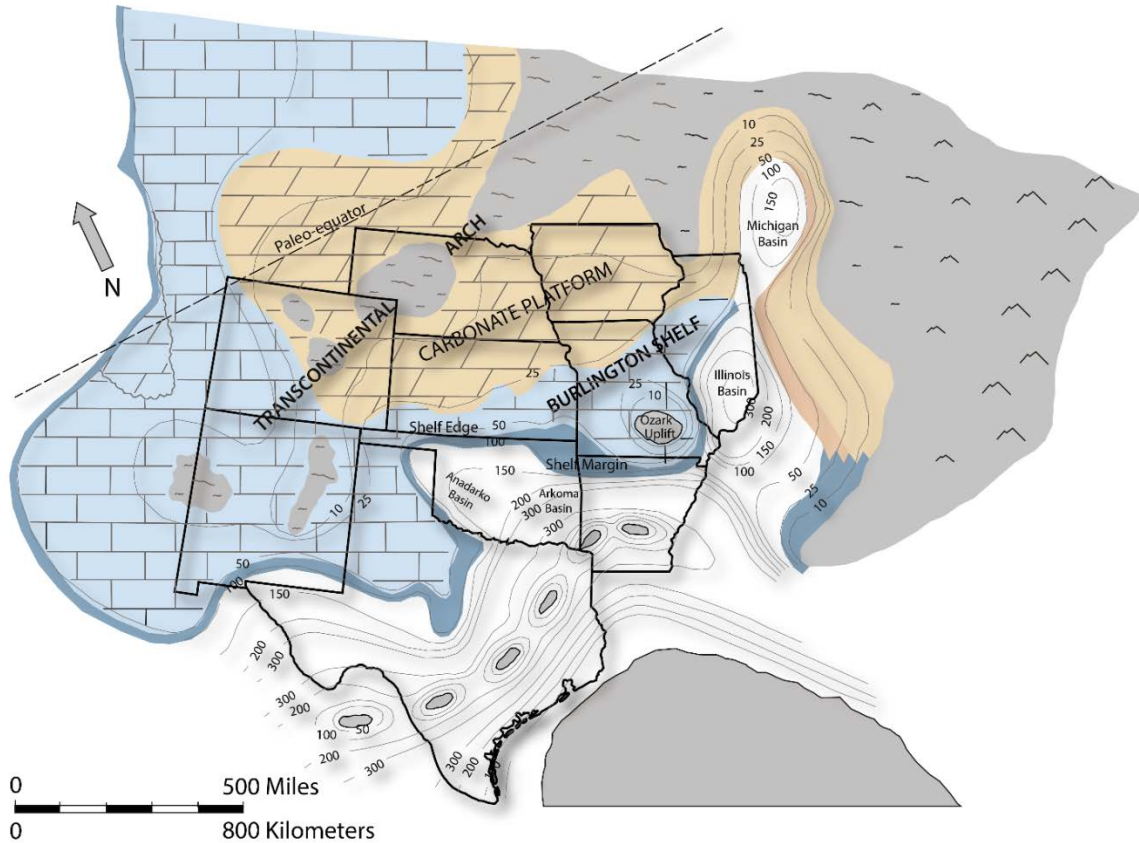


Figure 12. Paleo-depositional model of the Mid-Continent representative of the Early Mississippian (Tournasian) time. The carbonate system was bounded to the west and north by the Transcontinental Arch, to the east by the Ozark Uplift (Dome), and to the south by the ancestral Anadarko and Arkoma Basins. Generally speaking, the system trends west-east, with shallower water regions existing to the north and deeper water settings to the south. Although this paleo-depositional model is the most widely used, it is a very generalized static model that represents only a single and grossly generalized time slice of a dynamic system. Modified from Gutschick and Sandberg, 1983.

KINDERHOOKIAN

Kinderhookian-aged strata are mostly characterized by dark gray to greenish-gray silty shales and limestones (Jordan and Rowland, 1959). Generally speaking, Kinderhookian strata are less cherty than the overlying Osagean-aged strata and are

thought to have been deposited on a carbonate ramp or a distally steepened ramp (Wilhite et al., 2011).

BACHELOR FORMATION

The Bachelor Formation is composed of a lower quartzose sandstone with an upper green, glauconitic silty shale that is typically less than 2ft (0.6m) thick (Shoeia, 2012). This formation is not developed in northeastern Oklahoma outcrops.

The Bachelor Formation is thought to represent the initial flooding phase of the Burlington Shelf as evidenced by the presence of glauconite (Evans et al., 2011). The presence of sand in the Bachelor Formation is thought to be related to the Ozark Uplift in Missouri due to the fact that it forms a circular rim around the Ozark Dome (Thompson and Fellows, 1970).

COMPTON FORMATION

Conodont biostratigraphy demonstrates that the Compton Formation, or St. Joe Limestone, conformably overlies the Bachelor Formation (Thompson and Fellows, 1970). Manger and Shanks (1976) describe the Compton Formation in outcrop in northern Arkansas as a light gray, crinoid-bryozoan mudstone to wackestone with allochem content decreasing from the base to the top. In addition to the abundance of crinoid fragments, Shoeia (2012) also notes the presence of echinoderms, bryozoans, and trilobites, all of which can be identified in thin section. Another feature to note about the Compton Formation is the existence of asymmetrical *in-situ* mounds and/or

transported talus/slump blocks that range in size from 3-10ft (1-3m) high and 3-33ft (1-10m) long (Jackson and Evans, 2009; Unrast, 2013). For the most part, these mounds are composed of lime mud and contain wispy silt seams (Jackson and Evans, 2009). The mound cores are homogeneous, composed of disarticulated brachiopods and crinoids, and do not show any internal framework or obvious flank facies (Jackson and Evans, 2009; Unrast, 2013). Where mounds are present, the thickness of the Compton Formation can exceed 50ft (15m) (Huffman, 1960).

Based on paleogeographic reconstructions by Lane (1978) the Compton Formation is thought to have been deposited in a shelf margin environment. Wilhite et al. (2011) describe the Compton Formation as a series of aggrading transgressive and highstand system tract deposits on a distally steepened ramp. Due to the composition and lack of internal framework in their core and flanking facies, the mounds are interpreted to be derived from upslope slumping (Jackson and Evans, 2009).

NORTHVIEW FORMATION

The Northview Formation is generally described as a green-gray shaley limestone or laminated calcareous siltstone of wackestone to packstone texture (Kreman, 2011; Krueger, 1965; Mazzullo et al., 2009b; Shoeia, 2012). The uppermost bed identified in outcrops in Missouri is described as a silty dolomitic packstone that becomes more shale-rich to the north and more calcareous to the south (Shoeia, 2012). The Northview Formation has a maximum thickness of 80ft (25m) in southwest Missouri, but thins to less than 5ft (1.5m) to the north and south of Springfield, Missouri, and eventually

pinches out to the southwest in Cherokee County, Oklahoma (Huffman, 1960; Krueger, 1965; Shoeia, 2012). Conodont biostratigraphy suggests that the Northview Formation was deposited fairly continuously with no significant time breaks (Shoeia, 2012).

The Northview is interpreted to represent the transgressive to highstand systems tract of a very shallow-water nearshore marine environment, possibly the distal portion of a tidal flat (Mazzullo et al., 2011b). Generally speaking the Northview Formation is thought to represent deposition on a carbonate ramp from silty shale in a landward direction (north/northwest) to calcareous mudstones and wackestones in a seaward direction (south/southwest) (Wilhite et al., 2011).

OSAGEAN

In general, it is thought that depositional environments during the Osagean, from central Kansas southward, occurred on a southward dipping, gently sloping ramp toward the Anadarko Basin (Franseen, 2006; Rogers et al., 1996; Wilhite et al., 2011). Fluctuations in sea level during this time resulted in basinward progradation of Osagean strata (Wilhite et al., 2011).

PIERSON FORMATION

The Pierson Formation is lithologically similar to the Compton Formation. It consists mostly of gray lime packstones and grainstones containing brachiopod molds and corals lithified with carbonate mud (Kreman, 2011; Spreng, 1952; Wilhite et al., 2011). A glauconite interval present at the base of the Pierson Limestone serves as a

marker bed that defines the base of the Osage (Heinzelmann, 1964; Krueger, 1965). Minor amounts of dark-gray to black, blocky, and opaque chert are present within the basal Osagean (Thornton, 1961-1964). Dolomite has been found within the lower portion of the Pierson Formation in west-central Missouri (Mazzullo et al., 2011b). Similarly to the Compton Formation, the Pierson Formation contains what are interpreted by some as carbonate mud mounds. The Pierson Formation has an average thickness of 4-18ft (1.2-5.5m), but reaches 30ft (9m) in thickness near the Ozark Uplift region (Huffman, 1960; Kreman, 2011; Krueger, 1965; Wilhite et al. 2011). The limestones and dolomites of the Pierson Formation are northward dipping and erosionally truncated in southern Kansas (Wilhite et al., 2011). Here, the Pierson significantly increases in thickness to 75ft (23 meters) and consists of coarse to very coarse crinoid grainstones that downlap and prograde northward (Wilhite et al. 2011). Wilhite et al. (2011) describe the Pierson Formation as a series of deposits formed on a distally steepened ramp.

REEDS SPRING FORMATION

The Reeds Spring Formation conformably and unconformably overlies the Pierson Formation in outcrop and subsurface, and occasionally unconformably overlies the Northview Formation or the Woodford Shale (Kreman, 2011; Mazzullo et al., 2011a). The contact between the Reeds Spring and the underlying St. Joe Group is characterized by a change from grain dominated rocks (St. Joe Group) to mud dominated rocks (Reeds Spring) (Kreman, 2011). The Reeds Spring Formation is described as a medium to dark

gray, dense, fine crystalline limestone interbedded with thin beds of black to dark gray or blue-gray chert in outcrop and the subsurface (Curtis and Champlin, 1959; Huffman, 1960; Kreman, 2011; Mazzullo et al., 2011a; McFarland, 2004). Small and faint, horizontal to sub-horizontal burrows are characteristic of the upper half of the formation (Mazzullo et al., 2011a). The chert occurs in laterally continuous and discontinuous beds as well as in layers and lenses of anastomosing chert nodules that vary in thickness from a few inches to a few feet, and thicken in a basinward (south/southwest) direction (Mazzullo et al., 2011b). Narrow, deformed fractures are found within gray chert beds, but are commonly filled with white chert (Kreman, 2011; Mazzullo et al., 2011a). Branching *Thalassinoides* burrows can be found at the base of some of the chert beds (Mazzullo et al., 2011a). Dolomite is rarely observed in outcrops, but can sometimes be seen immediately beneath the unconformity present at the top of the Reeds Spring Formation (Mazzullo et al., 2011a). Dolomite has also been observed in the subsurface in southern Kansas (Mazzullo et al., 2011a). Total measured thickness of the formation in Missouri and Oklahoma outcrops is anywhere from 75-185ft (23-56m) (Mazzullo et al., 2011a). The Reeds Spring Formation thins southward in outcrops and eventually pinches out in northern Sequoyah County, Oklahoma (Huffman, 1958; Laudon, 1939; Mazzullo et al., 2011a).

The overall dark coloring, regionally extensive lithology, thin bedding, organic-rich nature, and lack of fossils in the Reeds Spring Formation suggests deposition occurred on a moderate depth ramp during a maximum sea-level highstand in Osagean time (Mazzullo et al., 2011a). Dark gray to black, shaley lime mudstone has been

identified in cores from northeast Oklahoma, indicative of deepening and pinching out depositionally to the south-southwest (Mazzullo et al., 2011a). Because the formation is not composed of pelagic skeletal grains, sediment may have been derived from an up-dip shallow-water carbonate shelf where sediment production and off-bank sediment transport were high (Mazzullo et al., 2011a). Based on conodont evidence, the Reeds Spring moderate-depth ramp passed up-dip, to the north, into shallow-water, high-energy crinoidal limestone in the lower part of the Bentonville/Burlington-Keokuk Formation (Boardman et al., 2010; Mazzullo et al. 2011a). Deposits of the Reeds Spring Formation prograde in a basinward (south/southwest) direction.

The top of the Reeds Spring Formation is characterized by an unconformity that is locally underlain by 50-60ft (15-18m) of tripolite referred to as the Pineville Tripolite (Mazzullo et al., 2011a). The Pineville Tripolite is highly fractured and has high microporosity as well as vuggy porosity (Mazzullo et al., 2011a). It can be seen on wireline logs as having high porosity and low to moderate resistivity values (Mazzullo et al., 2011a). The tripolite is light yellowish-tan in color, non-spiculitic, and common in outcrops in southwestern Missouri and northwestern Arkansas (Mazzullo and Wilhite, 2010; Mazzullo et al., 2011a). It grades downward into unaltered Reeds Spring lithologies (Mazzullo et al., 2011a).

The Pineville Tripolite is considered to be a diagenetic facies, as opposed to a depositional facies, and is therefore not indicative any specific environment of deposition (Mazzullo et al., 2013; Mazzullo et al., 2011a). The tripolite is believed to be a

product of meteoric alteration of preexisting chert present in the Reeds Spring Formation (Mazzullo et al., 2011a).

BENTONVILLE FORMATION (BURLINGTON-KEOKUK FORMATION)

The Bentonville/Burlington-Keokuk Formation is described as a thick to massively bedded, crinoid-rich lime packstone to grainstone interbedded with dolomitic mudstones and wackestones that unconformably overlie the Reeds Spring Formation (Choquette et al., 1992; Huffman, 1960). Crinoids and bryozoans are the most abundant fossils in this formation, but brachiopods and corals are also present (Choquette et al., 1992; Huffman, 1960; Mazzullo et al., 2011b). Thinly bedded green to black shale is commonly found in the uppermost part of the formation and typically transitions into the overlying Warsaw Formation (Banner and Kaufman, 1994; Choquette et al., 1992). Waulsortian-type buildups within the lower part of the Bentonville Formation are documented by King (1986) and Huffman (1960). These contain a core facies of dolomitized, bryozoan-crinoid lime mudstone and a flank facies of thin-bedded crinoidal packstone and grainstone (King, 1986). The flank facies show features such as Bouma intervals A and B, scours, flutes, and load casts (King, 1986). The maximum thickness of the Bentonville Formation is approximately 215ft (65.5m) in Missouri and 250ft (76m) in the Ozark Region, with average thicknesses ranging from 60-80ft (18-24m).

The lower portion of the Bentonville Formation is believed to represent the updip, shallower facies of the underlying Reeds Spring Formation (Handford, 2013).

Similarly to the Reeds Spring Formation, the Bentonville Formation deposits prograde in a basinward direction (Wilhite et al., 2011).

SHORT CREEK MEMBER

The Short Creek Member is an ooid-rich unit that lies directly above the Bentonville/Burlington-Keokuk Formation. The Short Creek Member typically ranges in thickness from 1-10ft (0.5-3m) where it is extensively developed, however localized thicknesses measuring up to 35ft (10.5m) thick and sporadic lenses measuring up to 25ft (7.5m) thick have been documented in northwest Arkansas and northeast Oklahoma (Braden and Ausbrooks, 2003; Lisle, 1983; McKnight and Fischer, 1970). The Short Creek Member is medium to light brown in color and weathers to a chalky white (McKnight and Fischer, 1970). The ooids exist within an opaque whitish matrix and are densely packed, mostly rounded, and slightly glauconitic (McKnight and Fischer, 1970).

The Short Creek Member is interpreted to be deposited in a high energy, shallow-water shelf margin environment during a regressive sequence of the Burlington Shelf (Greenberg, 1981; Lisle, 1983; Spreng, 1961). High ooid content and cross-bedding exist in the southwestern portion of Missouri, indicating deposition of the Short Creek Oolite as a marine sand belt or a tidal bar belt near an open shelf (Greenberg, 1981).

MERAMECIAN

Meramecian-aged strata has not been intensively studied and most reports do not distinguish individual units within the Meramecian. Rather, general observations

about the section are made. In northern and western Oklahoma, this unit is made up of gray-tan, medium to coarse-crystalline limestones that are commonly fossiliferous and partly oolitic (Jordan and Rowland, 1959; Thornton, 1961-1964). Chert is also observed in the section, but decreases in abundance in north central Oklahoma where calcareous siltstones and argillaceous limestones dominate (Jordan and Rowland, 1959; Thornton, 1961-1964). A glauconitic limestone unit observed in the tri-state district is present at the base on the Meramecian (Huffman, 1958; Thornton, 1961-1964). Meramecian strata has an average thickness of 240ft (73m) in the Stillwater-Chandler area in Oklahoma, but are missing due to pre-Pennsylvanian, or possibly pre-Chesterian, erosion to the west and northeast (Heinzelmann, 1964; Thornton, 1961-1964). Extreme differences in reported thicknesses are likely a result of complex structural and stratigraphic relationships. Although the Salem (Spergen) Limestone is clearly noted to be a separate formation within the Meramec section on most stratigraphic charts, detailed information regarding the facies, depositional environments or petrographic characteristics is rarely to never included in geologic reports of the Mississippian stratigraphy.

Curtis and Champlin (1959) hypothesize that most of the Meramecian deposits were deposited above wave base due to the presence of oolites and higher-energy deposits such as cross-bedded calcarenites and limestones with well sorted sand or silt content.

CHESTERIAN

The thickest section of Chesterian rocks was deposited in the Ardmore basin area (Curtis and Champlin, 1959). Chesterian rocks in northern Oklahoma are composed of varicolored silty and calcareous shales, and fine to coarse crystalline fossiliferous and oolitic limestones (Jordan and Rowland, 1959). In northwestern Oklahoma, sandstone or siltstone occur near the bottom of the section (Jordan and Rowland, 1959). In many places, the Chester-aged strata are absent, are thought to have either not been deposited, or have been removed by post-Mississippian erosion (Curtis and Champlin, 1959; Mikkelson, 1966; Jordan and Rowland, 1959).

HINDSVILLE FORMATION

The lithology of the Hindsville Formation is variable, but can be generally described as a gray or light to medium brown, medium-crystalline, thick-bedded oolitic and fossiliferous limestone in the Ozark Region and around the Tulsa area (Harris, 1987; Heinzelmann, 1964; Huffman, 1960; Krueger, 1965). The oolite content is highly variable and locally the ooid-rich limestones may show cross-lamination (Huffman, 1960; Krueger, 1965). The base of the formation is marked either by a thin (6in/15cm) zone of crushed brachiopod fragments, or a soft, green calcareous shale containing white limestone nodules (Heinzelmann, 1964; Huffman, 1960). However, where the Hindsville Formation rests unconformably above Osagean-aged chert, a basal conglomerate consisting of large, well-rounded pebbles of chert and limestone is typically present (Huffman, 1960; Daniels, 2012). Maximum thickness of the Hindsville Formation is

approximately 50ft (15m) and occurs in eastern Oklahoma, however, in some areas the formation has been removed completely by pre-Pennsylvanian erosion (Huffman, 1960; Kreman, 1965).

BATESVILLE FORMATION

The Batesville Formation is described as a siliciclastic sandstone and is thought to represent the near-shore facies of the underlying Hindsville Formation (Harris, 1987; Heinzelmann, 1964; Huffman, 1960; Krueger, 1965).

DATA AND METHODS

SEQUENCE STRATIGRAPHIC ANALYSIS

For this study, a sequence stratigraphic approach, as opposed to a lithostratigraphic approach, was utilized to establish the stratigraphic framework. Lithostratigraphy is the branch of stratigraphy that subdivides the rock record according to lithology. Lithostratigraphic units are generally time-transgressive and the resulting lithostratigraphic interpretations often result in a skewed view of the degree of lateral and vertical continuity of facies and may result in arbitrary formation names that may, in actuality, be related simply to facies mosaics during the same interval of time. Conversely, sequence stratigraphy is the branch of stratigraphy that divides the rock record using a succession of depositional sequences composed of genetically-related strata (i.e. – strata deposited during a single rise and fall of sea level). As a result,

sequence stratigraphy recognizes different facies that coexisted in the overall depositional environment during a given period of time. This allows for evaluation of depositional systems in a dynamic mode rather than a static one, which helps to explain the lateral variability of facies observed within a given system. The major strength of sequence stratigraphy is predictability. Sequence stratigraphy allows for the prediction of sedimentary packages, including sediment type, probable reservoir, source, or seal potential (i.e. – porosity, permeability, or total organic carbon content), geometry, and lateral and vertical continuity of strata across a sedimentary basin (Handford and Loucks, 1993). The sequence stratigraphic framework for the Mississippian section in north-central Oklahoma was established using core, thin section, and wireline log data as described in the following sections.

CORE DESCRIPTIONS

Describing core is critical for understanding the characteristics of the Mississippian section in the subsurface. Three cores were evaluated for detailed facies descriptions and include detailed observations regarding fossil content, sedimentary structures (i.e. – bedding, lamination, bioturbation, or burrows) and any visible pore types (Table 1). Descriptions of facies textures and pore types utilized the Dunham (1962) and Choquette and Pray (1970) classification schemes (Figures 13 and 14). Detailed core analysis was performed to 1) identify/confirm facies types, 2) interpret the depositional environment(s), 3) determine the effects of high frequency cyclicity on facies distribution and reservoir quality, and 4) identify reservoir heterogeneities.

Core #	Lease Name	Well No.	TD (ft)	Operator	County
1	Adkisson	1-33	6580	Devon Energy	Logan
2	Winney	1-8	5884	Devon Energy	Payne
3	Elinore	1-18	5076	Devon Energy	Payne

Table 1. List of wells that will be used in this investigation including lease name, well number, total depth (TD), operator, and county. Well information was taken from well log headers.

These three wells were chosen for this study because of their relatively close proximity to one another and because each well was cored continuously throughout the entire Mississippian section, showing contacts with both the underlying and overlying sediments. Cores #1 and #2 are approximately 11.1 miles (17.8 km) apart and Core #2 and Core #3 are 17.4 miles (28.0 km) apart (Figure 3). Studying closely-spaced cores allows for better correlation of high frequency sequences and cycles between wells and better identification of changes in reservoir facies that may occur across short distances. Mississippian cores from the three wells total 656.5ft (200m).

DEPOSITIONAL TEXTURE RECOGNIZABLE					DEPOSITIONAL TEXTURE NOT RECOGNIZABLE
Components not bound together during deposition				Components bound together during deposition	
Contains carbonate mud (clay/fine silt) (< 30 μm)			Lacks mud and is grain-supported		
Mud-supported		Grain-supported			
Less than 10% grains	More than 10% grains				
MUDSTONE	WACKESTONE	PACKSTONE	GRAINSTONE	BOUNDSTONE	CRYSTALLINE CARBONATE

Figure 13. Diagram showing the Dunham (1962) classification of carbonate rocks according to depositional textures. Modified from Scholle and Ulmer-Scholle, 2003.

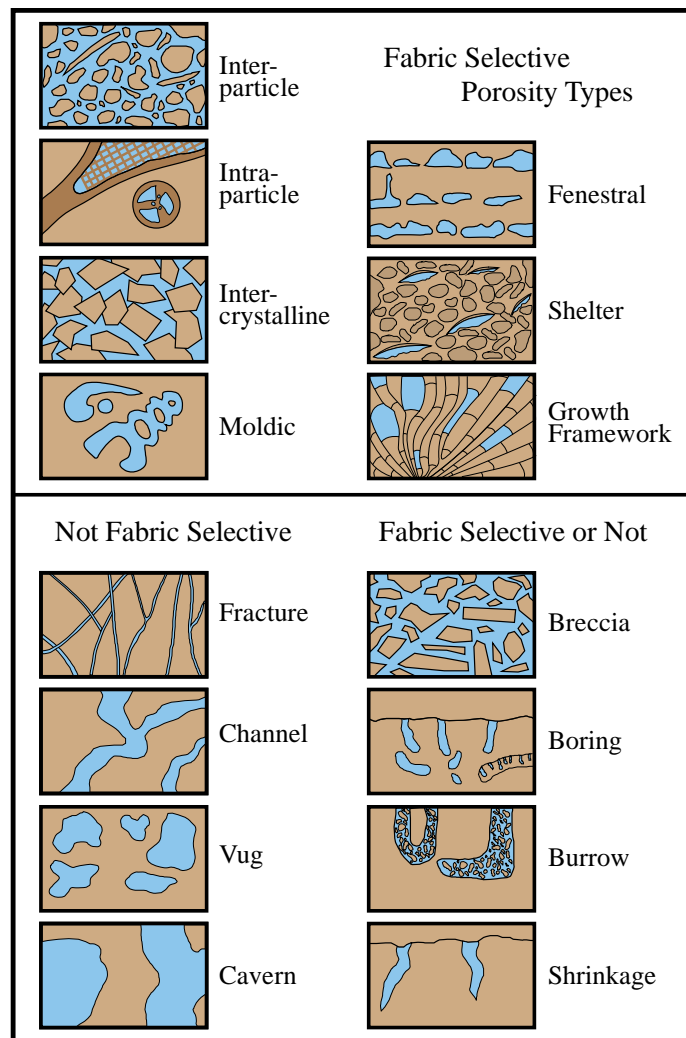


Figure 14. Diagrammatic representation of the Choquette and Pray (1970) classification of fabric selective and non-fabric selective porosity types observed in carbonate rocks. Modified from Scholle and Ulmer-Scholle, 2003.

PETROGRAPHIC ANALYSIS

Petrographic analysis is critical in determining the detailed variations in facies that is not visible in hand sample, but that may greatly affect reservoir quality.

Petrographic analysis focused on three wells and utilized thin-sections that were prepared by Weatherford Laboratories and Tulsa Thin Sections. A total of 191 thin sections covering 656.5ft (200m) of core were used in this study.

Petrographic analysis of thin-sections will primarily be used to identify key facies types. Thin-sections will allow for proper quantification of grain size using visual estimation charts as well as pore types and post-depositional alterations. As with the core descriptions, thin section descriptions will also utilize the Dunham (1962) and Choquette and Pray (1970) classification schemes (Figures 13 and 14) to describe observed textures and pore types. Porosity and permeability values measured by Weatherford Laboratories using core plugs are available for the majority of the thin sections. Additional thin sections cut for further facies analysis by Tulsa Thin Sections do not have laboratory measured porosity and permeability values, and porosity will be estimated using standard visual estimation charts.

These data were critical in identifying the environment of deposition, facies, and facies stacking patterns as well as high frequency cyclicity and its effects on reservoir quality. Relationships between porosity, permeability, facies, mineralogy, and biological constituents were examined in order to identify any patterns between these parameters and the sequence stratigraphic hierarchy in order to better understand and predict the distribution of reservoir-quality units.

X-RAY DIFFRACTION

X-ray diffraction (XRD) is an analytical method used to provide a qualitative or semi-quantitative estimation of whole rock and clay mineralogy. Core plugs sent to Weatherford Laboratories were analyzed using bulk XRD techniques and abundances of specific minerals (calcite, dolomite, quartz, and feldspars) were calculated using bulk x-ray diffraction patterns. A first order approximation of clay minerals was determined using bulk x-ray diffractions, however oriented mounts would be necessary for proper identification of specific clay minerals. For this study, XRD data were used to estimate mineralogy and add to interpretations of lithological variability, depositional cyclicity, and depositional setting.

WIRELIN LOGS

Wireline logs record physical attributes of a rock formation. These physical attributes are used as a proxy to estimate reservoir properties of the rock formation. Tool measurements and their relationships to rock characteristics are explained in depth by Asquith and Krygowski (2004). Core and thin section interpretations were used to ground-truth conventional wireline log data in order to provide a means of identifying and correlating high frequency sequences and cycles or facies based on petrophysical character.

Logs used in this study include caliper logs, gamma-ray logs, density and neutron porosity logs, and resistivity logs. Caliper logs measure borehole diameter and can indicate washout zones (increased borehole diameter) or permeable zones (decreased

borehole diameter due to mudcake build-up). Gamma-ray (GR) logs represent the natural radioactivity within a formation and give an indication of the elemental makeup of the rock material. The GR log is primarily used to differentiate lithologies and is particularly useful in identifying more shale-rich beds. Density logs indicate porosity by the measure of electron density in the formation, and neutron logs indicate porosity by the measure of hydrogen ion concentration. Together, density-neutron (D-N) porosity logs can be used to estimate porosity and identify lithologies and gas-bearing zones. Resistivity logs measure how a formation responds to current produced in an adjacent formation by electrode or induction tools. The primary use of the shallow, medium, and deep resistivity logs is to determine hydrocarbon-bearing versus water-bearing zones.

Both total spectral gamma-ray and borehole measured gamma-ray data were analyzed in this study to facilitate the correlation of facies, cycles, and sequences both vertically and laterally. In this study, spectral gamma-ray values represent laboratory measured gamma-ray values. Spectral gamma-ray methods measure the individual contributions of potassium, thorium, and uranium to the total amount of gamma-ray emission, which allows for a more detailed assessment of gamma-ray values associated with a particular unit (Doveton, 1994). Spectral gamma-ray data were analyzed in order to 1) identify trends between spectral gamma-ray signatures and sequences, cycles, and facies and 2) determine if spectral gamma-ray measurements (which may be obtained from outcrop sections) can be correlated to subsurface-measured gamma-ray signatures.

The use of wireline logs in combination with core and petrographic analyses can help to constrain high frequency sequence and cycle boundaries. Core and thin section data were compared to wireline log signatures in order to determine any relationship between facies types and wireline log signatures. Tying sequences, cycles, and/or facies to wireline log signatures allows for better prediction of reservoir-quality facies away from the study area.

DATASET LIMITATIONS

The reservoir characterization of the “Mississippian Limestone” in the study is limited in that it will integrate data from a set of only three representative wells. However, the spatial distribution of reservoir quality units likely exhibits regional and local variability between wells. The three wells used in this study are representative of the facies distribution within the study area, but may not serve as direct proxies to areas outside of the study area.

Although the contacts with the underlying Devonian-aged Woodford Shale and overlying Pennsylvanian-aged section is observed in each core, the exact age of the “Mississippian Limestone” in the studied cores is unknown. Determining the age of these cores would allow for better correlation to eustatic sea level curves and provide an enhanced understanding of the temporal range represented by the Mississippian section in the study area. Conodont biostratigraphic analysis, with a maximum resolution of one million years, has provided the most precise dataset for correlation in the Mississippian. Although conodont biostratigraphy is useful for identifying 3rd order

sequences, it cannot define the heterogeneities related to 4th and 5th order sea level variations. An idealized facies succession established for the study area was used to define high frequency sequence and cycle boundaries that are below the resolution of conodont biostratigraphy and, usually, wireline logs. Identifying these high frequency sequences and cycles is critical as they generally serve as individual flow and/or reservoir units in carbonate systems. These issues are obstacles for true reservoir characterization, but are not uncommon problems of reservoir characterization studies.

CHAPTER II

HIGH RESOLUTION SEQUENCE STRATIGRAPHY AND RESERVOIR CHARACTERIZATION OF THE “MISSISSIPPIAN LIMESTONE” IN NORTH-CENTRAL OKLAHOMA

INTRODUCTION

Mississippian reservoirs are significant unconventional hydrocarbon reservoirs (i.e. - reservoirs characterized by low porosities and/or low permeabilities) in central and northern Oklahoma and southern Kansas that have traditionally been developed using vertical wells. However, fairly recent developments and advancements in horizontal drilling and completion techniques have allowed for economic production of hydrocarbons from these reservoirs. Shallow drilling depths (3,000-6,000ft/915-1,825m) and low well costs (approx. \$3.5 million) makes the “Mississippian Limestone” an appealing unconventional prospect. Despite recent drilling efforts and renewed interest in the “Mississippian Limestone”, the vertical and lateral heterogeneity of the system is still poorly understood. Previous studies of the Mississippian section have not defined the control of high frequency sea level fluctuations on facies distribution, which in turn controls reservoir heterogeneity.

The primary goals of this research are to: 1) define the high-resolution sequence stratigraphic framework by identifying facies types and examining the vertical stacking patterns of facies using core and thin section data from three wells located in Logan and Payne Counties, Oklahoma; and 2) characterize variations in reservoir facies (textures, pore systems, porosity, and permeability) in order to establish controls on reservoir development. Incorporation of a detailed sequence stratigraphic framework into the reservoir characterization of the “Mississippian Limestone” increases the predictability of reservoir-quality units in the subsurface, allows for an enhanced understanding of reservoir and seal geometries and distributions, and ultimately leads to enhanced hydrocarbon production. This work not only has direct implications for understanding the “Mississippian Limestone” in north-central Oklahoma, but the methodologies followed and conclusions determined by this study may also be applied to other ancient carbonate systems deposited under similar environmental conditions.

GEOLOGIC SETTING

The study area is located in north-central/northeast Oklahoma on the Cherokee Platform in Logan and Payne Counties (Figure 15). Mississippian deposition occurred in relatively shallow, tropical to subtropical conditions 20-30° south of the paleoequator (Curtis and Champlin, 1959; Gutschick and Sandberg, 1983; Witzke, 1990). It is currently accepted that deposition occurred on a ramp to distally steepened ramp type environment, with strike trending roughly east-west (Mazzullo et al., 2011a). The ramp

system was regionally extensive and deposited Mississippian sediments across hundreds of square miles in portions of Colorado, Nebraska, Kansas, Oklahoma, Arkansas, Missouri, Iowa, and Illinois (Figure 16) (Gutschick and Sandberg, 1983; Lane, 1978). Proximal, shallower water conditions were present to the north, and deeper water, sediment starved conditions existed to the south (Gutschick and Sandberg, 1983; Lane and DeKyser, 1980). The entire ramp system was bounded to the north and northwest by the Transcontinental Arch, to the east by the Ozark Uplift, and to the south by the deep water settings of the ancestral Anadarko and Arkoma Basins (Lane and DeKyser, 1980).

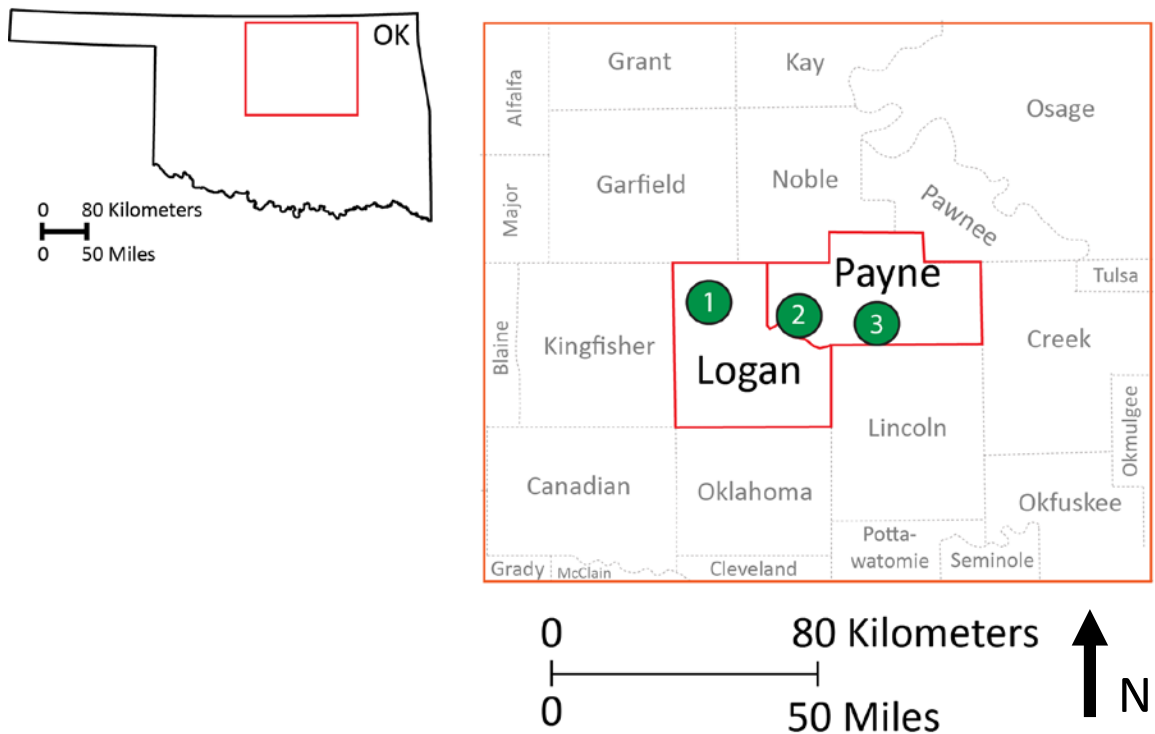


Figure 15. Map of Oklahoma showing the location of the study area and the three wells included in this study (green circles). Individual wells are, from west to east, the Adkisson #1-33, Winney #1-8, and Elinore #1-18.

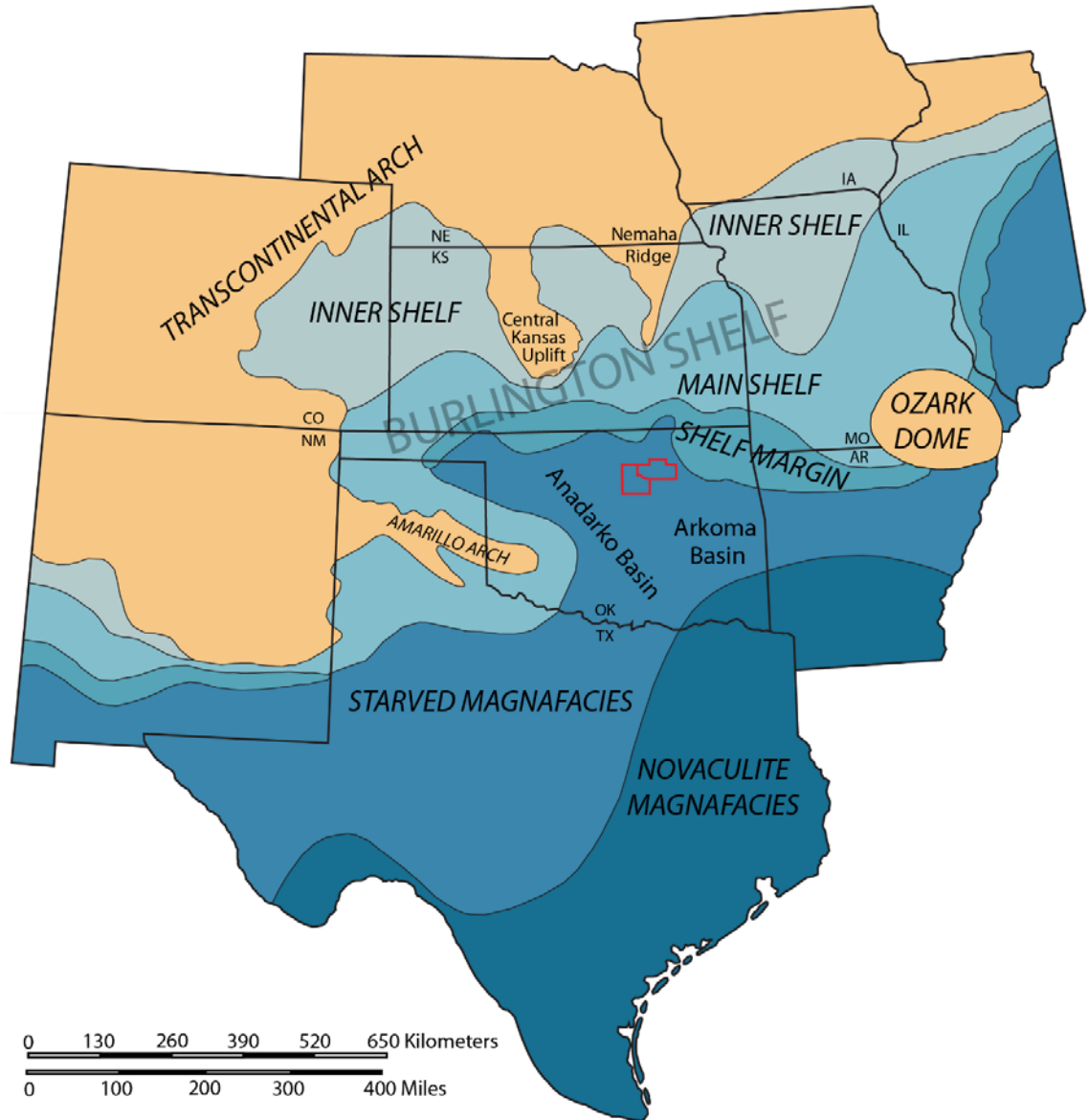


Figure 16. Generalized paleo-depositional model of the Mid-Continent representative of Early Mississippian time with the study area outline in red. Mississippian carbonates were deposited across hundreds of square miles across portions of Colorado, Nebraska, Kansas, Oklahoma, Arkansas, Missouri, Iowa, and Illinois on the ancient Burlington Shelf. The system was bounded to the west and north by the Transcontinental Arch, to the east by the Ozark Dome, and to the south by the ancestral Anadarko and Arkoma Basins. Modified from Lane and DeKyser, 1980.

During the Early (359Ma) and Middle Mississippian (345Ma), the Mid-Continent was relatively inactive in terms of structural deformation and tectonic activity.

However, during Late Mississippian or Early Pennsylvanian time, it is believed that the Nemaha Uplift or Nemaha Ridge, a north-south trending structural high extending from Kansas into Oklahoma, was active (Gay, 2003; Gay, 1999). Faulting associated with the Nemaha Uplift is believed to have affected Mississippian deposition and likely results in complex distribution of reservoir units laterally and vertically due to localized changes in accommodation related to tectonic movement.

STRATIGRAPHY

The term “Mississippian Limestone” is an informal term that refers to all Mississippian-aged strata across the Mid-Continent. Throughout the Mid-Continent, the Mississippian section unconformably overlies the Devonian-aged Woodford Shale and is capped by a regionally extensive, erosional unconformity. Although Mississippian strata in the Mid-Continent region are dominated by carbonate deposits, the rocks can be more accurately described as being composed of a mixture of carbonates and siliciclastics. Stratigraphy of the Mississippian-aged deposits is not well-defined and is further complicated by changes in nomenclature across short distances, as well as between outcrop and subsurface units. Although the exact stratigraphic range represented by the three cores used in this study is not known, the unconformable contacts between the Mississippian section and the underlying and overlying formations is observed in all three cores and a generalized sequence stratigraphic framework for the Mississippian section can still be defined using facies relationships. This sequence

stratigraphic framework can be used to explain the lateral and vertical variability observed throughout the region.

SEA LEVEL

The Mississippian represents a transitional period from greenhouse conditions that existed during the Devonian, to icehouse conditions that existed during the Pennsylvanian and Early Permian (Read, 1995). Long term (first-order) eustatic sea level was positioned between 165-328ft (50-100m) above present day sea level (Figure 17) (Haq and Schutter, 2008). Although little work has been done to quantify the amplitude of sea level fluctuations during the Mississippian, it is likely that amplitudes exceeded those typical of greenhouse conditions (5-15m). Even if sea level amplitudes were lower than estimated, small eustatic fluctuations experienced on low inclination carbonate ramp systems would still likely result in widespread, and geologically rapid, migration of facies. Numerous fluctuations in Mississippian sea level of probable 3rd order scale are noted on global sea level curves and likely influenced Mississippian deposition across the Mid-Continent (Haq and Schutter, 2008; Ross and Ross, 1988).

Although outcrop studies of the Mississippian across the Mid-Continent region have identified key exposure surfaces and sequences of strata indicative of cyclic deposition, these studies have not explored their significance in terms of high frequency cyclicity or determined their position within the overall sequence stratigraphic hierarchy – both of which play a major role in controlling the quality, aerial distribution, and

vertical heterogeneity of reservoir units. It is therefore necessary to identify the influence of sea level at various scales in order to determine its control on Mississippian reservoir development and distribution across the study area.

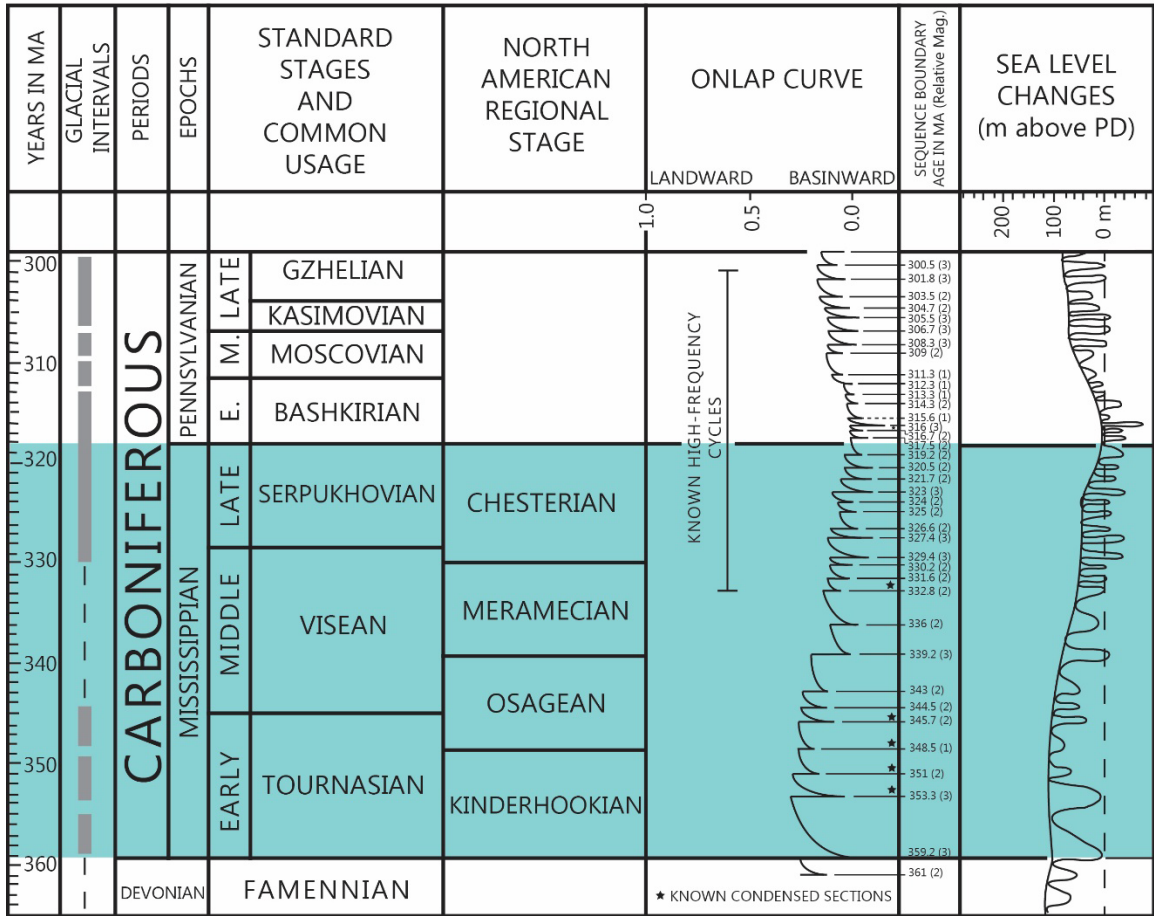


Figure 17. Diagram displaying global sea level and onlap curve for the Carboniferous Period. The Mississippian Epoch is highlighted in teal. North American regional stage names are usually used in literature when describing the age of Mississippian deposits. Length of high-frequency cycles decreases during Middle and Late Mississippian times and is possibly related to dominance of icehouse conditions and larger fluctuations in sea level, resulting in more distinct cycle boundaries. Modified from Haq and Schutter, 2008.

DATA AND METHODS

CORE DESCRIPTIONS

Core analysis is critical for understanding the characteristics of the Mississippian section in the subsurface as observations made in outcrop tend to differ greatly from those made in the subsurface. In order to better understand the Mississippian section in north-central Oklahoma, detailed core analysis was performed using three representative cores (Table 2) to: 1) identify/confirm facies types, 2) interpret the depositional environment(s), 3) determine facies successions and establish a hierarchical classification of vertical stacking patterns, 4) determine the effects of high frequency cyclicity on facies distribution and reservoir quality, and 5) identify reservoir heterogeneities throughout the Mississippian section. Mississippian cores from the three wells total 656.5ft (200m). Descriptions of facies textures and pore types utilized the Dunham (1962) and Choquette and Pray (1970) classification schemes. Detailed core descriptions include observations regarding fossil content, sedimentary structures (i.e. – bedding, lamination, bioturbation, or burrows) and any visible pore types.

Core #	Lease Name	Well No.	Core Length (ft)	TD (ft)	Operator	County
1	Adkisson	1-33	323.7	6580	Devon Energy	Logan
2	Winney	1-8	189.6	5884	Devon Energy	Payne
3	Elinore	1-18	143.2	5076	Devon Energy	Payne

Table 2. List of wells that were used in this investigation including lease name, well number, core length, total depth (TD), operator, and county. Well information was taken from well log headers.

These three cores were selected for this study based upon the following criteria:

1) relatively close proximity to one another given the available core dataset, 2) completeness of cored interval, and 3) availability of conventional wireline log suites (i.e. – gamma-ray, caliper, density and neutron porosity, and resistivity logs). Cores #1 and #2 are approximately 11.1 miles (17.8km) apart and Core #2 and Core #3 are 17.4 miles (28.0km) apart (Figure 15). A transect connecting these three cores roughly parallels the shelf margin during deposition and illustrates an along-strike or oblique-to-strike profile. Each of the three wells was cored continuously throughout the entire Mississippian section, showing contacts with both the underlying and overlying formations. Studying closely-spaced and continuous cores allows for better correlation of high frequency sequences and cycles between wells and better identification of changes in reservoir facies that may occur across short distances.

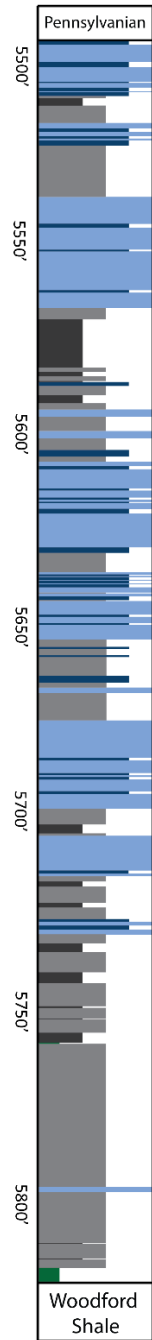
PETROGRAPHIC ANALYSIS

A detailed understanding of the facies distribution in the subsurface is critical to the interpretation of depositional environments and the understanding of facies types

and stacking patterns demonstrated within the Mississippian section in north-central Oklahoma. Due to the fine-grained nature and microscopic variabilities observed in outcrop and subsurface facies, the Mississippian section cannot be accurately described using only hand samples. Thin section analysis of the cores used in this study allows for more accurate facies descriptions and proper quantification of grain size, and helps to determine detailed variations in facies that are key in understanding changes in environmental setting due to high frequency sea level fluctuations.

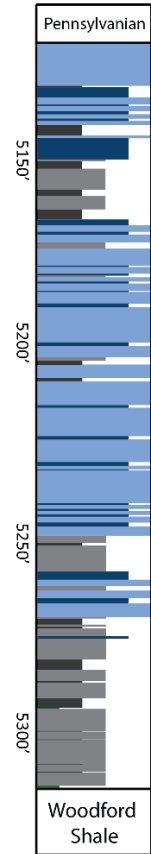
In this study, petrographic analysis focuses on three wells with Mississippian cores and utilizes 191 thin sections prepared by Weatherford Laboratories and Tulsa Thin Sections. All thin sections were alizarin red stained and/or blue epoxy impregnated (Figure 18). Thin section locations were chosen based on identifiable changes in the rock fabric. As with the core descriptions, thin section descriptions also utilized the Dunham (1962) and Choquette and Pray (1970) classification schemes to describe observed textures and pore types. Porosity (NCS) and permeability (Klinkenberg) values measured by Weatherford Laboratories using core plugs are available for the majority of the thin sections. Porosity was estimated using standard visual estimation charts for the remaining thin sections. These porosity and permeability data were utilized to determine patterns between reservoir development and position within the overall sequence stratigraphic framework.

Adkisson #1-33
 323.7ft core
 94 thin sections

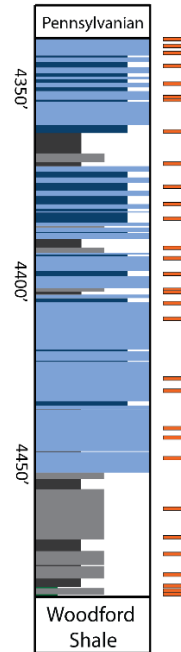


TOTAL:
656.5ft of core
191 thin sections

Winney #1-8
 189.6ft core
 66 thin sections



Elinore #1-18
 143.2ft core
 31 thin sections



■ Facies 1 ■ Facies 2 ■ Facies 3 ■ Facies 4 ■ Facies 5

Figure 18. Measured sections showing the lengths of each core and the distribution of thin sections (rectangles to the right of the measured sections) throughout the Mississippian interval. Sample locations were chosen based on identifiable changes in the rock fabric. This sample density captures the variability of facies well.

X-RAY DIFFRACTION (XRD)

X-ray diffraction (XRD) is an analytical method used to provide a qualitative or semi-quantitative estimation of whole rock and clay mineralogy. Core plugs sent to Weatherford Laboratories were analyzed using bulk XRD techniques and abundances of specific minerals (calcite, dolomite, quartz, and feldspars) were calculated using bulk x-ray diffraction patterns. A first order approximation of clay minerals was determined using bulk x-ray diffractions, however oriented mounts would be necessary for proper identification of specific clay minerals. For this study, XRD data were used to estimate mineralogy and add to interpretations of lithological variability, depositional cyclicity, and depositional setting.

WIRELINE LOGS

Core and thin section data were used to ground-truth conventional wireline log data in order to provide a means of identifying and correlating sequences based on petrophysical character. This is important as core data is not usually readily available and, as a result, subsurface correlations are primarily made using wireline logs. Logs utilized for each of the three cores used in this study include: 1) gamma-ray (total spectral and borehole measured), 2) caliper, 3) density porosity, 4) neutron porosity, and 5) shallow, medium, and deep resistivity. The use of wireline logs in combination with core and petrographic analyses can serve as a powerful tool that helps to constrain the high frequency sequence stratigraphic framework and allow for the correlation of high frequency sequence and cycle boundaries into areas where core and thin section data may be lacking.

FACIES ASSOCIATIONS

Five facies were identified through the analyses of the three cores (656.5ft; 200m) and defined on the basis of texture, grain types, sedimentary structures, environmental indicators, and color. Observations from core descriptions were supplemented using 191 thin sections. XRD analyses were integrated to aid in the determination of mineralogical abundance within each facies identified. Table 3 provides a detailed summary of each facies and their characteristics. Colors were determined using the GSA rock color designation chart (Table 4) (Goddard et al., 1951). Additional core photos and thin section photomicrographs of each facies can be found in Appendices C and D.

	Facies	Color	Mineralogy (Avg. %)			Sedimentological Character	Primary Grain Constituents	TOC (Avg. %)	Permeability (Avg. mD)	Porosity (Avg. %)	No. of Samples
			Clays	Carbonates	Other						
5	Skeletal Packstone-Grainstone	Medium to Dark Gray and Dark Yellowish Brown	1.5	45.0	53.5	Cross-Bedded Skeletal Debris, Mineralized Fractures	Crinoid, Brachiopod, and Bryozoan Fragments, Sponge Spicules, and Peloids	0.32	0.049	3.32	74
4	Peloidal Packstone-Grainstone	Olive Gray	2.1	59.8	38.1	Massive Bedded, Bioturbated, Mineralized Fractures	Peloids, Crinoids, Sponge Spicules, and Brachiopod Fragments	0.10	0.003	1.42	40
3	Bioturbated Wackestone-Packstone	Dusky Yellowish Brown	6.4	49.6	44.0	Bioturbated and Burrowed, Locally Thinly Bedded	Crinoid and Brachiopod Fragments and Sponge Spicules	0.52	0.045	1.57	55
2	Burrowed Calcareous Mudstone-Wackestone	Brownish Black to Grayish Black	16.1	32.5	51.4	Planar Laminae, Locally Burrowed to Bioturbated	Brachiopods and Sponge Spicules	1.49	0.019	1.64	14
1	Glauconitic Sandstone	Dark Greenish Gray	23.0	17.5	59.5	Massive Bedded, Burrowed	Conodonts and Brachiopod Fragments	2.28	0.358	9.45	5

Table 3. Outline of the facies identified in Mississippian cores including the sedimentological characteristics, dominant grain constituents, and average total organic carbon (TOC) associated with each facies. Key reservoir properties (permeability and porosity) are also reported and represent an average calculated using core data from all three wells.

The facies are ordered and described in a shallowing/shoaling-upward sequence, beginning with what is interpreted to be the deepest or most restricted depositional

environment and ending with what is interpreted as the shallowest depositional environment. Facies 1 is a glauconitic sandstone facies that is interpreted to represent deposition in a moderately anaerobic, or restricted, submarine environment characterized by normal salinities, low energy conditions, and low or no sedimentation rates. Facies 2 is a mm-scale burrowed calcareous mudstone that is interpreted to represent deposition below fair weather wave base in a low-energy and/or restricted environment. Facies 3 is a sparsely to completely bioturbated mudstone-wackestone that indicates deposition in a low to moderate energy setting where well-circulated, normal marine conditions existed. Facies 4 is a peloidal packstone-grainstone facies that is interpreted to represent deposition within a moderately high-energy environment just below fair weather wave base. Facies 5 is a skeletal grainstone facies representing deposition within a high-energy environment and is interpreted to be associated with a distal, yet active, portion of a skeletal shoal.

Based on the presence of these facies types, it is interpreted that deposition occurred on a gently sloping carbonate ramp with facies ranging from muddy, distal outer-ramp deposits to high-energy, shallow subtidal deposits in the outermost ramp crest environment (Figure 19).

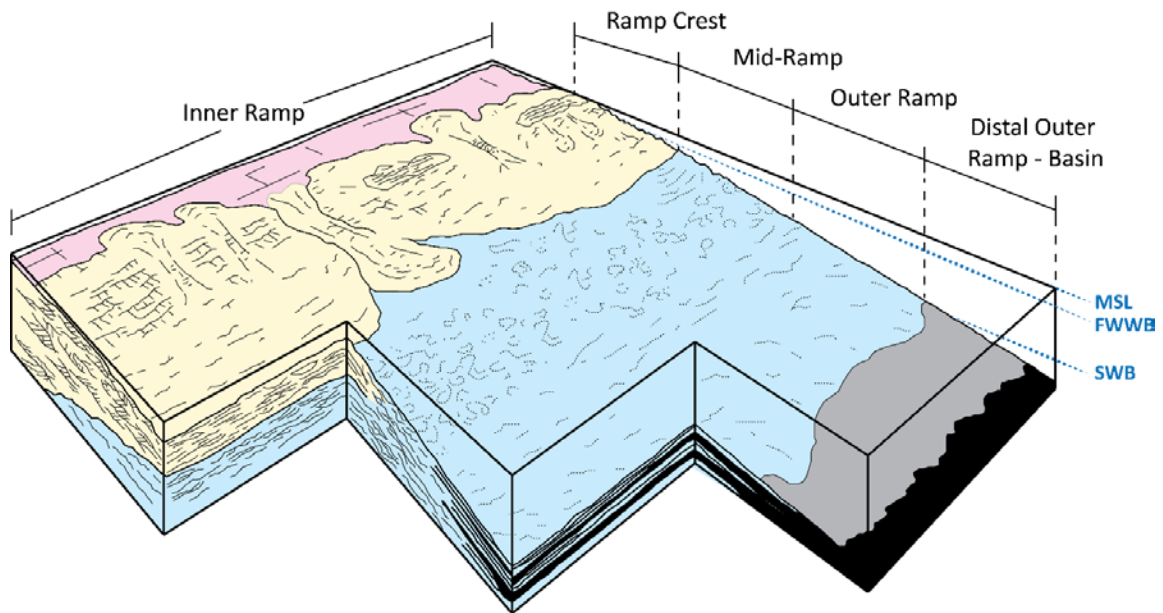


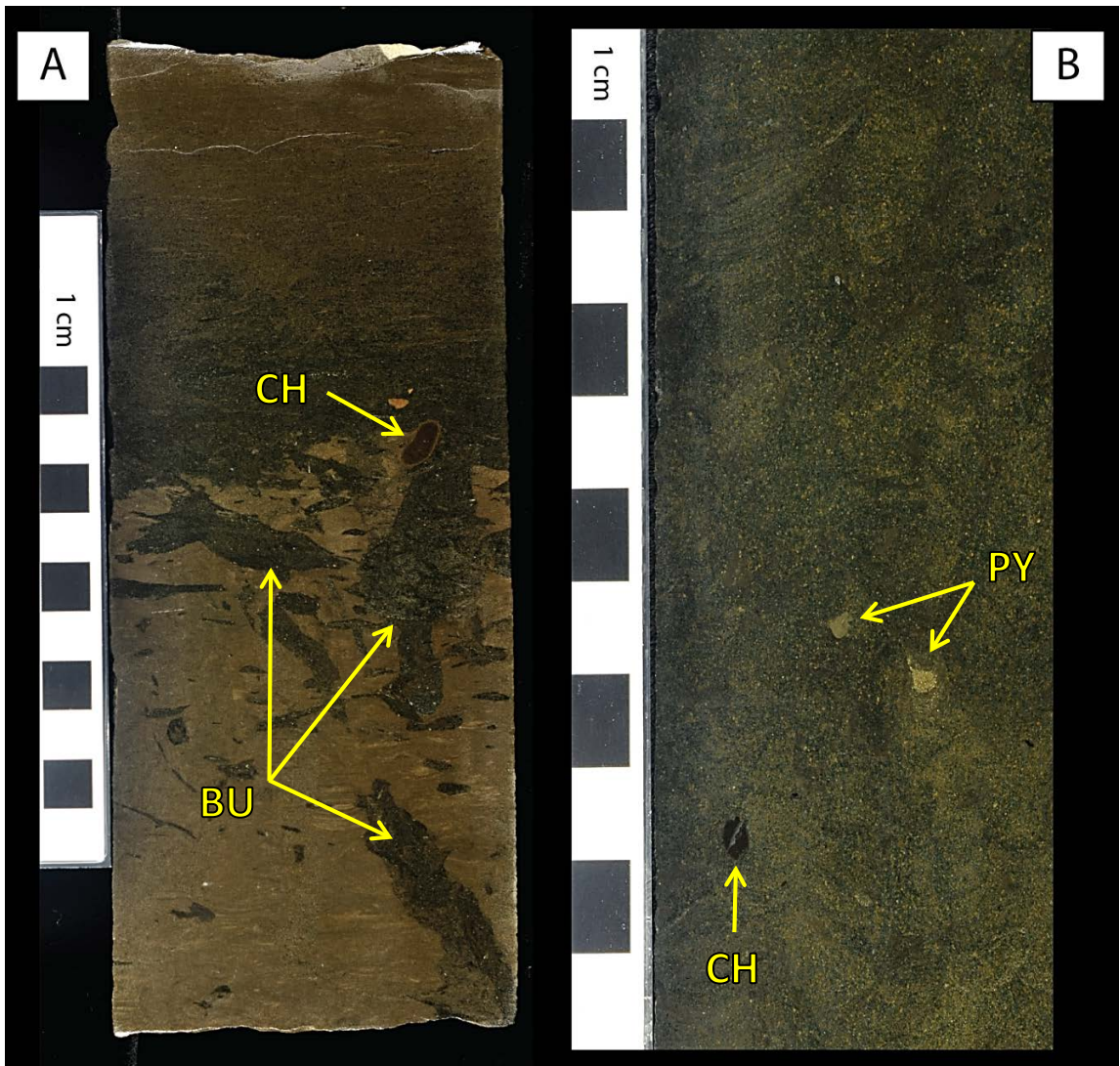
Figure 19. Schematic diagram illustrating the interpreted distribution of depositional facies and environments for the “Mississippian Limestone” in the studied cores. Facies types range from carbonate mudstones deposited in the distal outer ramp environment (Facies 1) through peloidal and skeletal grainstones (Facies 4 and 5) deposited in a higher-energy, shallow subtidal environment. Modified from Handford, 1986.

FACIES 1: GLAUCONITIC SANDSTONE

OBSERVATIONS – FACIES 1

The glauconitic sandstone facies (Figure 20) is a dark greenish gray, grain-dominated facies composed primarily of well-rounded to sub-rounded, well-sorted, silt-sized quartz grains (30-60%), rounded to sub-rounded, moderately sorted, sand-sized glauconite grains (40-50%), clays (10-20%), and dolomite (0-10%). This facies also contains sand-sized phosphate and pyrite grains (5%), sparse thin-shelled brachiopod fragments (5%), bone fragments (1-5%), and chert nodules. Facies 1 is characterized by good intraparticle and interparticle porosity (average 9.45%) and possesses the highest average permeability (0.36 mD). In all cores, the thickness of Facies 1 decreases

vertically with each occurrence. Thicknesses range from a maximum of 3.9ft (1.2m) to a minimum of 0.2ft (0.06m). The glauconitic sandstone facies is observed in all three wells, but only occurs within the lowermost 62.5ft (19m) of Core #1, 21ft (6.4m) of Core #2, and 2.5ft (0.76m) of Core #3.



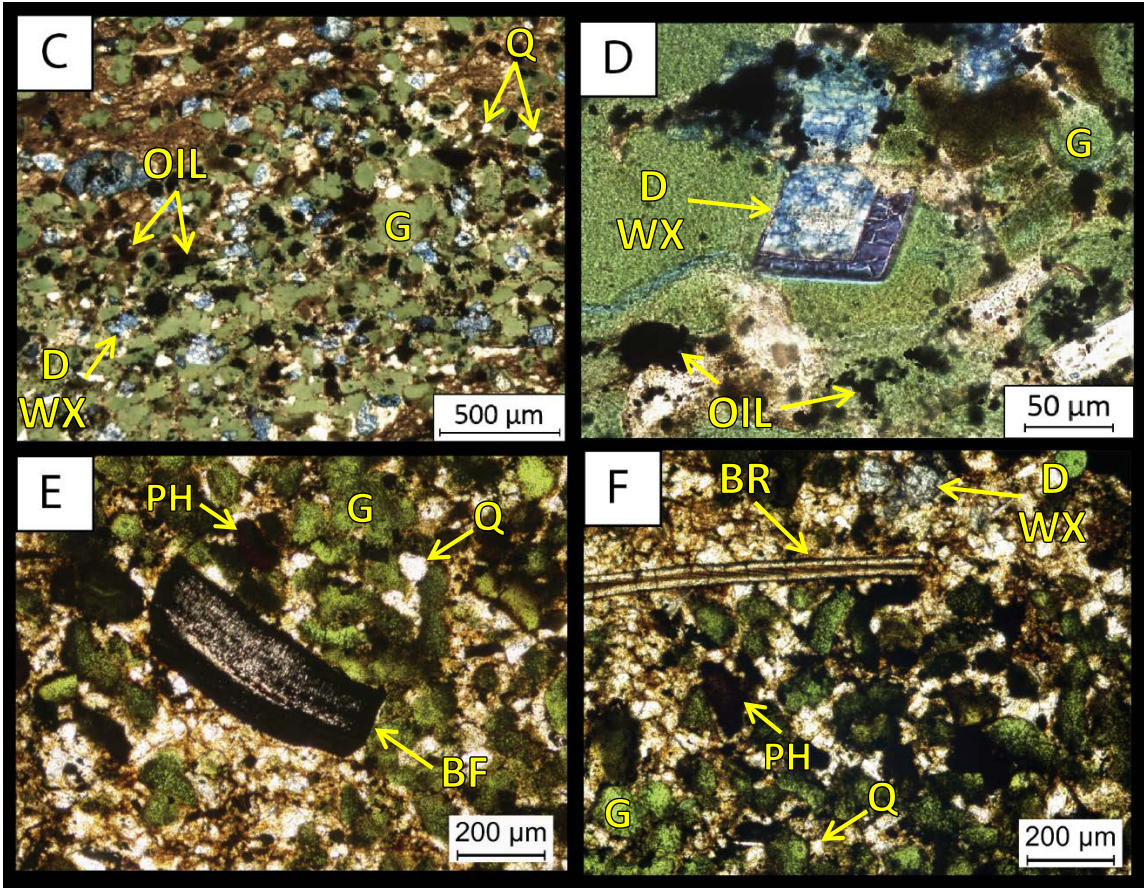


Figure 20. Facies 1: Glauconitic Sandstone Facies. **A)** Core photograph of Facies 1 under white light from Core #3 at a depth of 4479.0'. Scale is in centimeters. Facies 1 is dark greenish gray in hand sample. In this sample glauconite-rich sand is concentrated in cm-scale burrows (BU) within a bioturbated matrix. Chert nodule (CH) present. **B)** Core photograph of Facies 1 under white light from Core #1 at a depth of 5817.5'. Scale is in centimeters. Visible, very coarse sand-sized pyrite grains (PY) and chert nodules (CH) are scattered throughout the sample. **C-D)** Thin section photomicrograph of Facies 1 in plane light from Core #1 at a depth of 5819.8'. The sample is blue epoxy impregnated. This sample displays intracrystalline porosity (WX) within dolomite grains (D) and minor amounts of interparticle porosity between silt- to very fine sand-sized quartz (Q) and glauconite (G) grains. Dead oil can be seen throughout the sample (OIL). **E-F)** Thin section photomicrograph of Facies 1 in plane light from Core #2 at a depth of 5312.75'. The sample is blue epoxy impregnated. This sample displays intraparticle (WX) porosity (blue) within dolomite crystals (D) and lesser amounts of interparticle porosity between quartz (Q) and glauconite (G) grains. Phosphatic bone fragments (BF) and phosphate debris (PH) are scattered throughout the sample.

INTERPRETATION – FACIES 1

Glauconite is an authigenic mineral that forms from potassium-rich, iron-poor smectite clay (Middleton et al., 2003). Although glauconite can form in a number of marine environments, it is most commonly interpreted to indicate deposition within a moderately anaerobic, submarine environment extending over a large area characterized by normal salinities, low energy conditions, and low or no sedimentation rates (Middleton et al., 2003). Glauconite is rarely found in sediments above 60ft (18m) or below 2,400ft (730m). Due to the presence of thin-shelled brachiopod fragments it is inferred that deposition occurred within a fairly low-energy environment. Although conodont fragments are observed in some of these samples, the presence of conodonts does not indicate a particular water depth, energy level, or depositional environment (Clark, 1984). Based on these observations, Facies 1 is interpreted to represent deposition in a restricted, low-energy environment where circulation was limited. Because it is only present in the lowermost portions of each core, it is also interpreted to represent the initial stages of flooding on a regional scale.

FACIES 2: BURROWED CALCAREOUS MUDSTONE-WACKESTONE

OBSERVATIONS – FACIES 2

The burrowed calcareous mudstone facies (Figure 21) is a weakly-laminated calcareous mudstone with localized millimeter-scale burrows. Facies 2 possesses a characteristic brownish black to grayish black color due to its high clay content (average

16%) and has an average TOC (total organic carbon) of 1.49%. This facies is characterized by sponge spicules (5-10%) and thin-shelled brachiopod fragments (5%), but also contains silt-sized quartz grains (10-50%), pyrite crystals (3%), and occasional crinoid beds (average 1 cm thick) visible in hand sample. This facies contains moldic pores and has an average porosity of 1.64% and an average permeability of 0.019mD. Facies 2 may show either a gradational or sharp bedding contact with overlying and underlying facies. The burrowed calcareous mudstone facies is observed in all three cores and ranges in thickness from a maximum of 13ft (4m) to a minimum of 0.1ft (0.03m).

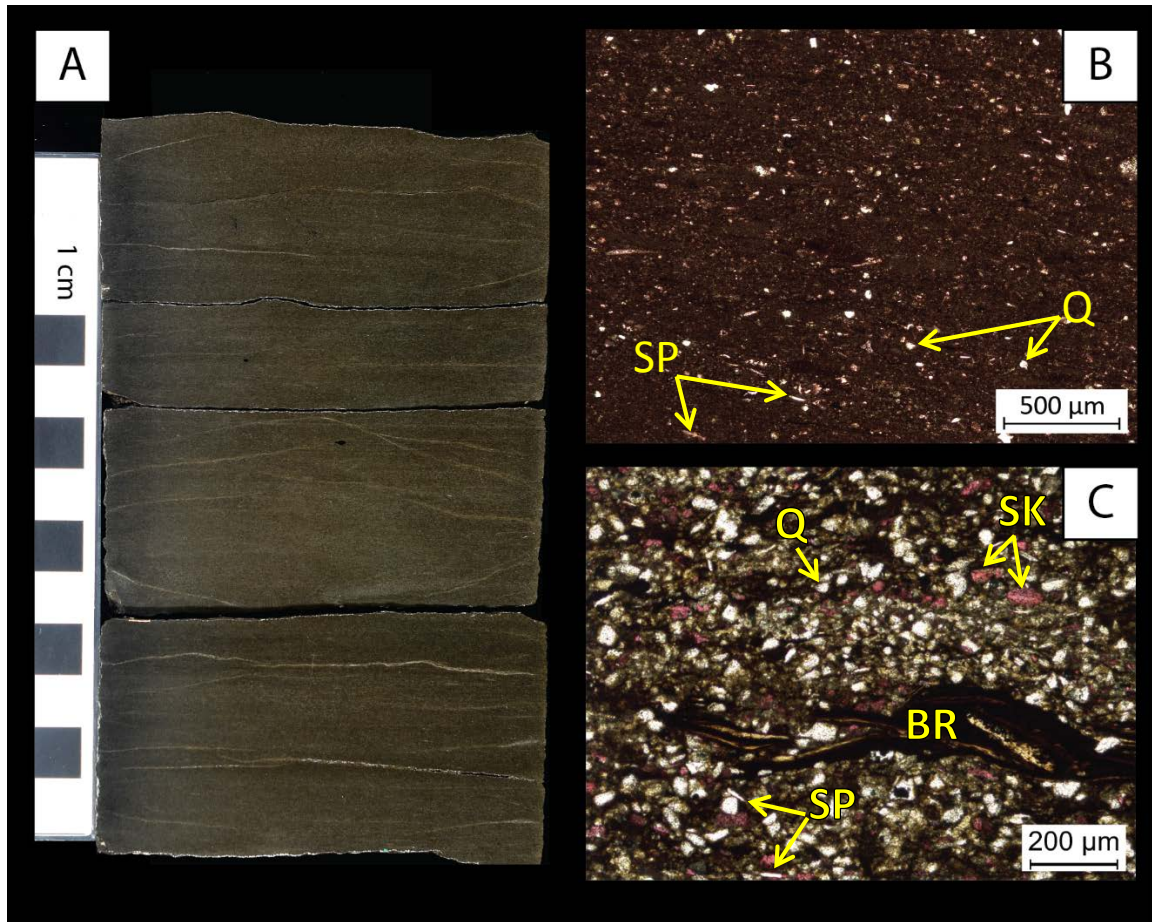


Figure 21. Facies 2: Burrowed Calcareous Mudstone-Wackestone Facies. **A)** Core photograph of Facies 2 under white light from Core #3 at a depth of 4355.5'. Scale is in centimeters. Facies 2 is brownish black to grayish black in hand sample. It is thinly bedded and, in some instances, crinoid fragments and thin-shelled brachiopods are visible in hand sample. **B)** Thin section photomicrograph of Facies 2 mudstone in plane light from Core #1 from 5512.00-5512.25'. Sample is alizarin red stained. Siliceous sponge spicules (SP), silt-sized quartz grains (Q), and calcareous grains (pink) are scattered throughout a muddy, organic-rich matrix. **C)** Thin section photomicrograph of Facies 2 wackestone in plane light from Core #2 from 5144.0-5144.2' with abundant silt-sized quartz grains (Q), brachiopod fragments (BR), and calcareous skeletal fragments (SK; crinoid fragments?) and some scattered sponge spicule fragments (SP). XRD: 23% clays (1% chlorite, 17% illite, and 5% mixed layer illite/smectite), 18% carbonates (17% calcite and 1% dolomite), and 59% other minerals (47% quartz, 2% potassium feldspar, 5% plagioclase feldspar, 4% pyrite, and 1% apatite).

INTERPRETATION – FACIES 2

This facies is interpreted to represent outer to distal outer ramp deposition below fair weather wave base or deposition in a low-energy, restricted environment that represents intermediate environmental conditions between the underlying glauconitic sandstone facies and the overlying bioturbated mudstone to wackestone facies. Limited abundance and diversity of skeletal grains (sponge spicules and thin-shelled brachiopods) indicates that conditions were not yet suitable for a diverse, normal-marine fauna (Flügel, 2010). Alternations of preserved laminations with millimeter-scale burrows suggests fluctuating environmental conditions between restricted environmental conditions and oxygen enriched conditions (Ekdale et al., 1984). Contacts between this facies and the overlying bioturbated facies are gradational as the diversity and abundance of skeletal content increases.

FACIES 3: BIOTURBATED WACKESTONE-PACKSTONE

OBSERVATIONS – FACIES 3

The bioturbated mudstone to wackestone-packstone facies (Figure 22) is a sparsely to completely bioturbated facies that contains local, centimeter-scale vertical burrows (*Cruziana*- or *Skolithos*-type). It contains abundant fine sand-size peloids (30-40%), and silt-sized quartz grains (average ~40%) and lesser amounts of pyrite grains (1.5%), sponge spicules (5%), brachiopods (5%), and crinoid fragments (10%). Occasionally sand-sized glauconite grains (1%) are observed. In hand sample, Facies 3 is a dusky yellowish brown color. This facies is characterized by moldic pores creating a range of porosities (minimum = 0.10%, maximum = 4.75%, and average = 1.57%) and an even wider range of permeabilities (minimum = <0.0001mD, maximum = 0.37mD, and average = 0.04mD). Contacts between this facies and Facies 2 are generally gradational whereas contacts between this facies and Facies 4 or 5 are sharp. The bioturbated mudstone to wackestone facies is observed in all three cores and ranges in thickness from 0.5ft (0.15m) to 39ft (11.9m).

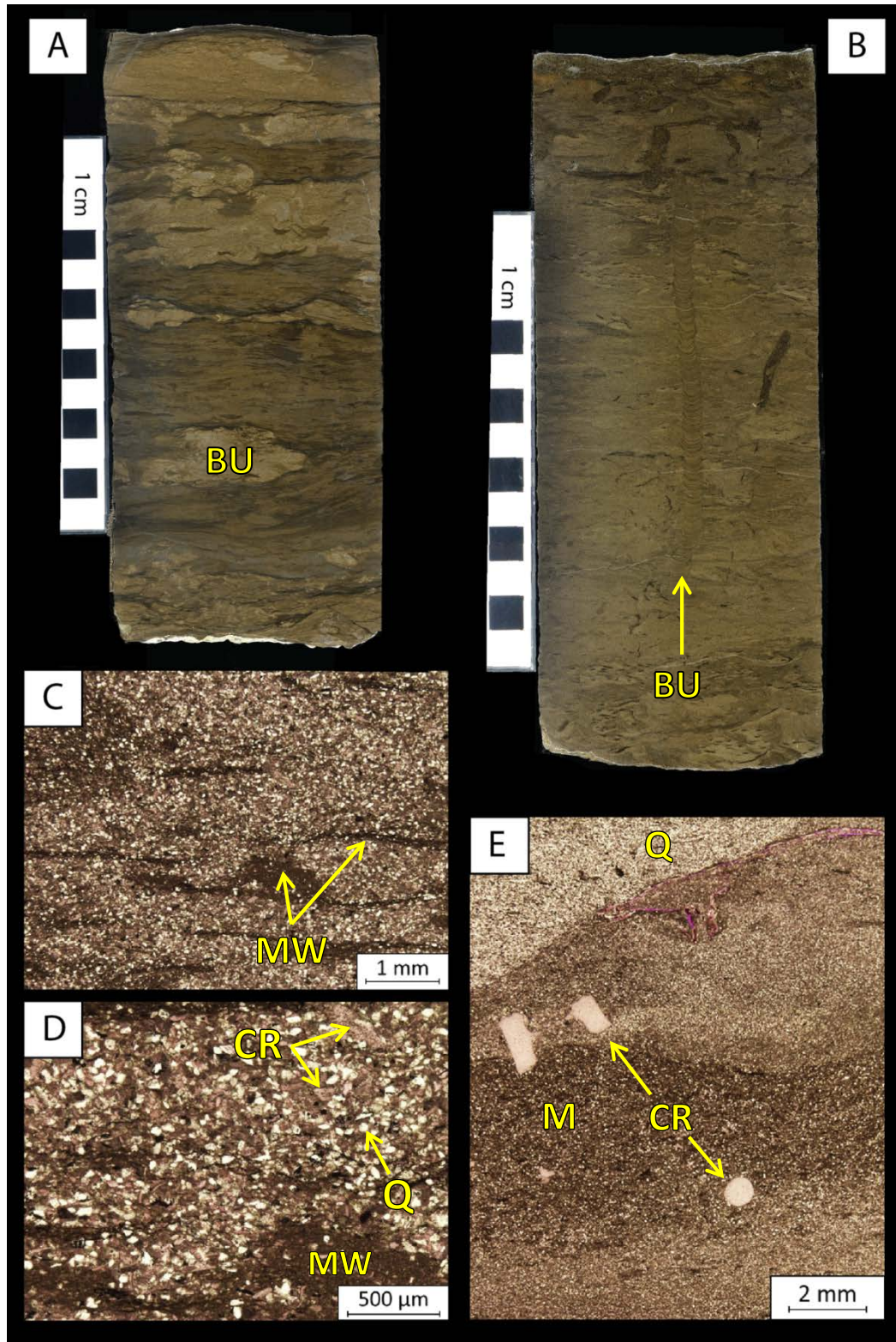


Figure 22. Facies 3: Bioturbated Wackestone to Packstone Facies. **A)** Core photograph of Facies 3 under white light from Core #1 at a depth of 5799.6'. Scale is in centimeters. Facies 3 is dusky yellowish brown and dark yellowish brown in this hand sample and is

heavily bioturbated showing cm-scale burrows (BU) filled with grainier sediment than surrounding material. **B)** Core photograph of Facies 3 under white light from Core #1 at a depth of 5748.8'. This sample is moderately bioturbated and captures a long vertical burrow (BU) representing the proximal expression of the *Cruziana* ichnofacies or the distal expression of the *Skolithos* facies (MacEachern et al., 2009). **C-D)** Thin section photomicrograph of Facies 3 in plane light from Core #1 at a depth of 5596.8' at 2X (**C**) and 5X (**D**). Sample is alizarin red stained. Mud wisps (MW) can be seen throughout grain-rich sample composed dominantly of silt-sized quartz (Q) grains and crinoid fragments (CR). XRD: 15% clays (1% chlorite, 9% illite, and 5% mixed layer illite/smectite), 39% carbonates (32% calcite and 4% dolomite), and 49% other minerals (41% quartz, 1% potassium feldspar, 3% plagioclase feldspar, 2% pyrite, 1% apatite, and 1% marcasite). **E)** Thin section photomicrograph of Facies 3 in plane light from Core #1 at a depth of 5526.05'. Sample is alizarin red stained. Sample is heavily bioturbated and ranges from mud-supported (M) near the base to grain-supported at the top. Large (1-2 mm) crinoid fragments (CR) are scattered throughout. XRD: 4% clays (3% illite and 1% mixed layer illite/smectite), 49% carbonates (45% calcite and 4% dolomite), and 47% other minerals (42% quartz, 1% potassium feldspar, 3% plagioclase feldspar, and 1% pyrite).

INTERPRETATION – FACIES 3

Facies 3 is interpreted as mid- to outer-ramp sediments deposited under low to moderate energy settings. Well-circulated, normal marine conditions during deposition are indicated by the presence of more diverse skeletal material (brachiopod and crinoid fragments), an overall high degree of bioturbation, and the presence of vertical burrows resembling proximal expressions of the *Cruziana* ichnofacies or distal expressions of the *Skolithos* ichnofacies (MacEachern et al., 2009). The presence of these ichnofacies suggests that clean, silty and muddy sand substrates existed during the time of deposition (MacEachern et al., 2009).

FACIES 4: PELOIDAL PACKSTONE-GRAINSTONE

OBSERVATIONS – FACIES 4

The peloidal packstone to grainstone facies (Figure 23) is an olive gray, grain-dominated facies characterized by abundant fine sand-sized peloids (~50%), silt- to fine sand-sized quartz grains (~35%), and skeletal debris (~15%). Some thin sections show a mottled texture. The skeletal debris is composed of crinoid, brachiopod, and lesser amounts of bryozoan fragments. Significant amounts (>50% abundance) of quartz is present in some samples. In core, Facies 4 is massive-bedded and is commonly interbedded with skeletal grainstones (Facies 5). Facies 4 demonstrates mainly fracture porosity and some solution-enhanced moldic porosity. Facies 4 has an average porosity of 1.4% and an average permeability of 0.003mD. Contacts between this facies and the underlying and overlying facies are generally sharp. Facies 4 is observed in all three cores and ranges in thickness from 0.1ft (0.03m) to 6ft (1.8m).

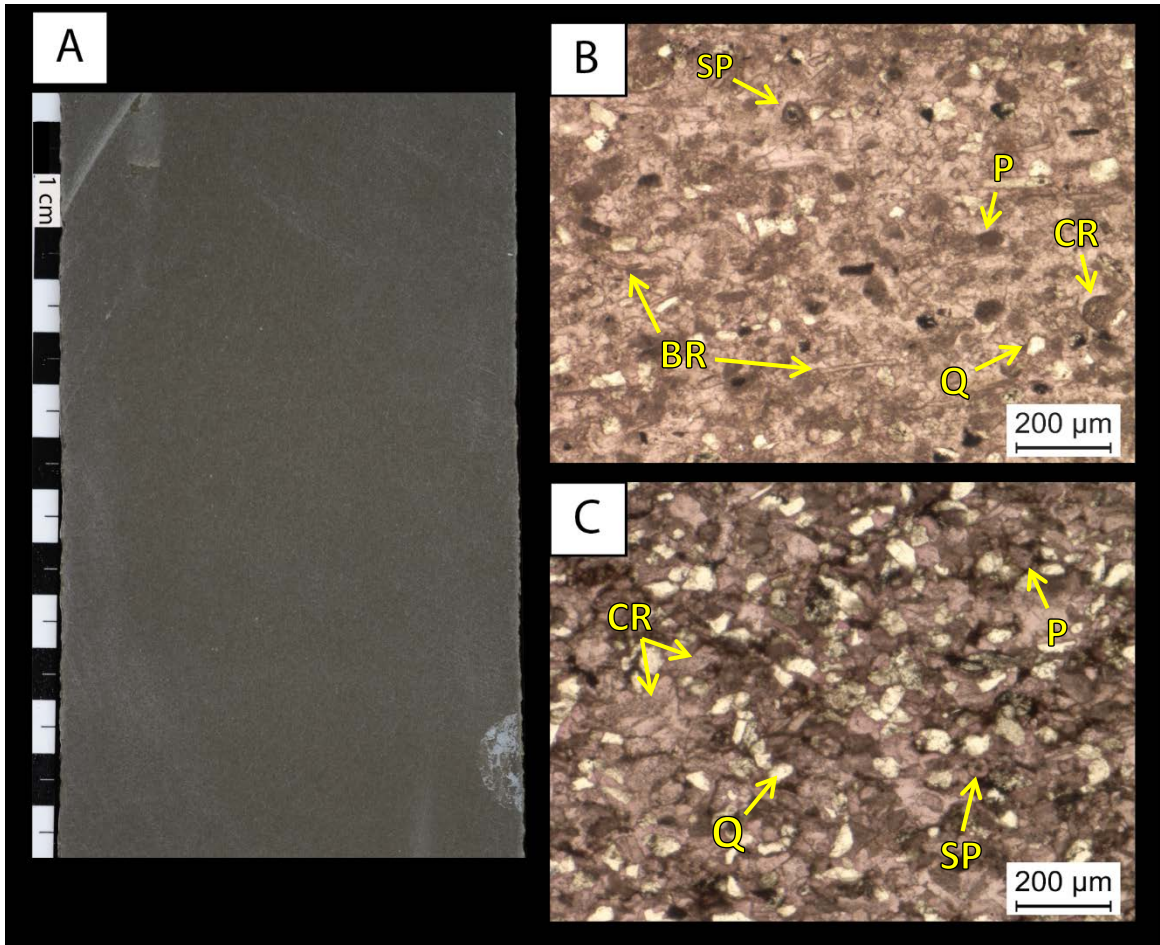


Figure 23. Facies 4: Peloidal Packstone to Grainstone Facies. **A)** Core photograph of Facies 4 in white light from Core #3 at a depth of 4384.0'. Scale is in centimeters. Facies 4 is olive gray in color and is characterized by massive bedding. **B)** Thin section photomicrograph of Facies 4 in plane light from Core #2 at a depth of 5219.75'. Sample is alizarin red stained. Composed of fine sand-sized peloids (P), brachiopod (BR) and crinoid (CR) fragments, sponge spicules (SP), and silt-sized quartz grains (Q). XRD: 1% clays (1% illite), 75% carbonates (74% quartz and 1% dolomite), and 24% other minerals (21% quartz, 1% potassium feldspar, and 2% plagioclase feldspar). **C)** Thin section photomicrograph of Facies 4 in plane light from Core #2 at a depth of 5149.8'. Composed of peloids (P), crinoid (CR) fragments, and silt-sized quartz grains (Q). XRD: 2% clays (1% illite and 1% mixed layer illite/smectite), 62% carbonates (59% calcite and 3% dolomite), and 36% other minerals (26% quartz, 2% potassium feldspar, 6% plagioclase feldspar, 1% pyrite, and 1% apatite).

INTERPRETATION – FACIES 4

The peloidal packstone to grainstone facies is interpreted to represent deposition within the mid-ramp or more distal portion of the ramp crest environment near fair weather wave base, proximal to skeletal shoals. The presence of more diverse skeletal material (brachiopods,

crinoids, and bryozoans) suggest that well-circulated, fairly normal marine conditions existed during deposition, and the mottled texture observed in thin section is indicative of bioturbation (Dodd and Stanton, 1981). These observations suggest that Facies 4 is a distal expression of the inactive portion of a skeletal shoal.

FACIES 5: SKELETAL PACKSTONE-GRAINSTONE

OBSERVATIONS – FACIES 5

The skeletal grainstone facies (Figure 24) is characterized by skeletal debris consisting of brachiopod, crinoid, and bryozoan fragments as well as sponge spicules. The skeletal grains are typically disarticulated and range in size from very fine sand to medium-sand size. Facies 5 is variable in color, ranging from medium and dark grays to a dark yellowish brown. Intermittent muddy intervals, burrowed firmgrounds, bioturbated intervals, or shell beds are occasionally observed (0.5in or 1.27cm thick). Quartz abundance is highly variable and significant amounts (>50% abundance) of subrounded to well-rounded silt-sized quartz grains are present in some samples. In core, cross-bedding, occasional hummocky and swaley cross stratification, and inclined bedding planes are commonly observed. Facies 5 is characterized by sharp basal contacts, but no direct evidence of scour was observed. The dominant pore types observed in thin section are solution-enhanced molds and vugs, with lesser amounts of fracture porosity observed. Facies 5 possesses the second highest average porosity (3.3%) and permeability (0.049mD). Under ultraviolet lighting, the grainstone intervals commonly show bright yellow or light blue fluorescence. The skeletal grainstone facies is observed in all three cores and ranges in thickness from 0.3ft (0.09m) to 12.2ft (3.7m).

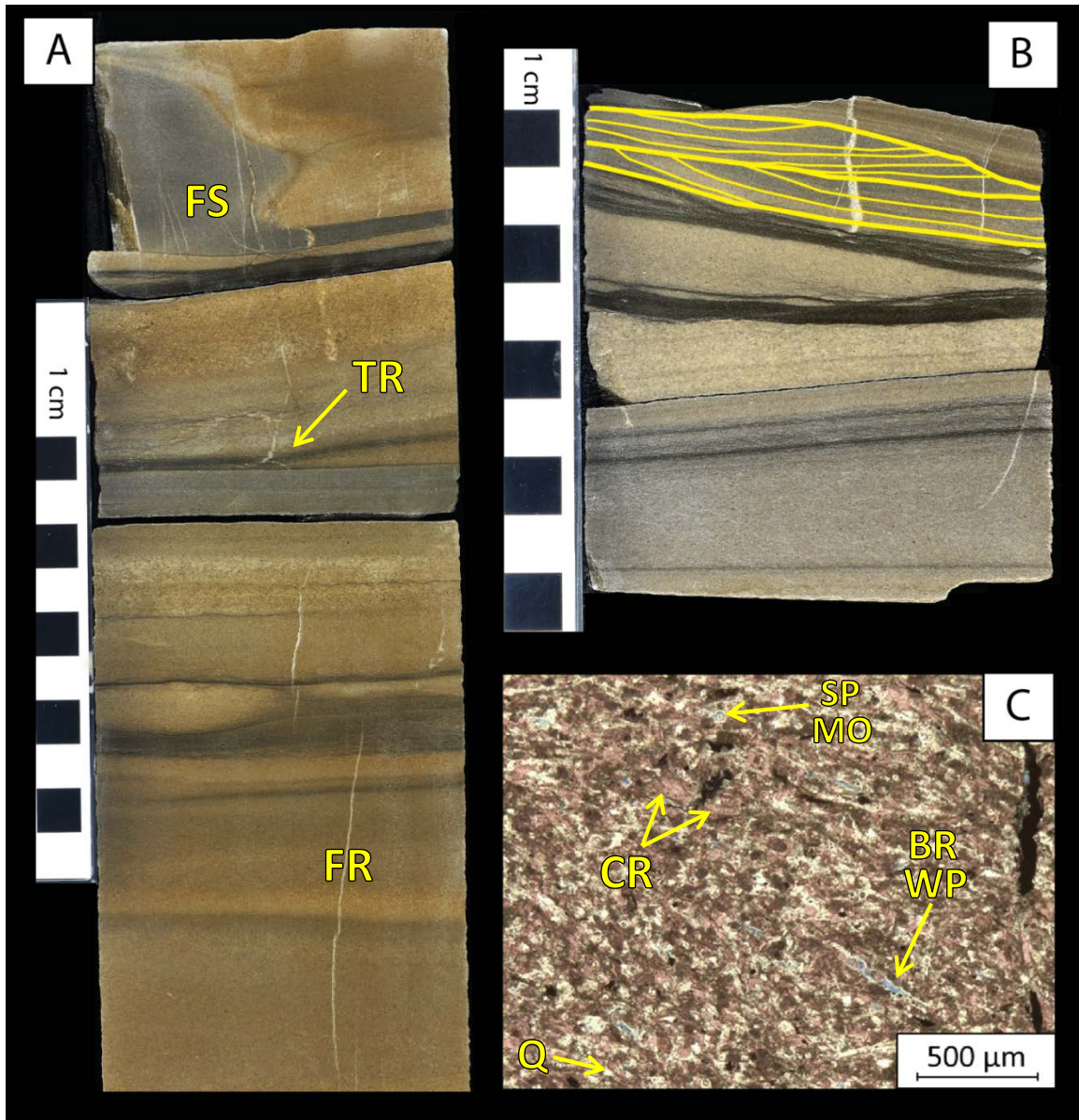


Figure 24. Facies 5: Skeletal Grainstone Facies. **A)** Core photograph of Facies 5 in white light from Core #3 at a depth of 4419'. Facies 5 is highly variable in color and contains interbedded intervals of dusky yellowish brown, dark yellowish brown, medium gray, olive gray, and light olive gray packstones and grainstones with intermittent brownish black muddy intervals. Sample is oil stained (yellowish brown tint). Traction current features showing truncation surfaces (TR) are commonly observed. Fractures (FR) and fracture swarms (FS) are commonly observed Facies 5 and usually terminate into thin, intermittent mud-rich intervals. **B)** Core photograph of Facies 5 in white light from Core #1 at a depth of 5620.1'. Hummocky cross stratification, traced in yellow, is occasionally observed within Facies 5 indicating storms sporadically influenced deposition. **C)** Thin section photomicrograph of Facies 5 in plane light from Core #1 at a depth of 5507.9'. Composed dominantly of crinoid (CR) and brachiopod (BR) fragments. Intraparticle porosity (WP)

observed within crinoid and brachiopod fragments and moldic porosity observed from the dissolution of sponge spicules. XRD: 1% clays (1% illite), 54% carbonates (47% calcite and 7% dolomite), and 45% other minerals (42% quartz, 1% potassium feldspar, and 2% plagioclase feldspar).

INTERPRETATION – FACIES 5

This facies is interpreted to represent deposition within the mid-ramp or more distal portion of the ramp crest environment near fair weather wave base. The presence of cross bedding and truncation surfaces suggests that these skeletal grainstones may have been deposited in the active portion of a skeletal shoal. However, the overall small grain size (silt to medium sand-size) and intermittent mud-rich intervals suggest that this facies may represent a more distal expression of the active portion of a skeletal shoal complex. The presence of hummocky cross-stratification indicates that deposition was occasionally influenced by storm processes (Middleton et al., 2003). Fluorescence under ultraviolet lighting indicates the presence of hydrocarbons in many of these deposits.

SEQUENCE STRATIGRAPHIC FRAMEWORK

IDEALIZED FACIES SUCCESSION

The sequence stratigraphic framework for the Mississippian section in north-central Oklahoma was determined using the idealized vertical stacking pattern of facies developed using facies data from three subsurface cores as described in the previous section. The idealized facies succession established for the study area exhibits a shoaling- or shallowing-upwards profile consisting of a transgressive and regressive phase (Figure 25). This idealized facies stacking pattern was used to understand the controls on the variability of facies and to identify a hierarchy of depositional sequences and cycles. Once the vertical variability of facies was constrained, sequence and cycle boundaries were correlated laterally between the three cores used in this study.

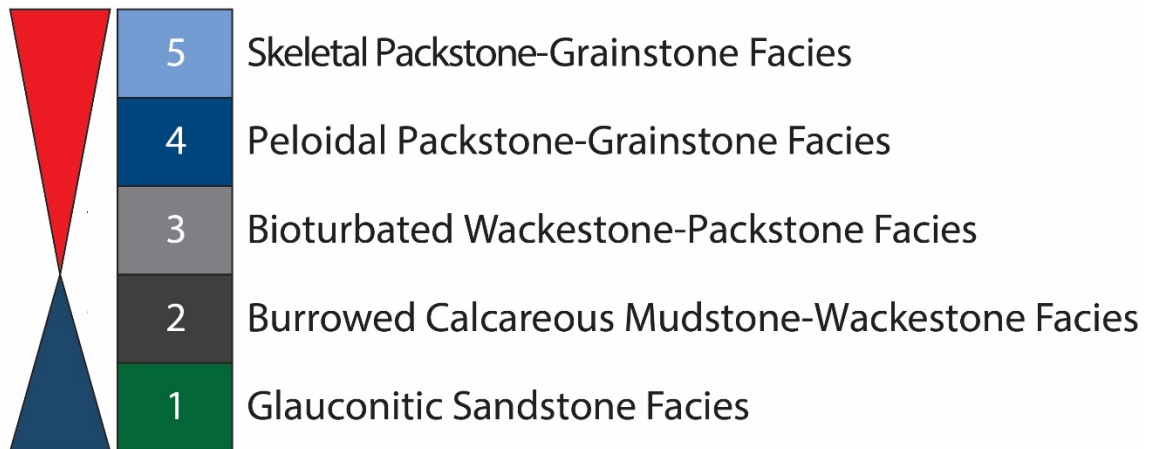


Figure 25. Idealized shallowing-upward facies succession established for the “Mississippian Limestone” section for the study area in north-central Oklahoma. The blue triangle represents the transgressive phase of the system and the red triangle represents the regressive phase. Deviations in the idealized facies stacking pattern may occur as a result of autocyclic processes.

SEQUENCE STRATIGRAPHIC HIERARCHY

The three cores analyzed in this study demonstrate at least three levels of sequence stratigraphic hierarchy. It is important to note that the sequences are not yet constrained by biostratigraphy and that characterization of 3rd, 4th, and 5th order cyclicity in this study is meant to illustrate the relative increase in the frequency of cycles and the hierarchy of the stratigraphic architecture, without assuming any specific time interval or duration. Integrating conodont biostratigraphic analyses, with a maximum resolution of one million years, would be useful in defining 3rd order sequences, but cannot define the heterogeneities related to 4th and 5th order high frequency sequences and cycles.

THIRD-ORDER SEQUENCES

A larger-scale (interpreted as 3rd order) sequence is represented by the entire cored interval. This overall shallowing-upward sequence is characterized by a general change in facies from deeper-water, lower-energy facies at the base, to shallow-water, higher-energy facies at the top. This trend is consistent with global sea level curves that show a gradual falling of sea throughout the Mississippian (Haq and Schutter, 2008).

HIGH FREQUENCY FOURTH-ORDER SEQUENCES

Each of the cores in this study exhibit four regionally correlative sequences of probable 4th order duration. These 4th order sequences display a well-defined shoaling upwards succession of depositional facies and are bounded at their bases by deeper-

water, transgressive facies (Facies 1, 2, or 3), and at their top by higher-energy, regressive facies (Facies 4 or 5). Observed 4th order sequences range in thickness from approximately 25ft (7.5m) to 115ft (35m). All four high frequency sequences are thickest in Core #1 and show some degree of thinning in an eastward direction, with the lowermost (S1) and uppermost (S4) sequences experiencing the most drastic changes in thickness. These thickness variations are likely related to the locations of the cores relative to the Nemaha Uplift and associated faults which likely created or reduced accommodation locally. Identification of these high frequency sequences is important as they likely control the distribution of reservoir-quality units (Grammer et al., 2004).

HIGH FREQUENCY FIFTH-ORDER CYCLES

High frequency 5th order cycles are the thinnest cycles identified in core and, generally speaking, and in this study, are an average of 10ft (3m) thick. Identification of these units is important as they often represent the fundamental reservoir flow units in many carbonate reservoirs (Grammer et al., 2004). However, the lack of high-resolution biostratigraphy, spacing of cores, and the uncertainty as to the controlling mechanism(s) at the 5th order scale makes these high frequency cycles the most problematic for regional correlation.

High frequency cycles were identified following the idealized vertical succession of facies and commonly consist of alternating mudstone to wackestone facies (Facies 2 and 3) and peloidal or skeletal packstone to grainstone facies (Facies 4 and 5). The distribution of the high frequency cycles lacks the regional consistency and correlativity

observed in the 4th order high frequency sequences, and the number of high frequency cycles varies both within and between each of the identified 4th order sequences. The inconsistencies in these cycles are likely related to high frequency sea level fluctuations and/or variations in accommodation (Eberli et al., 2004). The lateral continuity and thickness variations of these cycles are a function of carbonate production rates and the rate of sea level rise (Eberli et al., 2004). Although these 5th order cycles cannot be correlated across the study area, it is still important to identify these cycles as they provide insight and an enhanced predictability of sedimentary packages, probable reservoir or source potential, geometry, and the lateral and vertical continuity of sedimentary packages in the subsurface.

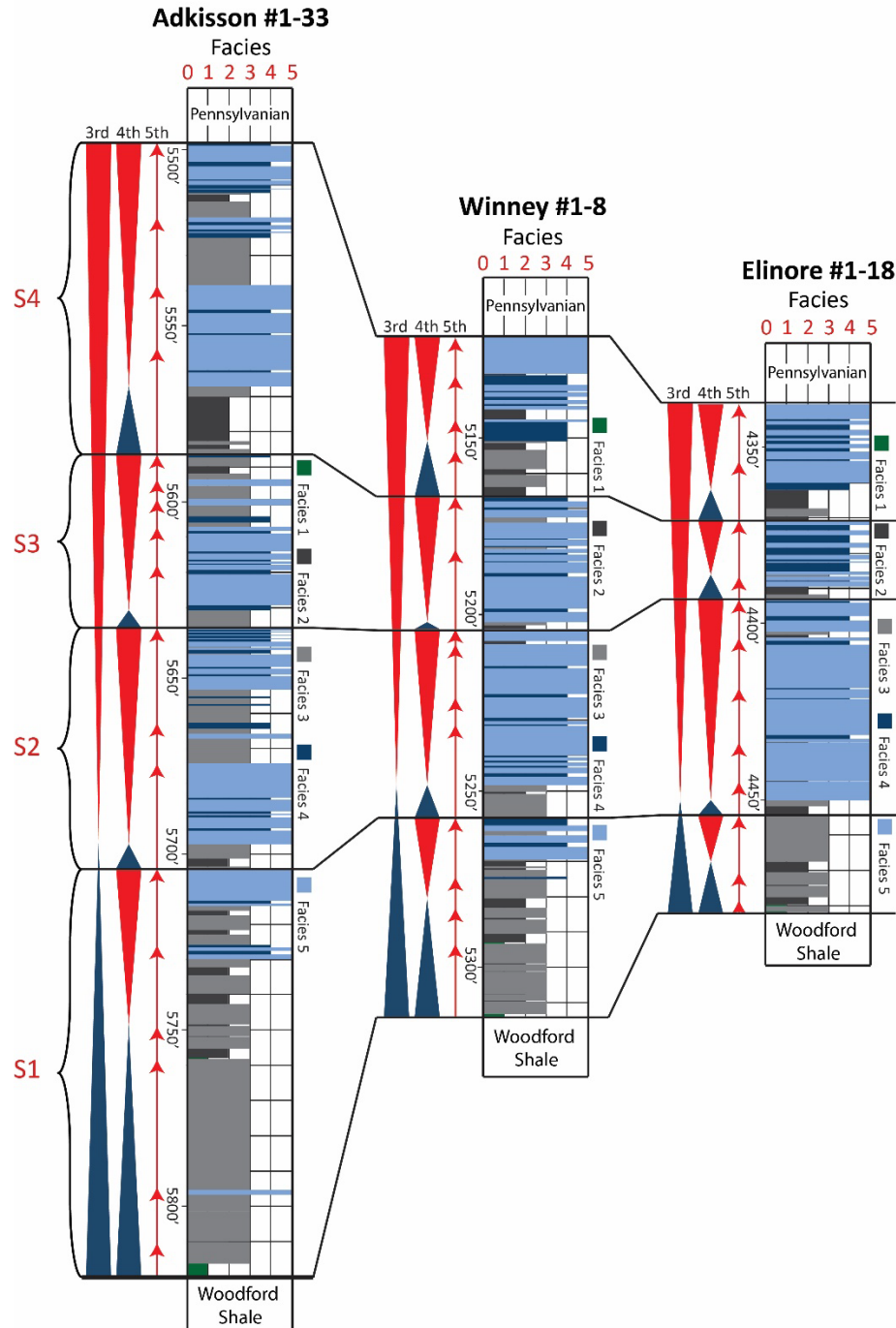


Figure 26. West to east cross section of depositional facies and 3rd, 4th, and 5th order sequences and cycles identified in core. Refer to Figure 23 for facies names. This cross section illustrates the regional continuity and eastward thinning of the 3rd order sequence and 4th order high frequency sequences (S1-S4). Regional variations in thickness suggests an influence of eustatic sea level changes and possible autocyclic processes. Thickness variations of S1 and S4 may be related to the unconformable surfaces above and below the Mississippian section. 5th order high-frequency cycles are regionally discontinuous and may be greatly influenced by autocyclic processes.

WIRELIN LOG CORRELATION

In order to correlate sequences and cycles laterally across the study area, a number of different datasets were used. Facies, cycles, and sequences were compared to available core data and wireline log signatures to determine any vertically and/or laterally repeating patterns that may facilitate facies, cycle, or sequence correlation within and beyond the study area.

WHOLE ROCK MINERALOGY/XRD

Whole rock mineralogy was determined for core plug samples analyzed by Weatherford Laboratories using bulk x-ray diffraction techniques. 169 samples from the three cores used in this study have associated XRD data. Petrophysicists at Devon Energy utilized XRD data from these samples to generate gross mineralogy curves that interpolate between measured samples. These curves were developed to illustrate the relative abundance of quartz, calcite, dolomite, and total clays throughout each core. These curves were plotted adjacent to measured sections to infer general trends between mineralogy and high frequency sequences and cycles (Figure 27). XRD data associated with specific thin sections were used to analyze relationships between mineralogy and facies.

It was predicted that a correlation between the volume of quartz silt and transgressive/regressive phases existed. It was expected that the amount of silt-sized quartz grains would be highest during the latest regressive phase or earliest transgressive phase. However, the volume of quartz is highly variable throughout the

observed sequences and cycles and there is no apparent trend between gross mineralogy and position within the sequence stratigraphic framework. Although there is a variable amount of quartz silt observed within each facies, generally speaking, Facies 4 contains the least amount of quartz silt (average 32%), Facies 1 and 5 contain the greatest amounts (average 48% and 43% respectively), and Facies 2 and 3 contain intermediate amounts (40% and 37% respectively). Thin section analysis reveals that some intervals of Facies 5 are completely silicified due to diagenetic processes. These samples show anomalously high volumes of quartz that are related to diagenetic processes, not specific depositional processes, that skew the dataset making interpretations between quartz abundance and the sequence stratigraphic framework difficult to determine.

Although oriented mounts were not prepared for more accurate determination of clay mineralogy, Weatherford Laboratories reports significant volumes (trace amounts to 15%) of illite throughout the section and lesser amounts of mixed-layer illite/smectite (trace amounts to 7%). The presence, or absence, of these clays may be important in terms of reservoir development and production as some clays (i.e. – smectite) are swelling clays that absorb drilling fluids and proppants that can result in the occlusion of porosity or inability to utilize hydraulic fracturing techniques within the interval of interest. A more detailed determination of clay minerals present throughout the section would be useful for identifying more desirable reservoir intervals.

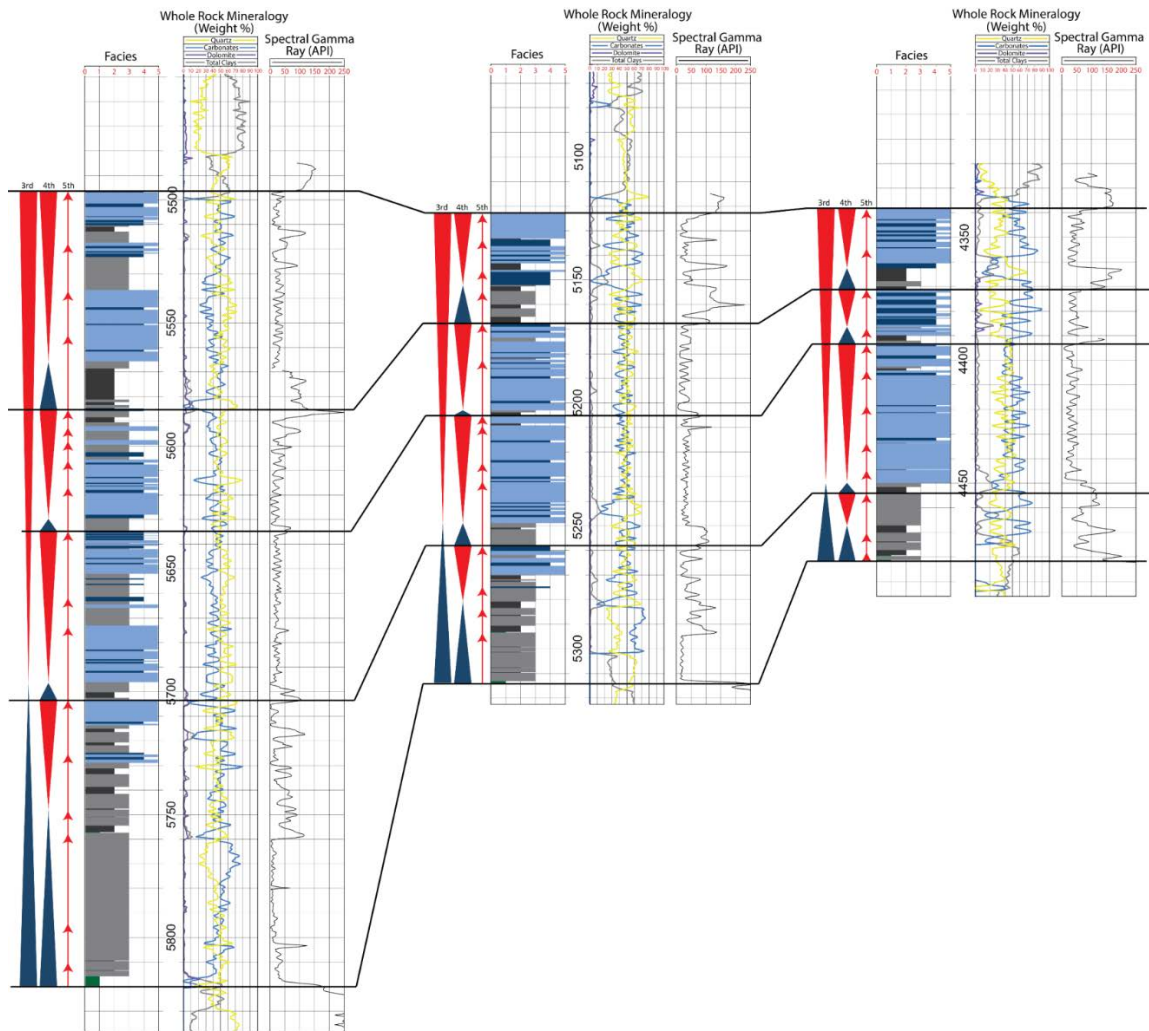


Figure 27. West to east cross section of depositional facies, 3rd, 4th, and 5th order sequences and cycles, whole rock mineralogy, and spectral (laboratory measured) gamma-ray. Refer to Figure 23 for facies names and color associations. Whole rock mineralogy curves are displayed on the center track. Quartz is represented by the yellow curve, calcium carbonate by the blue curve, dolomite by the purple, and total clays by the gray. There is no obvious correlation between gross mineralogy and the sequence stratigraphic framework. Spectral gamma-ray is plotted on the far right track. 4th order high frequency sequences appear to correlate well with spectral gamma-ray signatures, with the base of the 4th order sequences corresponding to pronounced spikes in spectral gamma-ray values. Although some 5th order high frequency cycle boundaries occasionally correspond to slight increases in spectral gamma-ray readings, the trend is highly inconsistent.

GAMMA-RAY

Both total spectral gamma-ray and borehole measured gamma-ray data were analyzed in this study to facilitate the correlation of facies, cycles, and sequences vertically and laterally. Overall, there is a good correlation between high frequency 4th order sequences and spectral and borehole-measured gamma-ray values.

Fourth-order sequence boundaries correlate well with spikes in total spectral gamma-ray signatures (Figure 25 and 26). However, high frequency 5th order cycles do not consistently correlate to spectral gamma-ray signatures. A similar trend is observed with borehole-measured gamma-ray values where 4th order sequence boundaries correlate to peaks in gamma-ray signatures, but 5th order cycles are below the resolution of the tool. The four 4th order high frequency sequences resolvable on wireline logs can be regionally correlated using spectral or borehole-measured gamma-ray characterized by elevated values at the base of the sequences (transgressive phase) and show an overall decreasing upward trend towards the top of the sequence (regressive phase).

Although 4th order high frequency sequences are readily identifiable on gamma-ray curves and 5th order high frequency cycles are occasionally visible, correlations based on gamma-ray signatures alone cannot be used blindly to define and correlate facies, cycle, and sequence boundaries. This practice will likely result in erroneous correlations. For example, the gamma-ray signature of the upper half of sequence one shows multiple spikes that are not associated with 4th order high frequency sequences (Figure 27 and 28). Correlation of these spikes could result in an erroneous sequence

stratigraphic correlation and an erroneous assumption that reservoir-quality packstone-grainstone facies exist at the tops of these sequences.

DENSITY AND NEUTRON POROSITY

Both density and neutron porosity logs were used to determine a relationship between high frequency sequences and cycles and units characterized by reservoir-quality porosity. Density and neutron porosity logs for each core were plotted using a limestone matrix (Figure 28). However, using a limestone matrix to calibrate density-neutron porosity throughout the Mississippian section is problematic as a number of zones are characterized by quartz abundances of >50%. Using a sandstone matrix for calibration in these zones may be more appropriate. If the formation's actual density is less than the matrix density used to calculate porosity (i.e. – calculating a sandstone porosity using a limestone matrix density), the log shows porosity values that are higher than the actual porosity of the formation.

Density logs typically plot within the range of 5-20% porosity while neutron logs generally plot between 0-10% porosity. Generally speaking, there is a gross trend of increasing porosity at the top of high frequency 4th order sequences associated with the regressive phase. As with observations made using gamma-ray logs, density and neutron porosity logs demonstrate inconsistent trends between wireline log signatures and facies types and the sequence stratigraphic framework. As a result, correlations of reservoir-quality units based solely upon density and neutron porosity log signatures will likely result in erroneous interpretations.

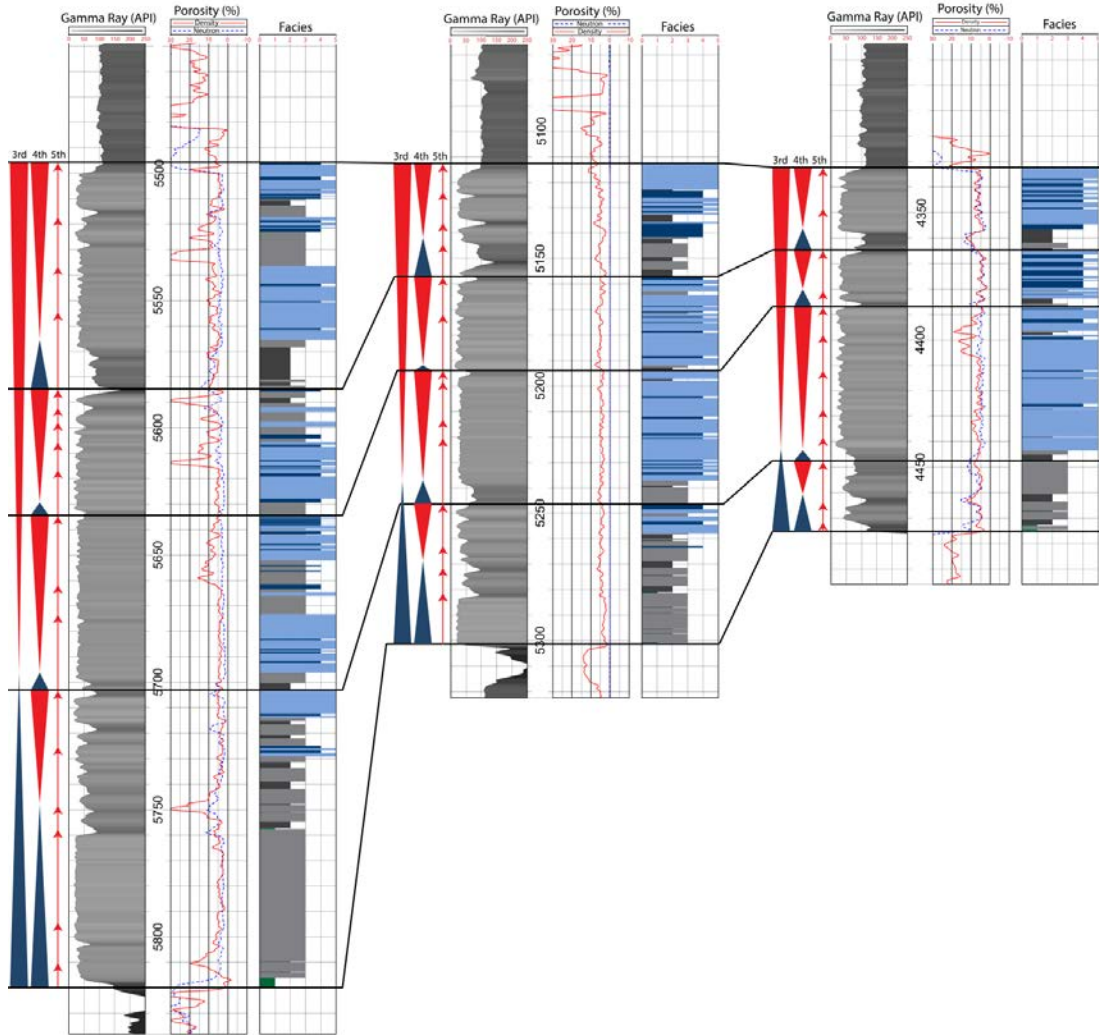


Figure 28. West to east cross section of depositional facies, 3rd, 4th, and 5th order sequences and cycles, and conventional wireline logs (gamma-ray, density porosity, and neutron porosity). Refer to Figure #23 for facies names and color associations. Gamma-ray is plotted on the left track. Fourth-order high frequency sequences appear to correlate well with gamma-ray signatures, with the base of the 4th order sequences corresponding to pronounced spikes in gamma-ray values. Some 5th order high frequency cycles also appear to correlate with elevated gamma-ray values, but this trend is inconsistent. These trends are comparable to those observed in spectral gamma-ray readings. Density and neutron porosity logs are displayed on the center track. The density porosity log is displayed as a blue dashed line and the neutron porosity log is displayed as a solid red line. Both logs are calibrated to a limestone matrix. There is a gross, yet inconsistent, trend of increased porosity values in the regressive phases of the 4th order high frequency sequences.

DEPOSITIONAL ANALOGS

Integration of ancient and modern analogs into a reservoir characterization study is helpful in characterizing and predicting the lateral and vertical distribution of both reservoir and non-reservoir facies in the subsurface (Grammer et al., 2004). Ancient analogs (e.g. – outcrop analogs) are commonly used as a 2-D proxy for subsurface reservoir distribution, but are limited by exposure and may be altered by surface processes that create an exaggerated diagenetic overprint (Grammer et al., 2004). Modern analogs illustrate the spatial distribution and geometry of facies within a single time slice, but do not demonstrate the effects compaction and later diagenesis may have on reservoir units (Grammer et al., 2004). Nevertheless, the use of analogs in a carbonate reservoir characterization study allows for an enhanced understanding of reservoir heterogeneity and can aid in predicting the distribution of reservoir facies in the subsurface (Grammer et al., 2004).

ANCIENT (OUTCROP) ANALOG: SAN ANDRES FORMATION, PERMIAN BASIN, TX

Facies types and stacking patterns similar to those observed in the “Mississippian Limestone” have been recorded in the Permian-aged San Andres Formation in West Texas. The San Andres Formation in the Permian Basin is interpreted to represent deposition on a distally steepened carbonate ramp (Kerans et al., 1994). According to the model developed by Kerans et al. (1994), the facies observed in the three cores used in this study are comparable to the carbonate facies observed in the San Andres

Formation in the distal ramp crest, outer ramp, and distal outer ramp environments (Figure 29). Both the ramp crest and outer ramp settings are dominated by bioclastic packstones and grainstones composed of diverse marine fauna (Kerans et al., 1994). Distal outer ramp facies are described as having millimeter-scale laminations, darker coloration, and minimal bioturbation indicating deposition in a deeper, lower-oxygen environment (Kerans et al., 1994). Deposition of grainstones within the ramp crest setting is thought to have occurred in water depths of 0-10ft (0-3m) while outer ramp and distal outer ramp packstones are interpreted to have been deposited between 30-200ft (10-60m) and greater than 200ft (60m) water depth, respectively (Kerans et al., 1994).

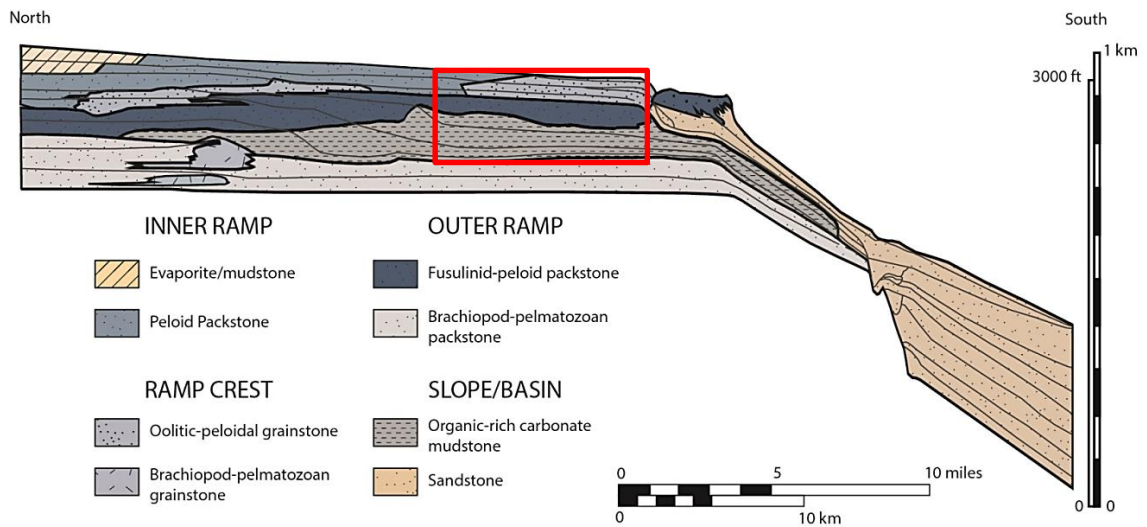


Figure 29. 2-D facies distribution observed in the Permian-aged San Andres Formation outcrop, Algerita Escarpment, Guadalupe Mountains, West Texas. This dip elongate section illustrates the distribution of facies across a distally steepened ramp. The facies and stacking patterns observed in the carbonate deposits of San Andres Formation are similar to those observed in the “Mississippian Limestone” of the Mid-Continent. Facies stacking patterns observed in the three cores used in this study suggest Mississippian deposition occurred within the ramp crest, outer ramp, and distal most portion of the outer ramp environments (outlined in red). Modified from Kerans et al., 1994.

The highest degree of heterogeneity is observed in the ramp crest zone. Cycles observed in the ramp crest environment demonstrate an overall shallowing-upwards (shoaling-upwards) profile consisting of dense mudstone-wackestone at the base that transitions into vertically into skeletal packstone and grainstone facies (Kerans et al., 1994). Facies stacking patterns observed in the “Mississippian Limestone” cores used in this study resemble those recorded in the San Andres Formation ramp crest and outer ramp environment (Figure 30). Similar depositional environments and facies stacking patterns suggest that facies geometries may be similar, therefore the San Andres Formation could serve as a predictive tool used to identify facies types and distributions in the subsurface.

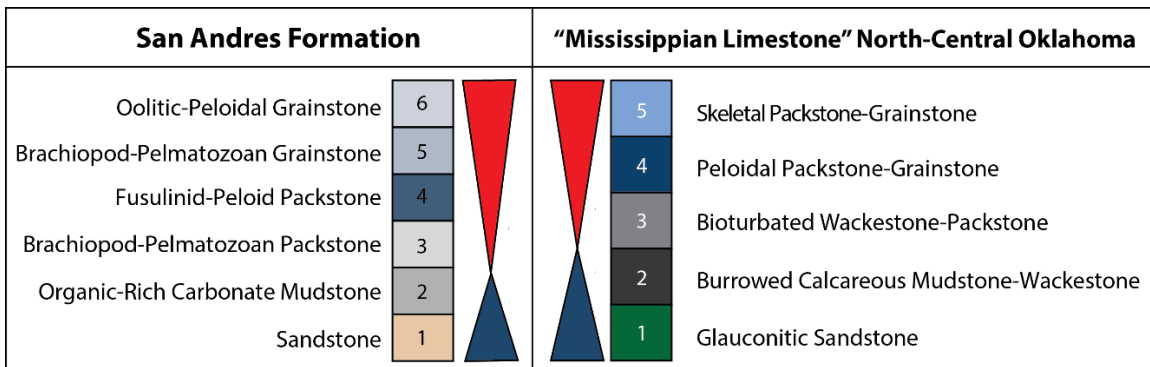


Figure 30. Diagram showing stacking patterns observed in the San Andres Formation (left) and the “Mississippian Limestone” in north-central Oklahoma (right). Facies types and textures observed in the “Mississippian Limestone” resemble those observed in the San Andres Formation suggesting that the San Andres Formation may serve as a good depositional analog for the “Mississippian Limestone” of north-central Oklahoma. Using the San Andres Formation as an analog, it is interpreted that the Mississippian section was deposited in the distal ramp crest, outer ramp, and distal outer ramp environments as illustrated in Figure 29.

Although the facies stacking patterns and depositional environments observed in the San Andres Formation resemble those observed in the “Mississippian Limestone”,

differences between the two systems exist. Fourth-order high frequency sequences recorded in the San Andres Formation are 100's of feet thick whereas those observed in the studied Mississippian cores are generally 10's of feet thick. Additionally, high frequency sequences in the San Andres Formation show a broader spectrum of fauna and facies than that observed in the "Mississippian Limestone" in north-central Oklahoma, and there is no note of hummocky or swaley cross stratification. These differences may be attributed to differences in geological and environmental conditions during the time of deposition (e.g. – amplitude of sea level fluctuations or arid v. humid climates). Nevertheless, the San Andres Formation exhibits similar facies stacking patterns to those observed in the "Mississippian Limestone" and is a suitable analog that may help to explain the regional-scale geometry and spatial distribution of facies.

MODERN ANALOG: PERSIAN (ARABIAN) GULF

Comparing ancient deposits to modern depositional environments is a valuable practice that helps to conceptualize the spatial distribution and geometry of reservoir facies during a single time slice (Grammer et al., 2004). For this study, the Persian Gulf, a modern example of carbonate deposition on a gently sloping ramp in an arid climate, is used as an analog for the "Mississippian Limestone". By using the Persian Gulf as a modern analog to the "Mississippian Limestone" it is possible to observe not only the regional facies distribution, but the high degree of heterogeneity associated with the system that may be present at any given time. This is something that cannot be observed using generalized paleodepositional models such as Lane and Dekyser (1980).

The Persian Gulf is a northwest-southeast trending body of water that is bordered by Oman, the United Arab Emirates (USE), Qatar, and Saudi Arabia to the south and southwest, and Kuwait, Iraq, and Iran to the northwest and north. The Persian Gulf carbonate ramp is part of the gently sloping Saudi Arabian shield where water depths range from largely exposed sabkhas to depths greater than 260ft (80m) in the Zagros Mountain foredeep in Iran (Wilkinson and Drummond, 2004). Holocene sediments have accumulated over an area that is 310 miles (500km) long and up to 37 miles (60km) wide (Alsharhan and Kendall, 2003). Sedimentation in the Persian Gulf is believed to be controlled by a number of factors including an arid climate, wave energy, orientation with respect to NW prevailing winds, and offshore barriers (Alsharhan and Kendall, 2003).

General facies types observed in the Persian Gulf consist of supratidal sabkha deposits, various types of bioclastic carbonate sands composed of skeletal fragments, peloids, and ooids, muddy carbonate sands, and carbonate mud (Figure 31) (Alsharhan and Kendall, 2003; Wilkinson and Drummond, 2004). Bioclastic and oolitic sands deposited in high-energy settings are dominant on the southern margin of the Arabian coast (Alsharhan and Kendall, 2003). These bioclastic sediments are found as deep as 20m, suggesting that storm wave base is at least this deep (Alsharhan and Kendall, 2003). Generalized facies types observed in the Persian Gulf occur in wide facies belts paralleling the shoreline, with the highest energy facies (carbonate sands) being deposited closest to the shore (Alsharhan and Kendall, 2003).

Comparison of Mississippian facies to those observed in the Persian Gulf allows for a first order interpretation of the spatial distribution of facies and possible water depths at the time of deposition. Peloidal and skeletal packstones to grainstones observed in the Mississippian cores used in this study are similar in composition and texture to the bioclastic carbonate sands observed in the Persian Gulf. Similarly, bioturbated wackestones and carbonate mudstones observed in the Mississippian section are comparable to the muddy carbonate sands and carbonate mud observed in the Persian Gulf, respectively. Using the Persian Gulf as an analog, it is possible that the peloidal and skeletal packstone and grainstone facies observed in the “Mississippian Limestone” were deposited in 3-65ft (1-20m) water depth, are strike elongated, and decrease in thickness in a basinward direction. It is also possible that the carbonate mudstone facies observed in the “Mississippian Limestone” was deposited in greater than 65ft (20m) water depth, is extensive in a strike and dip direction, and increases in thickness in a basinward direction.

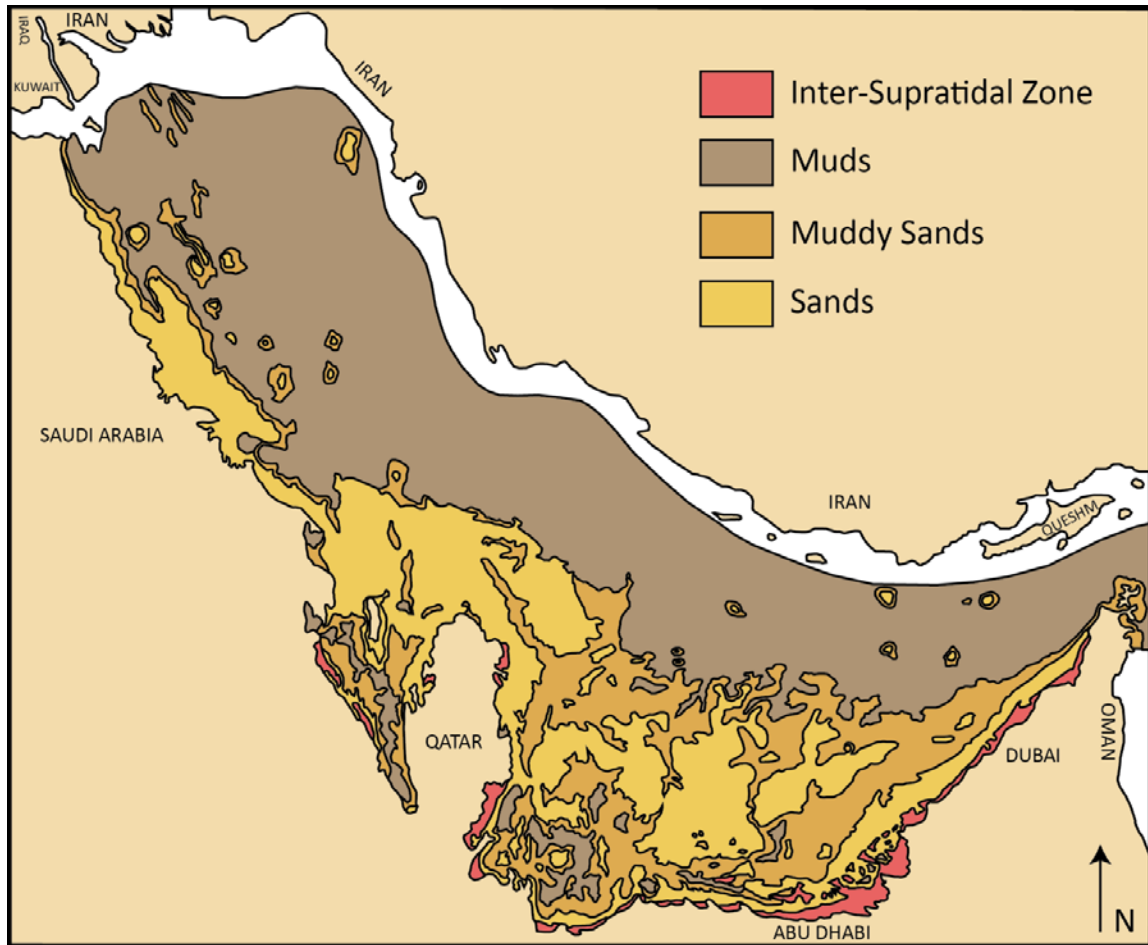


Figure 31. Regional map of the Persian Gulf illustrating the distribution and variation of facies textures. Using the Persian Gulf carbonate ramp system as a modern depositional analog to the “Mississippian Limestone” provides a means to visualize possible facies distributions and heterogeneities that may be present in the subsurface. This facies map shows a single time slice of general facies trends and illustrates the high degree of heterogeneity within the system due to local variations in environmental conditions (i.e. – a facies mosaic). Peloidal and skeletal packstones to grainstones observed in the Mississippian subsurface cores used in this study are similar in composition and texture to the bioclastic carbonate sands (yellow) observed in the Persian Gulf. Bioturbated wackestones and carbonate mudstones observed in the Mississippian section are comparable to the muddy carbonate sands (dark yellow-orange) and carbonate mud (brown) observed in the Persian Gulf, respectively. Modified from Wagner and Togg, 1973.

3-D SEQUENCE MODELING

Three-dimensional sequence modeling of a depositional system allows for the integration of multiple datasets to create a visualization of sequence continuity and geometry. These models help to guide geologic interpretations and also aid in the communication between geoscientists and non-geoscientists (Coburn et al., 2006; Pyrcz and Deutsch, 2014; Tinker, 1996). The output visualization is ultimately constrained by the sequence stratigraphic framework developed previously from core and thin section analysis. Constraining the data using the sequence stratigraphic framework allows for more geologically accurate modeling that takes into consideration the vertical and lateral heterogeneities that cannot be accurately modeled using lithostratigraphy (Pyrcz and Deutsch, 2014; Tinker, 1996). For this study, a 3-D sequence model was created to observe the vertical and lateral continuity and regional geometries of the high frequency 4th order sequences across the study area.

DATASET

The software used for 3-D modeling in this study is Petrel by Schlumberger. Petrel is a geostatistical reservoir modeling program that incorporates a suite of data including seismic, wireline logs, petrophysical data, lithology, and facies. The numerical data input into Petrel for this study consists of well information (i.e. – latitude and longitude), a log suite including gamma-ray and density and neutron porosity logs, and surfaces (4th order high frequency sequence boundaries). The study area defined for

this 3-D model is a rectangle that extends 43.5 miles (70.1km) in a west-east direction and 20.1 miles (32.4km) in a north-south direction and encompasses most of Logan and Payne Counties (Figure 32). The three wells used in this study cover a west-east distance of 28.5 miles (45.9 km). Core #1 and Core #2 are 11.1 miles (17.8km) apart and Core #2 and Core #3 are 17.4 miles (28.0 km) apart. Seventy-eight additional raster logs were used to infill between the three cored wells at an average spacing of 0.5 miles (0.8km).

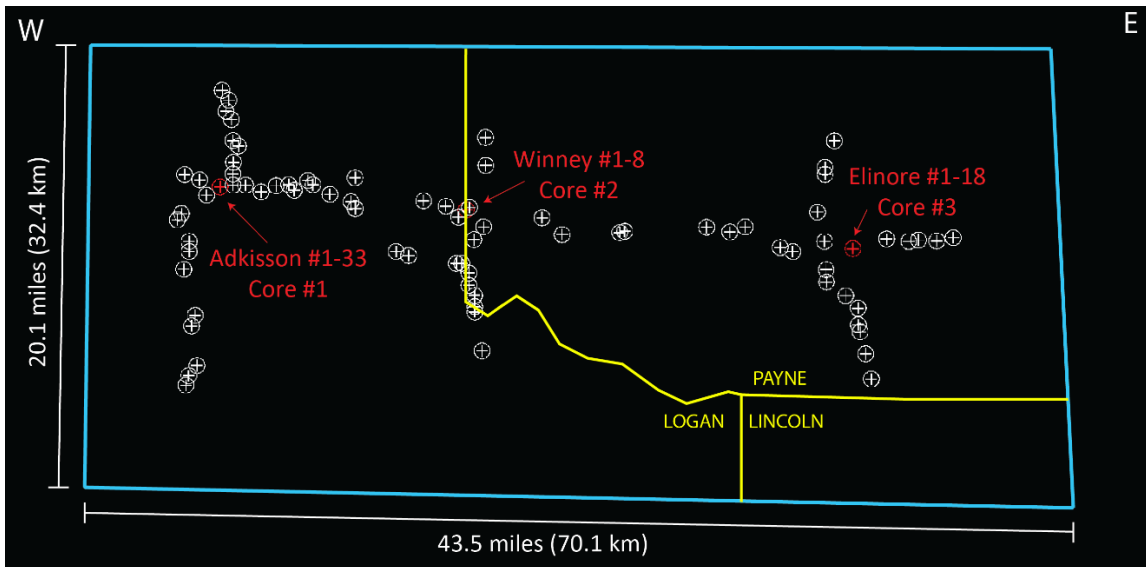


Figure 32. Map showing the locations of wells used to construct the 3-D model for the Mississippian depositional system in the Mid-Continent. The three cores used in this study are highlighted in red. Wells with raster logs used to infill between wells with cores are shown in white. The study area (outlined in light blue) extends 20.1 miles (32.4km) in and dip (N-S) direction and 43.5 miles (70.1km) in a strike (W-E) direction and encompasses most of Logan and Payne Counties (outlined in yellow).

SURFACE MODELING

High frequency 4th order sequences originally identified in core were correlated throughout the study area using wireline logs and input in Petrel to create a sequence

stratigraphic framework for the 3-D model. Surfaces were modeled using the convergent interpolation algorithm because of its simplistic representation of the surface geometries. Modeling these surfaces helps to constrain the lateral and vertical variability and geometries of the high frequency sequences throughout the study area. The surfaces and horizons used in the modeling process are as follows (Figure 33):

Sequence Boundary 0 (S_0)

S_0 represents the contact between the Devonian-aged Woodford Shale and the overlying “Mississippian Limestone”. This boundary is easily identified in core as a dark greenish gray glauconitic sandstone overlying a dark grayish black shale interval. This contact is observed in all three cores used in this study and is readily identified in a gamma-ray log signature. The Woodford Shale possesses a distinctive “hot” gamma-ray log signature (15-400 API units) whereas the “Mississippian Limestone” is characterized by a significantly lower gamma-ray signature (10-100 API units). This contact was picked in all 81 wells primarily using gamma-ray signatures. Mississippian deposition initiated on the unconformity surface on top of the Woodford Shale, which makes this surface the ideal bounding surface for the base of the model.

Sequence Boundaries 1-4 (S_1 - S_4)

Sequence boundaries 1 through 4 were identified based upon facies stacking patterns observed in the three cores used in this study. S_1 - S_4 correlate to the tops of the four high frequency sequences identified in the cores used in this study.

Sequence Boundary 5 (S₅)

Sequence boundary 5 is a regionally extensive erosional unconformity that represents the boundary between the top of the Mississippian section and the overlying Pennsylvanian-aged shales and sandstones. The unconformable boundary between the “Mississippian Limestone” and Pennsylvanian sediments is the uppermost bounding surface of the model. This boundary was observed in each of the three cores used in this study and was identified on all additional raster logs using differences in the gamma-ray signature. The Mississippian carbonate deposits are characterized by a relatively low gamma-ray log signature (15-30 API units) and the overlying Pennsylvanian sediments are characterized by distinctively higher gamma-ray log readings (generally 75-90 API units). Throughout most of the study area S₅ and S₄ are the same surface with S₅ only separating from S₄ in the south-central region of the study area. This is likely because S₅ was either eroded or was not deposited across the rest of the study area.

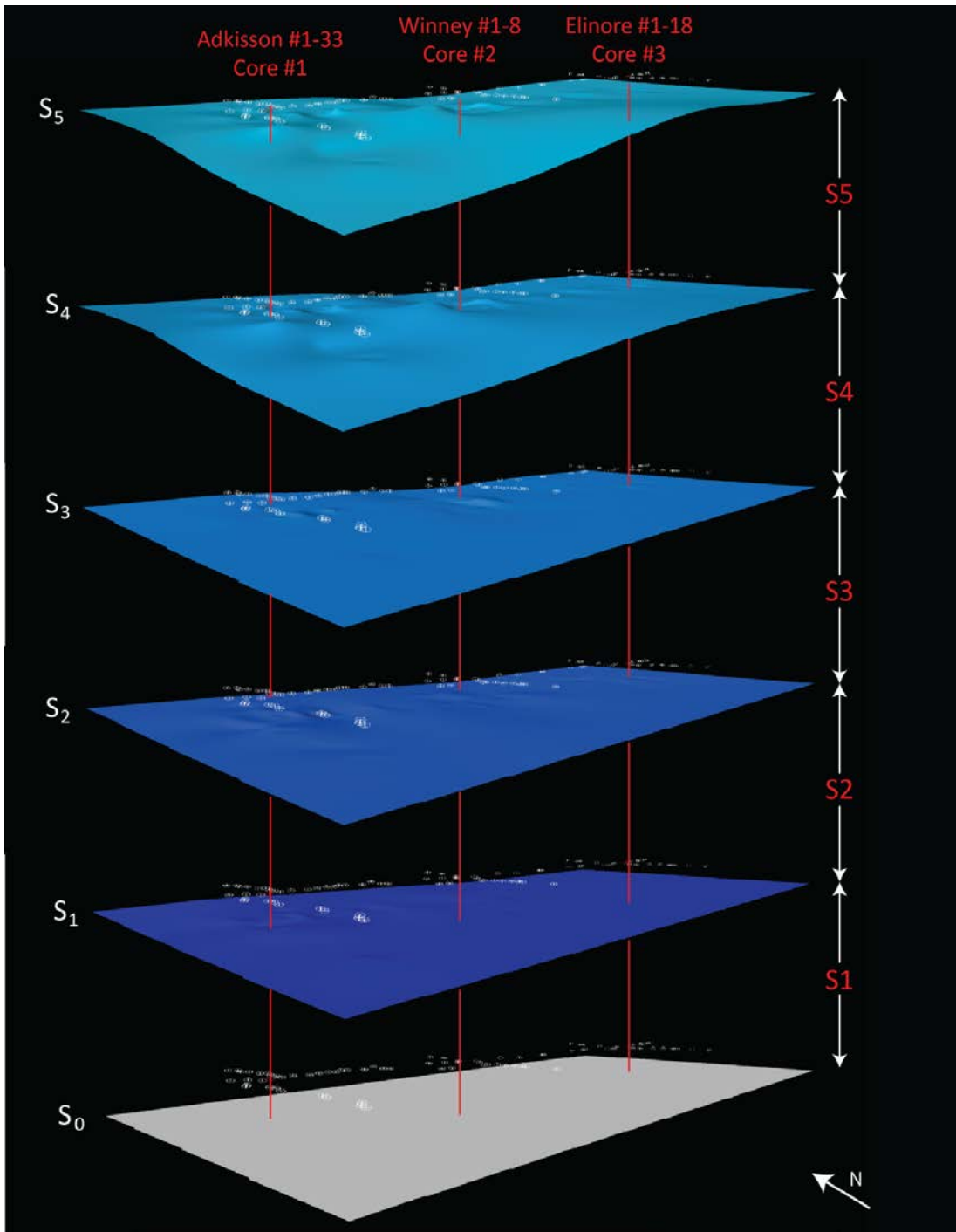


Figure 33. Figure showing all surfaces used in constructing the 3-D model for the Mississippian section within the study area. All surfaces extend across the entire study area and have been vertically exaggerated 50X to better illustrate surface features. Surfaces (S₀-S₅) are displayed at an even vertical spacing in this figure and do not reflect the thickness variations in the sequences (S₁-S₅). The three wells with cores used in this study are highlighted in red. Locations of wells with raster logs used to infill between wells with cores are shown in white. S₀ representing the top of the Woodford

Shale/base of the “Mississippian Limestone” is a completely flat surface. S_1 and S_2 do not show a high degree of topographic variation and are relatively flat surfaces compared to S_3 , S_4 , and S_5 . S_4 and S_5 are uneven surfaces as these represent the regionally extensive erosional unconformity at the top of the Mississippian section.

STRATIGRAPHIC AND STRUCTURAL MODELING FRAMEWORK

The grids and zones within the Petrel model are defined based on 4th order sequences derived from core analysis. The interpreted grid provides the stratigraphic and structural framework for the model. Based on aerial extent of the model and the spacing between data points, the length and height of the individual cells used for this project was 50ft by 50ft, resulting in a total of 592,020 grid cells that were used for model generation.

Isopach (thickness) maps were constructed for each high frequency sequence and were used to generate surfaces. Surfaces generated using structural depth points produced anomalous interpolations such as sharp structural peaks and overlap or crossing of the high frequency sequence boundaries. Using isopach maps to create surfaces resolved these issues and allowed more control to be placed on the geometry of each layer.

The base of the model (S_0) was gridded as a flat surface to simulate “flattening” on the top of the Woodford Shale (or base of the “Mississippian Limestone”). This helps to better illustrate the regional geometries associated with the overlying high frequency sequences defined in the Mississippian section. Using the calculator function, the S_1 isopach was added to the flat S_0 surface to create the S_1 surface. This methodology was followed for each high frequency sequence boundary to generate the S_1 - S_5 surfaces.

S₀-S₅ surfaces were used as horizons to create zones for the 3-D grids in the model. Zones were created between each of the high frequency sequence boundaries using S₀ (top of the Woodford Shale/base of the “Mississippian Limestone”) as the basal surface as described below. A total of five 4th order sequences were interpreted throughout the Mississippian section, each of which was modeled as a distinct zone (S1-S5) to construct a 3-D model (Figure 34).

Layering options utilized in this study were “proportional” and “follow base.” Proportional maintains the same number of layers throughout the model regardless of thickness and was used for this study in the three lowermost zones. Because the top of the “Mississippian Limestone” is an uneven, regionally unconformable surface that is represented by S₃, S₄, or S₅ depending on its location in the study area, these layers utilized the follow base option to reduce the jaggedness of each zone likely resulting from its unconformable top.

RESULTS

Zones, or sequences, 1-4 are present throughout the entire study area and have an average thickness of 54ft (16.5m). Zone, or sequence, 5 is present only in the south central portion of the study area and is interpreted to represent a sequence that was likely eroded away, or not deposited, across the rest of the study area. The 3-D model of the Mississippian section within the study area reveals that sequences 1-4 (S1-S4) are fairly continuous in a strike direction (W-E) and show a gradual decrease in thickness in an eastward direction (Figure 35). In the dip direction (N-S), the sequences show

progradational geometries with progressive thinning towards the north and thickening towards the central and southern portions of the study area (Figure 36). Overall, this 3-D model shows that the Mississippian section was deposited as a series of low-relief, southward-prograding wedges on a gently sloping surface (i.e. – a carbonate ramp). These results are consistent with depositional environment interpretations made using facies analysis.

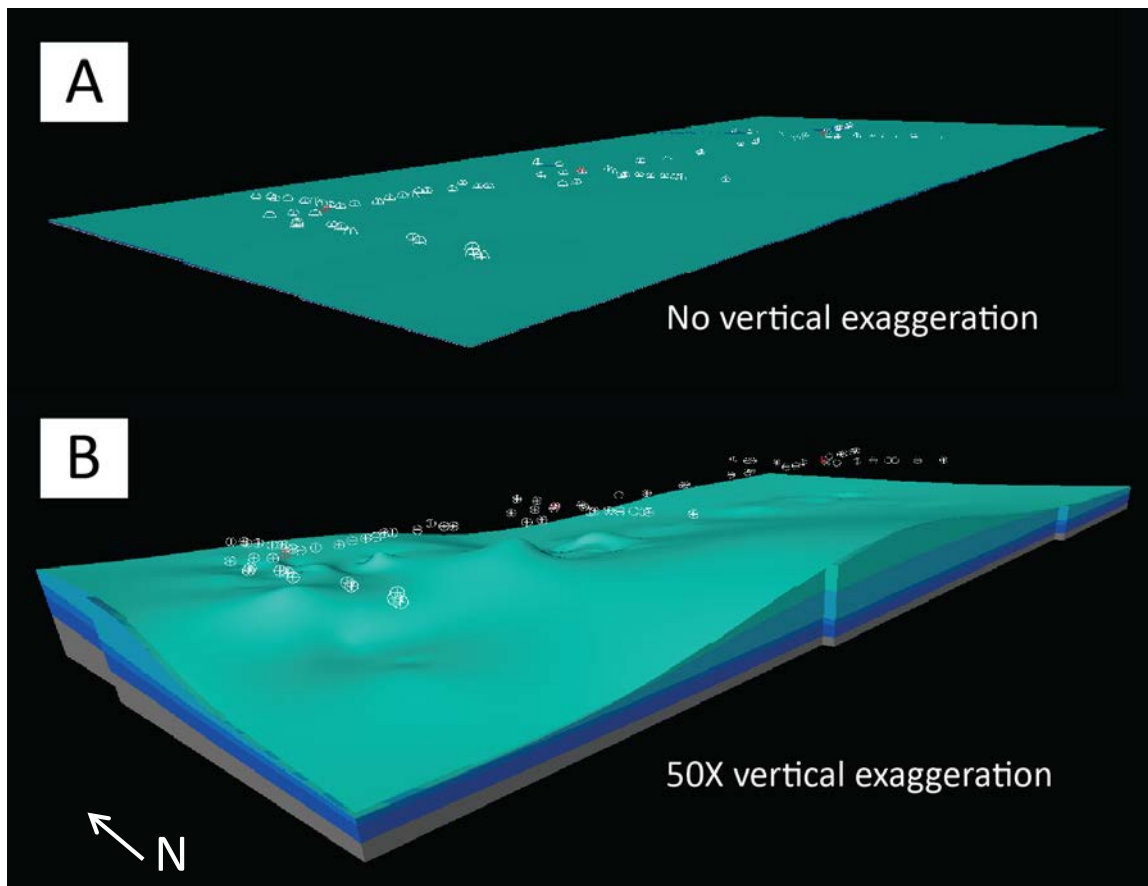


Figure 34. **A)** Three-dimensional model of the Mississippian section across the study area. No vertical exaggeration has been applied to this model. As a result, the model appears to be completely flat. **B)** 3D model of the Mississippian section across the study area that has been vertically exaggerated by 50X. High frequency sequence geometries can only be observed if the model is vertically exaggerated. Topographic highs and lows appear more dramatic as a result of vertical exaggeration.

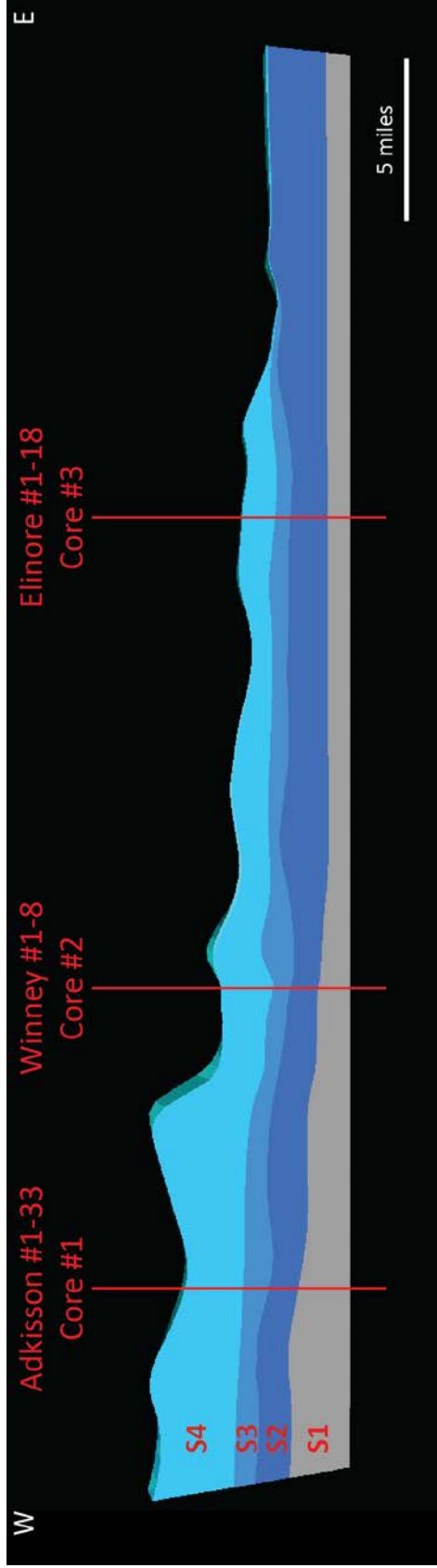


Figure 35. Strike-oriented (W-E) slice through the 3-D model showing sequences 1-4 (S1-S4) and the locations of the 3 cores used in this study. Slice has been vertically exaggerated by 100X to better illustrate sequence geometries. S1, S2, S3, and S4 are fairly continuous in a strike direction. Although thicknesses do not vary much (<10ft), S3 and S4 appear to thin slightly in an eastward direction. This is likely the result of erosion of the uppermost sequences associated with the Mississippian-Pennsylvanian

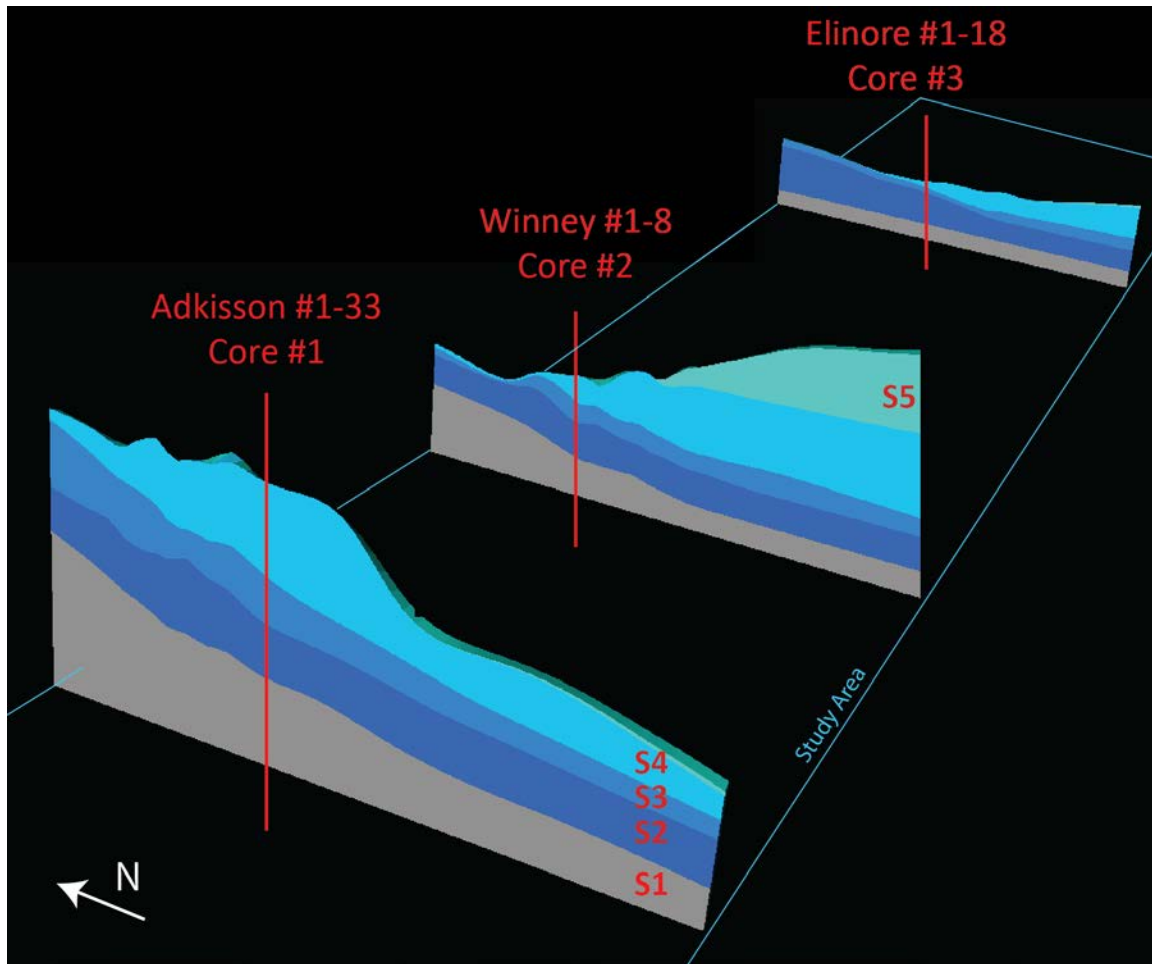


Figure 36. A series of dip-oriented (N-S) slices passing through each of the three cores used in this study. Slices have been vertically exaggerated by 100X to better illustrate sequence geometries. S1-S4 are present in all three dip sections and demonstrate progradational geometries in a southward (basinward) direction. S5 is present only in the center dip section and is interpreted to represent another prograding wedge that was either not deposited or eroded away across the rest of the study area. These dip sections suggest that Mississippian deposition occurred as a series of prograding wedges on a regionally-extensive, gently sloping ramp system.

LIMITATIONS

Although 3-D modeling has helped to identify high frequency sequence geometries across the study area, there are some limitations associated with the dataset. As previously discussed, the three wells used in this study span across two

counties (Logan and Payne Counties), and cover a west-east distance of 28.5 miles (45.9km). Core #1 and Core #2 are 11.1 miles (17.8km) apart and Core #2 and Core #3 are 17.4 miles (28.0km) apart. Spaces between the wells were infilled with raster logs downloaded from IHS at an average spacing of 0.5 miles (0.8km) in the strike and dip directions. This spacing of cores, and wireline logs, is not ideal for facies or sequence modeling as heterogeneities in carbonate depositional systems are known, and expected, to occur at a finer scale. Realistic facies heterogeneities are unresolvable using this dataset. However, an understanding of the facies stacking patterns related to the high frequency 4th order sequences and the overall depositional environment allows for the prediction of facies types away from wells with core. Additionally, these three cores are interpreted to be oriented along, or oblique to, depositional strike. As a result, the model is poorly constrained by rock data in a dip direction. It must be emphasized that this model is only constrained using three cores and 79 wireline logs. Integration of more datasets (i.e. – outcrop, seismic, additional cores or logs, etc.) can be used to better constrain the 3-D model to maintain its geologic integrity.

CHAPTER III

DISCUSSION

RESERVOIR CONSIDERATIONS

Consideration of reservoir potential within depositional and stratigraphic trends provides insight in to how reservoir quality and distribution is related to those aspects in the “Mississippian Limestone” in north-central Oklahoma. Observations and interpretations from core and wireline log analyses indicate a strong depositional control on facies distribution. If a relationship between depositional facies and reservoir aspects can be determined, the established vertical stacking patterns of facies and insight of depositional geometries from modern and ancient analogs can be used to better understand and predict the spatial distribution of reservoir quality units in the subsurface both vertically and laterally. Relationships between reservoir properties and depositional aspects may then be related to wireline log signatures in order to extrapolate interpretations away from the study area.

The reservoir aspect of this study is based on data collected from three cores. Analysis of core data show weak trends between porosity and permeability development and depositional facies (Figure 37). These observations indicate that

reservoir development may be related to other factors (e.g. – structural or diagenetic processes). General relationships between reservoir properties and depositional facies interpreted using average values are outlined below.

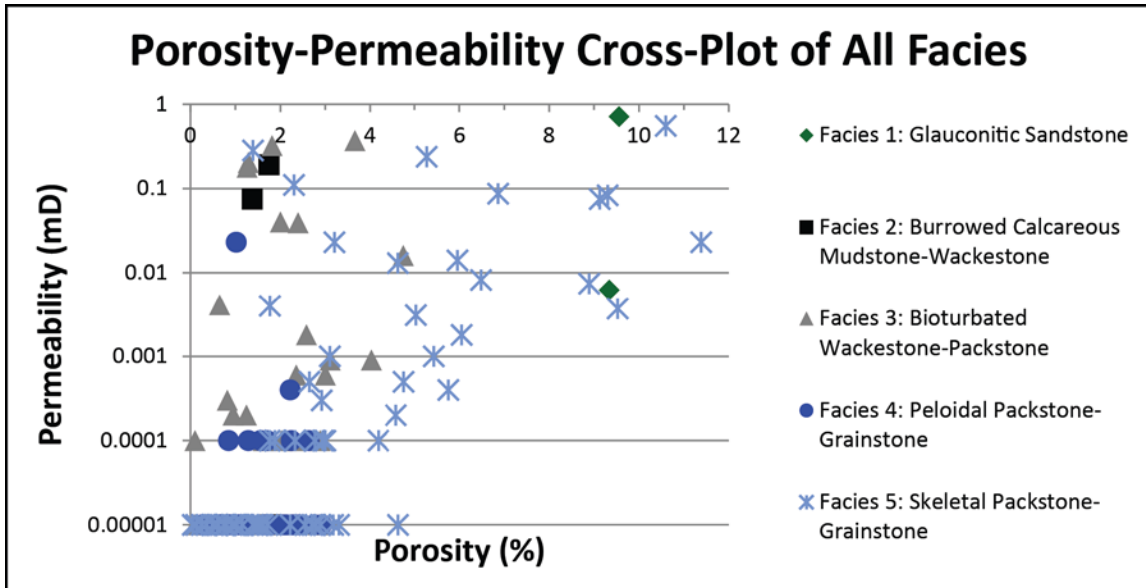


Figure 37. Cross-plot of whole core porosity and permeability by depositional facies for all three wells used in this study. Porosity (%) is plotted on the x-axis and permeability (mD) is plotted on a log scale on the y-axis. This cross-plot illustrates the scatter between depositional facies and their corresponding petrophysical properties making any patterns difficult to identify.

Porosity-permeability cross-plots show that the glauconitic sandstone facies (Facies 1) and the skeletal grainstone facies (Facies 5) have the highest reservoir potential (Figure 38). Facies 1 is of the highest reservoir quality and has an average porosity of 9.5% and an average permeability of 0.358 mD. Facies 1 is characterized by intracrystalline porosity within dolomite crystals, intraparticle porosity within skeletal fragments, and interparticle porosity between quartz and glauconite grains. Facies 1 only occurs near the base of each of the cores and is associated with the transgressive

phase of the overall inferred 3rd order sequence. Although Facies 1 is of good reservoir quality, it is volumetrically insignificant throughout the cores (1.1% of Core #1, 0.55% of Core #2, and 0.77% of Core #3).

Facies 5 has a lower average porosity (3.3%) and permeability (0.049 mD) than Facies 1. The dominant pore types in Facies 5 are solution enhanced moldic porosity developed from the dissolution of skeletal grains, vuggy porosity, and fracture porosity (Figure 39). Facies 5 is associated with the regressive phase of 4th and 5th order high frequency sequences and cycles. Oil staining is commonly observed in Facies 5 and is heaviest in the uppermost high frequency sequences (sequences 3 and 4). Facies 5 occurs throughout all three cores and is volumetrically significant in each (31.3% of Core #1, 45.6% of Core #2, and 53.8% of Core #3).

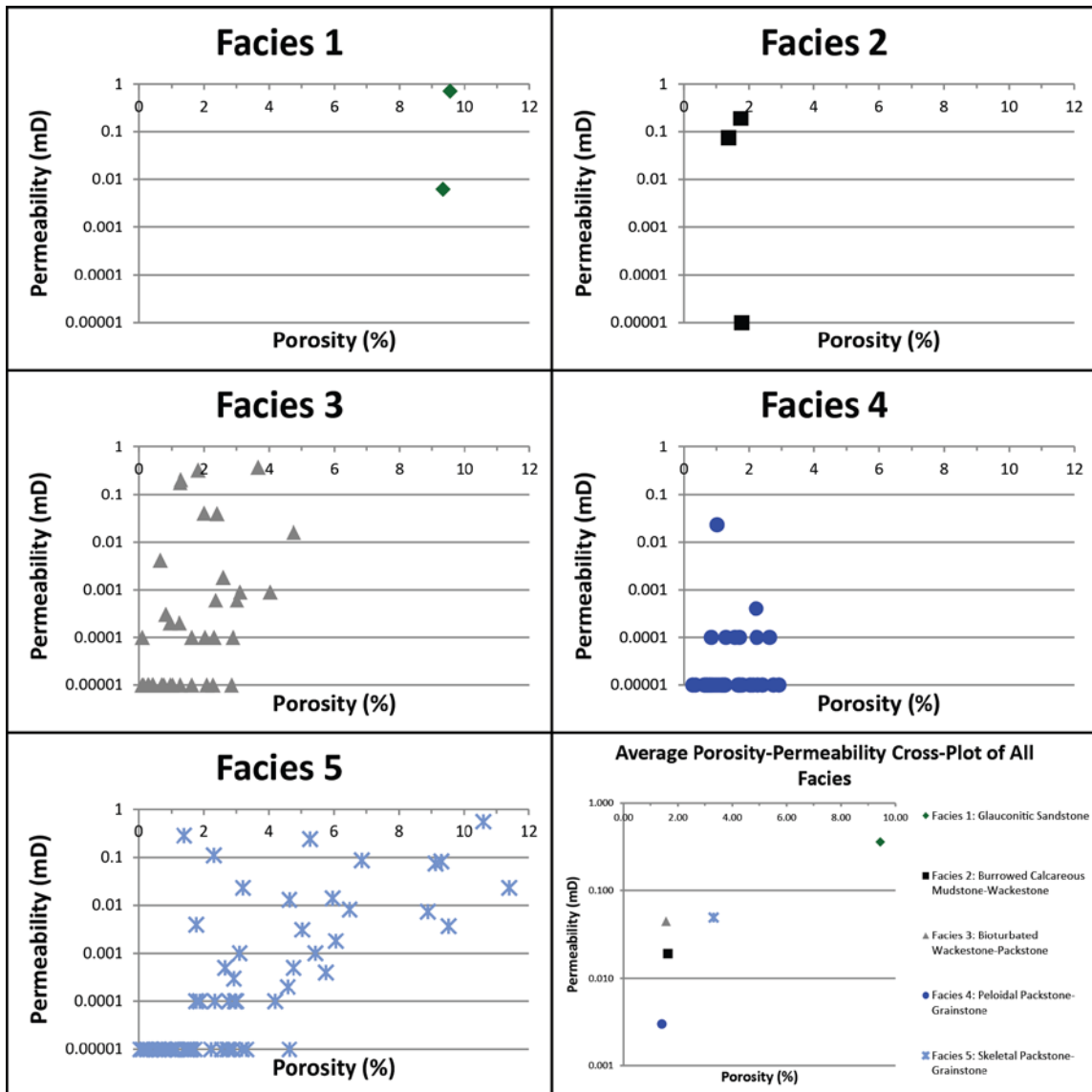


Figure 38. Cross-plots of each depositional facies (Facies 1-5) on the same scale (0-12% porosity on the x-axis and 0.00001-1.0 mD permeability on a log scale on the y-axis) with the average whole core porosity and permeability for each depositional facies plotted on the lower-right graph (0-10% porosity on the x-axis and 0.001-1.0 mD permeability on a log scale on the y-axis). This figure illustrates the wide distribution of porosity and permeability values for each facies individually across the study area, but also shows a relationship between reservoir and non-reservoir quality facies when average porosity and permeability values for each facies are plotted.

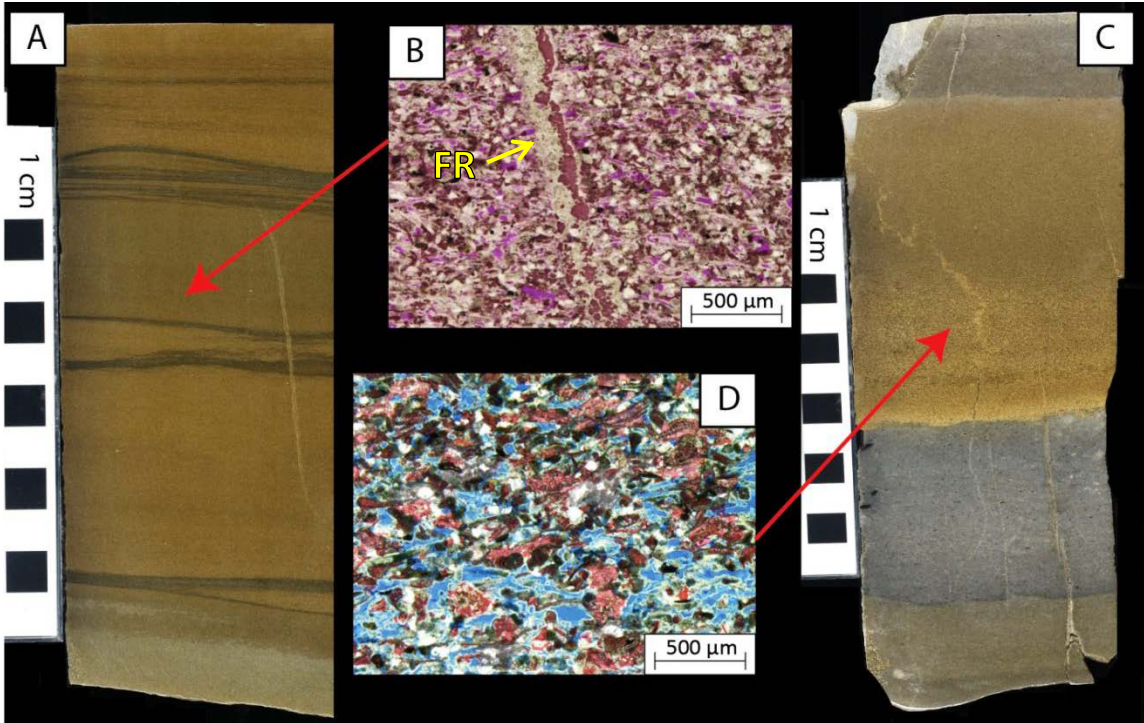


Figure 39. **A-B)** Core photograph and thin section photomicrograph of Core #3 at 4353.9'. This sample shows Facies 5 with a measured porosity of 8.9%. In core the sample is visibly oil stained (yellowish brown tint) and shows a vertical fracture. Thin section is alizarin red stained and porosity is shown in bright fuchsia. This sample is characterized by solution enhanced moldic and vuggy porosity formed by the dissolution of skeletal fragments. The thin section also shows a partially filled fracture. XRD: 1% clays, 33% carbonates (calcite and minimal amounts of iron-rich dolomite), and 66% other minerals (dominantly quartz with minor amounts of potassium feldspar, plagioclase feldspar, and pyrite). **C-D)** Core photograph and thin section photomicrograph of Facies 5 from Core #1 at 5599.4' with a measured porosity of 10.6%. In core the sample is visibly oil stained and contains multiple fractures. Thin section is blue epoxy impregnated. This sample is characterized by solution enhanced moldic and vuggy porosity formed by the dissolution of skeletal fragments. XRD: 0% clays, 59% carbonates (calcite and lesser amounts of iron-rich dolomite), and 41% other minerals (dominantly quartz with minor amounts of potassium feldspar, plagioclase feldspar, and pyrite).

In contrast, the peloidal packstone to grainstone facies (Facies 4) and the burrowed calcareous mudstone facies (Facies 2) possess the lowest porosity and permeability values and may control the vertical variability and compartmentalization of

reservoir units (Figure #29). Facies 4 has the lowest average permeability of 0.003 mD and an average porosity of 1.4%. Facies 4 is most common in the regressive phase of 4th and 5th order high frequency sequences and cycles. Facies 2 has a slightly higher average permeability of 0.019 mD and average porosity of 1.6%. Facies 2 is associated with the transgressive phase of 4th and 5th order high frequency sequences and cycles.

Analysis of core data shows a weak trend between reservoir development and position within the sequence stratigraphic framework. However, a generalized trend can be observed when comparing reservoir development to the 4th order high frequency sequences (Figure 40). Similar to the cross-plot of porosity and permeability and depositional facies, the cross-plot of porosity and permeability and high frequency sequence number shows a high degree of scatter within the data. However, if an average porosity and permeability for each sequence is plotted, sequences 3 and 1 possess the highest reservoir potential. This is likely due to the abundance of reservoir-quality Facies 5 in sequence 3 and Facies 1 in sequence 1. Although sequence 4 has a slightly higher average porosity value than sequence 1, sequence 4 is characterized by a significantly lower average permeability value. The development of porosity and/or permeability does not seem to be directly related to transgressive or regressive phases of the 4th order high frequency sequences (Figure 41). This is likely because the highest quality reservoir facies, Facies 1 and Facies 5, are associated with the transgressive and regressive phases of the high frequency sequences, respectively.

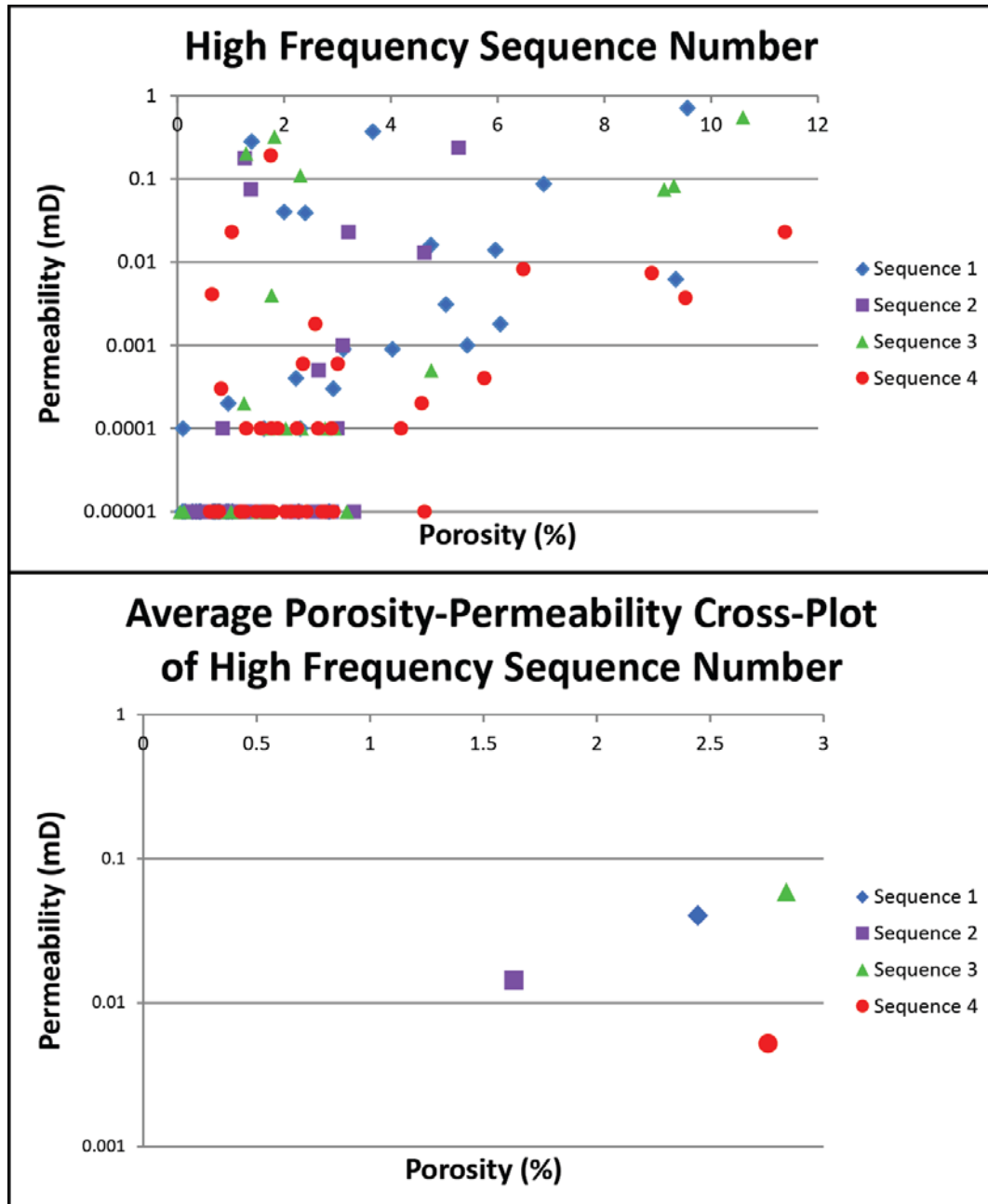


Figure 40. Cross-plot of whole core porosity and permeability by high frequency sequence for all three wells used in this study. Porosity (%) is plotted on the x-axis and permeability (mD) is plotted on a log scale on the y-axis. This cross-plot illustrates the scatter between reservoir and non-reservoir quality facies in each high frequency sequence and their corresponding petrophysical properties making any patterns difficult to identify. A plot of average porosity and permeability values for each high frequency sequence indicates that sequence 3 and sequence 1 possess the highest porosity and permeability values. Although sequence 4 has a slightly higher average porosity value than sequence 1, sequence 4 is characterized by a significantly lower average permeability.

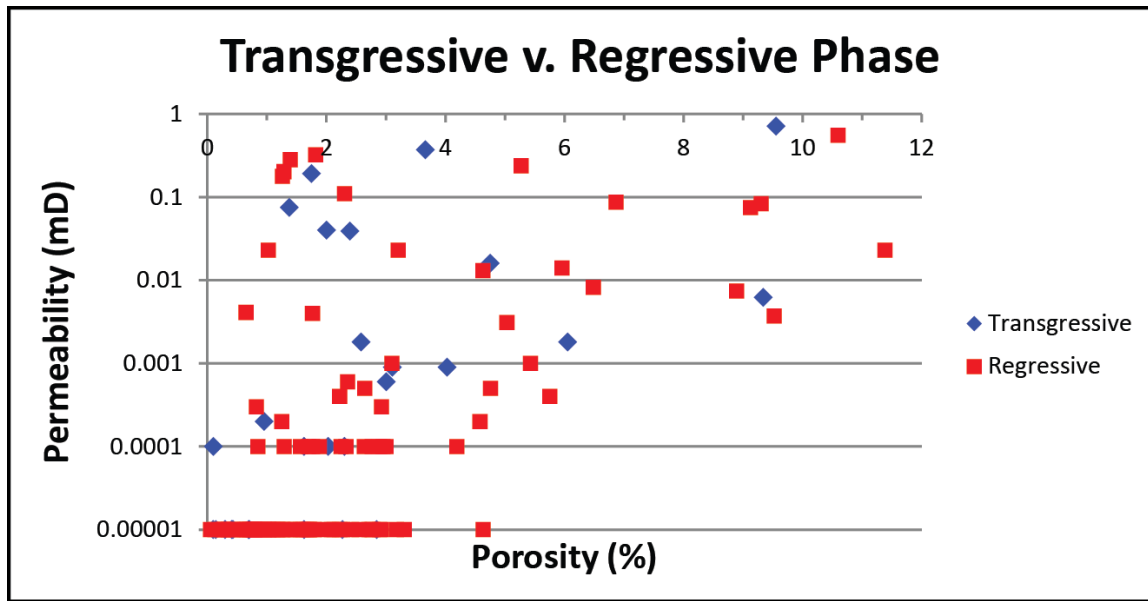


Figure 41. Cross-plot of whole core porosity and permeability by transgressive versus regressive phase of high frequency sequences for all three wells used in this study. Porosity (%) is plotted on the x-axis and permeability (mD) is plotted on a log scale on the y-axis. This cross-plot illustrates the scatter between reservoir and non-reservoir quality facies in each high frequency sequence and their positions within the high frequency sequence. There is no apparent trend between porosity and permeability development and position within the high frequency sequence. However, in general, the data suggest that porosity is better developed in the regressive phase.

NEMAHA FAULT ZONE AND STRUCTURALLY CONTROLLED ACCOMMODATION

Marine accommodation is governed by changes in relative sea level, which are controlled by both eustatic sea level fluctuations and tectonic subsidence/uplift.

Because structural movement during deposition can result in relative changes in sea level (and therefore accommodation), a definite relationship can be drawn between syndepositional geologic structure and depositional facies. Therefore, it is important to examine structures in and around the study area that may have been active during the Mississippian.

The Nemaha Uplift/Ridge is a structural high located just to the west of the study area that is generally believed to have initiated during the Late Mississippian or Early Pennsylvanian (Gay, 2003). It is therefore interpreted that the Nemaha Ridge and associated faults are responsible for post-depositional erosion of the “Mississippian Limestone”. However, the sequence stratigraphic framework established for the study area suggests that the Nemaha Uplift and associated structures were active not only after, but also during the time of deposition.

As illustrated by Lane and DeKyser (1980), the depositional strike of the system is interpreted to trend roughly west-east. Therefore, a transect connecting the three cores used in this study would represent an along strike or oblique to strike profile. Assuming a west-east trending strike and little tectonic activity during the time of deposition, it was expected that the sequences would maintain a relatively uniform thickness in the strike direction. However, the cores show an overall thickening of the Mississippian section in a westward direction, towards the Nemaha Ridge, with the “Mississippian Limestone” doubling in thickness from Core #3 (143.2ft; 43.6m) to Core #1 (323.7ft; 98.7m). Despite this difference in thickness, the four 4th order high frequency sequences are correlative across the study area. This suggests a possible syndepositional tectonic control on Mississippian deposition within the study area.

Within the study area, the axis of the Nemaha Ridge trends roughly north-south, exhibiting a strike-slip movement with a slight upthrow to the east (Figure 42). The thickest Mississippian cores within the study area (Cores #1 and #2) occur on the downthrown side of a large west-east trending fault (Figure 42 and Figure 43, B), and

the thinnest core (Core #3) is positioned on the upthrown block of a nearby, smaller northeast-southwest trending fault (Figure 42 and Figure 43, D). These variations in thickness suggest that the Nemaha Uplift/Ridge and associated faults within the study area were active during deposition and controlled deposition across the study area by locally creating accommodation on their downthrown sides and diminishing accommodation on their upthrown sides.

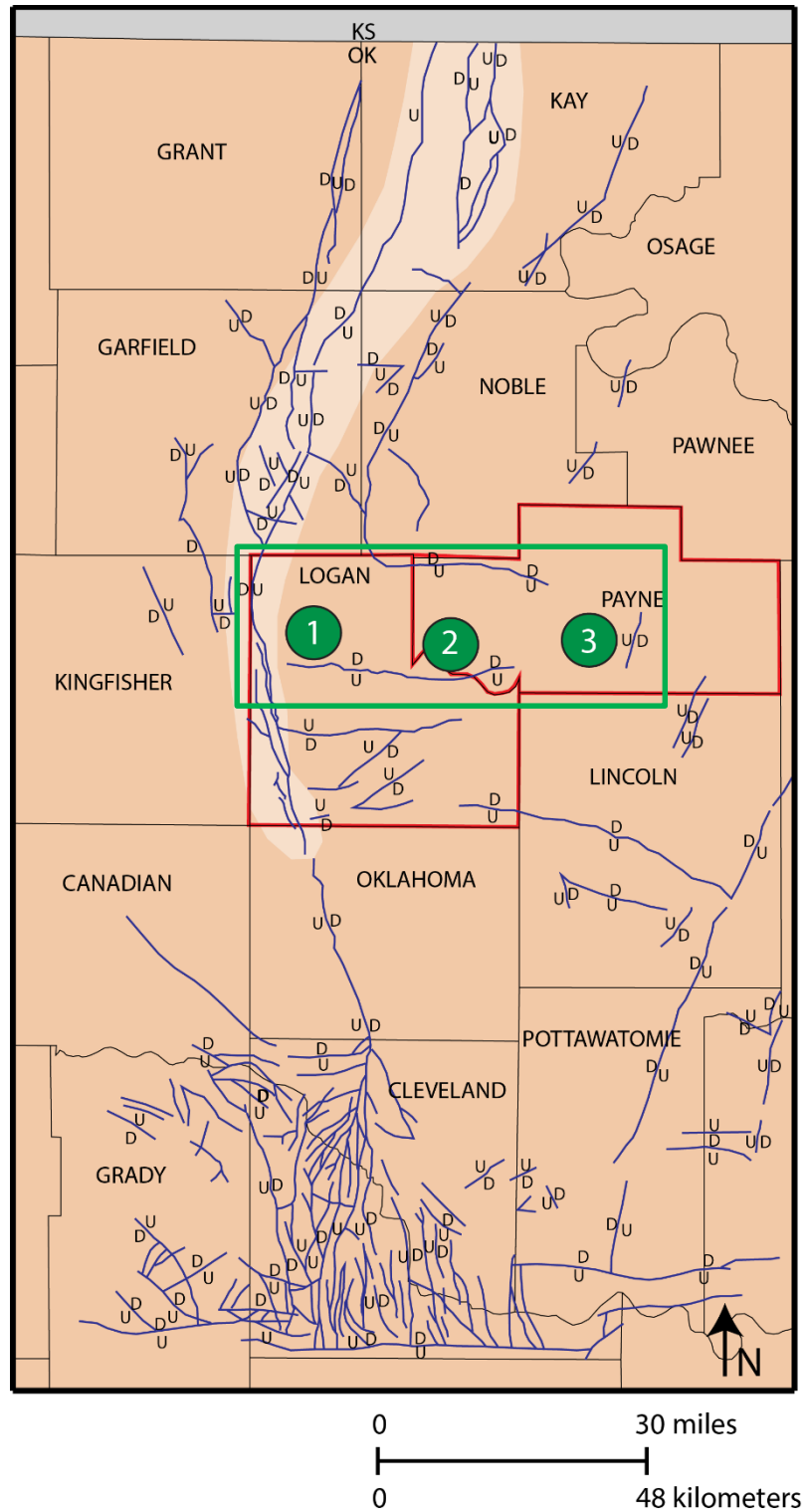


Figure 42. Map showing faulting (blue) associated with the Nemaha Uplift (off-white) in central Oklahoma. The study area is outlined in red. Faulting associated with the Nemaha Uplift is believed to have affected Late Mississippian deposition. This study focuses on the area outlined in green for structural interpretations. Modified from Gay, 2003.

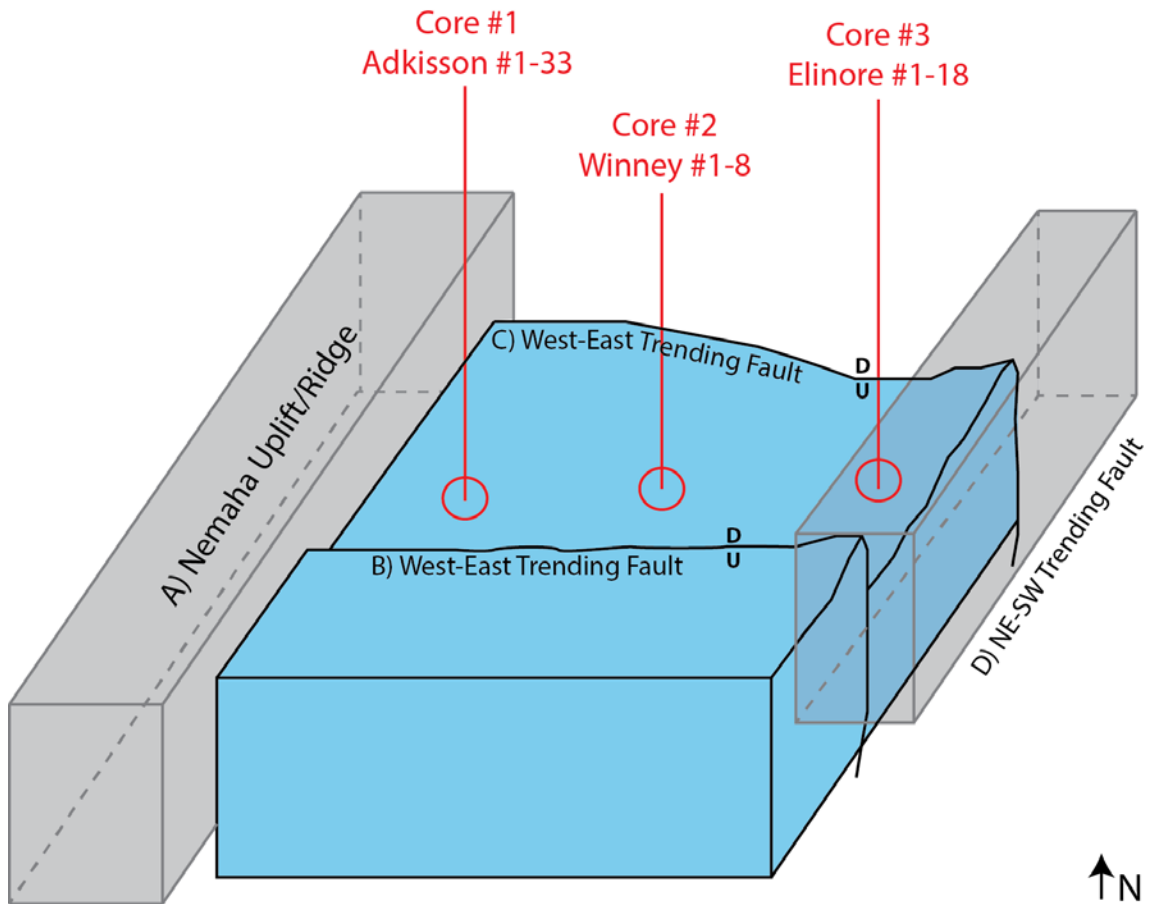


Figure 43. Schematic block diagram illustrating structures within the area of focus (outlined in green in Figure 42). The Nemaha Uplift/Ridge (A) is located to the west of the study area and is upthrown on its eastern flank. Two large west-east trending faults (B and C) pass through the study area and are bounded to the east by a smaller, northeast-southwest trending fault that is upthrown on its western edge. The cores show an overall thickening of the Mississippian section in a westward direction with the “Mississippian Lime” doubling in thickness from Core #3 (143.2ft; 43.6m) to Core #1 (323.7ft; 98.7m). The location of the thickest cores (Cores #1 and #2) adjacent to the downthrown side of a large west-east trending fault (B) and the thinnest core (Core #3) on the upthrown side of a northeast-southwest trending fault (D) and the continuity of high frequency sequences between the three cores suggests that these faults were active during Mississippian deposition and locally created or diminished accommodation.

If a series of these faults were active around the Nemaha fault zone during deposition, it is likely they too had a significant control on accommodation, which in turn led to changes in thickness and facies types. Not only would widespread faulting result in facies variations across relatively short distances, but these faults could also serve as fluid conduits that localize karst formation and diagenetic processes as well as affect the formation of stratigraphic and structural traps and hydrocarbon charging, storage, and expulsion.

Activity of the Nemaha Ridge during the Mississippian may also help explain the abundance of quartz throughout the section (generally 30-45% throughout the section). Well-rounded as well as sub-angular silt to very fine sand-sized quartz grains are observed throughout the Mississippian section in the study area. This suggests that some quartz grains (i.e. – the well-rounded, silt sized quartz grains) are windblown, while others (i.e. – sub-angular grains) may have originated from a closer source area. It is known that uplifts associated with the Nemaha fault system were created in Kansas and Oklahoma (Gay, 2003). If these uplifts existed during Mississippian deposition, they may have served as nearby sources of quartz, and lesser amounts of feldspars and micas, that were brought into the system.

Tectonism related to the Nemaha Ridge may have also affected sedimentation rates in the study area. In general, 3rd order sequences are described as being 100's of meters thick, 4th order high frequency sequences as 10's of meters thick, and 5th order high frequency cycles as few meters thick. 4th order high frequency sequences observed in the San Andres Formation in the Permian Basin are upwards of 200ft thick (10's of m

thick) whereas those observed in the studied Mississippian cores are thinner and range in thickness from approximately 25ft (7.5m) to a maximum of 115ft (35m) (a few m thick to 10's of m thick). In addition to accommodation, the thickness of these individual high frequency sequences is also controlled by carbonate sedimentation rates, which are highly dependent on environmental conditions such as sunlight, salinity, nutrients, and turbidity (Read, 1995). If the uplifts in Kansas and Oklahoma were present during the time of deposition and were significant sources of siliciclastic input, the Mississippian section in north-central Oklahoma may have suffered, to some degree, from clastic poisoning due to turbidity reducing light or suffocating filter feeders (Read, 1995). Therefore, tectonic uplift along the Nemaha Ridge and subsequent siliciclastic input may have resulted in reduced carbonate sedimentation rates and thinner than expected high frequency sequences within the study area.

FAIR WEATHER WAVE BASE FLUCTUATIONS

The reservoir quality skeletal packstone to grainstone facies and sealing peloidal packstone to grainstone facies observed in the Mississippian section in north-central Oklahoma are both interpreted to have been deposited at or just below fair weather wave base. Fair weather wave base is the water depth below which surface wave action no longer stirs or moves the sediment (Flügel, 2010). The depth of fair weather wave base varies widely depending on wave amplitude and fetch, bottom topography, storm activity, latitude, and overall morphology of the depositional system (e.g. – ramp, shelf, or rimmed platform) and its orientation in relation to the prevailing wind direction

(Flügel, 2010). In the skeletal grainstone facies, hummocky cross stratification was observed, indicating that storms intermittently influenced deposition. Based on observations made in this study (i.e. – correlations of high frequency sequences across the study area, orientation of the ramp system, and sequence thickening and thinning in relation to structure) it has been suggested that faults may have been active during the time of deposition. Storm influence and changing bottom topography due to tectonic activity could have influenced the position of fair weather wave base across the study area throughout Mississippian deposition. The alteration of fair weather wave base may have resulted in facies variations that differ from the idealized vertical succession and created facies patterns unrelated to sea level change. This may have been particularly true during the regressive phase where facies are generally thinner and facies changes occur more rapidly, making high frequency cycles difficult to identify. However, larger-scale 4th order high frequency sequences still exhibit repetitive shoaling upwards packages that are identifiable and correlative on wireline log signatures.

CHAPTER IV

SUMMARY AND CONCLUSIONS

This study uses an integrated approach to aid in the understanding of reservoir development within the “Mississippian Limestone” of the Mid-Continent. A better understanding of the depositional environment, facies type and distribution, and reservoir quality was gained by establishing a sequence stratigraphic framework utilizing detailed core descriptions, thin section data, and geostatistical modeling. Key conclusions from this study are:

1. Core and thin section analysis indicate the presence of 5 different facies types that repeatedly stack into a shoaling-upward (shallowing-upward) succession.
2. Analysis of facies stacking patterns demonstrates a three-tiered hierarchy of stratigraphic organization consisting of a large-scale sequence (3rd order), high frequency sequences (4th order), and high frequency cycles (5th order). The large-scale, 3rd order sequence represents the overall lowering of sea level throughout the Mississippian. Four interpreted 4th order high frequency sequences are identified within the Mississippian section and are correlative

across the study area. Higher frequency cycles of probable 5th order are superimposed within the 4th order sequences, but are not correlative between the three cores used in this study, which is believed to be due to autocyclic processes. Correlative 4th order sequences appear to control the overall facies distribution while 5th order high frequency cycles control internal facies heterogeneity.

3. Depositional facies and 4th order high frequency sequences correlate to wireline log signatures and are best identified using gamma-ray and density-neutron porosity curves. 4th order high frequency sequences usually show an upward decrease in gamma-ray values and, generally, an upward increase in density-neutron porosity values. 5th order high frequency cycles do not consistently coincide with gamma-ray signatures and cannot be correlated using wireline log signatures. Although high frequency 4th order sequences are generally observable on wireline logs, correlations based solely on wireline log signatures will likely result in erroneous correlations. Wireline logs must be ground-truthed to rock data to accurately identify high frequency sequences and cycles.
4. Deposition occurred on a ramp to distally steepened ramp. This was inferred from facies types and stacking patterns and comparison with ancient and modern analogs. This interpretation contrasts greatly from the commonly used paleodepositional models that suggest deposition on a platform/rimmed platform or within a starved basin. This highlights the

inaccuracies of the current depositional models and illustrates the need to revise paleogeographic reconstructions.

5. The San Andres Formation located in the Guadalupe Mountains may serve as a good regional analog to the Mississippian system of the Mid-Continent. Facies observed in three Mississippian cores used in this study are comparable to ramp crest, outer ramp, and distal outer ramp deposits of the San Andres and likely exhibit similar facies geometries.
6. The Persian Gulf may serve as an adequate modern depositional analog to the “Mississippian Limestone”. Comparison of Mississippian facies observed in the study area to those observed in the Persian Gulf allows for a first order approximation of water depth and facies geometries.
7. Three-dimensional modeling of high frequency 4th order sequences reveals that interpreted 4th order high frequency sequences are regionally continuous, but thin from west to east (strike direction). These sequences also demonstrate progressive thinning towards the north and thickening towards the south (dip direction). Three-dimensional modeling results show that the Mississippian section was deposited as a series of low-relief, southward prograding wedges on a gently sloping surface.
8. Primary reservoir quality porosity values show a correlation, although weak, to depositional facies and position within the stratigraphic framework. Facies 1 (average porosity of 9.5% and permeability of 0.358 mD) and Facies 5 (average porosity of 3.3% and permeability of 0.049 mD) possess the highest

reservoir quality, whereas Facies 4 and Facies 2 act as seals that compartmentalize reservoir units. Overall, high frequency Sequence 3 possesses the highest reservoir potential.

REFERENCES

- Alsharhan, A.S., and Kendall, C.G.St.C., 2003, Holocene Coastal Carbonates and Evaporites of the Southern Arabian Gulf and Their Ancient Analogues, Elsevier Earth-Science Reviews 61, p. 191-243.
- Asquith, George and Krygowski, Daniel, 2004, Basic Well Log Analysis, 2nd Edition, AAPG Methods in Exploration Series, No. 16, 244 p.
- Bann, K.L., Tye, S.C., MacEachern, J.A., Fielding, C.R., and Jones, B.G., 2008, Ichnological Signatures and Sedimentology of Mixed Wave- and Storm-dominated Deltaic Deposits: Examples from the Early Permian, Southern Sydney Basin of Southeastern Australia, in Hampson, G., Steel, R., Burgess, P., and Dalrymple, R. (eds.), Recent Advances in Models of Siliciclastic Shallow-Marine Stratigraphy, SEPM Special Publication 90, p. 293-332.
- Banner, J.L, and Kaufman, J., 1994, The Isotopic Record of Ocean Chemistry and Diagenesis Preserved in Non-Luminescent Brachiopods from Mississippian Carbonate Rocks, Illinois and Missouri, Geological Society of America Bulletin 106, p. 1074-1082.
- Bates, R.L. and Jackson, J.A., 1987, Glossary of Geology Third Addition, Alexandria, VA, American Geological Institute, 788p.

- Blakey, Ron, 2013, Paleogeography and Geologic Evolution of North America, <http://www2.nau.edu/rcb7/nam.html>. Accessed October 2013.
- Boardman, D.R., Mazzullo, S.J., Wilhite, B.W., Puckette, J.O., Thompson, T.L., and Woolsey, I.W., 2010, Diachronous Prograding Carbonate Wedges from the Burlington Shelf to the Southern Distal Shelf/Basin in the Southern Flanks of the Ozarks, Abstracts with Programs, North-Central and South-Central Meeting, Geological Society of America, v. 42, no. 2, p.41.
- Braden, Angela K., and Ausbrooks, Scott M., 2003, Geologic Map of the Snowball Quadrangle, Searcy County, Arkansas, Arkansas Geological Commission, Digital Geologic Map, DGM-AR-00800, 1 p.
- Buggisch, Werner, Joachimski, Michael M., Sevastopulo, George, and Morrow, Jared R., 2008, Mississippian $\delta^{13}\text{C}_{\text{carb}}$ and Conodont Apatite $\delta^{18}\text{O}$ Records – Their Relation to the Late Palaeozoic Glaciation, *Palaeogeography, Palaeoclimatology, Palaeoecology* 268, p. 273-292.
- Choquette, Phillip W., Cox, Ann, and Meyers, William J., 1992, Characteristics, Distribution and Origin of Porosity in Shelf Dolostones: Burlington-Keokuk Formation (Mississippian), U.S. Mid-Continent, *Journal of Sedimentary Petrology*, v. 62, no. 2, p. 167-189.
- Choquette, Philip W., and Pray, Lloyd C., 1970, Geologic Nomenclature and Classification of Porosity in Sedimentary Carbonates, *AAPG Bulletin*, v. 54, no. 2, p. 207-250.
- Clark, David L., 1984, Conodont Biofacies and Provincialism, *The Geological Society of America*, Special Paper 196, 345 p.

- Coburn, T. C., Corbett, P. W. M., Datta-Gupta, A., Jensen, J. L., Kelkar, M., Oliver, D. S., and White, C. D., 2006, A virtual conversation on the impact of geostatistics in petroleum, production, and reservoir engineering, in Coburn, T. C., Yarus, J. M., and Chambers, R. L., eds., *Stochastic modeling and geostatistics: Principles, methods, and case studies, volume II*, AAPG Computer Applications in Geology 5, p. 23-33.
- Cowan, C.A., and James, N. P., 1996, Autogenic Dynamics in Carbonate Sedimentation: Meter-Scale Shallowing Upward Cycles, Upper Cambrian, Western Newfoundland, Canada, *American Journal of Science*, v. 296, p. 1175-1207.
- Curtis, Doris M. and Champlin, Stephen C., 1959, Depositional Environments of Mississippian Limestones of Oklahoma, *Tulsa Geological Society Digest*, v. 27, no. 1, p. 90-103.
- Daniels, Terryl G., 2012, Outcrop Investigation of the Reeds Spring (Boone, Mississippian) of the Hindsville Quarry Using Terrestrial LIDAR, Master of Science, University of Arkansas, ProQuest, UMI Dissertation Publishing. 87 p.
- Dodd, J.R., and Stanton, Jr. R.J., 1981, *Paleoecology, Concepts and Applications*, Wiley-Interscience Publication, New York, 559 p.
- Doveton, J. H., 1994, *Geologic Log Interpretation: reading the rocks from wireline logs*, SEPM Short Course 29, 169 p.
- Drummond, C. N., and Wilkinson, B. H., 1993, Carbonate Cycle Stacking Patterns and Hierarchies of Orbitally-Forced Eustatic Sea Level Change, *Journal of Sedimentary Petrology*, v. 63, p. 369-377.

- Dunham, R.J., 1962, Classification of Carbonate Rocks According to Depositional Texture, AAPG Special Volumes, Memoir 1: Classification of Carbonate Rocks, v. 1, p. 108-121.
- Eberli, G. P., P. M. Harris, and G. M. Grammer, 2004, Carbonate sequence stratigraphy: American Association of Petroleum Geologists Field Guide, Tulsa, Oklahoma, p. 1–15.
- Ekdale, A.A., Bromley, R.G., and Pemberton, S.G., 1984, Ichnology – Trace Fossils in Sedimentology and Stratigraphy, SEPM Short Course No. 15, 317 p.
- Evans, K.R., Mickus, K.L., and Jackson, J.S., 2010, Geology of the Branson Area, Southwestern Missouri: AIPG Missouri Section Annual Meeting Field Trip Guidebook, 40 p.
- Evans, Kevin R., Jackson, Jeremiah S., Mickus, Kevin L., Miller, James F., and Cruz, Dulce, 2011, Enigmas and Anomalies of the Lower Mississippian Subsystem in Southwestern Missouri, Search and Discovery Article #50406, 47 p.
- Flügel, Erik, 2010, Microfacies of Carbonate Rocks: Analysis, Interpretation, and Application, 2nd Ed., Springer-Verlag, Berlin, Heidelberg, New York, 1007 p.
- Franseen, E.K., 2006, Mississippian (Osagean) Shallow-Water, Mid-Latitude Siliceous Sponge Spicule and Heterozoan Carbonate Facies: An Example from Kansas with Implications for Regional Controls and Distribution of Potential Reservoir Facies, Current Research in Earth Sciences, Bulletin 252, pg. 1-23.
- Gay, Parker S. Jr., 1999, Strike-Slip, Compressional Thrust-Fold Nature of the Nemaha System in Eastern Kansas and Oklahoma, Kansas Geological Society, Transactions

- of the 1999 American Association of Petroleum Geologists Midcontinent Section Meeting (Geoscience for the 21st Century), p. 39-50.
- Gay, Parker S. Jr., 2003, The Nemaha Trend – A System of Compressional Thrust-Fold, Strike-Slip Structural Features in Kansas and Oklahoma, Part 1, Shale Shaker, July-August, p. 9-49.
- Goddard, E. N., Trask, P. D., De Ford, R. K., Rove, O. N., Singewald, J. T., and Overbeck, R. M., 1951, Rock Color Chart, Geological Society of America, Boulder, Colorado.
- Grammer, G. M., P. M. Harris, G. P. Eberli, 2004, Integration of Outcrop and Modern Analogs in Reservoir Modeling: Overview with Examples from the Bahamas, in G. M. Grammer, P. M. Harris, and G. P. Eberli, eds., Integration of Outcrop and Modern Analogs in Reservoir Modeling: American Association of Petroleum Geologists Memoir 80, p. 1-22.
- Greenberg, Dallas W., 1981, Sedimentology and Diagenesis of the Short Creek Oolite, Master of Science Thesis, University of Missouri, Columbia, 72 p.
- Gutschick, Raymond, and Charles A. Sandberg, Charles A., 1983, Mississippian Continental Margins of the Conterminous United States, SEPM Special Publication, N. 33, p. 79-96.
- Haq, B. U., and Schutter, S. R., 2008, A Chronology of Paleozoic Sea-Level Changes, Science, v. 322, p. 64-68.
- Handford, C. Robertson, 1986, Facies and Bedding Sequences in Shelf-Storm-Deposited Carbonates – Fayetteville Shale and Pitkin Limestone (Mississippian), Arkansas, Journal of Sedimentary Petrology, v. 56, no. 1, p. 123-137.

- Handford, Robert, 2013, Carbonate Ramps, Clastic Lowstands and Organic-Rich Transgressive Shales – Hallmarks of Mississippian Sequences in North Arkansas and Southern Missouri, AAPG Mississippian Lime Play Forum, Oral Presentation, Oklahoma City, Oklahoma.
- Handford, C. Robertson, and Loucks, Robert G., 1993, Carbonate Depositional Sequences and Systems Tracts-Responses of Carbonate Platforms to Relative Sea-Level Changes, In: Loucks, Robert G., and Sarg, Frederick (eds.), Carbonate Sequence Stratigraphy: Recent Developments and Applications, AAPG Memoir 57, p. 3-42.
- Harris, S.A., 1987, Hydrocarbon Accumulation in “Meramec-Osage” (Mississippian) Rocks, Sooner Trend, Northwest-Central Oklahoma, Tulsa Geological Society, Special Publication No. 3: Petroleum Geology of the Mid-Continent.
- Heinzelmann, Gerald Mathias, 1964, Mississippian Rocks in the Stillwater-Chandler Area, Oklahoma City Geological Society, The Shale Shaker Digest V, v. XV-XVII, p. 195-207.
- Huffman, George G., 1958, Geology of the Ozark Uplift, Northeastern Oklahoma, Oklahoma City Geological Society, The Shale Shaker Digest I, v. I-V, p. 36-42.
- Huffman, George G., 1960, Geology of the Oklahoma Ozark Region, North-Eastern Oklahoma: Guidebook, 25th Field Conference, p. 82-109.
- Jackson, J.S. and Evans, K.R., 2009, Allochthonous Origin of Small Carbonate Mud Mounds in the Compton Limestone (Mississippian, Kinderhookian), Southwest Missouri, AAPG Search and Discovery Article #90095, 1 p.

- Jordan, Louise and Rowland, T.L., 1959, Mississippian Rocks in Northern Oklahoma, Tulsa Geological Society Digest, v. 27, p. 124-136.
- Kerans, C., Lucia, F. Jerry, and Senger, R.K., 1994, Integrated Characterization of Carbonate Ramp Reservoirs Using Permian San Andres Formation Outcrop Analogs, AAPG Bulletin, v. 78, no. 2, p. 181-216.
- King, D. T., Jr., 1986, Waulsortian-Type Buildups and Resedimented (Carbonate-Turbidite) Facies, Early Mississippian Burlington Shelf, Central Missouri, Journal of Sedimentary Petrology, v. 56, p. 471-479.
- Kreman, Drew Michael, 2011, Characterization of Kinderhookian and Osagean Strata of Northeast Oklahoma, Master of Science Thesis, ProQuest, UMI Dissertation Publishing, 160 p.
- Krueger, Robert Carl, 1965, Subsurface Study of Mississippian Rocks in the Tulsa Area, Oklahoma City Geological Society, The Shale Shaker Digest V, v. XV-XVII, p. 217-239.
- Lane, H. R., 1978, The Burlington Shelf (Mississippian, North-Central United States): Geologica et Palaeontologica, v. 12, p. 165-175.
- Lane, H. R., and DeKyser, T. L., 1980, Paleogeography of the Late Early Mississippian (Tournasian 3) in the Central and Southwestern United States, Paleozoic Paleogeography of West-Central United States: Rocky Mountain Paleogeography Symposium 1, p. 149-162.
- Laudon, L. R., 1939, Stratigraphy of Osage Subseries of Northeastern Oklahoma, AAPG Bulletin 23, p. 325-338.

- Lisle, Barbara A., 1983, Short Creek Oolite (Lower Mississippian) Deposition, War Eagle Quarry, Madison County, Arkansas, Arkansas Academy of Science Proceedings, v. XXXVII, p. 47-49.
- MacEachern, James A., Bann, Kerrie L., Gingras, Murray K., and Pemberton, S. George, 2009, Applied Ichnology, SEPM Short Course Notes 52: Revised Edition, Society for Sedimentary Geology (SEPM), Tulsa, OK, 145 p.
- Manger, Walter L., and Shanks, Jack L., 1976, Lower Mississippian Lithostratigraphy, Northern Arkansas, Arkansas Academy of Science Proceedings, v. XXX, p. 78-80.
- Mazzullo, S.J., Boardman, Darwin R., Wilhite, Brian W., Godwin, Cory, and Morris, Beau T., 2013, Revisions of Outcrop Lithostratigraphic Nomenclature in the Lower to Middle Mississippian Subsystem (Kinderhookian to Basal Meramecian Series) Along the Shelf-Edge in Southwest Missouri, Northwest Arkansas, and Northeast Oklahoma, Shale Shaker, v. 63, no. 6, p. 414-454.
- Mazzullo, S.J., and Wilhite, Brian W., 2010, Chert, Tripolite, Spiculite, Chat – What’s in a Name?, Kansas Geological Society Bulletin, v. 85, no. 1, p. 21-25.
- Mazzullo, S.J., Wilhite, B.W., and Boardman, D.R., 2011, Lithostratigraphic Architecture of the Mississippian Reeds Spring Formation (Middle Osagean) in Southwest Missouri, Northwest Arkansas, and Northeast Oklahoma: Outcrop Analog of Subsurface Petroleum Reservoirs, Shale Shaker, March/April, p.254-269.
- Mazzullo, S.J., Wilhite, Brian W., Boardman, Darwin R., Morris, Beau, Turner, Robert, and Godwin, Cory, 2011b, Field Trip Guidebook: Lithostratigraphy and Conodont

Biostratigraphy of the Kinderhookian to Osagean Series on the Western Flank of the Ozark Uplift, Sponsored by the Tulsa Geological Society, 48 p.

Mazzullo, S.J., Wilhite, Brian W., and Woolsey, I. Wayne, 2009a, Rhythmic Carbonate Versus Spiculite Deposition in Mississippian Hydrocarbon Reservoirs in the Midcontinent USA: Causative Factors and Resulting Reservoir Petrophysical Attributes, AAPG Search and Discovery Article #10209, 6 p.

Mazzullo, S.J., Wilhite, Brian W., and Woolsey, I. Wayne, 2009b, Petroleum Reservoirs within a Spiculite-Dominated Depositional Sequence: Cowley Formation (Mississippian: Lower Carboniferous), South-Central Kansas, AAPG Bulletin, v. 93, no. 12, p. 1649-1689.

McFarland, John David, 2004, Stratigraphic Summary of Arkansas, Arkansas Geological Commission, Information Circular 36, 44 p.

McKnight, E.T., and Fischer, R.P., 1970, Geology and Ore Deposits of the Picher Field, Oklahoma and Kansas, United States Geological Survey Professional Paper 588, 165 p.

Mehl, Maurice G., 1961, Basal Relationships of the Mississippian in Northeastern Missouri, Kansas Geological Society, Northeastern Missouri and West Central Illinois: Guidebook, 26th Annual Field Conference in Cooperation with the Missouri Geological Survey and the Illinois Geological Survey, p. 89-94.

Middleton, Gerard V., Church, Michael J., Coniglio, Mario, Hardie, Lawrence A., and Longstaffe, Frederick J., 2003, Encyclopedia of Sediments and Sedimentary Rocks, Kluwer Academic Publishers, The Netherlands, 821 p.

- Mikkelson, D.H., 1966, The Origin and Age of the Mississippian "Chat" in North-Central Oklahoma, Oklahoma City Geological Society, The Shale Shaker Digest V, v. XV-XVII, p. 255-265.
- Northcutt, R. A., and Campbell, J. A., 1996, Geologic Provinces of Oklahoma, Transactions of the 1995 AAPG Mid-Continent Section Meeting, 1996, p. 128-134.
- Pyrzcz, M. J. and Deutsch, C. V., 2014, Geostatistical Reservoir Modeling, Oxford University Press, Oxford, N.Y., 448 p.
- Rankey, Eugene C., 2002, Spatial Patterns of Sediment Accumulation on a Holocene Carbonate Tidal Flat, Northwest Andros Island, Bahamas, Journal of Sedimentary Research, v. 72, p. 591-601.
- Read, J.F., 1995, Overview of Carbonate Platform Sequences, Cycle Stratigraphy and Reservoirs in Greenhouse and Icehouse Worlds, In: Read, J. F., Kerans, C., Weber, L. J., Sarg, J. F., and Wright, F. M. (eds.), Milankovitch Sea Level Changes, Cycles, and Reservoirs on Carbonate Platforms in Greenhouse and Ice-House Worlds: SEPM Short Course 35, p. 1-102.
- Rogers, James P., Longman, Mark W., and Lloyd, R. Michael, 1996, Spiculitic Chert Reservoir in Glick Field, South-Central Kansas, Tulsa Geological Society, Transactions of the 1995 AAPG Mid-Continent Section Meeting, 31 p.
- Ross, C. A., and Ross, J. R., 1988, Late Paleozoic Transgressive-Regressive Deposits, in Wilgus, Cheryl K., Hastings, Bruce S., Posamentier, Henry, Wan Wagoner, John,

- Ross, Charles A., and Kendall, Christopher G. St. C., eds., Sea-Level Changes - An Integrated Approach, SEPM Special Publication No. 42, p. 227-247.
- Roundtree, R., Wright, J., and Miskimins, J., 2010, Unconventional Resource Recovery Improvement Using Conventional Reservoir Engineering Strategies, AAPG Search and Discovery Article #80088, 15 p.
- Scholle, P.A., and Ulmer-Scholle, D.S., 2003, A Color Guide to the Petrography of Carbonate Rocks: Grains, Textures, Porosity, Diagenesis, AAPG Memoir 77, Tulsa, The American Association of Petroleum Geologists, 474 p.
- Shoeia, Osama Khalifa, 2012, High resolution stratigraphy of Lower Mississippian Strata near Jane, Missouri, Master of Science Thesis, Oklahoma State University, unpublished, 262 p.
- Sloss, L. L., 1963, Sequences in the Cratonic Interior of North America, Geological Society of America Bulletin 74, p. 93-114.
- Spreng, A.C., 1952, The Lower Pierson Fauna of West-Central Missouri, Kansas Geological Society, West-Central and Southwestern Missouri: Guidebook, 16th Regional Field Conference, 6 p.
- Spreng, A.C., 1961, Mississippian System, In: The Stratigraphic Succession in Missouri, Missouri Geological Survey and Water Resources, 2nd Series, v. 40, p. 49-78.
- Thompson, T.L., and Fellows, L.D., 1970, Stratigraphy and Conodont Biostratigraphy of Kinderhookian and Osagean (Lower Mississippian) Rocks of Southwestern Missouri and Adjacent Areas, Missouri Geological Survey and Water Resources Report of Investigations 45, 263 p.

- Thornton, Wayne D., 1961-1964, Mississippian Rocks in the Subsurface of Alfalfa and Parts of Woods and Grant Counties, Northwestern Oklahoma, Oklahoma City Geological Society, The Shale Shaker Digest IV, v. XII-XIV, p. 117-128.
- Tinker, S.W., 1996, Building the 3-D Jigsaw Puzzle: Applications of Sequence Stratigraphy to 3-D Reservoir Characterization, Permian Basin, AAPG Bulletin, v. 80, no. 4, p. 460-485.
- Unrast, M., 2013, Composition and Classification of Mississippian Carbonate Mounds in the Ozark Region, North America, Shale Shaker, v. 63, no. 4, p. 254-273.
- Wagner, C.W, and Toghiani, C. Van Der, 1973, Holocene Sediment Types and Their Distribution in the Southern Persian Gulf, In: Purser, Burce H. (ed), The Persian Gulf, Springer-Verlag, Berlin, Heidelberg, New York, p. 123-155.
- Wilhite, Brian W., Mazzullo, S.J., Morris, Beau T., and Boardman, Darwin II, 2011, Syndepositional Tectonism and its Effects on Mississippian (Kinderhookian to Osagean) Lithostratigraphic Architecture: Part 1 – Based on Exposures in the Midcontinent USA, AAPG Search and Discovery Article #30207, 43 p.
- Wilkinson, Bruce H. and Drummond, Carl N., 2004, Facies Mosaics Across the Persian Gulf and Around Antigua – Stochastic and Deterministic Products of Shallow-Water Sediment Accumulation, Journal of Sedimentary Research, v. 74, no. 4, p. 513-526.
- Witzke, B. J., 1990, Paleoclimatic constraints for Paleozoic paleolatitudes of Laurentia and Euramerica, W. S. McKerrow and C. R. Scotese, eds. Paleogeography and biogeography: Geological Society (London) Memoir 12, p. 57-73.

APPENDICES

APPENDIX A

WRITTEN CORE DESCRIPTIONS

Colors described from core relate to the standardized color chart key (Table 4), which has been abbreviated from the rock-color chart developed by the Rock-Color Chart Committee (1970). Locations of thin section samples are indicated by “TS” below each written description. Descriptions of the degree of bioturbation refer to the bioturbation index from Bann et al., 2008 (Table 5).

Rock-Color Chart			
Color Name	Numerical Designation	Color Name	Numerical Designation
Black	N1	Medium Gray	N5
Brownish Black	5 YR 2/1	Moderate Yellowish Brown	10 YR 5/4
Dark Gray	N3	Olive Black	5 Y 2/1
Dark Yellowish Brown	10 YR 4/2	Olive Gray	5 Y 4/1
Dark Yellowish Orange	10 YR 6/6	Very Light Gray	N8
Dusky Yellowish Brown	10 YR 2/2	Yellowish Gray	5 Y 8/1
Grayish Black	N2		
Grayish Yellow Green	5 GY 7/2		
Greenish Black	5 GY 2/1		
Light Gray	N7		
Light Olive Gray	5 Y 6/1		
Medium Dark Gray	N4		

Table 4. Rock-Color Chart listing color names and associated numerical designations. Modified from Goddard et al., 1951.

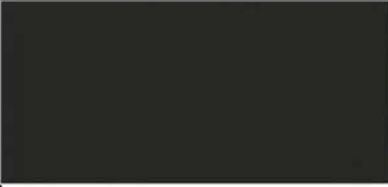


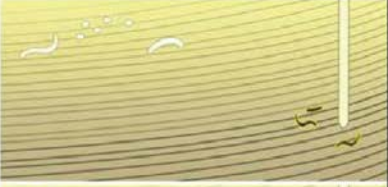


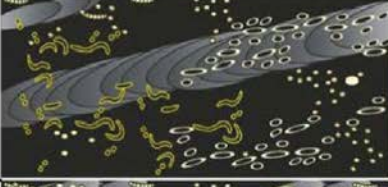

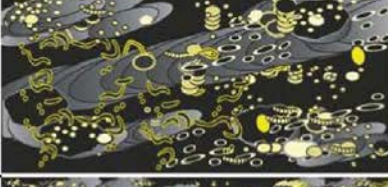

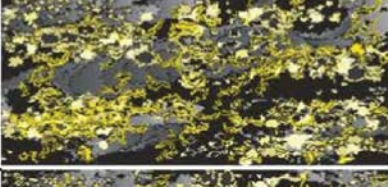



Bioturbation Index			
#	Characteristics	Mud-Dominated Facies	Grain-Dominated Facies
0	Bioturbation absent		
1	Sparse bioturbation, bedding distinct, few discrete traces		
2	Uncommon bioturbation, bedding distinct, low trace density		
3	Moderate bioturbation, bedding boundaries sharp, traces discrete, overlap rare		
4	Common bioturbation, bedding boundaries indistinct, high trace density with overlap common		
5	Abundant bioturbation, bedding completely disturbed (just visible)		
6	Complete bioturbation, total biogenic homogenization of sediment		

Table 5. Bioturbation index used for written and illustrative core descriptions. Modified from Bann et al., 2008.

Fracture Density

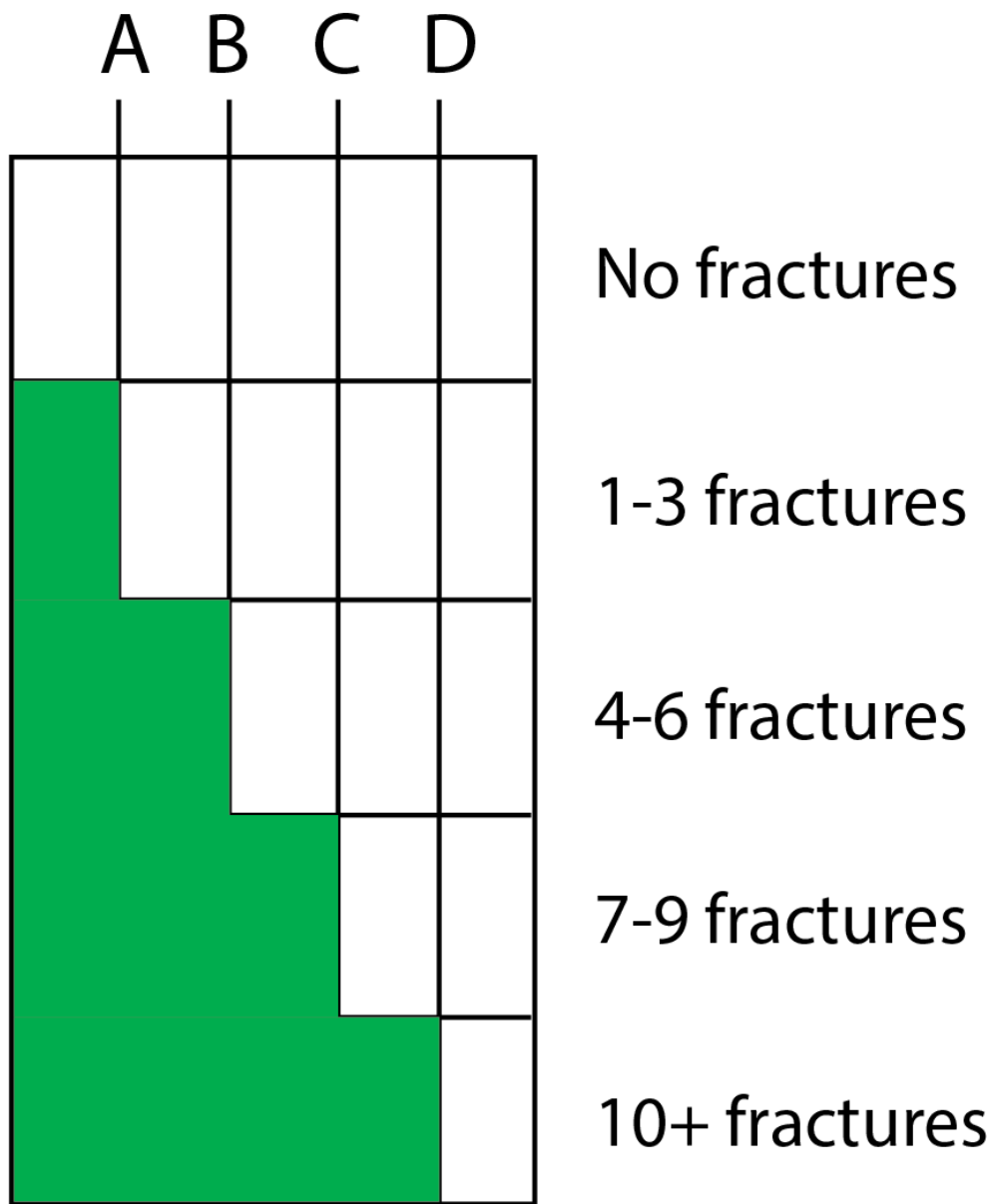


Table 6. Fracture density chart used for written and illustrative core descriptions. Letters A-D correspond to the number of fractures per foot.

Core #1: Adkisson #1-33 SWD – Devon Energy

Logan County, OK

Cored Interval: 5827.0'-5485.0'

Examined Interval: 5819.9'-5496.2'

Top "Mississippian Limestone": 5819.9' (from core)

Formations: Woodford Shale, "Mississippian Limestone", and Pennsylvanian

5819.9' – 5816.2' = Facies #1. Glauconitic sandstone. Dark gray and greenish black. Contact between Woodford Shale and "Mississippian Limestone" at 5819.9'. Abundant bioturbation. Very fine sand-sized glauconite grains. Very fine sand-sized pyrite crystals grading into very coarse sand-sized crystals (~30%) from base to top of interval. Scattered, grayish black chert nodules throughout the interval (~1 inch in diameter). No visible porosity or oil staining (or fluorescence under ultraviolet light) in hand sample.

TS 5819.8'

5816.2' – 5799.0' = Facies #3 and #2. Bioturbated wackestones and occasional packstones with intermittent burrowed calcareous mudstones. Olive gray, light olive gray, olive black, and yellowish gray. Generally uncommon to moderate bioturbation, but some intervals are abundantly bioturbated (5810'-5805' and 5800'-5898'). Silty and sandy wackestones present. Intervals of burrowed calcareous mudstone facies (approximately 0.15' thick) at 5813.5', 5810.3', and 5801.1'. Scattered, visible very coarse sand-sized crinoid fragments and coarse to very coarse sand-sized pyrite crystals throughout interval (<5%). Brachiopod fragments (~0.5-1 inch) visible at 5807.5'. Sparse vertical to sub-vertical fractures ranging in length from 0.4' to 0.1' that are partially to completely cemented with calcite. Porosity visible within partially cemented vertical fractures. Oil staining and fluorescence under ultraviolet light observed in moderately bioturbated zones (5810', 5808', 5806', and 5802.5'), vertical fracture at 5807', and brachiopod fragments at 5807.5'.

TS 5810.4'

TS 5807.75'

TS 5801.4'

5799.0' – 5797.3' = Facies #5. Bioturbated skeletal packstone to grainstone. Olive gray, light olive gray, brownish black, and grayish orange. Common to moderate bioturbation. Heavily fractured with most fractures occurring as partially filled vertical fractures (approximately 0.2' long). Porosity visible in partially cemented fractures. Oil staining and fluorescence under ultraviolet light observed throughout the interval and concentrated in lighter-colored, grainier intervals and fractures. No visible skeletal fragments in hand sample.

TS 5797.55'

5797.3' – 5757.9' = Facies #3. Bioturbated wackestones. Olive gray, light gray, dusky yellowish brown, brownish black, and brownish gray. Sparsely to moderately bioturbated. Coarse to very coarse sand-size crinoid fragments (~1mm) scattered throughout entire interval. Deposits are more thinly bedded at the base of the interval (5797.3'-5776') and transition upward into thicker or massively bedded deposits. Wispy laminations observed throughout interval. Overall low degree of fracturing. Faint oil staining and fluorescence under ultraviolet light observed near the base of the interval.

TS 5786.5'

TS 5775.0'

TS 5770.6'

TS 5763.15'

TS 5760.6'

5757.9' – 5757.6 = Facies #1. Glauconitic sandstone. Dark gray and greenish black. Abundant bioturbation. Glauconite grains concentrated in burrows. Very fine sand-sized glauconite grains and coarse sand-sized pyrite crystals. No visible porosity or oil staining (or fluorescence under ultraviolet light) in hand sample.

TS 5757.85'

5757.6' – 5754.8' = Facies #2. Burrowed calcareous mudstone. Grayish black and olive black. Moderately bioturbated with mm-scale burrows throughout. Interval contains visible, scattered brachiopod fragments (1-2 cm) and coarse sand-sized crinoid fragments. No visible porosity or oil staining (or fluorescence under ultraviolet light) in hand sample.

5754.8' – 5742.0' = Facies 3. Bioturbated wackestones with some intermittent burrowed calcareous mudstones. Olive gray, light gray, dusky yellowish brown, brownish black, and brownish gray. Moderately to commonly bioturbated. Overall low degree of fracturing, but some sub-vertical, filled fractures are present towards the top of the interval. Coarse sand-sized pyrite grains and crinoid fragments are observed in the uppermost intervals. Thin intervals of burrowed calcareous facies observed at 5751.1' (0.1' thick) and 5748.2' (0.5' thick). No visible porosity or oil staining (or fluorescence under ultraviolet light) in hand sample.

TS 5751.65'

TS 5750.6'

TS 5749.0

TS 5744.75'

5742.0' – 5729.0' = Facies #2 and #3. Burrowed calcareous mudstones and bioturbated wackestones. Olive gray, light olive gray, olive black, and yellowish gray. Generally sparse to uncommon bioturbation with some moderate bioturbation (5735.5'-5736.5'). Burrowed calcareous mudstone facies from 5742.0'-5738.3' and 5734.0'-5731.8'. Coarse to very coarse sand-sized crinoid fragments and pyrite crystals and mm-scale burrows observed in burrowed calcareous mudstone intervals. Overall moderate degree of fracturing with most fractures occurring in the bioturbated wackestone facies. Very faint oil staining (and associated fluorescence under ultraviolet light) observed in the bioturbated wackestone facies.

TS 5737.85'

TS 5735.0'

5729.0' – 5725.7' = Facies #4 and #5. Interbedded peloidal and skeletal grainstones. Dark gray, medium gray, brownish black, light olive gray, and dark yellowish brown. Some intervals of silty to sandy grainstones present. Most of the interval is not bioturbated, but a thin bioturbated interval occurs at 5727.0'. Few fractures are observed throughout this interval. Heavy oil staining observed in skeletal grainstone facies at the base of the interval with a lesser degree of oil staining observed in the peloidal grainstone facies interval just above.

TS 5728.8'

TS 5727.5'

TS 5725.75'

5725.7' – 5722.3' = Facies #3. Bioturbated wackestone. Olive gray, olive black, and medium dark gray. Wispy laminations scattered throughout interval. Characterized by uncommon bioturbation and a moderate degree of fracturing. No visible porosity or oil staining in hand sample. Minor occurrences of fluorescence under ultraviolet light in fractures at 5723.2'.

5722.3' – 5721.1' = Facies #2. Burrowed calcareous mudstone. Grayish black and olive black. Scattered very coarse sand-sized crinoid fragments and brachiopods (1-2 cm) scattered throughout interval. Uncommon bioturbation. No fractures were observed in this interval. No visible porosity or oil staining (or fluorescence under ultraviolet light) in hand sample.

TS 5722.0-5722.25'

5721.1' – 5717.3' = Facies #3. Bioturbated wackestone. Olive gray, olive black, and medium dark gray. Very coarse sand-sized crinoid fragments are scattered

throughout interval. Uncommon to moderate bioturbation. Moderate degree of fracturing. Porosity observed in partially filled fractures. Oil staining and fluorescence under ultraviolet light is observed in fractures at 5718.4'-5719.4'.

TS 5718.55'

TS 5717.5'

5717.3' – 5714.0' = Facies #2 and #3. Burrowed calcareous mudstones and bioturbated wackestones. Olive gray, light olive gray, olive black, grayish black, and medium dark gray. Sparse bioturbation. No fractures observed in this interval. No visible skeletal fragments of oil staining (or fluorescence under ultraviolet light) observed.

5714.0' – 5703.6' = Facies #5 and #4. Traction current skeletal packstones and grainstones and massive bedded peloidal grainstones. Dark gray, medium gray, brownish black, light olive gray and dusky yellowish brown. Some silty and sandy grainstones are present. Bioturbation absent. Low to moderate degree of fracturing observed throughout this interval. Fractures are vertical to sub-vertical (~0.3' long) and are partially filled with calcite cement. Heavy oil staining and fluorescence under ultraviolet light observed from 5710.6'-5706.3'. No visible skeletal fragments in hand sample.

TS 5712.55'

TS 5709.65'

TS 5707.5'

TS 5705.3'

TS 5704.45

5703.6' – 5696.1' = Facies #3 and #2. Bioturbated wackestones and burrowed calcareous mudstones. Olive gray, light olive gray, olive black, grayish black, black, and medium dark gray. Brachiopod fragment (1 cm) visible in hand sample. Interval transitions from dark mudstone facies at the base to interbedded dark and light mudstone and wackestone facies towards the top. Sparse to uncommon bioturbation. Some fractures observed at the top of the interval. Porosity visible in partially filled fractures. No oil staining observed. Very faint fluorescence under ultraviolet light in bioturbated wackestone facies.

TS 5701.65'

TS 5701.3-5701.55'

TS 5697.5'

5696.1' – 5673.8' = Facies #5 and #4. Interbedded skeletal and peloidal packstones and grainstones. Dark gray, medium gray, medium dark gray, brownish black, light olive gray, light gray, and dusky yellowish brown. Silty and sandy grainstones

present. Very fine pyrite granules (2-4 mm) and coarse sand-sized pyrite grains observed from 5686'-5682'. Cross-bedding and truncation surfaces occur throughout interval. Bioturbation is absent throughout most of the interval with some zones of sparse and uncommon bioturbation. The entire interval shows at least some degree of fracturing with some zones showing a high to very high degree of fracturing. Heaviest oil staining and fluorescence under ultraviolet light is observed at the base of the interval, with faint fluorescence under ultraviolet light occurring throughout the rest of the interval. No visible skeletal fragments in hand sample.

TS 5691.1'
TS 5688.85'
TS 5687.5'
TS 5683.4'
TS 5678.35'
TS 5676.7'

5673.8' – 5652.8' = Facies #3, #4, and #5. Bioturbated wackestones with intermittent massive bedded peloidal wackestones and traction current skeletal grainstones. Dark gray, medium gray, medium dark gray, brownish black, light olive gray, light gray, and dusky yellowish brown. Mostly moderately to commonly bioturbated wackestones with wispy laminations and very coarse sand-sized pyrite crystals. Moderately bioturbated skeletal grainstone and moderately to uncommonly bioturbated peloidal wackestones are interbedded with bioturbated wackestones. Entire interval displays some degree of fracturing with fractures being most abundant from 5666'-5660'. No visible skeletal fragments in hand sample. Faint oil staining (and fluorescence under ultraviolet light) is observed throughout the interval.

TS 5673.25
TS 5669.7'
TS 5666.2'
TS 5663.75'
TS 5657.1'
TS 5654.8'

5652.8' – 5635.0' = Facies #5 and #4. Traction current skeletal grainstones interbedded with massive bedded peloidal packstones and grainstones. Light olive gray, moderate yellowish brown, dusky yellowish brown, medium gray, medium dark gray, and light gray. Very coarse sand-sized pyrite crystals observed in the lower half of the interval. Intervals of moderately bioturbated packstones occur throughout. Overall low degree of fracturing. No skeletal fragments visible in hand sample. Faint oil staining and fluorescence under ultraviolet light is observed in the upper portion of the interval.

TS 5648.65'
TS 5646.65'
TS 5641.8'
TS 5638.5'
TS 5635.9'

5635.0' – 5630.0' = Facies #3. Bioturbated mudstone to wackestone. Olive gray, dusky yellowish brown, grayish black, and dark yellowish brown. Uncommon to moderate bioturbation. Moderate degree of fracturing. Lower half of the interval is thinly bedded and darker in color than upper half. Medium sand-sized pyrite crystals observed near the top of the interval. Oil staining and fluorescence under ultraviolet light observed at 5634.5'.

TS 5634.65'
TS 5630.75'

5630.0' – 5606.2' = Facies #5 and #4. Traction current skeletal packstones and grainstones interbedded with massive bedded peloidal grainstones. Light olive gray, moderate yellowish brown, dusky yellowish brown, medium gray, medium dark gray, olive gray, dark yellowish orange, and light gray. Sandy and silty grainstones. Cross bedding and traction current features observed throughout interval. Bioturbation is absent throughout most of the interval with some sparsely bioturbated zones present. Entire interval is heavily fractured (0.2' to 0.6' in length). Heavy oil staining and fluorescence under ultraviolet light is observed in traction current skeletal grainstone facies and partially filled vertical fractures. No visible skeletal fragments in hand sample.

TS 5628.5'
TS 5624.2'
TS 5616.95'
TS 5614.5'
TS 5610.75'
TS 5606.4'

5606.2' – 5592.7' = Facies #3, #4, and #5. Bioturbated wackestones and packstones with interbedded traction current skeletal grainstones and massive bedded peloidal packstone facies. Dark gray, medium gray, medium dark gray, brownish black, light olive gray, light gray, and dusky yellowish brown. Moderate bioturbation observed in bioturbated wackestones and packstones with bioturbation absent in skeletal grainstone and peloidal packstone facies. Highest degree of fracturing observed in grainier intervals. Oil staining and fluorescence under ultraviolet light occurs in skeletal grainstone interval. No visible skeletal fragments in hand sample.

TS 5505.5'
TS 5599.4'
TS 5596.8'
TS 5592.7'

5592.7' – 5564.20' = Facies #2 and #3. Interbedded burrowed calcareous mudstones and bioturbated wackestones. Olive black, olive gray, brownish black, and grayish black. Burrows, brachiopod fragments (1-2 cm), and coarse to very coarse sand-sized pyrite crystals are scattered throughout the entire interval. Skeletal debris beds observed at 5591.8', 5590.1', and 5581.7'. Overall low degree of fracturing, but, where present, fractures appear to be completely or partially filled. Sparse to moderate bioturbation. No oil staining or fluorescence under ultraviolet light observed in hand sample.

TS 5584.8'
TS 5581.7'
TS 5581.55-5581.80'
TS 5574.35'
TS 5569.65-5569.95'

5564.20' – 5537.0' = Facies #5 and #4. Traction current skeletal grainstones interbedded with massive bedded peloidal grainstones. Light olive gray, moderate yellowish brown, dusky yellowish brown, medium gray, medium dark gray, olive gray, dark yellowish orange, and light gray. Silty grainstones present. Wispy laminations and cross-bedding present throughout. Bioturbation is absent throughout most of the interval with occasional zones having sparse or uncommon bioturbation. Fractures present throughout entire interval.

TS 5559.5'
TS 5556.05'
TS 5546.55'
TS 5546.1'
TS 5544.65'

5537.0' – 5523.0' = Facies #3. Bioturbated wackestones and packstones. Olive gray, dusky yellowish brown, and grayish black. Thinly bedded bioturbated wackestones and packstones with wispy laminations. Some silty wackestones and packstones present. Bioturbation ranges from absent to moderate. Abundant partially filled fractures are present throughout the entire interval. Faint oil staining and fluorescence occurs throughout entire interval. No skeletal fragments visible in core.

TS 5536.6'

TS 5536.0'
TS 5532.1'
TS 5527.8'
TS 5526.05'
TS 5524.65-5524.90'

5523.0' – 5517.7' = Facies #4 and #5. Interbedded peloidal and skeletal grainstones.

Light olive gray, moderate yellowish brown, dusky yellowish brown, medium gray, medium dark gray, olive gray, dark yellowish orange, and light gray. Bioturbation absent to sparse. Sparse, but large, fractures observed throughout interval (~0.5' long). Cross-bedding and wispy laminations observed in skeletal grainstones. Heavy oil staining and fluorescence under ultraviolet light present in skeletal grainstone facies. No skeletal fragments observed in hand sample.

TS 5520.1'

5517.7' – 5510.6' = Facies #3 and #2. Bioturbated wackestones and burrowed

calcareous mudstones. Olive black, brownish black, and grayish black. Scattered coarse to very coarse sand-sized crinoid fragments. Brachiopod fragments (1-2 cm) concentrated in mudstone facies. Glauconite grains observed at the base of the interval. Sparse to moderate bioturbation. Very few fractures observed throughout interval. No oil staining or fluorescence under ultraviolet light observed in hand sample.

TS 5517.75'
TS 5516.1'
TS 5512.00-5512.25'

5510.6' – 5496.2' = Facies #5 and #4. Interbedded traction current skeletal and massive bedded peloidal grainstones.

Moderate yellowish brown, yellowish gray, very light gray, light gray, light olive gray, brownish black, and dark yellowish orange. Bioturbation generally absent, but some thin intervals of uncommon bioturbation are present. Cross-bedding and wispy laminations are observed in skeletal grainstones facies. Fractures are observed throughout the entire interval with the majority of the interval being heavily fractured. Oil staining is observed throughout the interval with the heaviest oil staining, and fluorescence, occurring at 5507'. The contact between the "Mississippian Limestone" and the overlying Pennsylvanian sediments occurs at 5496.2'.

TS 5509.1'
TS 5507.9'
TS 5506.1'
TS 5504.25'
TS 5501.65'

TS 5498.45'
TS 5496.7'
TS 5496.1' – Pennsylvanian
TS 5495.2' – Pennsylvanian
TS 5491.4' – Pennsylvanian

Core #2: Winney #1-18 SWD – Devon Energy

Payne County, OK

Cored Interval: 5401.95'-5115.0'

Examined Interval: 5125.0'-5313.0'

Top "Mississippian Limestone": 5123.4' (from core)

Formations: Woodford Shale, "Mississippian Limestone", and Pennsylvanian

5313' - 5312.2' = Facies #1. Glauconitic Sandstone. Dark gray and greenish black. Contact between Woodford Shale and "Mississippian Limestone" at 5313'. Abundant bioturbation. Glauconite appears to be concentrated in burrows. Very fine sand-sized glauconite grains. Interbedding of glauconitic sandstone with Facies #2 (burrowed calcareous mudstone) from 5313' to 5312.8'. Very fine sand-sized pyrite crystals grading into very coarse sand-sized crystals (~30%) from base to top of interval. Brachiopods (~0.5 cm in length) present along bedding plane at 5312.3'. No visible porosity or oil staining (or fluorescence under ultraviolet light) in hand sample.

TS 5312.75'-5312.95'

5312.2' – 5292.65' = Facies #2 and #3. Burrowed calcareous mudstones and bioturbated mudstones to packstones. Olive gray, light olive gray, olive black, and yellowish gray. Generally sparse to common bioturbation, but some intervals contain abundant bioturbation. Bioturbated wackestones and packstones interbedded with burrowed calcareous mudstone facies (approximately 0.15' thick) at 5308.7', 5307.6', 5303.75', 5301.3', 5300.55', 5298.25', 5297', and 5295.55'. Scattered, visible very coarse sand-sized crinoid fragments throughout interval (<5%). Medium sand-sized pyrite crystals present at 5305'. Sparse vertical to sub-vertical fractures ranging in length from 2.0' to 0.2' that are partially to completely cemented with calcite. Porosity within partially cemented vertical fractures. Fluorescence under ultraviolet light observed in bioturbated zones and vertical fractures from 5310'-5303'.

TS 5309.60'

TS 5305.35'

TS 5298.45'

5292.65' – 5292.4' = Facies #1. Glauconitic Sandstone. Dark gray and greenish black. Very fine sand sized glauconite grains decreasing in abundance upwards showing a gradational contact between this facies and the overlying facies. Sparse bioturbation. No fractures observed. No visible skeletal fragments, porosity, or oil staining (or fluorescence under ultraviolet light) in hand sample.

TS 5292.60'

5292.4' – 5269.1' = Facies #2 and #3. Burrowed calcareous mudstones interbedded with bioturbated mudstones to wackestones and packstones. Black, grayish black, olive black, olive gray, dusky yellowish brown, and moderate yellowish brown. Primarily moderately to abundantly bioturbated mudstones and wackestones interbedded with less frequent, thinner (approximately 1.0' thick) intervals of moderately burrowed calcareous mudstones at 5292', 5290.8', 5281', and 5280'. Interval contains scattered, visible brachiopod fragments (~10%) ranging from 1.5-2.0 cm in length. Occasional vertical fractures (average 0.2' long) and sparse sub-vertical calcite-filled ptigmatic fractures (average 0.3' long) present in bioturbated intervals. Fine sand-sized pyrite crystals around clasts at 5280.6'. Fracture porosity observed in partially filled fractures. No visible skeletal fragments or oil staining in hand sample. Some fluorescence in bioturbated intervals and vertical fractures.

TS 5289.55'
TS 5285.55'
TS 5282.80'
TS 5279.85'
TS 5274.60'
TS 5270.50'

5269.1' – 5262.3' = Facies #3, #4, and #5. Bioturbated wackestones interbedded with massive bedded peloidal and traction current skeletal packstones to grainstones. Olive gray, dusky yellowish brown, brownish black, dark yellowish brown, and moderate yellowish brown. Bioturbated (uncommon) wackestones interbedded with massively bedded silty to sandy packstones. Commonly bioturbated at the top of this interval with burrows approximately 4mm in diameter. Thin (<0.1' thick) intervals of Facies #1 present throughout. Marine hardgrounds. Abundant fractures. Sub-vertical fractures occur at the base of the interval whereas vertical, partially filled fractures (average 0.7' long and 1mm thick) occur in the grainier facies. Porosity observed in partially filled fractures. Skeletal fragments visible in hand sample. Fluorescence under ultraviolet light observed throughout interval, but concentrated in massive bedded packstone to grainstone facies and vertical, partially open fractures.

TS 5268.60'
TS 5263.90'
TS 5262.30'

5262.3' – 5261.65' = Facies #2. Burrowed calcareous mudstone. Black, grayish black, olive black, and brownish black. Thin-shelled brachiopod fragments (~2 cm long) present at the base of the interval. Mm-scale laminations and burrows exist throughout. Abundant fractures. Moderate bioturbation. No observed porosity or oil staining (or fluorescence under ultraviolet light) in hand sample.

5261.65' – 5257.5' = Facies #3 and #4. Bioturbated wackestones to packstones and massive bedded peloidal packstones to grainstones. Olive gray, dusky yellowish brown, and dark yellowish brown. Common to abundant bioturbation in wackestones and packstones with some massive bedded packstones and grainstones present. Abundant, partially filled vertical fractures (approximately 4 cm long). No skeletal fragments visible in hand sample. Oil staining from 5259'-5259.2' and 5265.3'-5265.6'. Fluorescence under ultraviolet light observed within vertical fractures and bioturbated zones.

TS 5260.10'

TS 5258.50'

5257.5' – 5248.3' = Facies #2 and #3. Burrowed and bioturbated mudstones to wackestones. Olive black, olive gray, brownish black, and grayish black. Uncommonly bioturbated mudstones and wackestones. Few (<5%) scattered crinoid fragments (~1mm) present at the base of the interval. Sparse ptymatic fractures (ranging from 0.2'-0.6' long) observed throughout the interval. No visible porosity or oil staining (or fluorescence under ultraviolet light) observed in hand sample.

TS 5253.80'-5254.00'

TS 5249.75'

5248.3' – 5208.95' = Facies #4 and #5. Massive bedded peloidal packstones to grainstones interbedded with traction current skeletal grainstones. Dark gray, medium gray, brownish black, light olive gray and dark yellowish brown. Dominantly silty and sandy traction current grainstones showing cross bedding. Intervals of silty and sandy massive bedded packstones to grainstones occur throughout this interval. Abundant, partially filled vertical fractures occur throughout this interval (average 0.5' long). Moderately bioturbated and/or vertically burrowed hardgrounds present at 5236.4', 5233.9', 5233.1', 5231.15', 5225.1', 5222.8', 5221.85', 5219.5', and 5217.4'. No visible skeletal fragments in hand sample. Porosity observed in partially filled vertical fractures. Oil staining observed throughout interval. Fluorescence under ultraviolet light observed mostly in Facies #5 and vertical fractures, but also seen in bioturbated and/or burrowed hardgrounds throughout interval.

TS 5212.55'-5215.75'

TS 5243.00'

TS 5239.30'

TS 5238.65'

TS 5234.60'

TS 5233.90'

TS 5232.90'
TS 5229.75'
TS 5229.35'
TS 5225.50'
TS 5222.85'
TS 5219.75'

5208.95' – 5208.1' = Facies #2. Burrowed calcareous mudstone. Black, grayish black, and brownish black. Abundant mm-scale laminations and sparse burrows. Sparse fractures. No visible skeletal fragments, porosity, or oil staining (or fluorescence under ultraviolet light) in hand sample.

5208.1' – 5204.8' = Facies #4 and #5. Massive bedded peloidal packstones and grainstones interbedded with traction current skeletal grainstones. Dark gray, dark yellowish brown, dusky yellowish brown, medium gray, and olive black. Cross bedding observed in traction current grainstone facies. Occasional (<5%) scattered crinoid fragments (~2 mm) observed throughout interval. Vertical to sub-vertical open and partially filled fractures are common. Bioturbation absent. Porosity observed in open and partially filled fractures. Oil staining (and fluorescence under ultraviolet light) observed at the base of the interval in traction current grainstone facies.

TS 5207.50'
TS 5205.30'

5204.8' – 5202.8' = Facies #2 and #3. Burrowed calcareous mudstones and bioturbated mudstones to wackestones. Black, grayish black, brownish black, olive gray, and olive black. Mm-scale laminations and burrows exist throughout this interval. Brachiopod fragments at 5203.8'. Mm-scale laminated and burrowed mudstones grade into commonly bioturbated mudstones and wackestones. Sparse fractures. No visible porosity or oil staining (or fluorescence under ultraviolet light) in hand sample.

5202.8' – 5167.6' = Facies #4, #5, and #2. Traction current skeletal grainstones interbedded with massive bedded peloidal packstones and grainstones and occasional mm-scale laminated mudstones. Dark gray, dark yellowish brown, dusky yellowish brown, medium gray, and olive black. Dominantly sandy and silty cross-bedded and massive bedded packstones and grainstones. Mm-scale laminated and moderately burrowed mudstones (approximately .01' thick) occur at 5176.75', 5174.85', and 5171.8'. Abundant filled and partially filled vertical fractures throughout ranging from 0.2'-2.0' long. Porosity observed within the partially filled vertical fractures. No skeletal fragments observed in hand sample. Oil staining and abundant fluorescence observed throughout interval and concentrated in Facies #5 and vertical fractures.

TS 5199.80'
TS 5198.75'
TS 5190.10'
TS 5187.90'
TS 5186.65'
TS 5184.15'
TS 5182.25'
TS 5179.80'
TS 5179.15'
TS 5177.95'
TS 5177.90'
TS 5176.35'
TS 5170.15'

5167.6' – 5165.0' = Facies #2. Burrowed calcareous mudstone. Black, grayish black, brownish black, and olive black. Mm-scale laminated and sparsely burrowed mudstone containing thin-shelled brachiopods (<5%) approximately 1 cm long. No visible porosity or oil staining (or fluorescence under ultraviolet light) in hand sample.

TS 5166.35'-5166.55'

5165.0' – 5163.4' = Facies #3 and #5. Bioturbated mudstones to wackestones and traction current skeletal grainstones. Olive gray, brownish black, and olive black. Uncommonly to moderately bioturbated mudstones and wackestones present in between cross-bedded grainstones. Moderate abundance of vertical, partially filled fractures. Minor fluorescence under ultraviolet light in vertical fractures. No visible skeletal fragments in hand sample.

5163.4' – 5152.2' = Facies #2/3. Burrowed calcareous mudstone to wackestone and bioturbated mudstone to wackestone. Black, grayish black, brownish black, olive black, and olive gray. Mm-scale laminated mudstone to wackestone containing brachiopods (~10%) that range in size from 1-3 cm. Abundant sub-vertical filled fractures (average 0.1' long) from 5158'-5157'. Fractures are otherwise sparse. Moderate to common bioturbation. No visible porosity or oil staining (or fluorescence under ultraviolet light) in hand sample.

TS 5161.70'
TS 5159.85'
TS 5158.70'-5158.90'
TS 5157.25'
TS 5155.65'
TS 5153.80'-5154.00'

TS 5152.90'

5152.2' – 5146.3' = Facies #4 and #5. Massive bedded packstones with some traction current grainstones. Olive gray with some olive black. Silty packstones with occasional mm-scale laminated mudstone facies (approximately 0.1' thick) occurring throughout. Fractures are common. Partially filled ptigmatic and vertical fractures (0.5' long) at 5149'. Porosity observed in partially filled fractures. Bioturbation absent. No visible skeletal fragments or oil staining in hand sample. Fluorescence under ultraviolet light in ptigmatic and vertical fractures.

TS 5149.80'

TS 5148.40'

5146.3' – 5145.4' = Facies #5 and #2. Skeletal grainstones interbedded with laminated mudstones. Olive black and olive gray. Abundance of laminated mudstones interbedded within traction current grainstones. Cross bedding observed in traction current grainstone facies (Facies #5). One filled ptigmatic fracture .03' long. Bioturbation absent. No skeletal fragments or porosity visible in hand sample. Oil staining (and fluorescence under ultraviolet light) observed in hand sample.

TS 5145.90'

5145.4' – 5143.5' = Facies #2. Calcareous mudstone. Black, grayish black, brownish black, and olive black. Mm-scale laminated mudstone containing thin-shelled brachiopods (~5%) approximately 1 cm long. Fractures are sparse. Bioturbation absent. No visible porosity or oil staining (or fluorescence under ultraviolet light) in hand sample.

TS 5144.75'-5145.00'

TS 5144.00'-5144.20'

5143.5' – 5133.85' = Facies #4 and #5. Massive bedded peloidal packstones and grainstones interbedded with traction current skeletal grainstones. Dark gray, dark yellowish brown, dusky yellowish brown, medium gray, and olive black. Low angle cross bedding observed in the traction current grainstone facies. Scattered mud wisps throughout interval. Sparsely to moderately fractured consisting of vertical, partially filled fractures (generally about 1.0' long) and calcite filled fractures. Bioturbation absent. Porosity observed in partially filled vertical fractures. No skeletal fragments visible in hand sample. Facies #5 and vertical fractures are highly fluorescent under ultraviolet light.

TS 5140.25'

TS 5139.15'
TS 5138.35'
TS 5136.60'
TS 5134.25'

5133.85' – 5133.45' = Facies #2. Burrowed calcareous mudstone. Black, grayish black, brownish black, and olive black. Mm-scale laminated and burrowed mudstone. Sparsely fractured. Sparse bioturbation. No visible skeletal fragments, porosity, or oil staining (or fluorescence under ultraviolet light) in hand sample.

TS 5133.60'-5133.80'

5133.45' -5124.7' = Facies #4 and #5. Massive bedded peloidal packstones and grainstones interbedded with traction current skeletal grainstones. Light olive gray, moderate yellowish brown, medium gray, and medium dark gray. Dominantly composed of low- angle, cross-bedded grainstone facies. Scattered mud wisps throughout interval. Moderate to abundant vertical, partially filled fractures (generally about 1.0' long) and calcite filled fractures. Porosity observed in partially filled vertical fractures. Bioturbation absent. No skeletal fragments visible in hand sample. Heavy oil staining and fluorescence under ultraviolet light throughout interval.

TS 5132.75'
TS 5132.25'
TS 5131.75'
TS 5129.70'
TS 5129.30'
TS 5127.35'
TS 5126.80'
TS 5126.40'

5124.7' – 5123.4' = Facies #5. Chert-rich grainstone. Moderate yellowish brown, yellowish gray, very light gray, light gray, brownish black, dark yellowish orange, and grayish yellow green. Cherty grainstone showing exposure features and some iron-rich areas around fractures. Abundant fractures. Bioturbation absent. No visible skeletal fragments or porosity in hand sample. Oil staining and fluorescence under ultraviolet light observed throughout interval. Contact with the "Mississippian Limestone" and overlying Pennsylvanian sediments at 5123.4'.

TS 5124.55'
TS 5124.10'
TS 5123.70'
TS 5123.20' – Pennsylvanian

Core #3: Elinore #1-18 SWD – Devon Energy

Payne County, OK

Cored Interval: 4481.7' – 4324.0'

Examined Interval: 4480.5' – 4338.5'

Top “Mississippian Limestone”: 4338.5' (from core)

Formations: Woodford Shale, “Mississippian Limestone”, and Pennsylvanian

4481.7' – 4481.0' = Facies #1. Glauconitic sandstone. Dark gray and greenish black. Contact between Woodford Shale and “Mississippian Limestone” at 4481.7'. Abundant bioturbation. Coarse to very coarse sand-sized pyrite crystals. Dark yellowish orange nodules present at the base of the interval (~1 inch in diameter). No visible porosity, fractures, or oil staining (or fluorescence under ultraviolet light) observed in hand sample.

TS 4481.5'

4481.0' – 4479.5' = Facies #3. Bioturbated wackestone. Olive gray and olive black. Abundant bioturbation. Few scattered brachiopod fragments (< 1 cm) and coarse sand-sized crinoid fragments. Gradual transition upwards into the overlying glauconitic sandstone facies. No fractures, porosity, or oil staining (or fluorescence under ultraviolet light) observed in hand sample.

TS 4480.5'

4479.5' – 4479.1' = Facies #1. Glauconitic sandstone. Dark gray and greenish black. Abundant bioturbation. Sand-sized glauconite grains concentrated within cm-scale burrows. Fine to very coarse sand-sized pyrite crystals present. Scattered, grayish black chert nodules throughout the interval (~1 inch in diameter). No fractures, porosity, or oil staining (or fluorescence under ultraviolet light) observed in hand sample.

TS 4479.4'

4479.1' – 4477.7' = Facies #2. Burrowed calcareous mudstone. Grayish black, greenish black, olive black, olive gray, and moderate yellowish brown. Abundant bioturbation and mm-scale burrows. Scattered very coarse sand-sized crinoid fragments throughout interval. Moderate yellowish brown nodule (~2 cm) and bed at 4478.2' (~1 cm thick). No fractures or oil staining (or fluorescence under ultraviolet light) observed in hand sample.

4477.7' – 4470.0' = Facies #3 and #2. Bioturbated wackestones with some burrowed calcareous mudstones. Olive gray, light olive gray, grayish black, and olive black. Long (~3.5' long) vertical fracture mostly filled with calcite cement showing multiple generations of fractures and terminating into wispy laminated burrowed calcareous mudstone facies at 4473.9'. Bioturbation decreases from base to top of interval.

Brachiopod fragments (1-2 cm) visible at 4472.7'. Moderate oil staining and fluorescence under ultraviolet light observed in bioturbated wackestones, with more intense fluorescence in fracture(s).

TS 4476.4'

TS 4471.3'

TS 4470.5'

4470.0' – 4466.3' = Facies #2. Burrowed calcareous mudstone. Brownish black and grayish black. Common bioturbation. Thin shelled brachiopods (1-5 cm) scattered throughout interval. Coral (3 cm) at 4469.9'. Mm-scale burrows and laminations occur throughout. Burrow size increases upwards throughout interval as this facies gradually transitions into the overlying facies. No porosity or oil staining observed in hand sample, however very faint fluorescence under ultraviolet light occurs.

4466.3' – 4448.5' = Facies #3 and #2. Bioturbated wackestones with some burrowed calcareous mudstones. Olive gray, brownish black, grayish black, and olive black. Wackestones with coarse to very coarse sand-sized crinoid fragments scattered throughout. Common bioturbation. Vertical, partially filled fractures (~0.6' long) present. Thin bedding and wispy laminations occur at the top of the interval as it transitions relatively sharply into the overlying facies. Faint fluorescence under ultraviolet light throughout interval with more intense fluorescence in a fracture at 4458.4'. No visible porosity observed in hand sample.

TS 4466.85'

TS 4459.0'

4448.5' – 4404.0' = Facies #5, #4 and #2. Traction current skeletal grainstones with intermittent intervals of massive bedded peloidal grainstones and some burrowed calcareous mudstones. Olive gray, dark yellowish brown, dusky yellowish brown, moderate yellowish brown, light olive gray, medium gray, and olive black. Bioturbation absent throughout most of the interval with some zones of sparse or uncommon bioturbation. Scattered mud whisps throughout. Overall high degree of fracturing characterized by fracture swarms and partially filled vertical to sub-vertical fractures (range in length from 0.2' to 1.0'). Interval alternates between thick-bedded and thin bedded (4436.0'-4434.0', 4426.0'-4425.0', 4418.0'-4417.0', and 4414.5'-4413.7') zones. Thin intervals of burrowed calcareous mudstone facies occur from 4444.2'-4444.4' and 4433.5'-4433.6'. Siliceous grainstones present at the top of the interval. Oil staining, and fluorescence under ultraviolet light) observed throughout the interval in traction current skeletal grainstone facies. No oil staining, or fluorescence under ultraviolet light, observed in peloidal grainstones of burrowed calcareous mudstones. Porosity visible in partially filled vertical fractures.

TS 4446.55'

TS 4441.24'
TS 4438.75'
TS 4429.1'
TS 4426.2'
TS 4410.55
TS 4407.1'
TS 4406.65'

4404.0' – 4403.5' = Facies #2 and #3. Burrowed mudstones and bioturbated wackestones.

Olive gray and olive black. Uncommon bioturbation. Thin bedded, interbedded bioturbated mudstones and wackestones. Fairly high degree of fracturing. No skeletal fragments, porosity, or oil staining (or fluorescence under ultraviolet light) visible in hand sample.

TS 4403.0'

4403.5' – 4393.75' = Facies #5 and #4. Interbedded traction current skeletal and massive

bedded peloidal grainstones. Olive gray, dark yellowish brown, dusky yellowish brown, moderate yellowish brown, light olive gray, medium gray, and olive black. Bioturbation absent throughout most of the interval with one zone of uncommon bioturbation from 4400.0'-4401.0'. Fairly low degree of fracturing observed. Large, mostly filled vertical fracture at 4402'. Cross-bedding and truncation surfaces are observed throughout this interval. Oil staining and fluorescence under ultraviolet light is observed in the traction current skeletal grainstone facies. No skeletal fragments observed in hand sample. Minor amounts of porosity visible within partially filled vertical fractures.

TS 4398.8'
TS 4395.0'

4393.75' – 4390.0' = Facies #2 and #3. Burrowed mudstones and bioturbated wackestones.

Olive gray and olive black. Uncommon to moderate bioturbation. Low degree of fracturing. Mm-scale laminations present at the top of the interval. No skeletal fragments, porosity, or oil staining (or fluorescence under ultraviolet light) visible in hand sample.

TS 4393.5'

4390.0' – 4371.1' = Facies #5 and #4. Interbedded traction current skeletal grainstones and

massive bedded peloidal grainstones and packstones. Olive gray, dark yellowish brown, dusky yellowish brown, moderate yellowish brown, light olive gray, medium gray, and olive black. Cross-bedding observed in skeletal grainstone facies. Bioturbation absent with the exception of one thin (0.6' thick) interval of bioturbated wackestone facies at 4386.5' and large (cm-scale) burrows at 4377.5'. Varying degrees of fracturing occurs throughout this interval, with some zones being heavily fractured. Significant oil staining

and fluorescence observed in traction current grainstone facies, burrows, and fractures. Visible porosity within partially filled vertical fractures. No visible skeletal grains observed in hand sample.

TS 4384.7'

TS 4380.95'

TS 4376.5'

4371.1' – 4362.5' = Facies #2 and #3. Burrowed calcareous mudstones and bioturbated wackestones. Olive gray, olive black, and brownish back. Sparse to moderate bioturbation with abundance decreasing upward. Wispy laminations and mm-scale burrows observed throughout. Brachiopod fragments (1-2 cm) visible at the base of the interval. Fractures observed in this interval appear to be almost completely filled. No oil staining, or fluorescence under ultraviolet light, observed in hand sample.

4362.5' – 4338.5' = Facies #4 and #5. Interbedded traction current skeletal grainstones and massive bedded grainstones. Olive gray, dark yellowish brown, dusky yellowish brown, moderate yellowish brown, light olive gray, medium gray, and olive black. Abundance of silty and sandy grainstones. Bioturbation absent. Generally thick bedded, but thin bedded intervals occur from 4348.5'-4348.0', 4347.5'-4345.5', and 4343.5'-4345.0'. Abundant vertical fractures (average 0.5' long) observed in this interval with general trends of 1) increased fractures in traction current grainstone facies and 2) an overall increase in fracture density from base to top. Oil staining and fluorescence under ultraviolet light observed in traction current skeletal grainstone facies and fractures. Visible porosity within partially filled vertical fractures.

TS 4362.35'

TS 4354.3'

TS 4353.9'

TS 4349.9'

TS 4345.5'


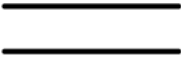
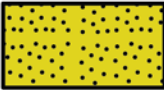

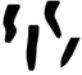



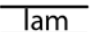


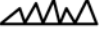







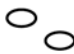
TS 4341.9'

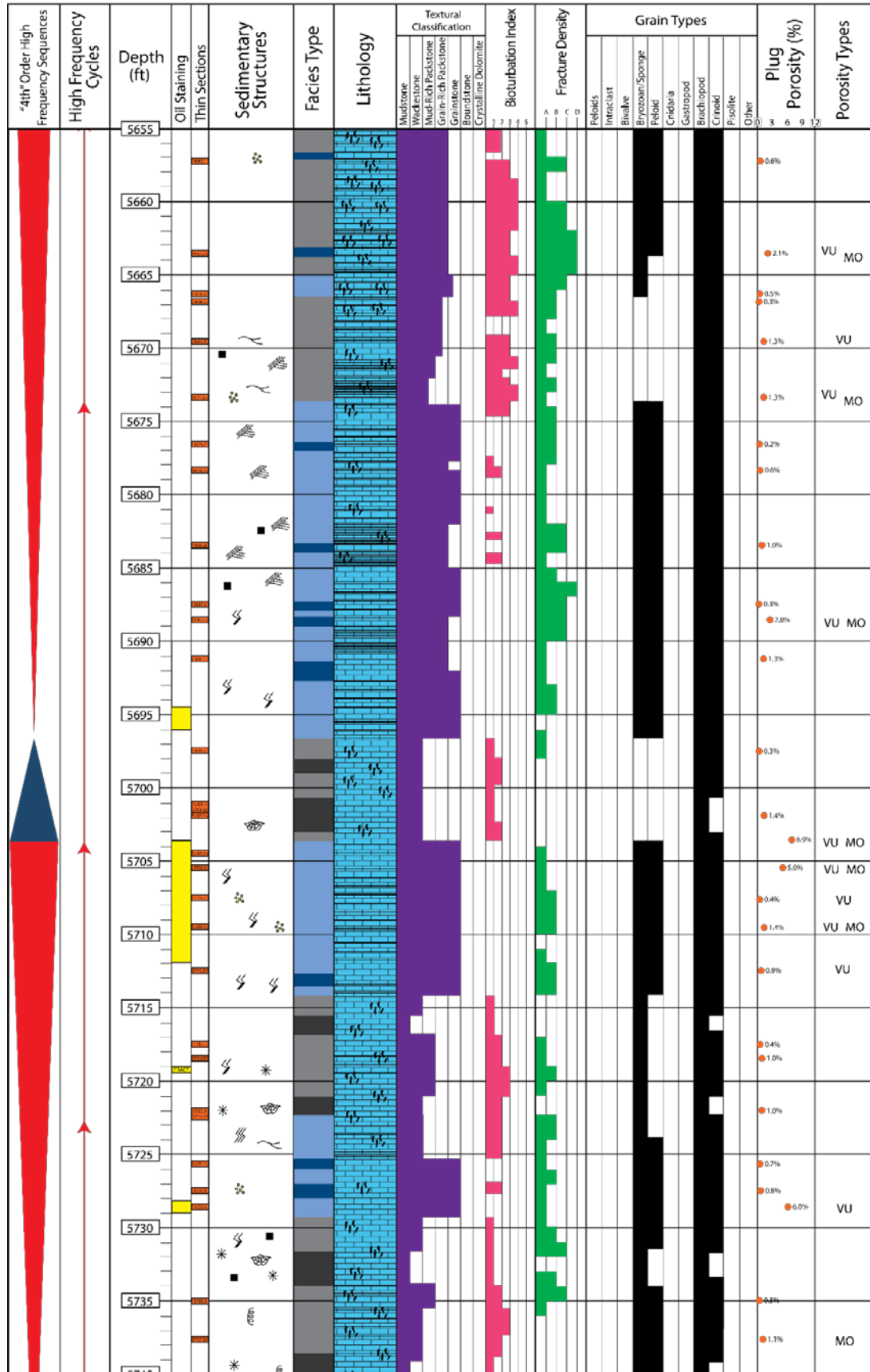
TS 4340.25'

TS 4338.5'

APPENDIX B

ILLUSTRATIVE CORE DESCRIPTIONS

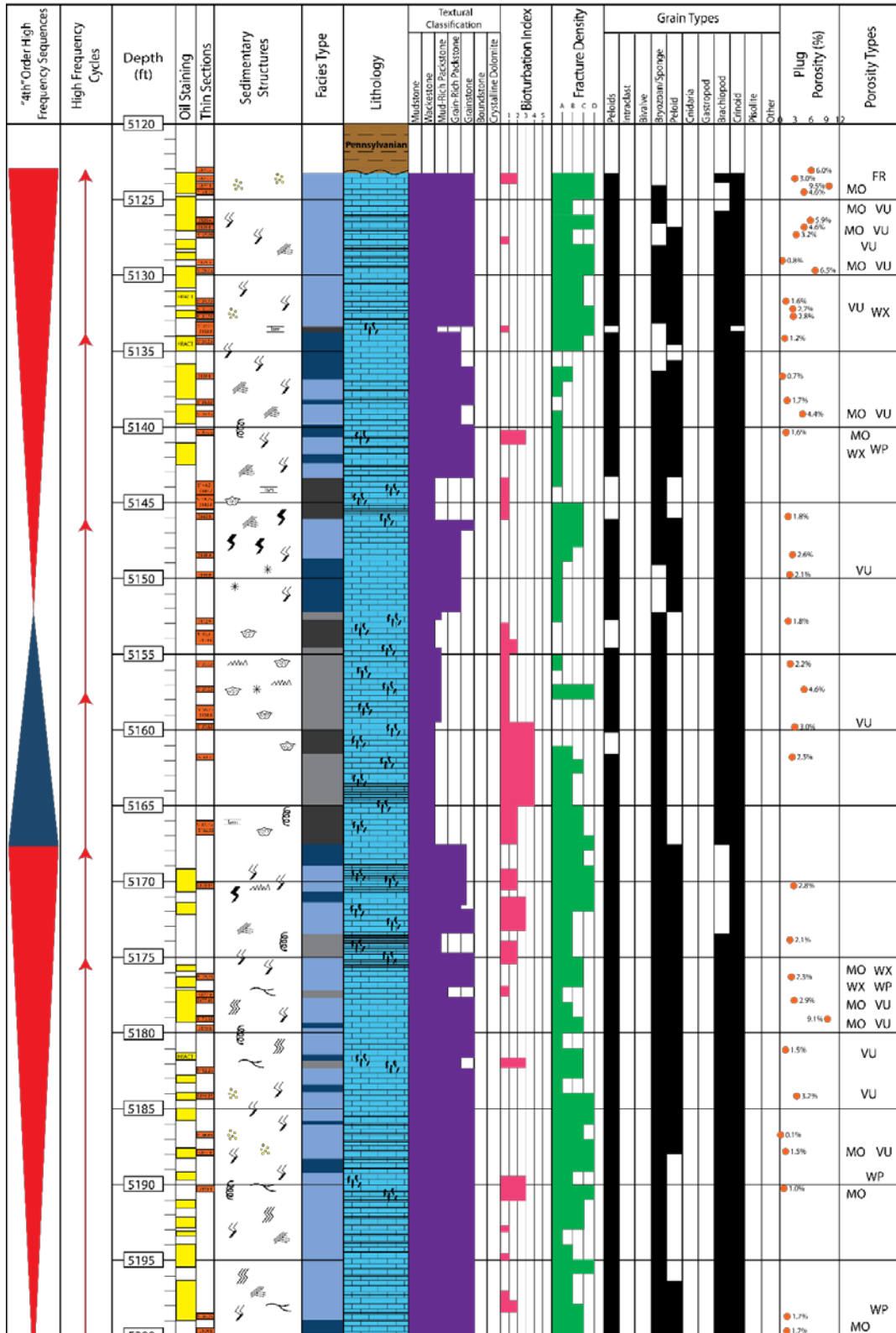
LITHOLOGIC SYMBOLS			
	Limestone		Thick Bedded
	Sandstone		Thin Bedded
			Bioturbated
GRAIN TYPES, SEDIMENTARY STRUCTURES, & DIAGENETIC FEATURES			
	Burrow		Cross-Bedded
	Brachiopod		Laminated
	Crinoid		Whispy Laminated
	Conodont		Filled Fracture
	Coral		Partially Filled Fracture
			Fracture Swarm
			Silica-Rich
			Glauconite
			Pyrite
			Intraclast
POROSITY TYPES			
WP - Intraparticle		MO - Moldic	
WX - Intracrystalline		VU - Vug	
BP - Interparticle		FR - Fracture	



Winney #1-8, Payne County, Oklahoma

Formation: Mississippian Limestone Depth Interval: 5120'-5315'

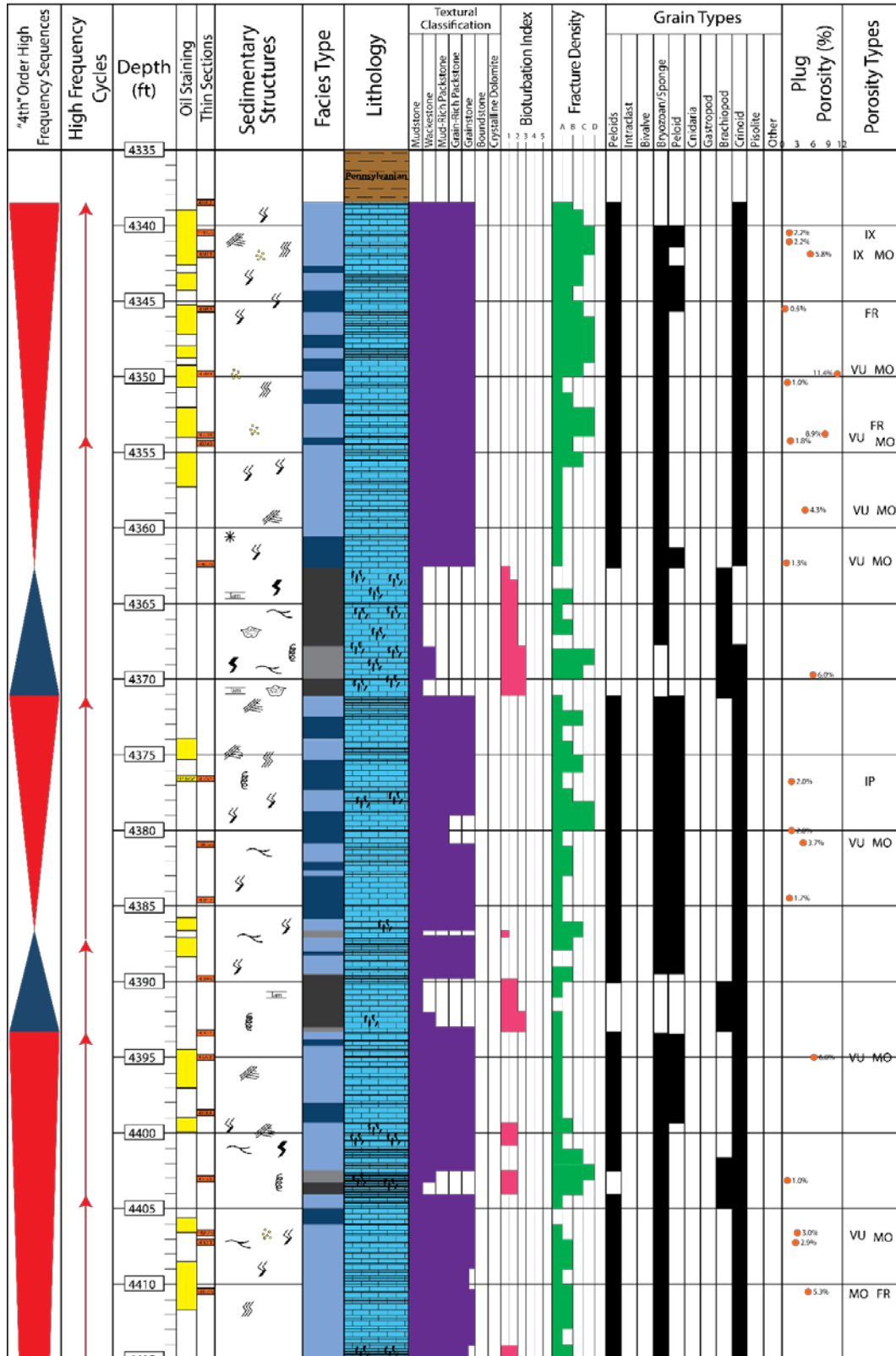
Core #2



Elinore #1-18, Payne County, Oklahoma

Formation: Mississippian Limestone Depth Interval: 4335'-4485'

Core #3



APPENDIX C

WHOLE CORE PHOTOGRAPHS

Core photographs are shown in white light and are labeled using the abbreviations outlined in the chart shown below. All cores are photographed in boxes that are 2 feet in length and are oriented with the shallowest depths at the top left of the image and the deepest depths at the bottom right. All scales are in feet with smaller dashes corresponding to tenths of a foot, not inches. To the left of each 2ft interval, facies types are displayed using a colored box. Facies colors correspond to idealized facies stacking pattern colors. The bottom and top of the “Mississippian Limestone” are marked using solid yellow lines. Fourth-order high frequency sequences are marked by a solid red line and 5th order high frequency cycles are marked by a dashed red line.

Core and Thin Section Image Labels							
Feature Key						Porosity Key	
BF	bone fragment	GB	grain bed	PY	pyrite	FR	fracture
BR	brachiopod	GST	gastropod	Q	quartz	IP	interparticle
BU	burrow	HCS	hummocky cross stratification	S	stylolite	IX	intercrystalline
BY	bryozoan	IC	intraclast	SK	undifferentiated skeletal fragments	MO	moldic
C	coral	L	lamination	SP	spicule	VU	vug
CH	chert	M	mud/mudstone	TS	truncation surface	WP	intraparticle
CON	conodont	ME	micritic envelope	XB	cross-bedding	WX	intracrystalline
CR	crinoid	MW	mud whisp				
D	dolomite	O	ostracode				
FG	firm ground	OIL	oil/dead oil				
FR	fracture	P	peloid				
G	glauconite	PH	phosphate				

Core #1

Adkisson #1-33 SWD

CORE 1

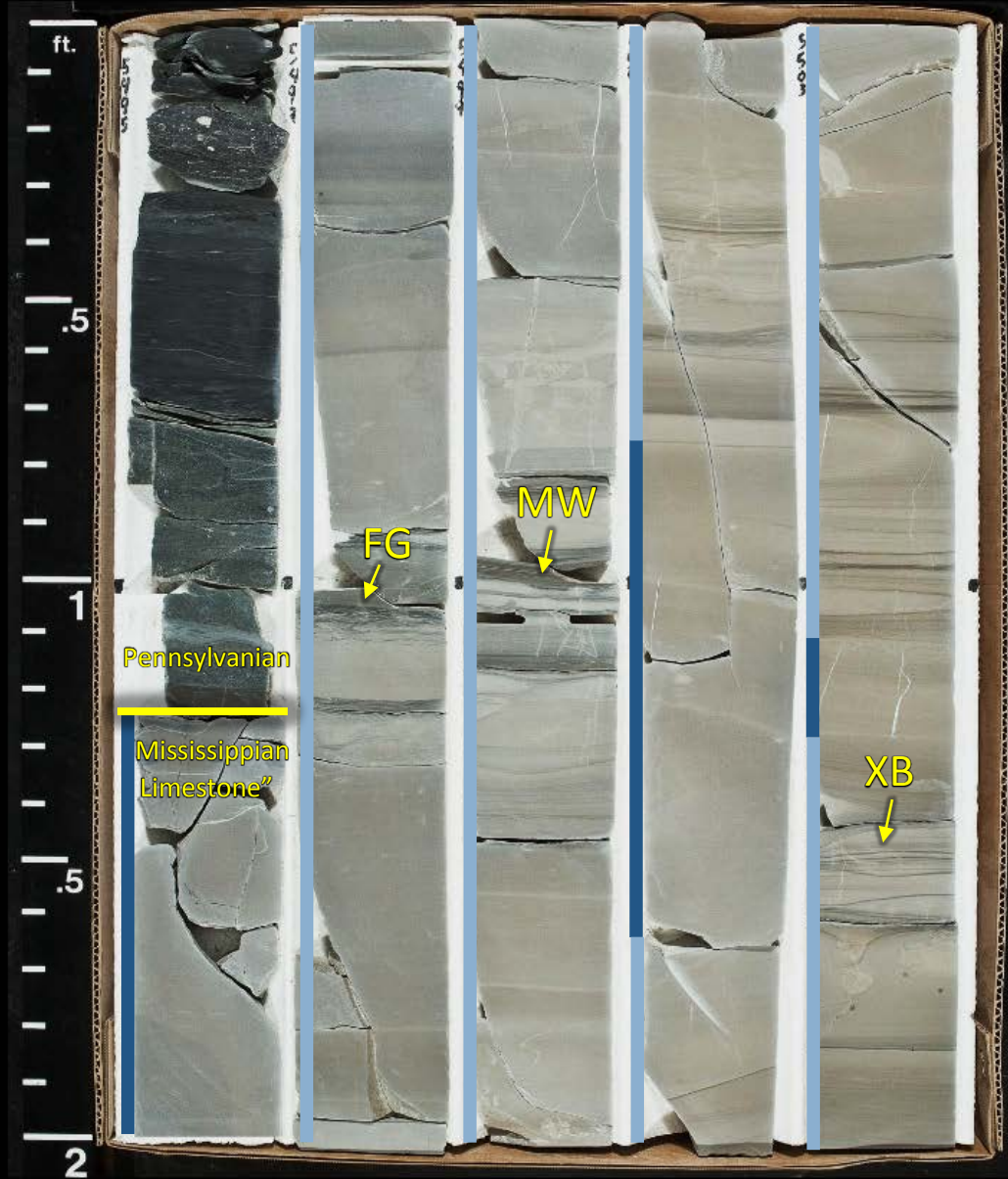
5495

5497

5499

5501

5503



CORE 1

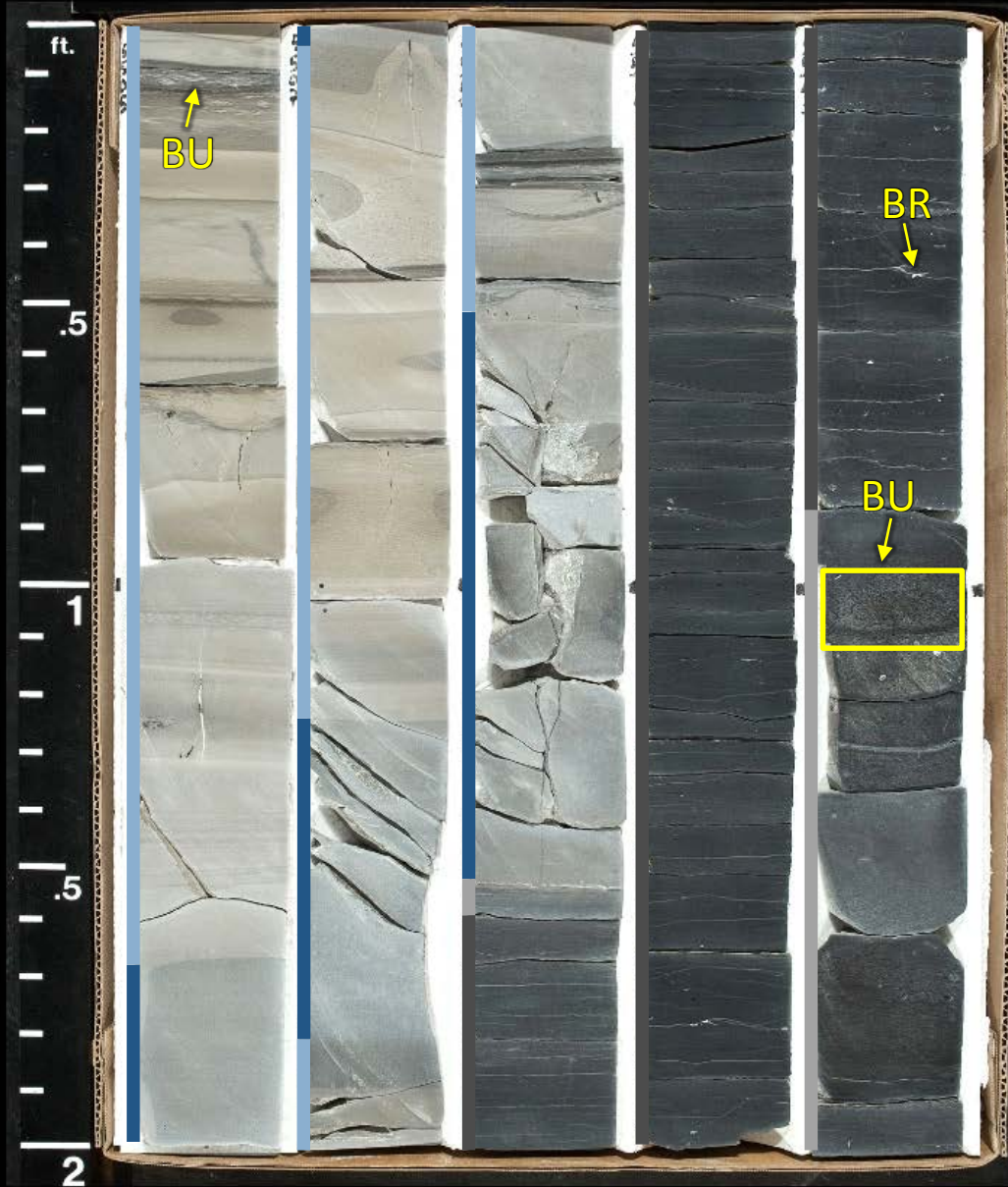
5505

5507

5509

5511

5513



CORE 1

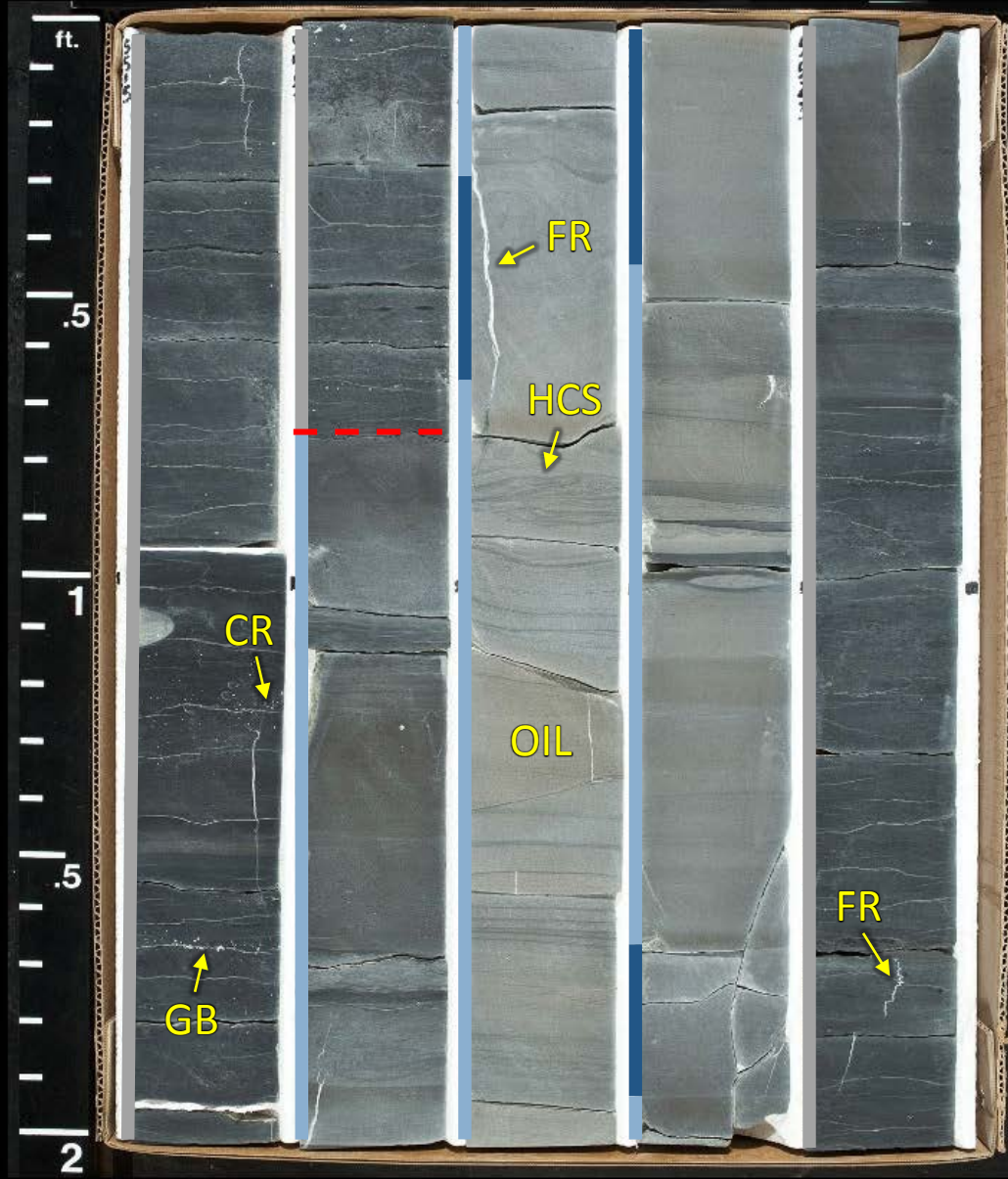
5515

5517

5519

5521

5523



CORE 1

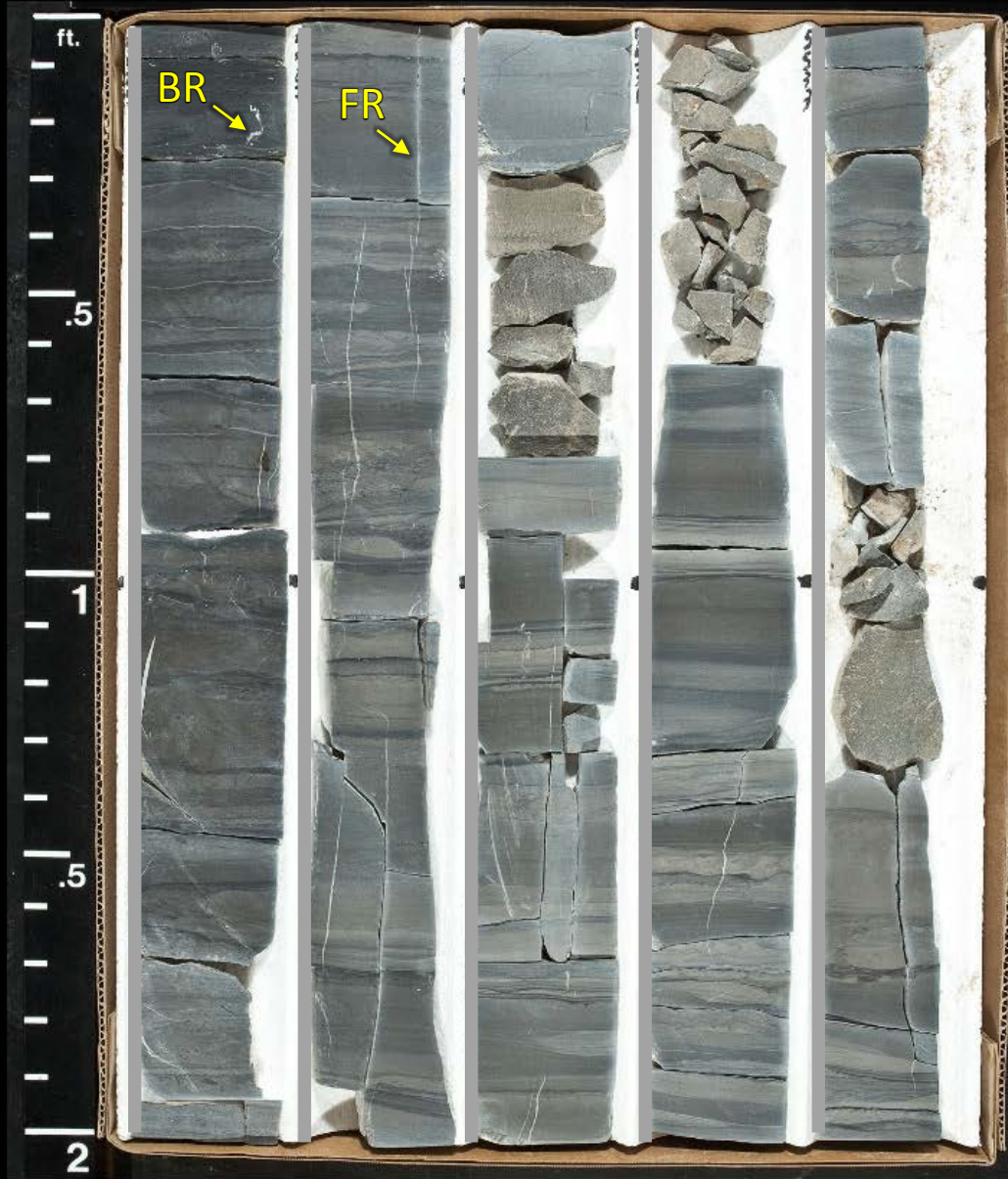
5525

5527

5529

5531

5533



CORE 1

5535

5537

5539

5541

5543



CORE 1

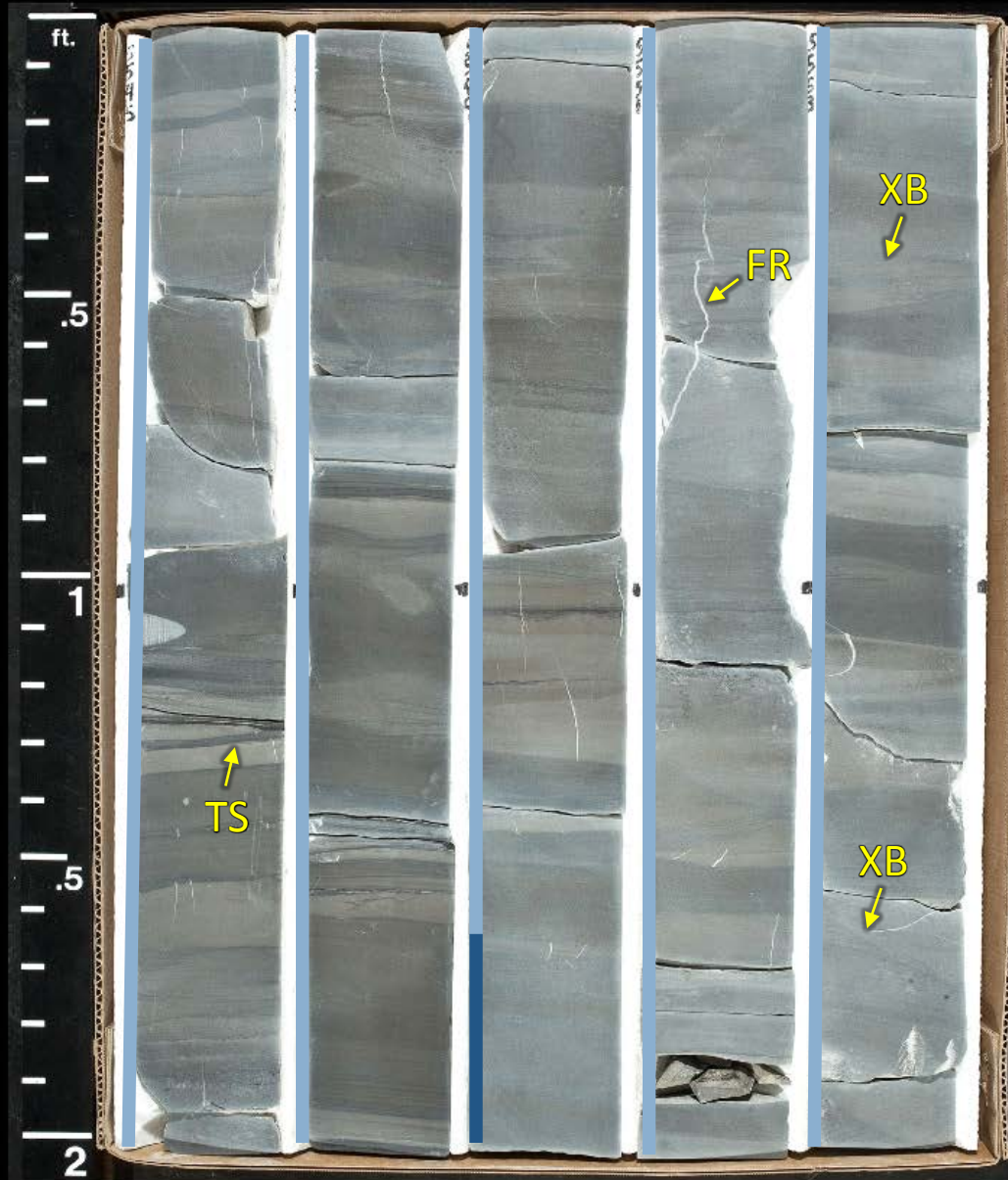
5545

5547

5549

5551

5553



CORE 1

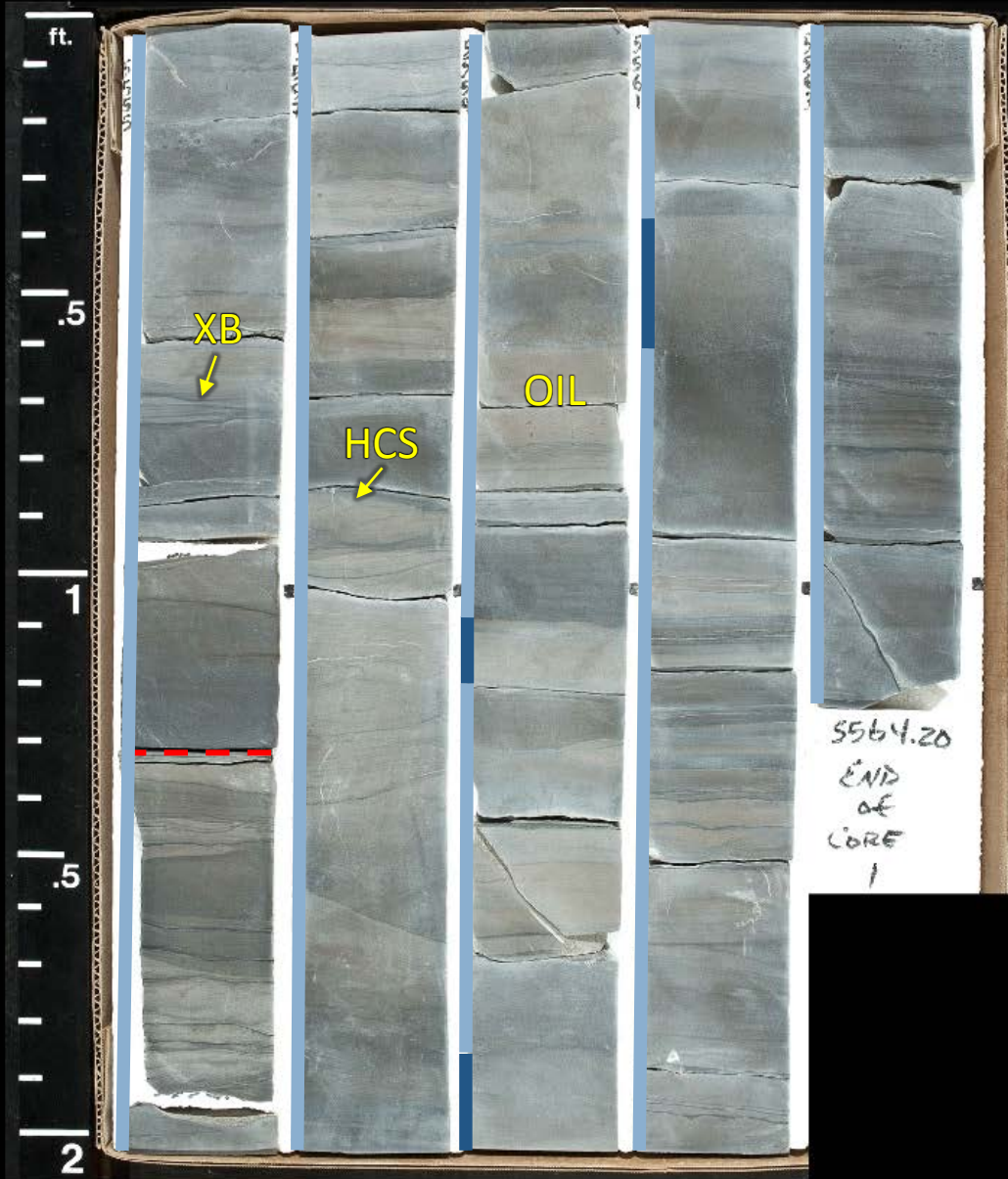
5555

5557

5559

5561

5563



CORE 2

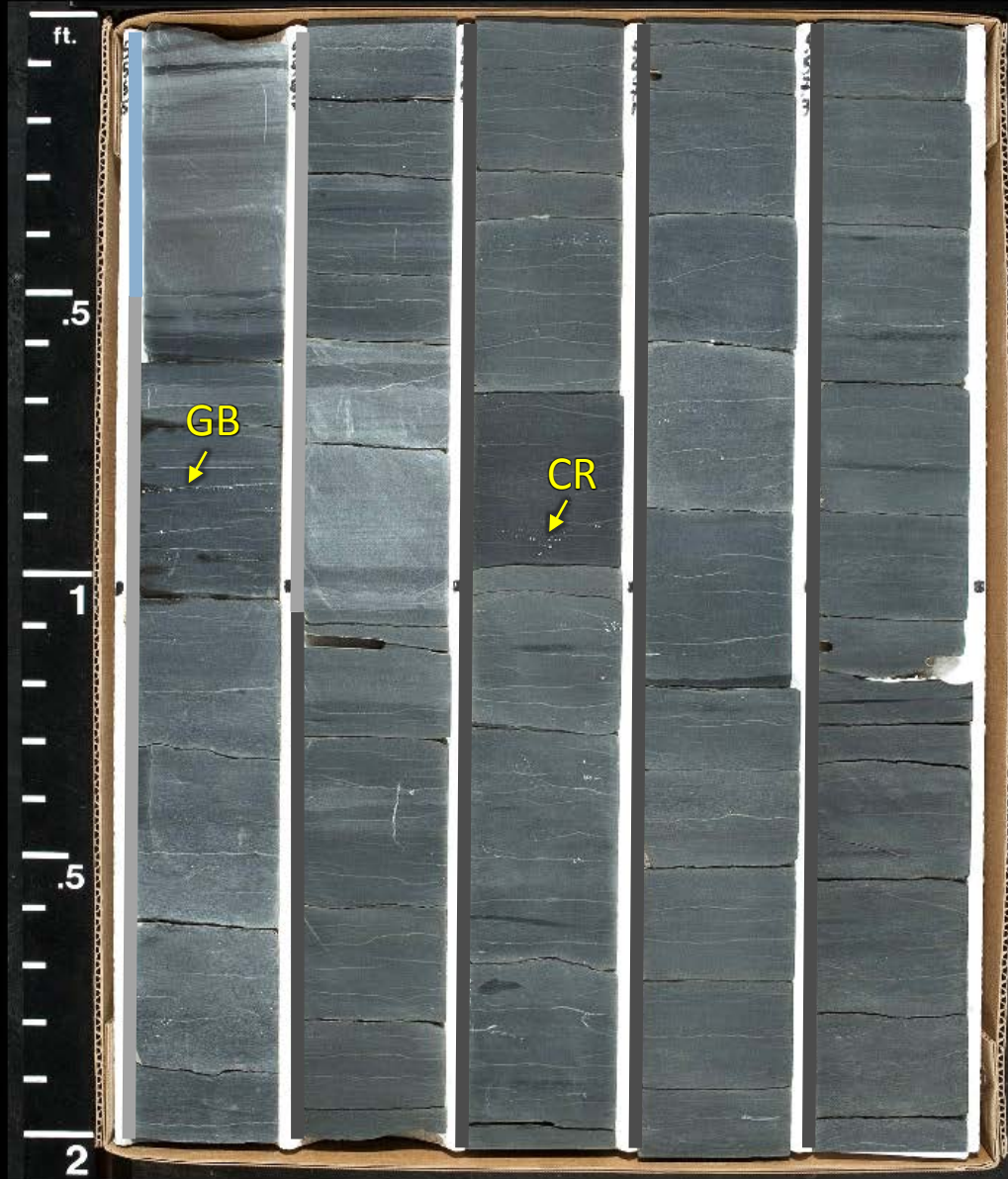
5565

5567

5569

5571

5573



CORE 2

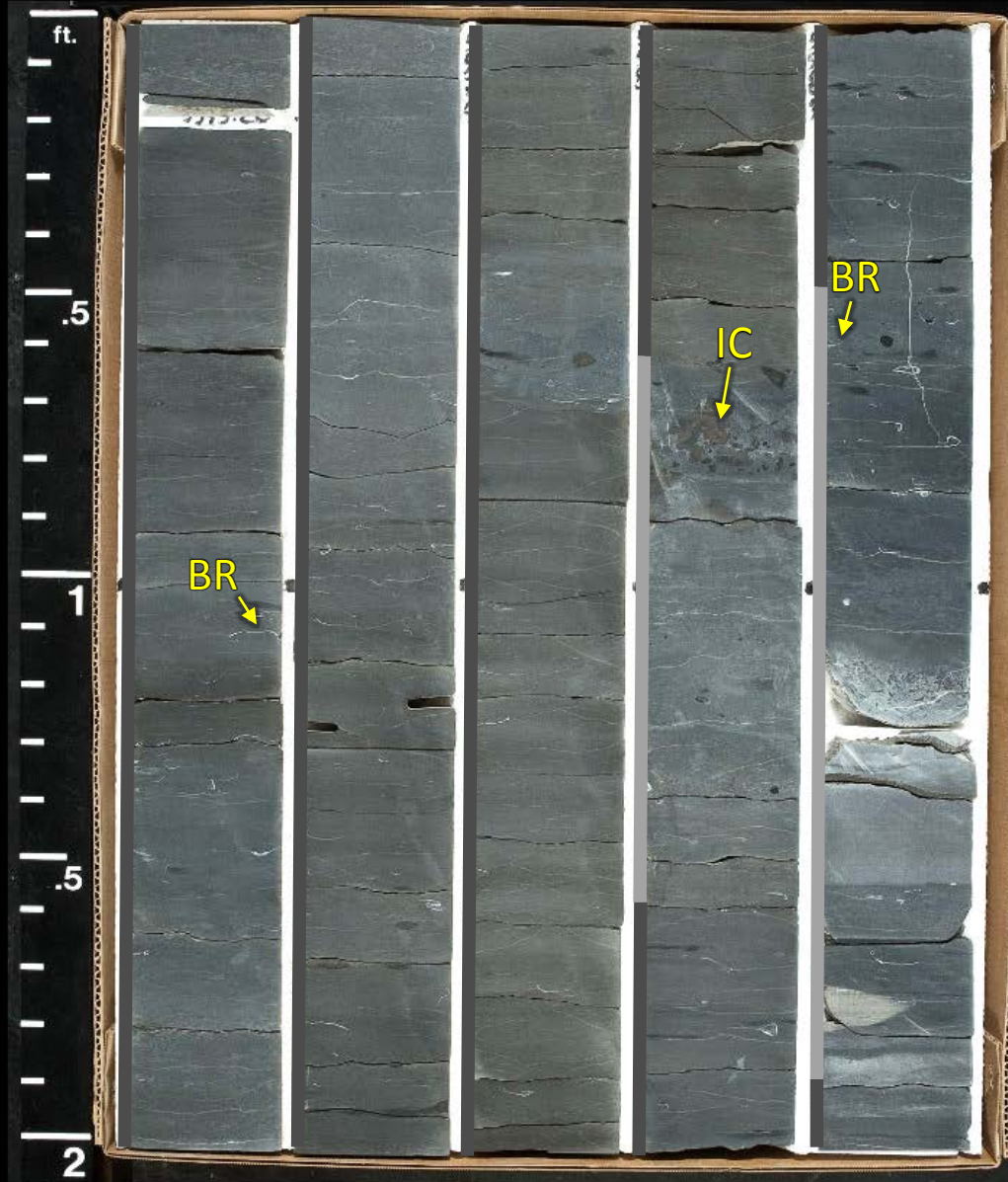
5575

5577

5579

5581

5583



CORE 2

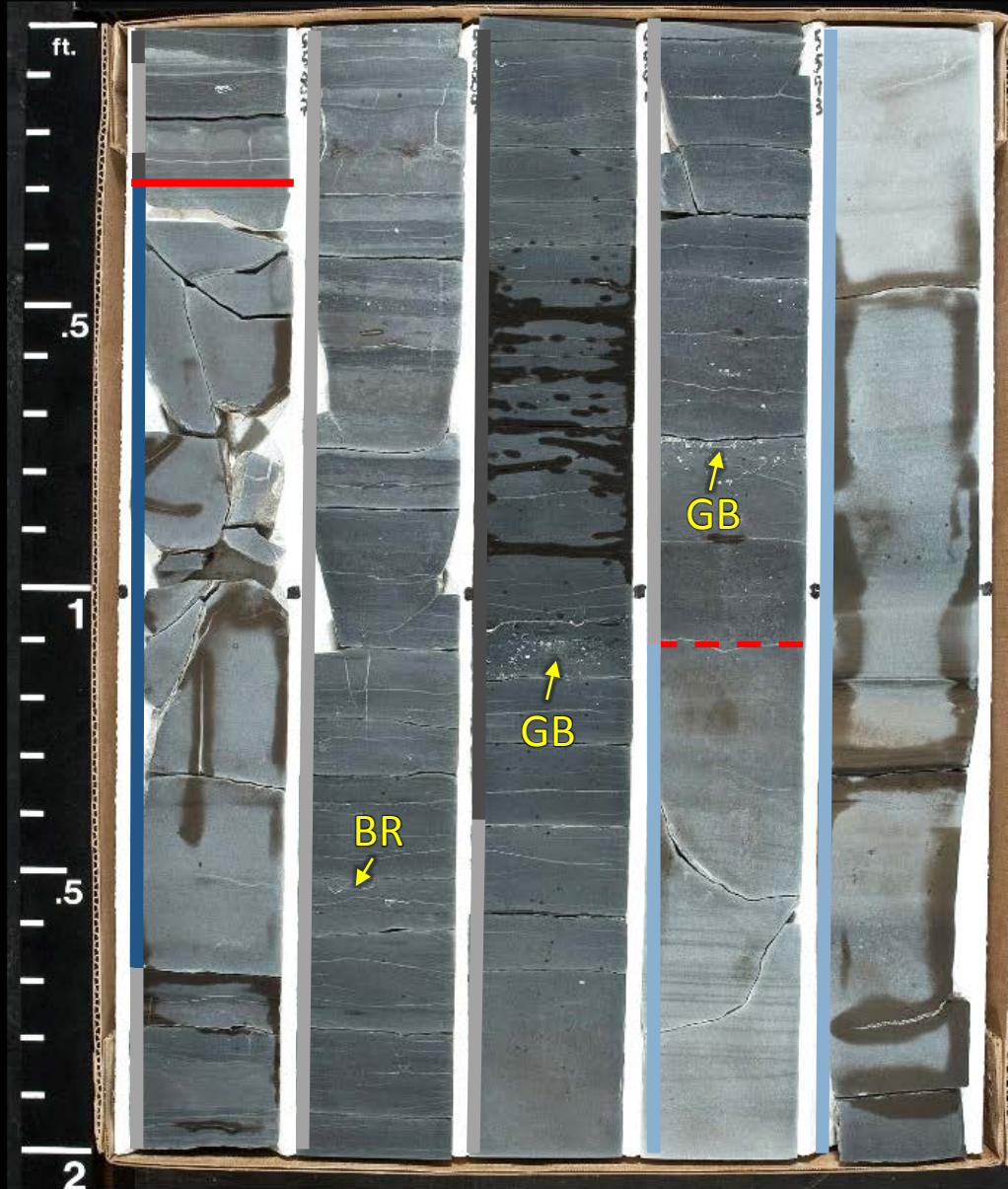
5585

5587

5589

5591

5593



CORE 2

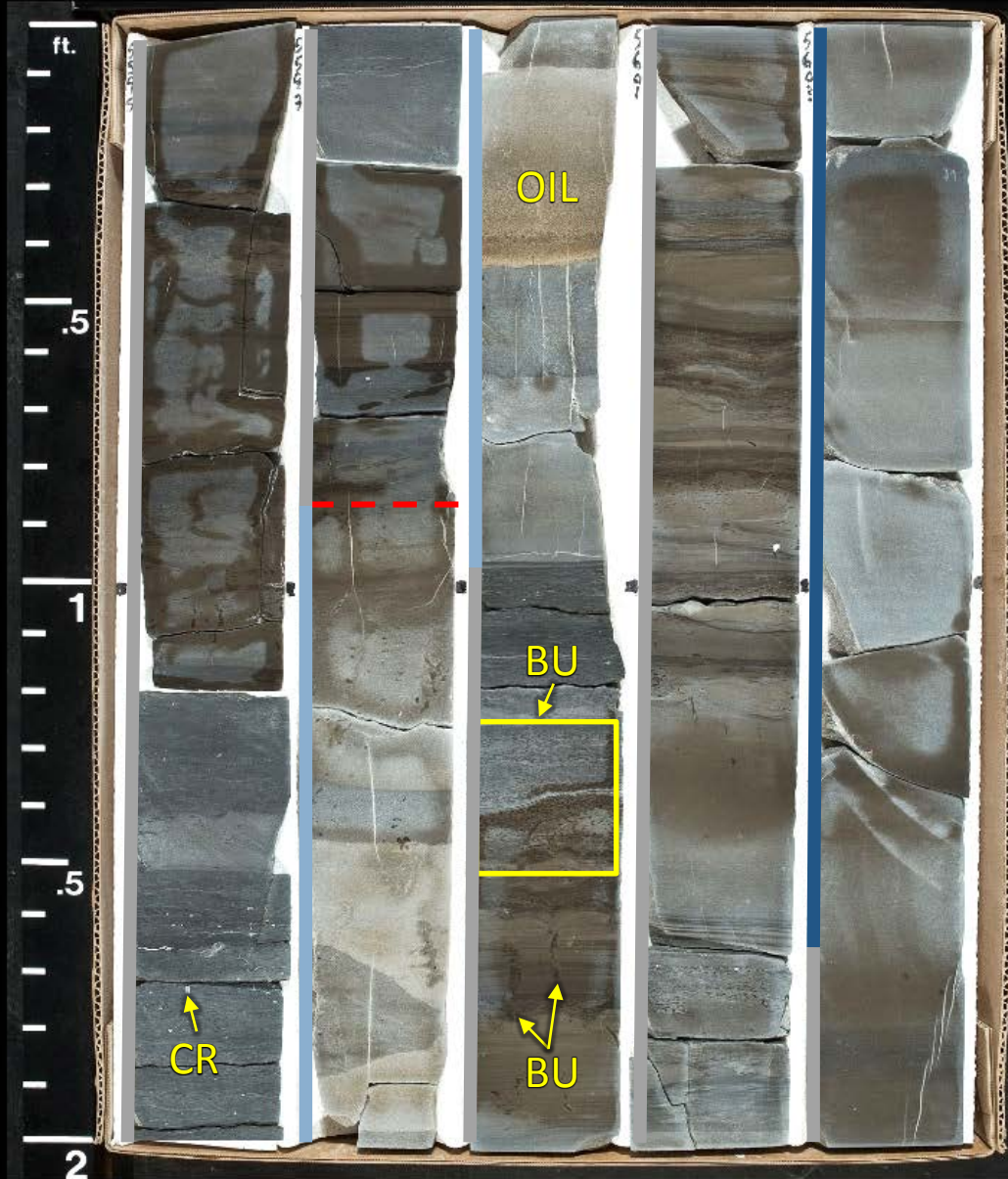
5595

5597

5599

5601

5603



CORE 2

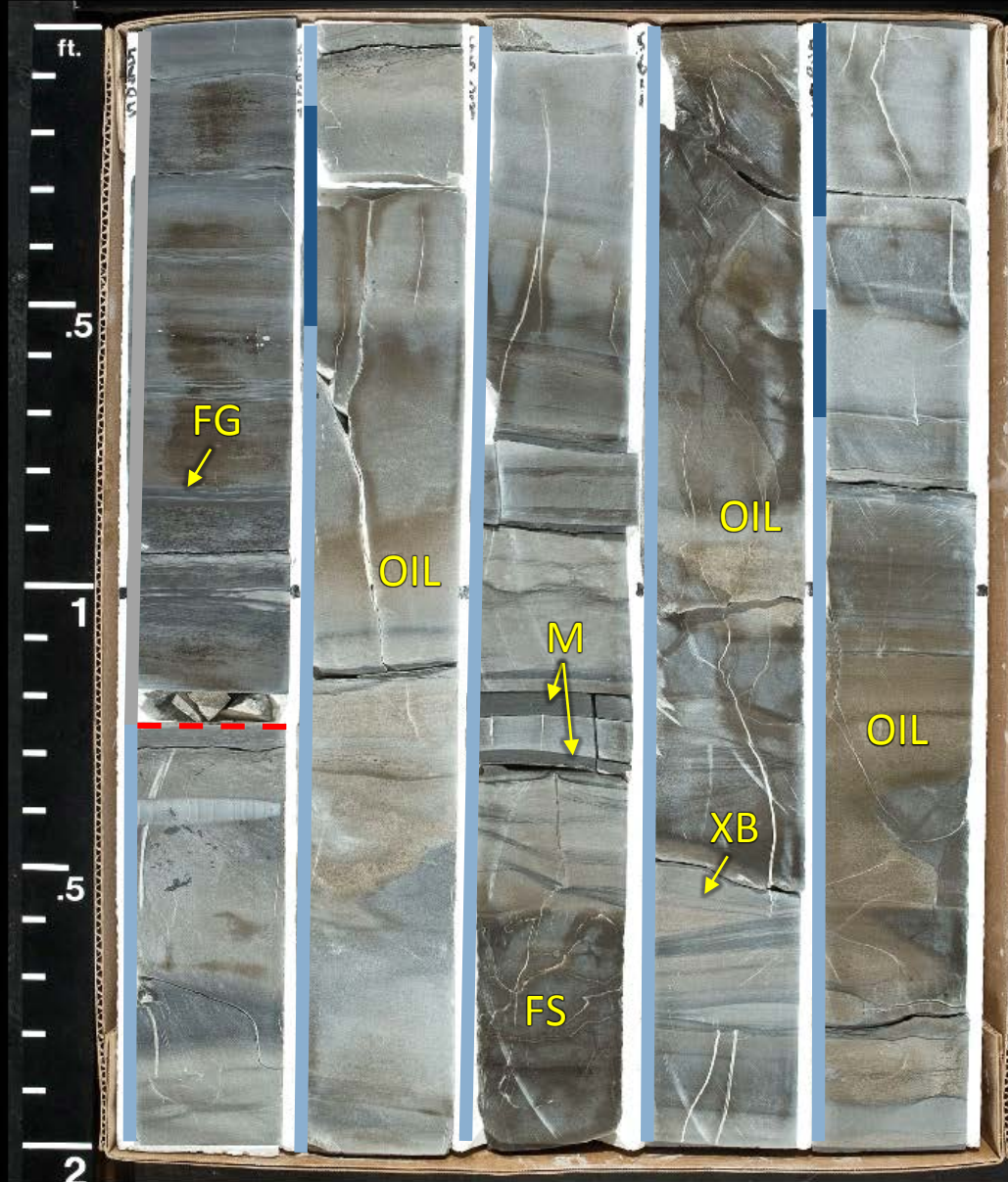
5605

5607

5609

5611

5613



CORE 2

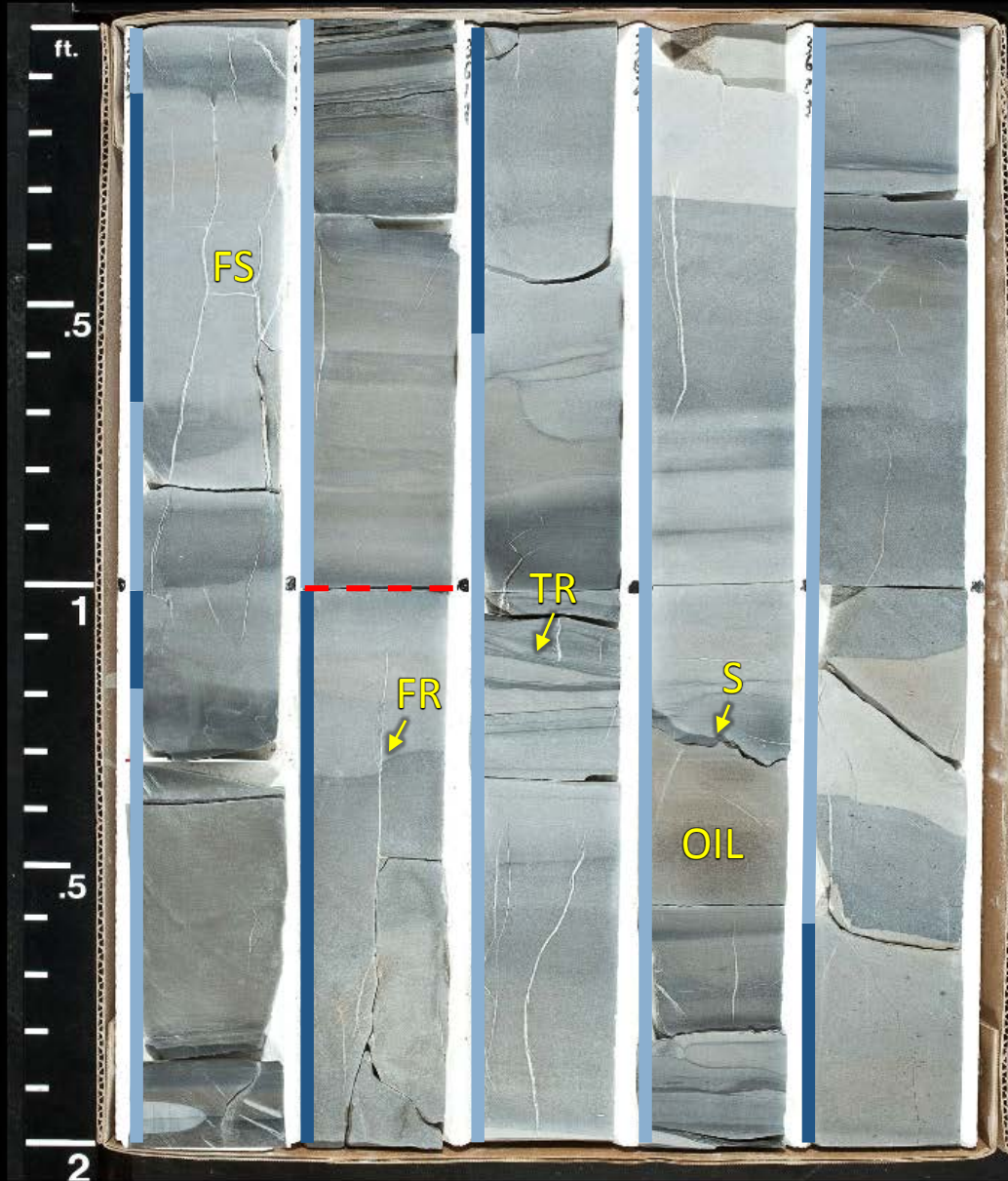
5615

5617

5619

5621

5623



CORE 2

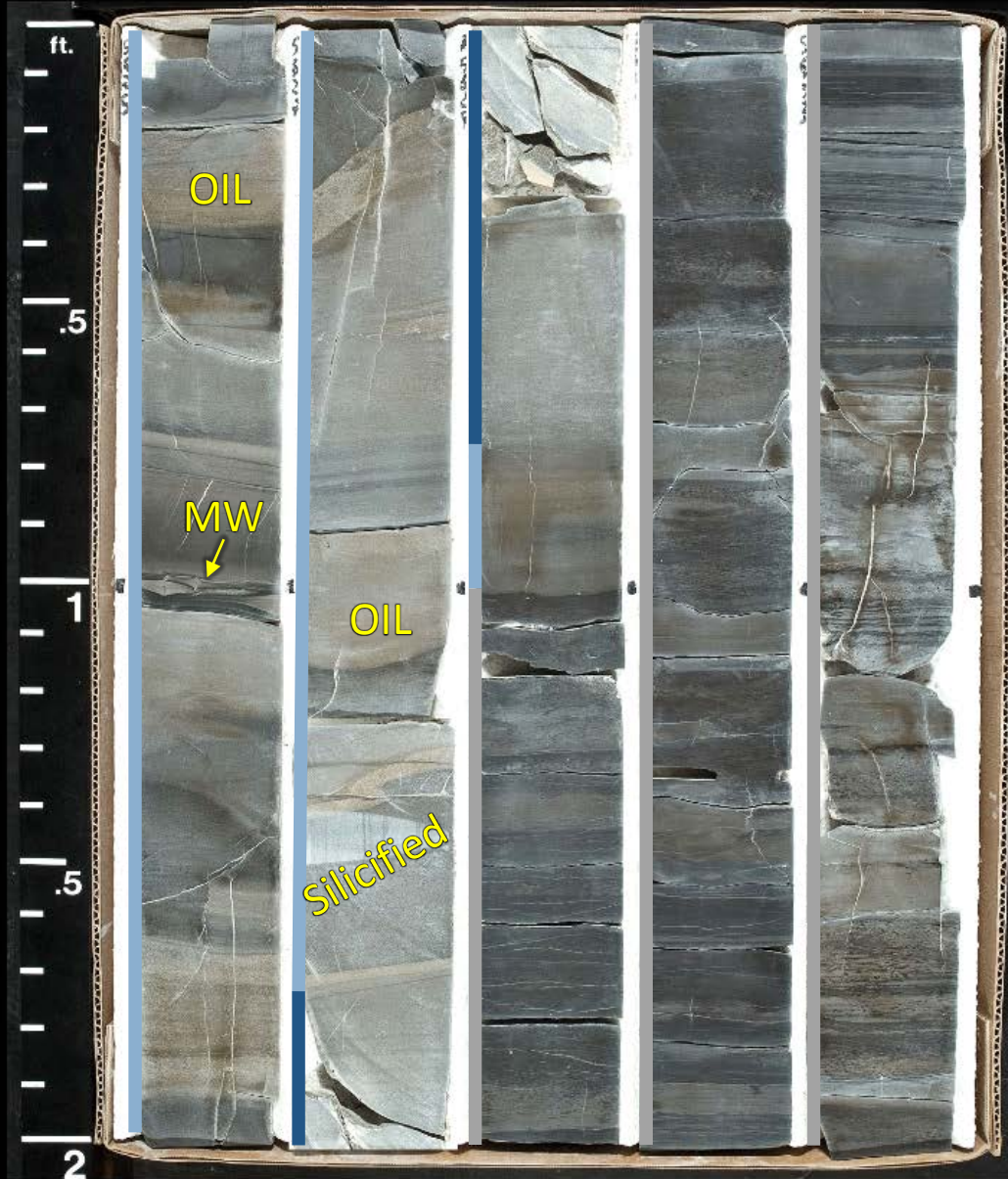
5625

5627

5629

5631

5633



CORE 2

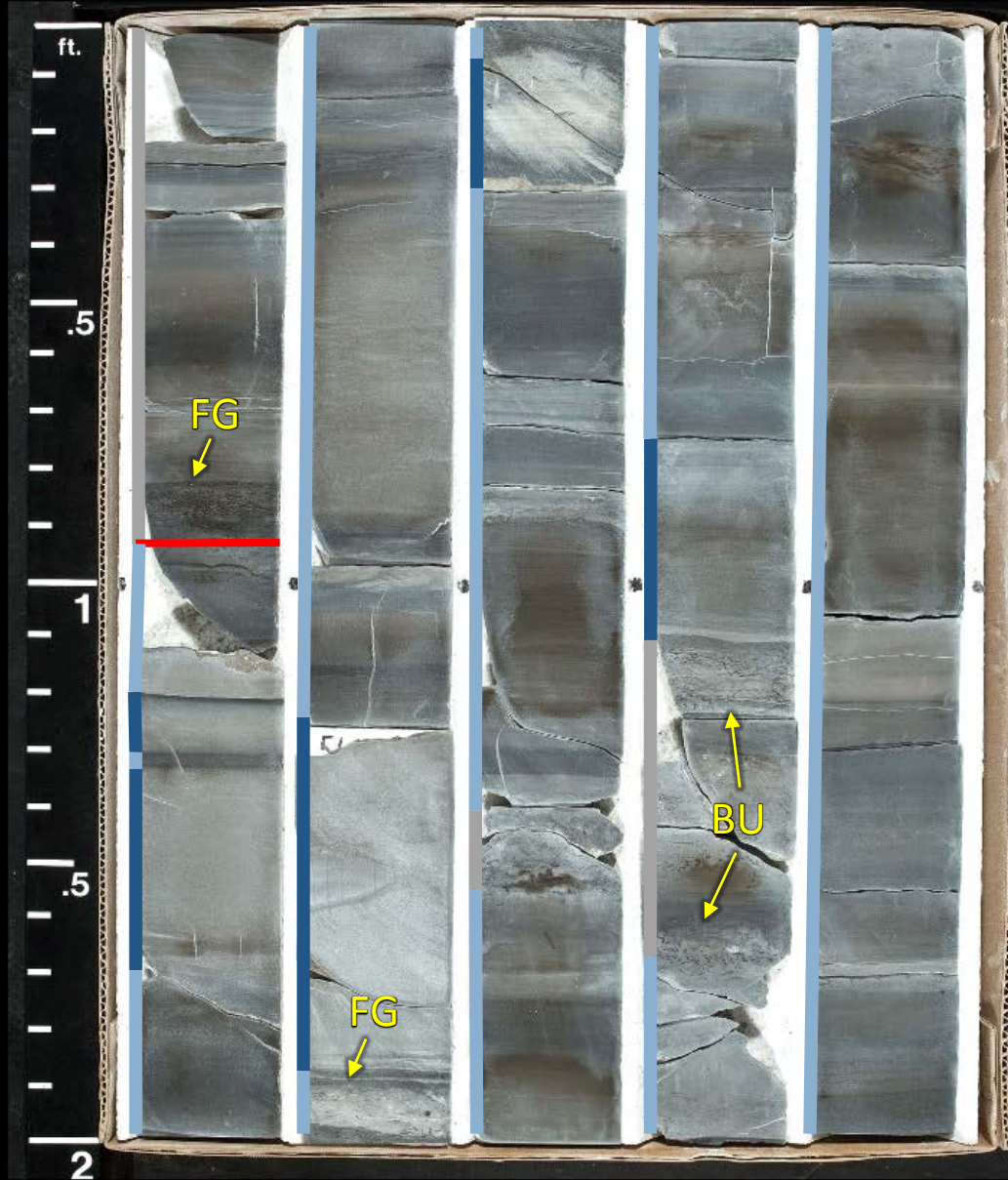
5635

5637

5639

5641

5643



CORE 2

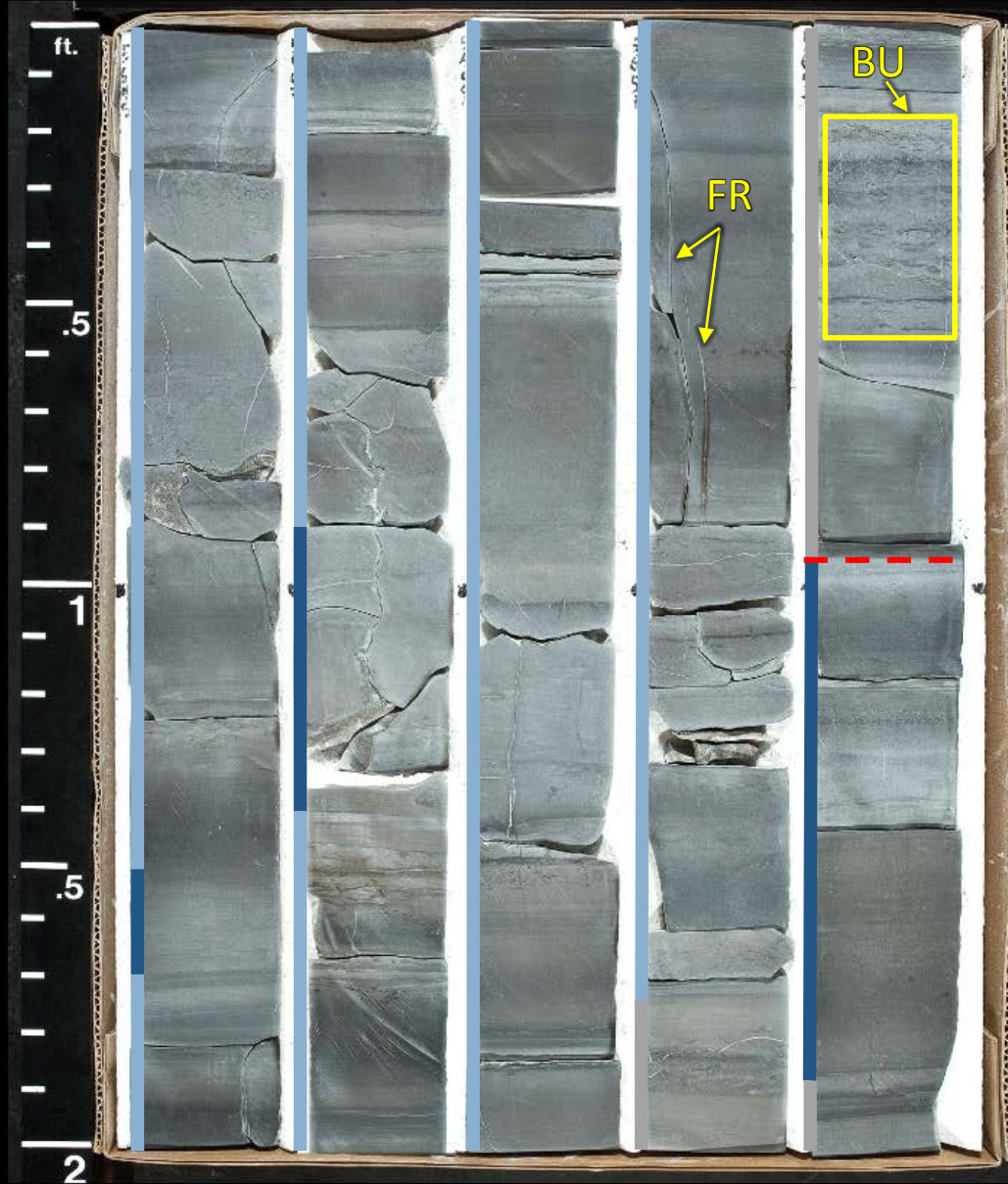
5645

5647

5649

5651

5653



CORE 2

5655



CORE 3

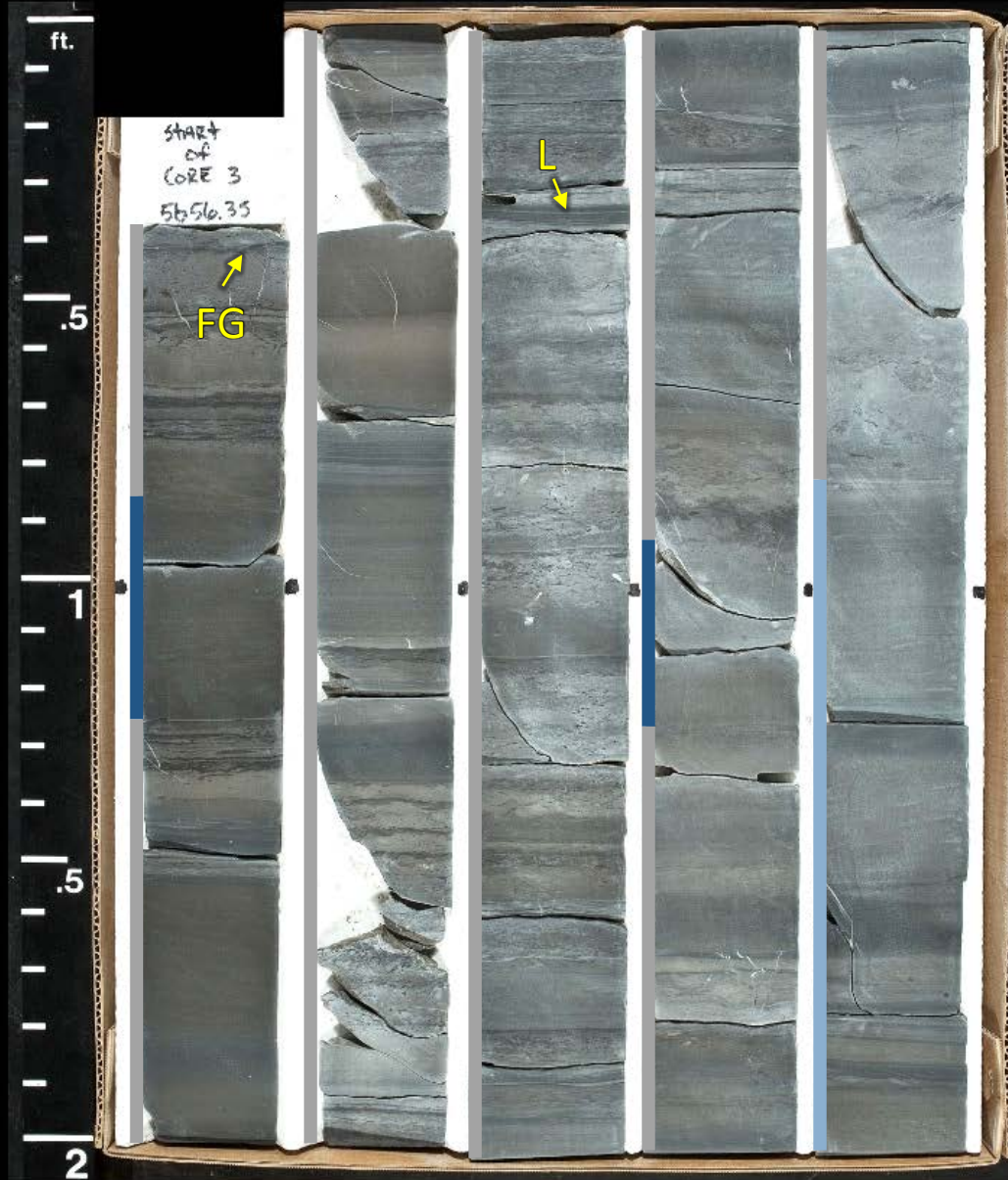
5656

5658

5660

5662

5664



CORE 3

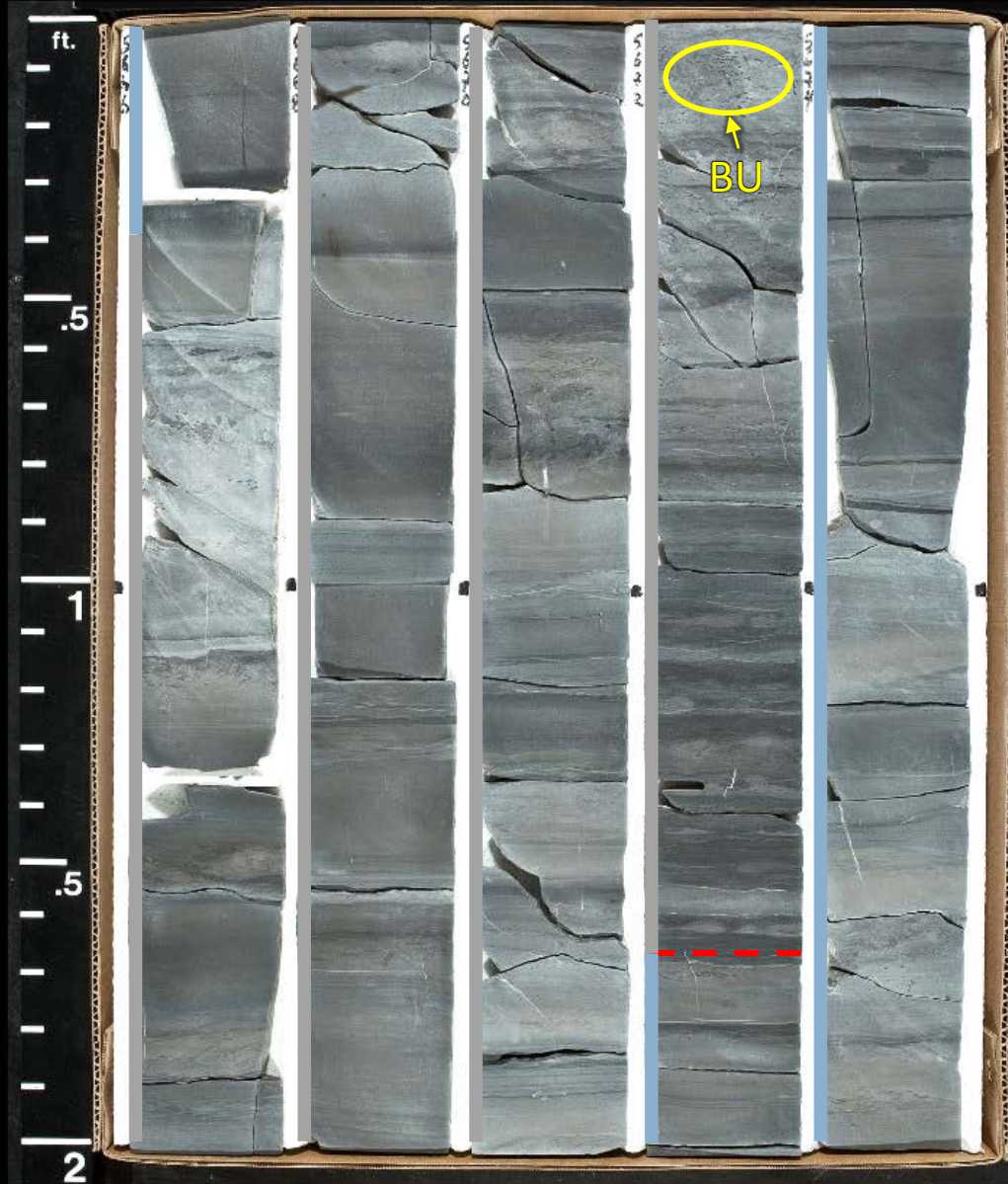
5666

5668

5670

5672

5674



CORE 3

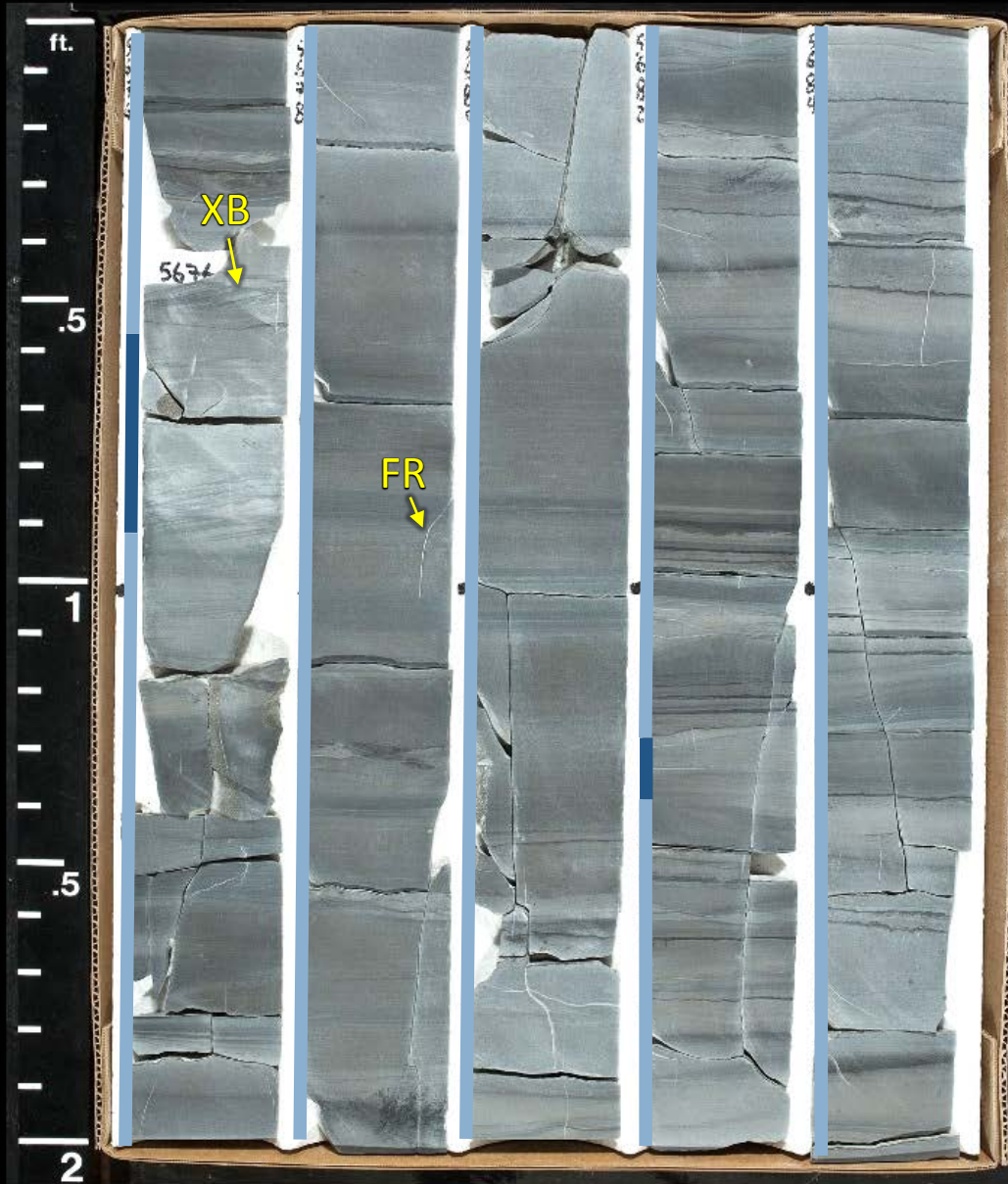
5676

5678

5680

5682

5684



CORE 3

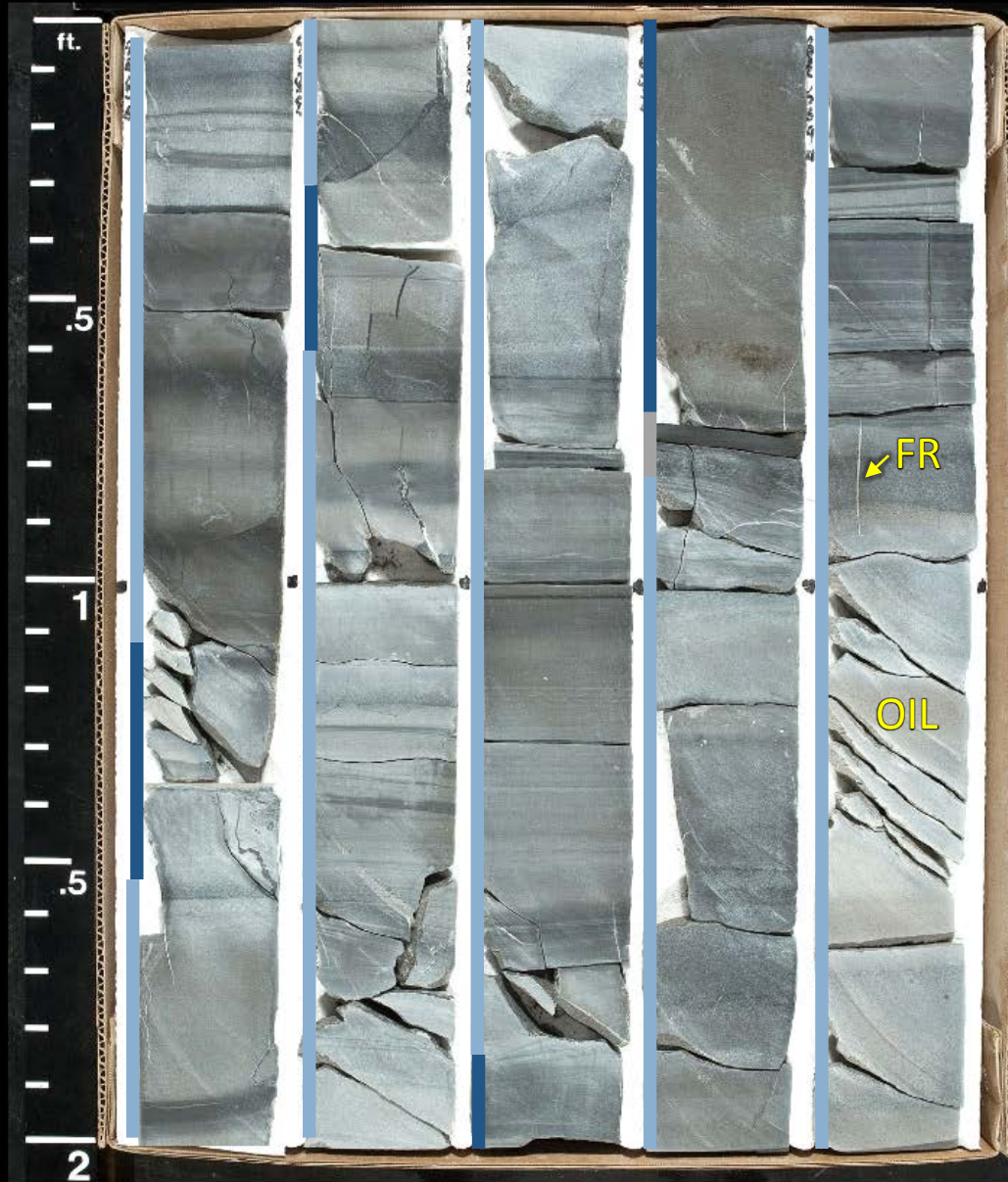
5686

5688

5690

5692

5694



CORE 3

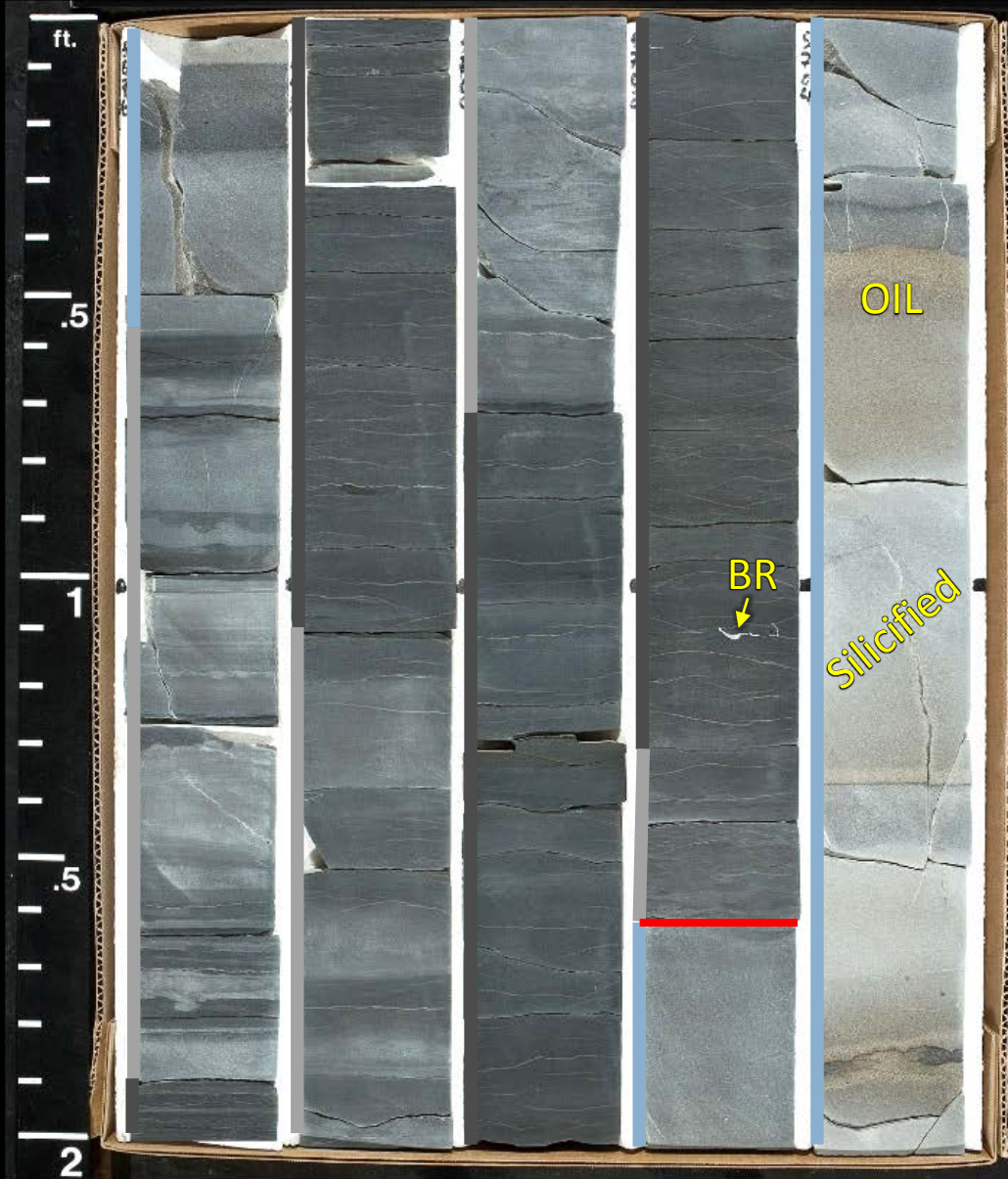
5696

5698

5700

5702

5704



CORE 3

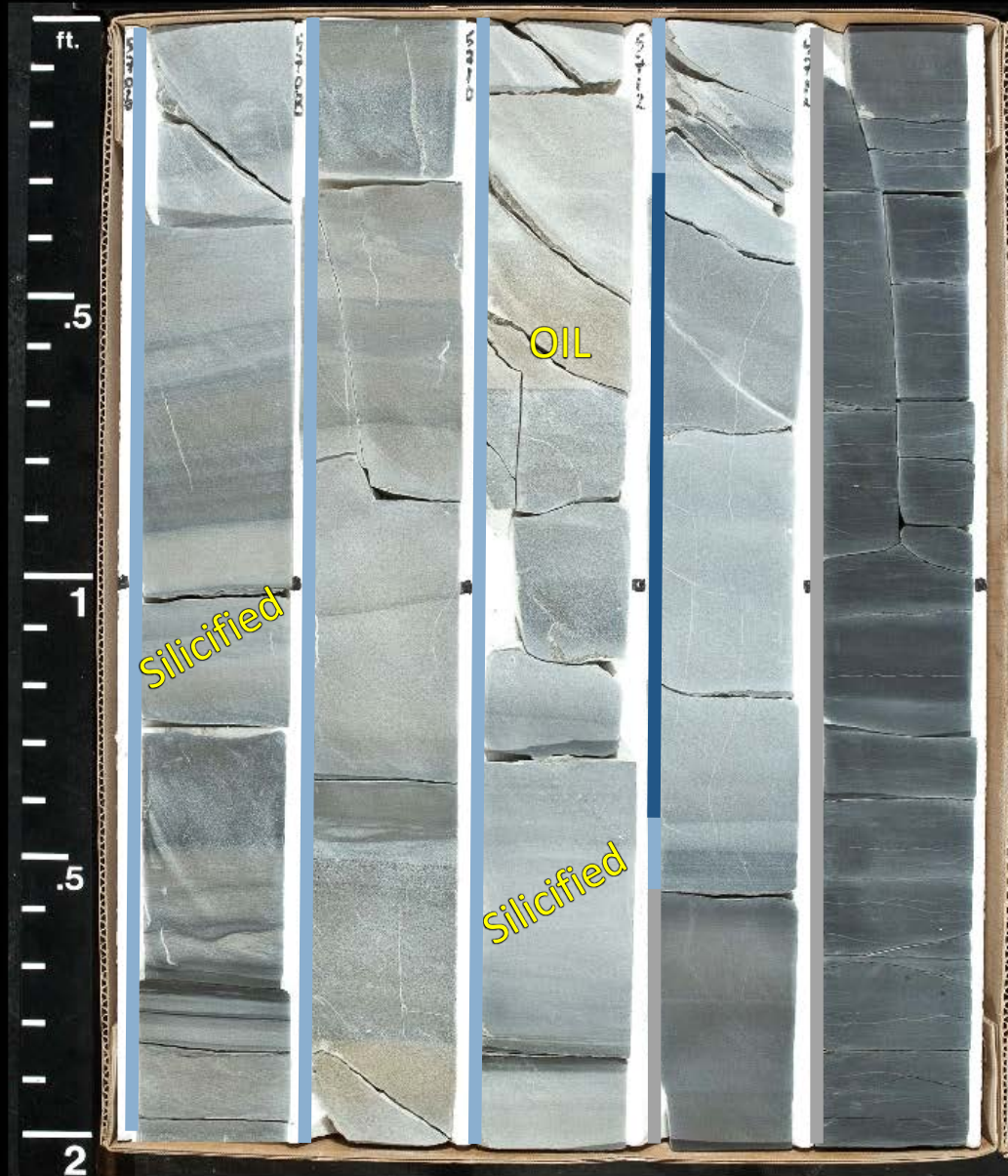
5706

5708

5710

5712

5714



CORE 3

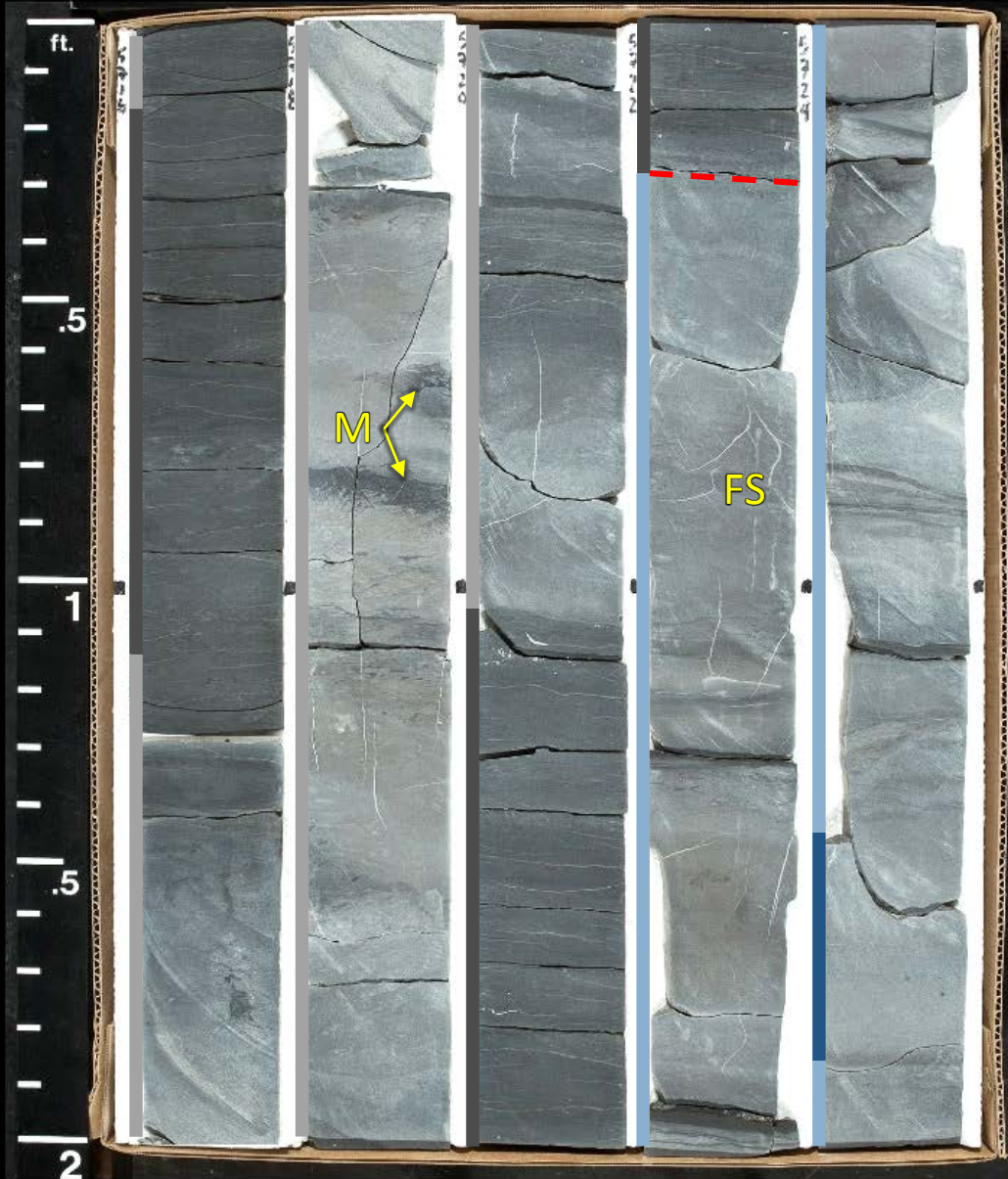
5716

5718

5720

5722

5724



CORE 3

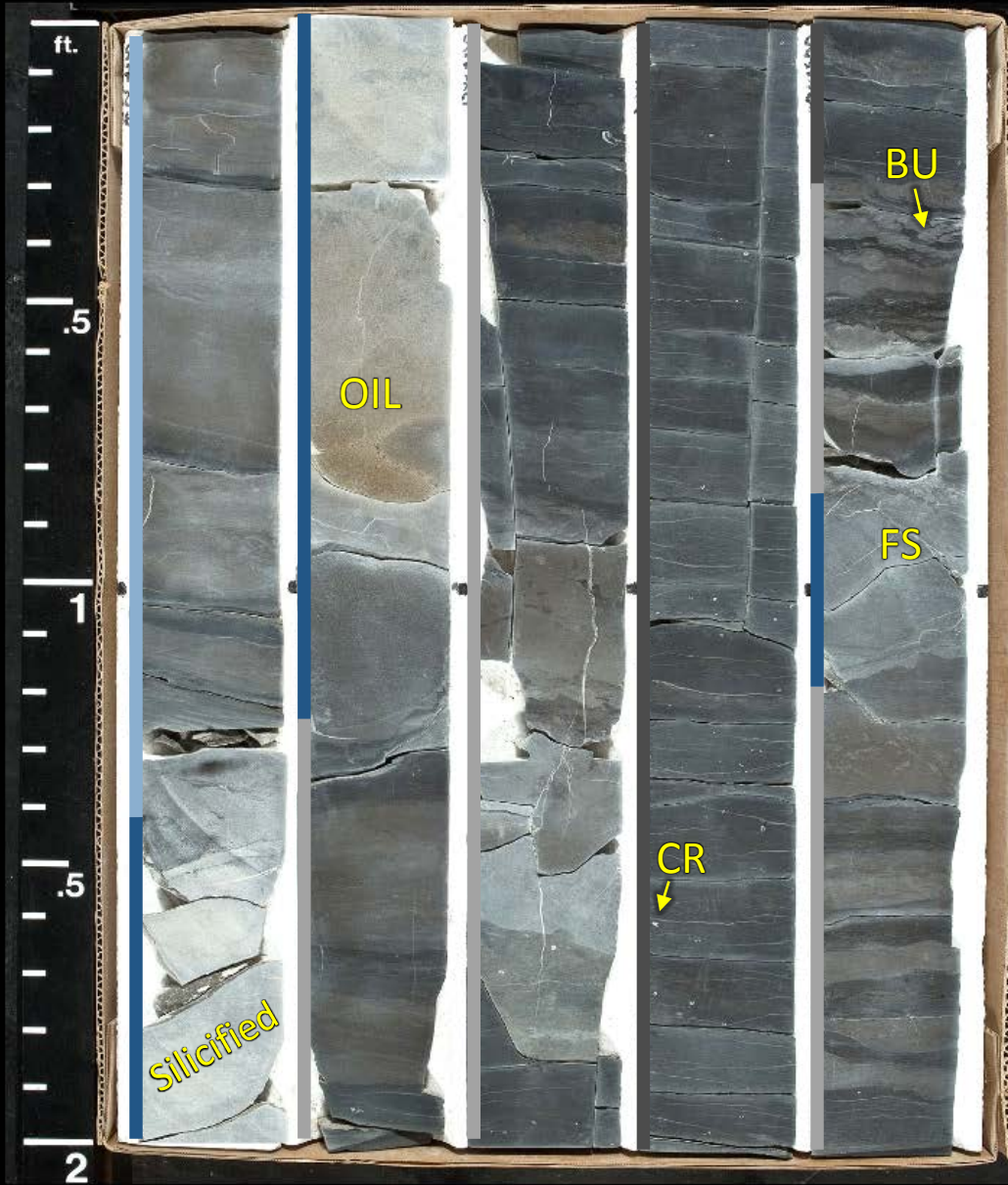
5726

5728

5730

5732

5734



CORE 3

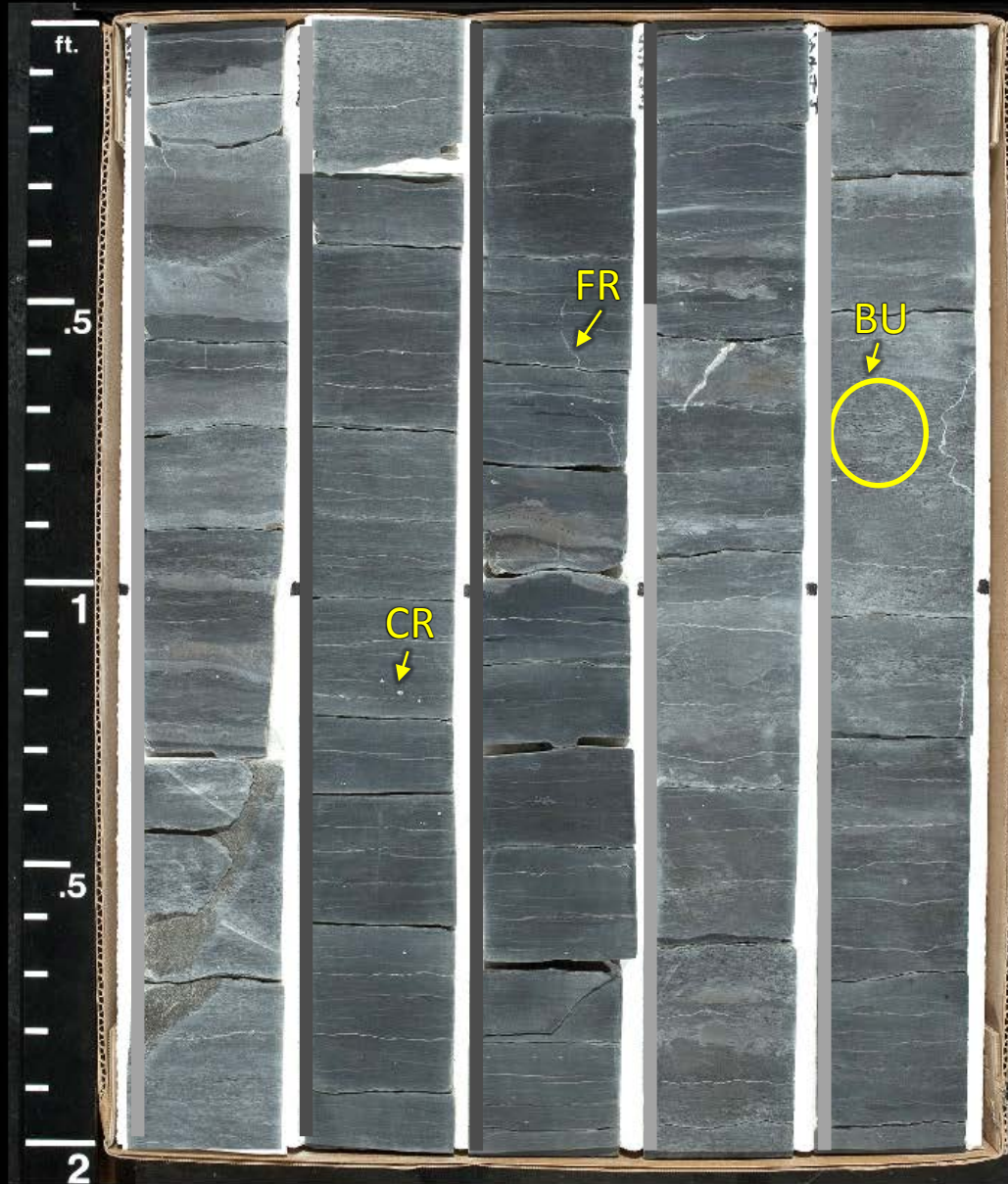
5736

5738

5740

5742

5744



CORE 3

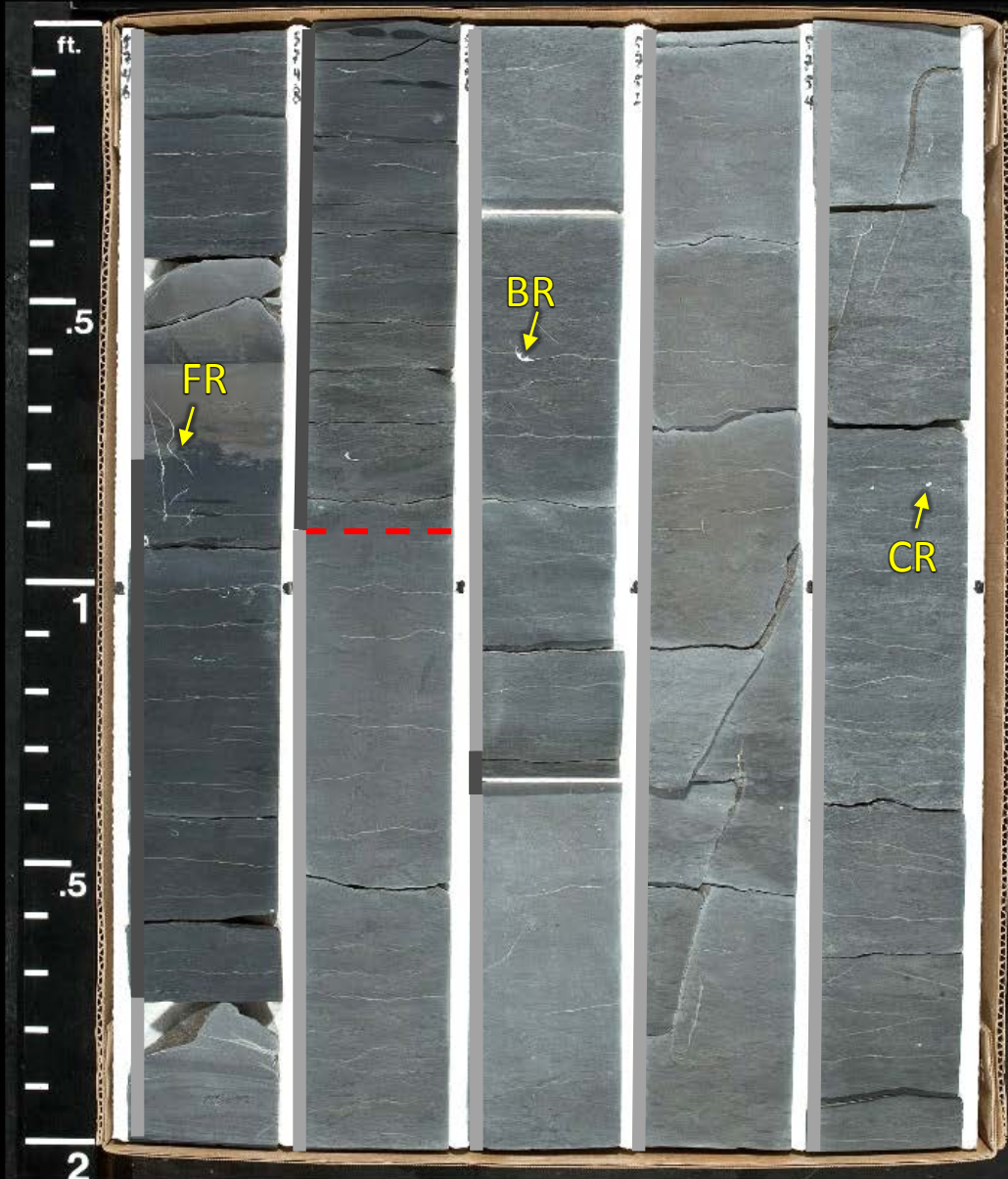
5746

5748

5750

5752

5754



CORE 3

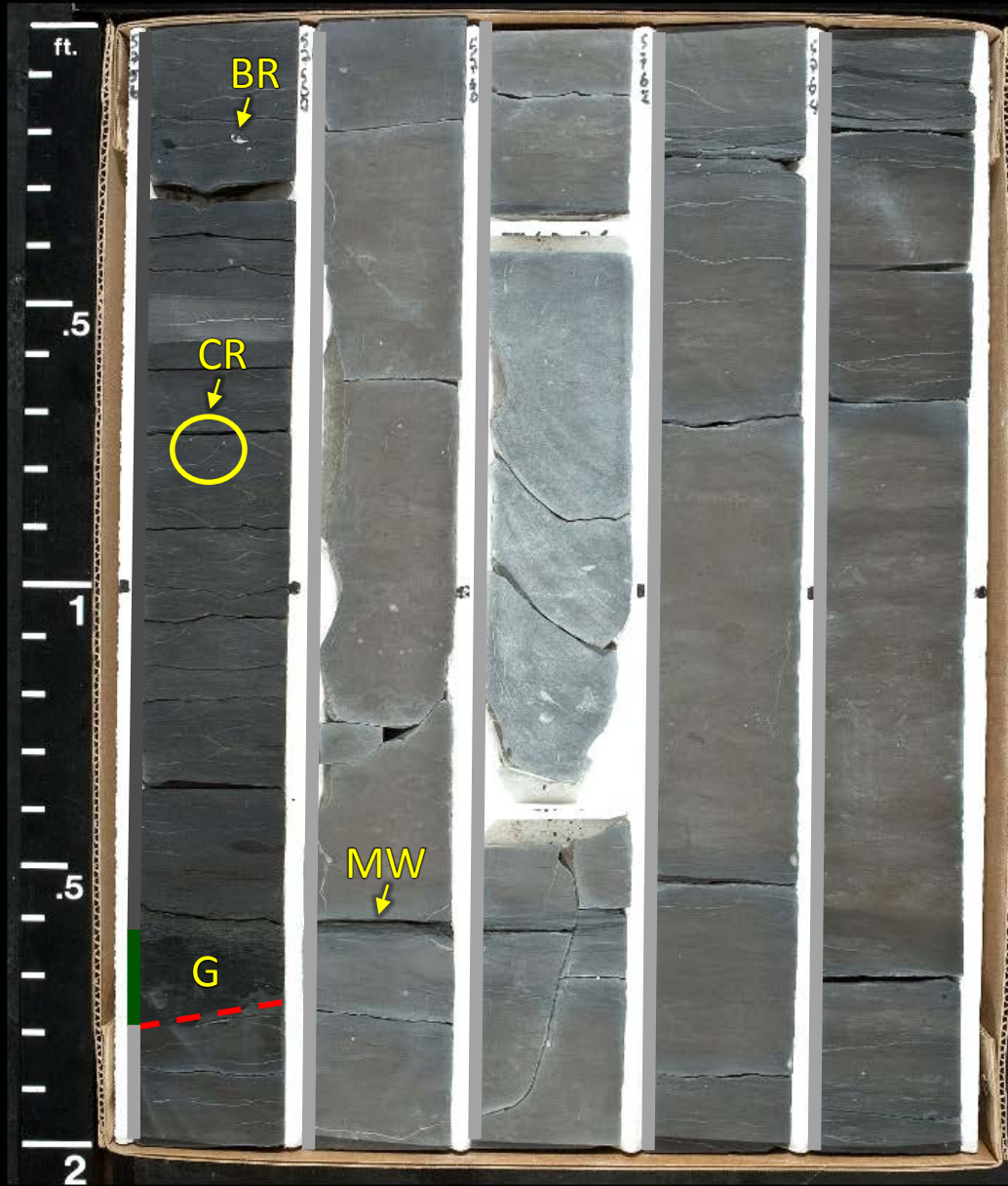
5756

5758

5760

5762

5764



CORE 3

5766

5768

5770

5772

5774



CORE 3

5776



CORE 4

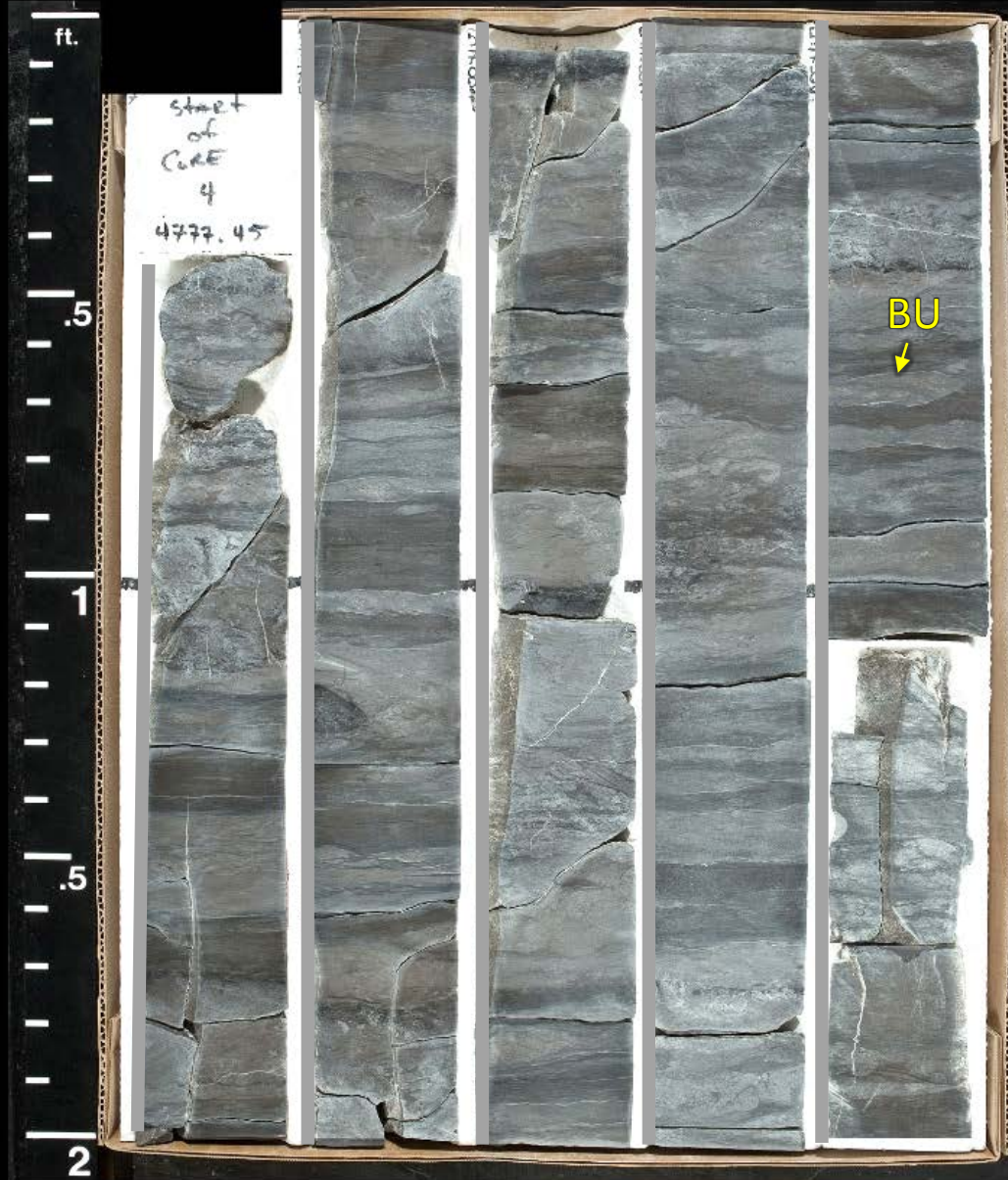
5777

5779

5781

5783

5785



CORE 4

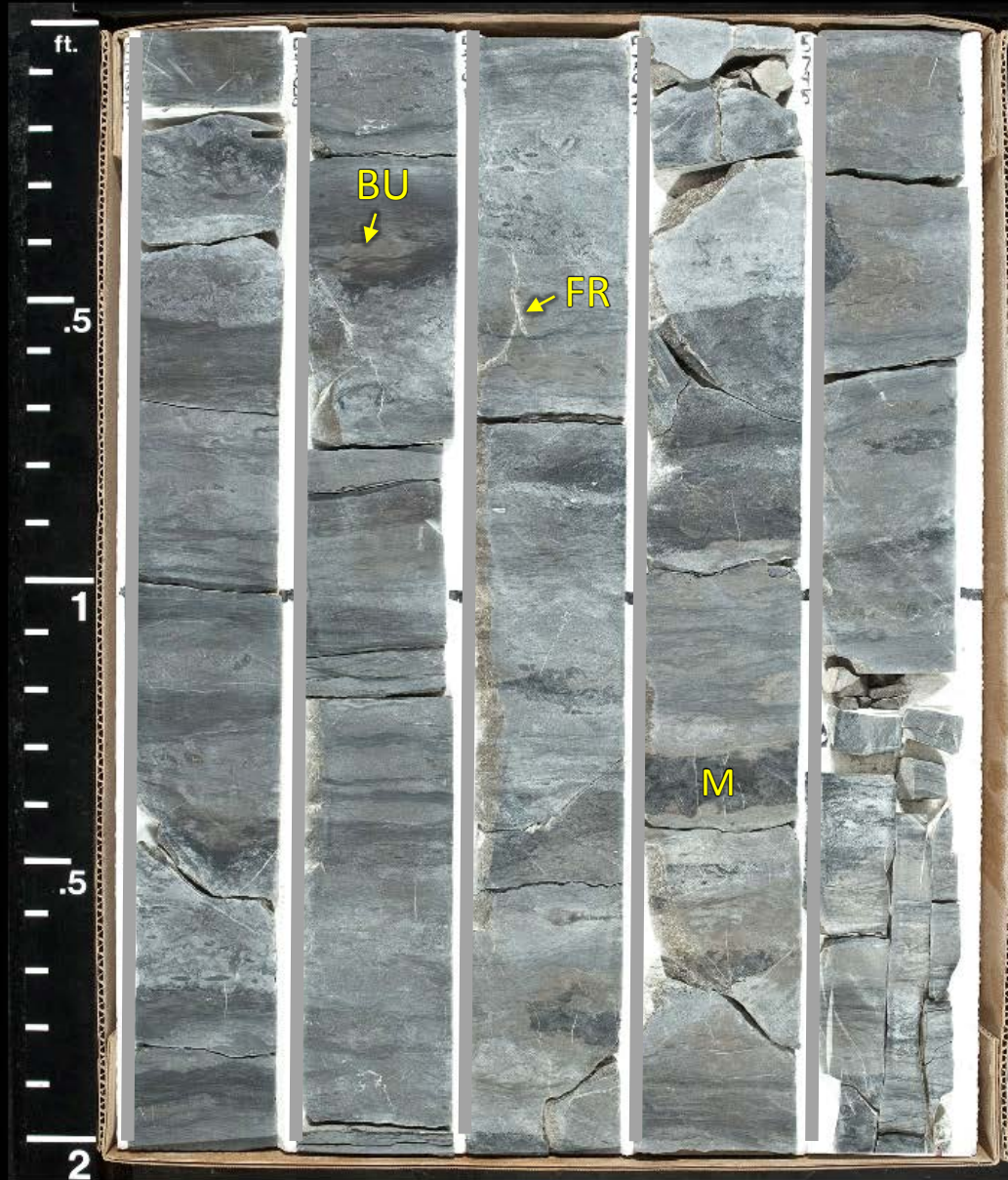
5787

5789

5791

5793

5795



CORE 4

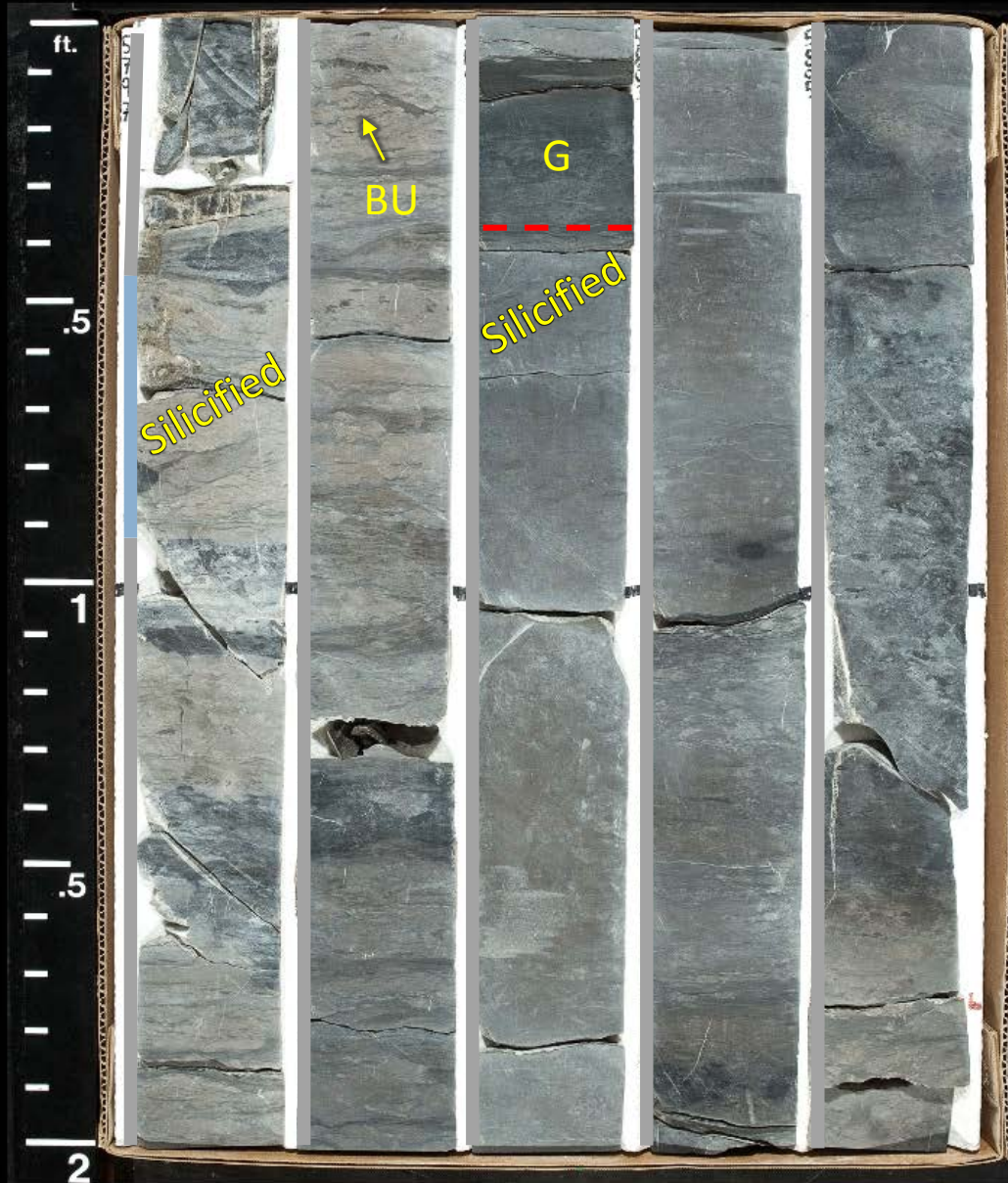
5797

5799

5801

5803

5805



CORE 4

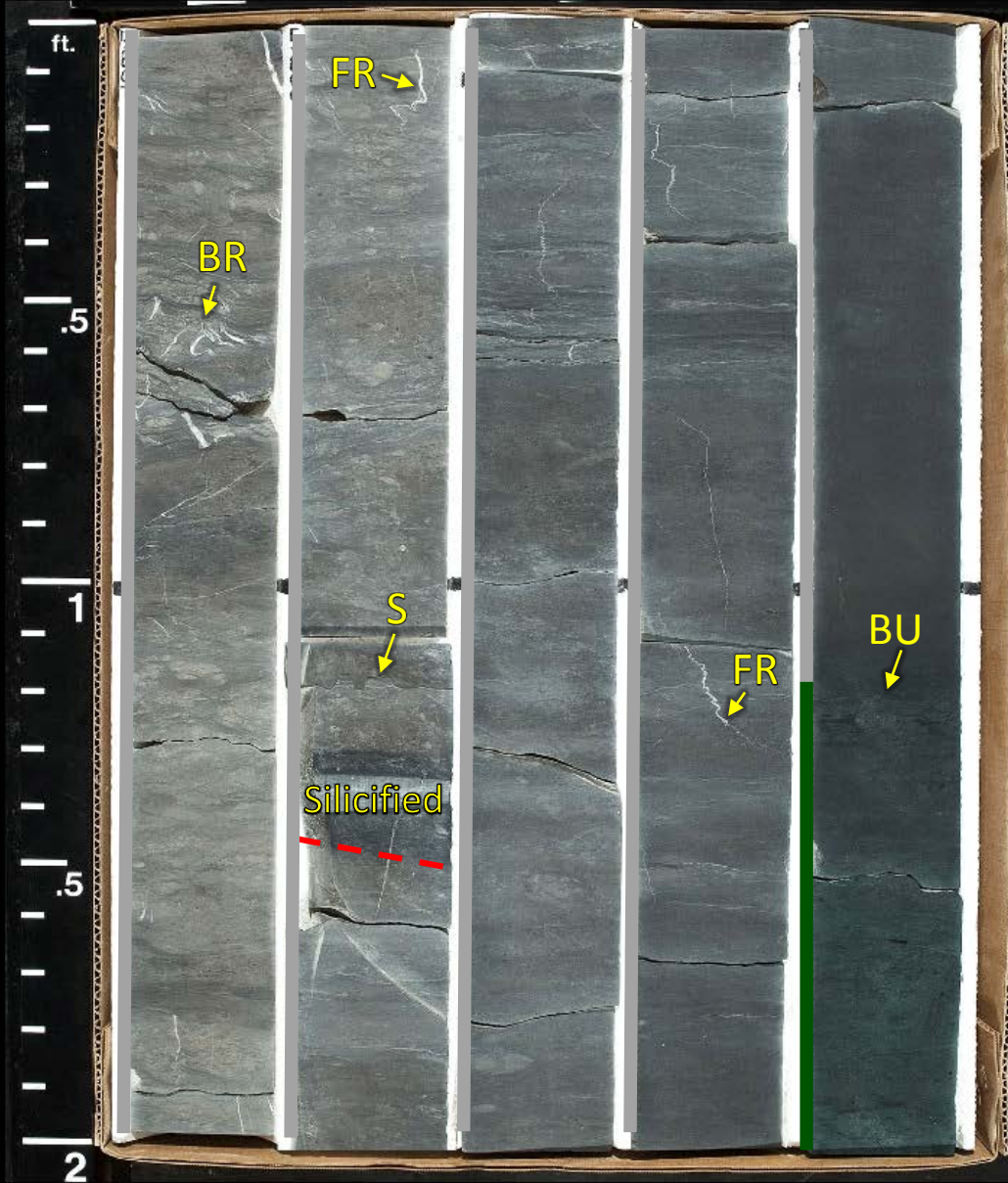
5807

5809

5811

5813

5815



CORE 4

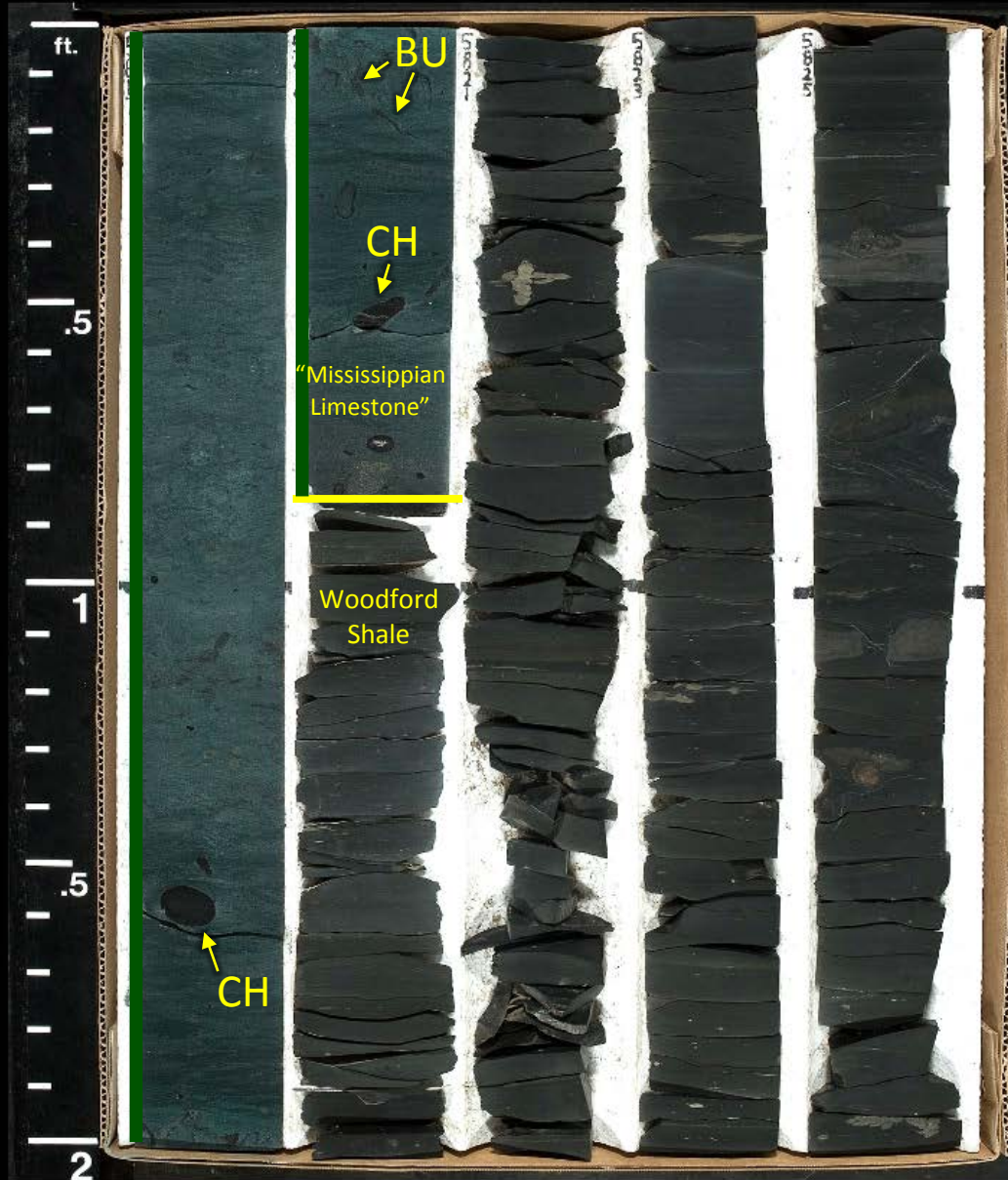
5817

5819

5821

5823

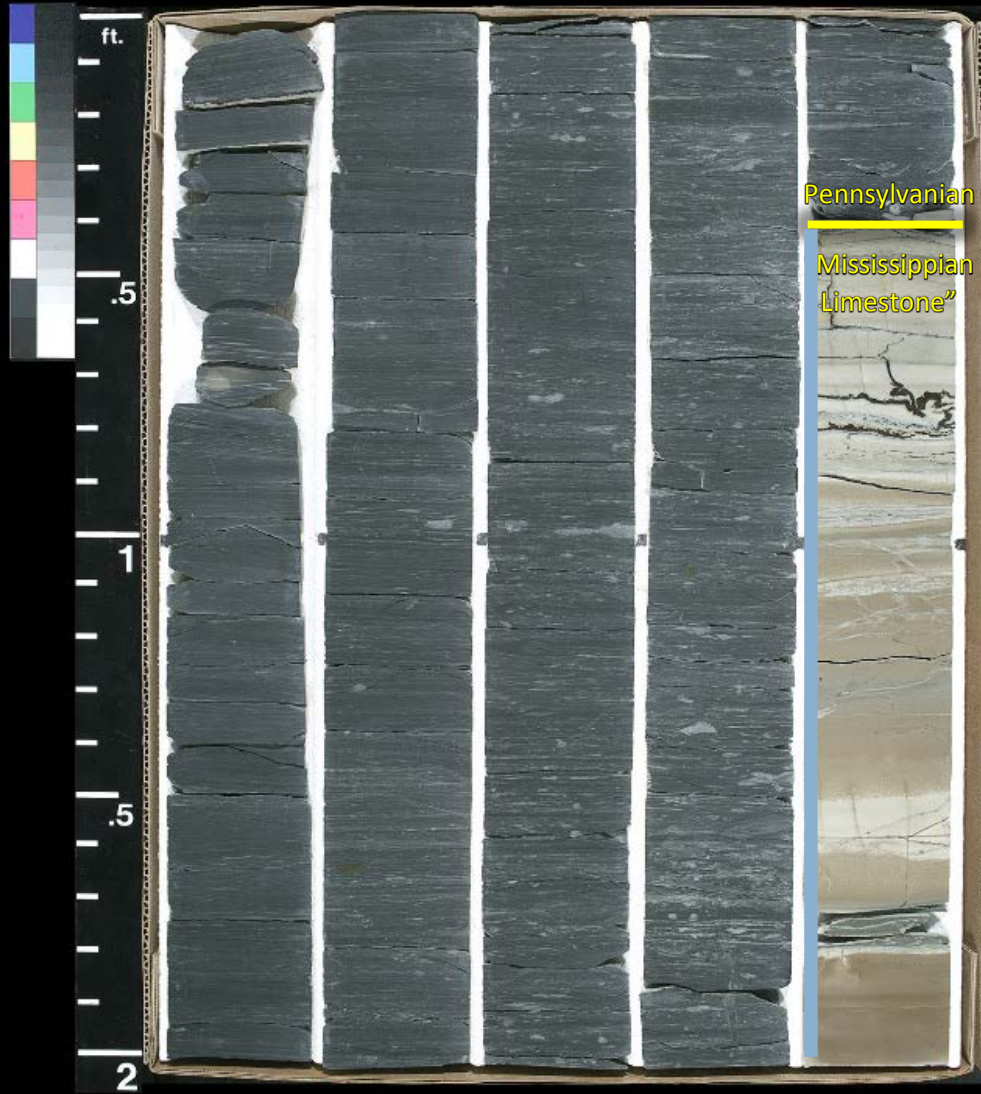
5825



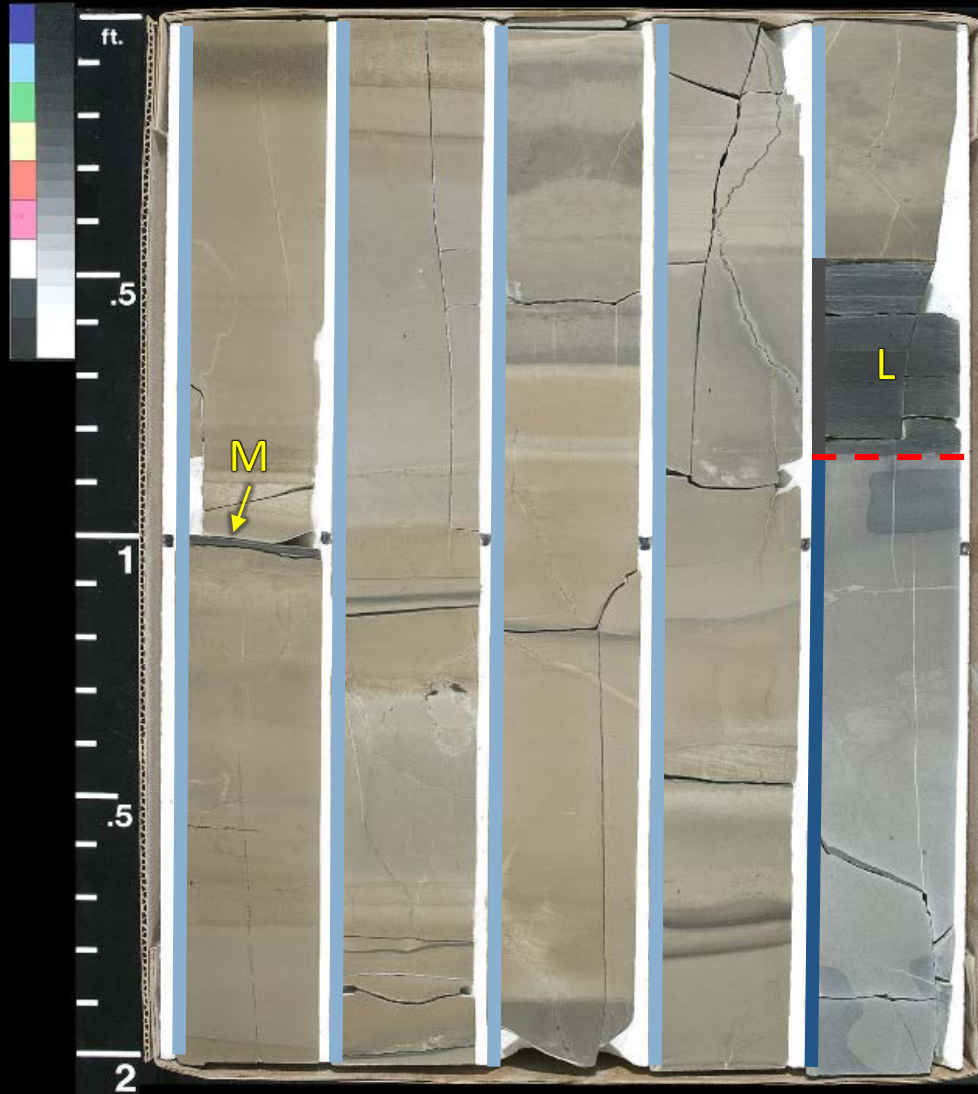
Core #2

Winney #1-8 SWD

CORE 1 5115 5117 5119 5121 5123

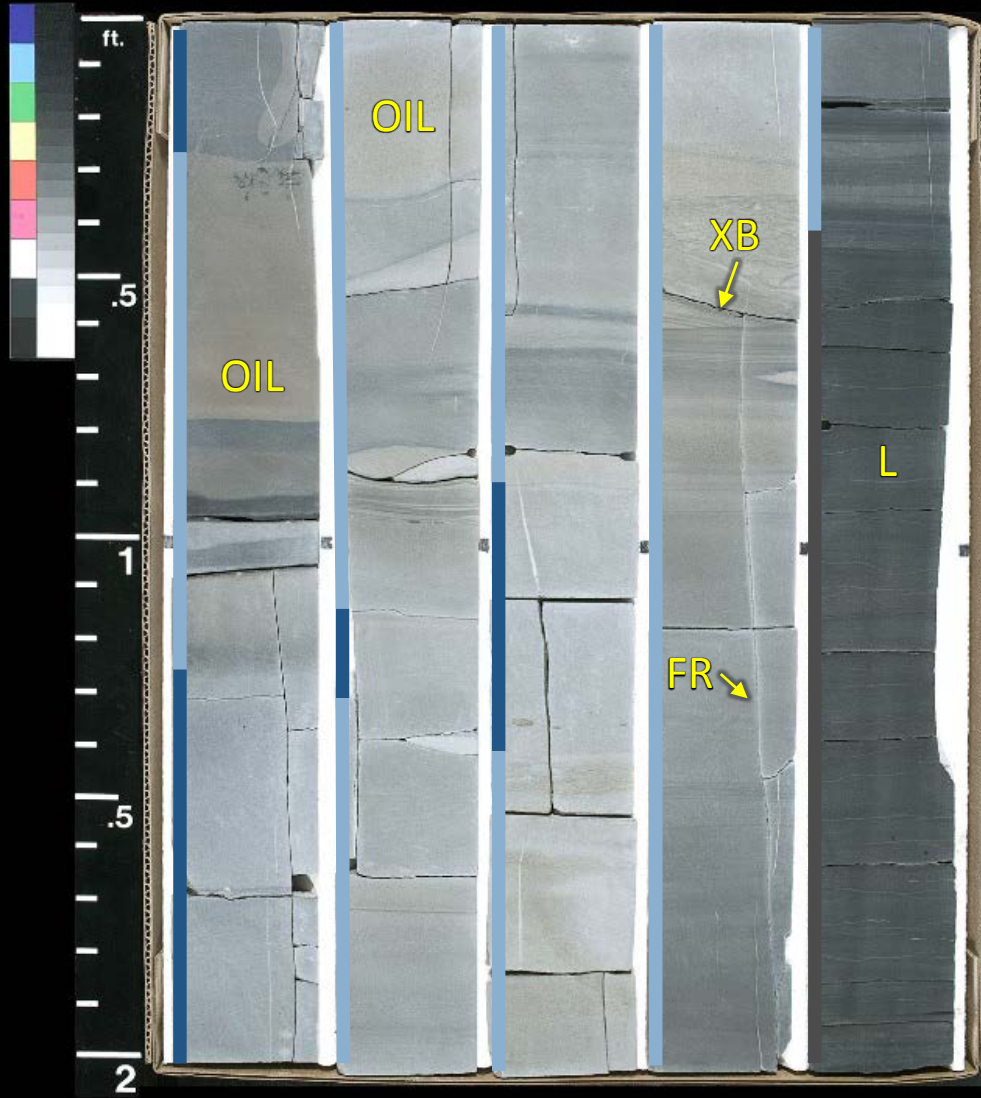


CORE 1 5125 5127 5129 5131 5133

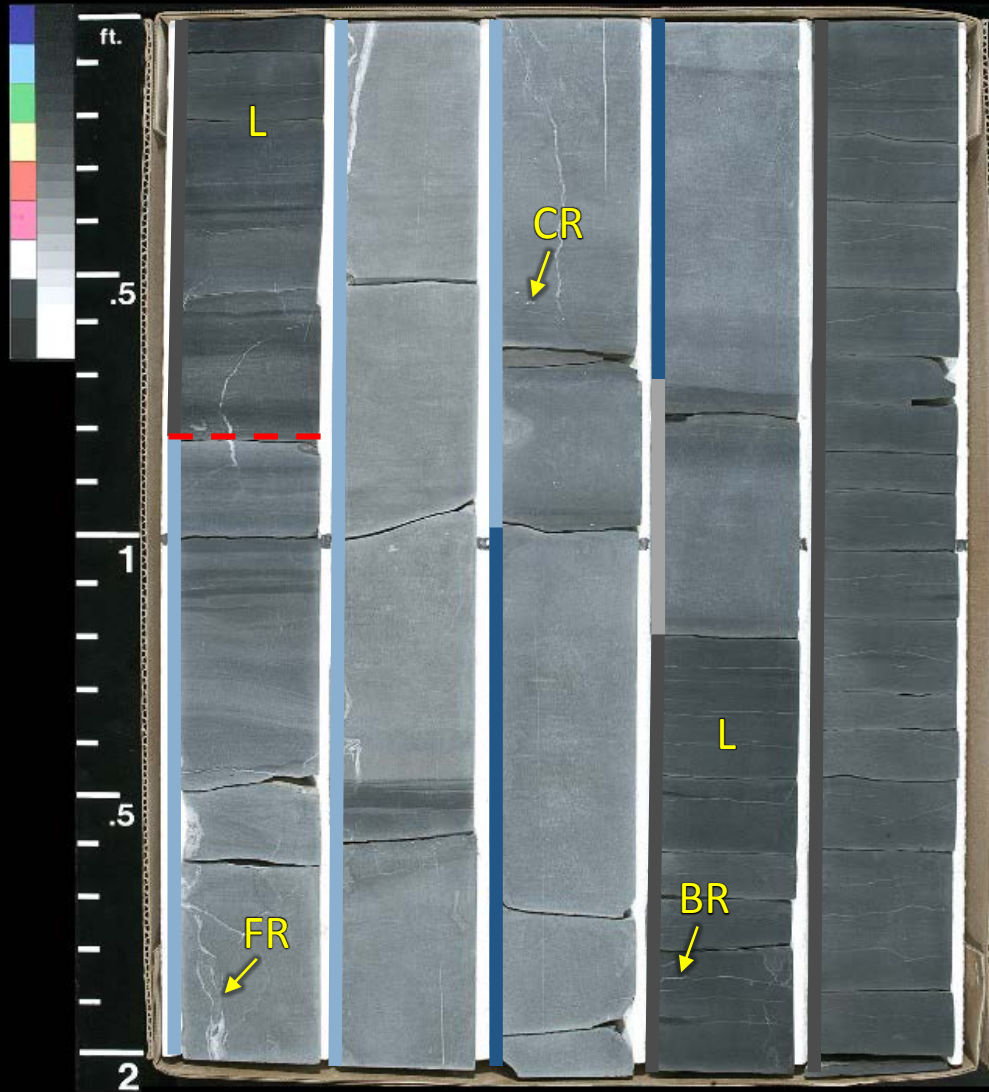


Heavy oil staining throughout interval

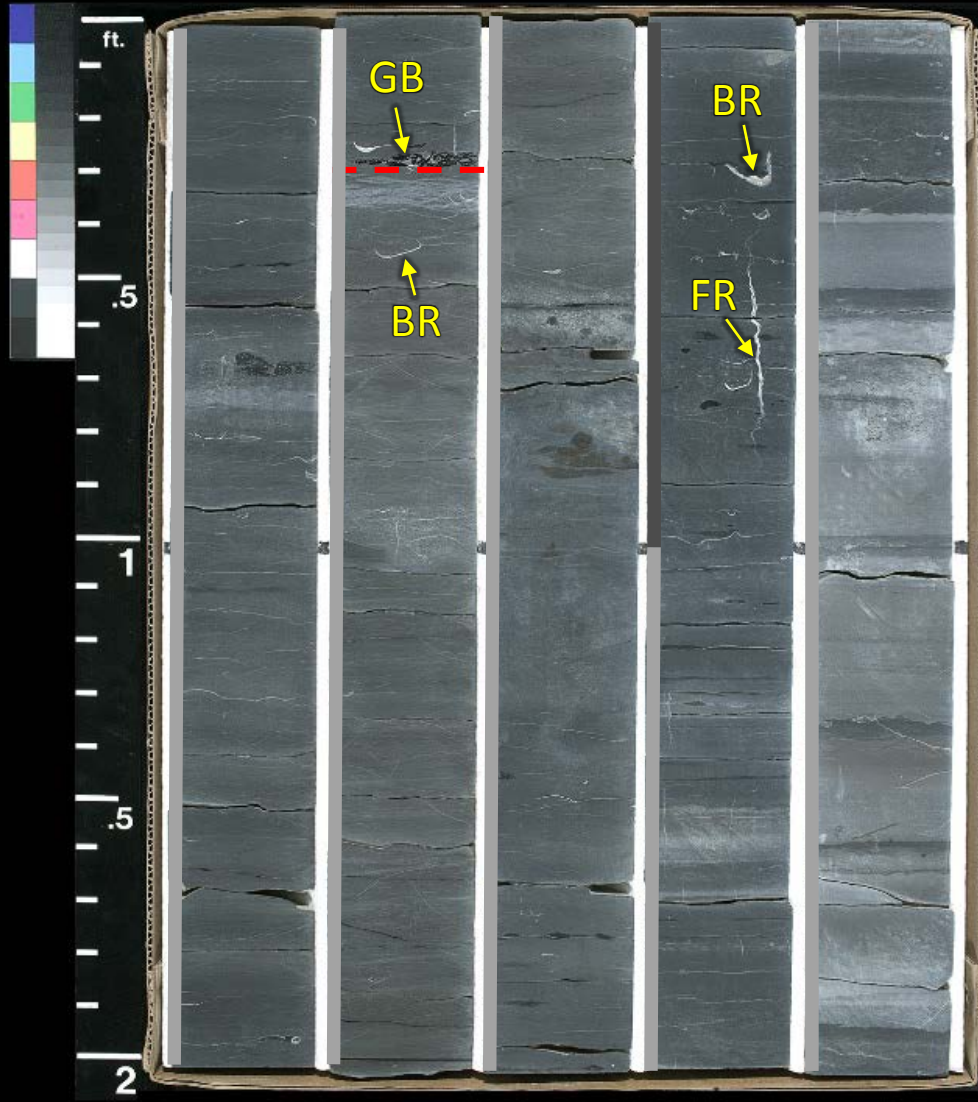
CORE 1 5135 5137 5139 5141 5143



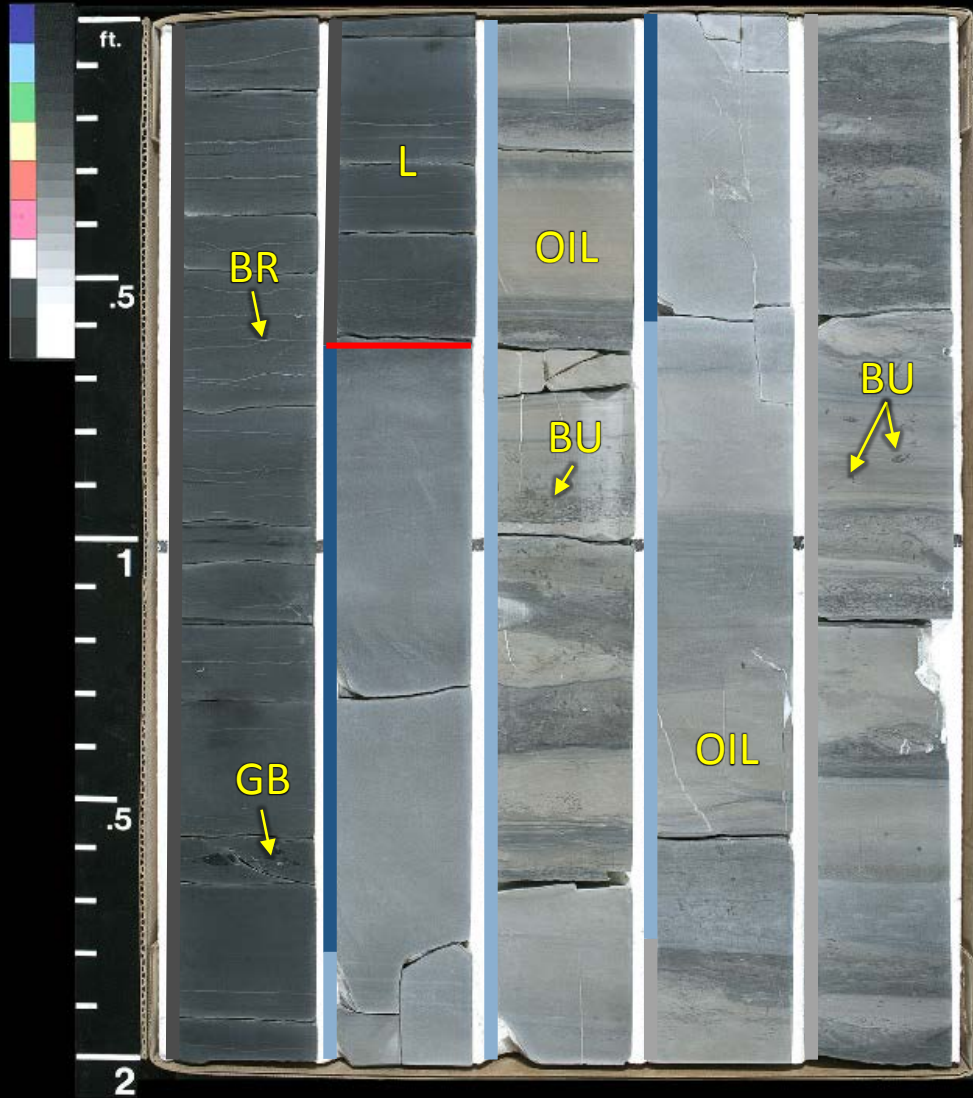
CORE 1 5145 5147 5149 5151 5153



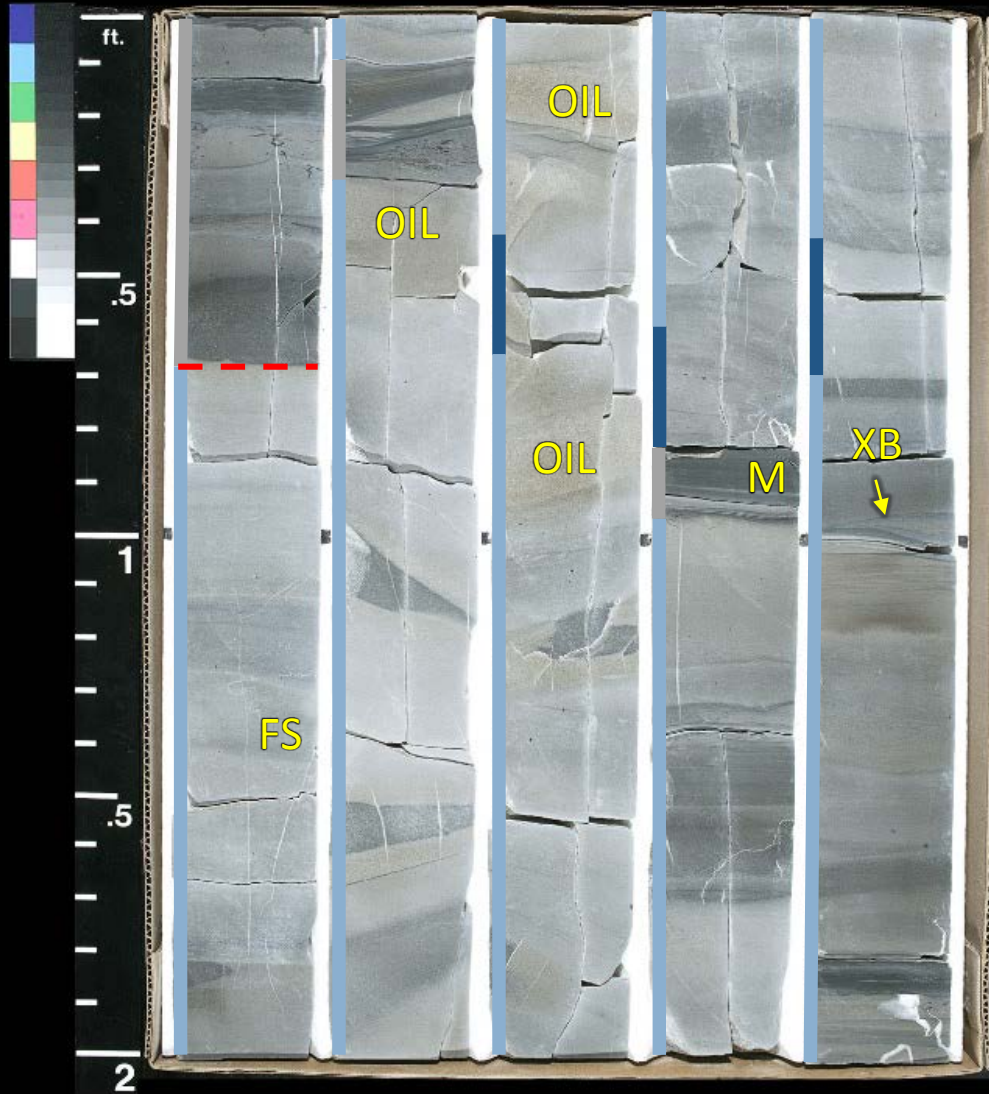
CORE 1 5155 5157 5159 5161 5163



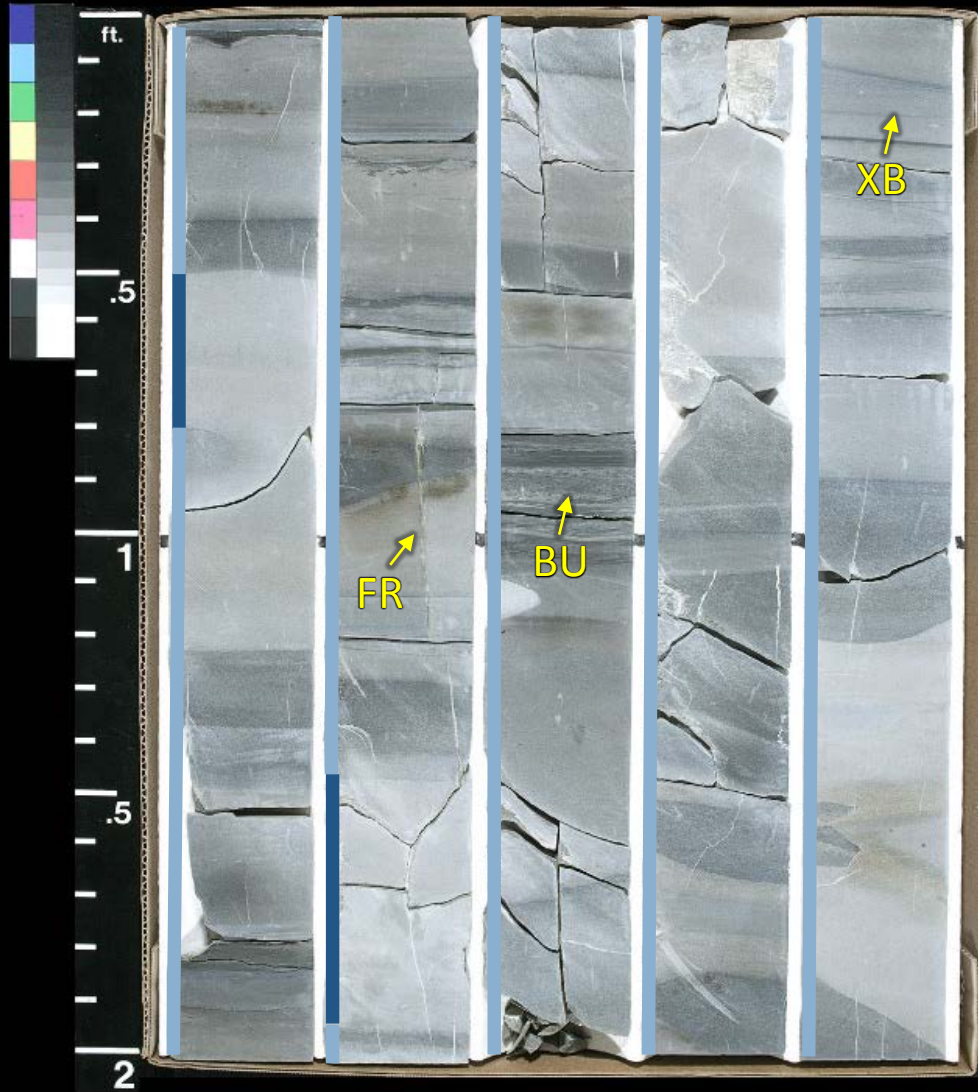
CORE 1 5165 5167 5169 5171 5173



CORE 1 5175 5177 5179 5181 5183



CORE 1 5185 5187 5189 5191 5193



CORE 1

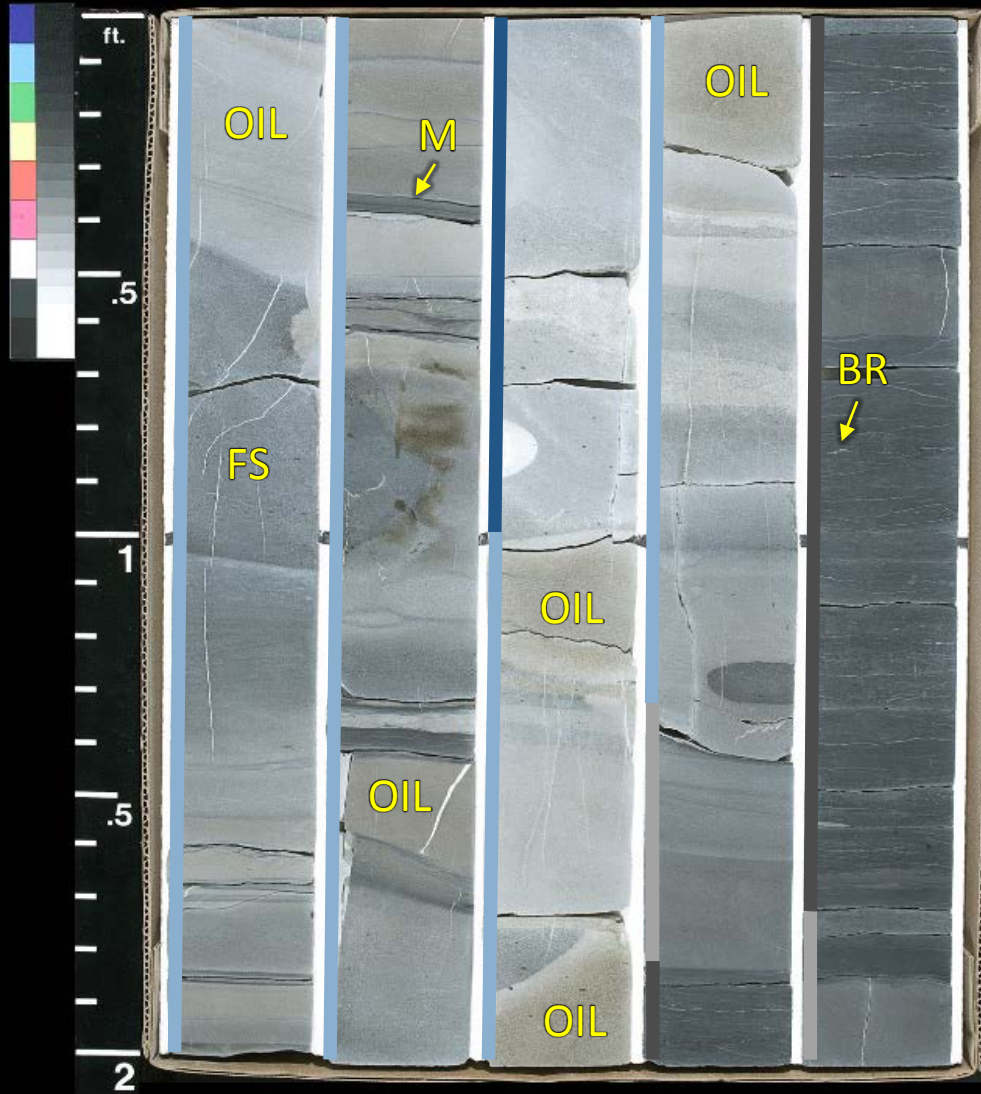
5195

5197

5199

5201

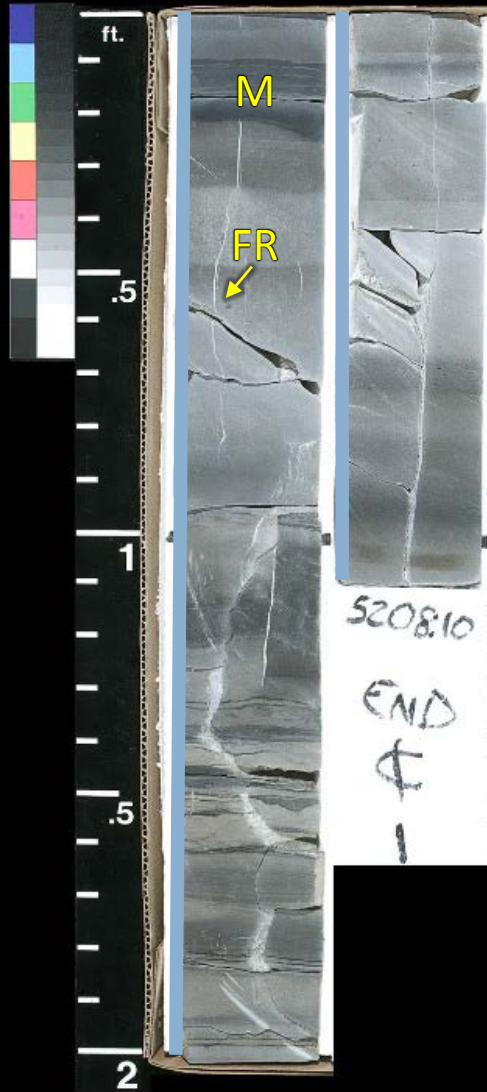
5203



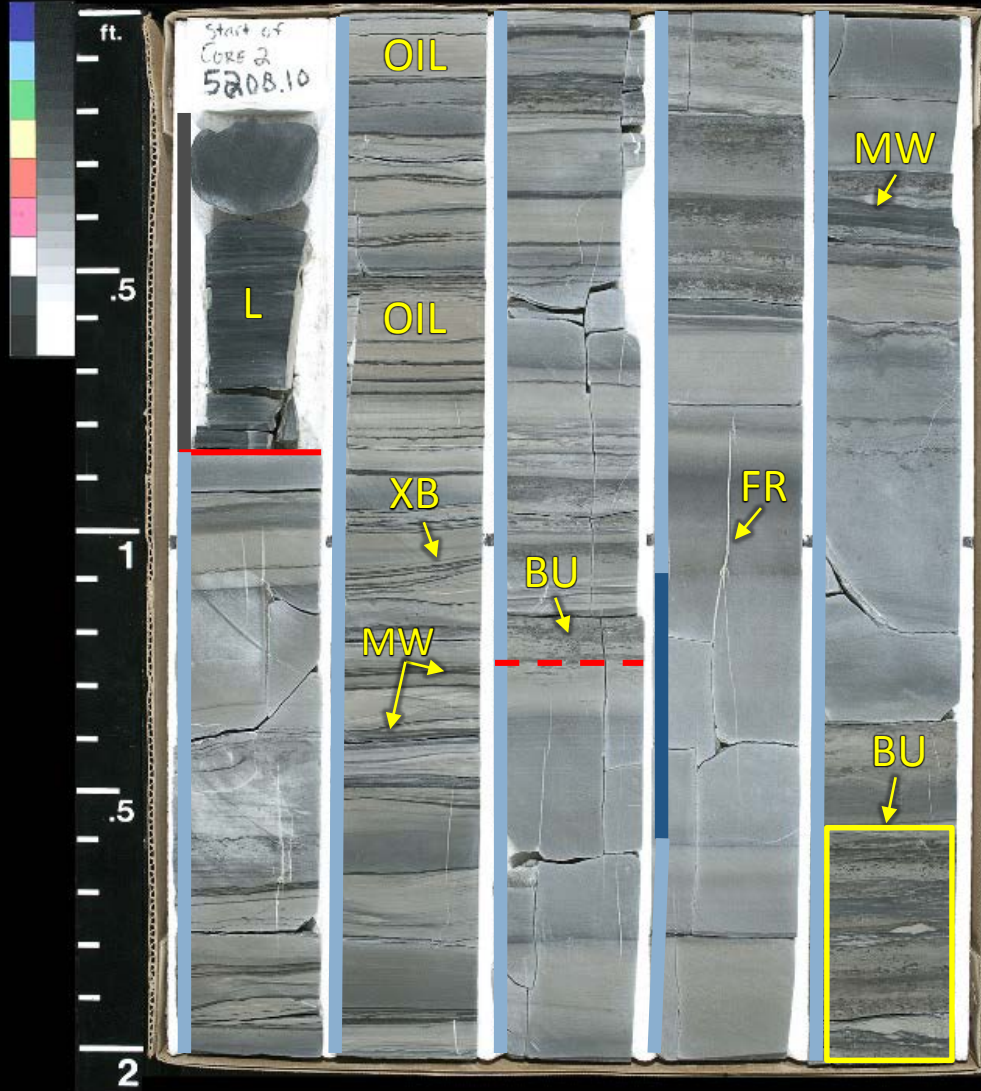
CORE 1

5205

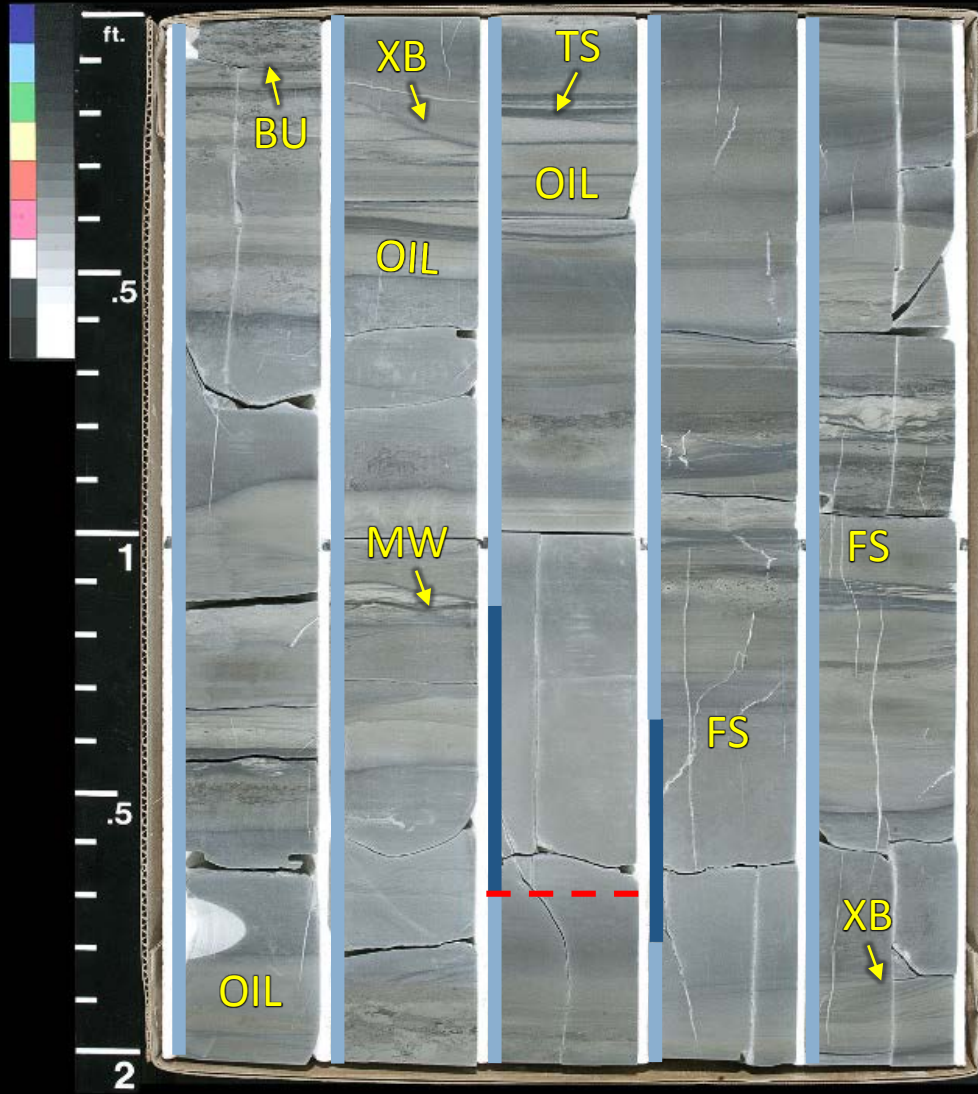
5207



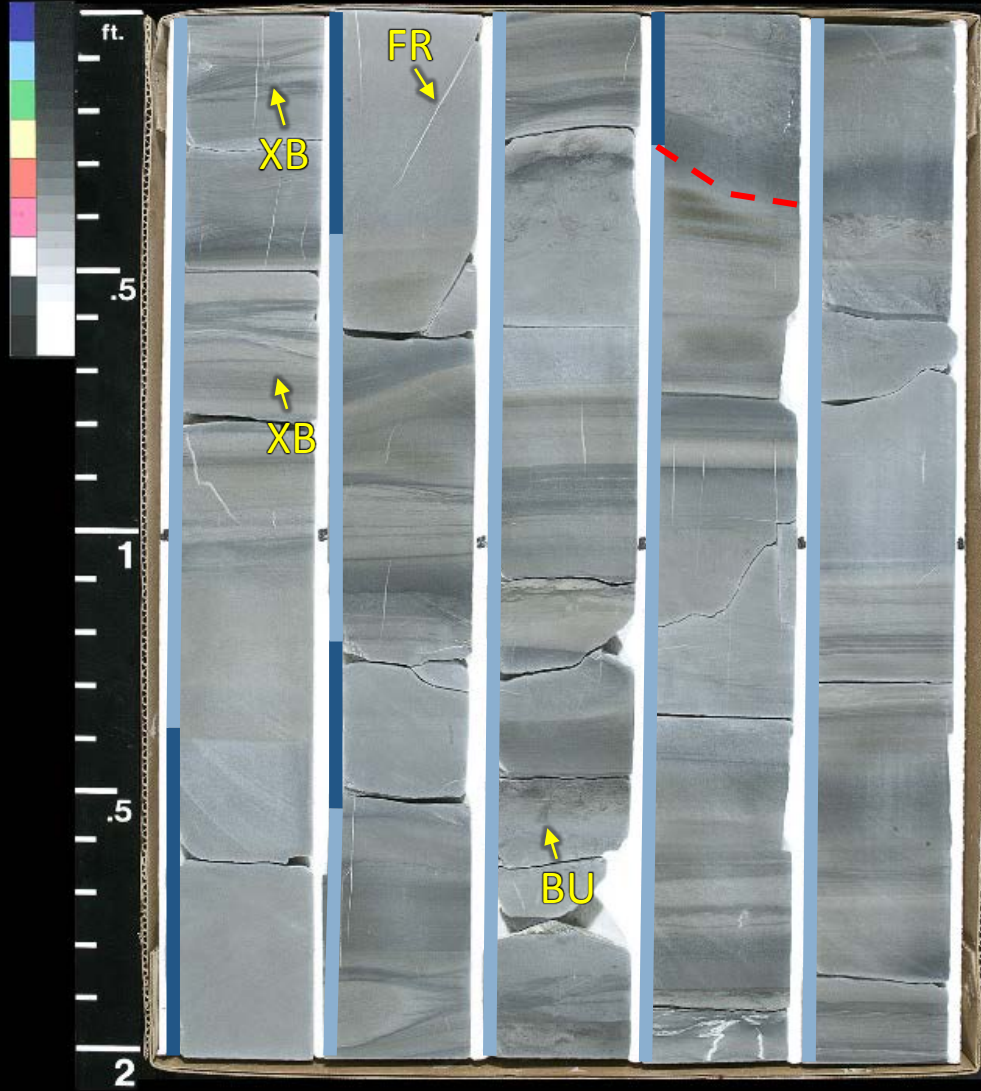
CORE 2 5208 5210 5212 5214 5216



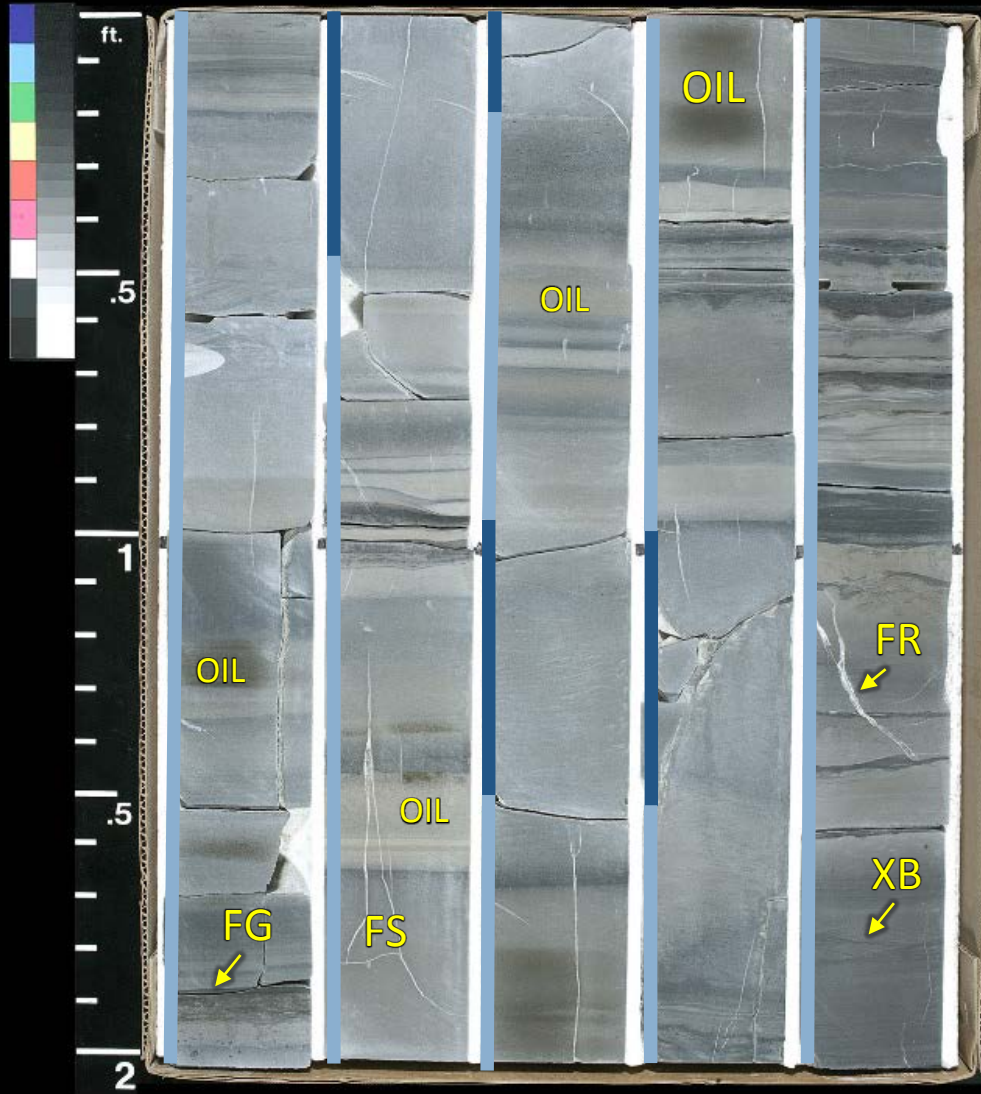
CORE 2 5218 5220 5222 5224 5226



CORE 2 5228 5230 5232 5234 5236



CORE 2 5238 5240 5242 5244 5246



CORE 2

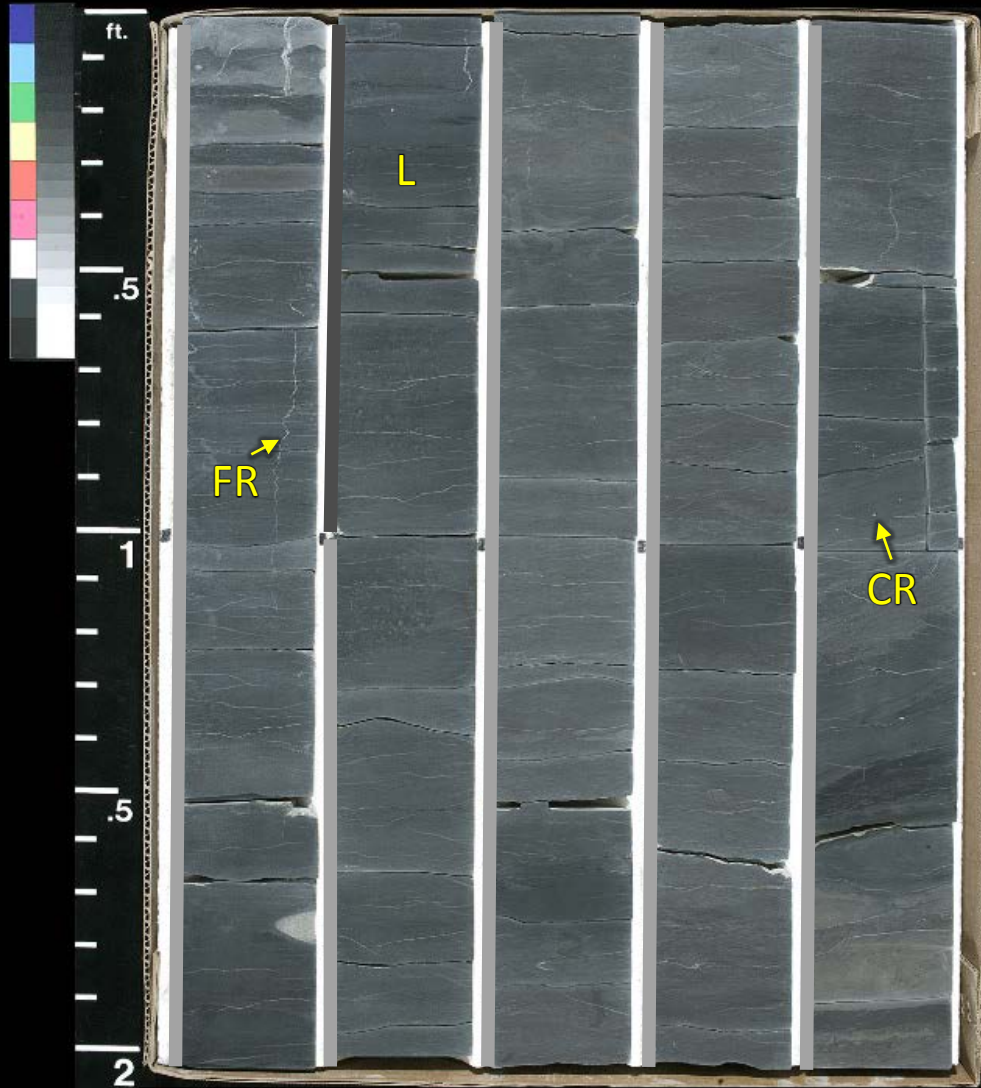
5248

5250

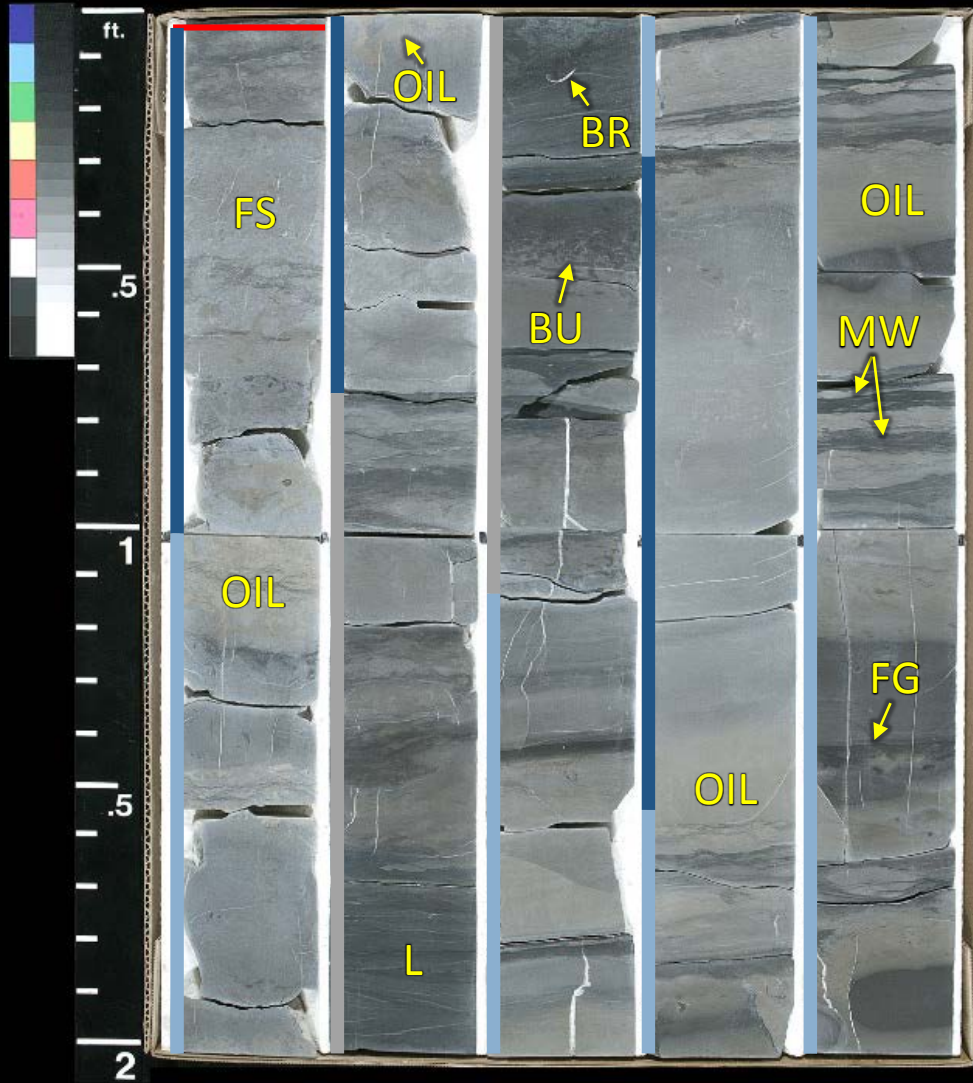
5252

5254

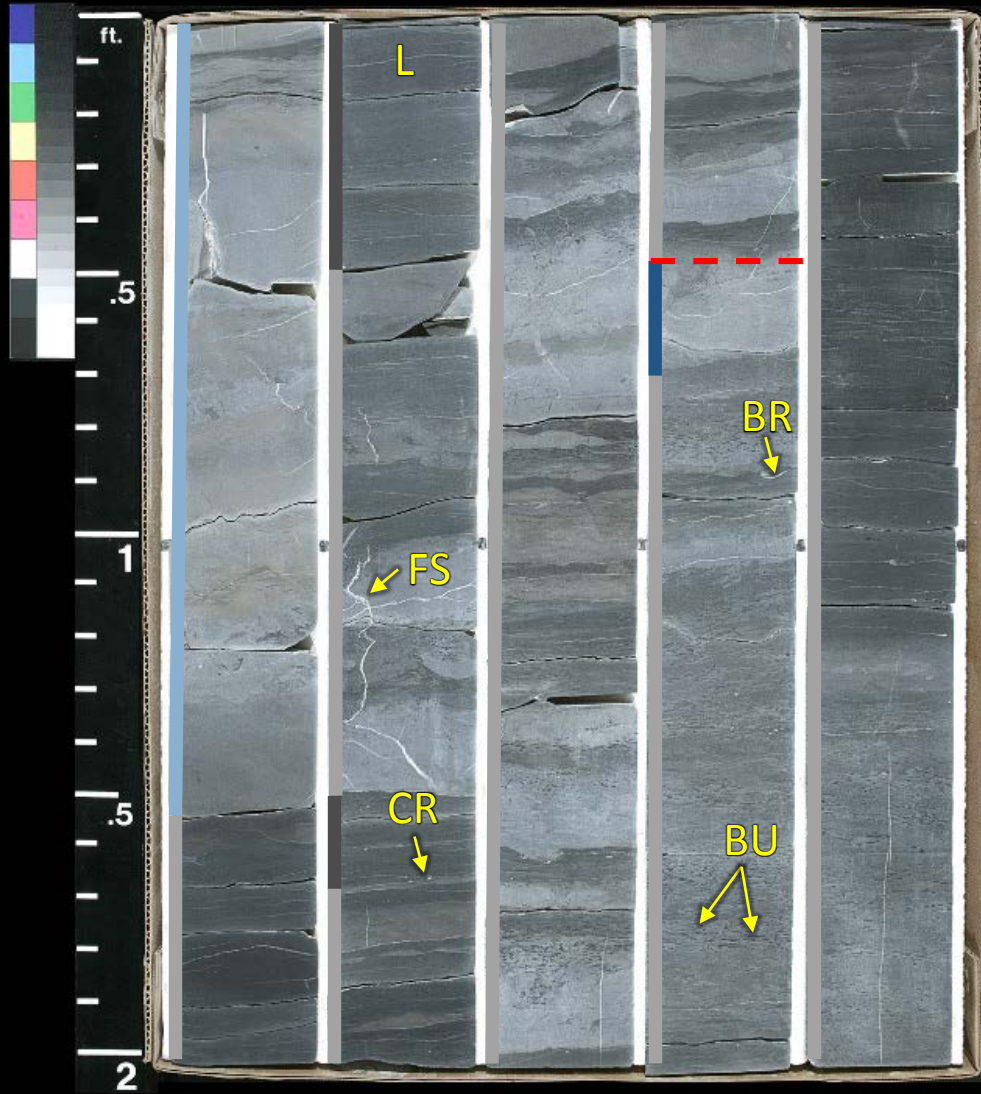
5256



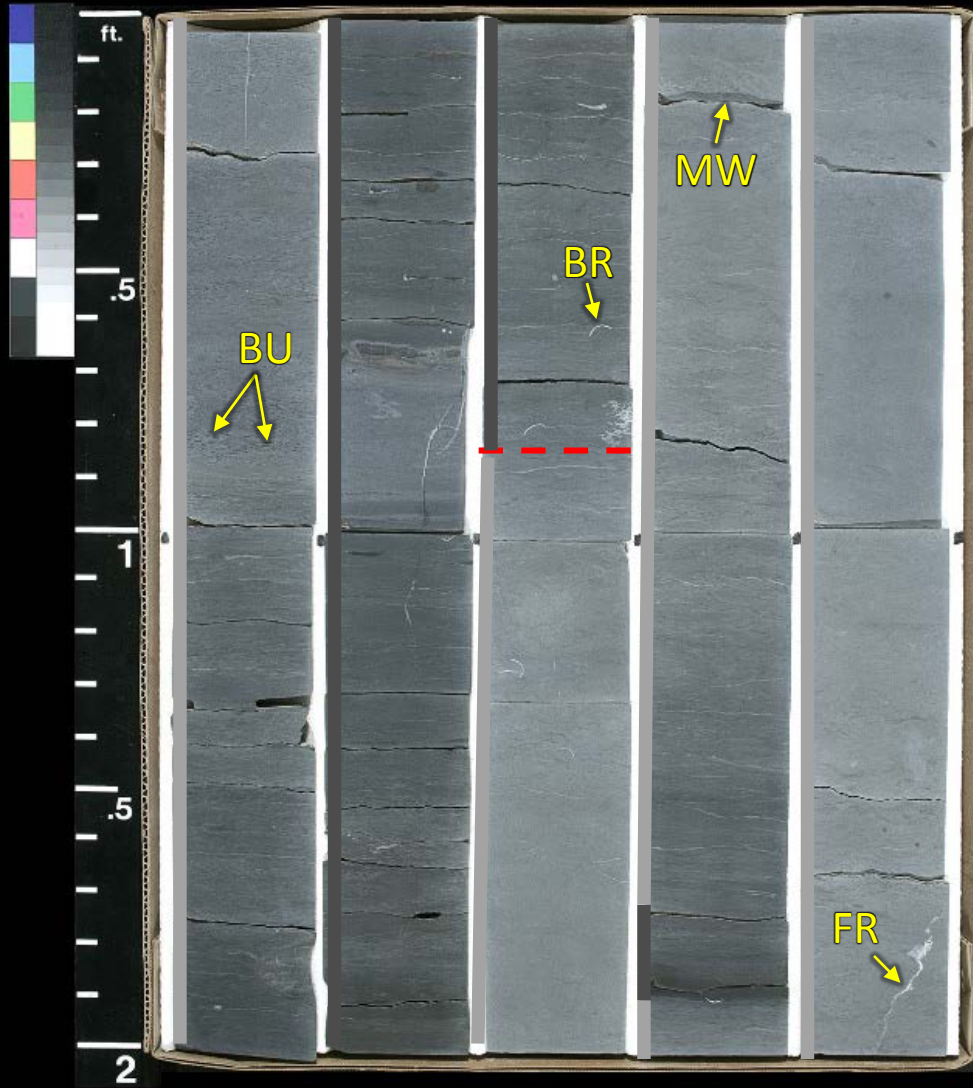
CORE 2 5258 5260 5262 5264 5266



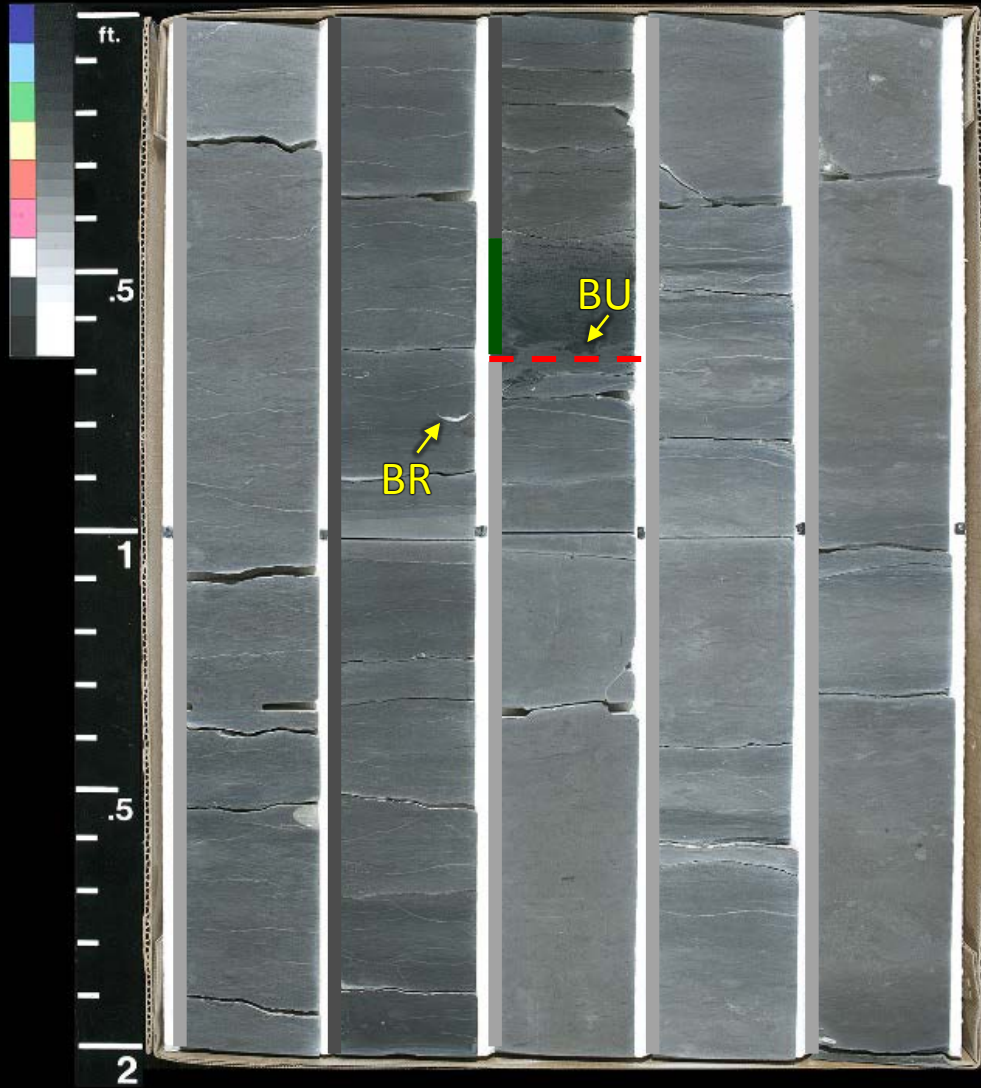
CORE 2 5268 5270 5272 5274 5276



CORE 2 5278 5280 5282 5284 5286



CORE 2 5288 5290 5292 5294 5296



CORE 2

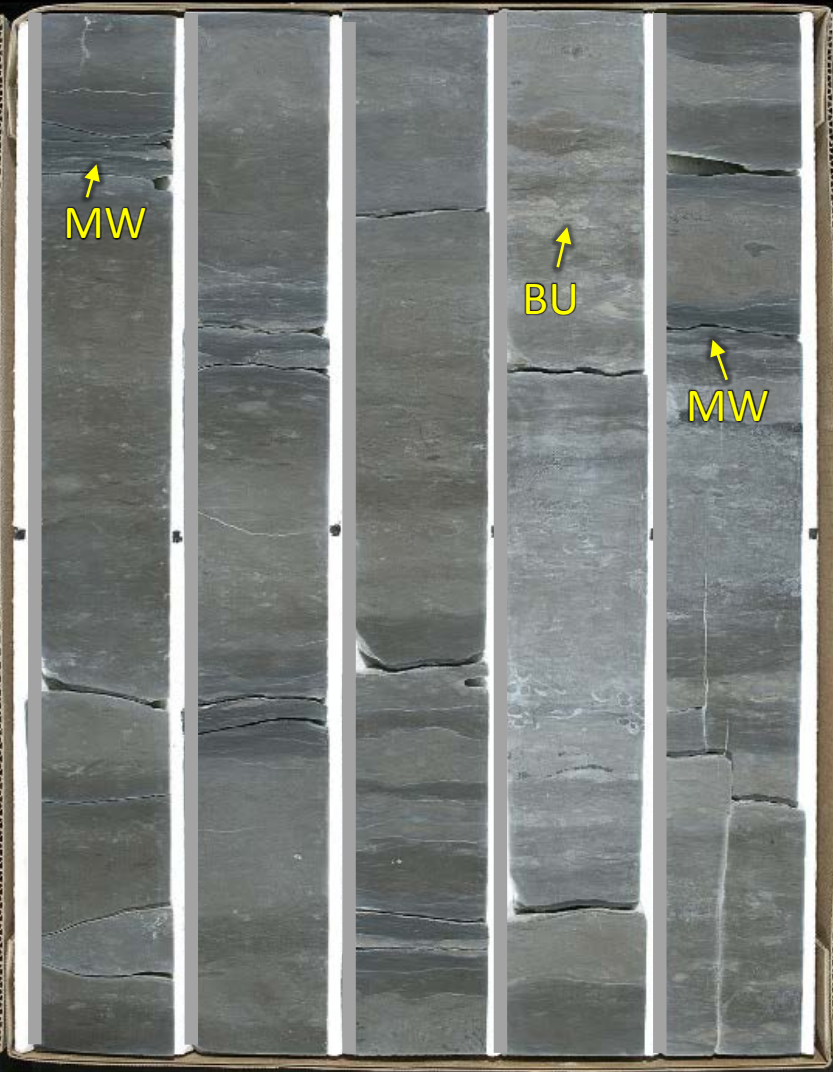
5298

5300

5302

5304

5306

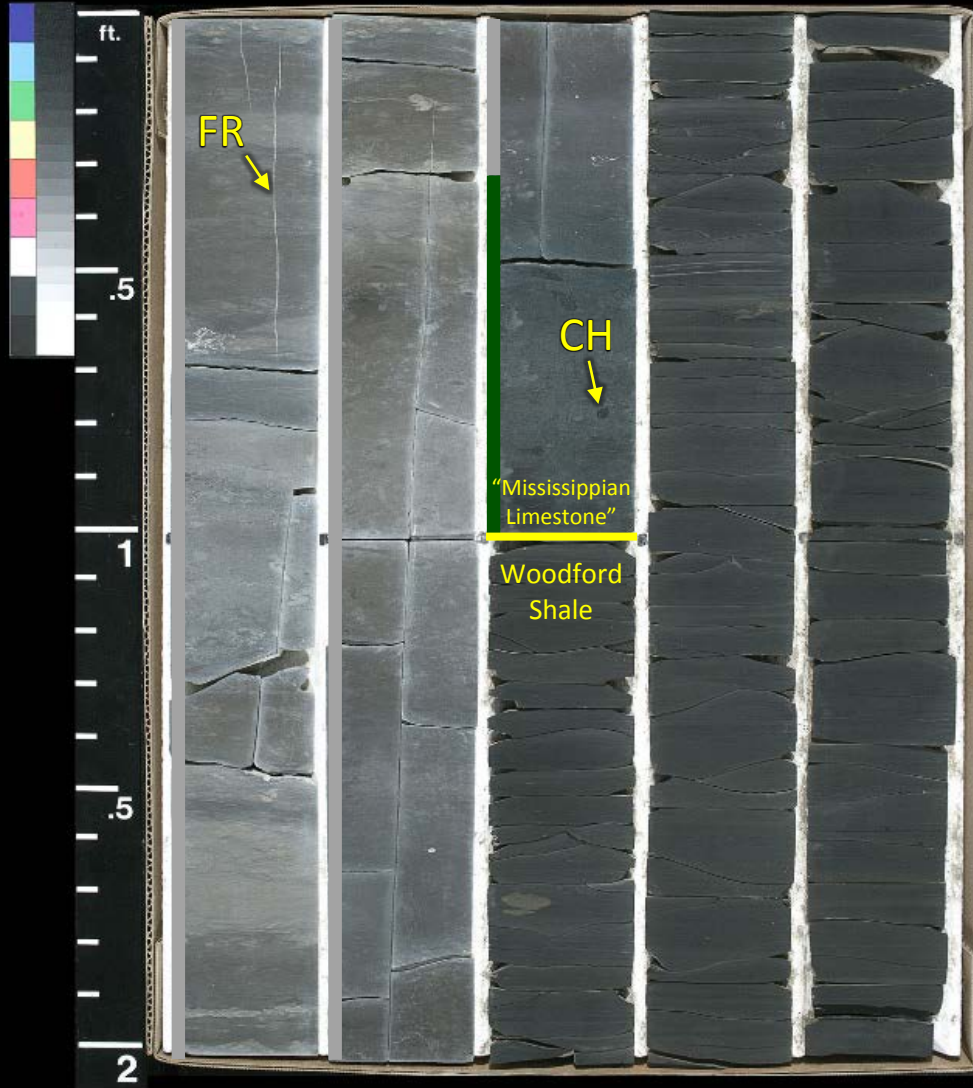


MW

BU

MW

CORE 2 5308 5310 5312 5314 5316



Core #3

Elinore #1-18 SWD

4331

4333

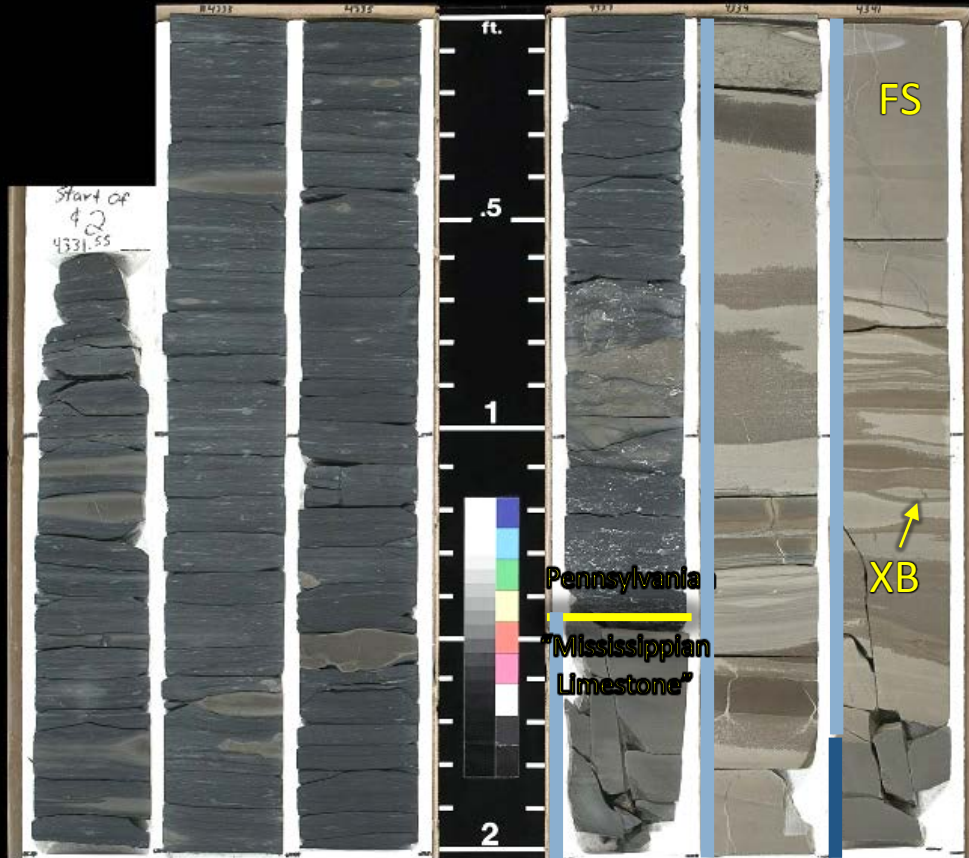
4335

CORE 2

4337

4339

4341



Heavy oil staining throughout interval

4343

4345

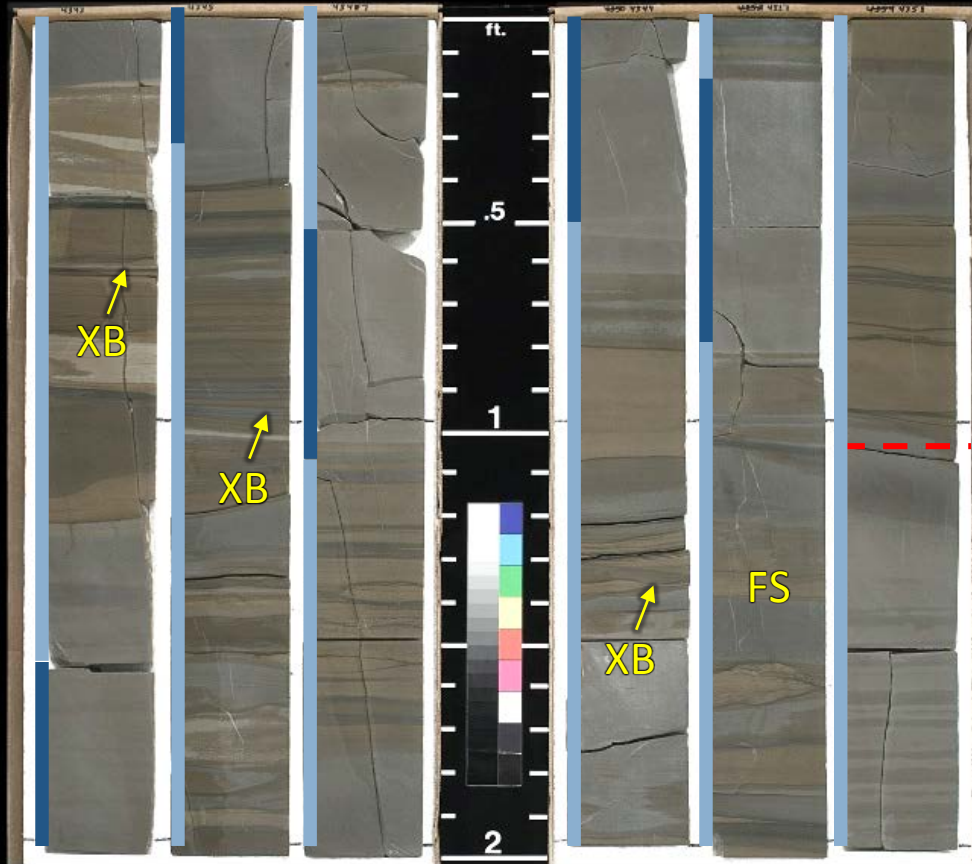
4347

CORE 2

4349

4351

4353



Heavy oil staining throughout interval



Devon Energy Corporation - OKC
Elinore No. 1-18 SWD Well
Logan County, Oklahoma

HH-55430

4355

4357

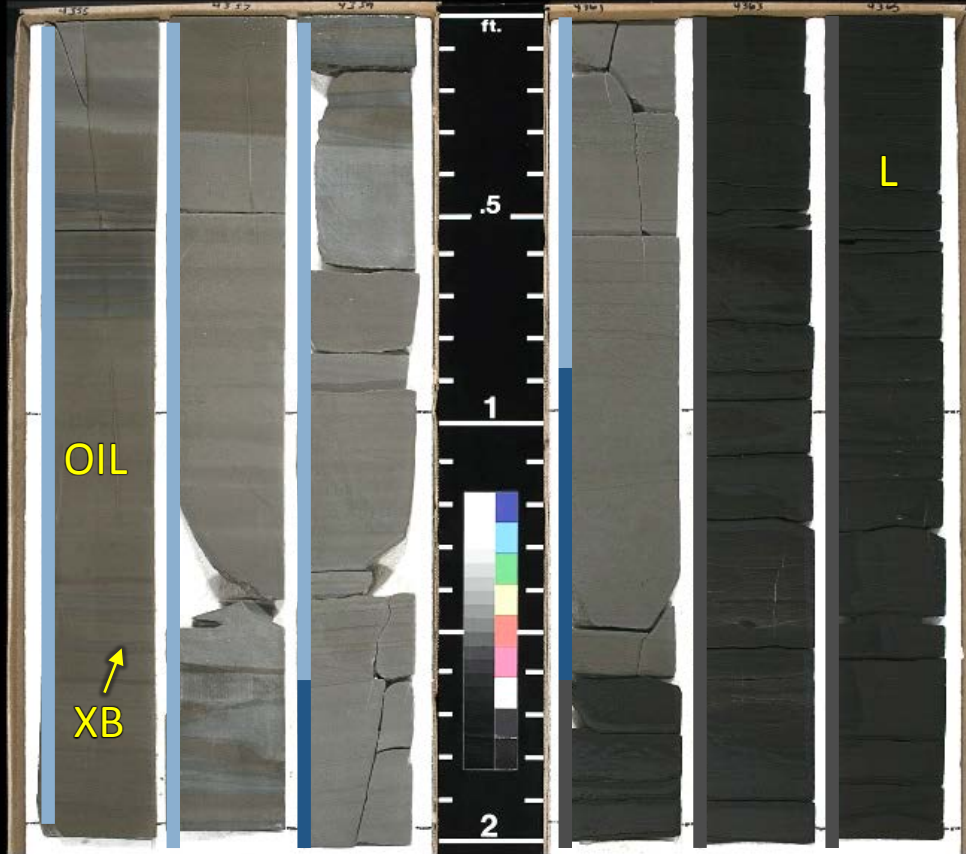
4359

CORE 2

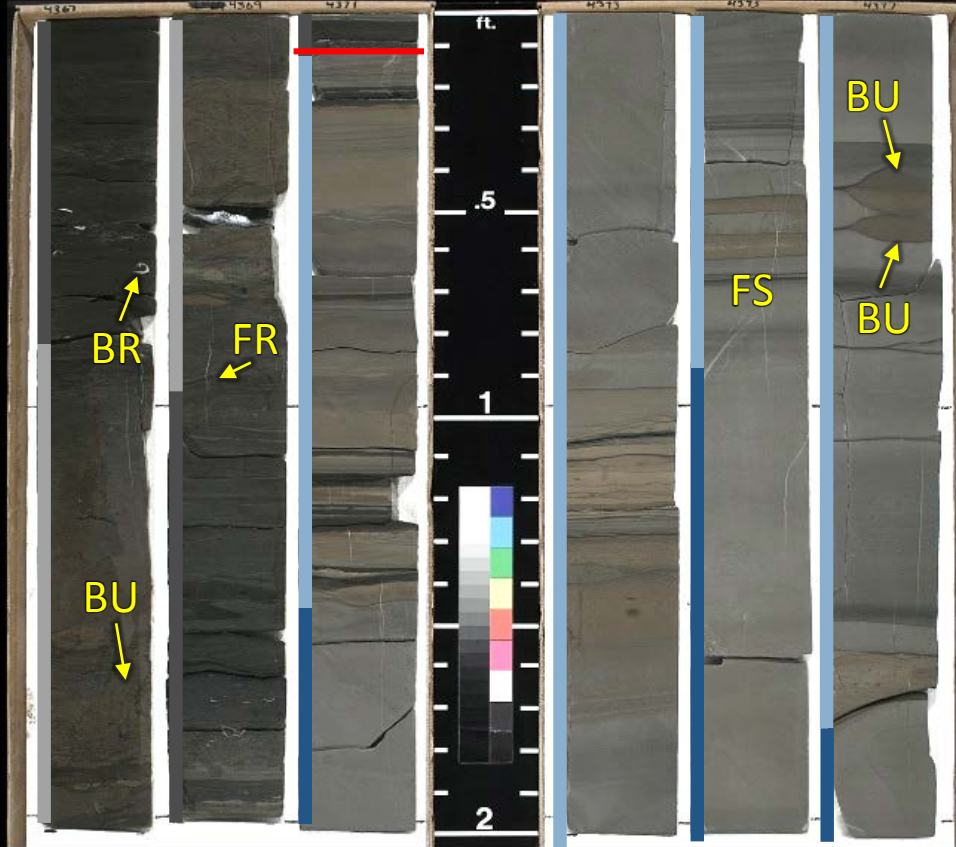
4361

4363

4365



4367 4369 4371 CORE 2 4373 4375 4377



4379

4381

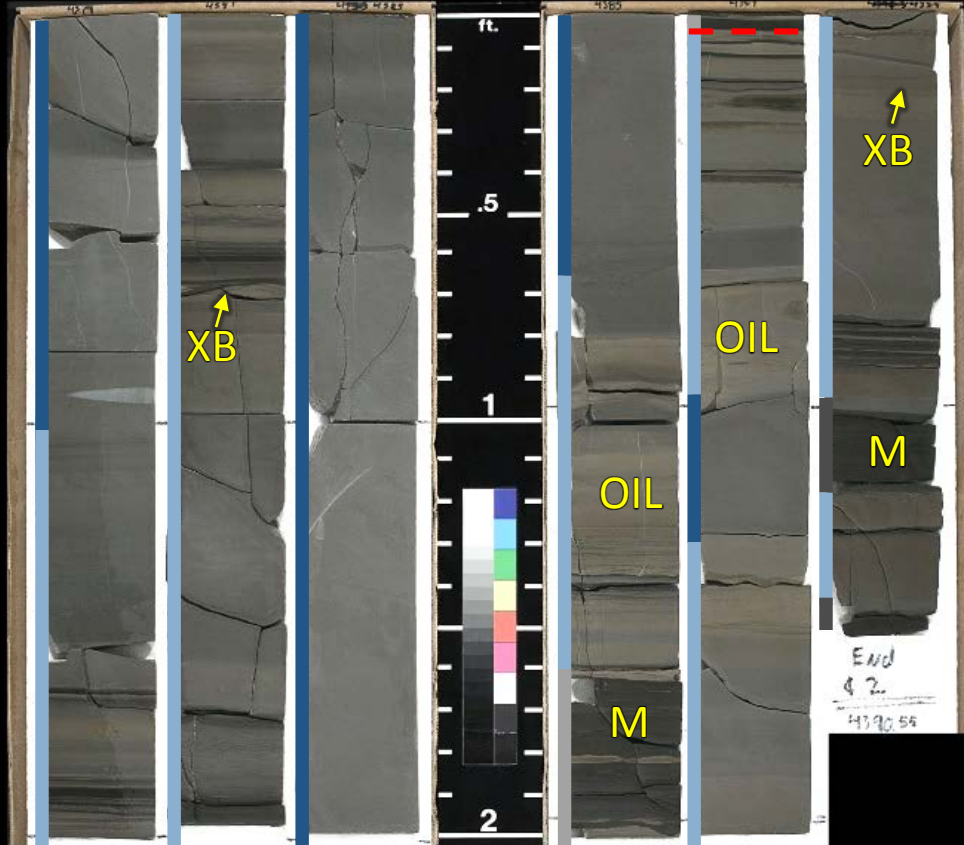
4383

CORE 2

4385

4387

4389



4391

4393

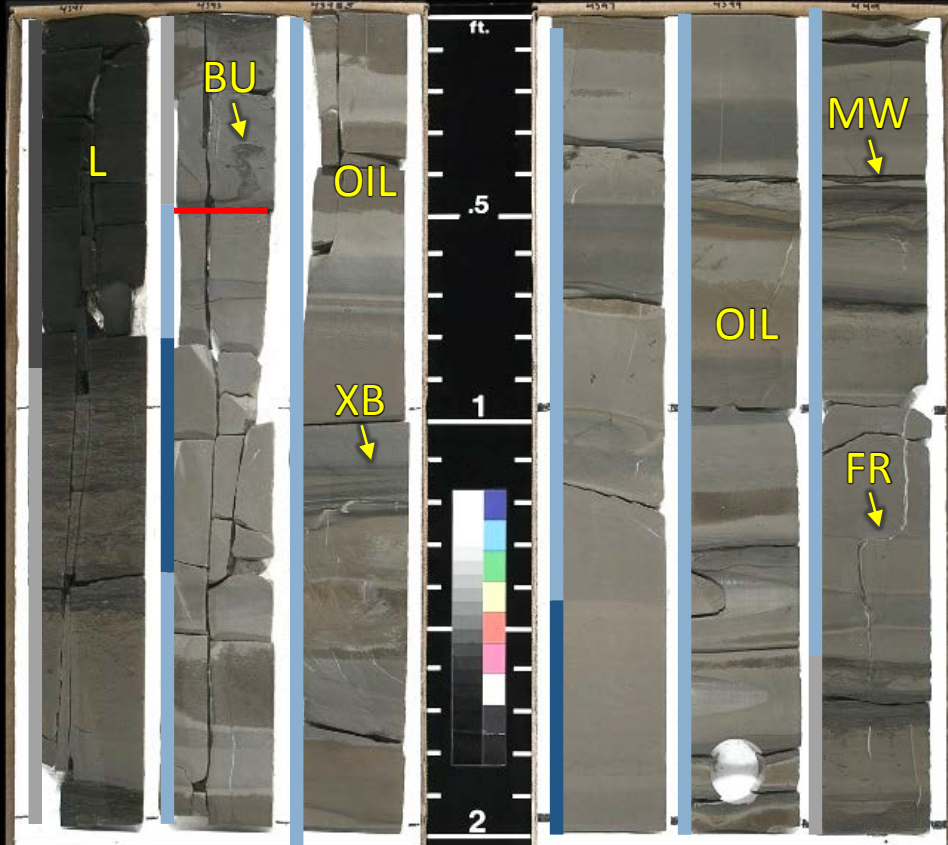
4395

CORE 3

4397

4399

4401



4403

4405

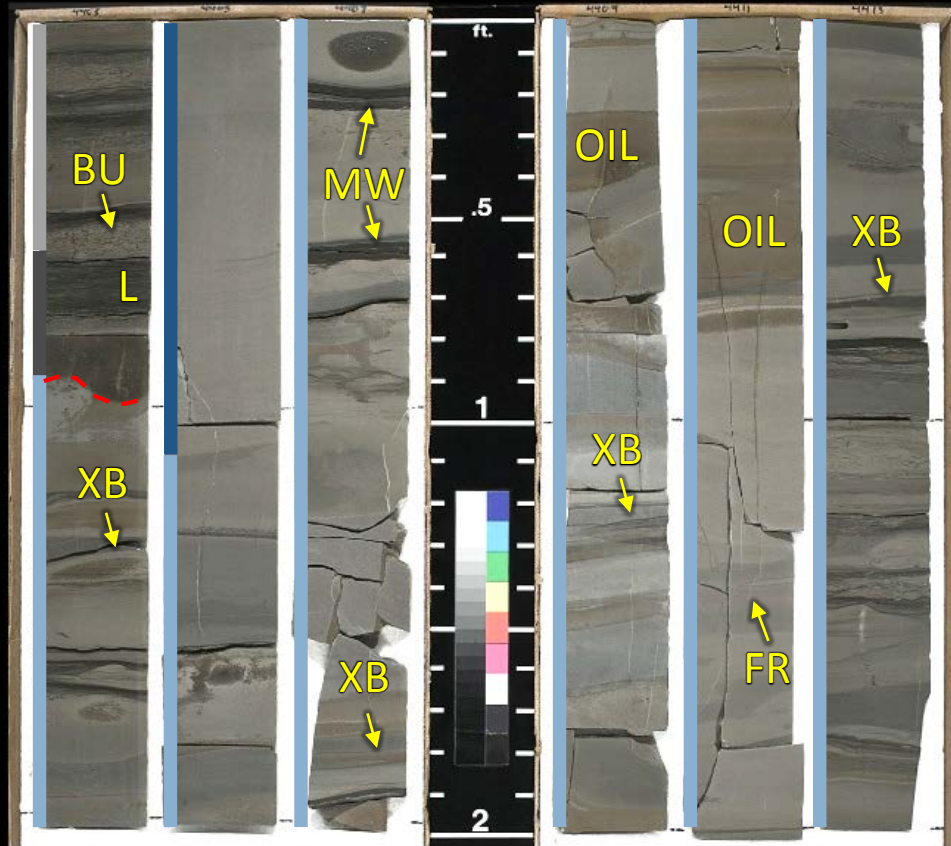
4407

CORE 3

4409

4411

4413



4415

4417

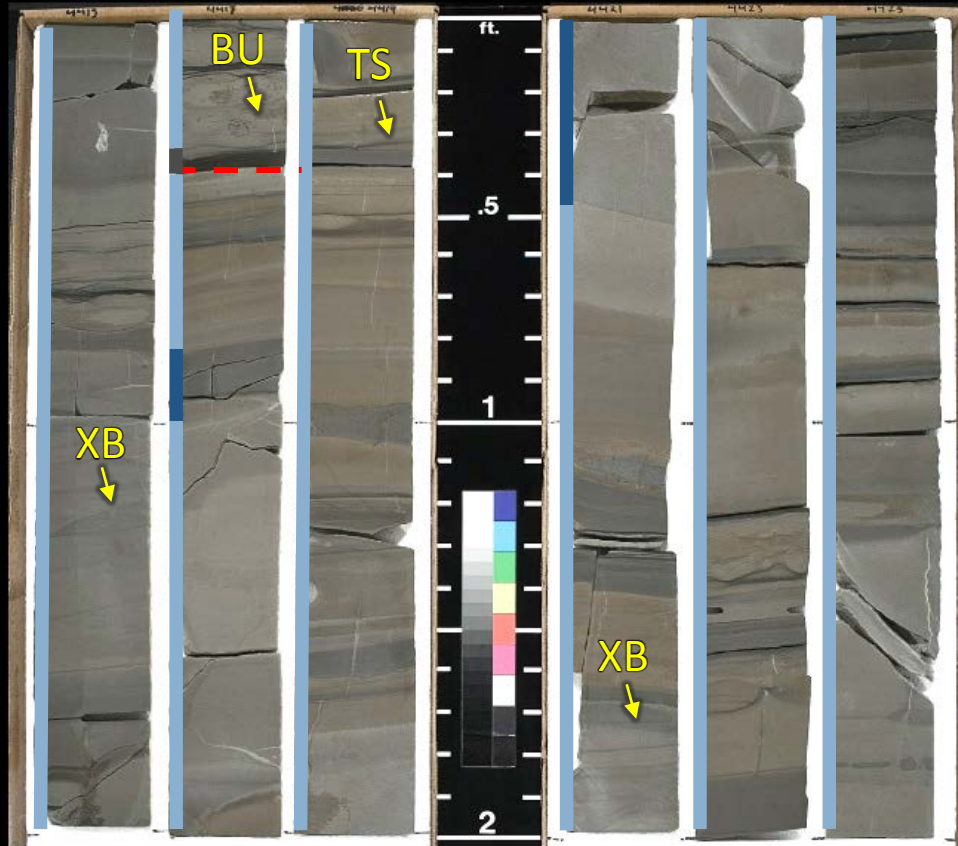
4419

CORE 3

4421

4423

4425



Heavy oil staining throughout interval

4427

4429

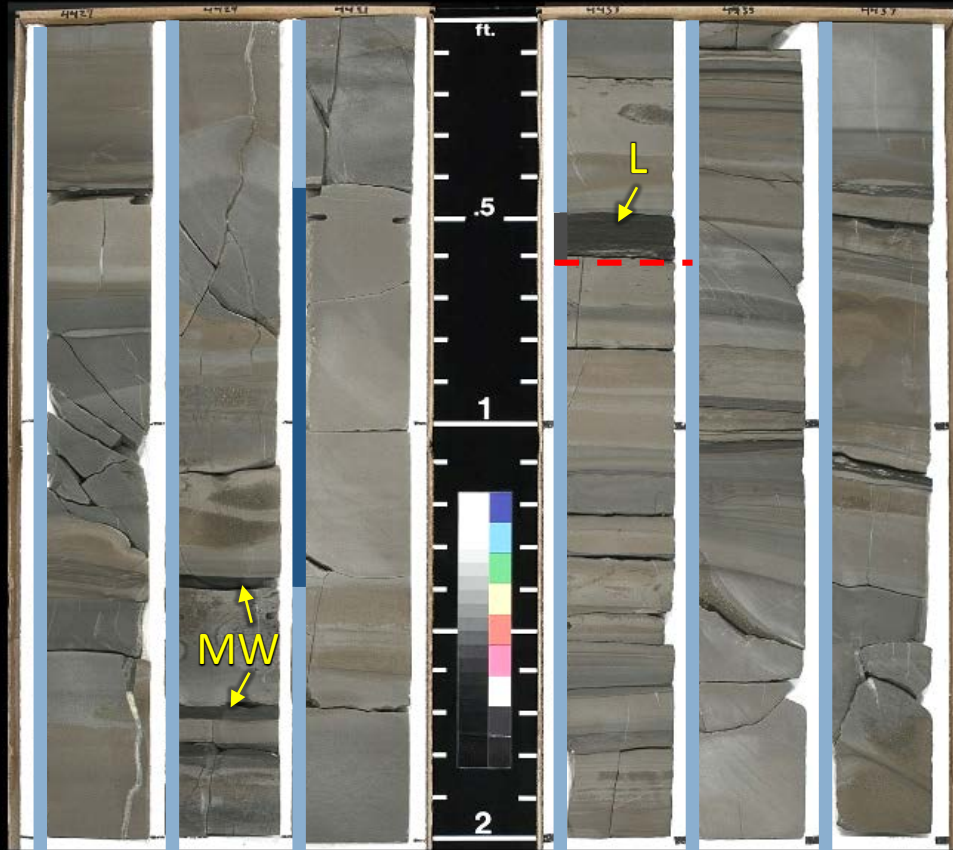
4431

CORE 3

4433

4435

4437



Heavy oil staining throughout interval

4439

4441

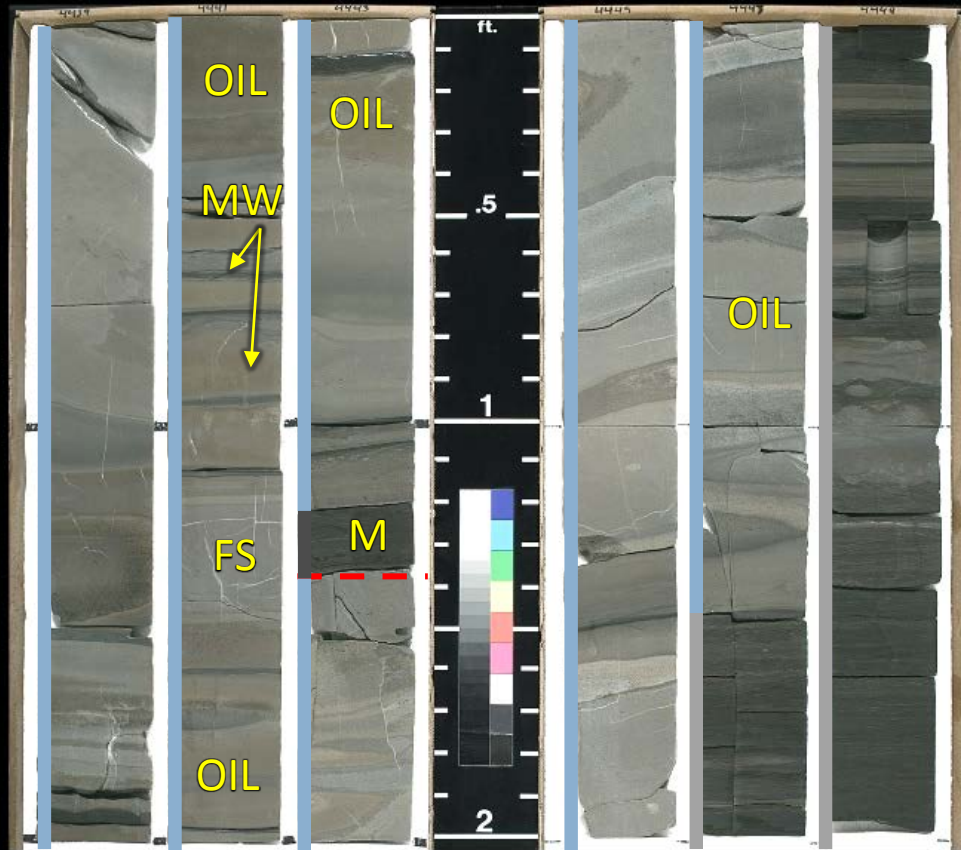
4443

CORE 3

4445

4447

4449





Devon Energy Corporation - OKC
Elinore No. 1-18 SWD Well
Logan County, Oklahoma

HH-55430

4451

4453

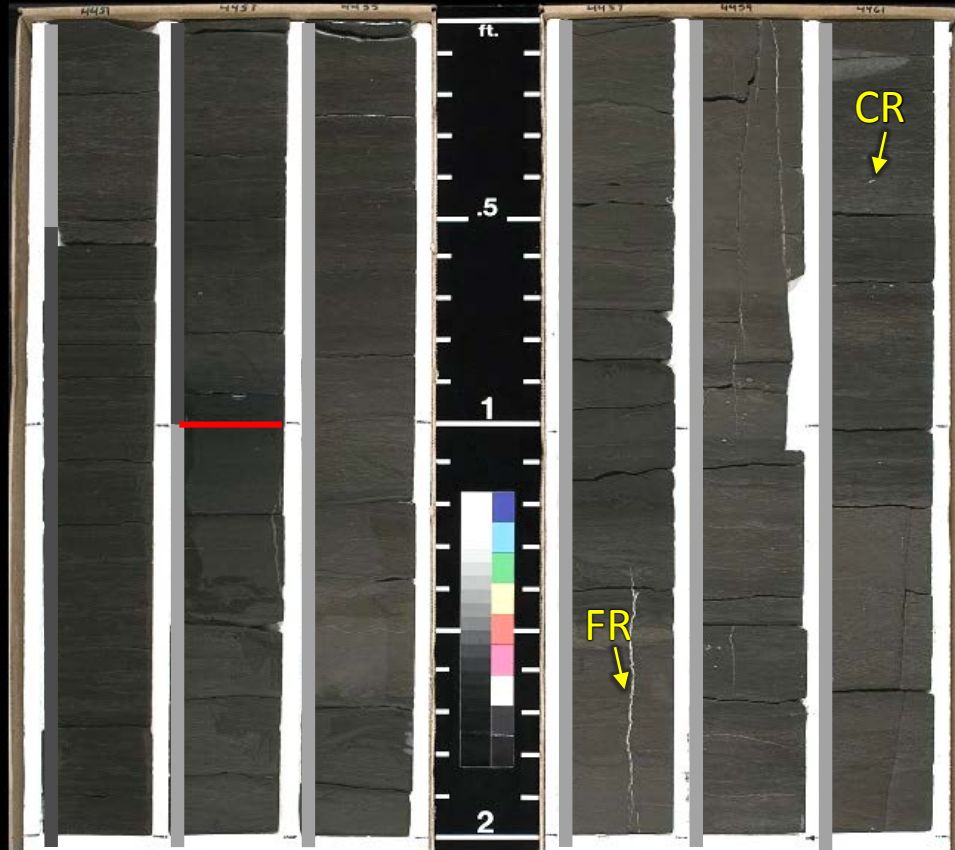
4455

CORE 3

4457

4459

4461



4463

4465

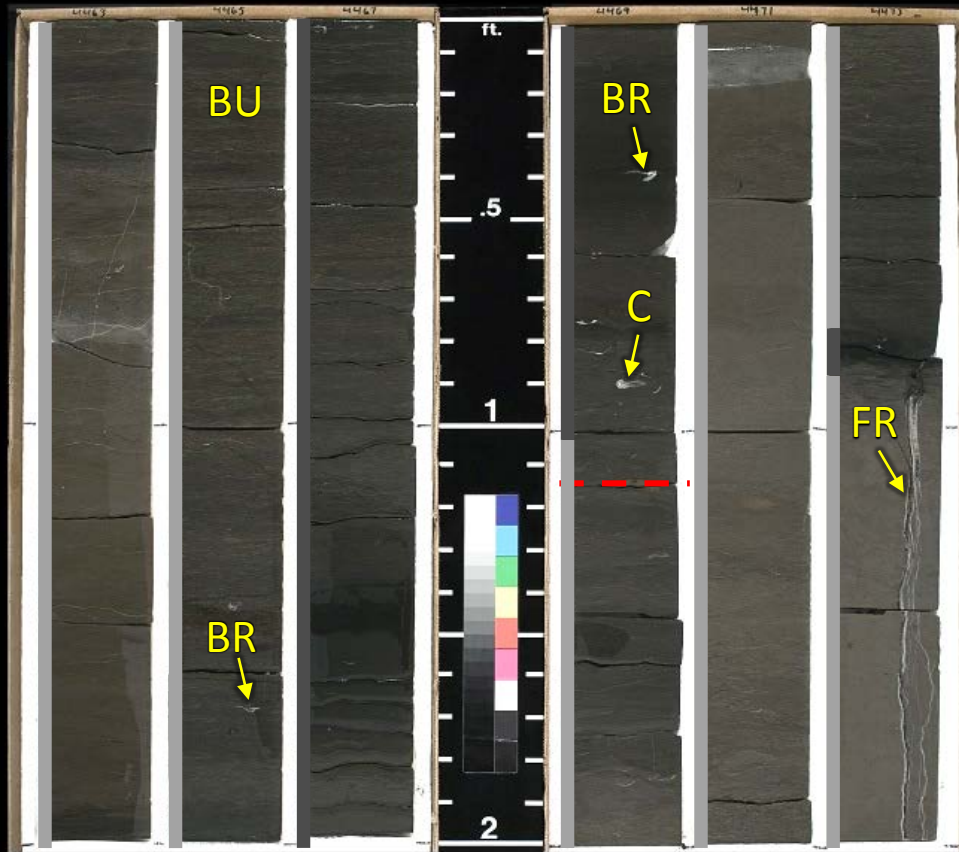
4467

CORE 3

4469

4471

4473



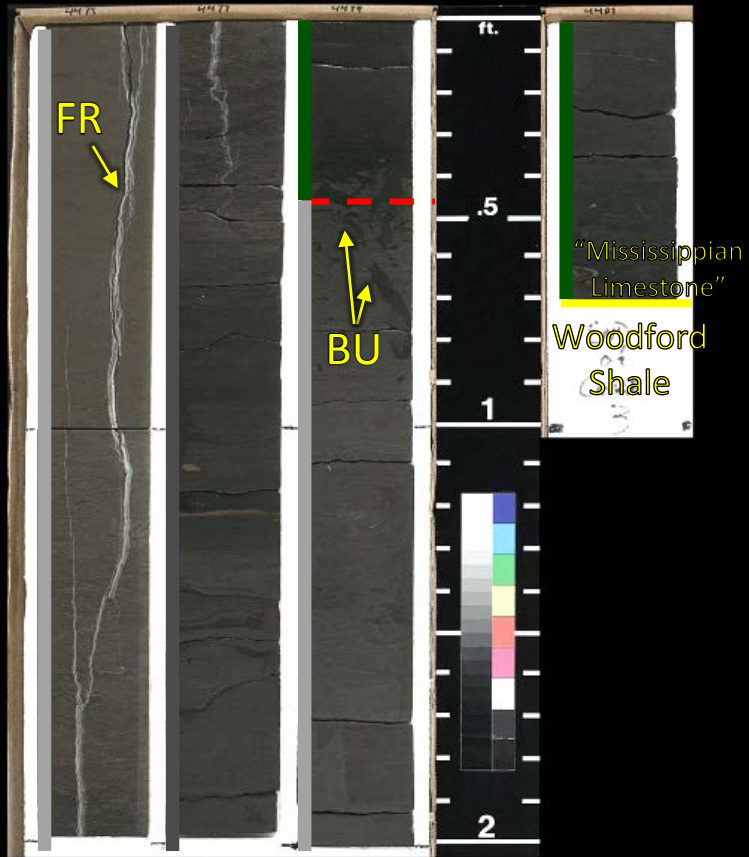
4475

4477

4479

CORE 3

4481



APPENDIX D

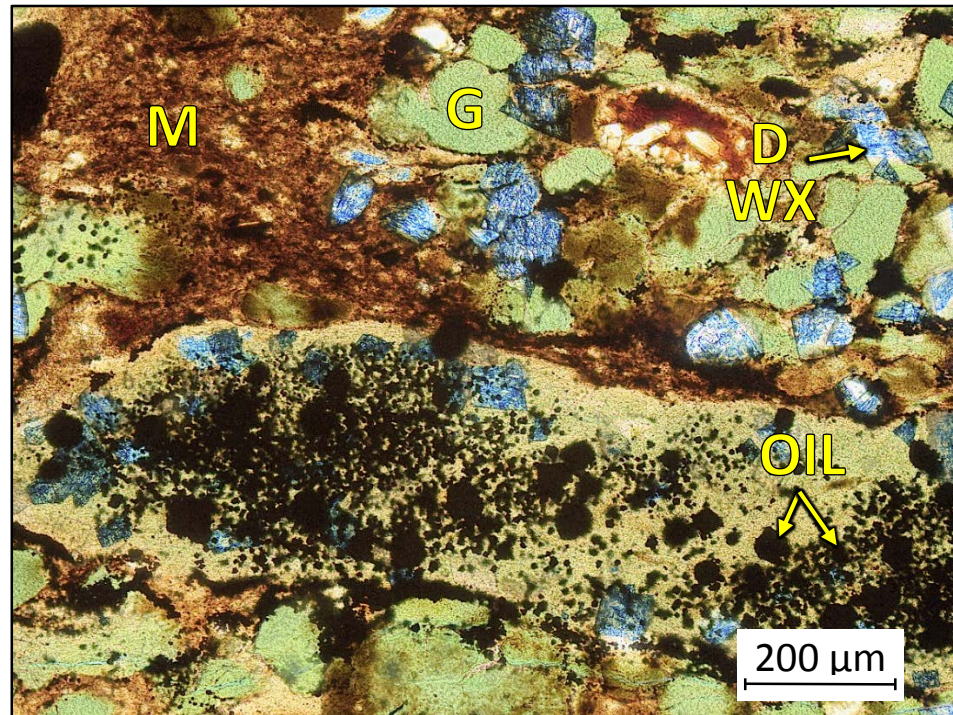
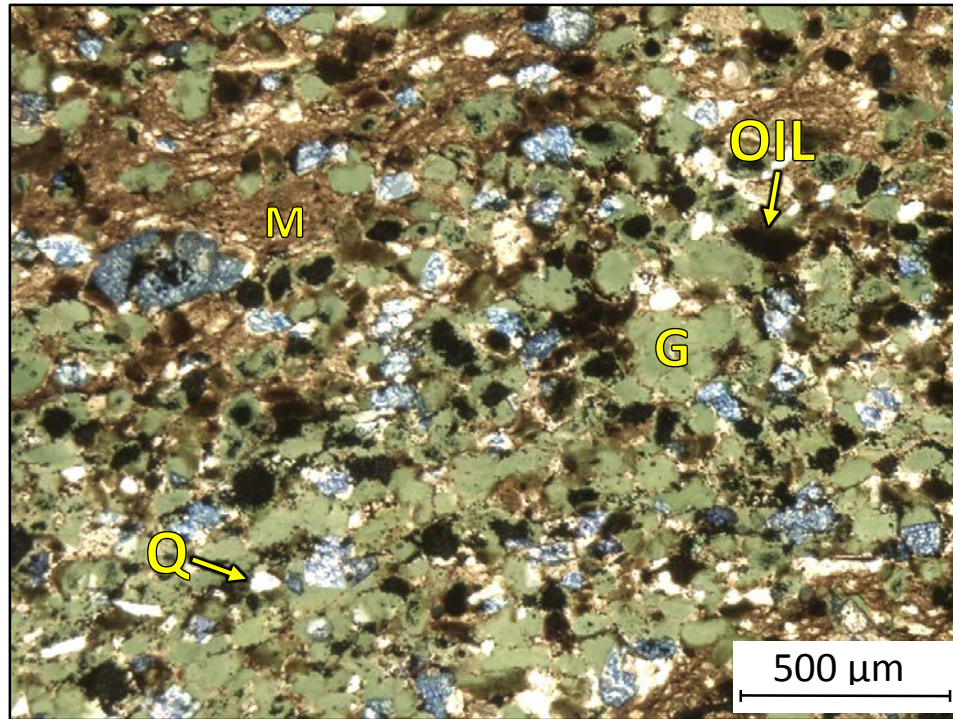
THIN SECTION PHOTOMICROGRAPHS

Thin section photomicrographs show magnified views of core samples. All samples are oriented with the horizontal core axis parallel with the long axis of the photomicrograph. Images are organized by well and show samples from deepest to shallowest. All samples are shown in plane polarized light (unless otherwise noted) and labeled using the key outlined below. Multiple photographs are shown for each thin section sample at different scales.

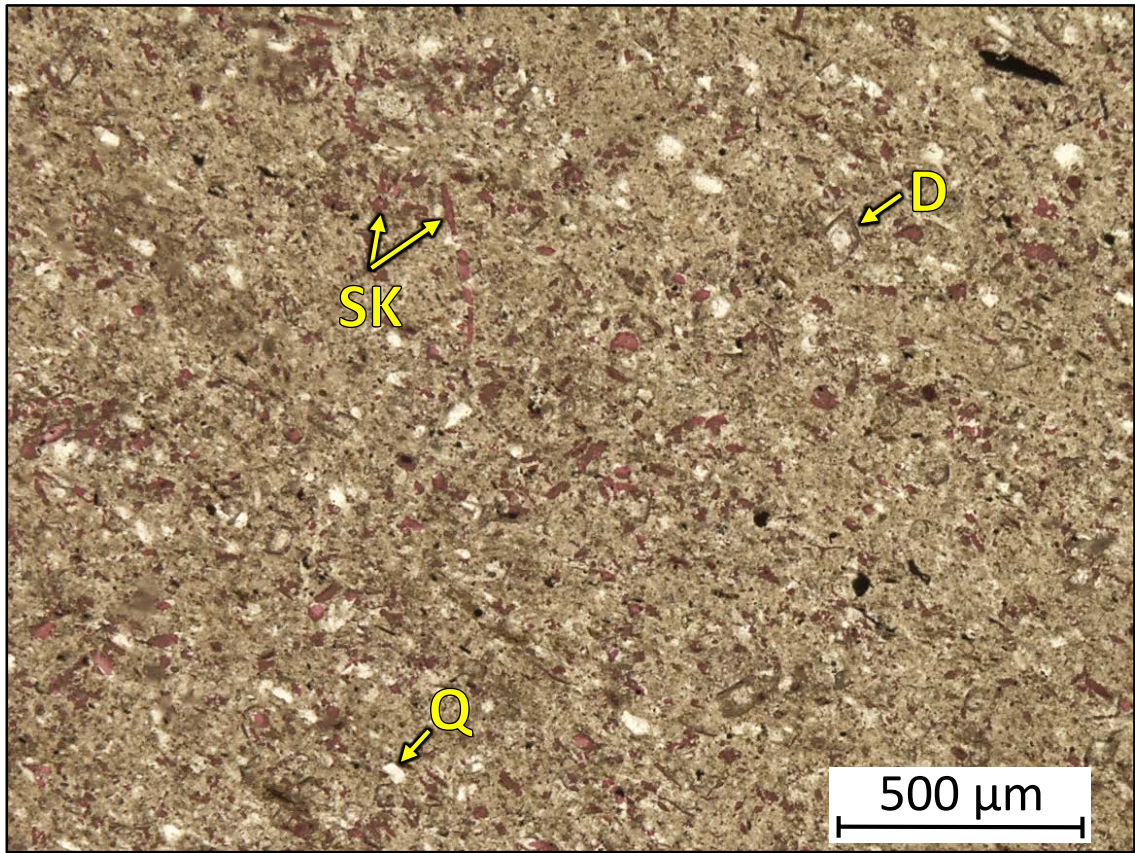
Core and Thin Section Image Labels							
Feature Key					Porosity Key		
BF	bone fragment	GB	grain bed	PY	pyrite	FR	fracture
BR	brachiopod	GST	gastropod	Q	quartz	IP	interparticle
BU	burrow	HCS	hummocky cross stratification	S	stylolite	IX	intercrystalline
BY	bryozoan	IC	intraclast	SK	undifferentiated skeletal fragments	MO	moldic
C	coral	L	lamination	SP	spicule	VU	vug
CH	chert	M	mud/mudstone	TS	truncation surface	WP	intraparticle
CON	conodont	ME	micritic envelope	XB	cross-bedding	WX	intracrystalline
CR	crinoid	MW	mud whisp				
D	dolomite	O	ostracode				
FG	firm ground	OIL	oil/dead oil				
FR	fracture	P	peloid				
G	glauconite	PH	phosphate				

Core #1

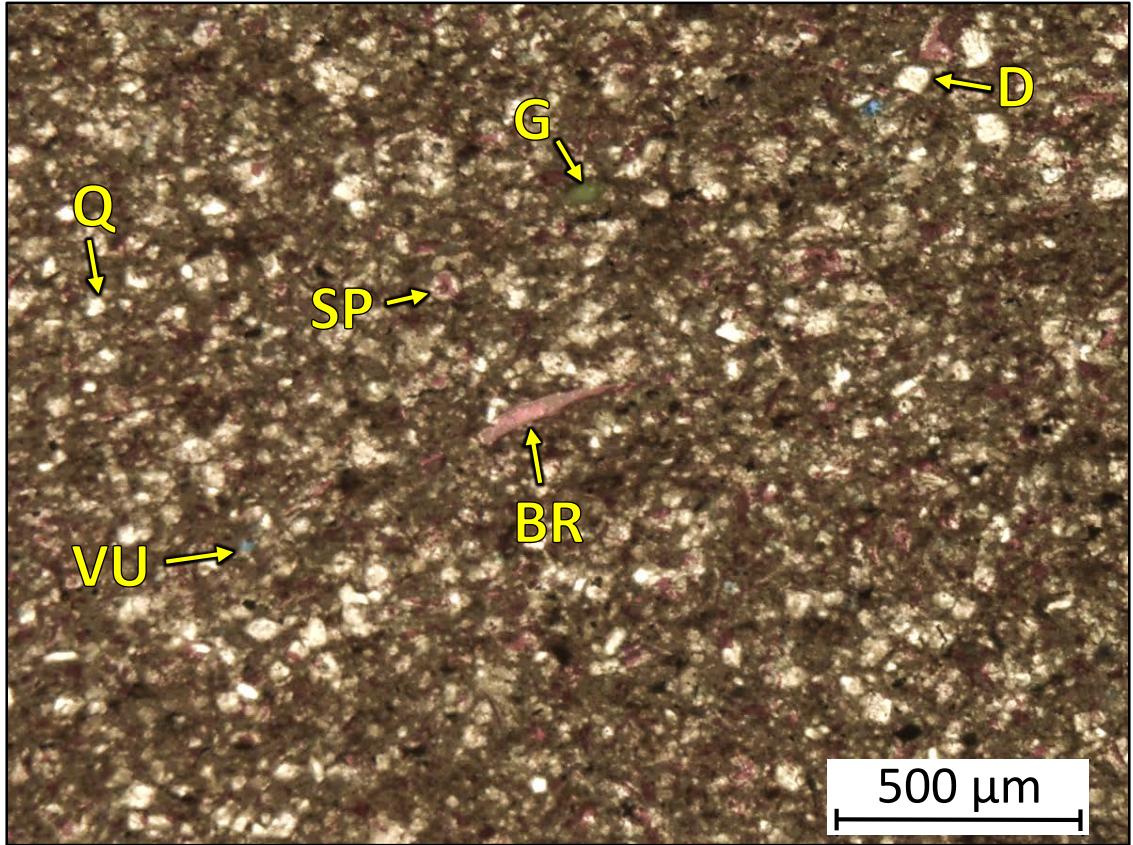
Adkisson #1-33 SWD



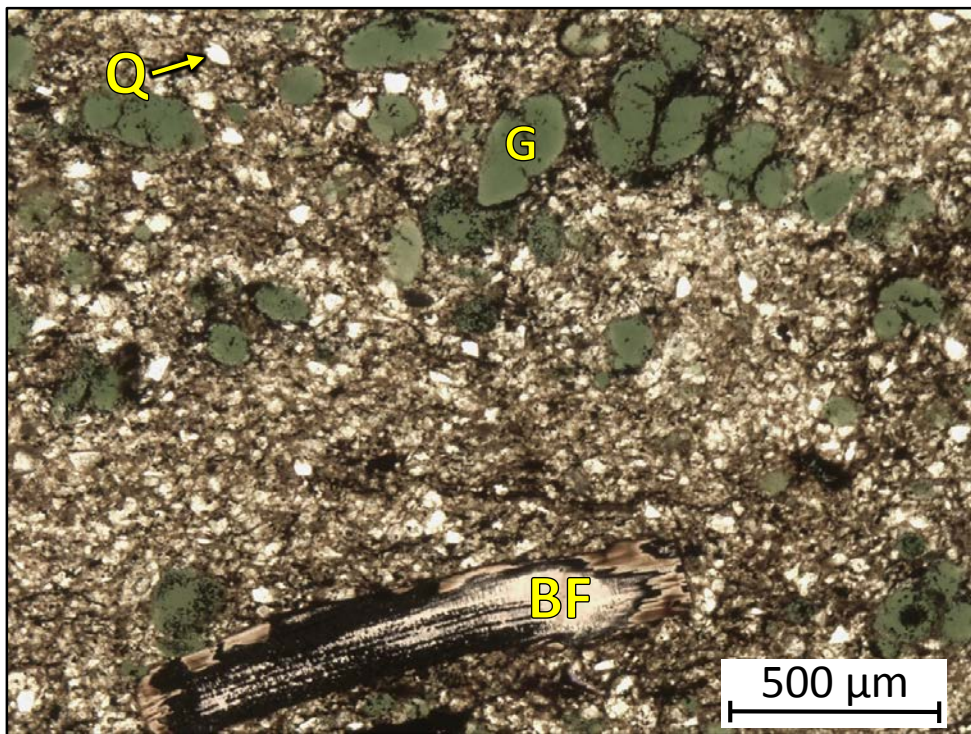
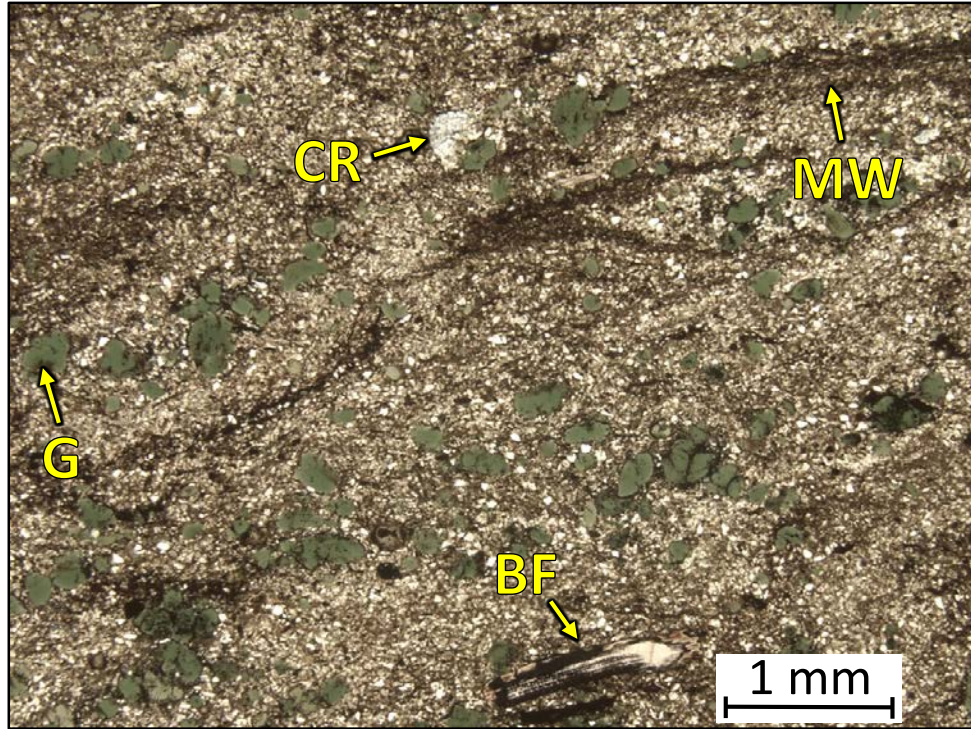
1AD – 5819.8' = Glauconitic sandstone. Porosity (visual estimation): 10.0%. Visual estimation: 17% clays, 18% carbonates, and 65% other minerals. Sample contains silt-sized quartz grains (20%), sand-sized glauconite grains (40%), and bone fragments (3%). Significant amounts of oil observed within sample. Intracrystalline porosity observed within dolomite crystals.



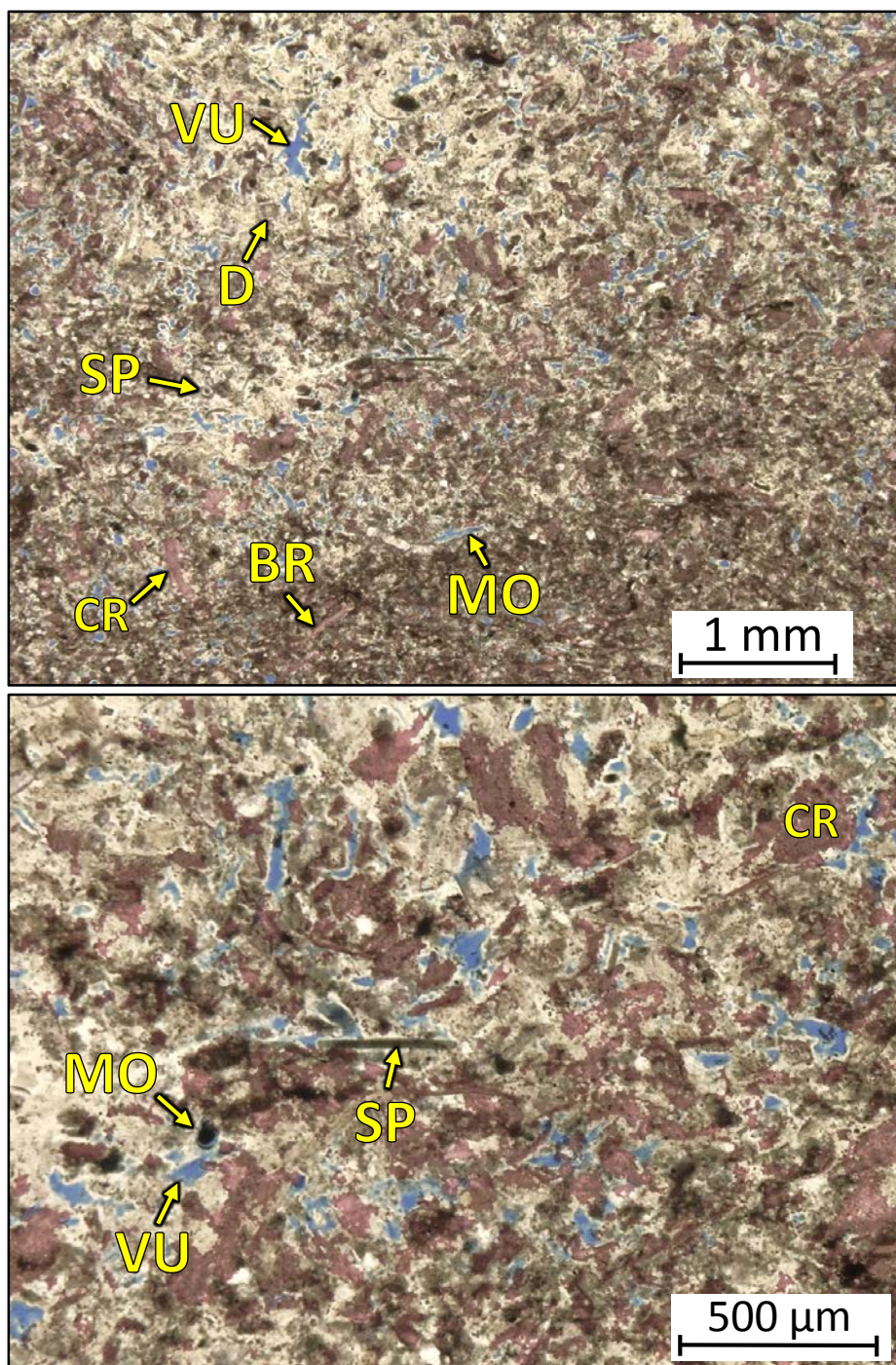
1AD – 5810.40' = Silicified bioturbated wackestone. Sample is alizarin red stained and blue epoxy impregnated. Porosity (NCS): 0.1%. Permeability (Klinkenberg): <0.0001 mD. TOC: 0.18%. XRD: 1% clays (1% illite), 25% carbonates (20% calcite and 5% dolomite), and 74% other minerals (71% quartz, 2% potassium feldspar, and 1% plagioclase feldspar). Sample contains silt-sized quartz grains and undifferentiated microbioclastic debris. Some spicules have been replaced by calcite.



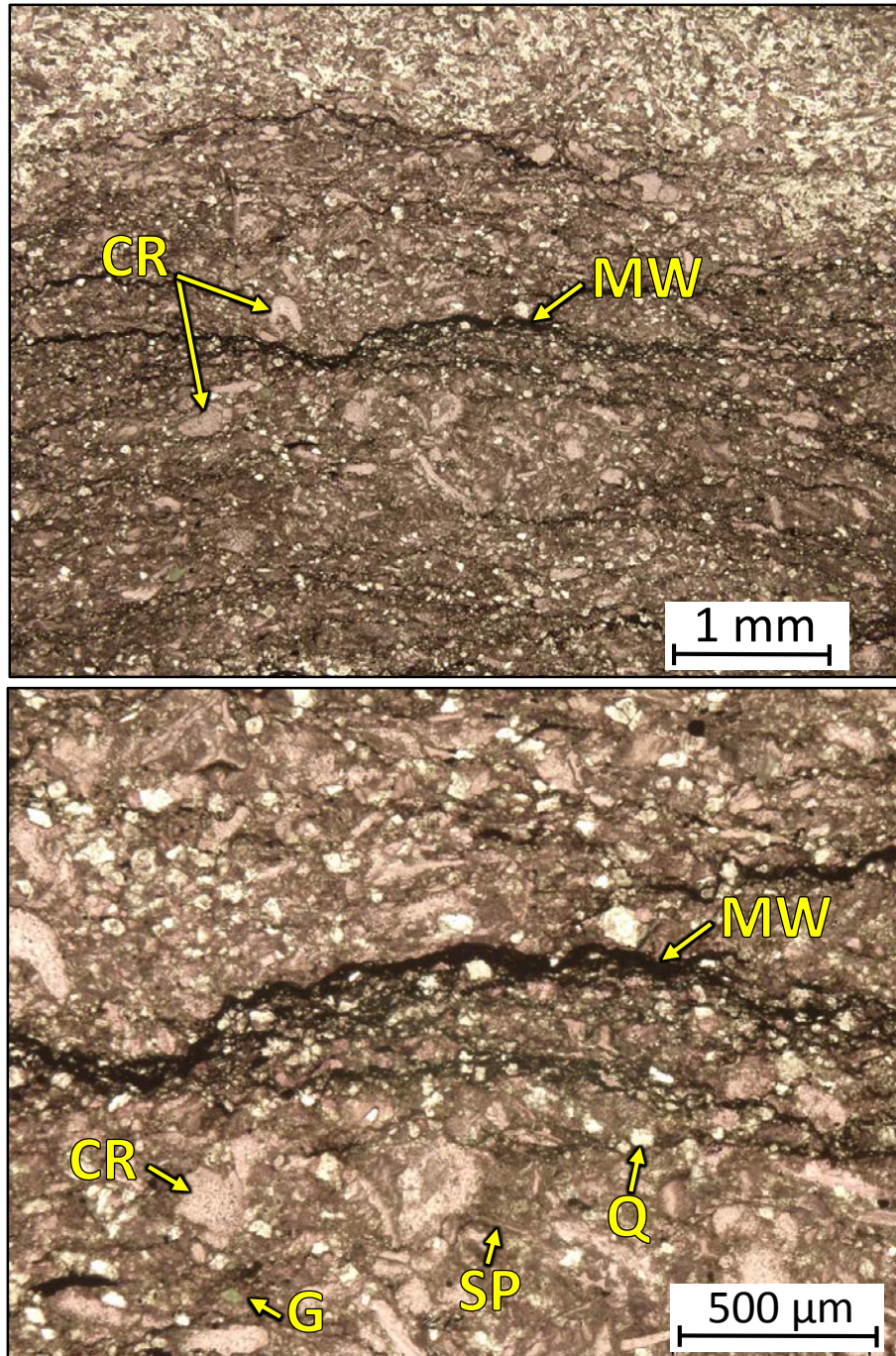
1AD – 5807.75' = Calcareous bioturbated wackestone. Sample is alizarin red stained and blue epoxy impregnated. Porosity (NCS): 4.8%. Permeability (Klinkenberg): 0.016 mD. TOC: 0.45%. XRD: 2% clays (1% illite and 1% mixed layer illite/smectite), 38% carbonates (21% calcite and 17% dolomite), and 60% other minerals (54% quartz, 3% potassium feldspar, 2% plagioclase feldspar, and 1% pyrite). Sample contains silt-sized quartz grains (50%), brachiopod fragments (5%), sponge spicules (1%), very fine sand-sized glauconite grains (1%), and undifferentiated microbioclastic debris. Some spicules have been replaced by calcite. Vug porosity observed.



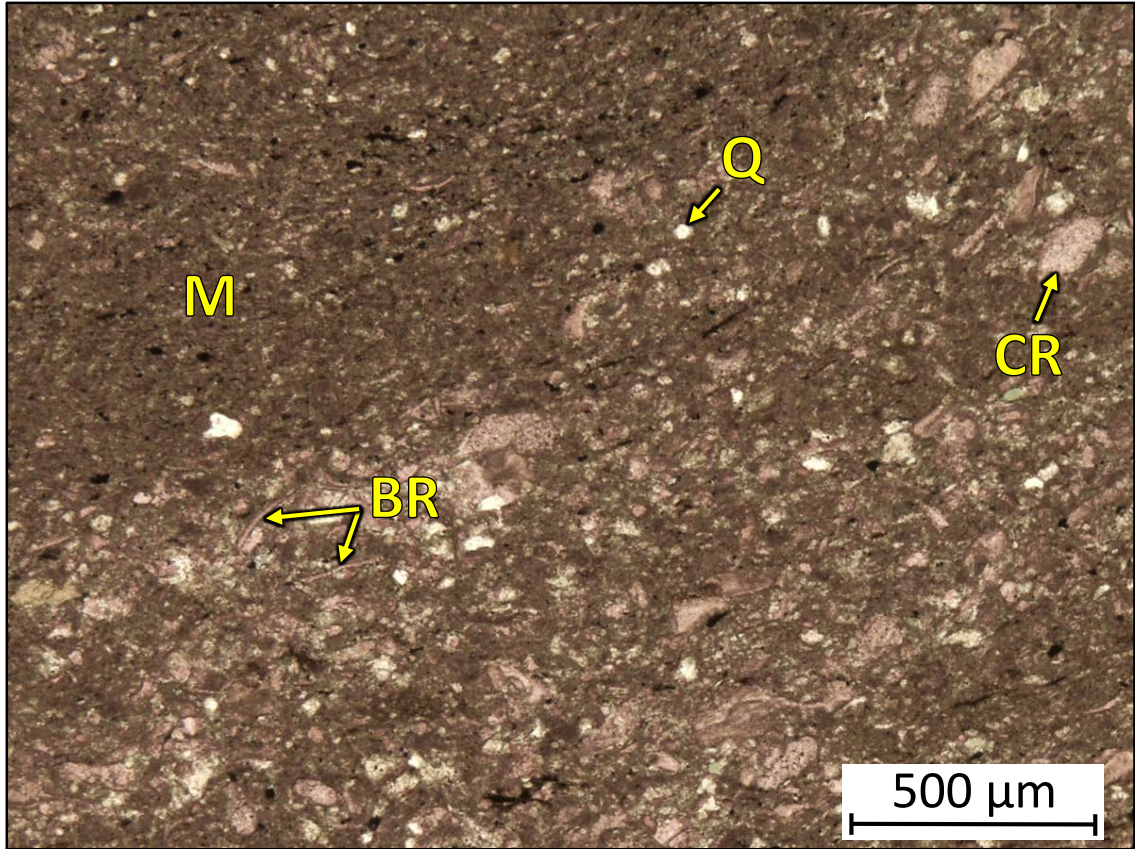
1AD – 5801.40' = Glauconitic wackestone-packstone. Sample is blue epoxy impregnated. Porosity (visual estimation): 5.0%. Visual estimation: 5% clays, 80% carbonates, and 15% other minerals. Sample contains very fine sand-sized glauconite grains (20%), bone fragments (5%), crinoid fragments (3%), and undifferentiated microbioclastic debris. Oil observed throughout sample.



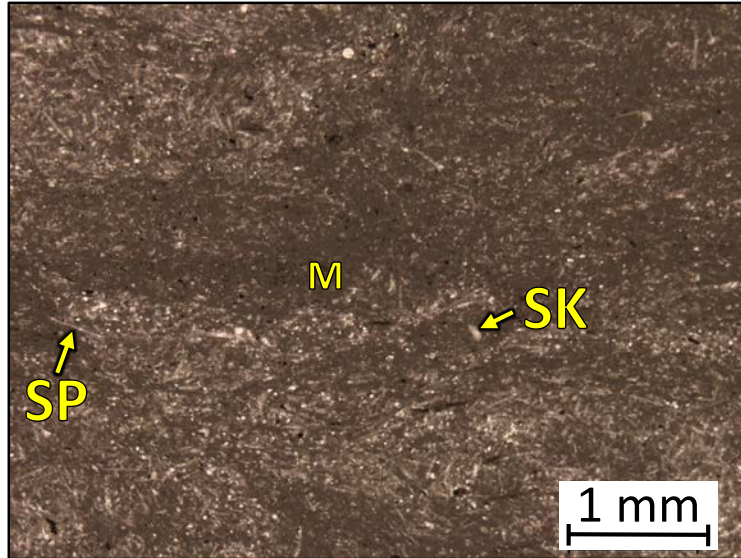
1AD – 5797.55' = Silicified packstone. Sample is alizarin red stained. Porosity (NCS): 6.1%. Permeability (Klinkenberg): 0.0018 mD. TOC: 0.46%. XRD: 1% clays (1% illite), 69% carbonates (53% calcite and 16% dolomite), and 30% other minerals (27% quartz, 1% potassium feldspar, 2% plagioclase feldspar, and trace amounts of pyrite). Sample is composed of crinoid fragments (20%), sponge spicules (20%), brachiopod fragments (10%), and undifferentiated microbioclastic debris. Some spicules have been replaced by calcite. Vug and moldic porosity observed.



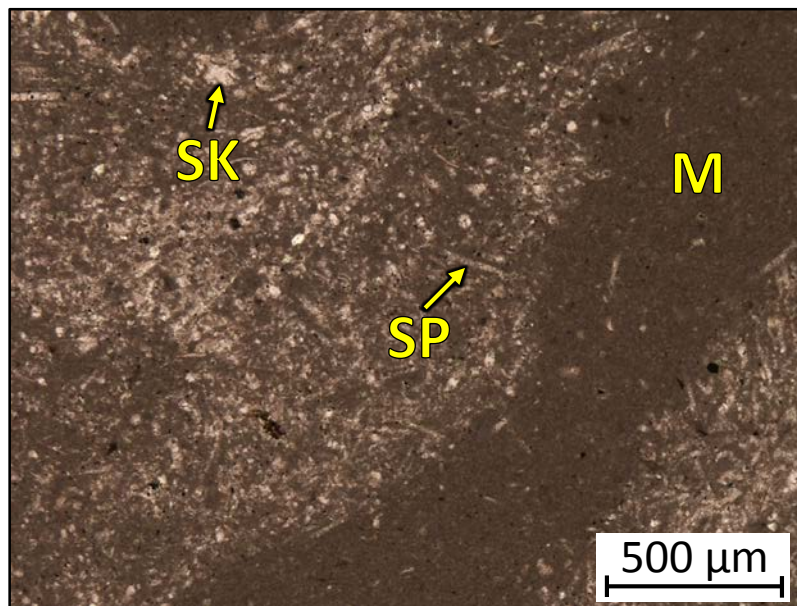
1AD – 5796.35' = Partially silicified crinoidal wackestone-packstone. Sample is alizarin red stained. Porosity (ambient): 1.7%. Permeability (Klinkenberg): Sample was unsuitable for this type of measurement. TOC: 0.78%. XRD: 1% clays (1% illite), 36% carbonates (29% calcite and 7% dolomite), and 63% other minerals (58% quartz, 2% potassium feldspar, 2% plagioclase feldspar, and 1% pyrite). Sample contains abundant crinoid fragments (30%), sponge spicules (10%), brachiopod fragments (7%), and silt-sized glauconite grains (1%). Some spicules have been replaced by calcite. Oil-filled moldic porosity observed.



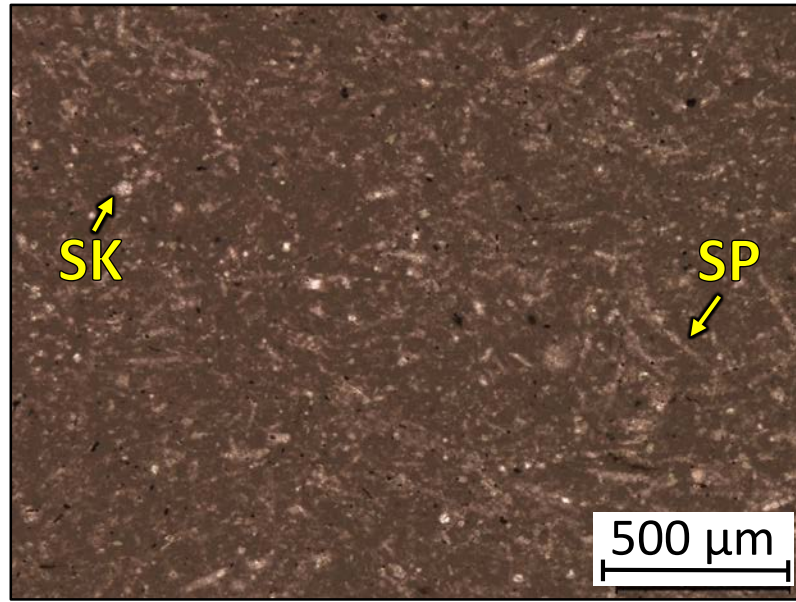
1AD – 5786.50' = Bioturbated mudstone-wackestone. Sample is alizarin red stained. Porosity (NCS): 1.0%. Permeability (Klinkenberg): 0.0002 mD. TOC: 0.20%. XRD: 4% clays (3% illite and 1% mixed layer illite/smectite), 53% carbonates (45% calcite and 8% dolomite), and 43% other minerals (40% quartz, 1% potassium feldspar, 1% plagioclase feldspar, and 1% pyrite). Sample contains silt-sized quartz grains (40%), crinoid fragments (15%), and brachiopod fragments (10%). Oil-filled moldic porosity observed.



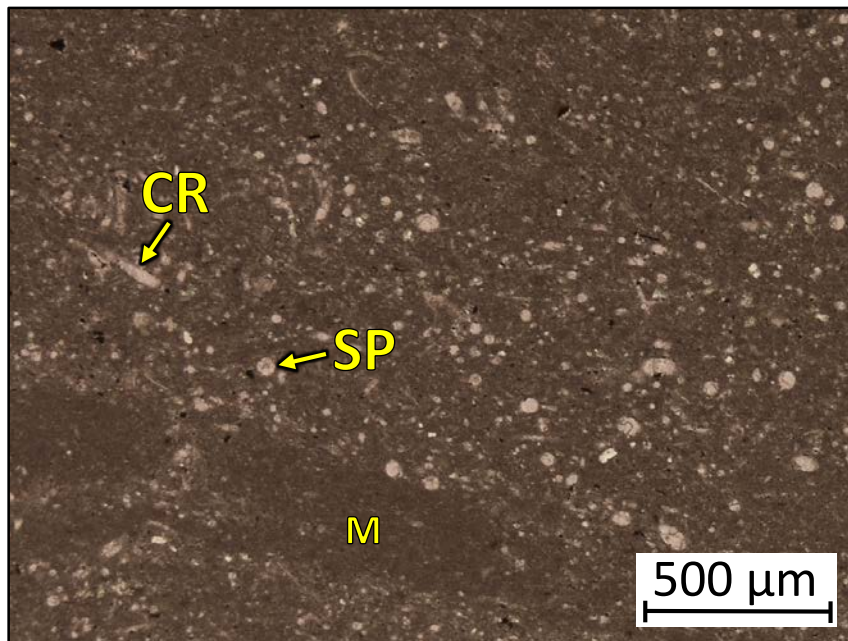
1AD – 5775.00' = Bioturbated mudstone-wackestone. Sample is alizarin red stained. Porosity (NCS): 0.4%. Permeability (Klinkenberg): <0.0001 mD. TOC: 0.07%. XRD: 1% clays (1% illite), 72% carbonates (72% calcite and trace amounts of dolomite), and 27% other minerals (24% quartz, 1% potassium feldspar, 1% plagioclase feldspar, and 1% pyrite). Sample contains sponge spicules (15%) and undifferentiated microbioclastic debris. Burrows concentrate sponge spicules.



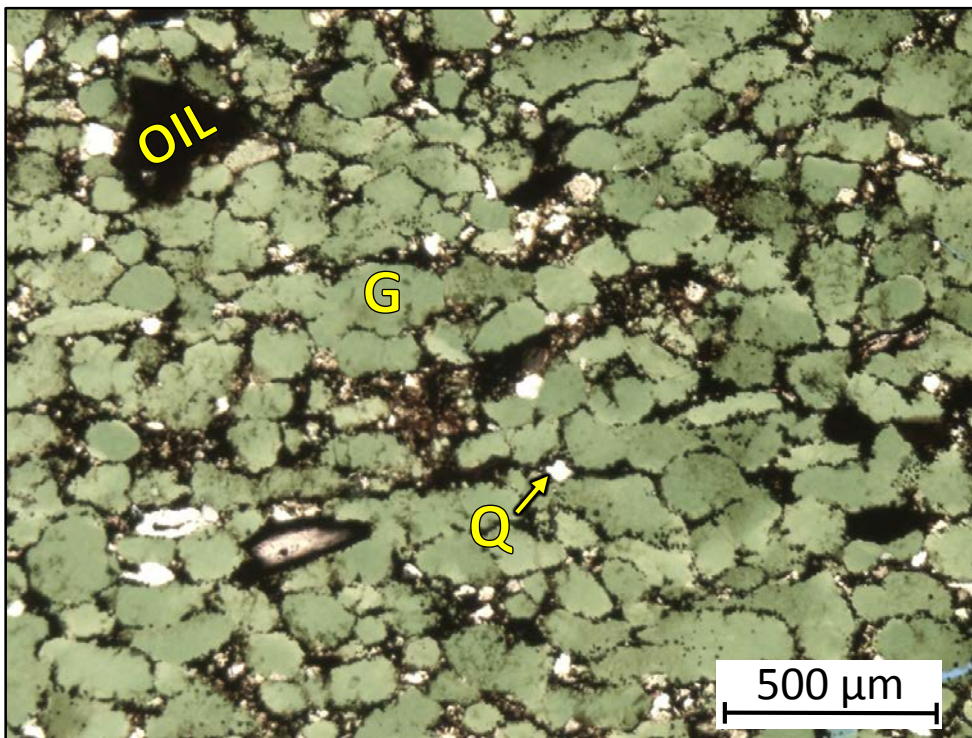
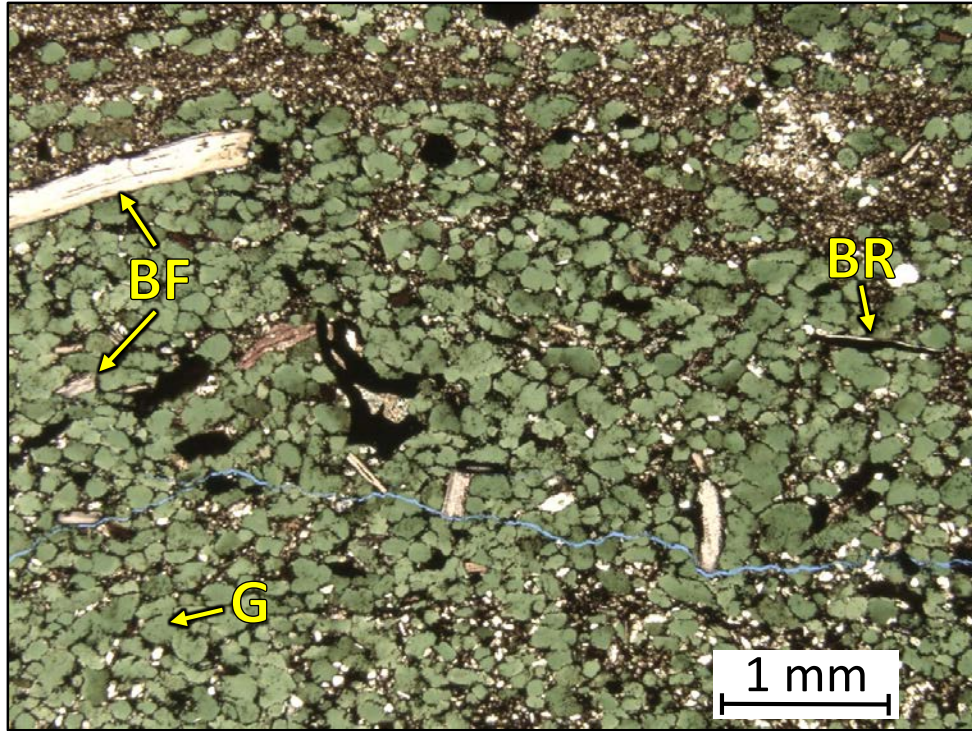
1AD – 5770.60' = Bioturbated wackestone-packstone. Sample is alizarin red stained. Porosity (NCS): 0.1%. Permeability (Klinkenberg): <0.0001 mD. TOC: 0.08%. XRD: 2% clays (1% illite and 1% mixed layer illite/smectite), 72% carbonates (71% calcite and 1% dolomite), and 26% other minerals (23% quartz, 1% potassium feldspar, 1% plagioclase feldspar, and 1% pyrite). Sample contains sponge spicules (15%) and undifferentiated microbioclastic debris. Burrows concentrate sponge spicules.



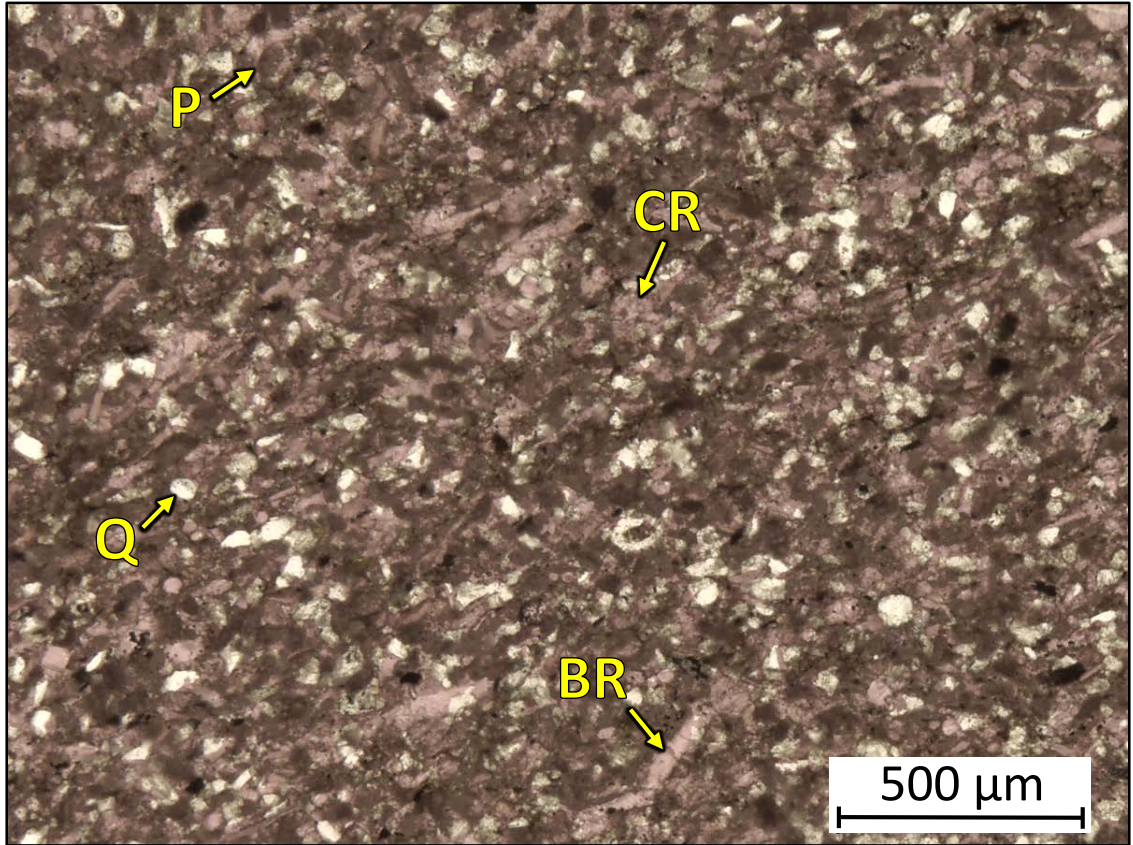
1AD – 5763.15' = Bioturbated mudstone-wackestone. Sample is alizarin red stained. Porosity (NCS): 0.7%. Permeability (Klinkenberg): <0.0001 mD. TOC: 0.03%. XRD: Trace amounts of clays, 87% carbonates (86% calcite and 1% dolomite), and 13% other minerals (9% quartz, 1% potassium feldspar, 3% plagioclase feldspar, and trace amounts of pyrite). Sample contains sponge spicules (10%) and undifferentiated microbioclastic debris.



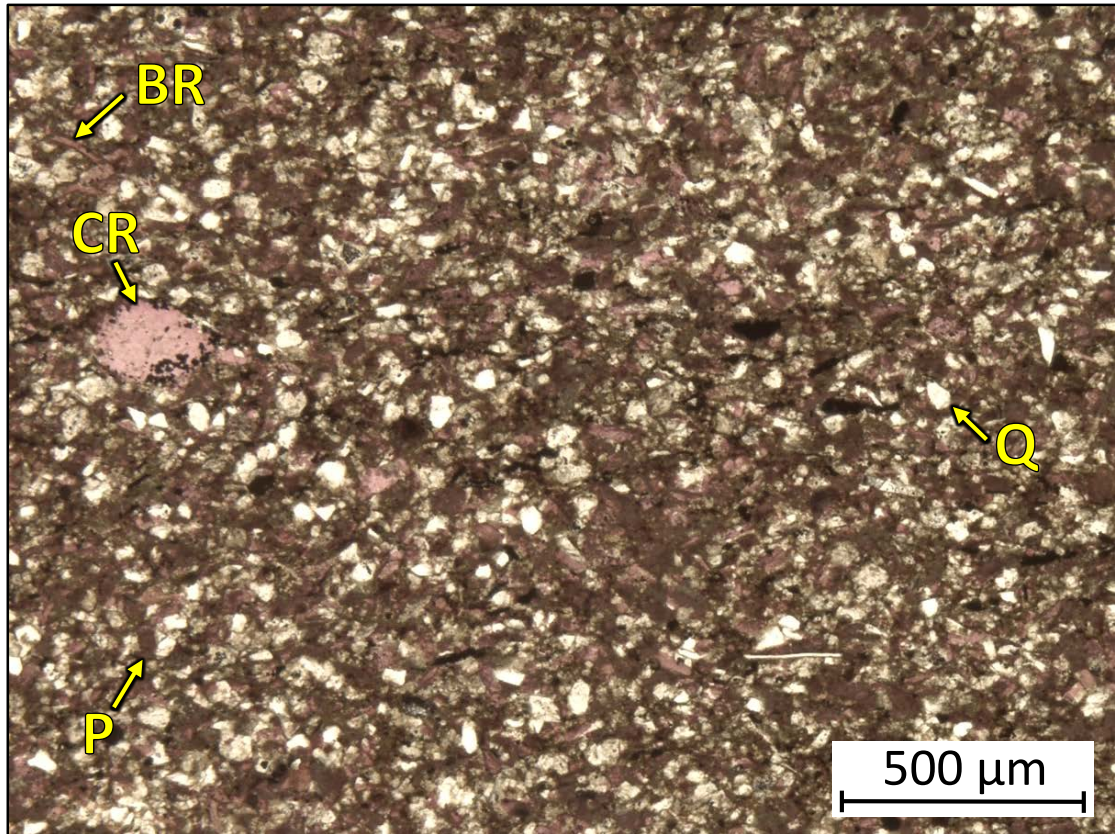
1AD – 5760.60' = Bioturbated mudstone-wackestone. Sample is alizarin red stained. Porosity (NCS): 0.1%. Permeability (Klinkenberg): 0.0001 mD. TOC: 0.08%. XRD: 2% clays (2% illite), 81% carbonates (80% calcite and 1% dolomite), and 17% other minerals (13% quartz, 1% potassium feldspar, 2% plagioclase feldspar, and 1% pyrite). Sample contains sponge spicules (5%), crinoid fragments (5%), and undifferentiated microbioclastic debris.



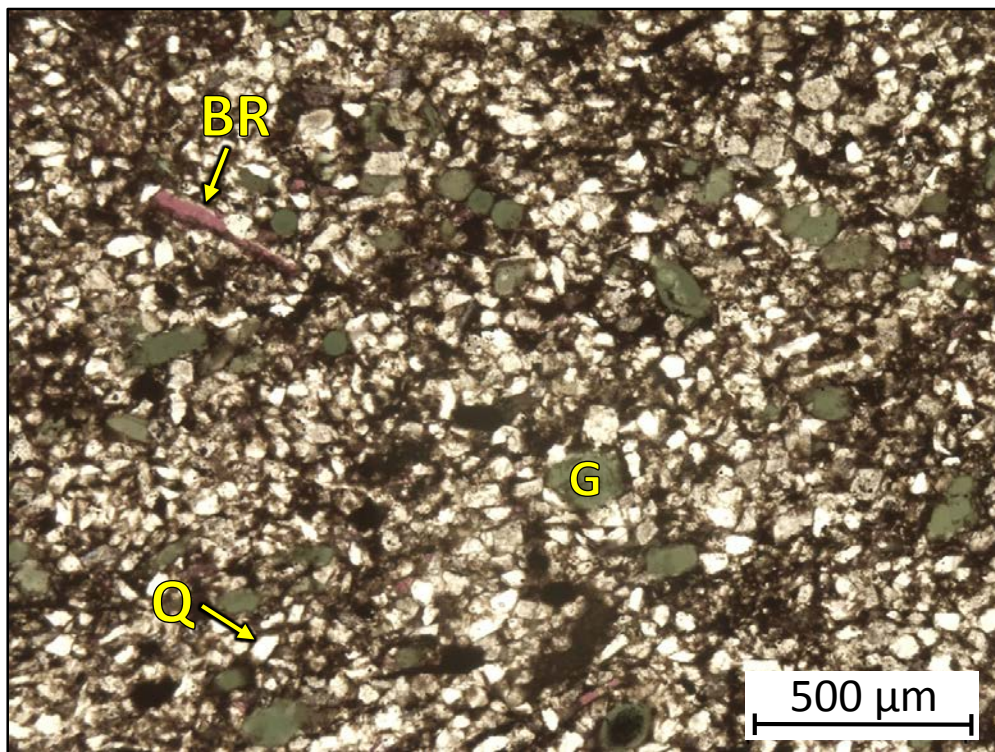
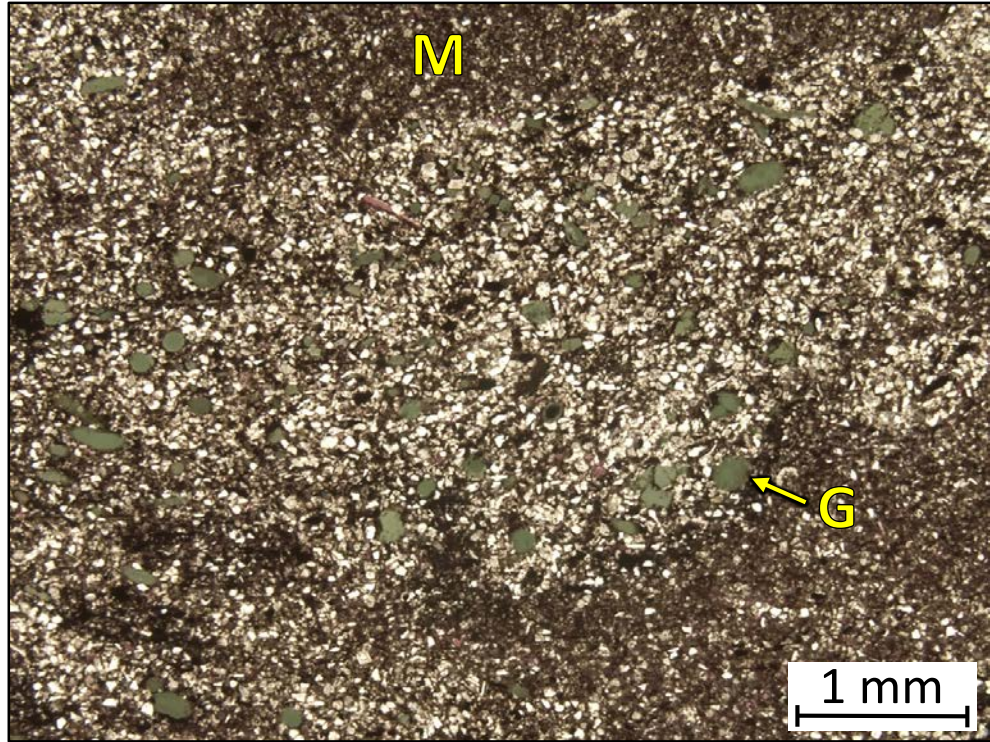
1AD – 5757.85 = Glauconitic sandstone. Sample is blue epoxy impregnated. Porosity (visual estimation): 5.0%. Visual estimation: 10% clays, 20% carbonates, and 70% other minerals. Sample contains fine to medium sand-sized glauconite grains (70%), silt-sized quartz grains (10%), bone fragments (10%), and brachiopod fragments (5%). Oil-filled vug porosity observed.



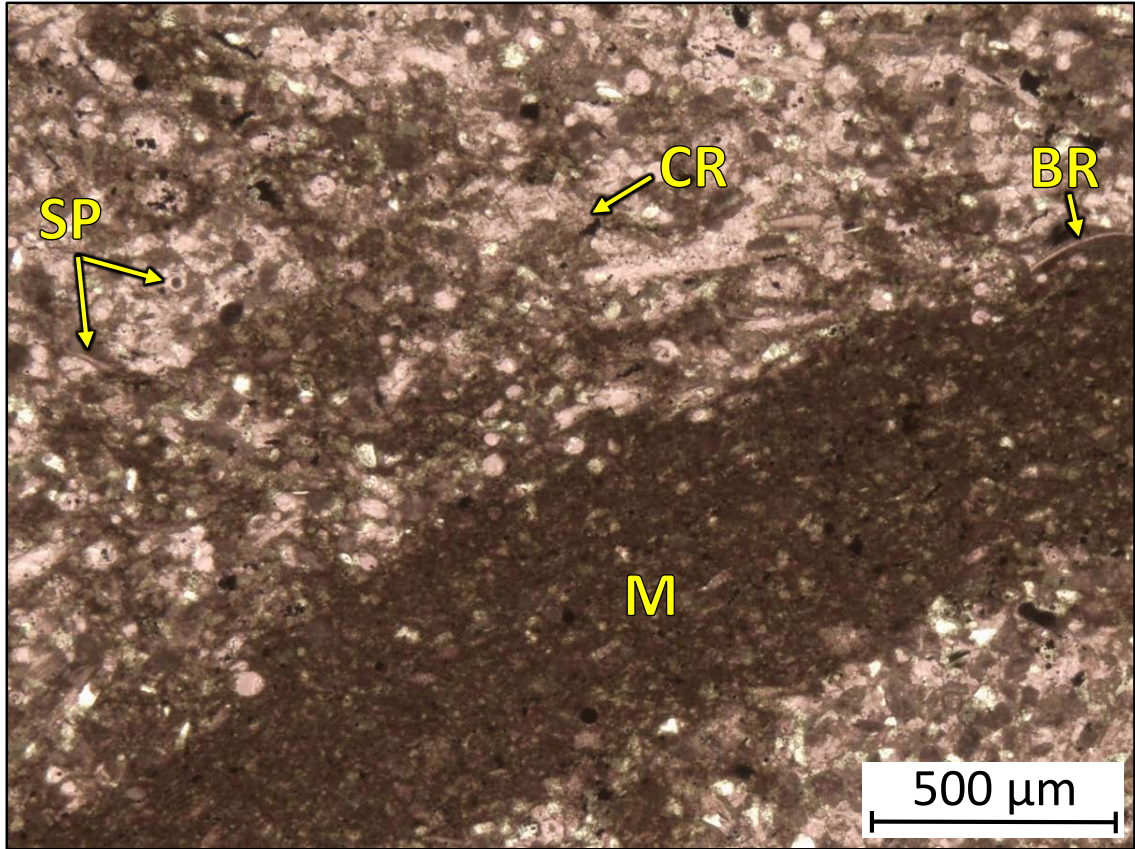
1AD – 5751.65' = Bioturbated wackestone-packstone. Sample is alizarin red stained. Porosity (NCS): 2.3%. Permeability (Klinkenberg): 0.0001 mD. TOC: 0.13%. XRD: 2% clays (1% illite and 1% mixed layer illite/smectite), 73% carbonates (65% calcite and 8% dolomite), and 25% other minerals (20% quartz, 1% potassium feldspar, 3% plagioclase feldspar, and 1% pyrite). Sample contains silt-sized quartz grains (20%), crinoid grains (15%), peloids (10%), and brachiopod fragments (5%). Oil-filled vug and moldic porosity observed.



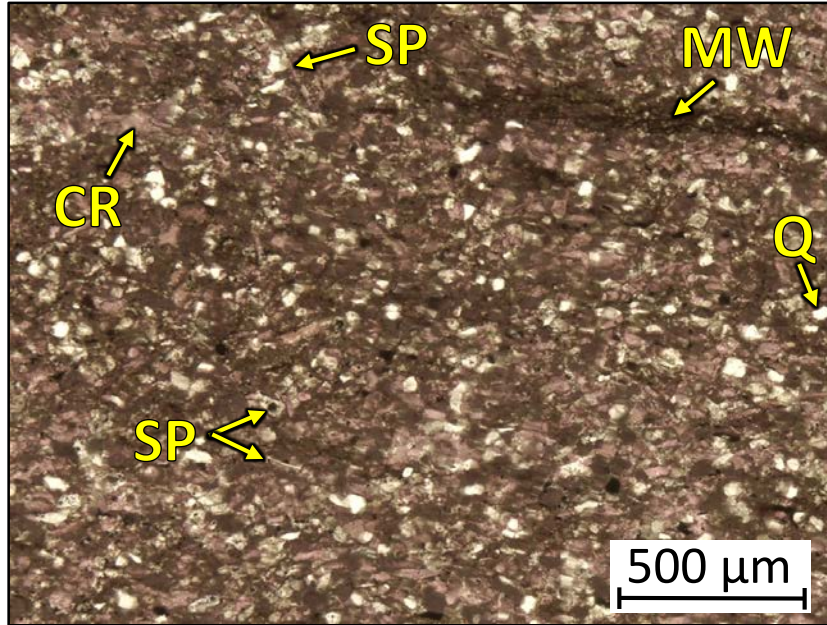
1AD – 5750.60' = Bioturbated wackestone-packstone. Sample is alizarin red stained. Porosity (NCS): 2.0%. Permeability (Klinkenberg): 0.040 mD. TOC: 0.50%. XRD: 7% clays (2% illite and 5% mixed layer illite/smectite), 50% carbonates (41% calcite and 9% dolomite), and 43% other minerals (37% quartz, 1% potassium feldspar, 3% plagioclase feldspar, and 2% pyrite). Sample contains silt-sized quartz grains (30%), crinoid fragments (15%), peloids (10%), and brachiopod fragments (5%). Oil-filled moldic and vug porosity observed.



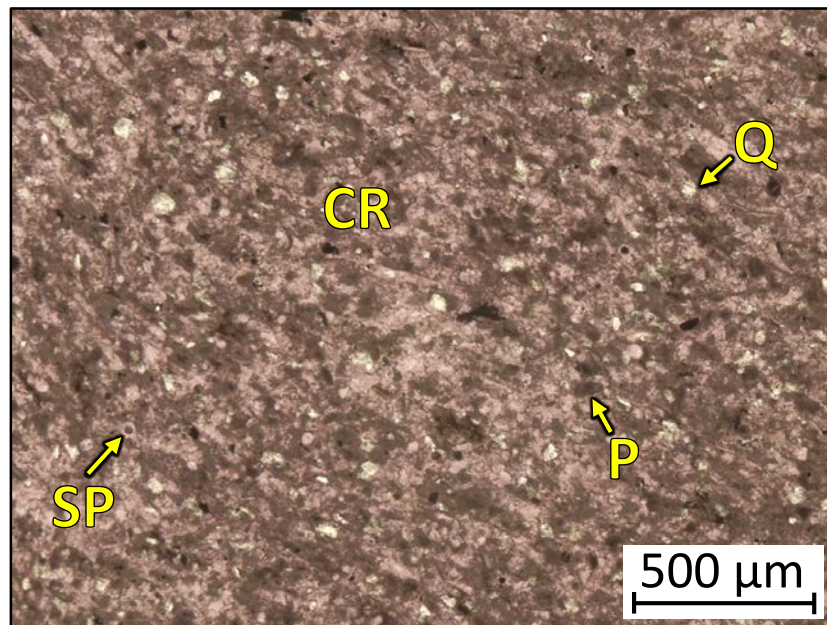
1AD – 5749.00' = Glauconitic siltstone. Sample is alizarin red stained. Porosity (visual estimation): 7.0%. Visual estimation: 10% clays, 5% carbonates, and 85% other minerals. Sample contains silt-sized quartz grains (80%), fine-sand sized glauconite grains (10%), and brachiopod fragments (3%).



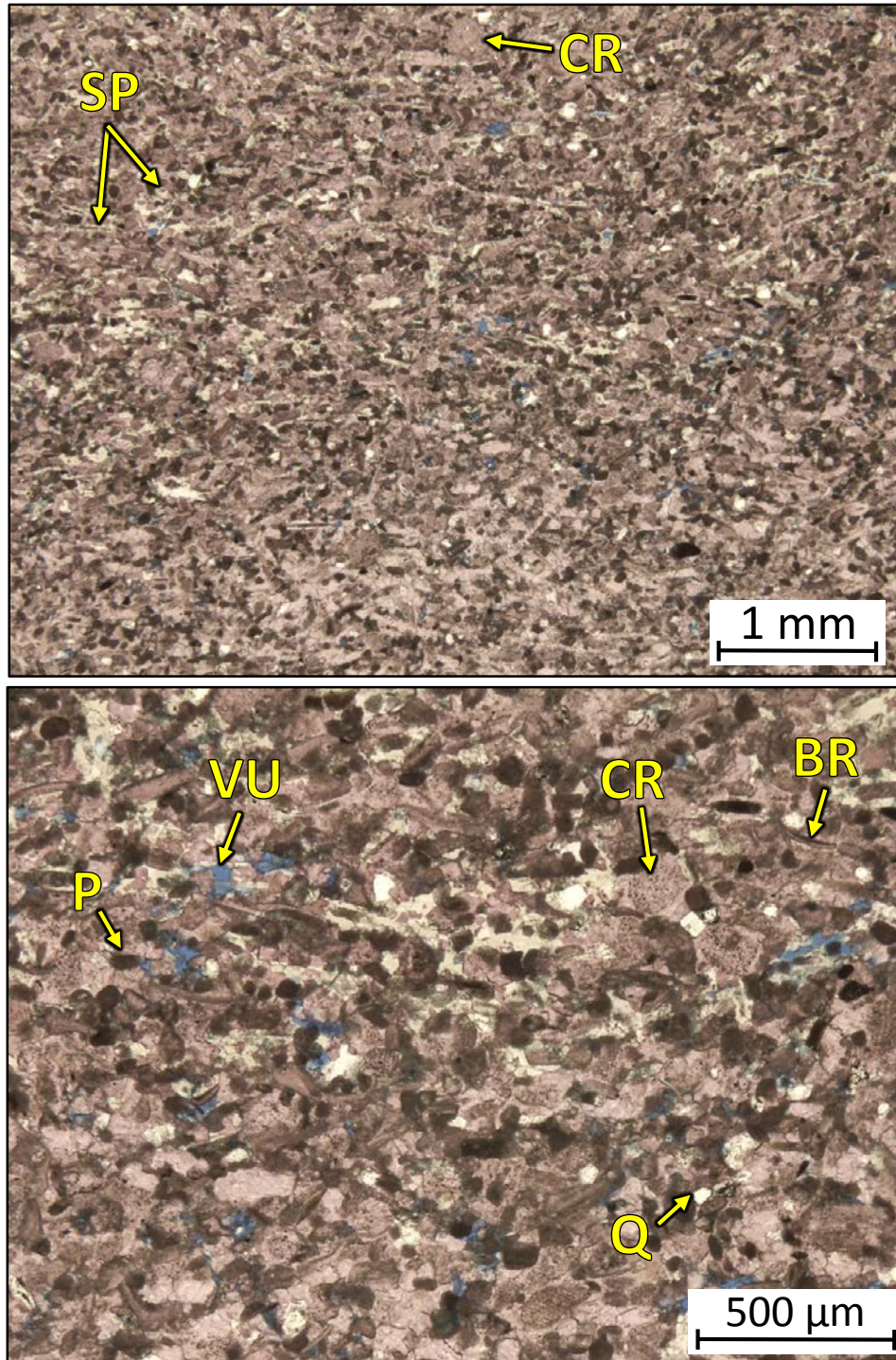
1AD – 5744.75' = Bioturbated mudstone-skeletal packstone. Sample is alizarin red stained. Porosity (NCS): 0.8%. Permeability (Klinkenberg): <0.0001 mD. TOC: 0.26%. XRD: 3% clays (2% illite and 1% mixed layer illite/smectite), 64% carbonates (61% calcite and 3% dolomite), and 33% other minerals (27% quartz, 2% potassium feldspar, 3% plagioclase feldspar, and 1% pyrite). Sample contains crinoid fragments (25%), brachiopod fragments (5%), and undifferentiated microbioclastic debris. Most spicules have been replaced with calcite.



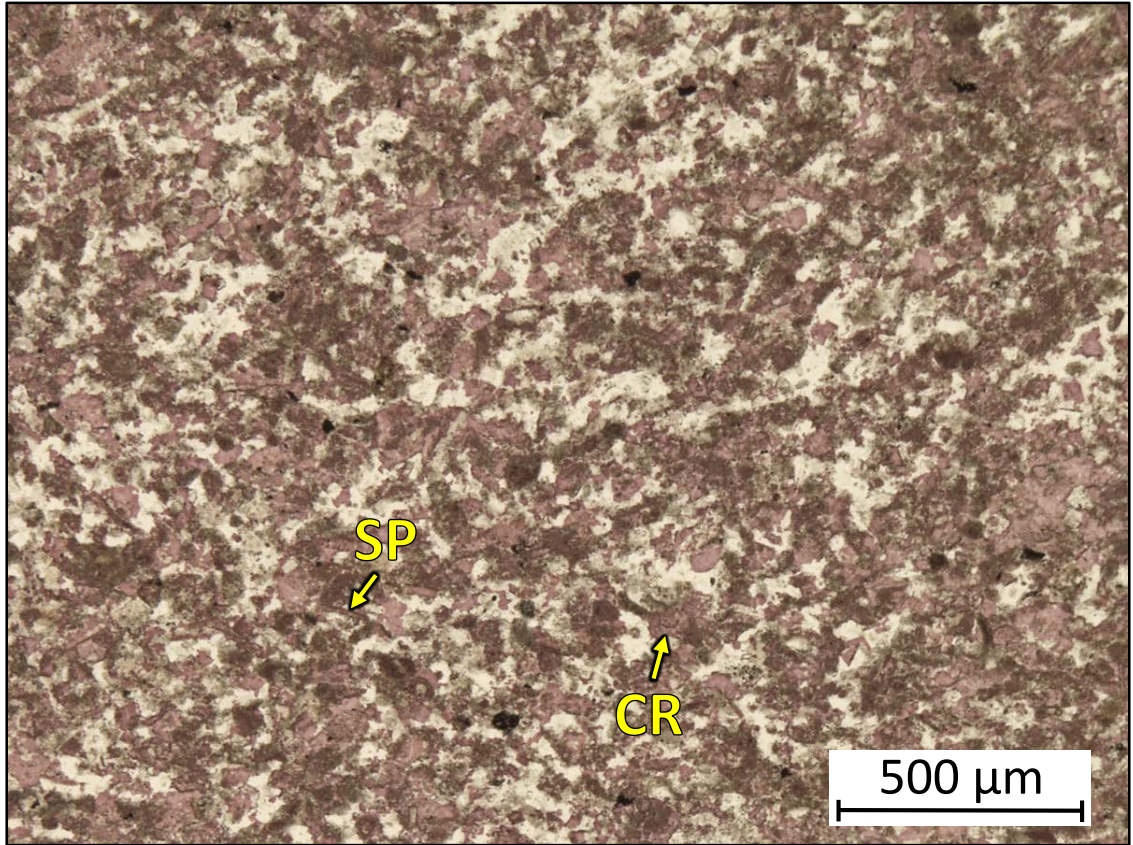
1AD – 5737.85' = Bioturbated wackestone-packstone. Sample is alizarin red stained. Porosity (NCS): 1.1%. Permeability (Klinkenberg): Sample was unsuitable for this type of measurement. TOC: 0.51%. XRD: 7% clays (5% illite and 2% mixed layer illite/smectite), 50% carbonates (43% calcite and 7% dolomite), and 43% other minerals (37% quartz, 1% potassium feldspar, 3% plagioclase feldspar, and 2% pyrite). Sample contains crinoid fragments (20%), sponge spicules (10%), and undifferentiated microbioclastic debris.



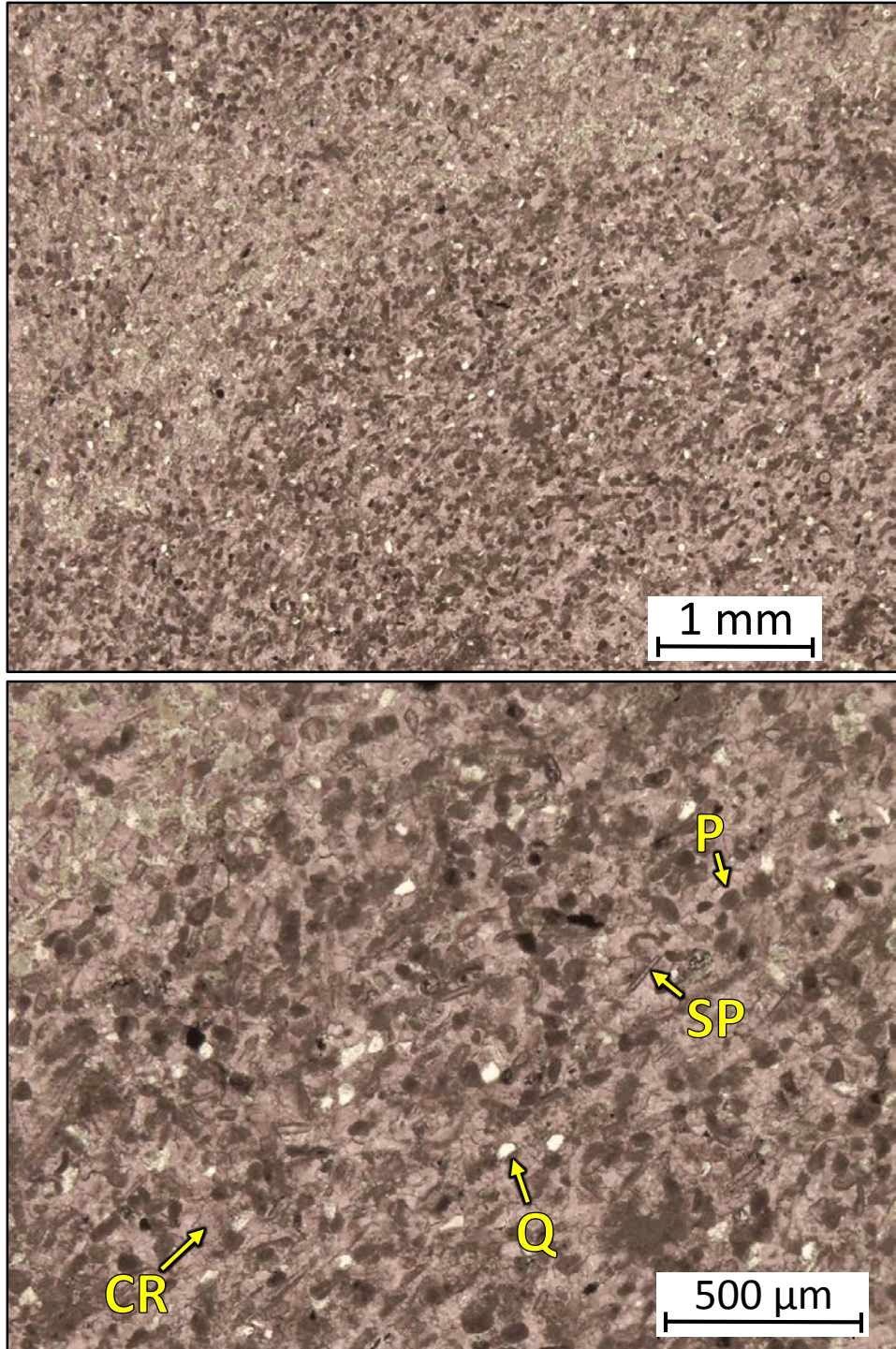
1AD – 5735.00' = Peloidal grainstone. Sample is alizarin red stained. Porosity (NCS): 0.3%. Permeability (Klinkenberg): <0.0001 mD. TOC: 0.02%. XRD: 1% clays (1% illite), 87% carbonates (87% calcite and trace amounts of dolomite), and 12% other minerals (9% quartz, trace amounts of potassium feldspar, 2% plagioclase feldspar, and 1% pyrite). Sample contains crinoid fragments (30%), peloids (15%), and sponge spicules (10%).



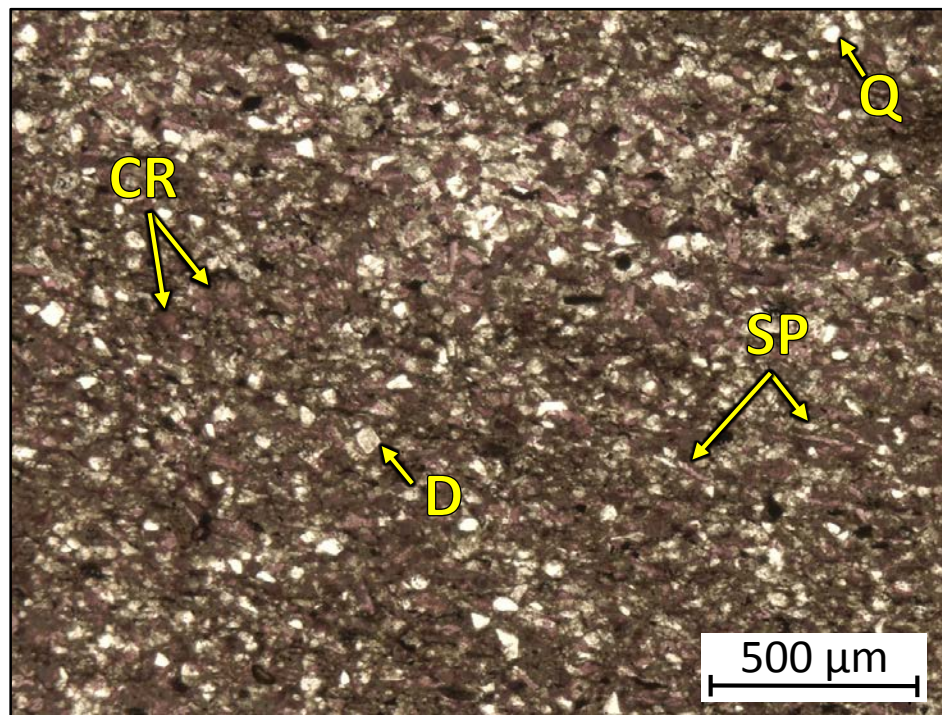
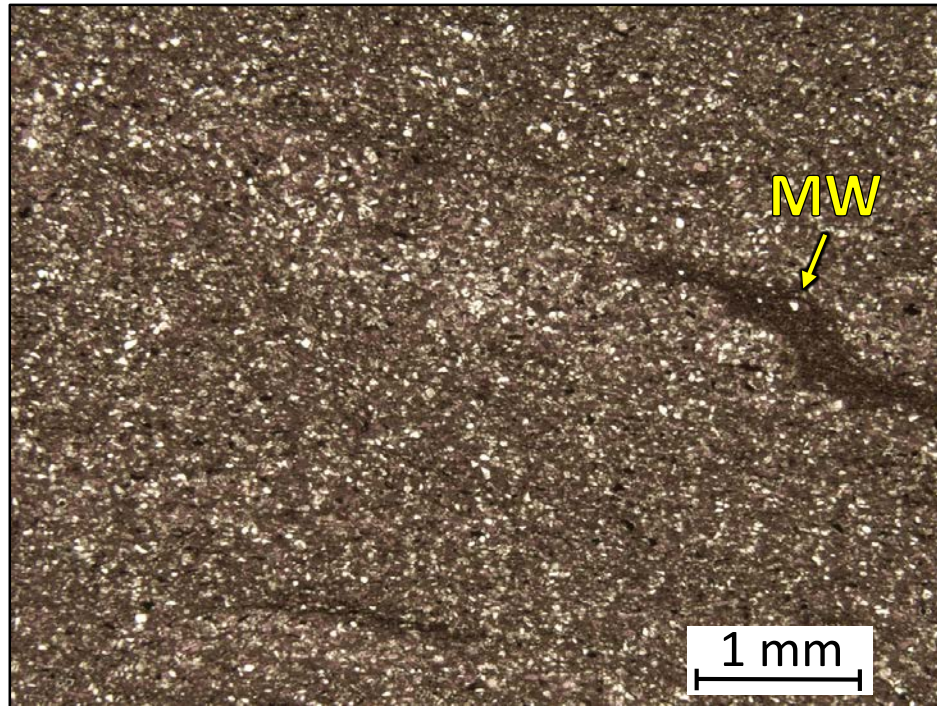
1AD – 5728.80' = Peloidal-skeletal grainstone. Sample is alizarin red stained and blue epoxy impregnated. Porosity (NCS): 6.0%. Permeability (Klinkenberg): 0.014 mD. TOC: 0.48%. XRD: 1% clays (1% illite), 82% carbonates (79% calcite and 3% dolomite), and 17% other minerals (12% quartz, 1% potassium feldspar, 2% plagioclase feldspar, trace amounts of pyrite, 1% apatite, and 1% marcasite). Sample contains crinoid fragments (35%), sponge spicules (20%), peloids (20%), silt-sized quartz fragments (10%), and brachiopod fragments (5%). Vug porosity observed.



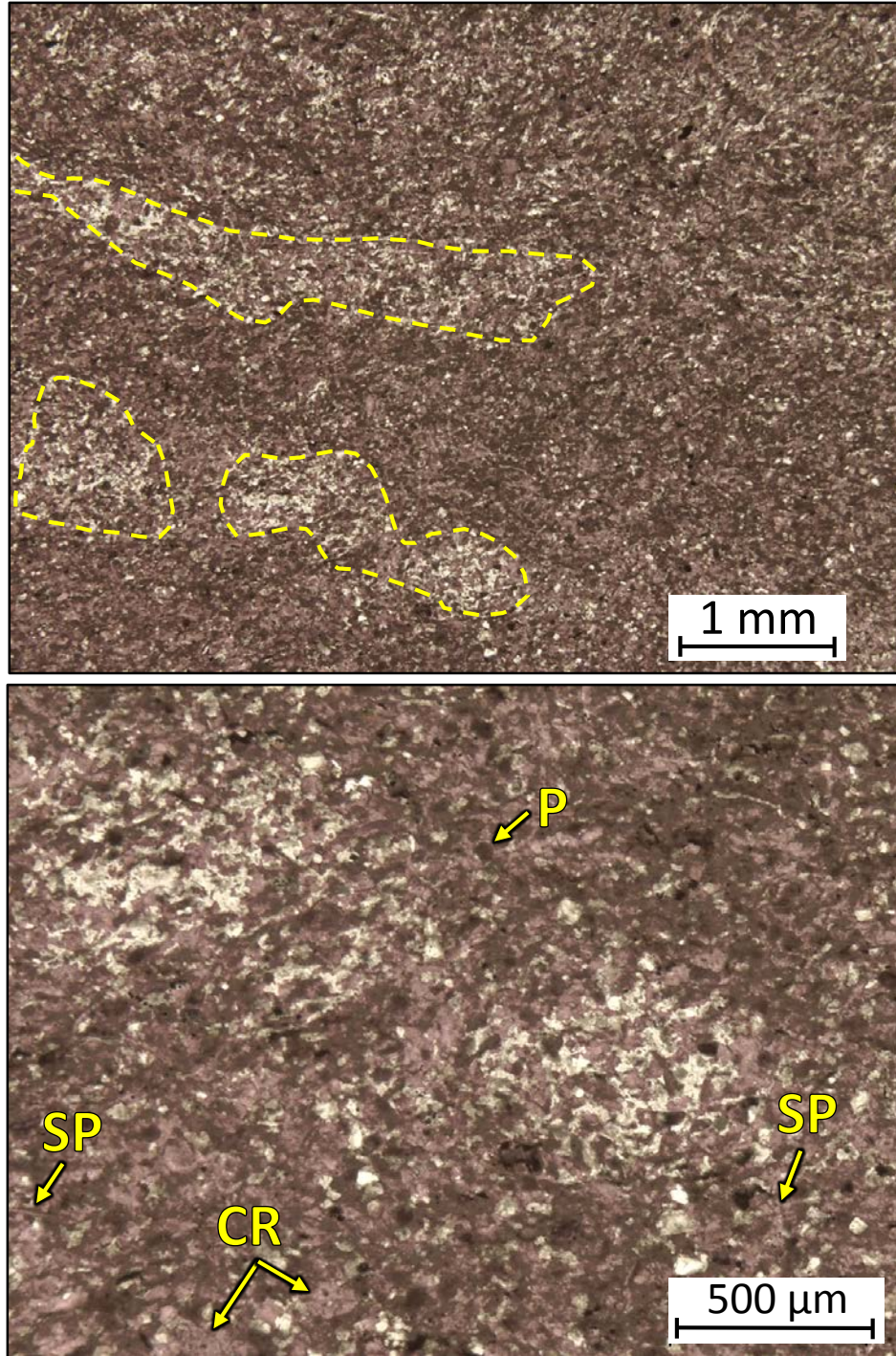
1AD – 5727.50' = Partially silicified skeletal grainstone. Sample is alizarin red stained. Porosity (NCS): 0.8%. Permeability (Klinkenberg): <0.0001 mD. TOC: 0.03%. XRD: Trace amounts of clays, 24% carbonates (23% calcite and 1% dolomite), and 76% other minerals (72% quartz, 3% potassium feldspar, 1% plagioclase feldspar, and trace amounts of pyrite). Sample contains crinoid fragments (15%), sponge spicules (10%), and undifferentiated microbioclastic debris.



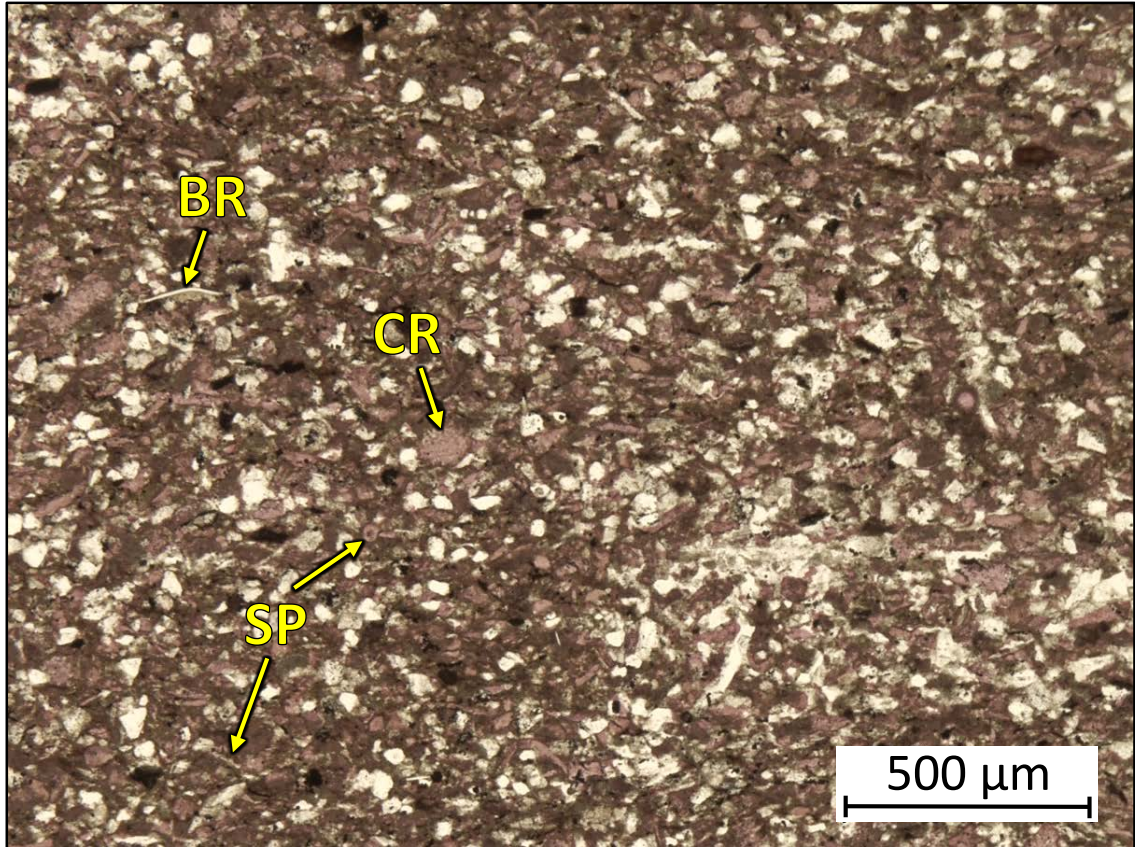
1AD – 5725.75' = Peloidal grainstone. Sample is alizarin red stained. Porosity (NCS): 0.7%. Permeability (Klinkenberg): <0.0001 mD. TOC: 0.01%. XRD: Trace amounts of clays, 79% carbonates (79% calcite and trace amounts of dolomite), and 21% other minerals (16% quartz, 2% potassium feldspar, 3% plagioclase feldspar, and trace amounts of pyrite). Sample contains crinoid fragments (20%), peloids (20%), sponge spicules (15%), and undifferentiated microbioclastic debris.



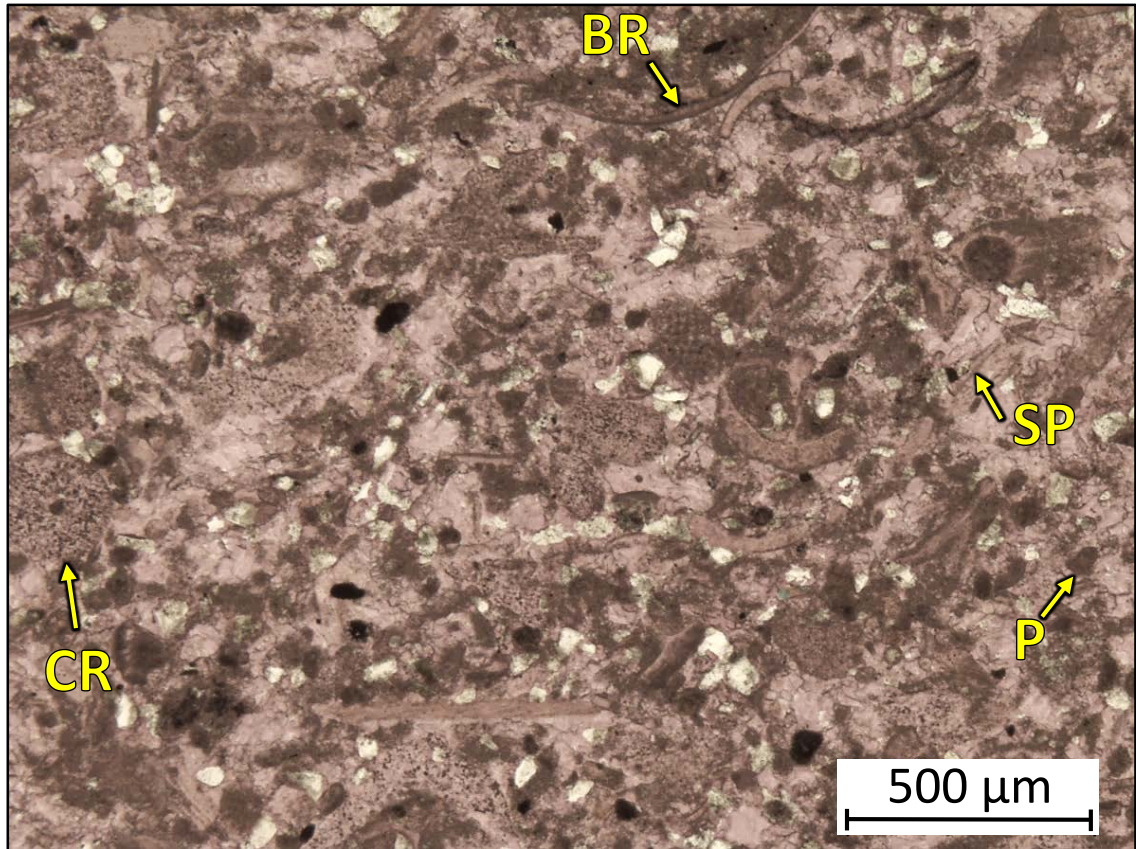
1AD – 5722.00-5722.25' = Bioturbated wackestone. Sample is alizarin red stained. Porosity (visual estimation): 1.0%. TOC: 0.63%. XRD: 7% clays (5% illite and 2% mixed layer illite/smectite), 57% carbonates (50% calcite and 7% dolomite), and 36% other minerals (28% quartz, 1% potassium feldspar, 4% plagioclase feldspar, 2% pyrite, and 1% apatite). Sample contains crinoid fragments (10%), sponge spicules (5%), and undifferentiated microbioclastic debris. Some spicules have been replaced by calcite. Minor amounts of vug and moldic porosity observed.



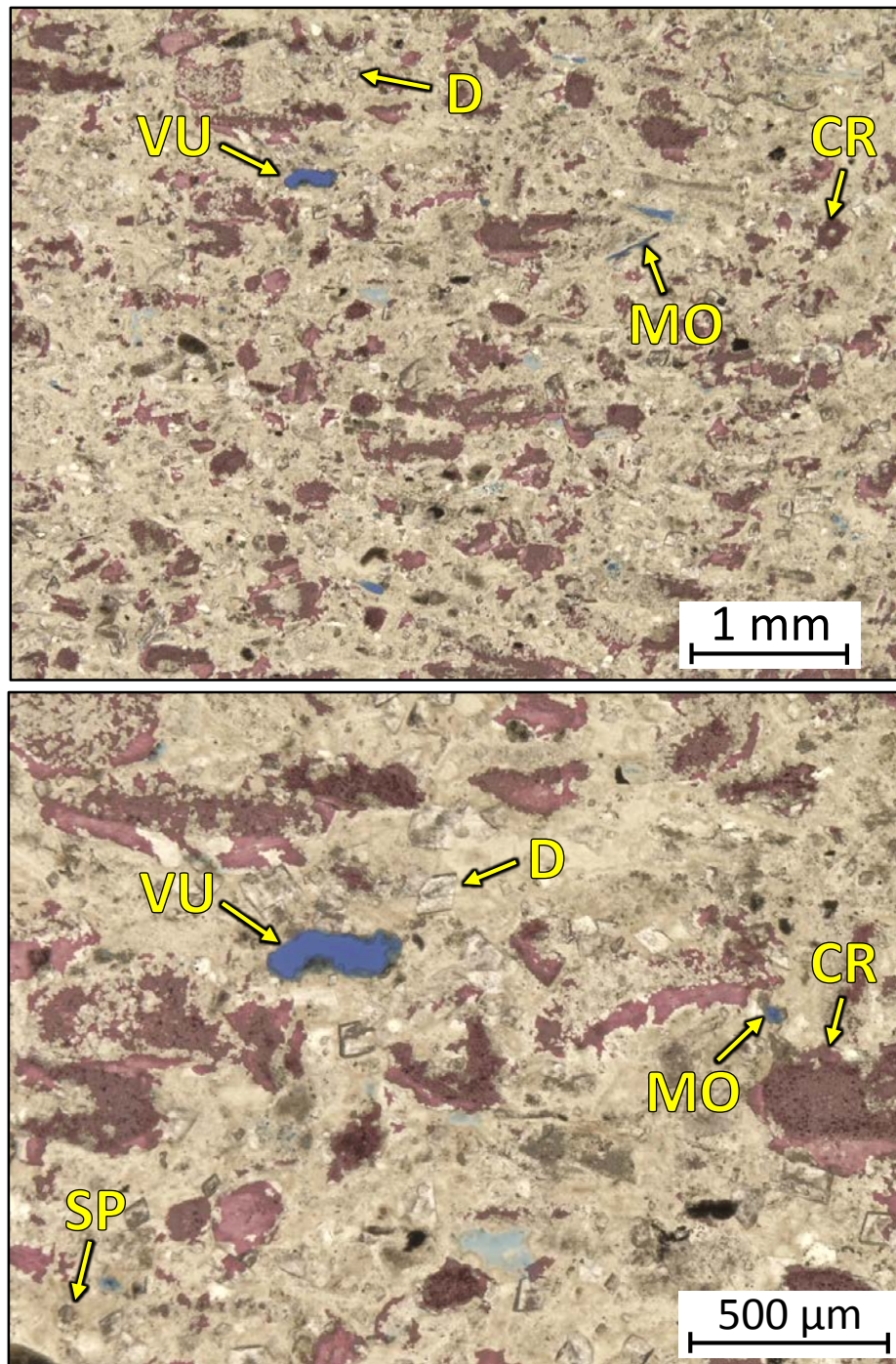
1AD – 5718.55' = Crinoidal wackestone-packstone with silicified skeletal grainstone wisps. Sample is alizarin red stained. Porosity (NCS): 1.0%. Permeability (Klinkenberg): <0.0001 mD. TOC: 0.10%. XRD: Trace amounts of clays, 65% carbonates (63% calcite and 2% dolomite), and 35% other minerals (30% quartz, 1% potassium feldspar, 3% plagioclase feldspar, and 1% pyrite). Sample contains crinoid fragments (30%), peloids (20%), sponge spicules (7%), and undifferentiated microbioclastic debris. Most spicules have been replaced by calcite. Wisps of silicified grainstone (outlined in dashed yellow line), possibly representative of burrow fill, are observed.



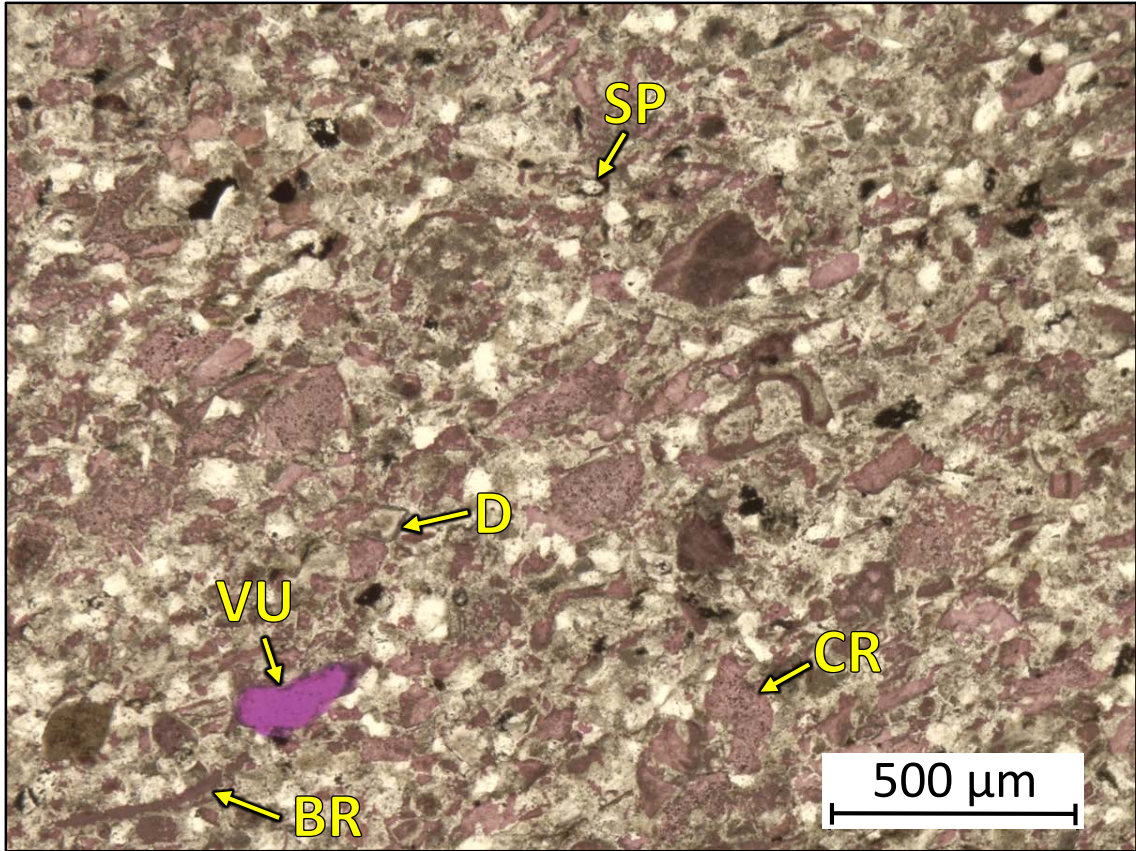
1AD – 5717.50 = Bioturbated packstone. Sample is alizarin red stained. Porosity (NCS): 0.4%. Permeability (Klinkenberg): <0.0001 mD. TOC: 0.12%. XRD: 5% clays (4% illite and 1% mixed layer illite/smectite), 48% carbonates (45% calcite and 3% dolomite), and 47% other minerals (40% quartz, 1% potassium feldspar, 2% plagioclase feldspar, 1% pyrite, 2% apatite, and 1% marcasite). Sample contains crinoid fragments (15%), sponge spicules (10%), brachiopod fragments (5%), and undifferentiated microbioclastic debris. Some sponge spicules have been replaced with calcite while other skeletal grains have been replaced by quartz.



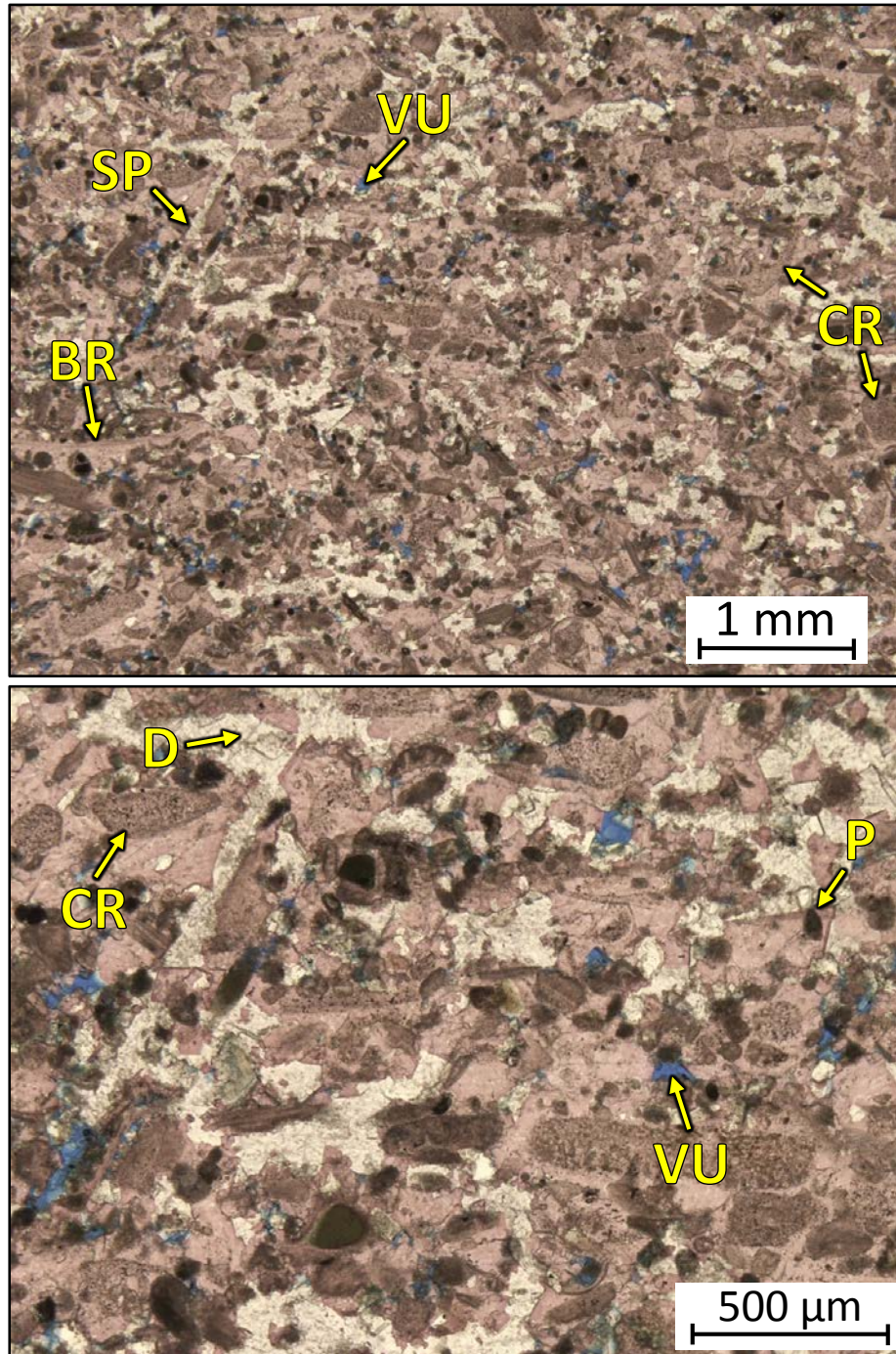
1AD – 5712.55 = Peloidal-skeletal grainstone. Sample is alizarin red stained. Porosity (NCS): 0.9%. Permeability (Klinkenberg): <0.0001 mD. TOC: 0.01%. XRD: 1% clays (1% illite), 84% carbonates (82% calcite and 2% dolomite), and 15% other minerals (12% quartz, 1% potassium feldspar, 2% plagioclase feldspar, and trace amounts of pyrite). Sample contains crinoid fragments (20%), sponge spicules (15%), brachiopod fragments (10%), and peloids (10%). Minor amounts of oil-filled vug porosity observed.



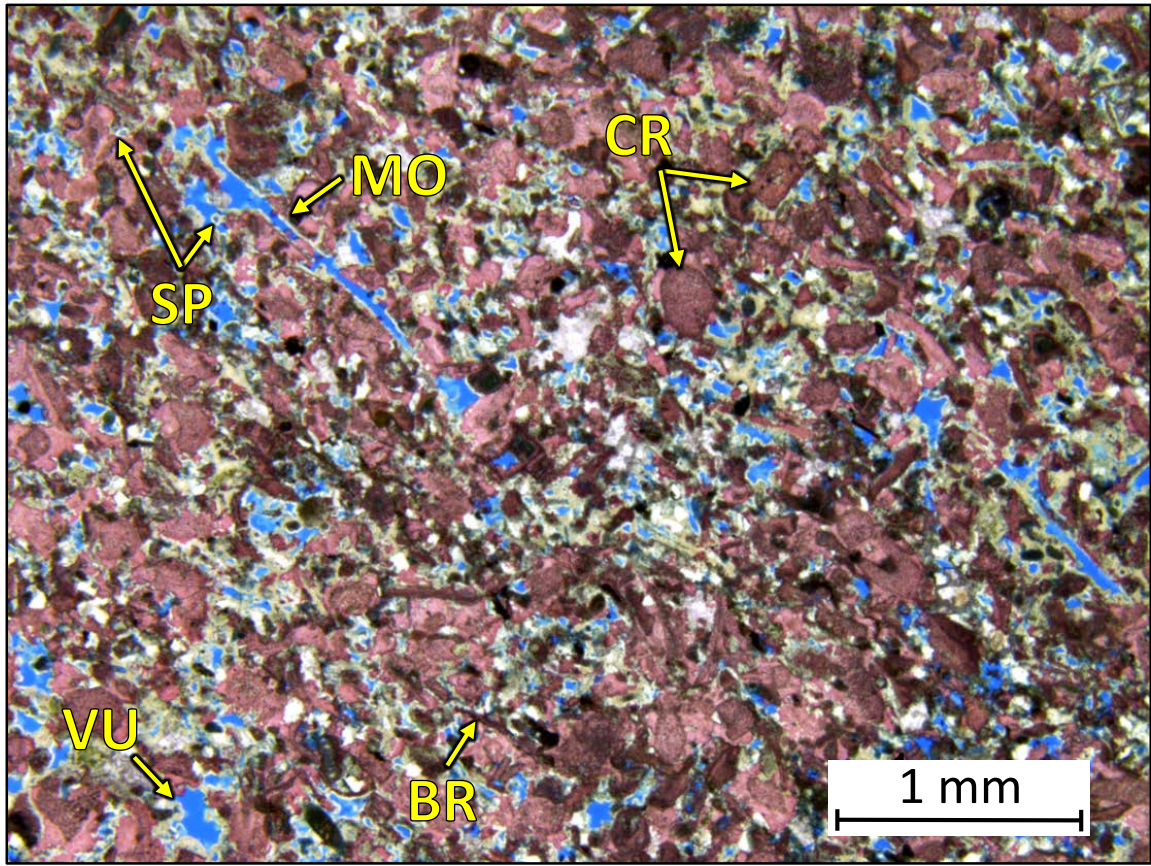
1AD – 5709.65 = Silicified grainstone. Sample is alizarin red stained. Porosity (NCS): 1.4%. Permeability (Klinkenberg): 0.282 mD. TOC: 0.01%. XRD: Trace amounts of clays, 28% carbonates (21% calcite and 7% dolomite), and 72% other minerals (71% quartz, 1% potassium feldspar, and trace amounts of plagioclase feldspar and pyrite). Sample contains crinoid fragments and sponge spicules. Vug and moldic porosity observed.



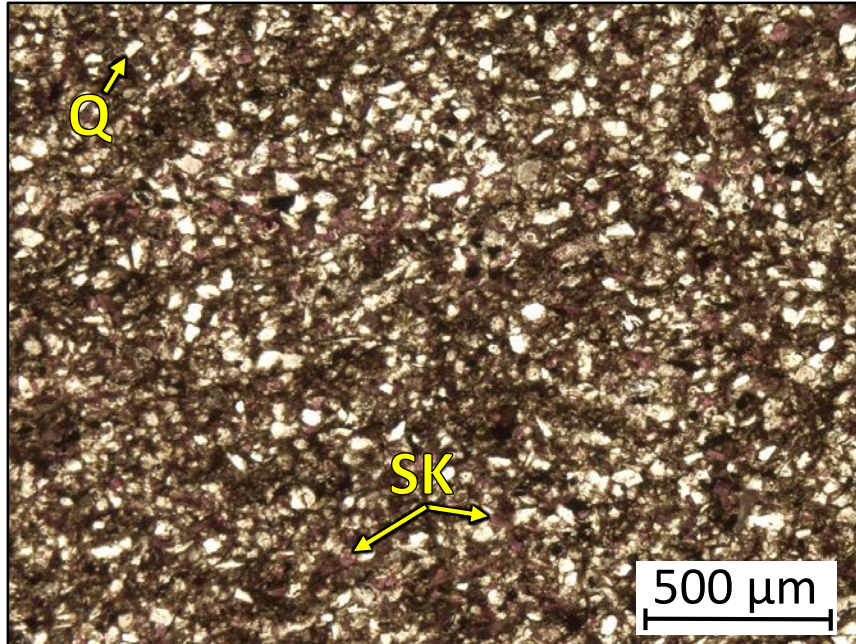
1AD – 5707.50 = Silicified grainstone. Sample is alizarin red stained. Porosity (NCS): 0.4%. Permeability (Klinkenberg): <0.0001 mD. TOC: 0.07%. XRD: 1% clays (1% illite), 41% carbonates (37% calcite and 4% dolomite), and 58% other minerals (56% quartz, 1% potassium feldspar, 1% plagioclase feldspar, and trace amounts of pyrite). Sample contains crinoid fragments (20%), brachiopod fragments (5%), sponge spicules, and undifferentiated microbioclastic debris. Vug porosity observed.



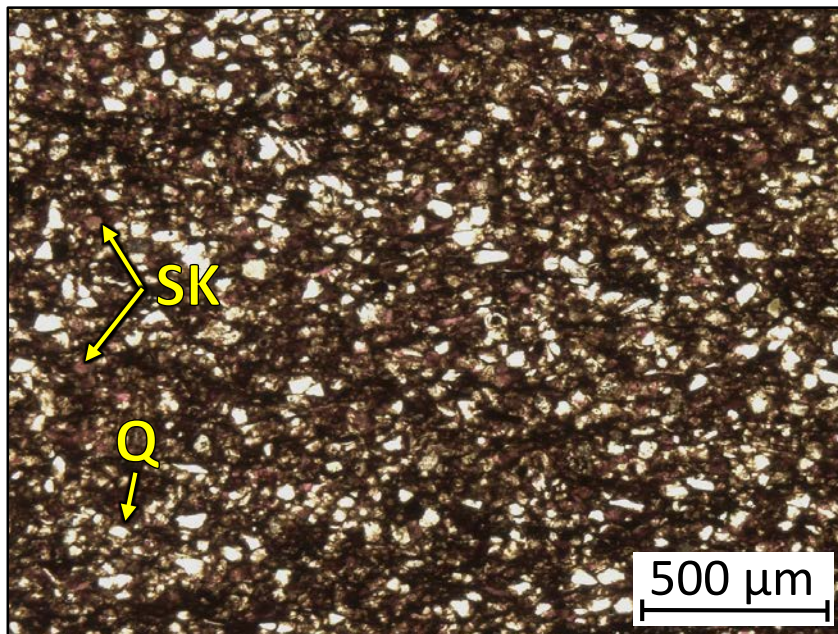
1AD – 5705.30' = Skeletal-peloidal grainstone. Sample is alizarin red stained and blue epoxy impregnated. Porosity (NCS): 5.0%. Permeability (Klinkenberg): 0.0031 mD. TOC: 0.12%. XRD: 1% clays (1% illite), 82% carbonates (69% calcite and 13% dolomite), and 17% other minerals (16% quartz, trace amounts of potassium feldspar, 1% plagioclase feldspar, and trace amounts of pyrite). Sample contains crinoid fragments (20%), peloids (15%), sponge spicules (15%), brachiopod fragments (5%) and undifferentiated microbioclastic debris. Vug and moldic porosity observed. Some dolomite has been replaced by calcite.



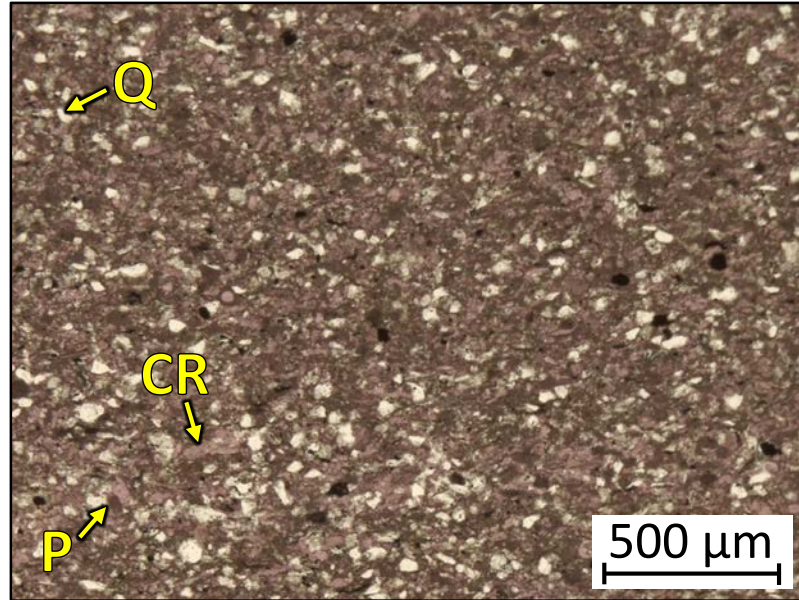
1AD – 5704.45' = Skeletal grainstone. Sample is alizarin red stained and blue epoxy impregnated. Porosity (NCS): 6.9%. Permeability (Klinkenberg): 0.087 mD. TOC: 0.29%. XRD: 1% clays (1% illite), 73% carbonates (68% calcite and 5% dolomite), and 26% other minerals (21% quartz, 2% potassium feldspar, 3% plagioclase feldspar, and trace amounts of pyrite). Sample contains crinoid fragments (30%), sponge spicules (10%), brachiopod fragments (3%), and undifferentiated microbioclastic debris. Abundant moldic and vug porosity observed.



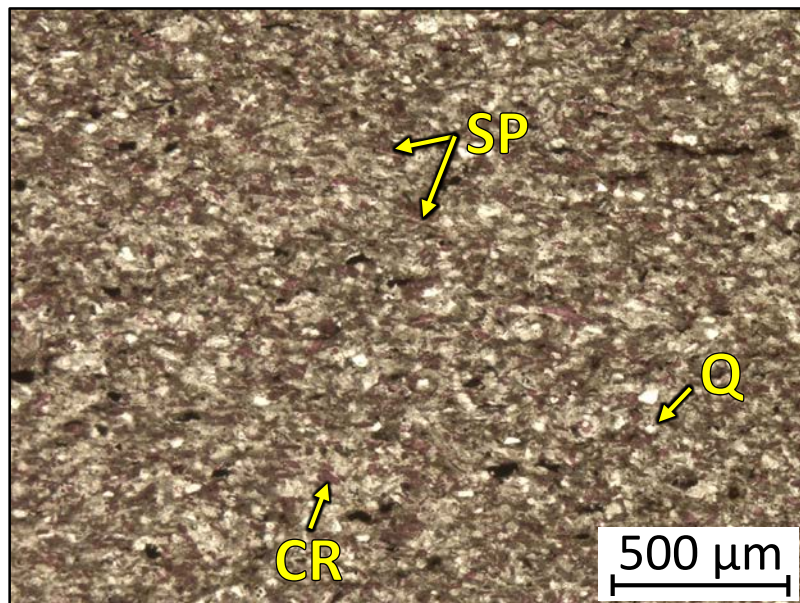
1AD – 5701.65' = Bioturbated wackestone. Sample is alizarin red stained. Porosity (NCS): 1.4%. Permeability (Klinkenberg): 0.075 mD. TOC: 1.06%. XRD: 12% clays (9% illite and 3% mixed layer illite/smectite), 30% carbonates (23% calcite and 7% dolomite), and 58% other minerals (45% quartz, 3% potassium feldspar, 6% plagioclase feldspar, 3% pyrite, and 1% apatite). Sample contains silt-sized quartz grains and undifferentiated microbioclastic debris.



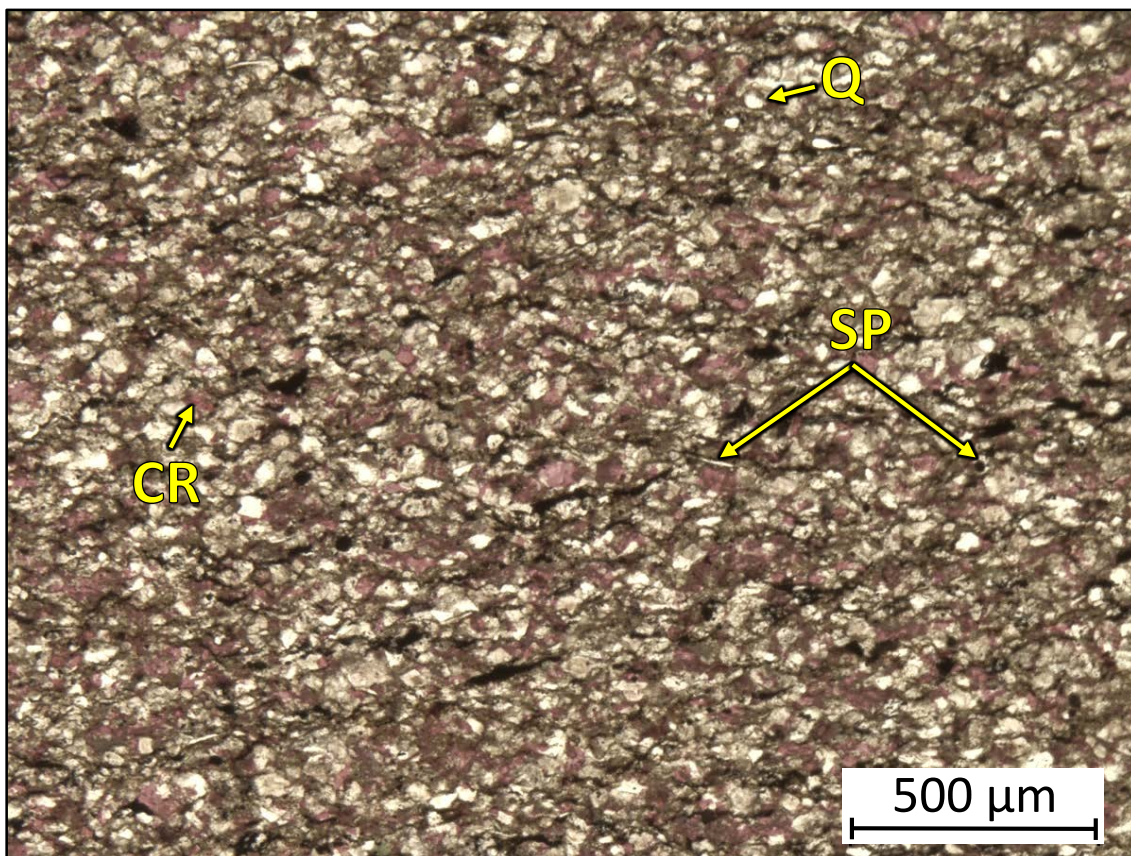
1AD – 5701.30-5701.55' = Bioturbated wackestone. Sample is alizarin red stained. TOC: 1.21%. XRD: 13% clays (9% illite and 4% mixed layer illite/smectite), 24% carbonates (20% calcite and 4% dolomite), and 63% other minerals (49% quartz, 4% potassium feldspar, 7% plagioclase feldspar, 3% pyrite, and trace amounts of apatite). Sample contains silt-sized quartz grains and undifferentiated microbioclastic debris.



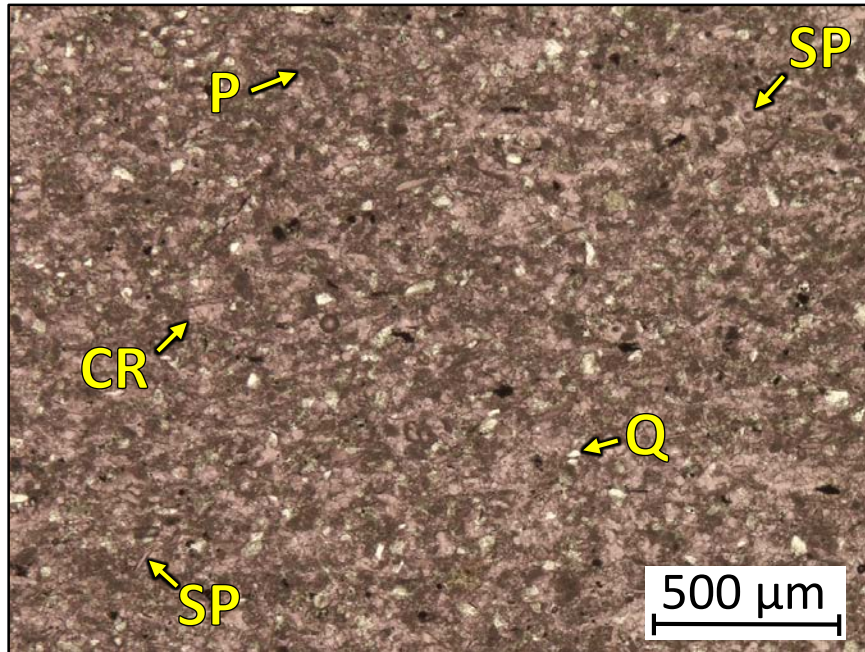
1AD – 5697.50' = Bioturbated wackestone. Sample is alizarin red stained. Porosity (NCS): 0.3%. Permeability (Klinkenberg): <0.0001 mD. TOC: 0.06%. XRD: 5% clays (4% illite and 1% mixed layer illite/smectite), 57% carbonates (51% calcite and 6% dolomite), and 38% other minerals (34% quartz, 1% potassium feldspar, 2% plagioclase feldspar, and 1% pyrite). Sample contains silt-sized quartz grains (30%), crinoid fragments (15%), peloids (5%), and undifferentiated microbioclastic debris.



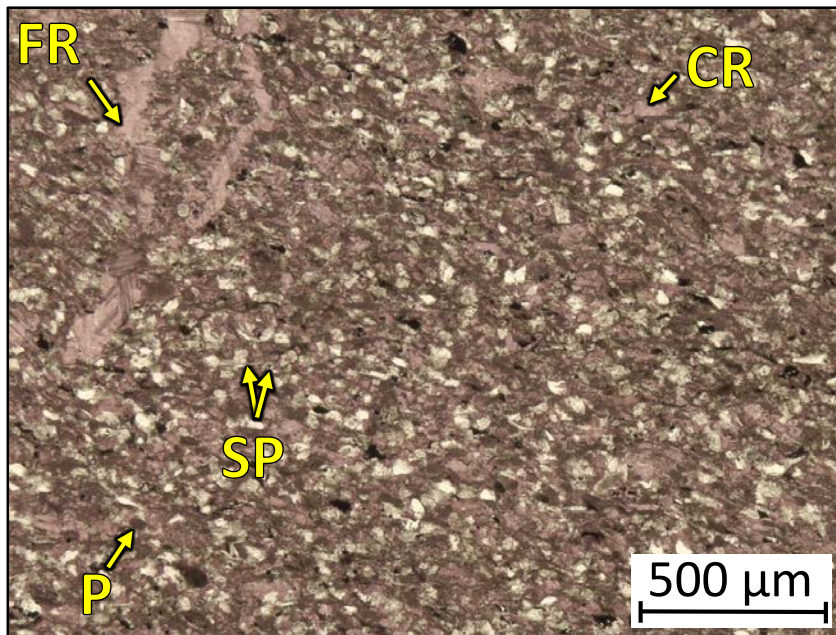
1AD – 5691.10' = Silicified skeletal packstone-grainstone. Sample is alizarin red stained. Porosity (NCS): 1.3%. Permeability (Klinkenberg): <0.0001 mD. TOC: 0.10%. XRD: 3% clays (2% illite and 1% mixed layer illite/smectite), 32% carbonates (26% calcite and 6% dolomite), and 65% other minerals (56% quartz, 3% potassium feldspar, 4% plagioclase feldspar, 1% pyrite, trace amounts of apatite, and 1% marcasite). Sample contains silt-sized quartz grains (15%), crinoid fragments (10%), sponge spicules (10%), and undifferentiated microbioclastic debris.



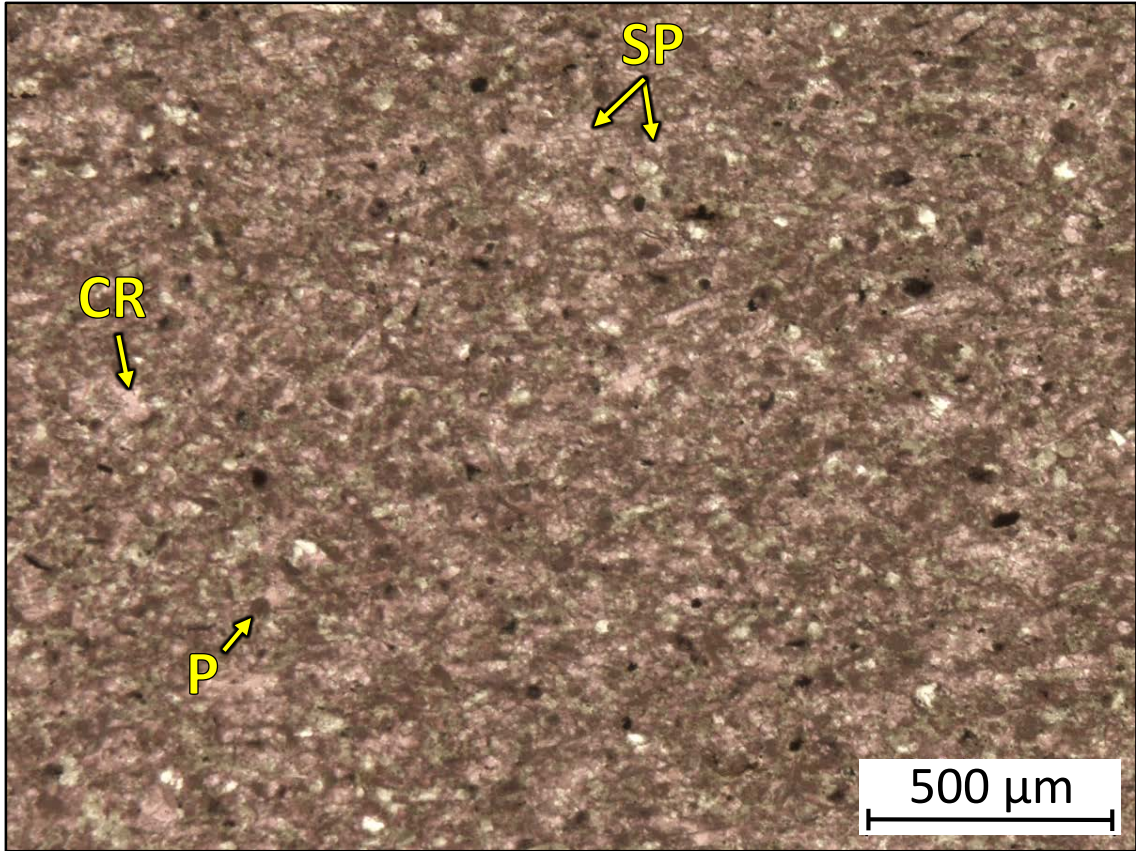
1AD – 5688.85' = Crinoidal packstone. Sample is alizarin red stained. Porosity (NCS): 2.8%. Permeability (Klinkenberg): <0.0001 mD. TOC: 0.14%. XRD: 5% clays (4% illite and 1% mixed layer illite/smectite), 47% carbonates (34% calcite and 13% dolomite), and 48% other minerals (38% quartz, 1% potassium feldspar, 6% plagioclase feldspar, 2% pyrite, and 1% apatite). Sample consists of silt-sized quartz grains (30%), crinoid fragments (15%), sponge spicules (7%), and undifferentiated microbioclastic debris. Oil-filled moldic and vug porosity observed.



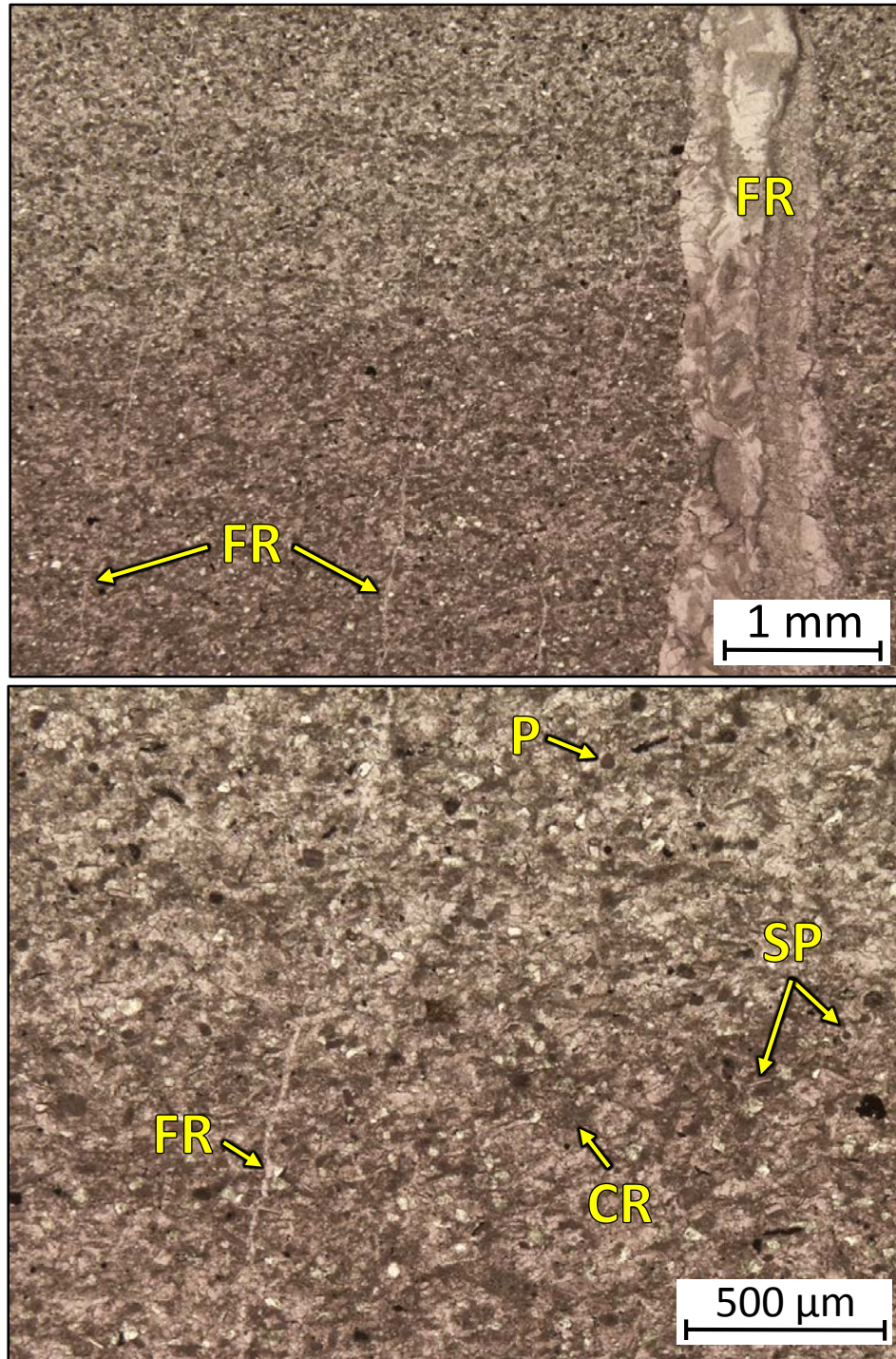
1AD – 5687.50' = Peloidal-skeletal packstone. Sample is alizarin red stained. Porosity (NCS): 0.3%. Permeability (Klinkenberg): <0.0001 mD. TOC: 0.06%. XRD: Trace amounts of clays, 75% carbonates (73% calcite and 2% dolomite), and 25% other minerals (22% quartz, 1% potassium feldspar, 2% plagioclase feldspar, and trace amounts of pyrite). Sample contains crinoidal debris (20%), sponge spicules (10%), peloids (10%), and silt-sized quartz grains (15%).



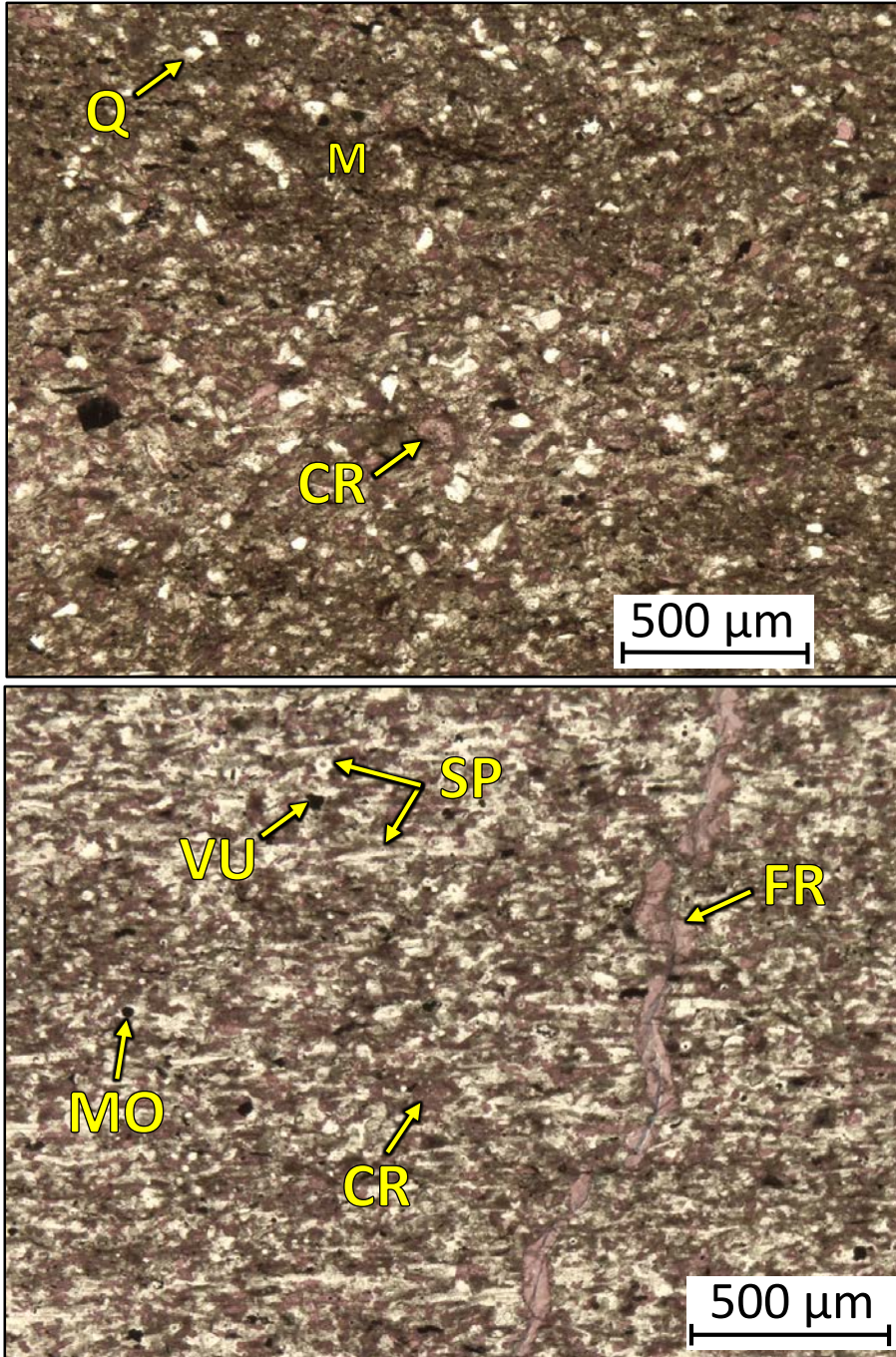
1AD – 5683.40' = Crinoidal-peloidal packstone-grainstone. Sample is alizarin red stained. Porosity (NCS): 1.0%. Permeability (Klinkenberg): <0.0001 mD. TOC: 0.03%. XRD: 2% clays (1% illite and 1% mixed layer illite/smectite), 54% carbonates (51% calcite and 3% dolomite), and 44% other minerals (39% quartz, 1% potassium feldspar, 3% plagioclase feldspar, and 1% pyrite). Sample contains peloids (20%), crinoid fragments (10%), and sponge spicules (10%).



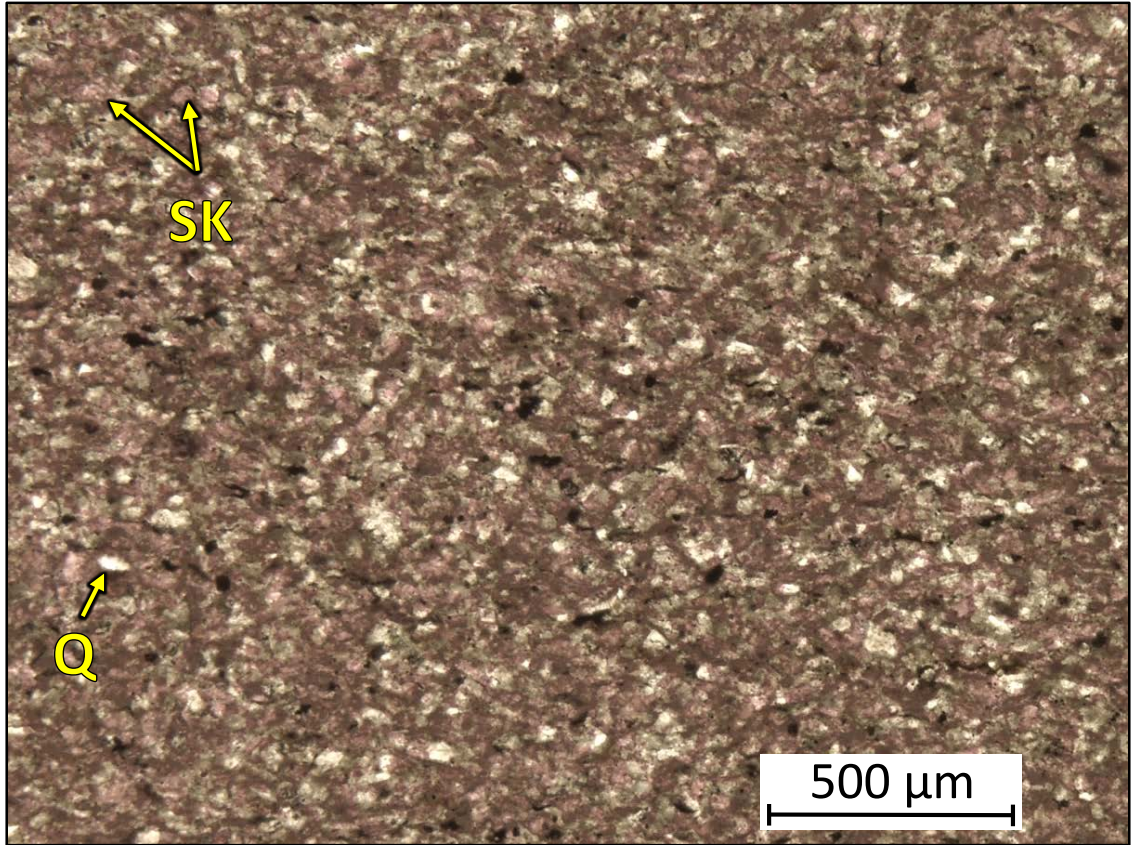
1AD – 5678.35' = Bioturbated skeletal packstone. Sample is alizarin red stained. Porosity (NCS): 0.6%. Permeability (Klinkenberg): <0.0001 mD. TOC: 0.01%. XRD: Trace amounts of clays, 69% carbonates (67% calcite and 2% dolomite), and 31% other minerals (27% quartz, 1% potassium feldspar, 2% plagioclase feldspar, 1% pyrite, and trace amounts of apatite). Sample contains crinoidal debris (20%), peloids (20%), sponge spicules (10%), and undifferentiated microbioclastic debris.



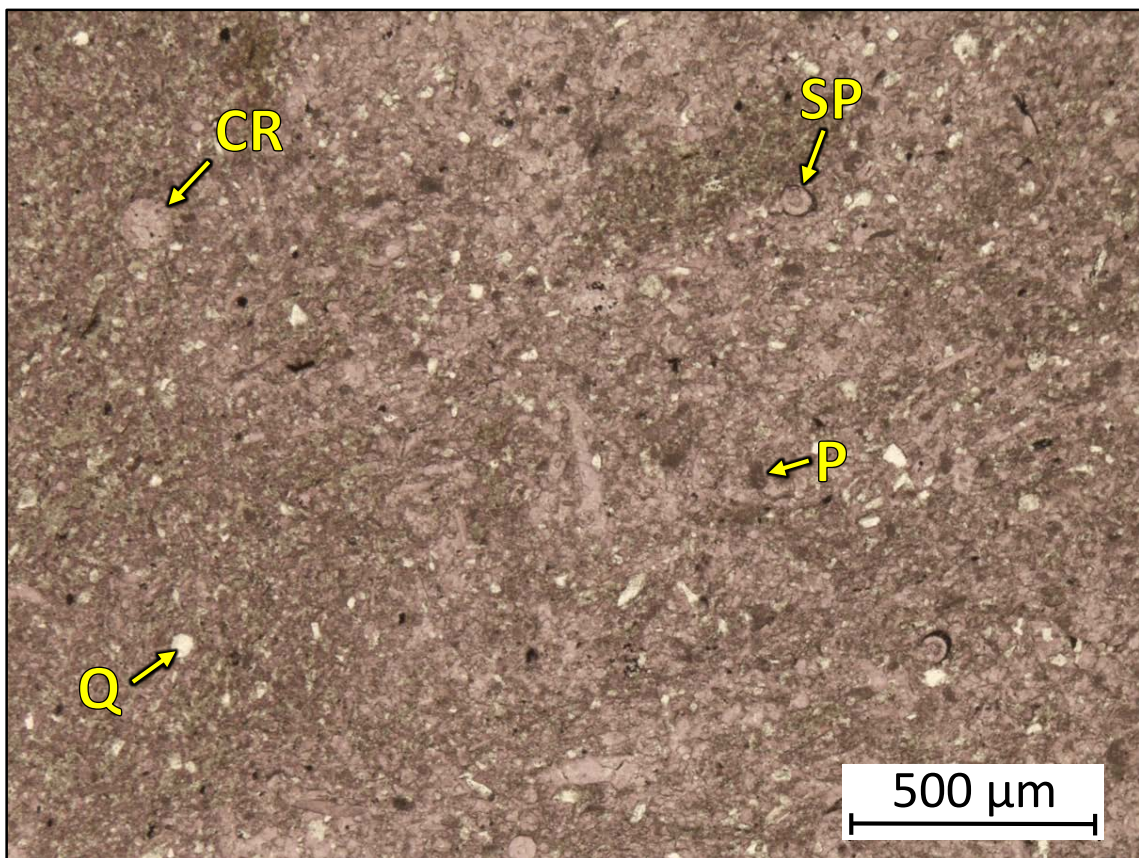
1AD – 5676.70' = Peloidal grainstone. Sample is alizarin red stained. Porosity (NCS): 0.2%. Permeability (Klinkenberg): <0.0001 mD. TOC: 0.01%. XRD: 1% clays (1% illite), 79% carbonates (77% calcite and 2% dolomite), and 20% other minerals (17% quartz, trace amounts of potassium feldspar, 3% plagioclase feldspar, and trace amounts of pyrite). Sample contains crinoidal debris (40%), peloids (20%), and sponge spicules (7%). Large fracture is calcite cemented and shows multiple cementation events. Micro-fractures are cemented with blocky calcite cement.



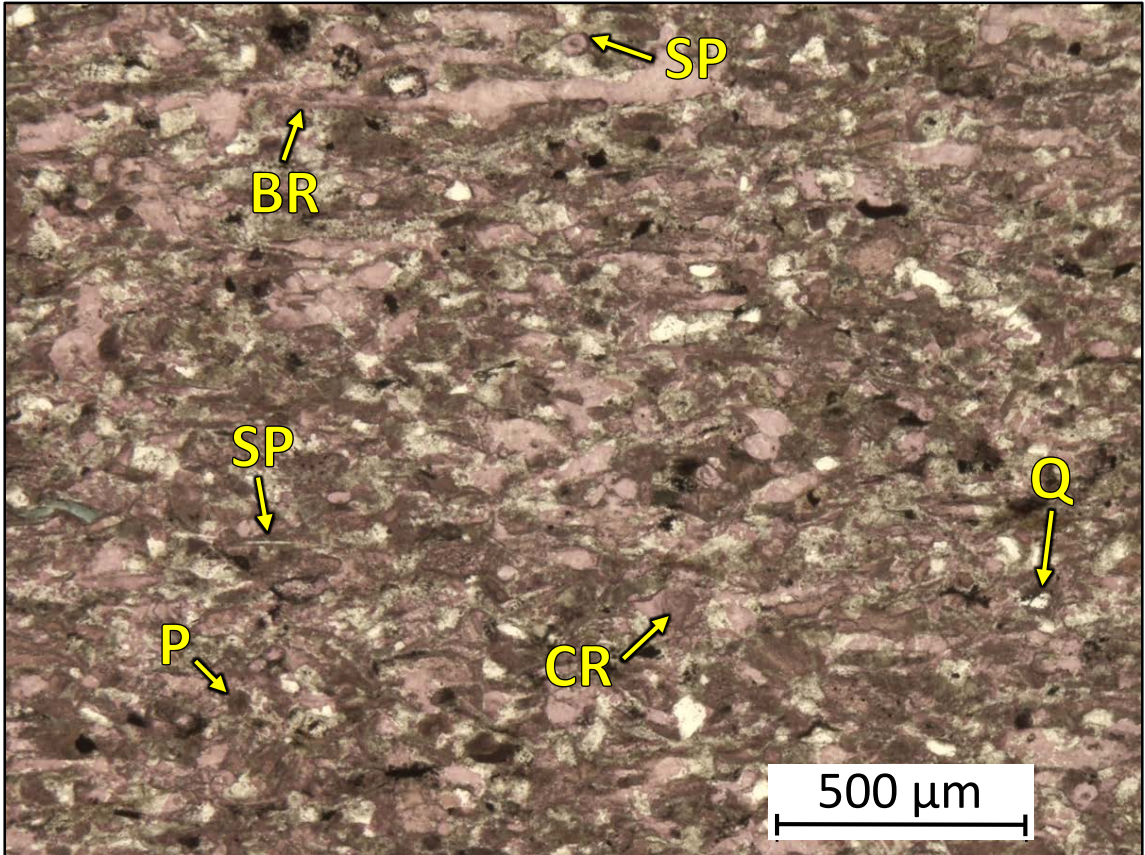
1AD – 5673.25' = Bioturbated wackestone-skeletal packstone. Sample is alizarin red stained. Porosity (NCS): 1.3%. Permeability (Klinkenberg): 0.178 mD. TOC: 0.05%. XRD: 5% clays (3% illite and 2% mixed layer illite/smectite), 33% carbonates (30% calcite and 3% dolomite), and 62% other minerals (51% quartz, 3% potassium feldspar, 6% plagioclase feldspar, 2% pyrite, and trace amounts of apatite). Sample is characterized by varying mineralogies and constituents depending on location. Sample contains crinoid fragments (10%), sponge spicules (10-35%), silt-sized quartz grains, and undifferentiated microbioclastic debris. Ptygmatic fracture in sample is filled with calcite cement and shows some evidence of available porosity and permeability. Vug and moldic porosity observed.



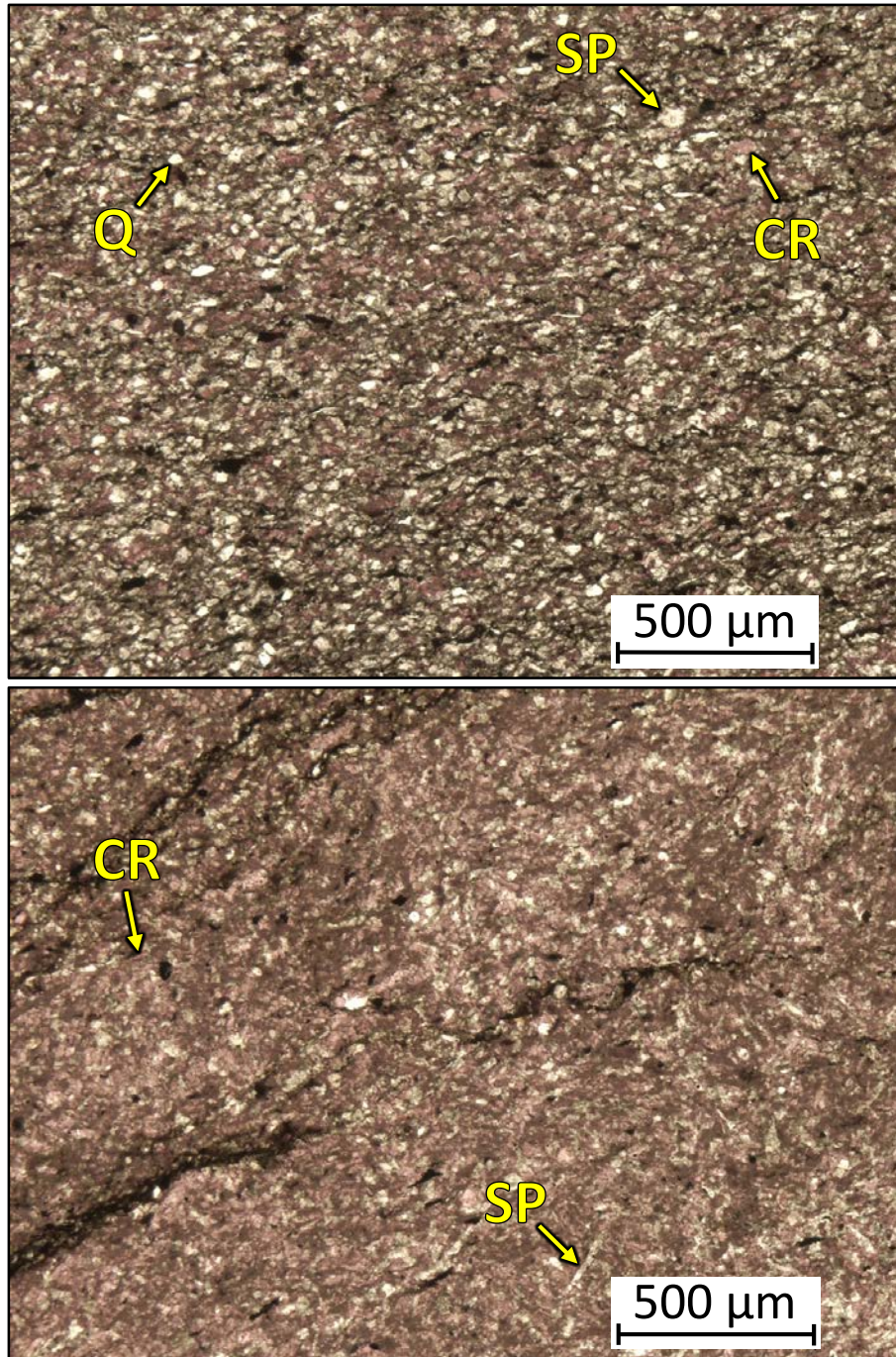
1AD – 5669.70' = Bioturbated wackestone-packstone. Sample is alizarin red stained. Porosity (NCS): 1.3%. Permeability (Klinkenberg): <0.0001 mD. TOC: 0.07%. XRD: 3% clays (2% illite and 1% mixed layer illite/smectite), 49% carbonates (44% calcite and 5% dolomite), and 48% other minerals (40% quartz, 2% potassium feldspar, 5% plagioclase feldspar, 1% pyrite, and trace amounts of apatite). Sample contains silt-sized quartz grains and undifferentiated microbioclastic debris composed mostly of crinoidal debris.



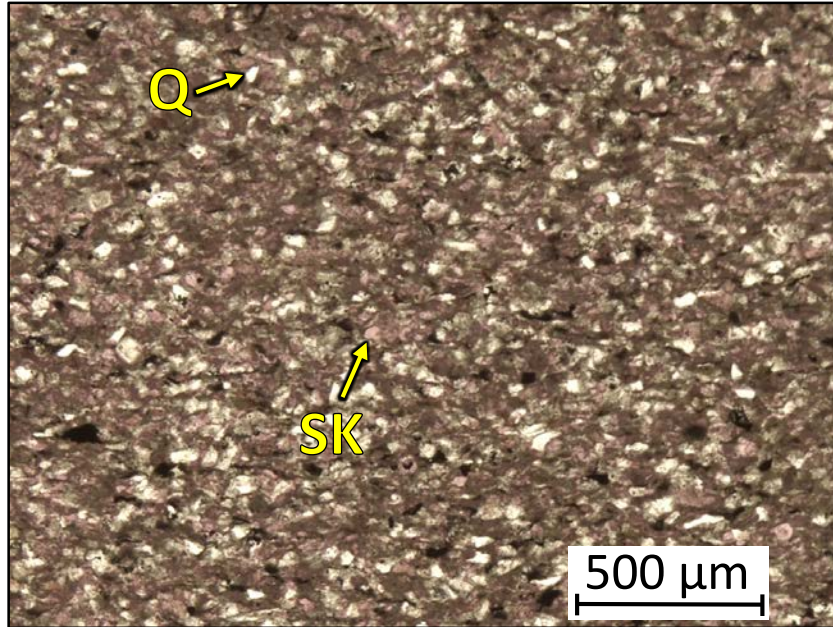
1AD – 5666.70' = Bioturbated wackestone-skeletal packstone. Sample is alizarin red stained. Porosity (NCS): 0.3%. Permeability (Klinkenberg): <0.0001 mD. TOC: 0.03%. XRD: 1% clays (1% illite), 75% carbonates (73% calcite and 2% dolomite), and 24% other minerals (21% quartz, 1% potassium feldspar, 2% plagioclase feldspar, and trace amounts of pyrite). Sample contains crinoid fragments (20%), silt-sized quartz grains (20%), peloids (15%), sponge spicules (10%), and undifferentiated microbioclastic debris. Some spicules are partially replaced by calcite.



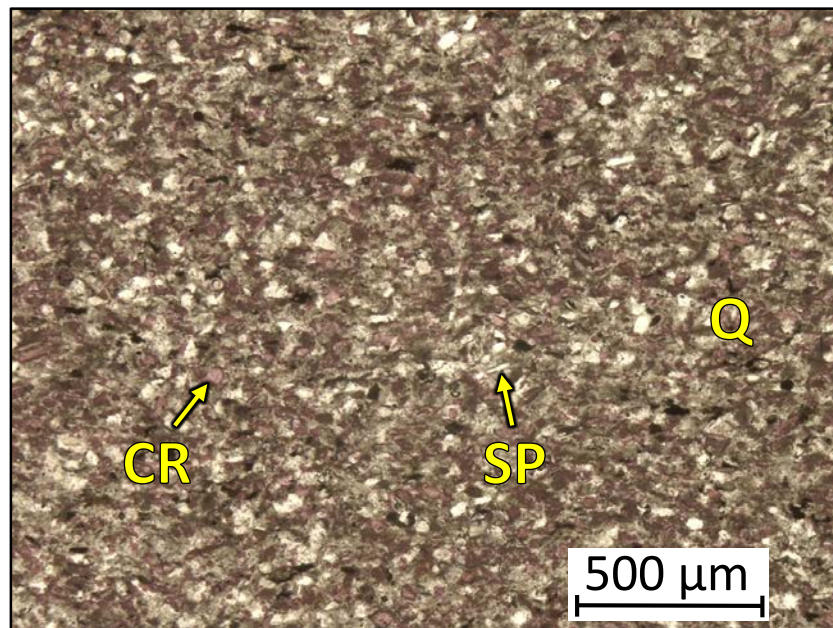
1AD – 5666.20' = Skeletal packstone-grainstone. Sample is alizarin red stained. Porosity (NCS): 0.5%. Permeability (Klinkenberg): <0.0001 mD. TOC: 0.03%. XRD: Trace amounts of clays, 51% carbonates (49% calcite and 2% dolomite), and 49% other minerals (45% quartz, 2% potassium feldspar, 2% plagioclase feldspar, and trace amounts of pyrite). Sample contains crinoid fragments (15%), peloids (10%), sponge spicules (10%), brachiopod fragments, and silt-sized quartz grains (40%).



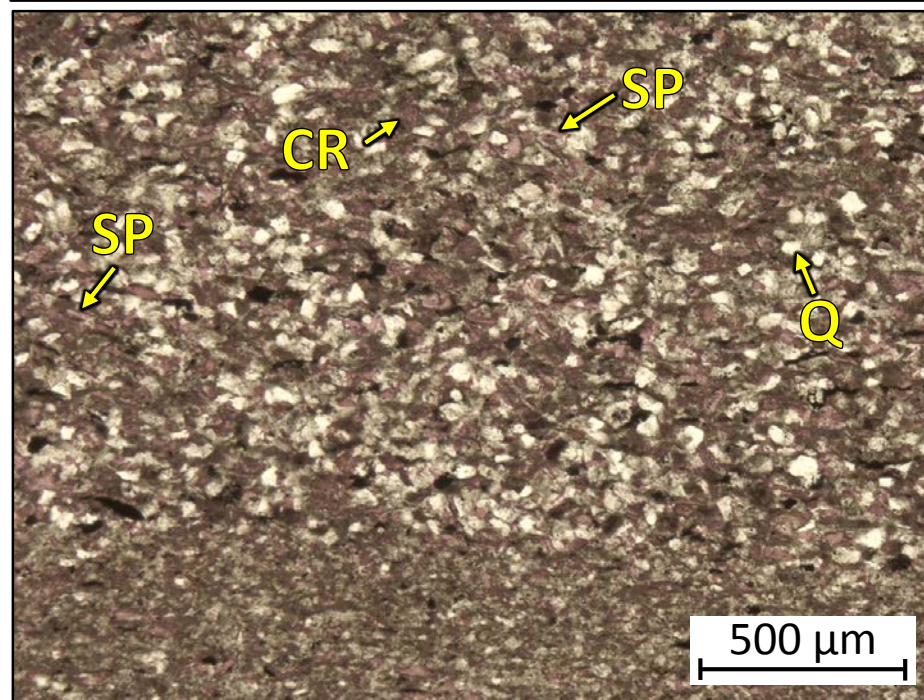
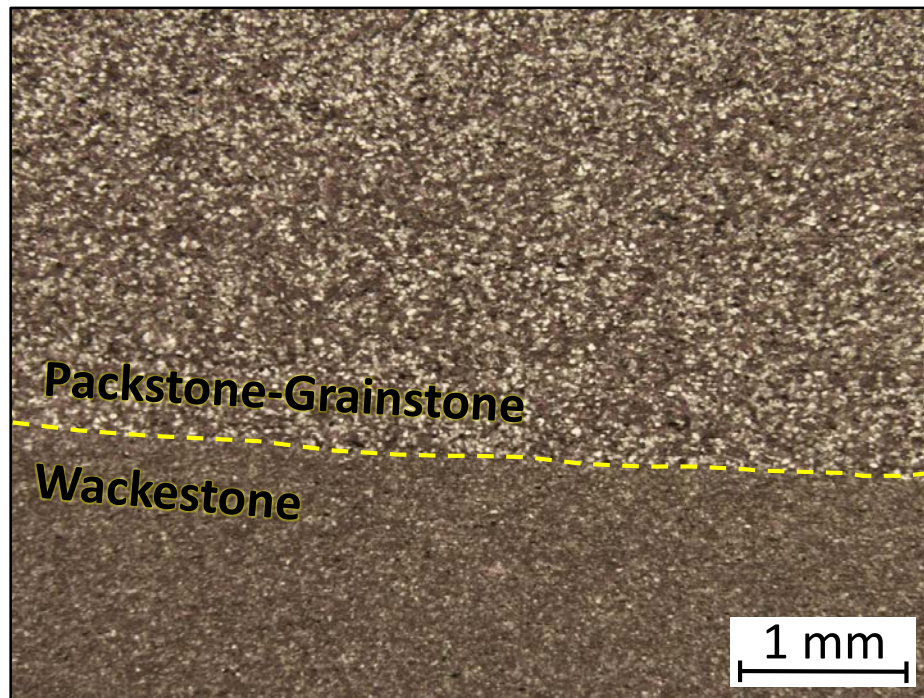
1AD – 5663.75' = Bioturbated packstone-skeletal packstone. Sample is alizarin red stained. Porosity (NCS): 2.1%. Permeability (Klinkenberg): <0.0001 mD. TOC: 0.08%. XRD: 2% clays (1% illite and 1% mixed layer illite/smectite), 53% carbonates (48% calcite and 5% dolomite), and 45% other minerals (39% quartz, 2% potassium feldspar, 3% plagioclase feldspar, 1% pyrite, and trace amounts of apatite). Sample is characterized by varying mineralogies and constituents. Sample contains crinoidal debris (10-30%), silt-sized quartz grains (20-10%), sponge spicules (5-15%), and undifferentiated microbioclastic debris. Moldic and vug porosity observed.



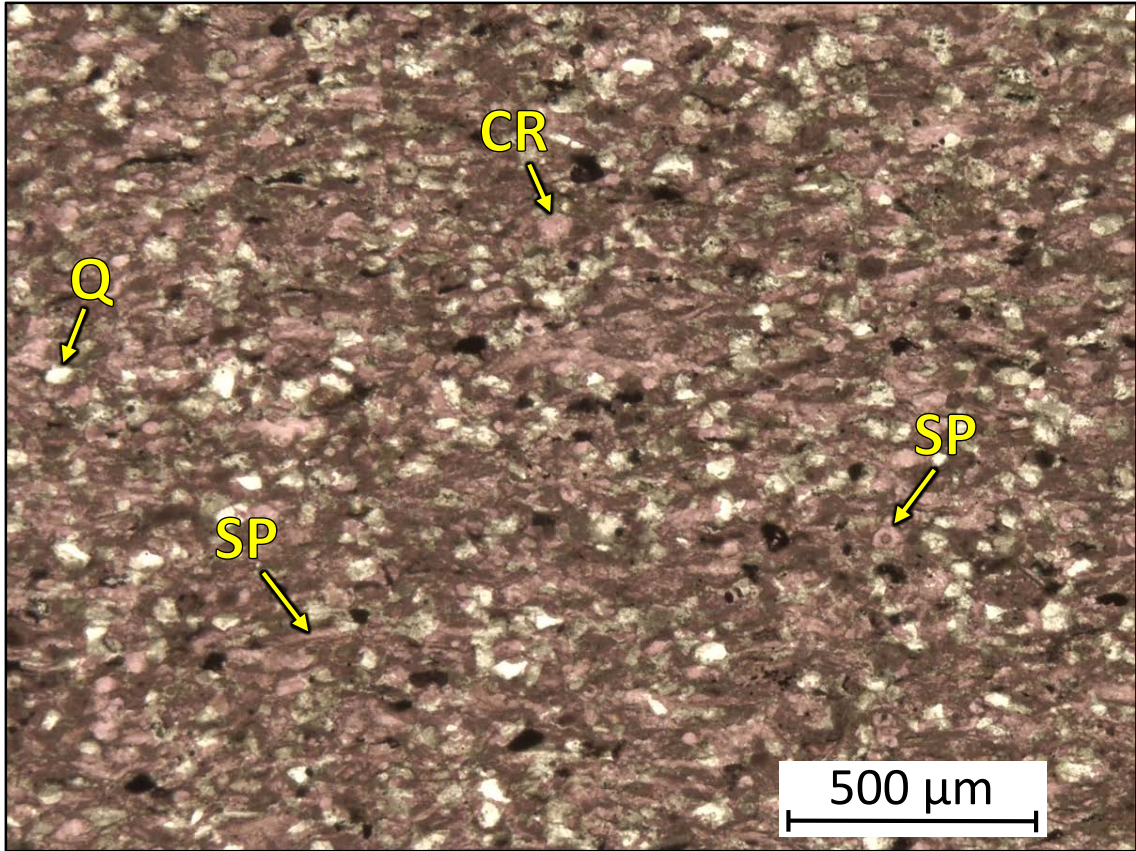
1AD – 5657.10' = Bioturbated wackestone-packstone. Sample is alizarin red stained. Porosity (NCS): 0.6%. Permeability (Klinkenberg): <0.0001 mD. TOC: 0.06%. XRD: 1% clays (1% illite), 39% carbonates (36% calcite and 3% dolomite), and 60% other minerals (53% quartz, 2% potassium feldspar, 4% plagioclase feldspar, 1% pyrite, and trace amounts of apatite). Sample contains silt-sized quartz grains and undifferentiated microbioclastic debris.



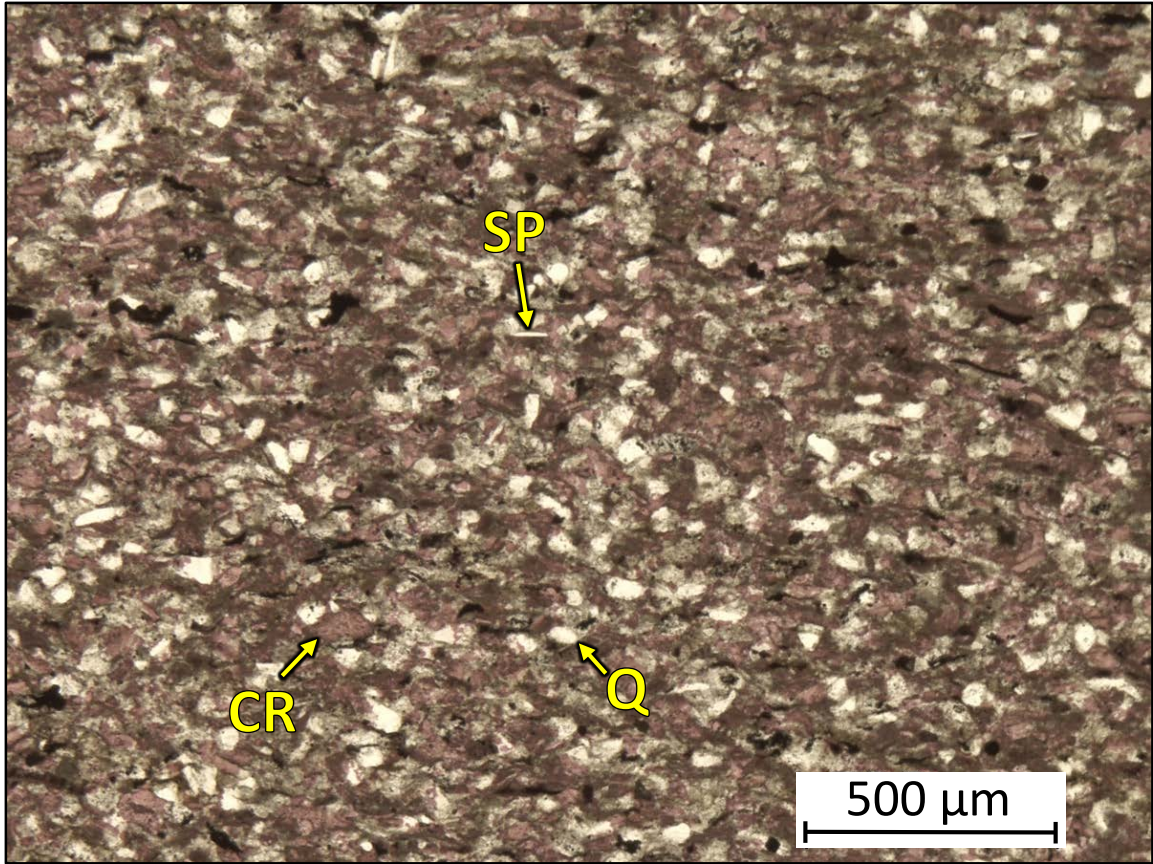
1AD – 5654.80' = Partially silicified, bioturbated peloidal packstone. Sample is alizarin red stained. Porosity (NCS): 0.8%. Permeability (Klinkenberg): <0.0001 mD. TOC: 0.07%. XRD: 1% clays (1% illite), 42% carbonates (39% calcite and 3% dolomite), and 57% other minerals (51% quartz, 2% potassium feldspar, 3% plagioclase feldspar, and 1% pyrite). Sample contains silt-sized quartz grains (30%), crinoid fragments (15%), sponge spicule fragments (10%), and undifferentiated microbioclastic debris.



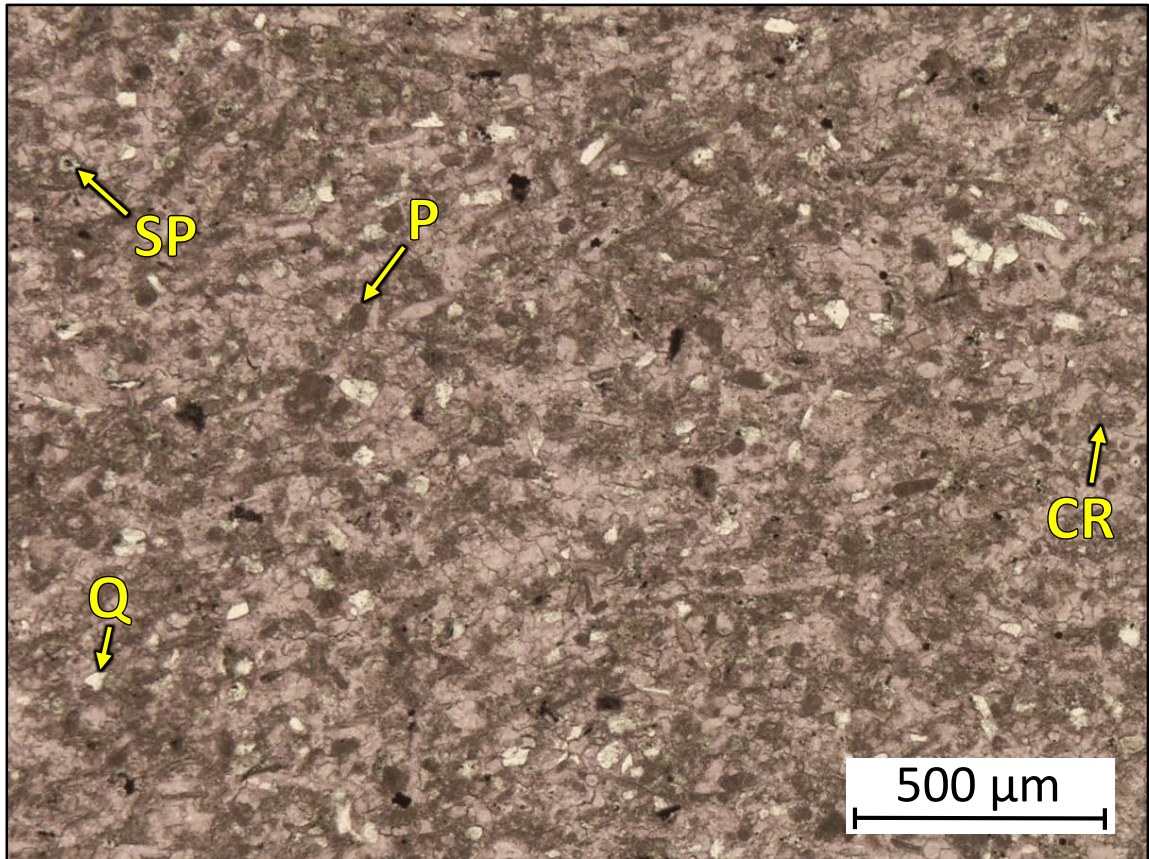
1AD – 5648.65' = Peloidal packstone to bioturbated wackestone-packstone. Sample is alizarin red stained. Porosity (NCS): 0.8%. Permeability (Klinkenberg): 0.0001 mD. TOC: 0.11%. XRD: 2% clays (1% illite and 1% mixed layer illite/smectite), 39% carbonates (37% calcite and 2% dolomite), and 59% other minerals (53% quartz, 2% potassium feldspar, 3% plagioclase feldspar, and 1% pyrite). Sample is characterized by varying mineralogies and constituents depending on location. Sample contains silt-sized quartz grains (50%), crinoid fragments (10%), sponge spicules (10%), and undifferentiated microbioclastic debris. Some sponge spicules have been replaced with calcite.



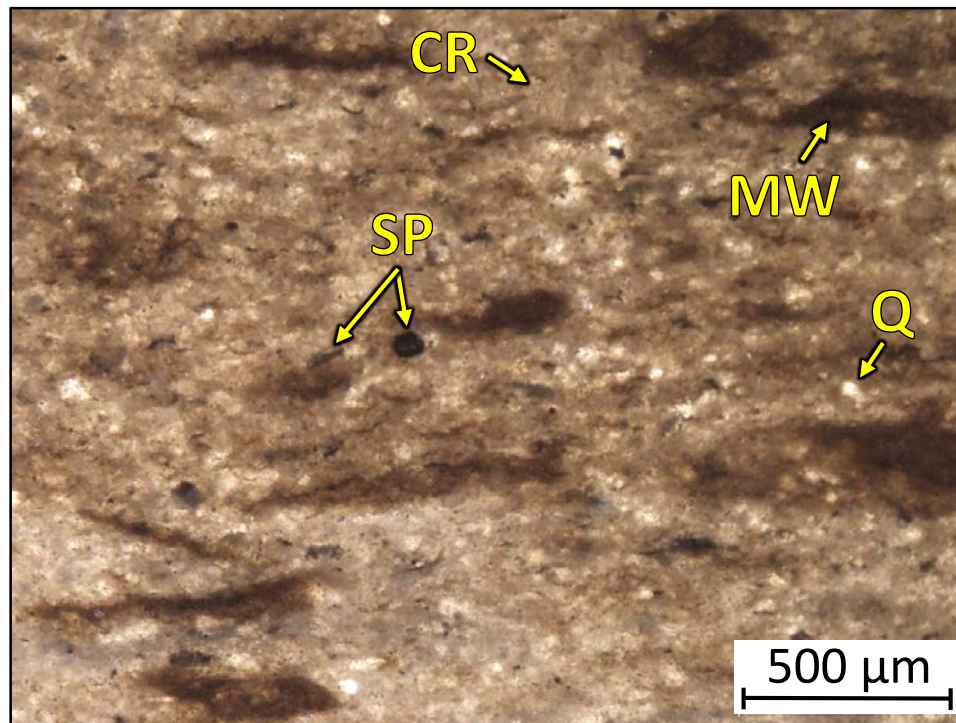
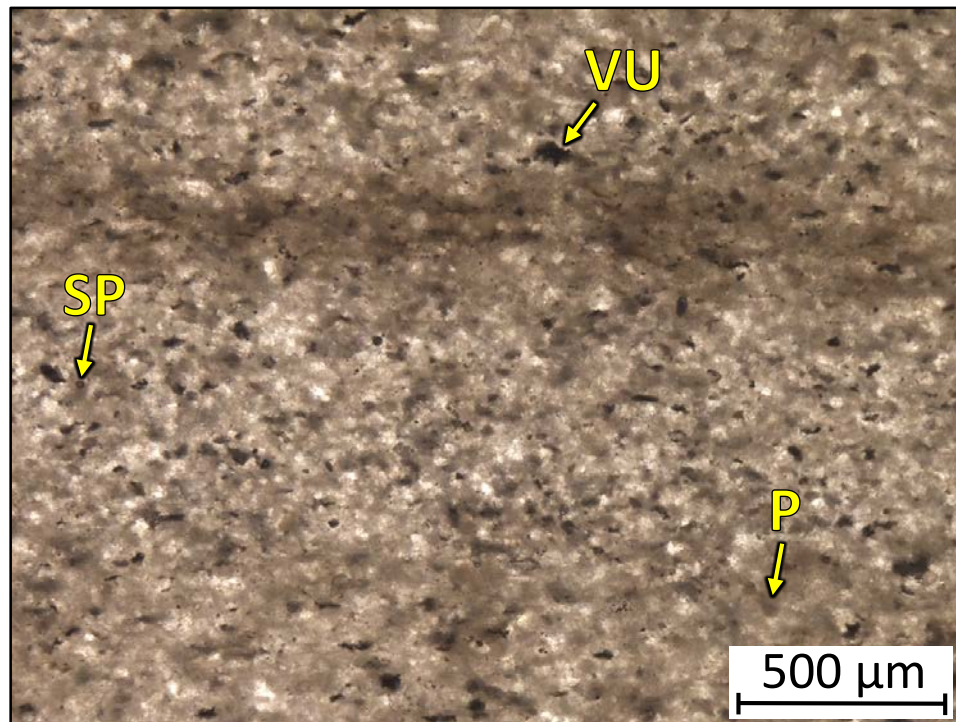
1AD – 5646.65' = Skeletal-peloidal packstone-grainstone. Sample is alizarin red stained. Porosity (NCS): 1.1%. Permeability (Klinkenberg): <0.0001 mD. TOC: 0.03%. XRD: 2% clays (1% illite and 1% mixed layer illite/smectite), 56% carbonates (54% calcite and 2% dolomite), and 42% other minerals (37% quartz, 1% potassium feldspar, 3% plagioclase feldspar, and 1% pyrite). Sample contains silt-sized quartz grains (35%), sponge spicules (15%), crinoid fragments (5%), and undifferentiated microbioclastic debris. Some sponge spicules are replaced by calcite. Minor amounts of moldic and vug porosity observed.



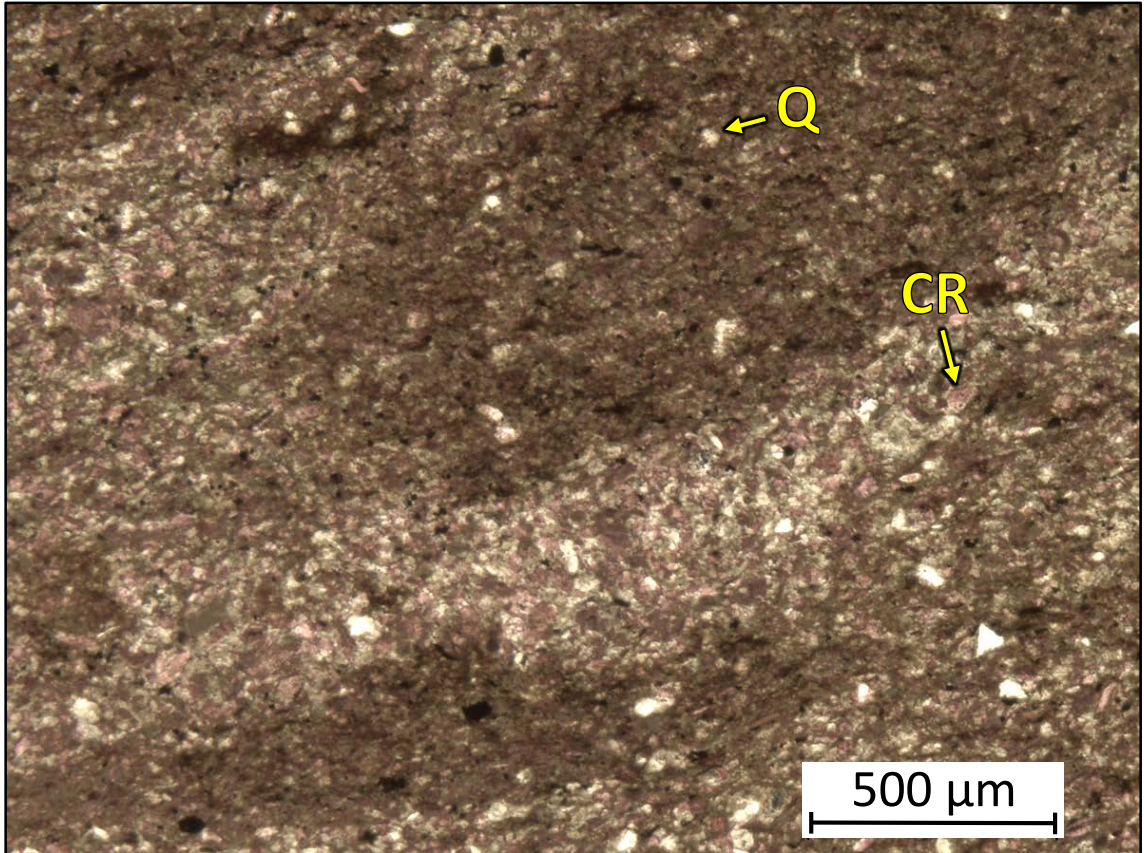
1AD – 5641.80' = Partially silicified, bioturbated peloidal packstone. Sample is alizarin red stained. Porosity (NCS): 1.0%. Permeability (Klinkenberg): <0.0001 mD. TOC: 0.05%. XRD: 1% clays (1% illite), 50% carbonates (47% calcite and 3% dolomite), and 49% other minerals (40% quartz, 3% potassium feldspar, 5% plagioclase feldspar, 1% pyrite, and trace amounts of apatite). Sample contains silt-sized quartz grains (35%), sponge spicule fragments (15%), crinoid fragments (10%), and undifferentiated microbioclastic debris. Oil-filled vug and moldic porosity observed.



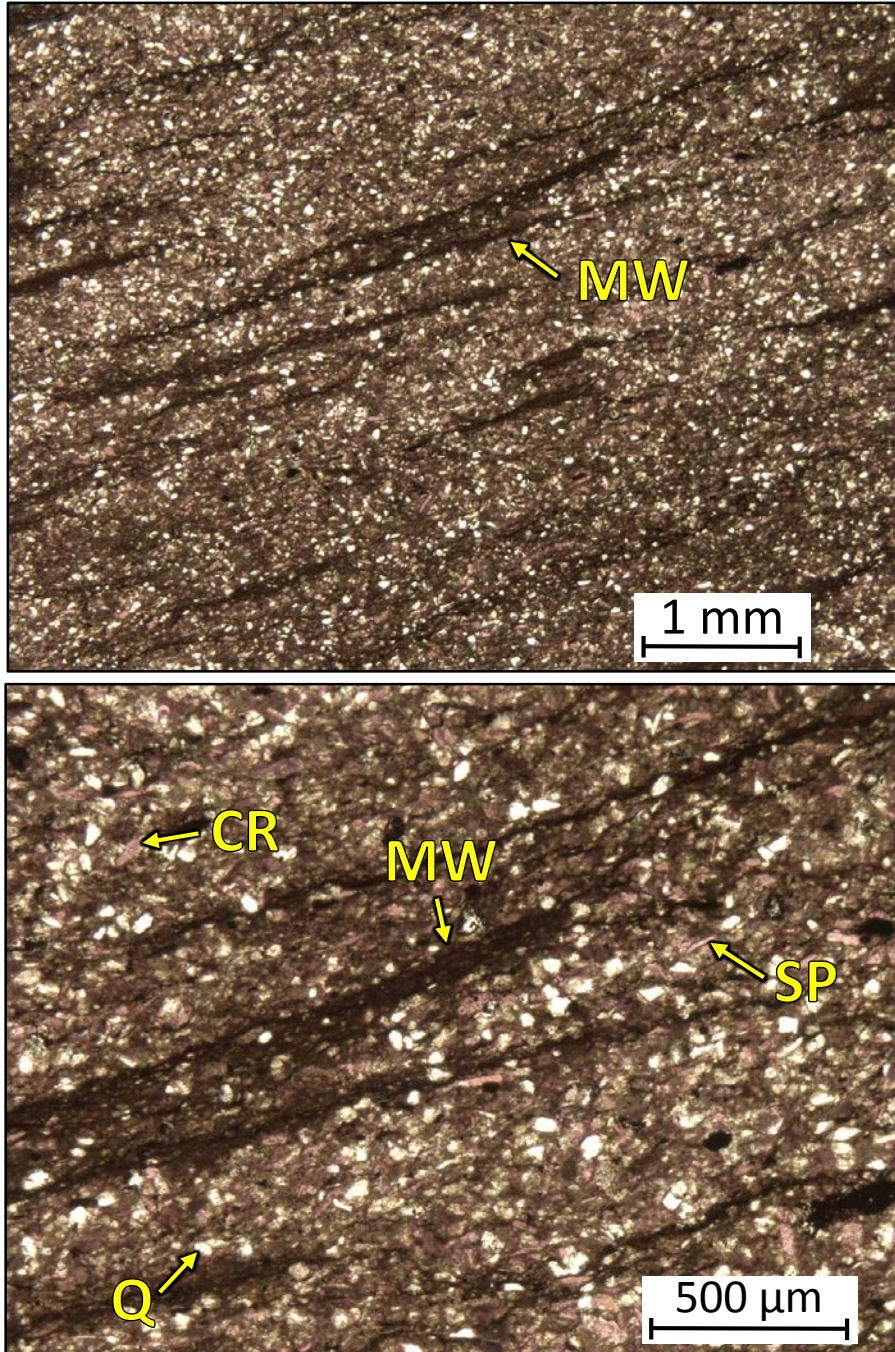
1AD – 5638.50' = Peloidal grainstone. Sample is alizarin red stained. Porosity (NCS): 0.4%. Permeability (Klinkenberg): <0.0001 mD. TOC: 0.02%. XRD: 1% clays (1% illite), 74% carbonates (72% calcite and 2% dolomite), and 25% other minerals (22% quartz, 1% potassium feldspar, 2% plagioclase feldspar, and trace amounts of pyrite). Sample contains crinoidal debris (30%), peloids (15%), sponge spicules (10%), silt-sized quartz grains (10%), and undifferentiated microbioclastic debris.



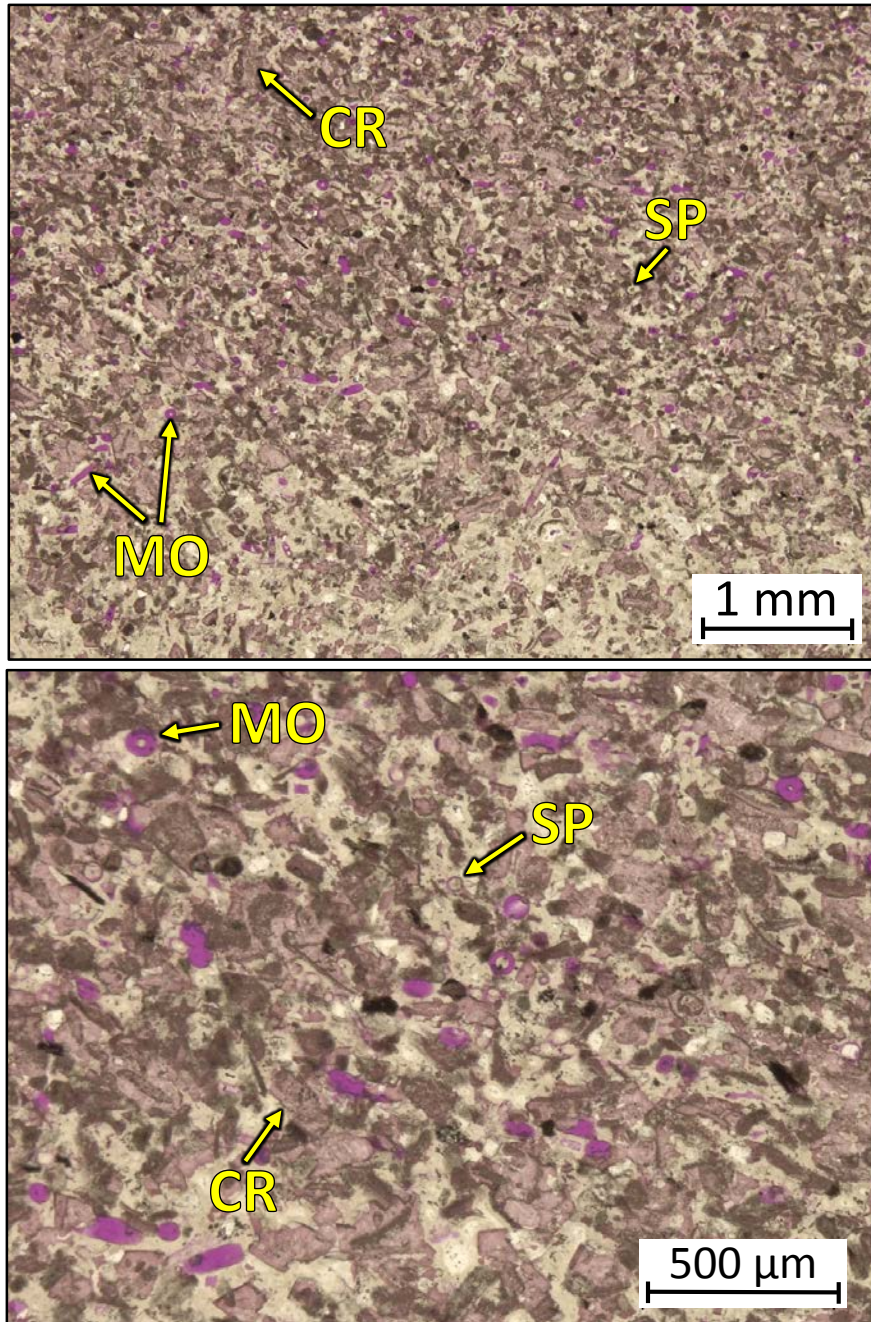
1AD – 5635.90' = Peloidal packstone-grainstone to bioturbated wackestone. Porosity (visual estimation): 1.5%. Visual estimation: 3% clays, 55% carbonates, and 42% other minerals. Sample contains silt-sized quartz grains, peloids, sponge spicules, crinoids, and undifferentiated microbioclastic debris. Vug and moldic porosity observed.



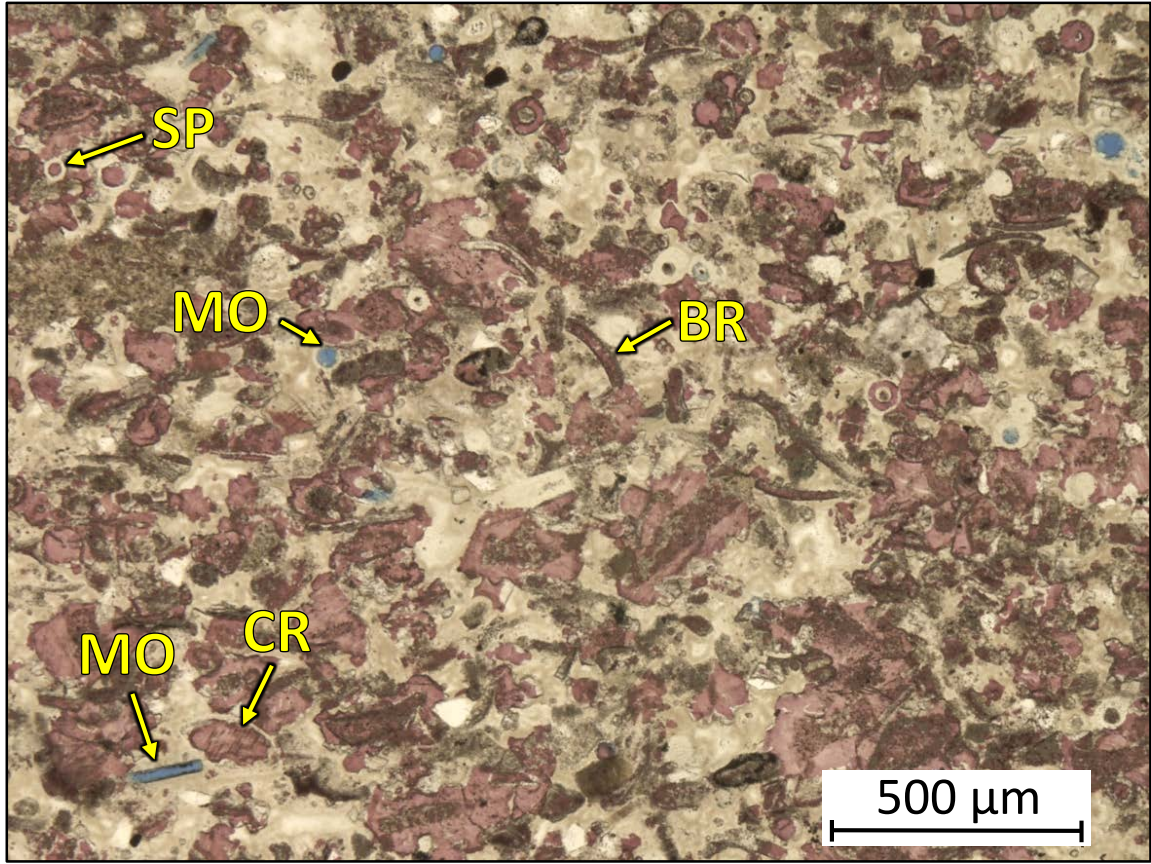
1AD – 5634.65' = Bioturbated wackestone with grainstone wisps. Sample is alizarin red stained. Porosity (NCS): 2.0%. Permeability (Klinkenberg): 0.0001 mD. TOC: 0.19%. XRD: 3% clays (2% illite and 1% mixed layer illite/smectite), 53% carbonates (49% calcite and 4% dolomite), and 44% other minerals (41% quartz, 1% potassium feldspar, 2% plagioclase feldspar, and trace amounts of pyrite and apatite). Sample is characterized by varying mineralogies and constituents depending on location. Sample contains crinoidal debris (10-30%), silt-sized quartz grains (20%), and undifferentiated microbioclastic debris. Oil-filled vug porosity observed.



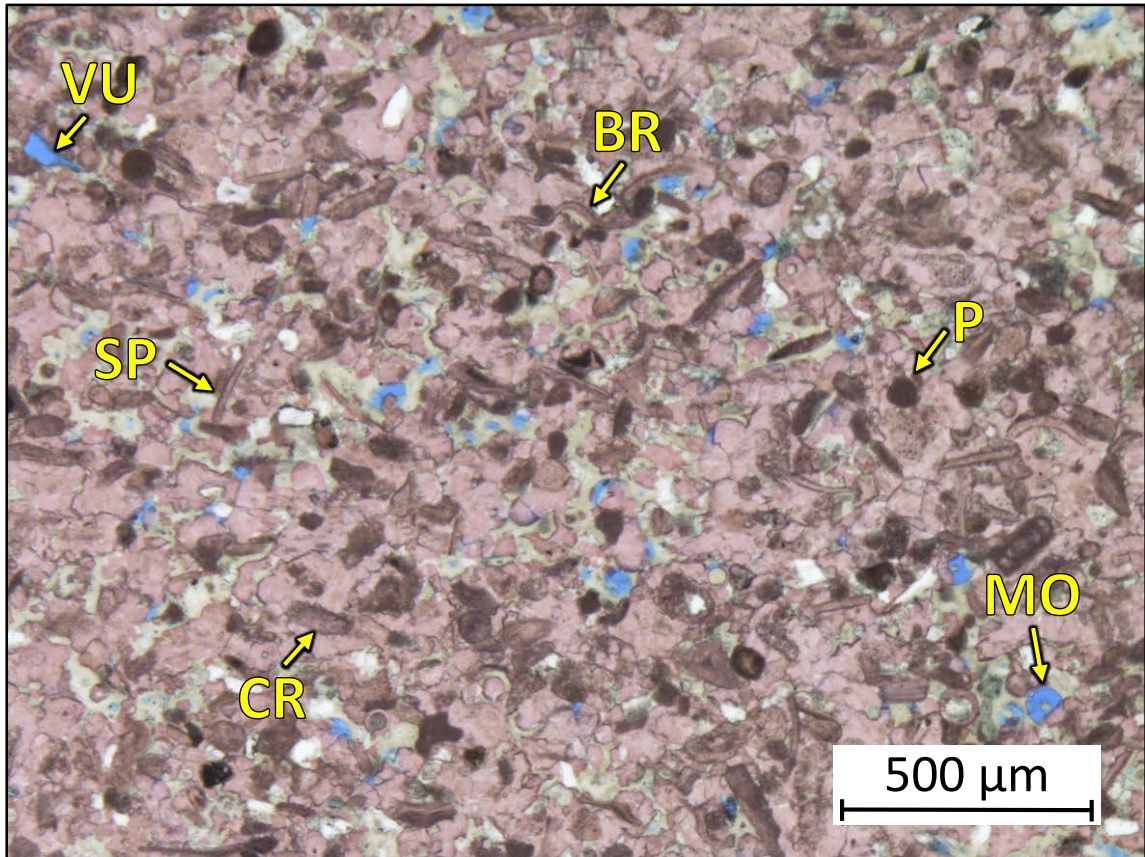
1AD – 5630.75' = Bioturbated wackestone. Sample is alizarin red stained. Porosity (ambient): 2.5%. Permeability (Klinkenberg): Sample was unsuitable for this type of measurement. TOC: 0.59%. XRD: 10% clays (8% illite and 2% mixed layer illite/smectite), 39% carbonates (33% calcite and 6% dolomite), and 51% other minerals (39% quartz, 4% potassium feldspar, 6% plagioclase feldspar, 2% pyrite, and trace amounts of apatite). Sample contains silt-sized quartz grains (20%), crinoid fragments (15%), brachiopod fragments (10%), sponge spicules (5%), and undifferentiated microbioclastic debris. Vug and minor amounts of moldic porosity observed.



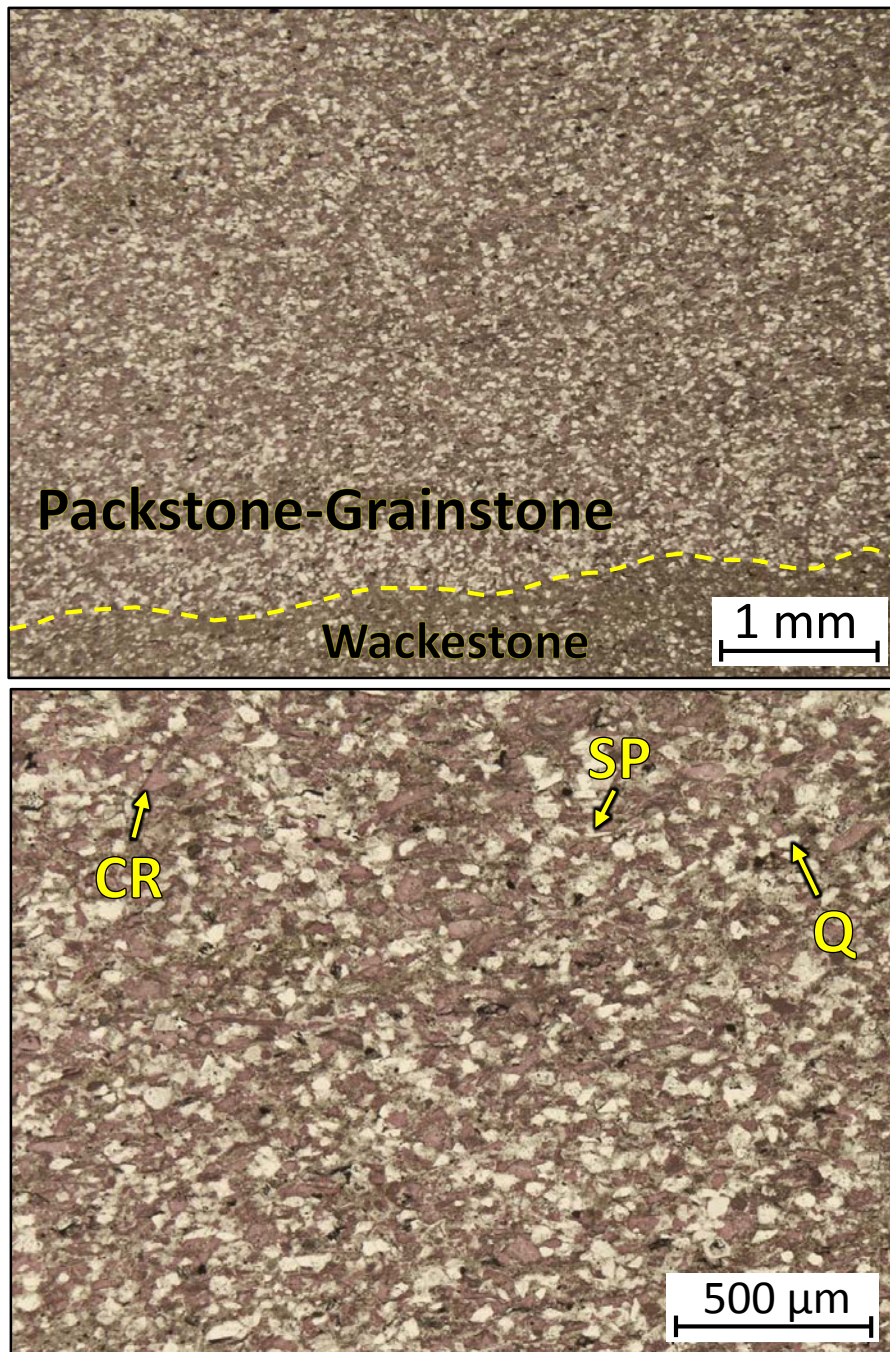
1AD – 5628.50' = Silicified skeletal grainstone. Sample is alizarin red stained. Porosity (NCS): 2.3%. Permeability (Klinkenberg): 0.110 mD. TOC: 0.02%. XRD: Trace amounts of clays, 32% carbonates (31% calcite and 1% dolomite), and 68% other minerals (66% quartz, 2% potassium feldspar, and trace amounts of plagioclase feldspar and pyrite). Sample contains crinoid fragments (20%), sponge spicules (10%), brachiopod (or ostracode?) fragments (5%), and minor amounts of calcite replaced dolomite. Moldic porosity observed.



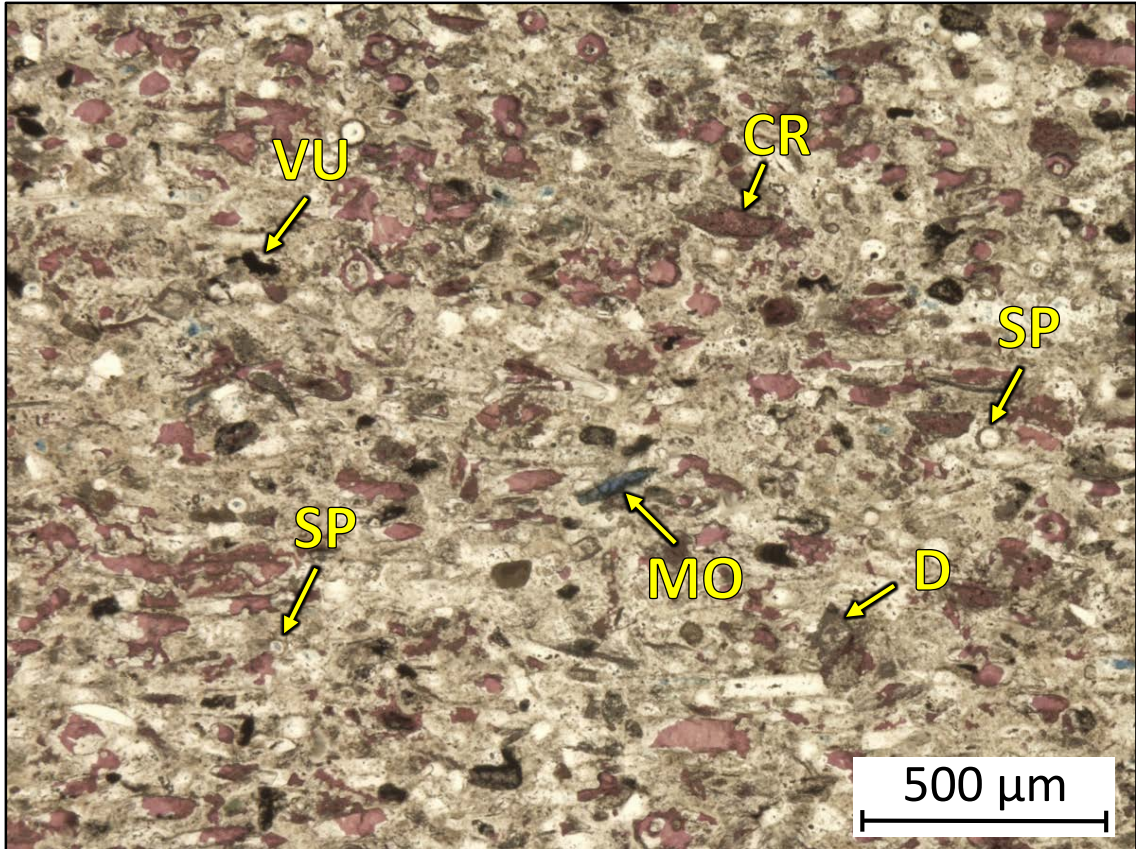
1AD – 5624.50' = Silicified skeletal grainstone. Sample is alizarin red stained. Porosity (ambient): 1.1%. Permeability (Klinkenberg): Sample was unsuitable for this type of analysis. TOC: 0.11%. XRD: 1% clays (1% illite), 32% carbonates (31% calcite and 1% dolomite), and 67% other minerals (64% quartz, 1% potassium feldspar, 2% plagioclase feldspar, and trace amounts of pyrite). Sample contains crinoid fragments (25%), sponge spicules (15%), and brachiopod fragments (10%). Moldic porosity observed.



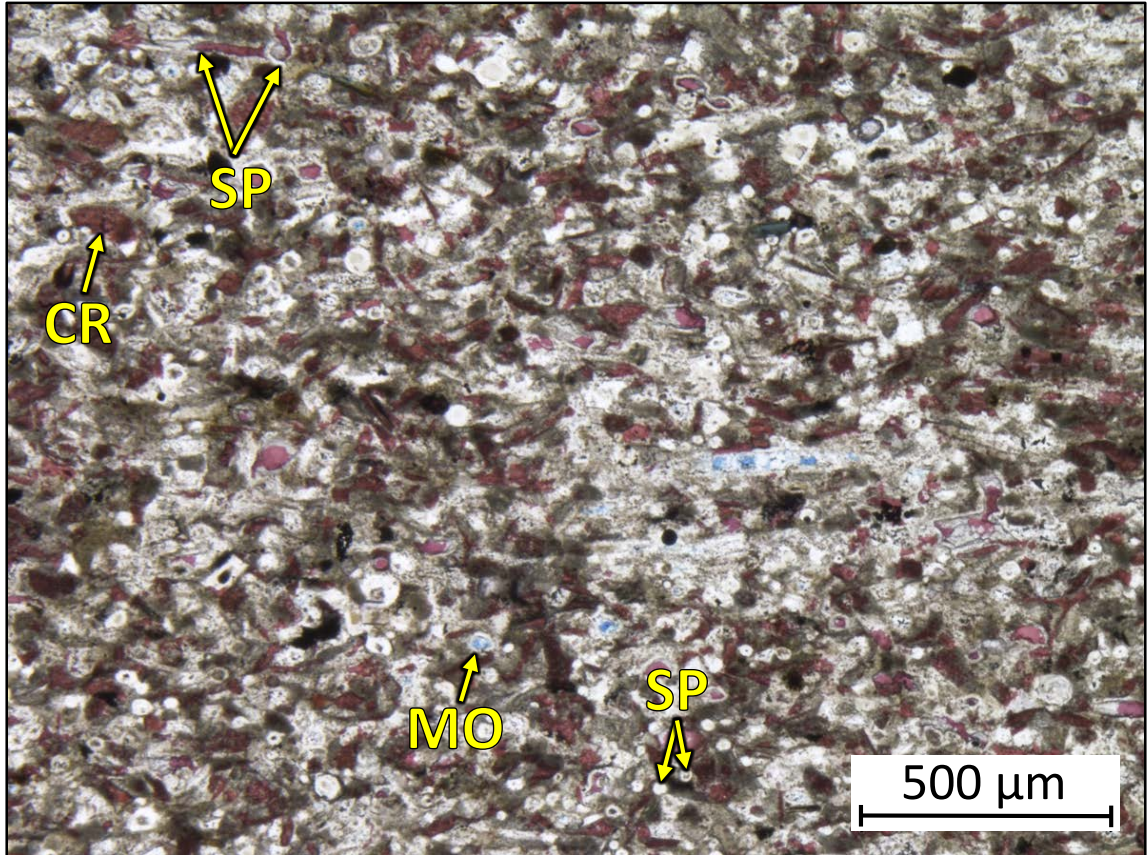
1AD – 5624.20' = Partially silicified skeletal-peloidal grainstone. Sample is alizarin red stained and blue epoxy impregnated. Porosity (NCS): 4.8%. Permeability (Klinkenberg): 0.0005 mD. TOC: 0.08%. XRD: 1% clays (1% illite), 60% carbonates (59% calcite and 1% dolomite), and 39% other minerals (36% quartz, 1% potassium feldspar, 2% plagioclase feldspar, and trace amounts of pyrite and apatite). Sample contains crinoid fragments (20%), sponge spicules (15%), peloids (10%), and brachiopod fragments (5%). Moldic and vug porosity observed.



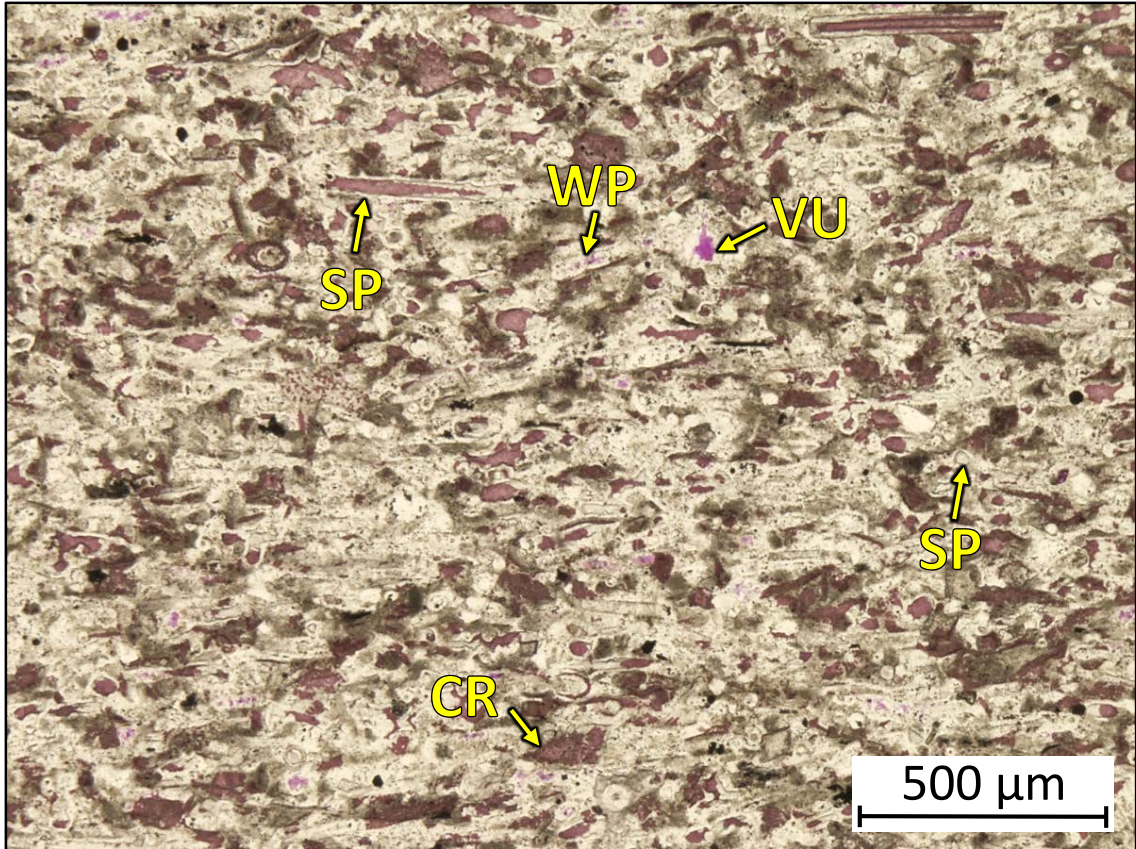
1AD – 5616.95' = Skeletal packstone-grainstone. Sample is alizarin red stained. Porosity (ambient): 7.7%. Permeability (Klinkenberg): Sample was unsuitable for this type of analysis. TOC: 0.19%. XRD: 5% clays (3% illite and 2% mixed layer illite/smectite), 37% carbonates (33% calcite and 4% dolomite), and 58% other minerals (52% quartz, 2% potassium feldspar, 3% plagioclase feldspar, 1% pyrite, and trace amounts of apatite). Sample contains silt-sized quartz grains (30%), crinoid fragments (20%), sponge spicules (5%), and undifferentiated microbioclastic debris. Oil-filled moldic and vug porosity observed.



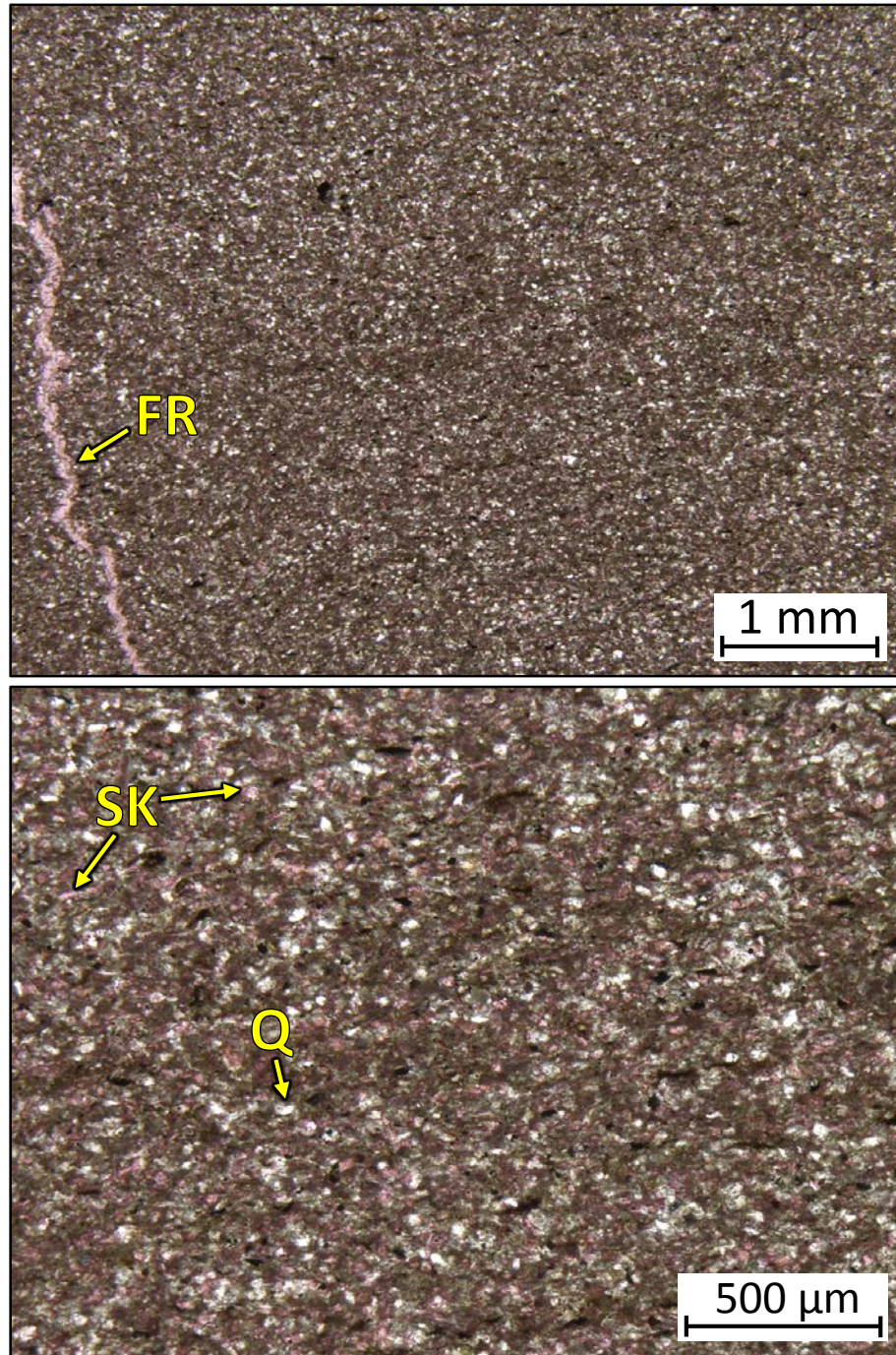
1AD – 5614.50' = Silicified skeletal grainstone. Sample is alizarin red stained. Porosity (NCS): 1.8%. Permeability (Klinkenberg): 0.0040 mD. TOC: 0.14%. XRD: Trace amounts of clays, 17% carbonates (16% calcite and 1% dolomite), and 83% other minerals (80% quartz, 2% potassium feldspar, 1% plagioclase feldspar, and trace amounts of pyrite). Sample contains sponge spicules (25%), crinoid fragments (10%), and undifferentiated microbioclastic debris. Oil-filled moldic and vug porosity observed.



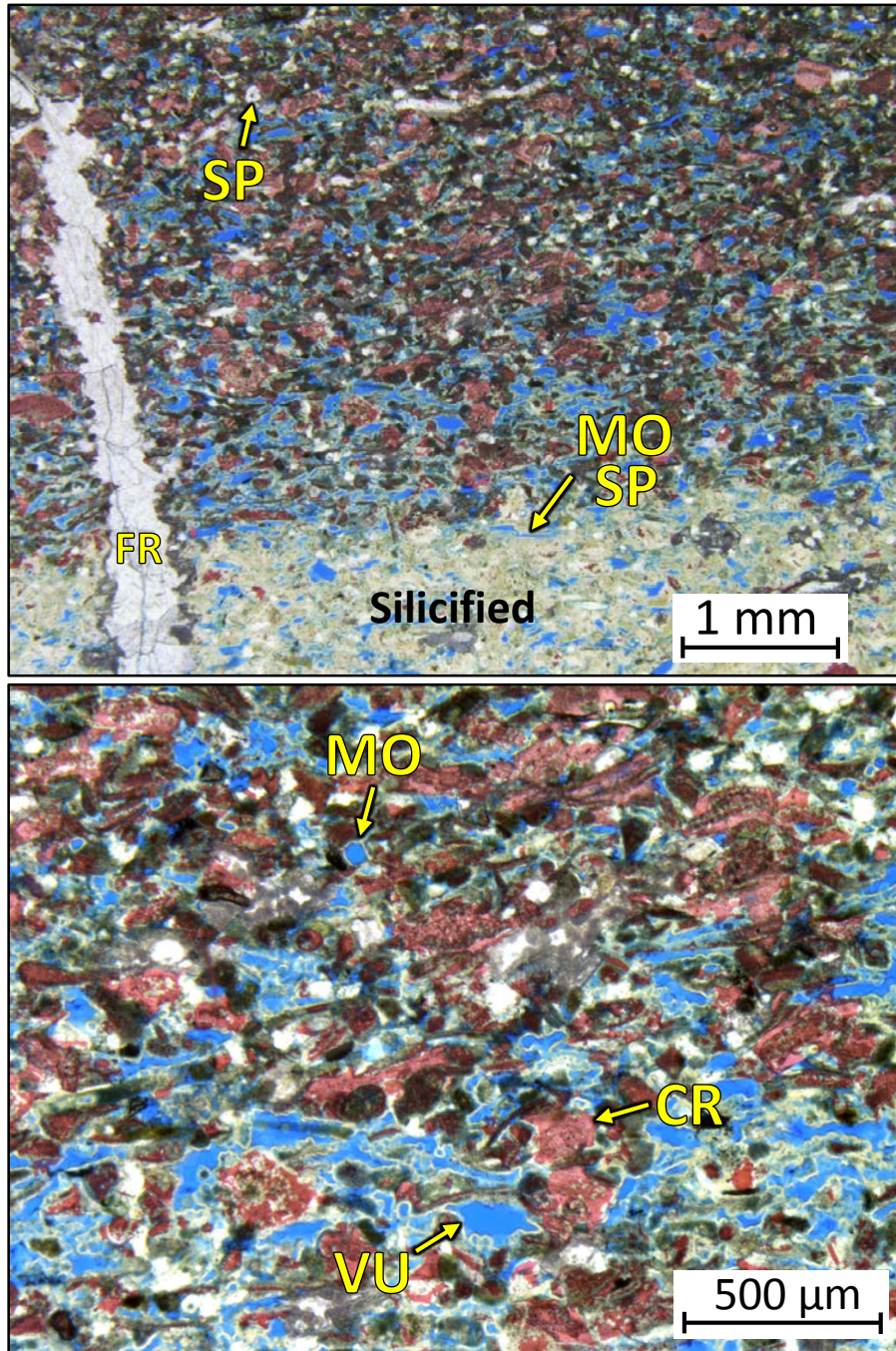
1AD – 5610.75' = Silicified skeletal grainstone. Sample is alizarin red stained and blue epoxy impregnated. Porosity (NCS): 0.8%. Permeability (Klinkenberg): <0.0001 mD. TOC: 0.09%. XRD: 1% clays (1% illite), 32% carbonates (31% calcite and 1% dolomite), and 67% other minerals (63% quartz, 2% potassium feldspar, 2% plagioclase feldspar, and trace amounts of pyrite and apatite). Sample contains sponge spicules (35%), crinoid fragments (5%), brachiopod fragments (5%), and undifferentiated microbioclastic debris. Moldic and vug porosity observed.



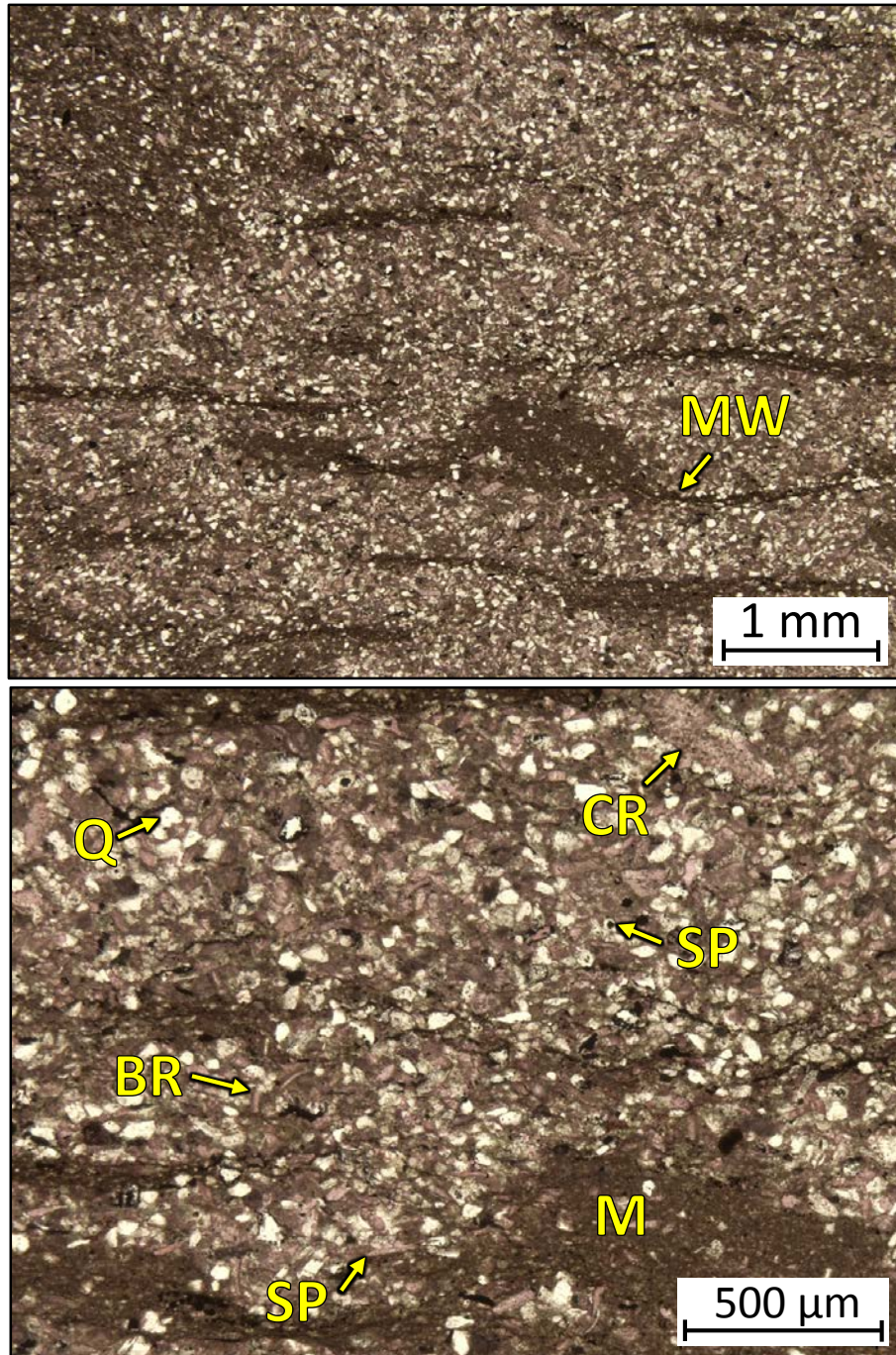
1AD – 5606.40' = Silicified skeletal grainstone. Sample is alizarin red stained. Porosity (NCS): 0.1%. Permeability (Klinkenberg): <0.0001 mD. TOC: 0.10%. XRD: 1% clays (1% illite), 18% carbonates (17% calcite and 1% dolomite), and 81% other minerals (73% quartz, 4% potassium feldspar, 2% plagioclase feldspar, and 2% pyrite). Sample contains sponge spicules (35%), crinoid fragments (10%), and undifferentiated microbioclastic debris. Moldic, vug, and intraparticle porosity observed.



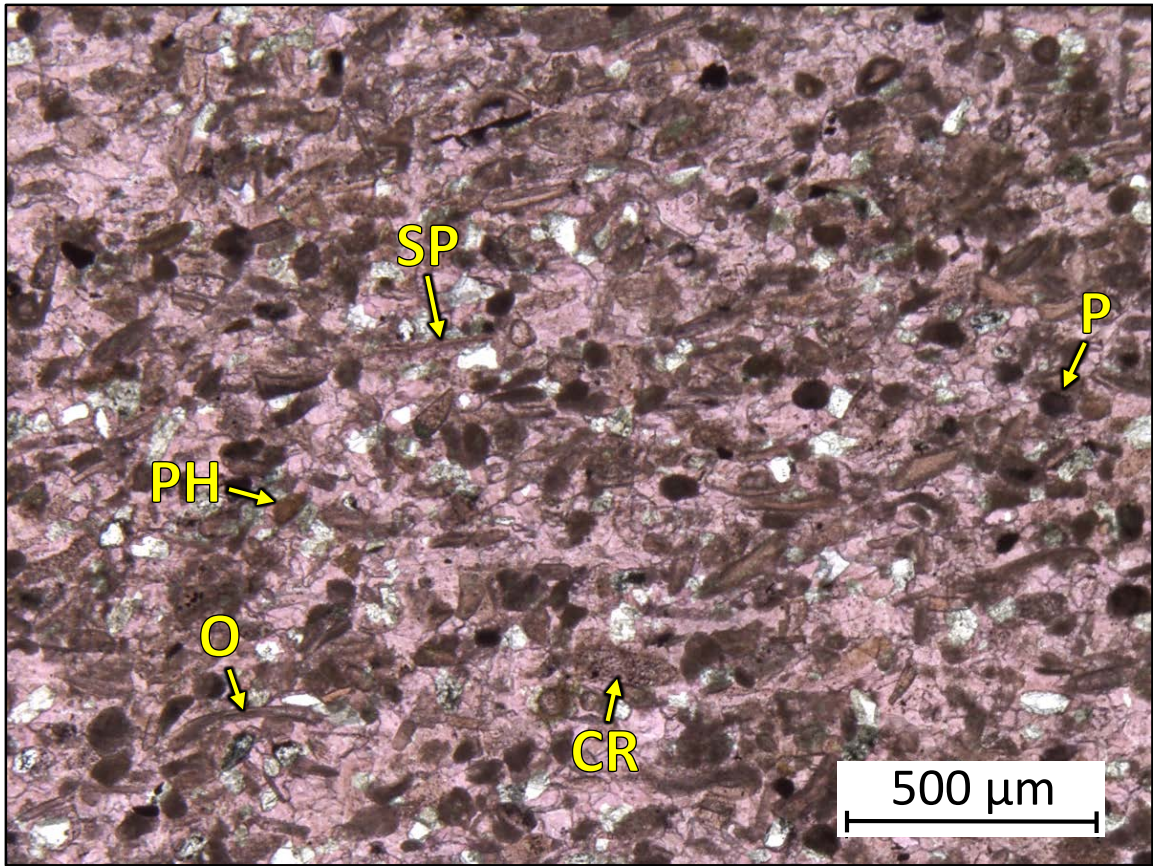
1AD – 5605.50' =Bioturbated wackestone. Sample is alizarin red stained. Porosity (NCS): 1.2%. Permeability (Klinkenberg): 0.0002 mD. TOC: 0.11%. XRD: 3% clays (2% illite and 1% mixed layer illite/smectite), 49% carbonates (45% calcite and 4% dolomite), and 48% other minerals (41% quartz, 2% potassium feldspar, 4% plagioclase feldspar, 1% pyrite, and trace amounts of apatite). Sample is composed of silt-sized quartz grains and undifferentiated microbioclastic debris. Ptygmatic fracture in sample is filled with blocky calcite cement.



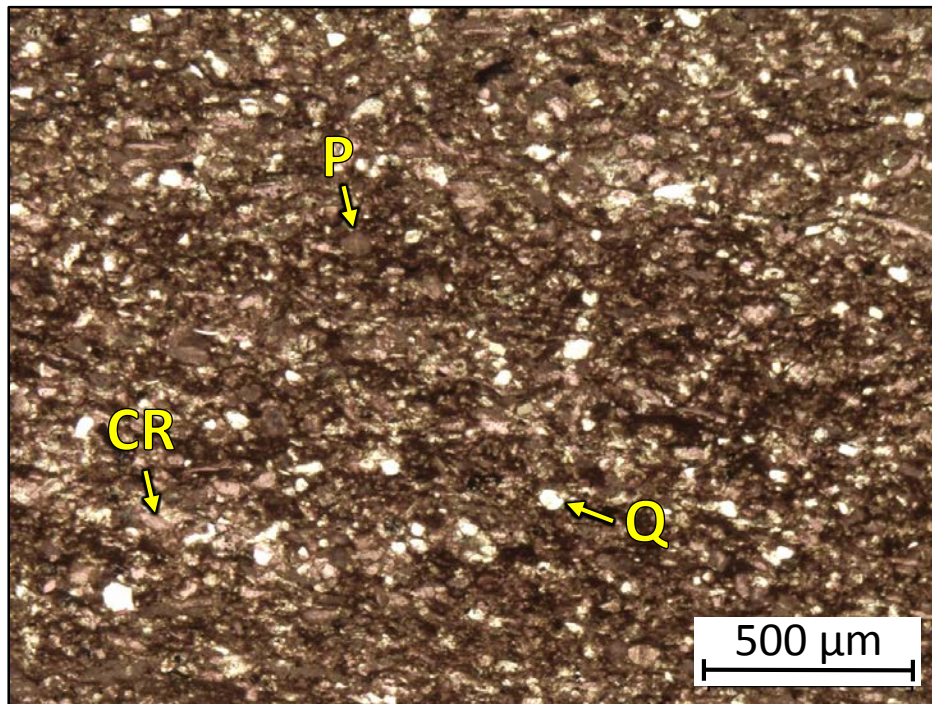
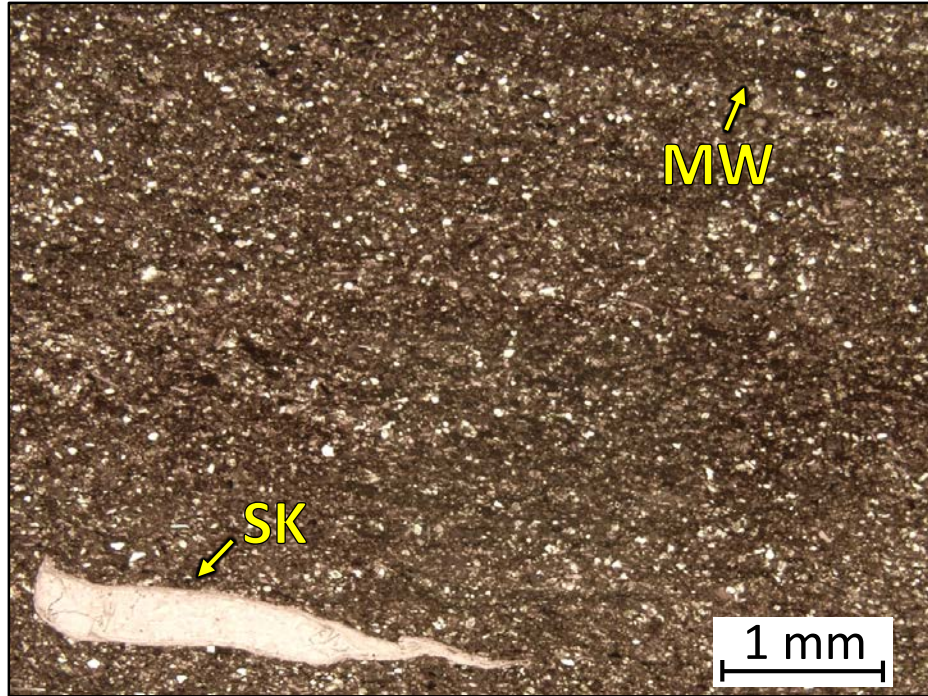
1AD – 5599.40' = Partially silicified skeletal grainstone. Sample is alizarin red stained and blue epoxy impregnated. Porosity (NCS): 10.6%. Permeability (Klinkenberg): 0.553 mD. TOC: 0.44%. Trace amounts of clays, 59% carbonates (50% calcite and 9% dolomite), and 41% other minerals (38% quartz, 1% potassium feldspar, 1% plagioclase feldspar, 1% pyrite, and trace amounts of apatite). Sample contains crinoid fragments (35%), sponge spicules (10%), and undifferentiated microbioclastic debris. Fracture in sample is filled with quartz cement. Abundant moldic and vug porosity observed.



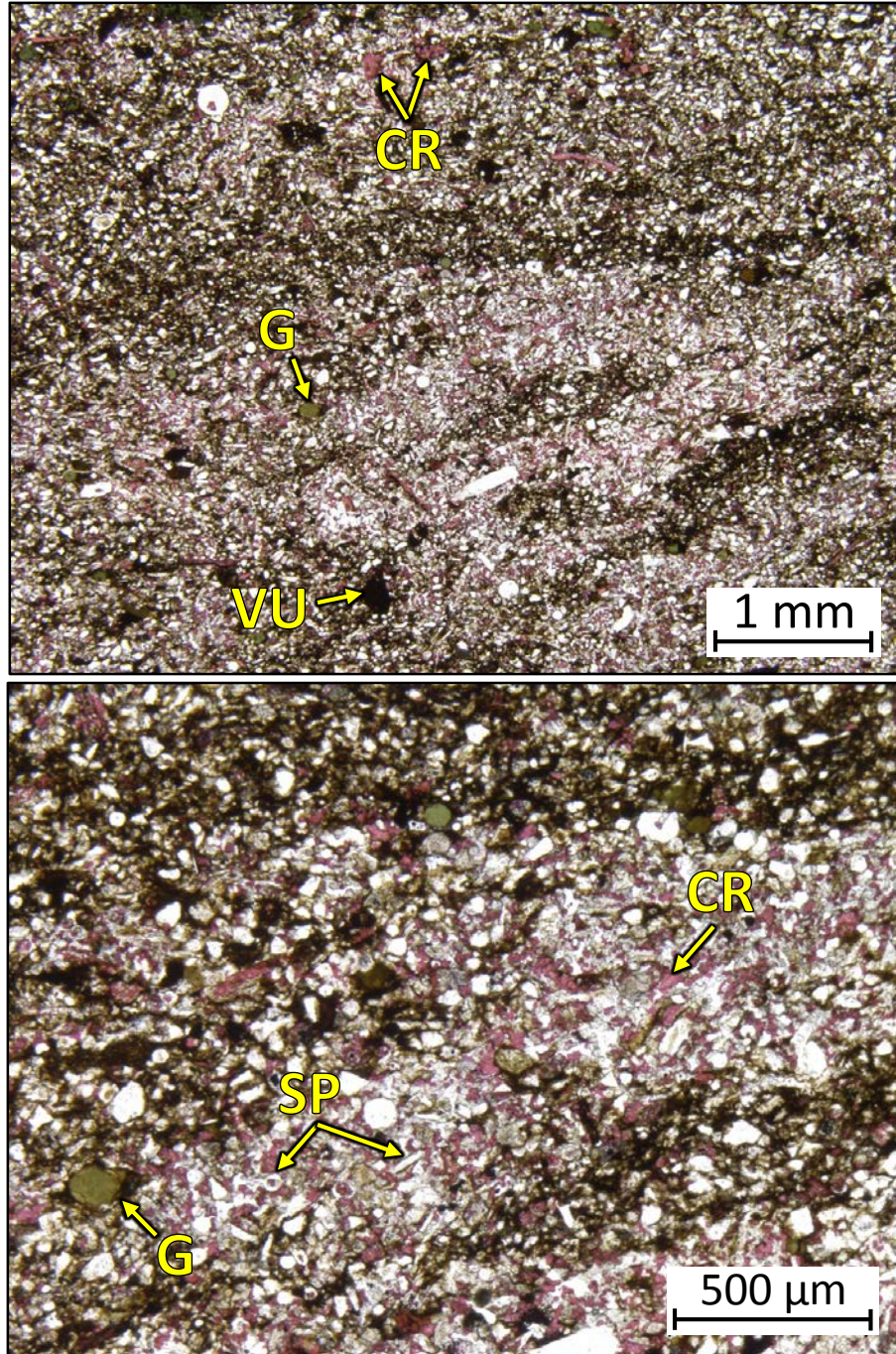
1AD – 5596.80' = Bioturbated mudstone-wackestone. Sample is alizarin red stained. Porosity (NCS): 1.8%. Permeability (Klinkenberg): 0.322 mD. TOC: 0.55%. XRD: 15% clays (1% chlorite, 9% illite, and 5% mixed layer illite/smectite), 36% carbonates (32% calcite and 4% dolomite), and 49% other minerals (41% quartz, 1% potassium feldspar, 3% plagioclase feldspar, 2% pyrite, 1% apatite, and 1% marcasite). Sample contains crinoid fragments (20%), sponge spicules (10%), brachiopod fragments (5%), and undifferentiated microbioclastic debris. Moldic and vug porosity observed.



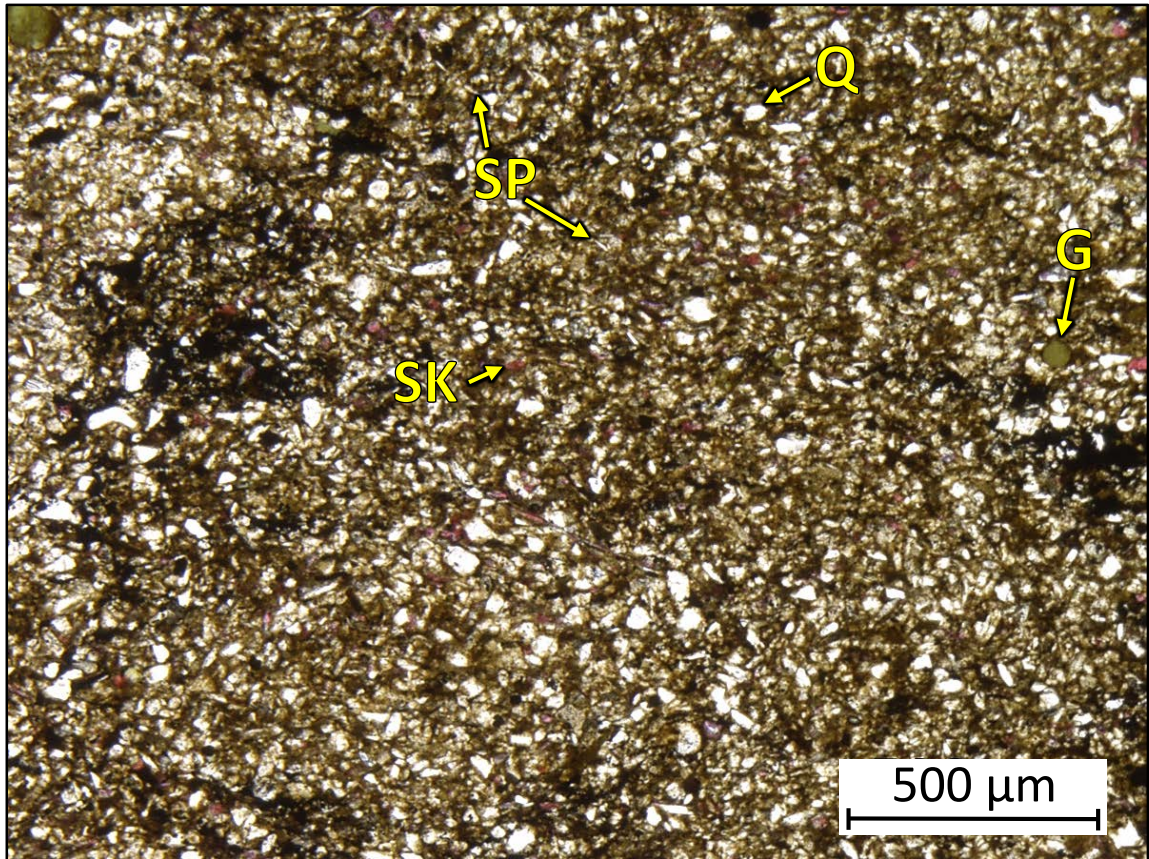
1AD – 5592.70' = Peloidal grainstone. Sample is alizarin red stained. Porosity (NCS): 1.2%. Permeability (Klinkenberg): <0.0001 mD. TOC: 0.01%. XRD: 1% clays (1% illite), 78% carbonates (77% calcite and 1% dolomite), and 21% other minerals (15% quartz, trace amounts of potassium feldspar, 5% plagioclase feldspar, trace amounts of pyrite, and 1% apatite). Sample contains crinoid fragments (15%), peloids (15%), sponge spicules (10%), ostracodes (2%), phosphatic grains (2%) and undifferentiated microbioclastic debris. Moldic and vug porosity observed.



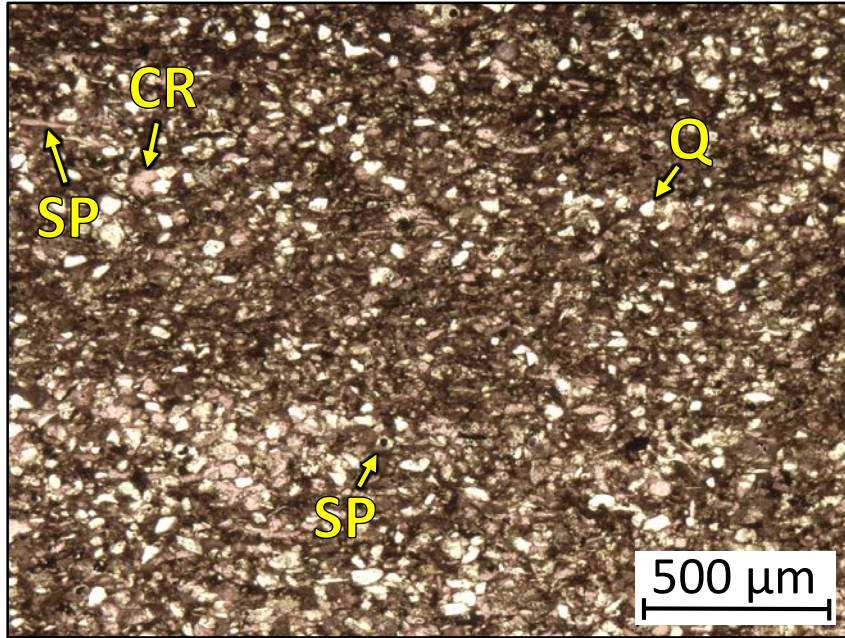
1AD – 5584.80' = Bioturbated wackestone-packstone. Sample is alizarin red stained. Porosity (NCS): 1.3%. Permeability (Klinkenberg): 0.203 mD. TOC: 0.82%. XRD: 9% clays (1% chlorite, 5% illite, and 3% mixed layer illite/smectite), 39% carbonates (34% calcite and 4% dolomite), and 52% other minerals (41% quartz, 1% potassium feldspar, 3% plagioclase feldspar, 3% pyrite, 3% apatite, and 1% marcasite). Sample contains crinoid fragments (10%), peloids (10%), and undifferentiated microbioclastic debris. Vug porosity observed.



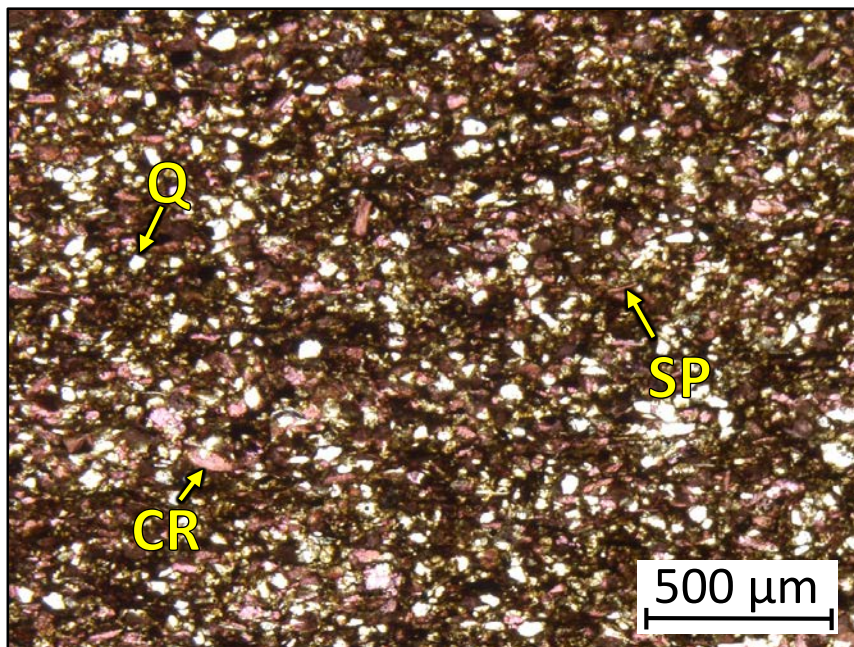
1AD – 5581.70' = Partially silicified, bioturbated wackestone to skeletal packstone. Sample is alizarin red stained. Porosity (NCS): 2.6%. Permeability (Klinkenberg): 0.0018 mD. TOC: 2.48%. XRD: 11% clays (8% illite and 3% mixed layer illite/smectite), 20% carbonates (19% calcite and 1% dolomite), and 69% other minerals (54% quartz, 3% potassium feldspar, 6% plagioclase feldspar, 3% pyrite, and 3% apatite). Sample contains crinoid grains (10%), sponge spicules (20%), minor amounts of very fine sand-size glauconite grains (3%) and brachiopod fragments (1%), and undifferentiated calcareous and silicified microbioclastic debris. Oil-filled vug porosity observed.



1AD – 5581.55-5581.80' = Bioturbated wackestone-packstone. Sample is alizarin red stained. TOC: 0.94%. XRD: 22% clays (1% chlorite, 15% illite, and 1% mixed layer illite/smectite), 12% carbonates (11% calcite and 1% dolomite), and 66% other minerals (49% quartz, 4% potassium feldspar, 9% plagioclase feldspar, 3% pyrite, and 1% apatite). Sample contains slit-sized quartz grains (30%), sponge spicules (10%), minor amounts of very fine sand-size glauconite grains (3%), and undifferentiated calcareous and silicified microbioclastic debris. Oil observed throughout sample.

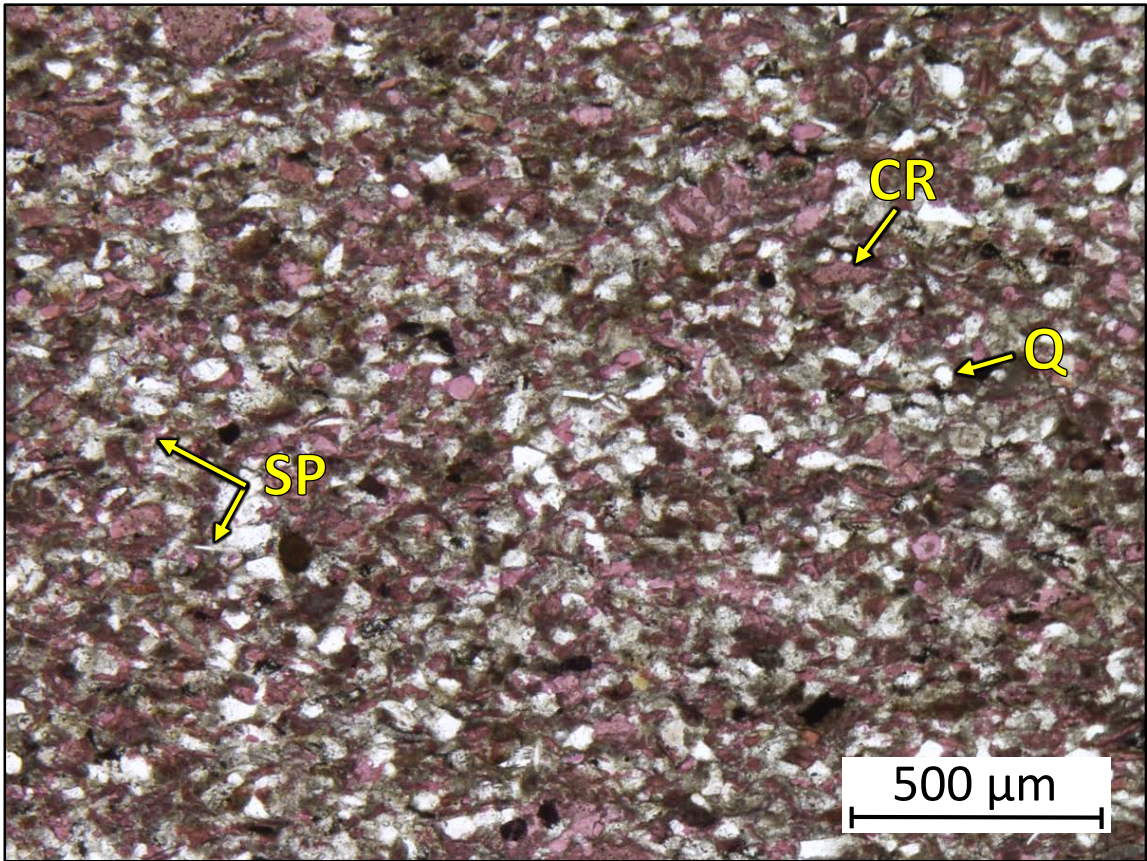


1AD – 5574.35' = Bioturbated wackestone-packstone. Sample is alizarin red stained. Porosity (ambient): 2.2%. Permeability (Klinkenberg): Sample was unsuitable for this type of measurement. TOC: 1.51%. XRD: 16% clays (1% chlorite, 8% illite, and 7% mixed layer illite/smectite), 34% carbonates (33% calcite and 1% dolomite), and 50% other minerals (37% quartz, 1% potassium feldspar, 5% plagioclase feldspar, 3% pyrite, 2% apatite, and 1% marcasite). Sample contains crinoid grains (15%), sponge spicules (10%), and undifferentiated calcareous and silicified microbioclastic debris. Oil-filled vug and moldic porosity.

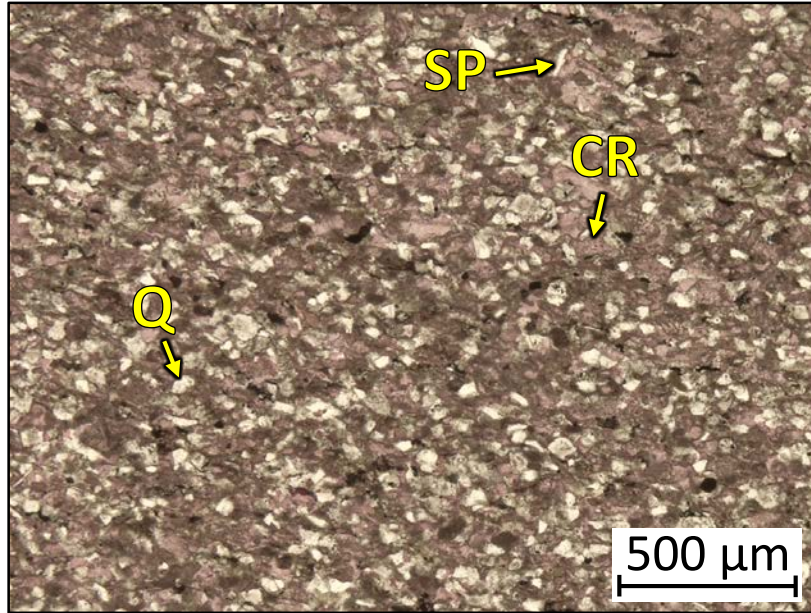


1AD – 5569.65-5569.95' = Bioturbated mudstone-wackestone. Sample is alizarin red stained. Porosity (visual estimation): 1.2%. TOC: 1.47%. XRD: 10% clays (1% chlorite, 8% illite, and 1% mixed layer illite/smectite), 43% carbonates (42% calcite and 1% dolomite), and 47% other minerals (36% quartz, 3% potassium feldspar, 5%

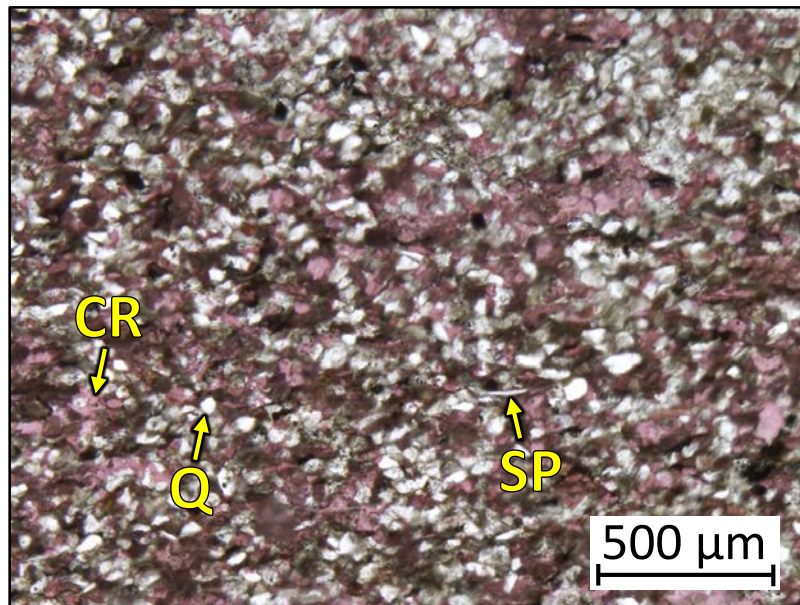
plagioclase feldspar, 2% pyrite, and 1% apatite). Sample contains crinoid grains (15%), sponge spicules (5%), and undifferentiated calcareous and silicified microbioclastic debris.



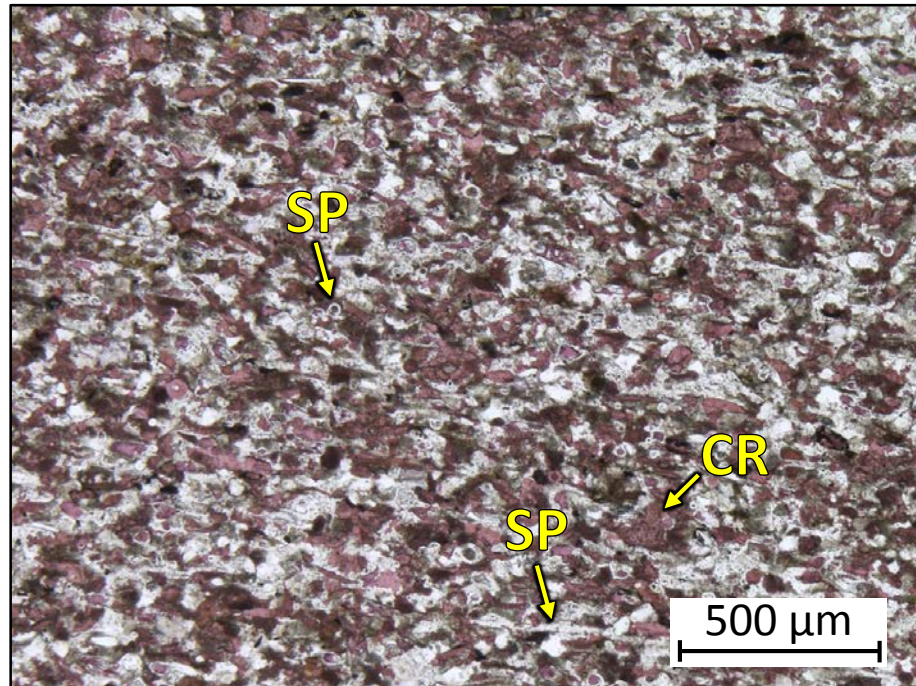
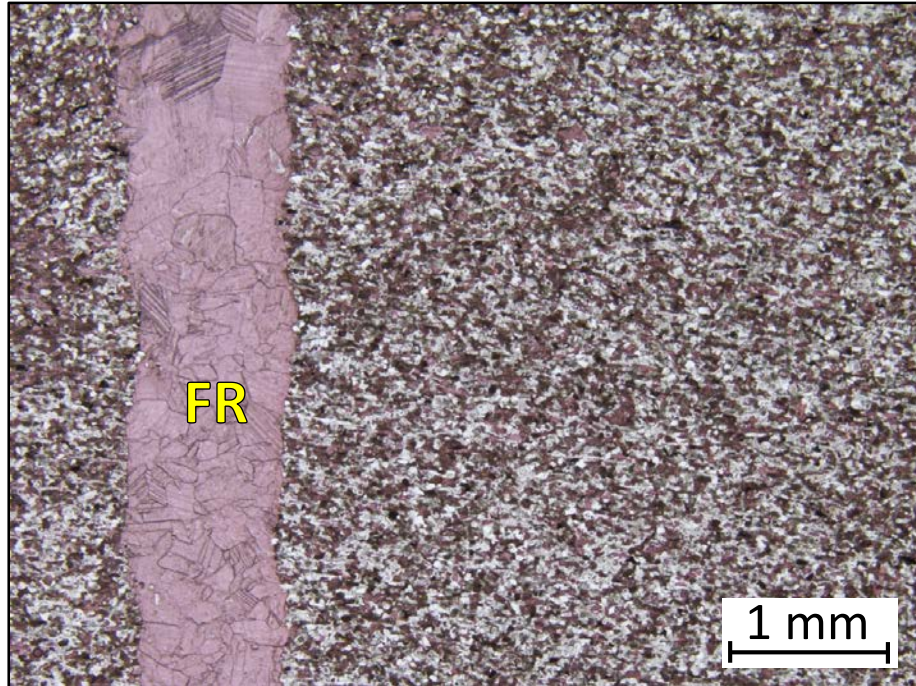
1AD – 5559.50' = Peloidal grainstone. Sample is alizarin red stained. Porosity (NCS): 1.7%. Permeability (Klinkenberg): <0.0001 mD. TOC: 0.14%. XRD: 2% clays (1% illite and 1% mixed layer illite/smectite), 46% carbonates (43% calcite and 3% dolomite), and 52% other minerals (46% quartz, 2% potassium feldspar, 3% plagioclase feldspar, 1% pyrite, and trace amounts of apatite). Sample contains crinoid grains (25%), silt-sized quartz grains (15%), sponge spicules (10%), and undifferentiated microbioclastic debris. Oil-filled moldic and vug porosity observed.



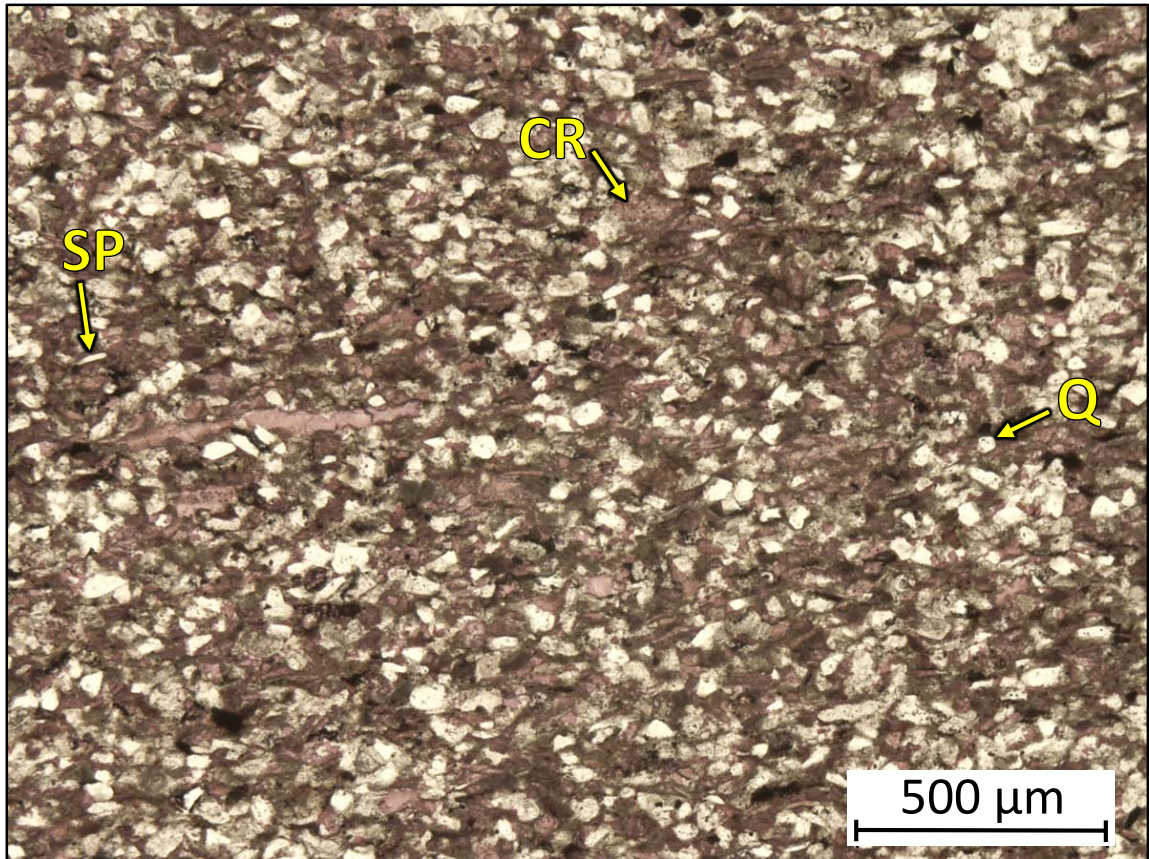
1AD – 5556.05' = Crinoidal grainstone. Sample is alizarin red stained. Porosity (NCS): 1.3%. Permeability (Klinkenberg): 0.0001 mD. TOC: 0.07%. XRD: 4% clays (2% illite and 2% mixed layer illite/smectite), 44% carbonates (41% calcite and 3% dolomite), and 52% other minerals (44% quartz, 2% potassium feldspar, 5% plagioclase feldspar, and 1% pyrite). Sample contains crinoid grains (20%), silt-sized quartz grains (10%), sponge spicules (5%), and undifferentiated microbioclastic debris. Oil-filled moldic and vug porosity observed.



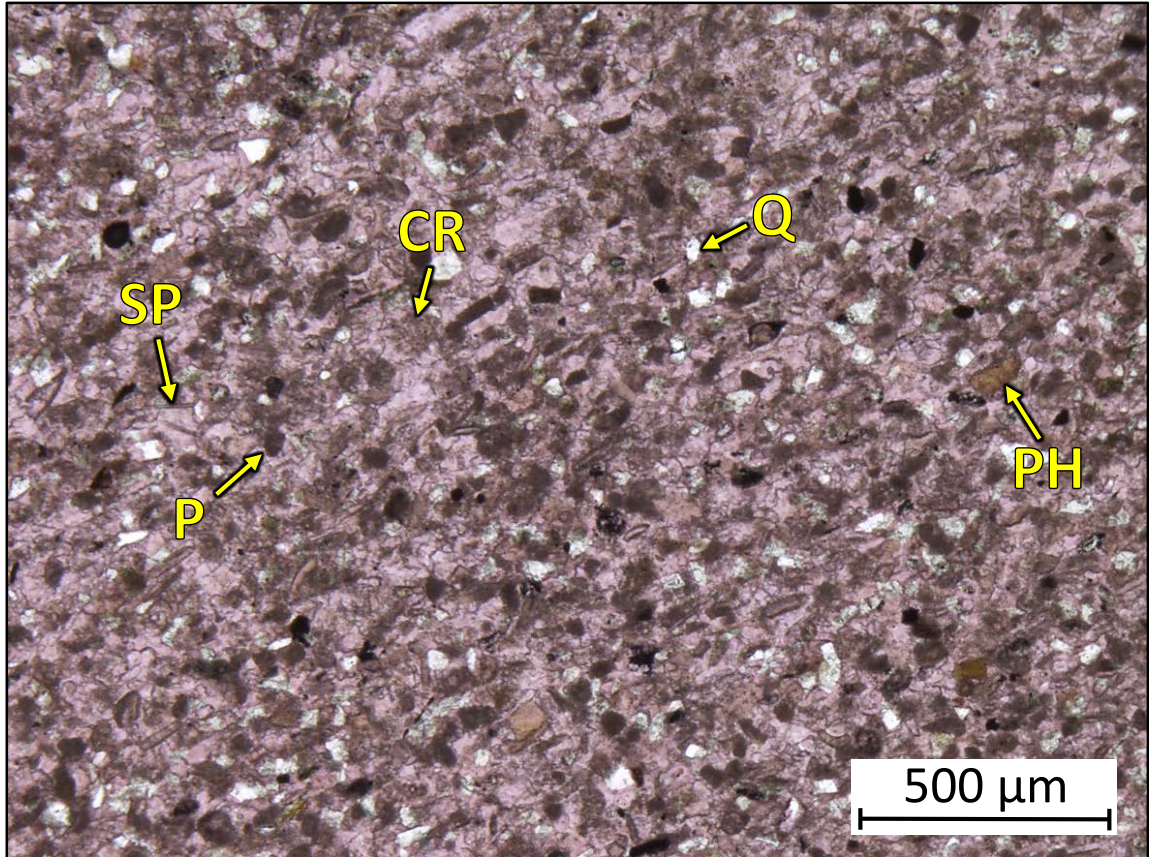
1AD – 5550.80' = Crinoidal grainstone. Sample is alizarin red stained. Porosity (NCS): 2.3%. Permeability (Klinkenberg): <0.0001 mD. TOC: 0.12%. XRD: 5% clays (4% illite and 1% mixed layer illite/smectite), 31% carbonates (28% calcite and 3% dolomite), and 64% other minerals (51% quartz, 3% potassium feldspar, 8% plagioclase feldspar, 1% pyrite, and 1% apatite). Sample contains crinoid grains (20%), silt-sized quartz grains (20%), sponge spicules (7%), and undifferentiated microbioclastic debris. Oil-filled moldic and vug porosity observed.



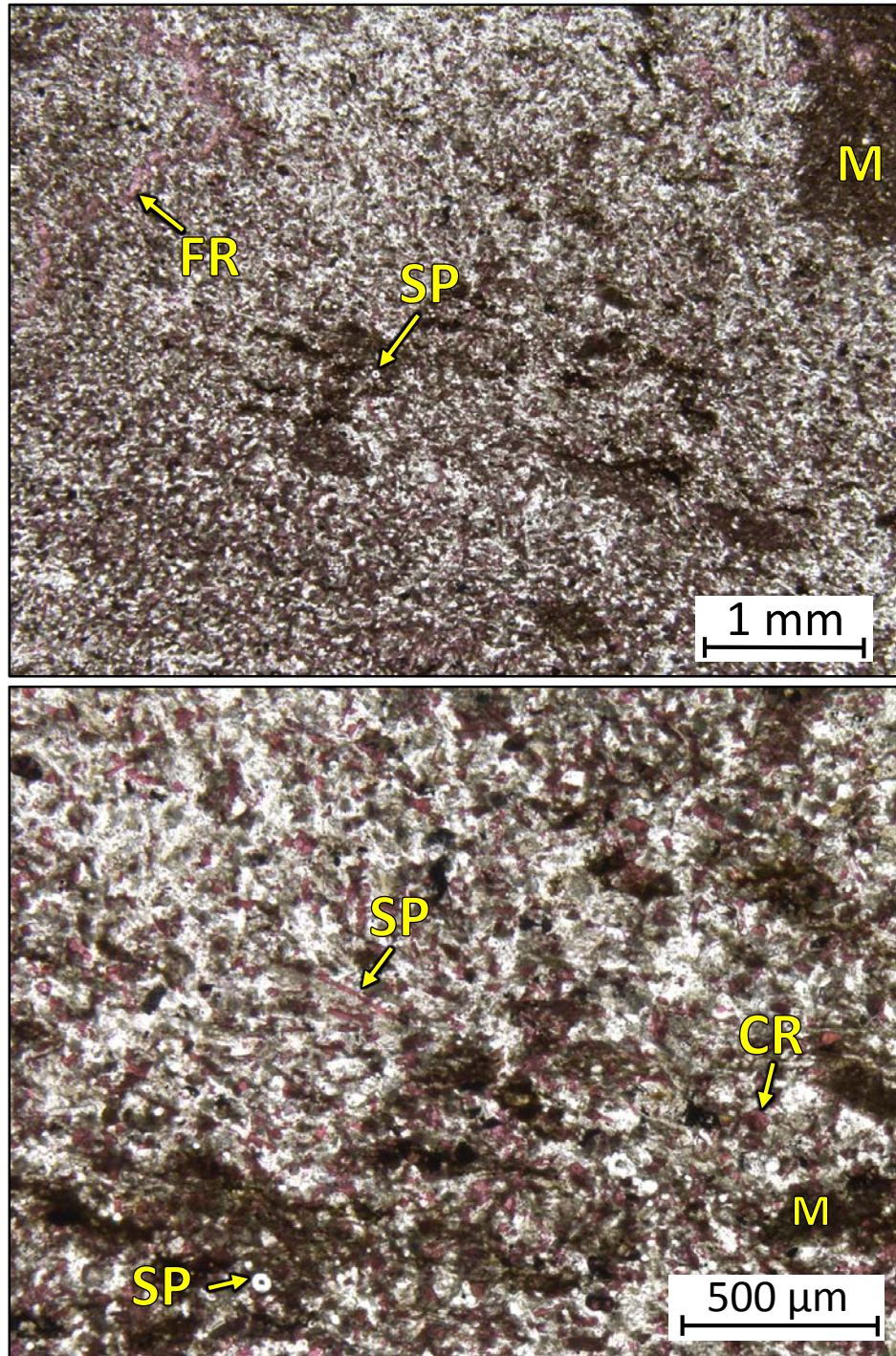
1AD – 5546.55' = Silicified skeletal grainstone. Sample is alizarin red stained. Porosity (NCS): 1.5%. Permeability (Klinkenberg): <0.0001 mD. TOC: 0.03%. XRD: 1% clays (1% illite), 35% carbonates (34% calcite and 1% dolomite), and 64% other minerals (58% quartz, 2% potassium feldspar, 4% plagioclase feldspar, and trace amounts of pyrite and apatite). Sample contains silt-sponge spicules (40%), crinoid grains (10%), and undifferentiated microbioclastic debris. Fracture is filled with calcite cement. Oil-filled moldic and vug porosity observed.



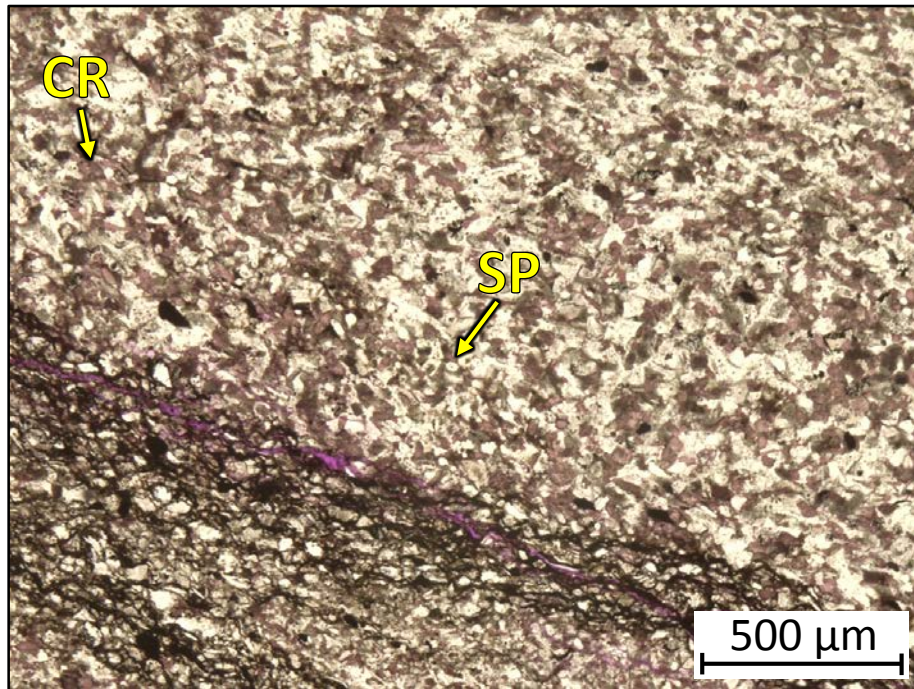
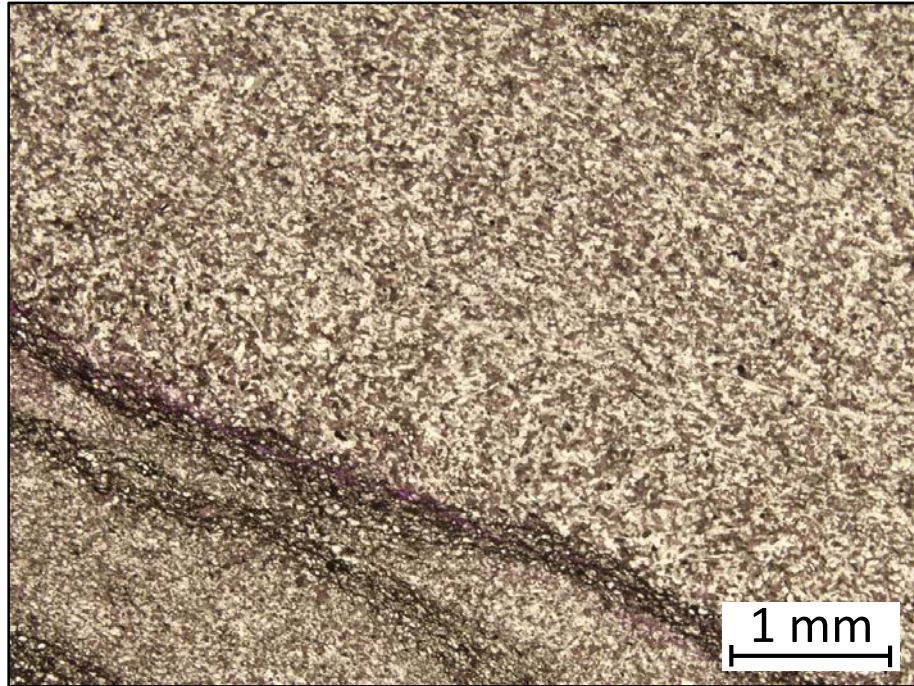
1AD – 5546.10' = Skeletal-peloidal packstone. Sample is alizarin red stained. Porosity (NCS): 1.8%. Permeability (Klinkenberg): 0.0001 mD. TOC: 0.07%. XRD: 4% clays (3% illite and 1% mixed layer illite/smectite), 36% carbonates (33% calcite and 3% dolomite), and 60% other minerals (53% quartz, 1% potassium feldspar, 5% plagioclase feldspar, and 1% pyrite). Sample contains crinoid grains (15%), silt-sized quartz grains (15%), sponge spicules (10%), and undifferentiated microbioclastic debris. Oil-filled moldic and vug porosity observed.



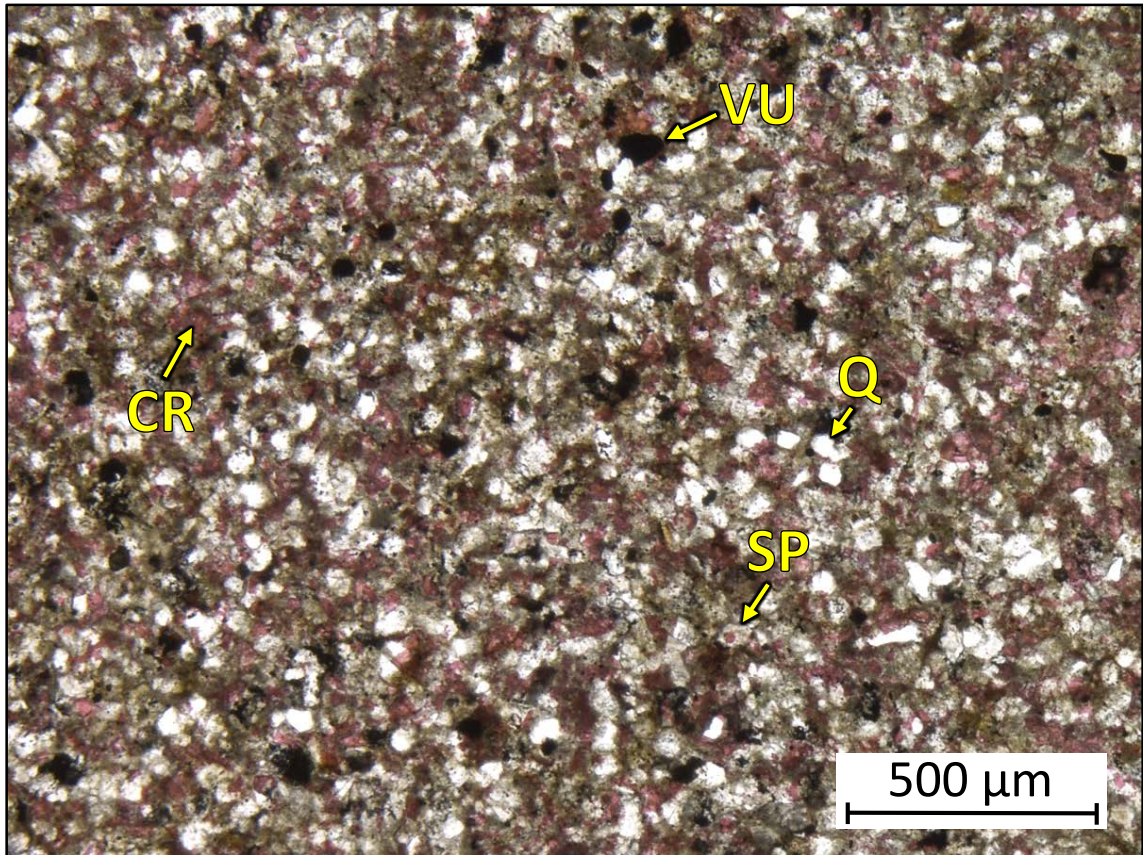
1AD – 5544.65' = Peloidal grainstone. Sample is alizarin red stained. Porosity (NCS): 0.8%. Permeability (Klinkenberg): <0.0001 mD. TOC: 0.01%. XRD: 1% clays (1% illite), 79% carbonates (78% calcite and 1% dolomite), and 20% other minerals (16% quartz, 1% potassium feldspar, 3% plagioclase feldspar, and trace amounts of pyrite and apatite). Sample contains crinoid grains (30%), sponge spicules (15%), peloids (15%), silt-sized quartz grains (10%), and phosphatic grains (3%). Oil-filled moldic and vug porosity observed.



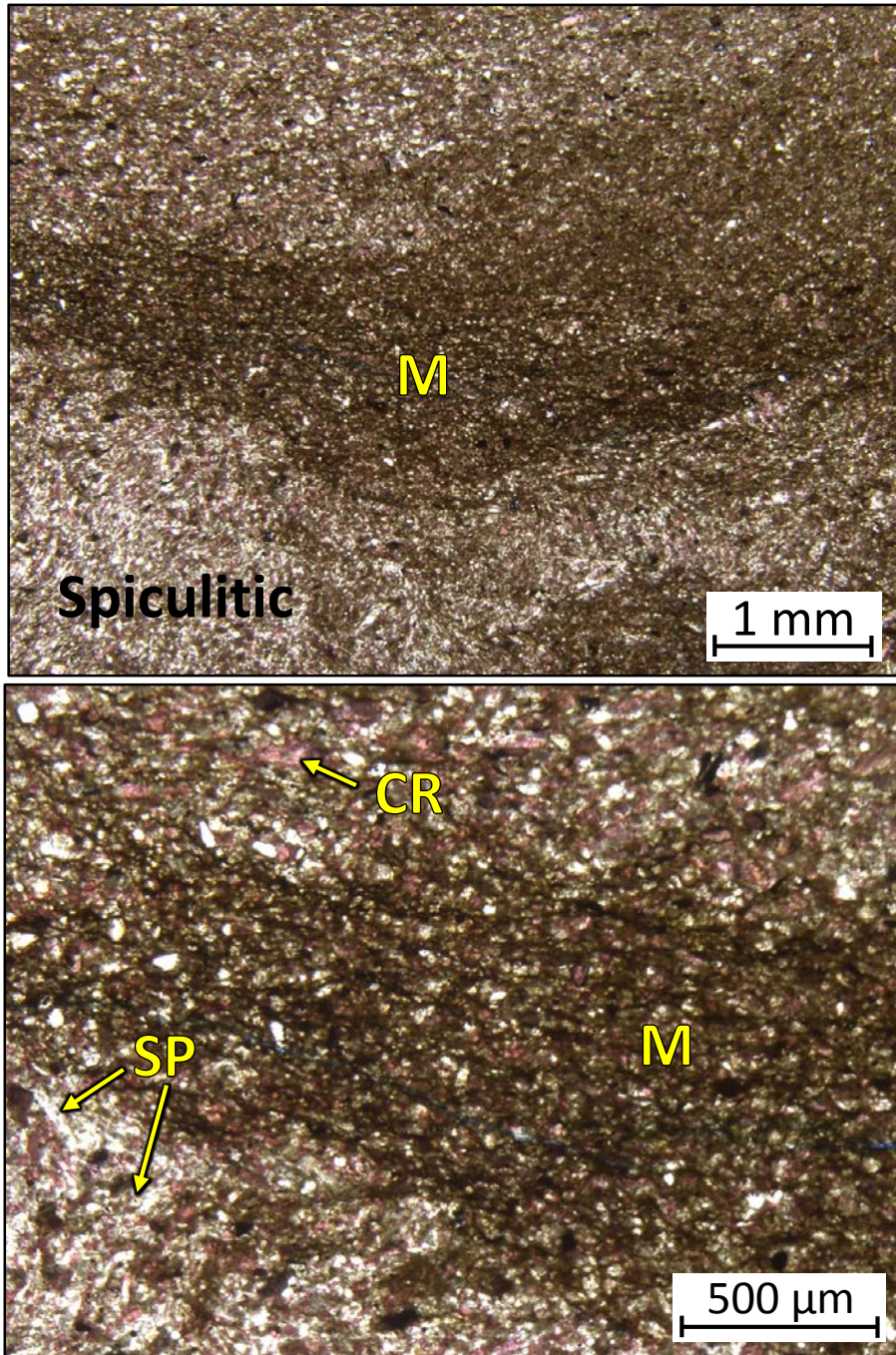
1AD – 5536.60' = Bioturbated wackestone to silicified skeletal packstone-grainstone. Sample is alizarin red stained. Porosity (NCS): 2.9%. Permeability (Klinkenberg): 0.0001 mD. TOC: 0.16%. XRD: 1% clays (1% illite), 31% carbonates (29% calcite and 2% dolomite), and 68% other minerals (62% quartz, 2% potassium feldspar, 3% plagioclase feldspar, 1% pyrite, and trace amounts of apatite). Sample contains crinoid grains (15%), sponge spicules (25%), peloids (15%), phosphatic grains (2%), and undifferentiated microbioclastic debris. Ptygmatic fracture in sample is filled with blocky calcite cement. Oil-filled moldic and vug porosity observed.



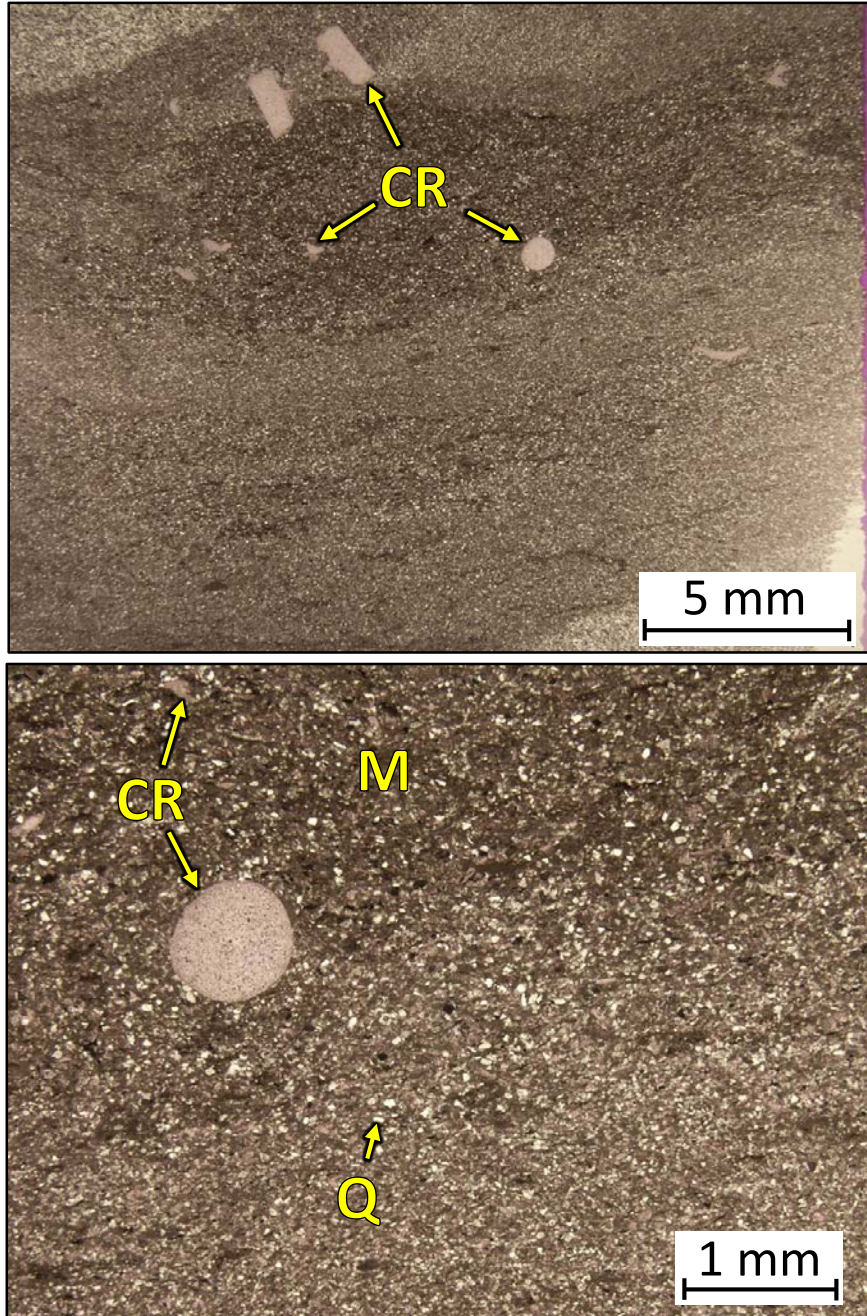
1AD – 5536.00' = Silicified skeletal packstone. Sample is alizarin red stained. Porosity (NCS): 2.4%. Permeability (Klinkenberg): 0.0006 mD. TOC: 0.15%. XRD: 4% clays (3% illite and 1% mixed layer illite/smectite), 29% carbonates (27% calcite and 2% dolomite), and 67% other minerals (63% quartz, 1% potassium feldspar, 2% plagioclase feldspar, and 1% pyrite). Sample contains crinoid grains (15%), sponge spicules (30%), and undifferentiated microbioclastic debris. Oil-filled moldic and vug porosity observed.



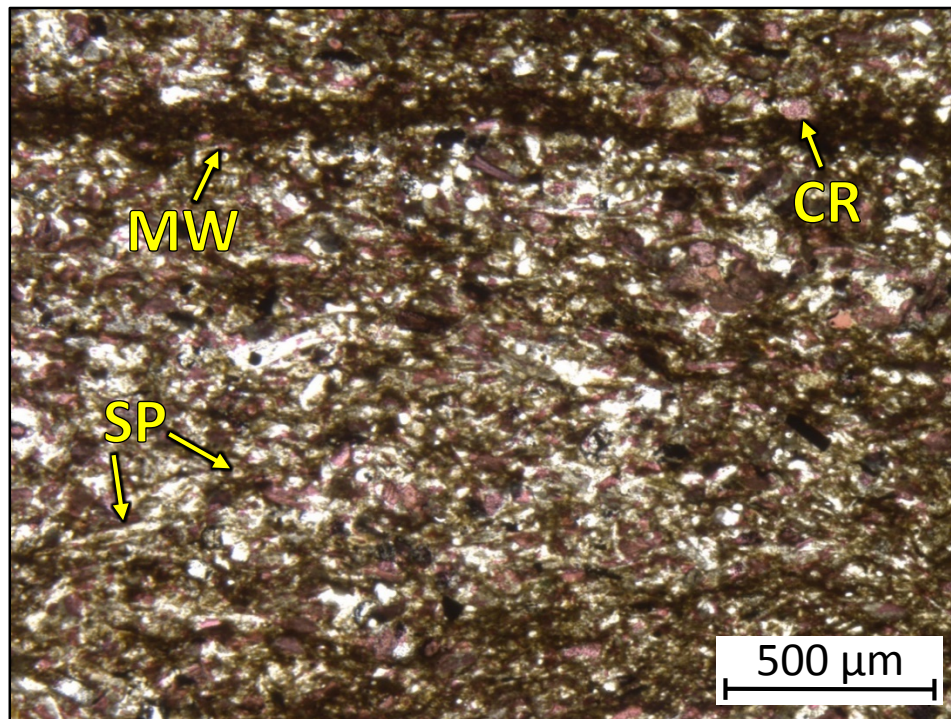
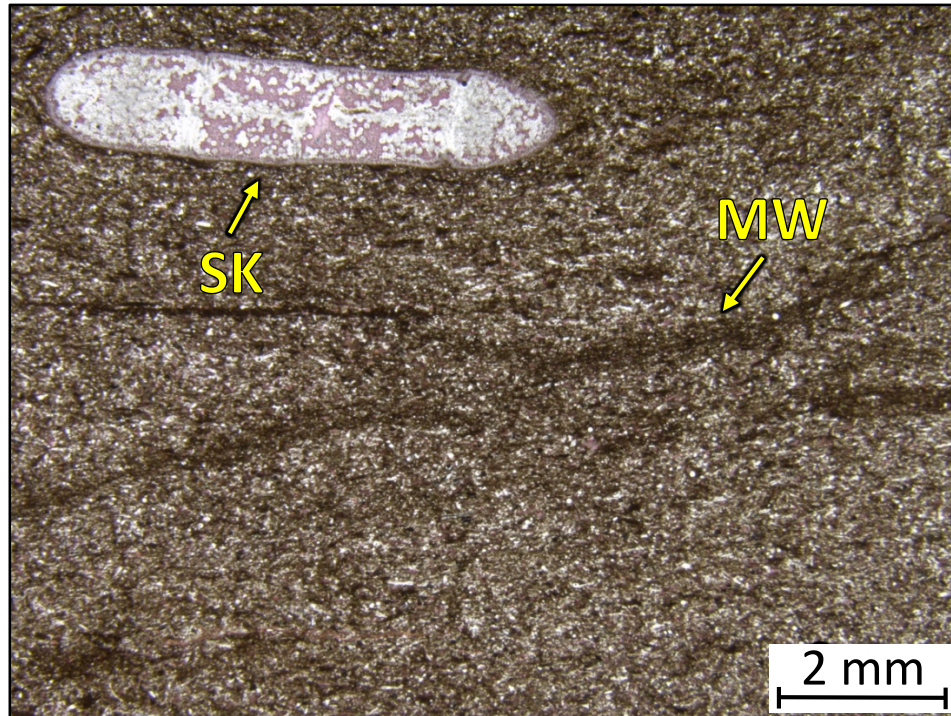
1AD – 5532.10' = Bioturbated packstone. Sample is alizarin red stained. Porosity (NCS): 2.0%. Permeability (Klinkenberg): <0.0001 mD. TOC: 0.15%. XRD: 3% clays (2% illite and 1% mixed layer illite/smectite), 38% carbonates (35% calcite and 3% dolomite), and 59% other minerals (50% quartz, 2% potassium feldspar, 4% plagioclase feldspar, 2% pyrite, and 1% apatite). Sample contains silt-sized quartz grains and undifferentiated microbioclastic debris. Oil-filled moldic and vug porosity observed.



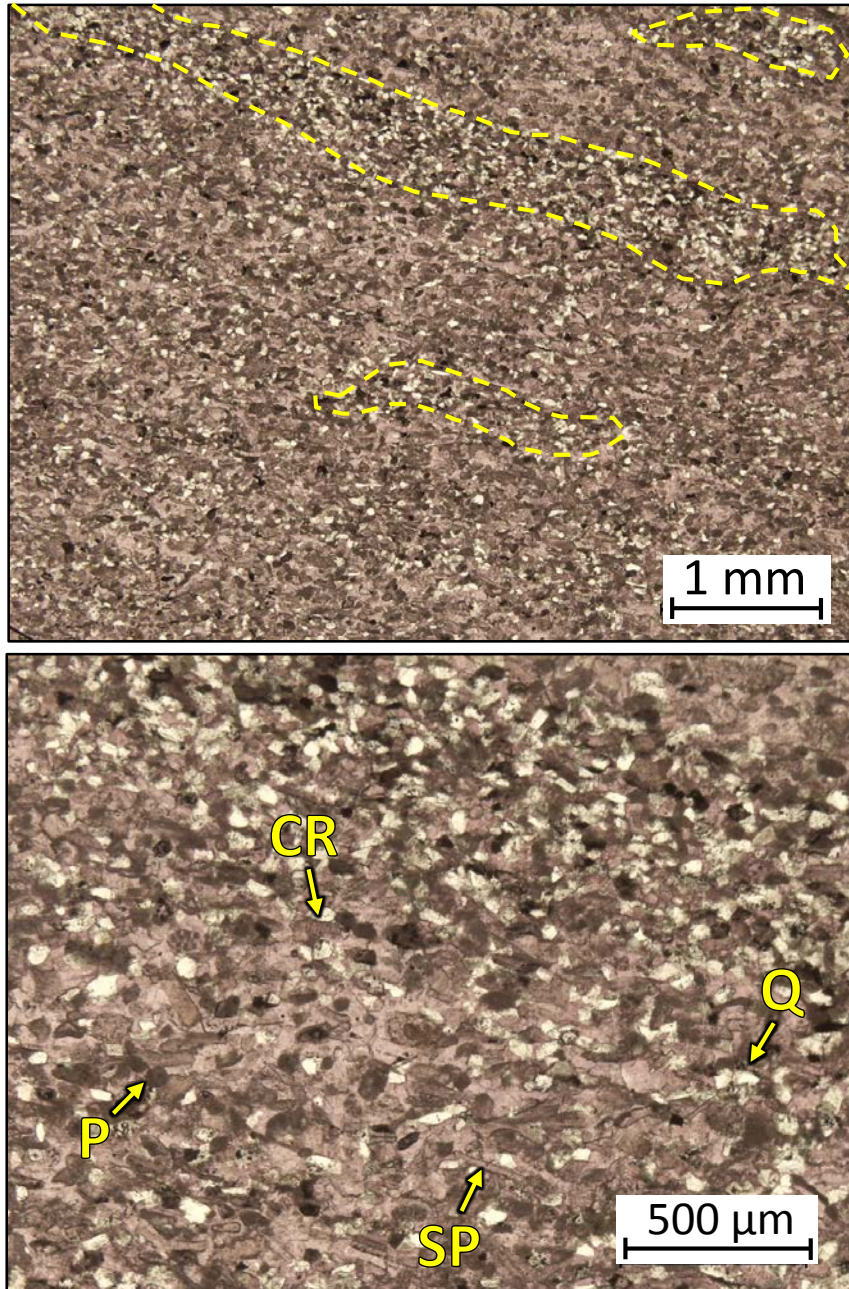
1AD – 5527.80' = Bioturbated wackestone to silicified skeletal grainstone. Sample is alizarin red stained and blue epoxy impregnated. Porosity (ambient): 2.8%. Permeability (Klinkenberg): Sample was unsuitable for this type of measurement. TOC: 0.09%. XRD: 2% clays (1% illite and 1% mixed layer illite/smectite), 34% carbonates (32% calcite and 2% dolomite), and 64% other minerals (59% quartz, 2% potassium feldspar, 3% plagioclase feldspar, and trace amounts of pyrite and apatite). Sample contains crinoid grains (10%), sponge spicules (20%), and undifferentiated microbioclastic debris. Grainy sediments concentrated in burrows. Oil-filled moldic and vug porosity observed.



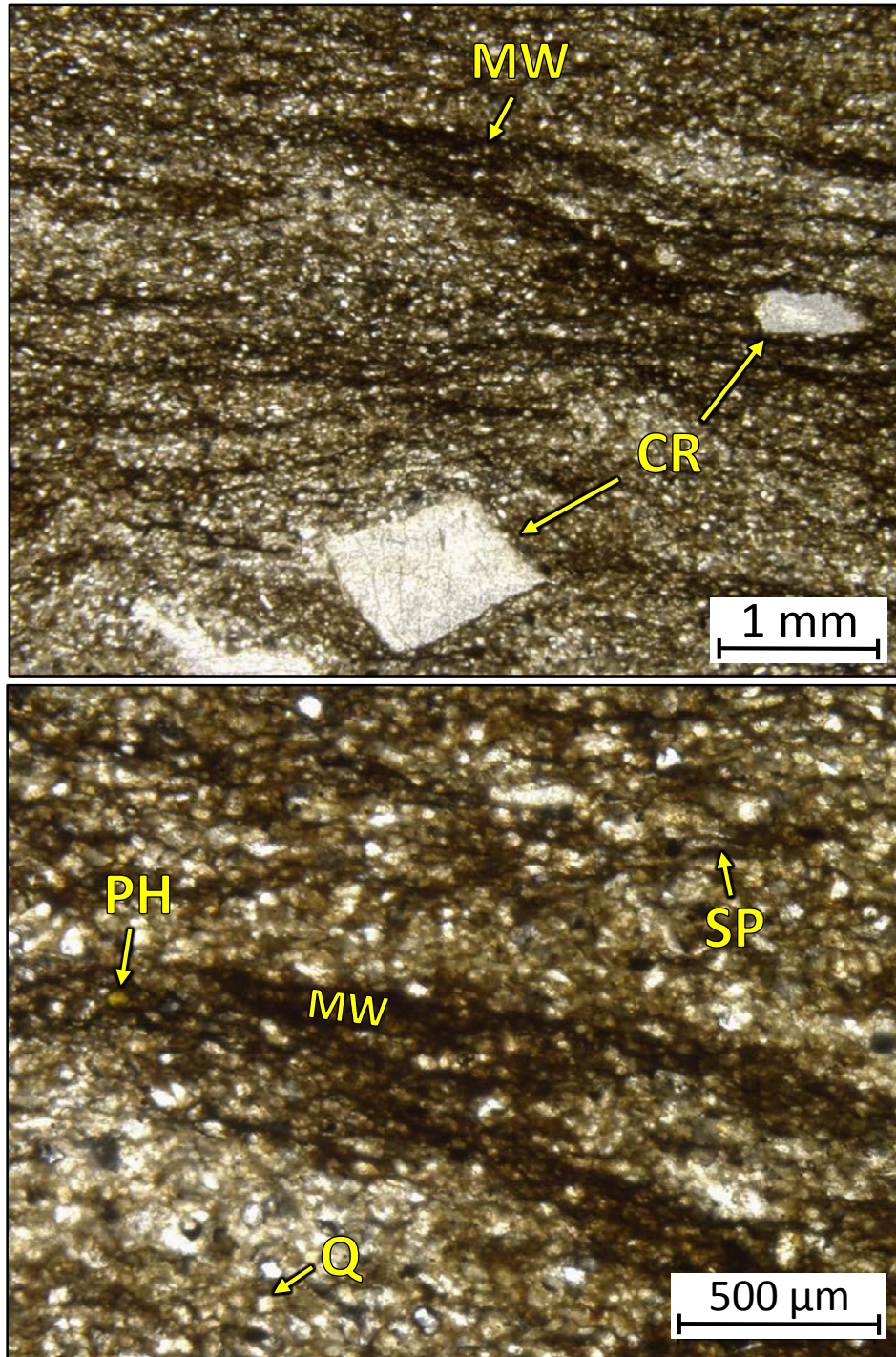
1AD – 5526.05' = Bioturbated wackestone-packstone. Sample is alizarin red stained. Porosity (NCS): 0.7%. Permeability (Klinkenberg): 0.0041 mD. TOC: 0.14%. XRD: 4% clays (3% illite and 1% mixed layer illite/smectite), 49% carbonates (45% calcite and 4% dolomite), and 47% other minerals (42% quartz, 1% potassium feldspar, 3% plagioclase feldspar, 1% pyrite, and trace amounts of apatite). Sample contains crinoid grains (20%), silt-sized quartz grains (50%), and undifferentiated microbioclastic debris.



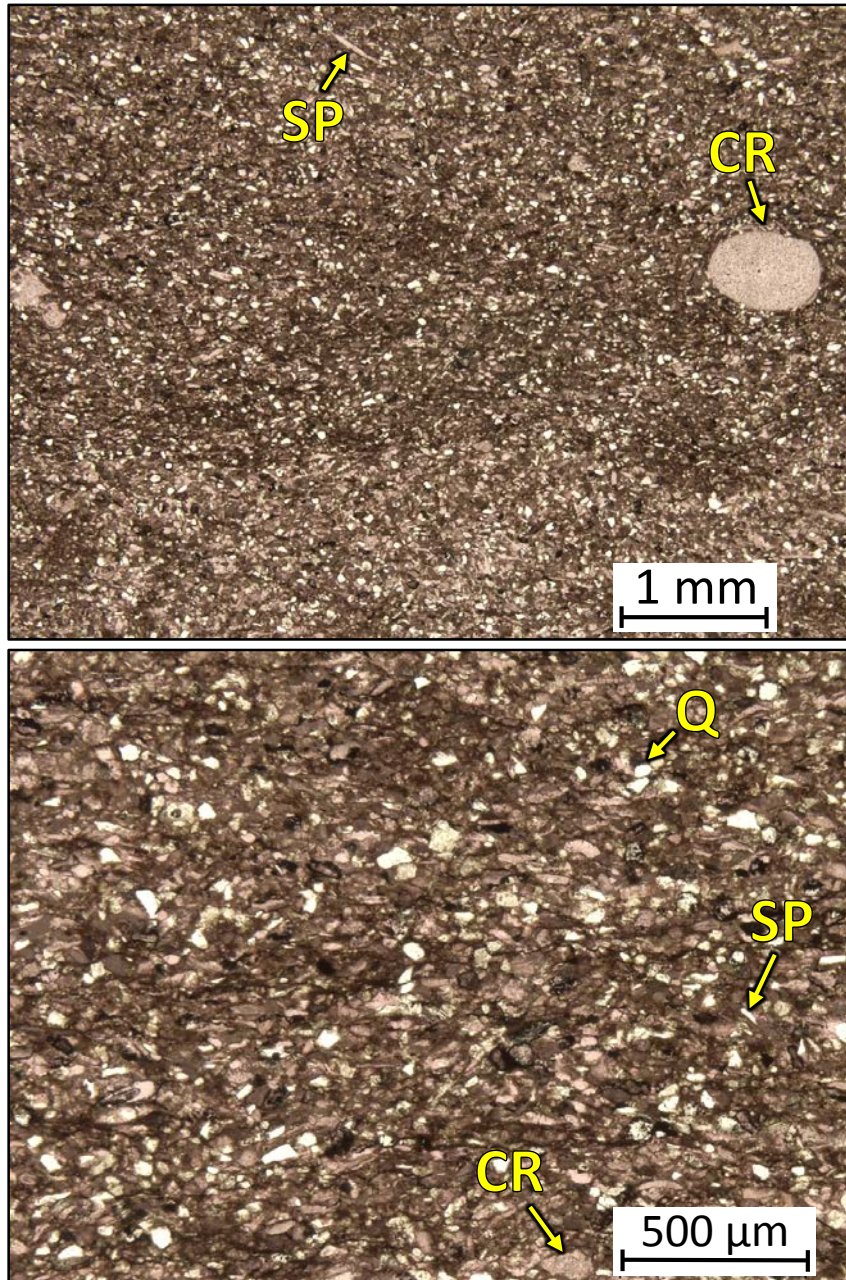
1AD – 5524.65-5524.90' = Bioturbated skeletal packstone. Sample is alizarin red stained. TOC: 0.71%. XRD: 13% clays (1% chlorite, 8% illite, and 4% mixed layer illite/smectite), 32% carbonates (30% calcite and 2% dolomite), and 55% other minerals (43% quartz, 2% potassium feldspar, 6% plagioclase feldspar, 3% pyrite, and 1% apatite). Sample contains crinoid grains (15%), sponge spicules (15%), brachiopod fragments (3%), and phosphatic grains (3%). Oil-filled moldic and vug porosity observed.



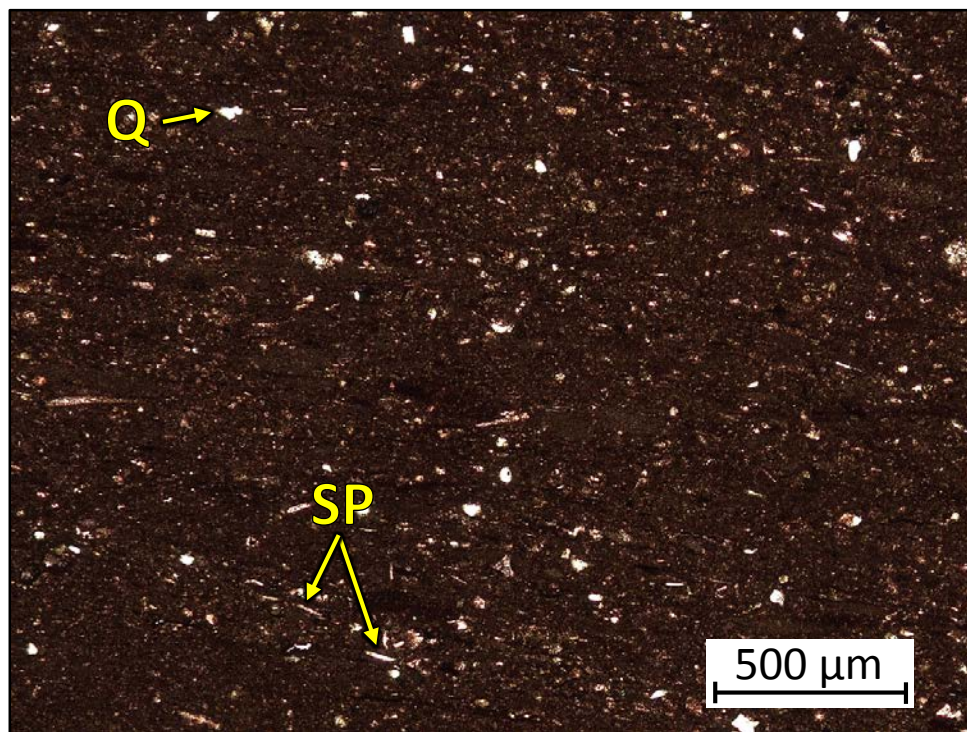
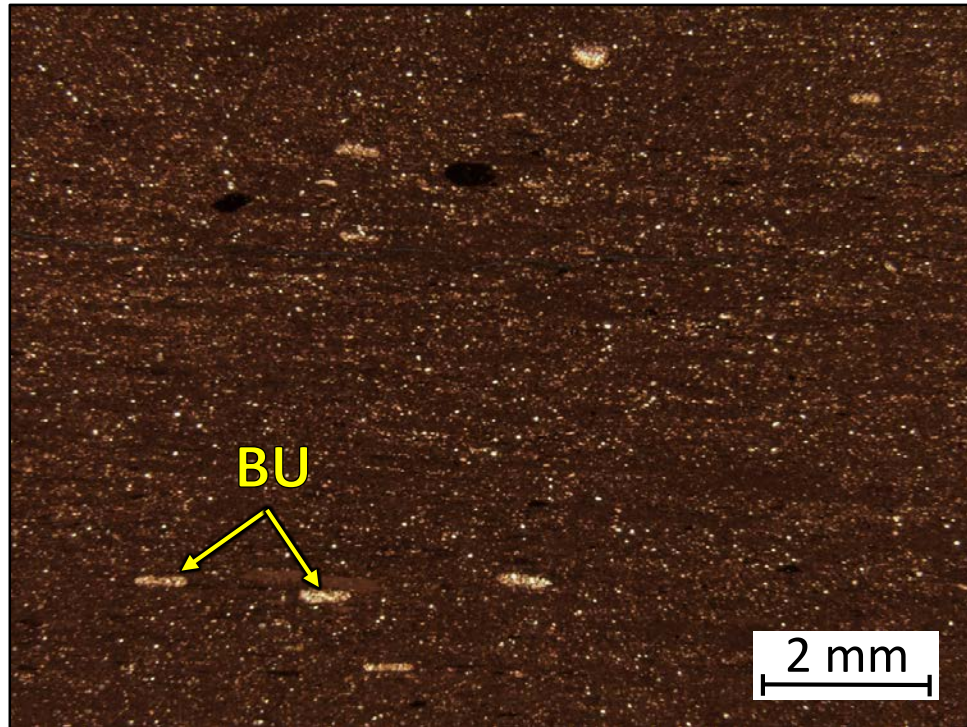
1AD – 5520.10' = Peloidal grainstone. Sample is alizarin red stained. Porosity (NCS): 1.9%. Permeability (Klinkenberg): 0.0001 mD. TOC: 0.01%. XRD: 1% clays (1% illite), 72% carbonates (71% calcite and 1% dolomite), and 27% other minerals (22% quartz, 1% potassium feldspar, 4% plagioclase feldspar, and trace amounts of pyrite and apatite). Sample contains crinoid grains (30%), peloids (20%), silt-sized quartz grains (20%), and sponge spicules (15%). Quartz-rich wisps (outlined in dashed yellow line) observed throughout sample. Oil-filled moldic and vug porosity observed.



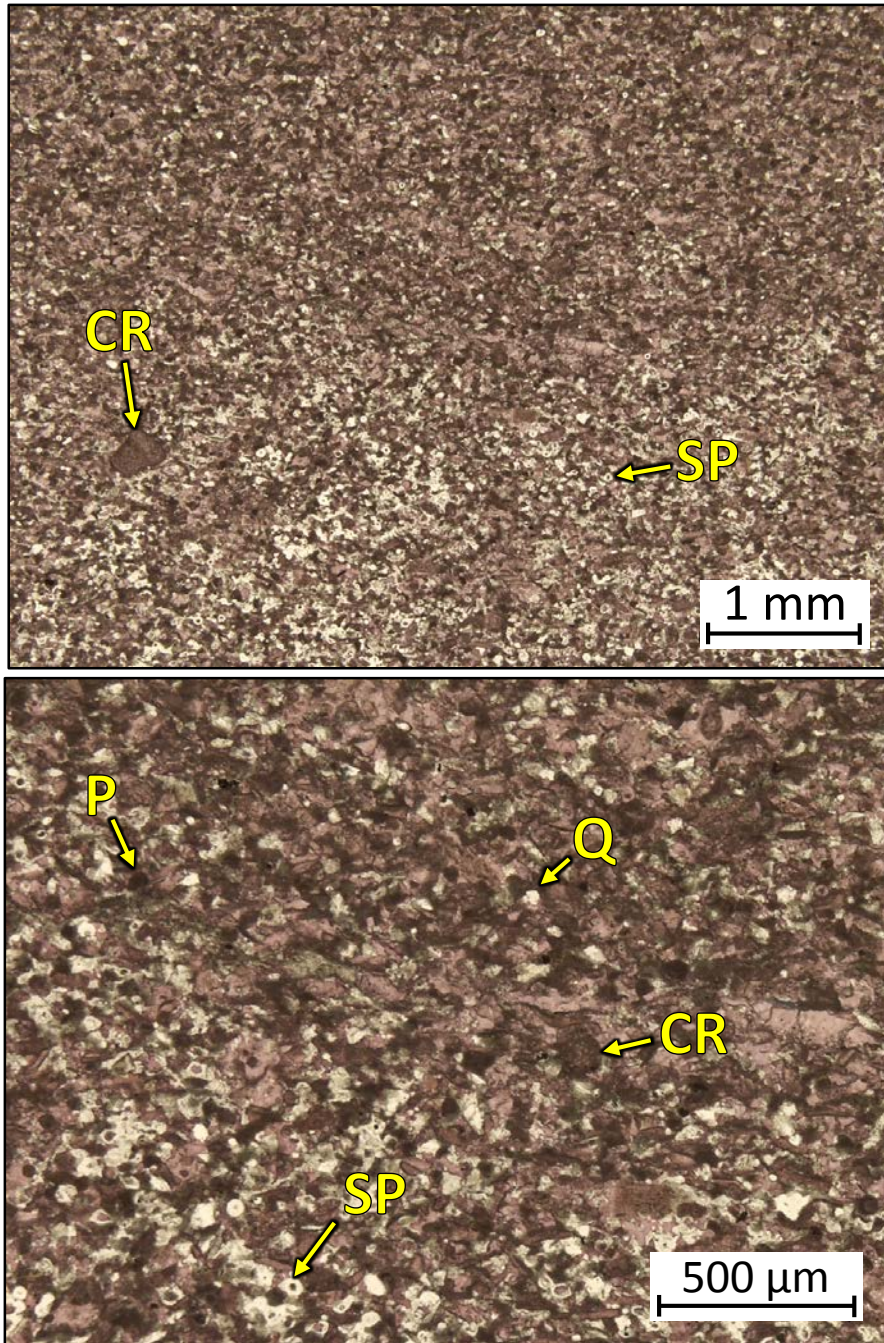
1AD – 5517.75' = Bioturbated wackestone-packstone. Sample is blue epoxy impregnated. Porosity (visual estimation): 1.0%. Visual estimation: 12% clays, 35 % carbonates, 53% other minerals. Sample contains crinoid grains (25%), silt-sized quartz grains (15%), phosphatic or glauconitic grains (5%), and undifferentiated microbioclastic debris.



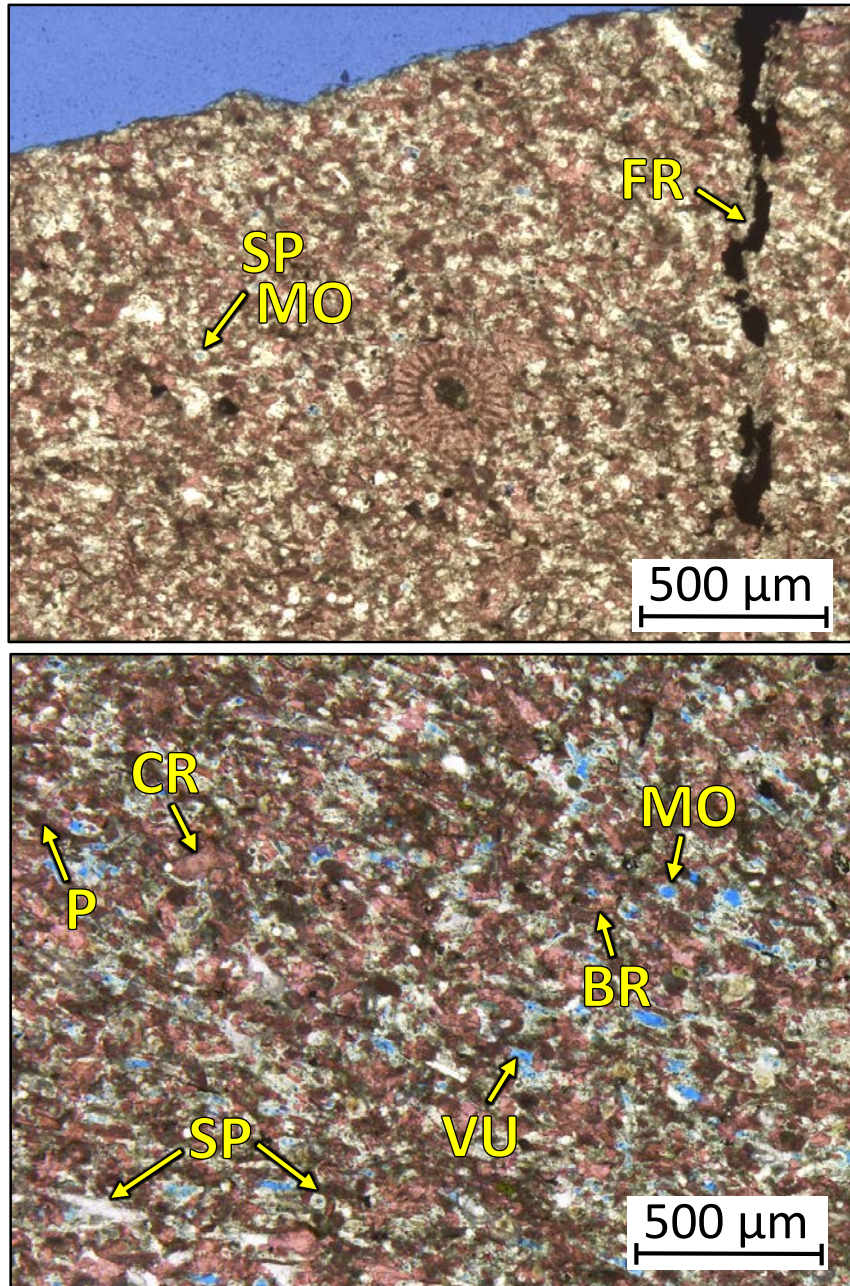
1AD – 5516.10' = Crinoidal wackestone-packstone. Sample is alizarin red stained. Porosity (NCS): 0.8%. Permeability (Klinkenberg): 0.0001-3 mD. TOC: 0.54%. XRD: 5% clays (3% illite and 2% mixed layer illite/smectite), 57% carbonates (56% calcite and 1% dolomite), and 38% other minerals (33% quartz, 1% potassium feldspar, 2% plagioclase feldspar, 2% pyrite, and trace amounts of apatite). Sample contains crinoid grains (25%), sponge spicules (10%), and silt-sized quartz grains (10%). Oil-filled moldic and vug porosity observed.



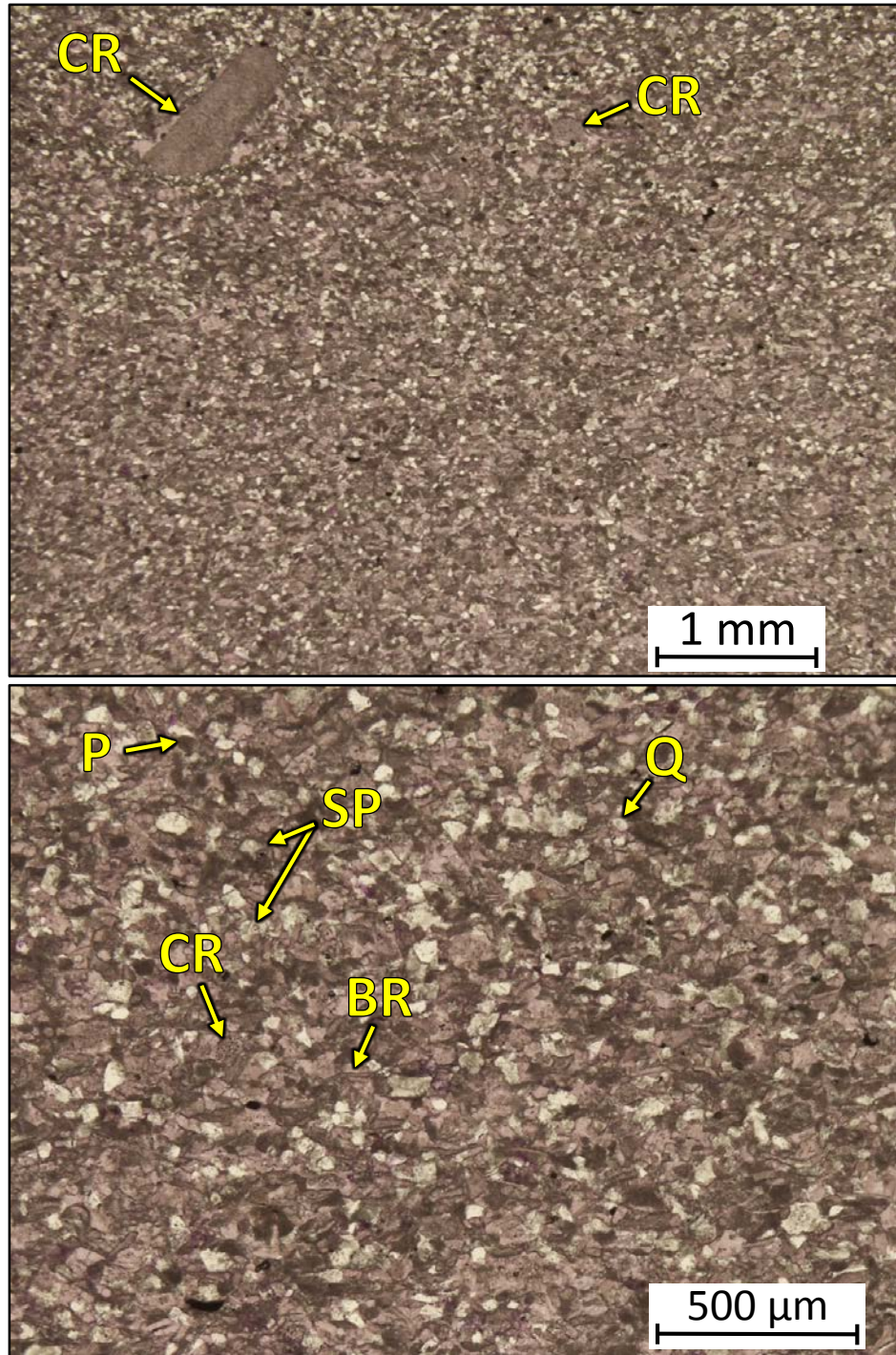
1AD – 5512.0-5512.25' = Laminated mudstone-wackestone. Sample is alizarin red stained. TOC: 1.41%. XRD: 10% clays (8% illite and 2% mixed layer illite/smectite), 58% carbonates (55% calcite and 3% dolomite), and 32% other minerals (26% quartz, 1% potassium feldspar, 1% plagioclase feldspar, 1% pyrite, 2% apatite, and 1% marcasite). Sample contains silt-sized quartz grains (10%), sponge spicules (10%), and undifferentiated microbioclastic debris.



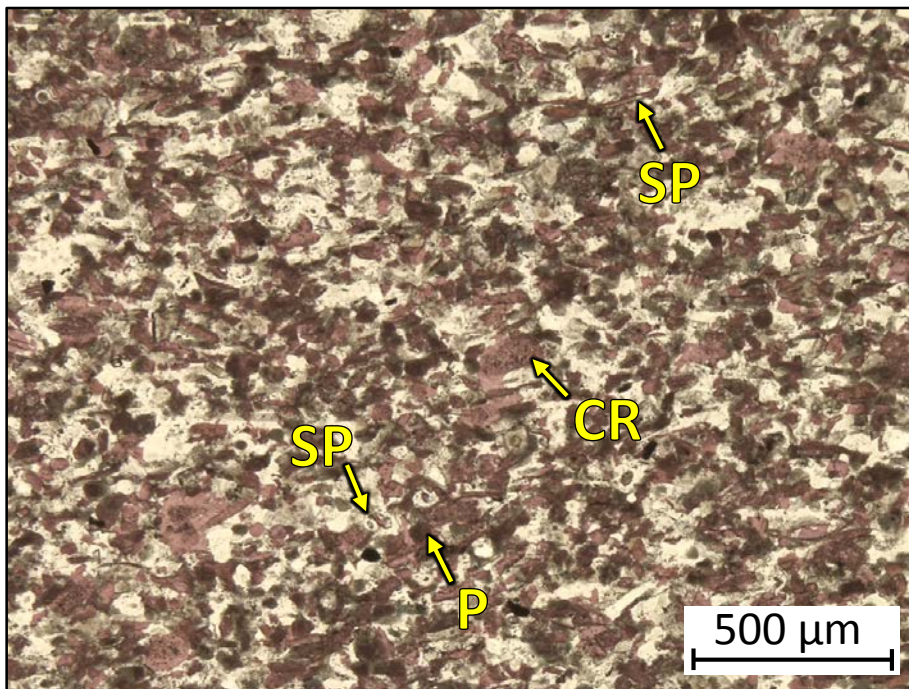
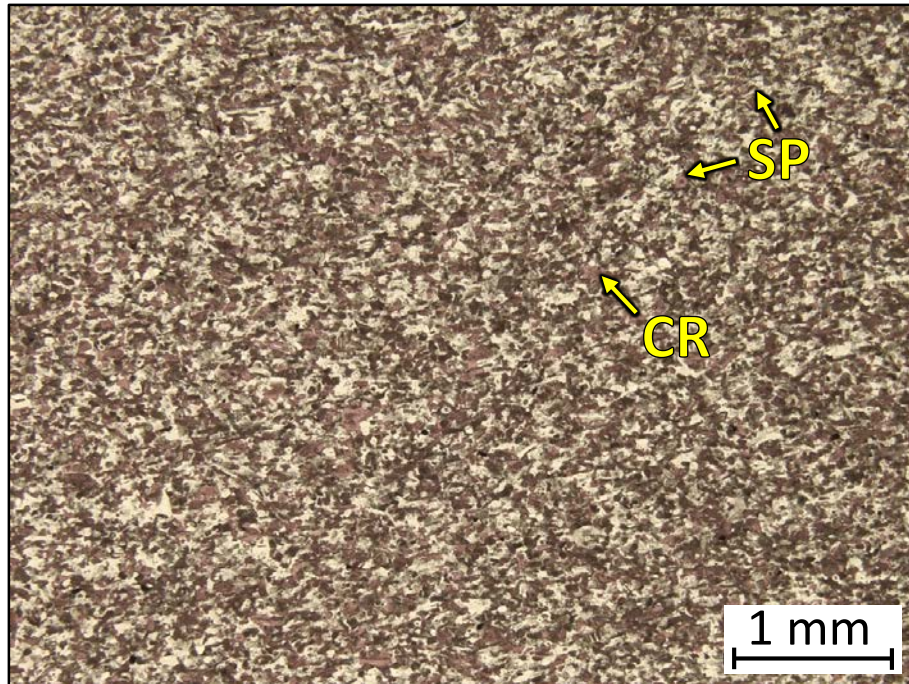
1AD – 5509.10' = Partially silicified skeletal grainstone. Sample is alizarin red stained. Porosity (NCS): 1.2%. Permeability (Klinkenberg): <0.0001 mD. TOC: 0.01%. XRD: 1% clays (8% illite and 2% mixed layer illite/smectite), 65% carbonates (60% calcite and 5% dolomite), and 34% other minerals (28% quartz, 1% potassium feldspar, 4% plagioclase feldspar, trace amounts of pyrite, and 1% apatite). Sample contains crinoid grains (25%), sponge spicules (20%), peloids (10%), and silt-sized quartz grains (10%). Increased abundance of sponge spicules in silicified portion. Oil-filled vug porosity observed.



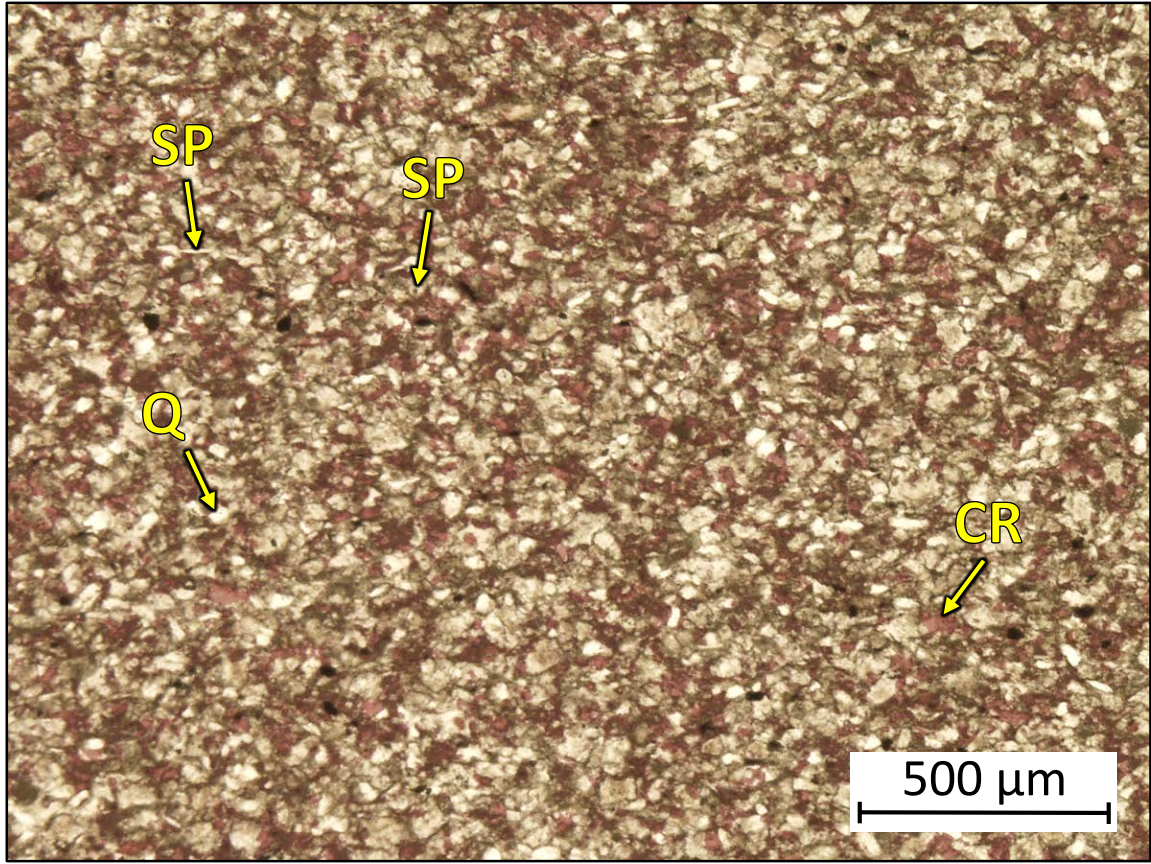
1AD – 5507.90' = Skeletal grainstone. Sample is alizarin red stained. Porosity (NCS): 4.2%. Permeability (Klinkenberg): 0.0001 mD. TOC: 0.23%. XRD: 1% clays (1% illite), 54% carbonates (47% calcite and 7% dolomite), and 45% other minerals (42% quartz, 1% potassium feldspar, 2% plagioclase feldspar, and trace amounts of pyrite and apatite). Sample contains crinoid grains (25%), sponge spicules (20%), peloids (15%), brachiopod fragments (10%), and undifferentiated microbioclastic debris. A bryozoan fragment or a transverse section of an echinoid spine is shown in the upper photomicrograph. Oil-filled and open fracture, moldic, and vug porosity observed.



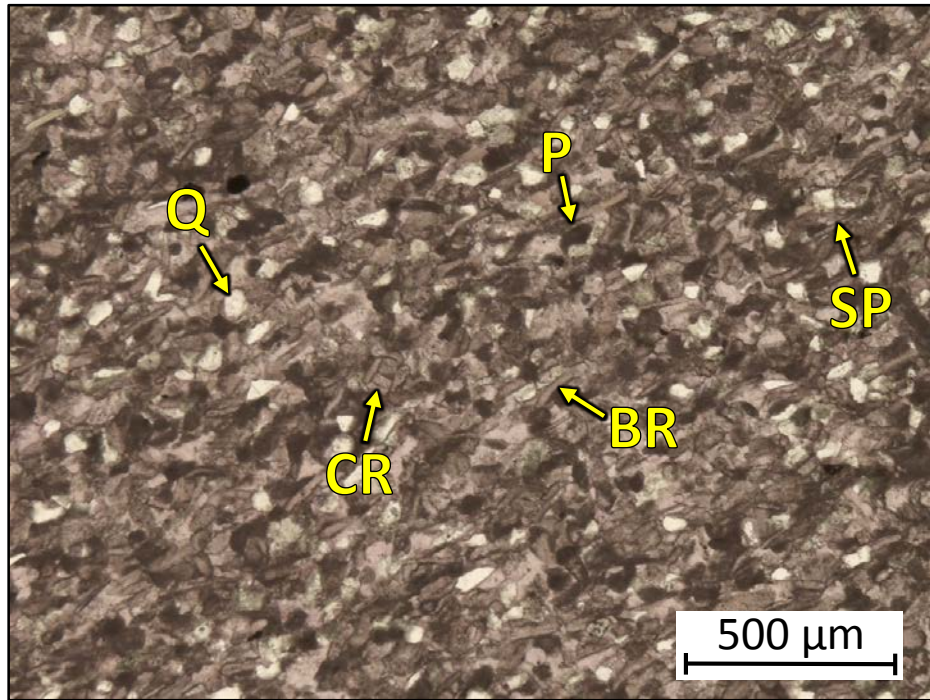
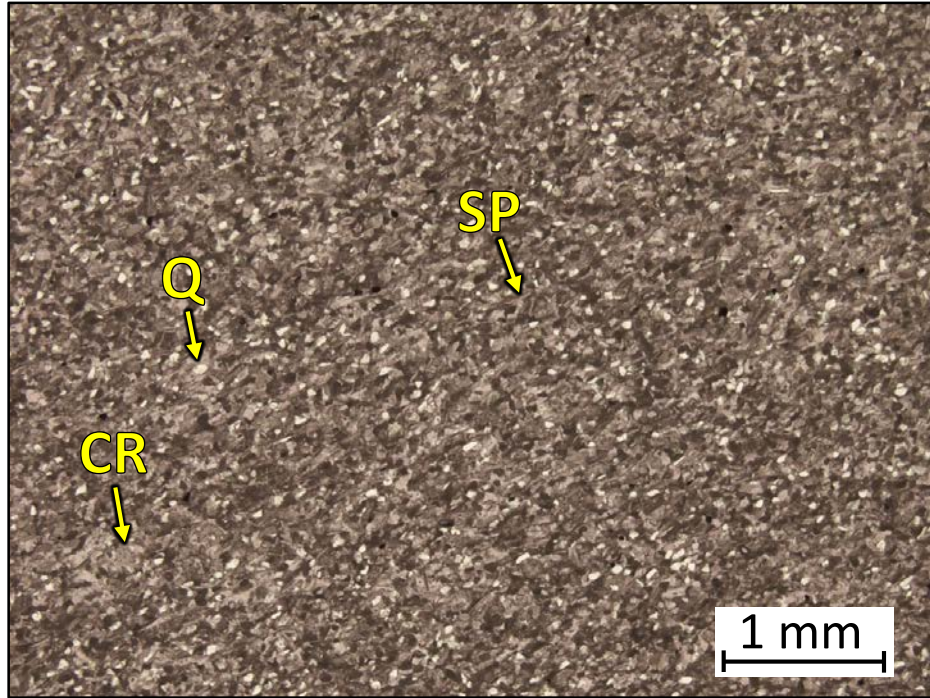
1AD – 5506.10' = Skeletal-peloidal grainstone. Sample is alizarin red stained. Porosity (NCS): 2.2%. Permeability (Klinkenberg): 0.0001 mD. TOC: 0.07%. XRD: 2% clays (1% illite and 1% mixed layer illite/smectite), 69% carbonates (64% calcite and 5% dolomite), and 29% other minerals (25% quartz, 1% potassium feldspar, 2% plagioclase feldspar, 1% pyrite, and trace amounts of apatite). Sample contains crinoid grains (25%), peloids (20%), brachiopod or ostracode fragments (10%), silt-sized quartz grains (10%), sponge spicules (5%), and undifferentiated microbioclastic debris. Oil-filled moldic porosity observed.



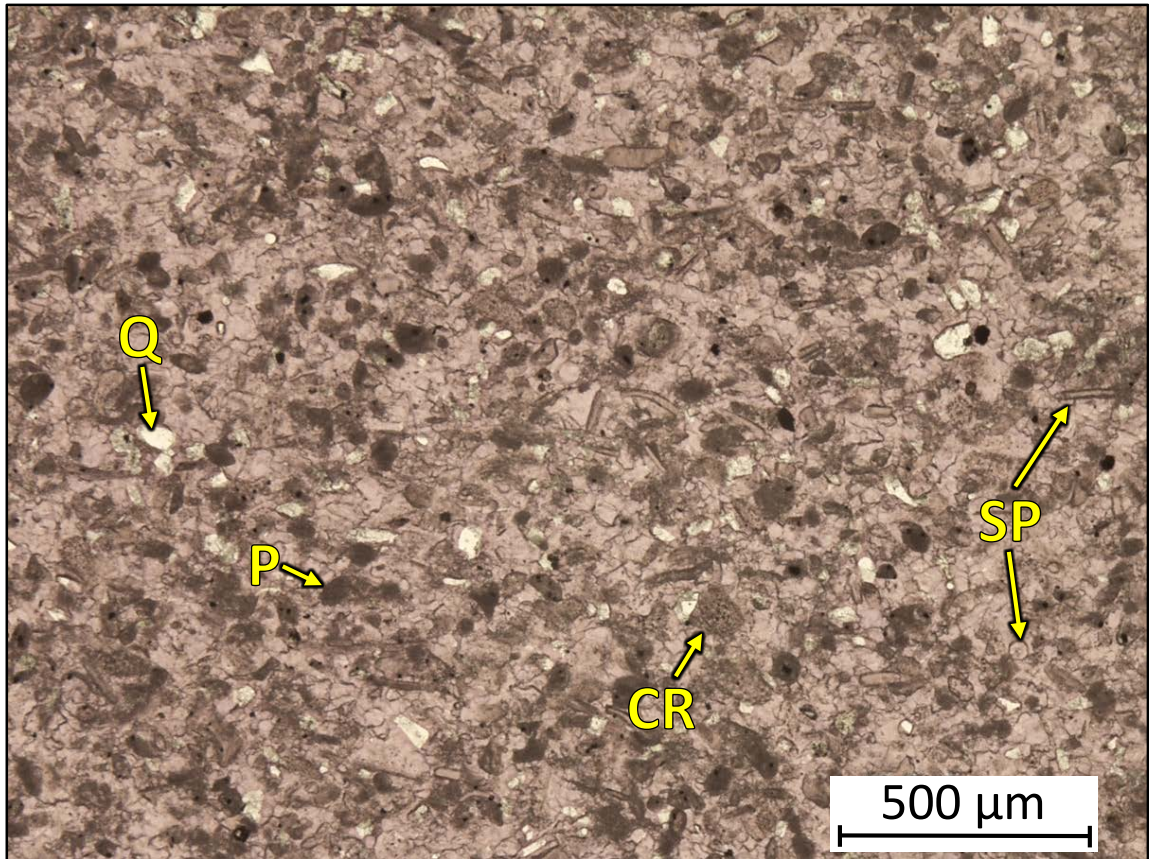
1AD – 5504.25' = Silicified skeletal grainstone. Sample is alizarin red stained. Porosity (NCS): 2.4%. Permeability (Klinkenberg): <0.0001 mD. TOC: 0.01%. XRD: 1% clays (1% illite), 67% carbonates (64% calcite and 3% dolomite), and 32% other minerals (29% quartz, 1% potassium feldspar, 2% plagioclase feldspar, and trace amounts of pyrite and apatite). Sample contains crinoid grains (20%), sponge spicules (30%), peloids (15%), and undifferentiated microbioclastic debris. Oil-filled moldic and vug porosity observed.



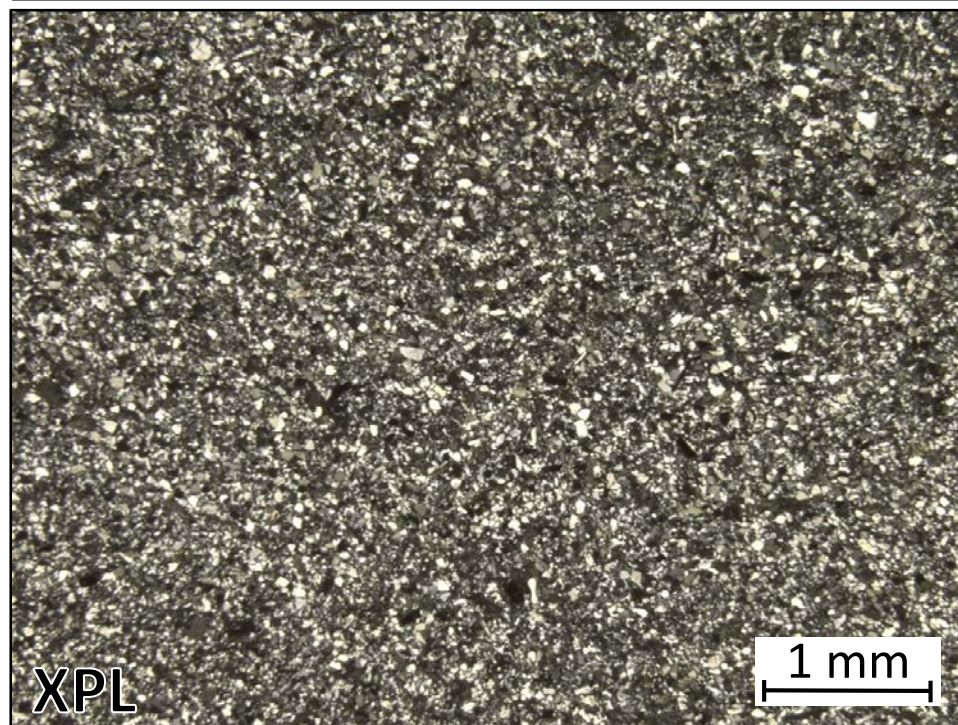
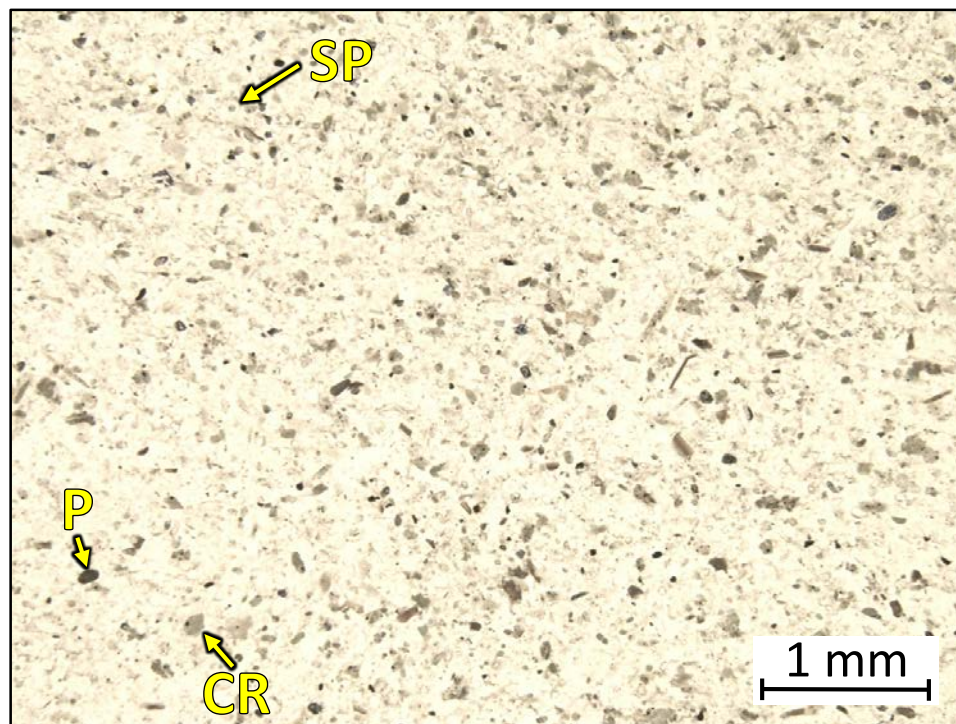
1AD – 5501.65' = Silica-rich skeletal-peloidal packstone-grainstone. Sample is alizarin red stained. Porosity (NCS): 2.9%. Permeability (Klinkenberg): <0.0001 mD. TOC: 0.01%. XRD: 4% clays (4% illite), 50% carbonates (28% calcite and 22% dolomite), and 46% other minerals (36% quartz, 2% potassium feldspar, 6% plagioclase feldspar, trace amounts of pyrite, 1% apatite, and 1% marcasite). Sample contains crinoidal debris (20%), sponge spicules (15%), and undifferentiated microbioclastic debris. Oil-filled moldic and vug porosity observed.



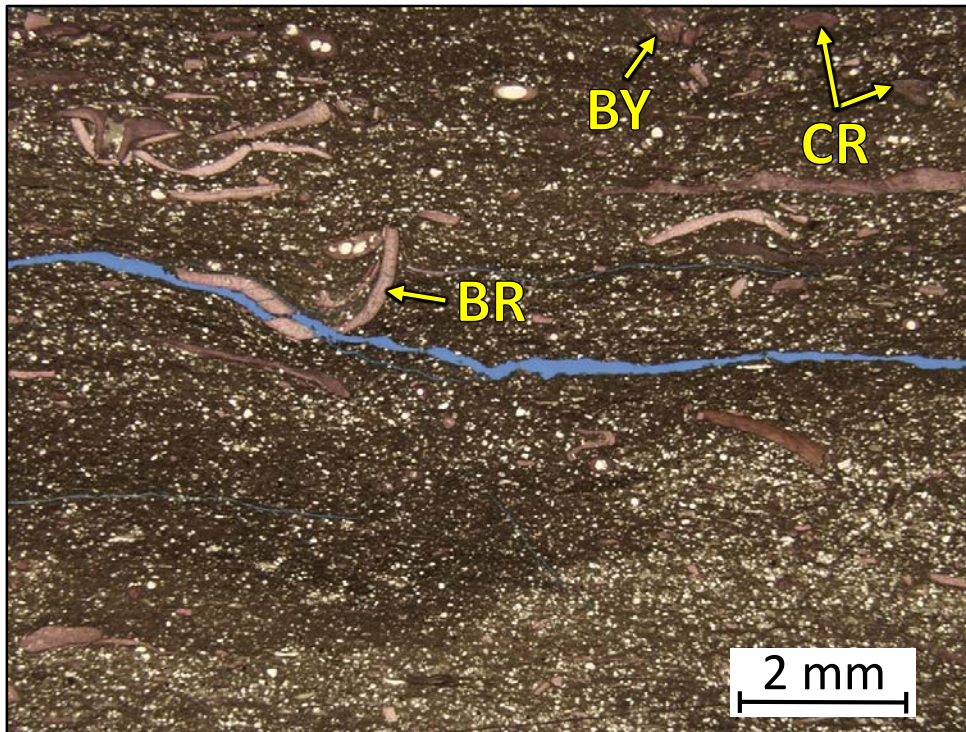
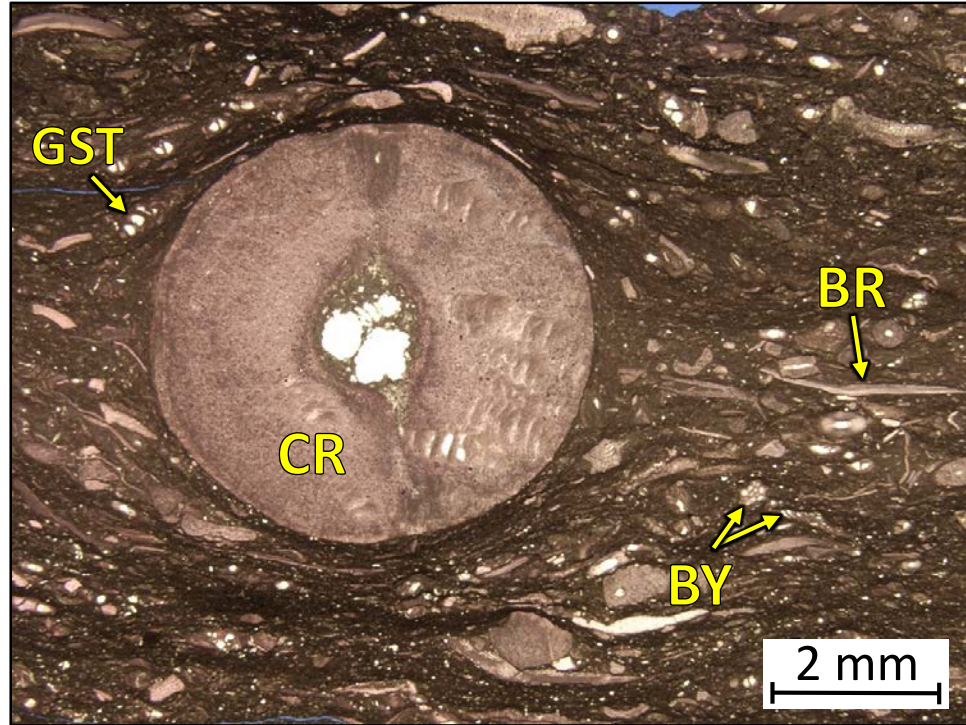
1AD – 5498.45' = Peloidal-skeletal grainstone. Sample is alizarin red stained. Porosity (NCS): 0.6%. Permeability (Klinkenberg): <0.0001 mD. TOC: 0.01%. XRD: 1% clays (1% illite), 71% carbonates (71% calcite), and 28% other minerals (22% quartz, 1% potassium feldspar, 4% plagioclase feldspar, trace amounts of pyrite, and 1% apatite). Sample contains crinoid grains (15%), sponge spicules (10%), peloids (20%), silt-sized quartz grains (20%), and brachiopod fragments (3%). Oil-filled moldic and vug porosity observed.



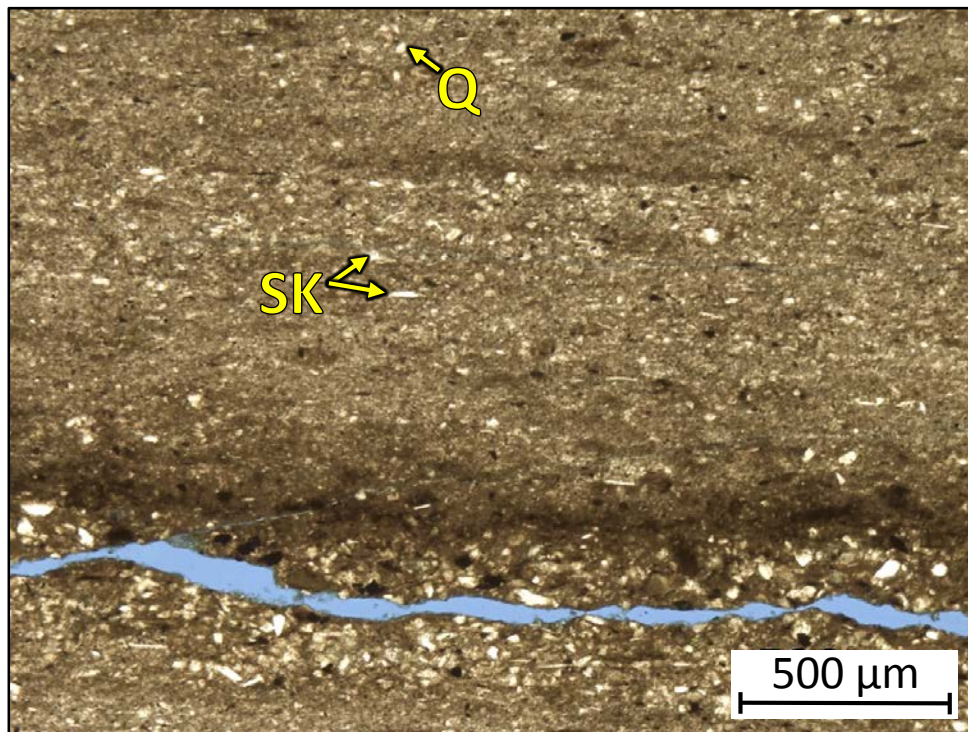
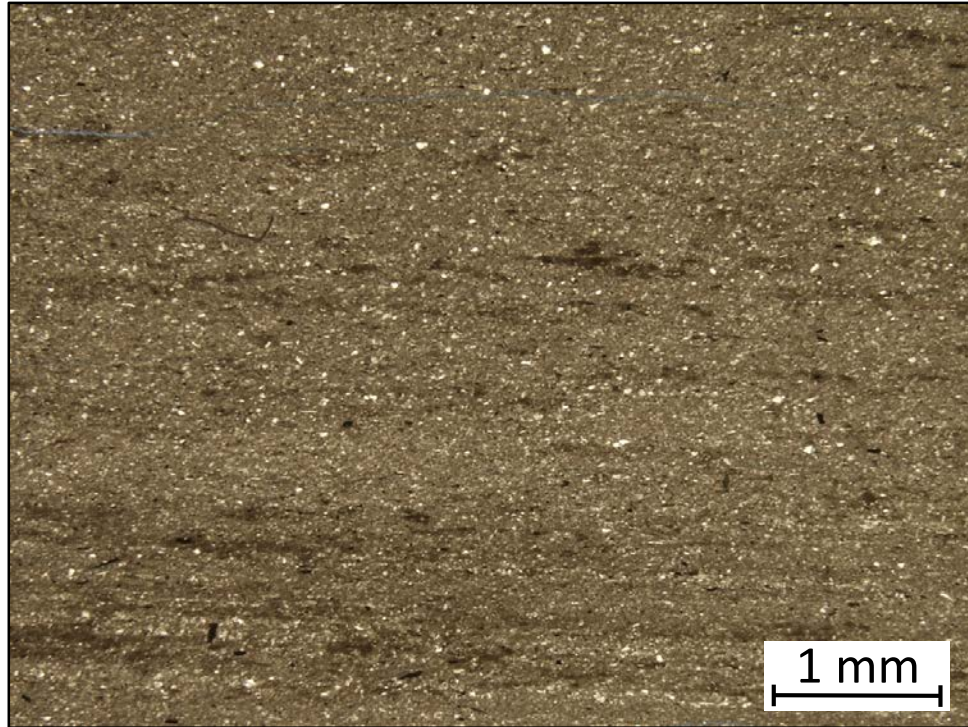
1AD – 5496.70' = Peloidal grainstone. Sample is alizarin red stained. Porosity (NCS): 1.0%. Permeability (Klinkenberg): 0.023 mD. TOC: 0.03%. XRD: 1% clays (1% illite), 84% carbonates (84% calcite), and 15% other minerals (10% quartz, 1% potassium feldspar, 3% plagioclase feldspar, 1% pyrite, and trace amounts of apatite). Sample contains crinoid fragments (30%), sponge spicules (15%), peloids (10%), silt-sized quartz grains (10%), and undifferentiated microbioclastic debris. Minor amounts of oil-filled moldic and vug porosity observed.



1AD – 5496.10' = Chert/silicified grainstone. Sample is alizarin red stained and blue epoxy impregnated. Sample has been completely silicified. Original skeletal components were composed of crinoid fragments, sponge spicules, and other undifferentiated microbioclastic debris.



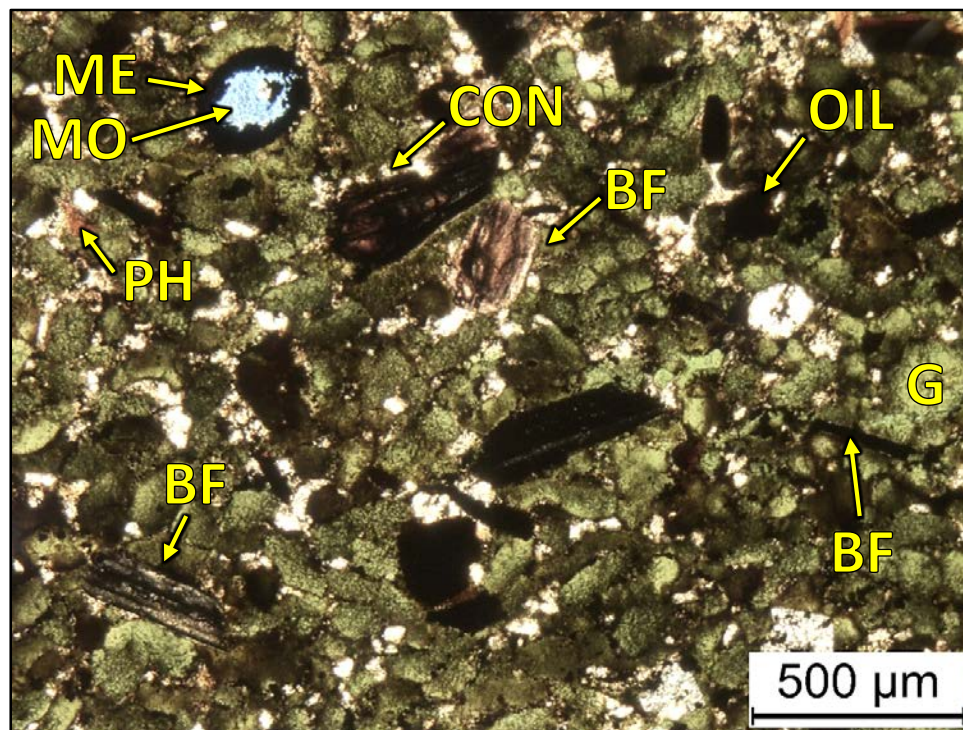
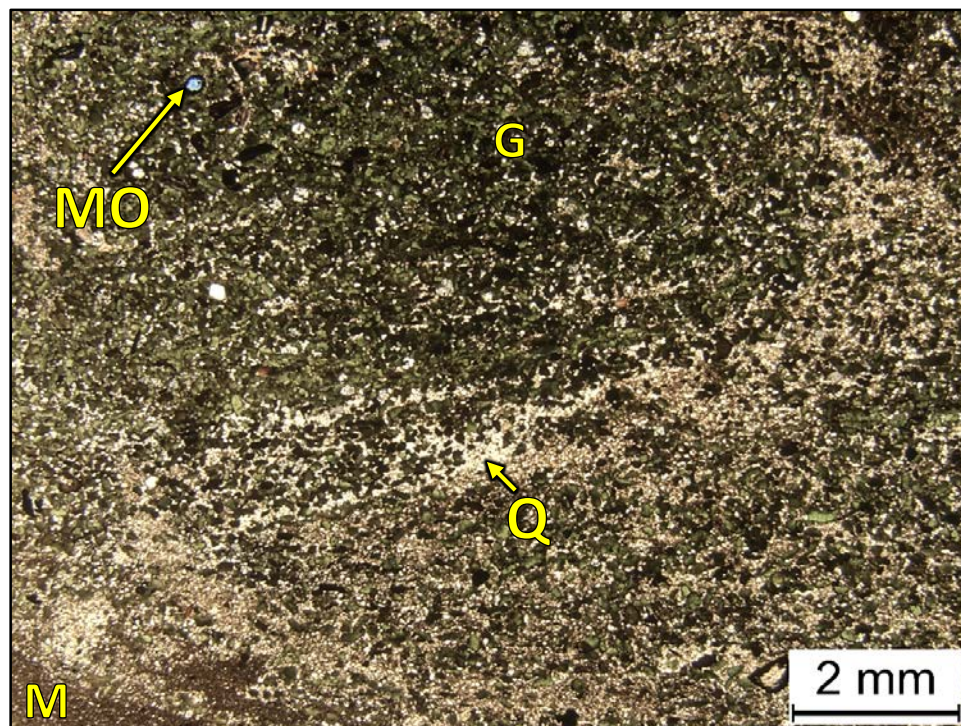
1AD – 5495.2' = Pennsylvanian wackestone-floatstone. Sample is alizarin red stained and blue epoxy impregnated. Sample contains silt-sized quartz grains (25%), crinoid fragments (20%), brachiopod fragments (15%), and bryozoans (10%).



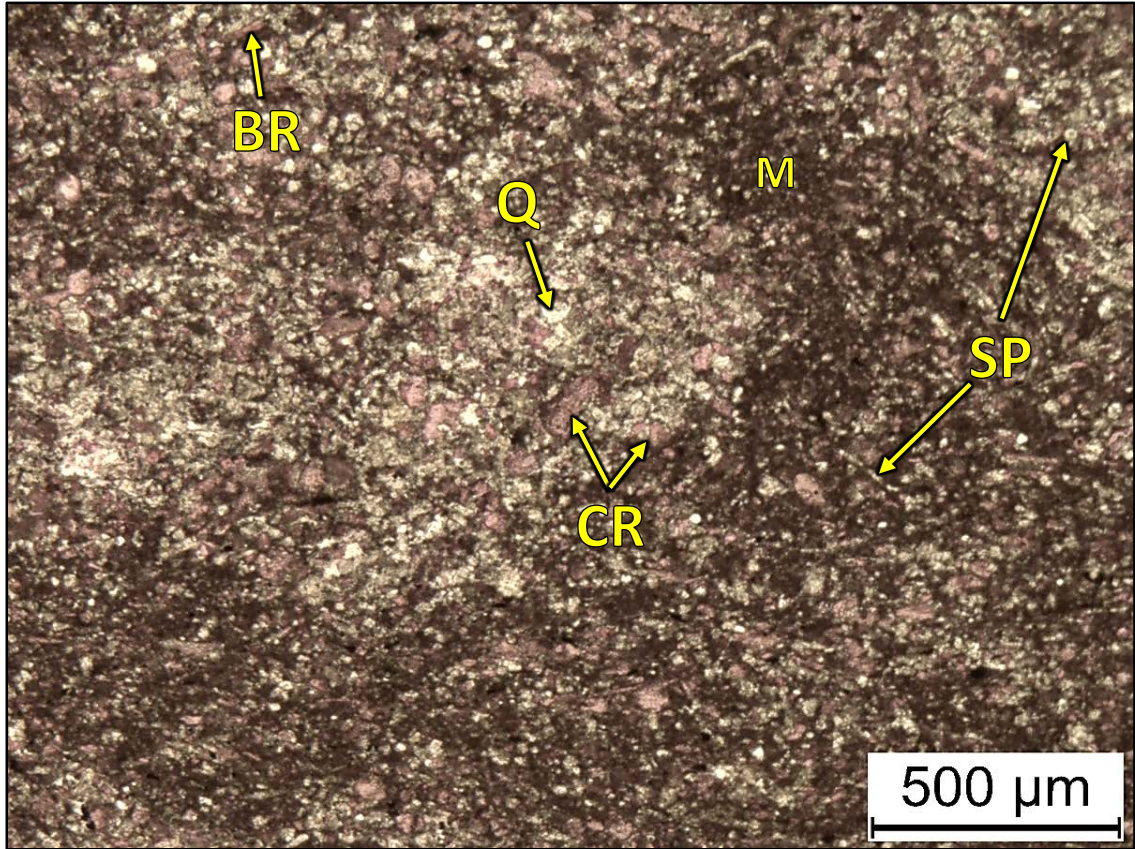
1AD – 5491.4' = Pennsylvanian wackestone-packstone. Sample is blue epoxy impregnated. Sample contains silt-sized quartz fragments and undifferentiated skeletal material likely composed of crinoid and sponge spicule fragments.

Core #2

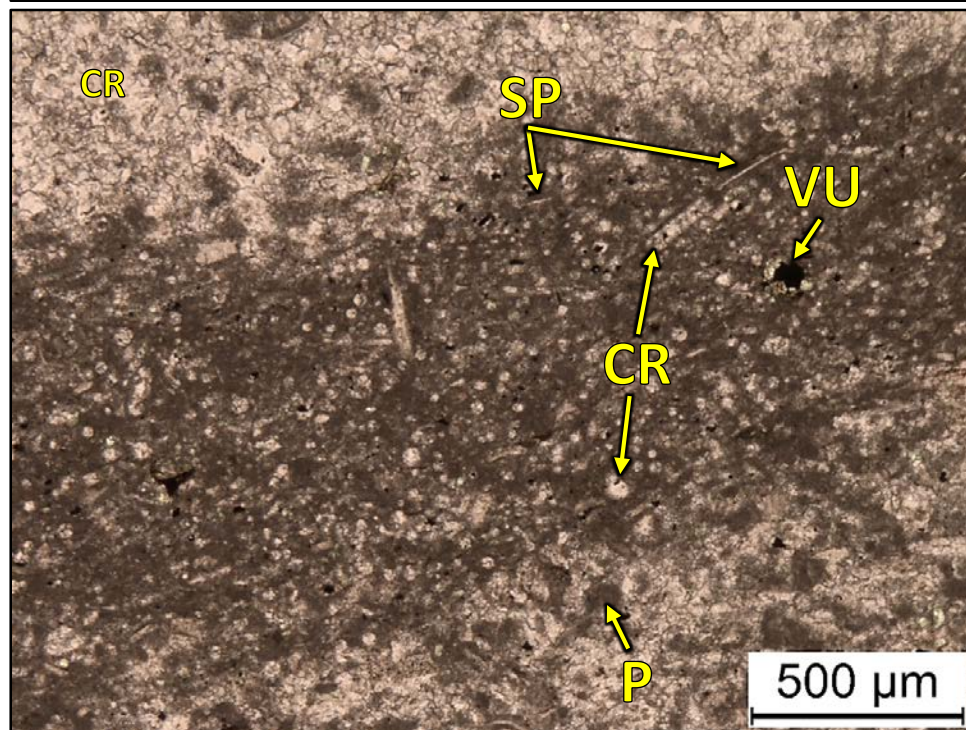
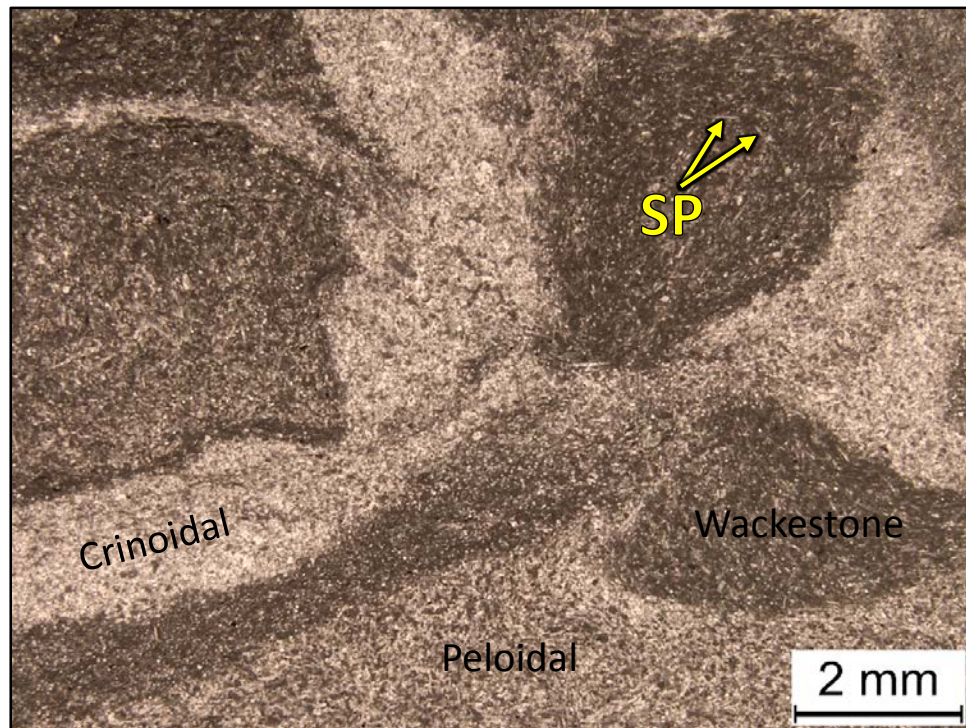
Winney #1-8 SWD



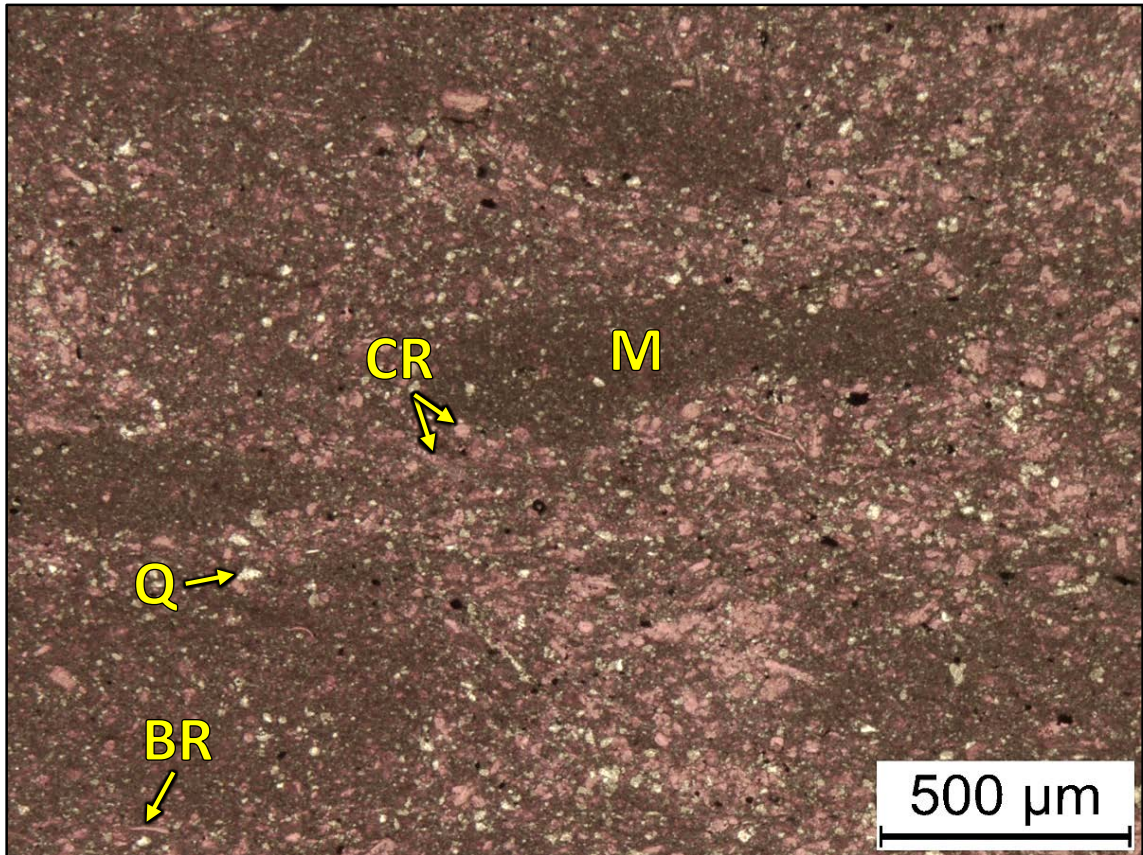
2WN – 5312.75' = Glauconitic sandstone. Sample is blue epoxy impregnated. Porosity (visual estimation): 5.0%. Visual estimation: 10% clays, 35% carbonates, and 55% other minerals. Sample contains slit-sized quartz grains (50%), fine sand-sized glauconite grains (40%), brachiopod fragments (3%), bone fragments (5%), and some phosphate, sponge spicule, and conodont fragments. Moldic porosity from dissolution skeletal grains. Oil present throughout sample.



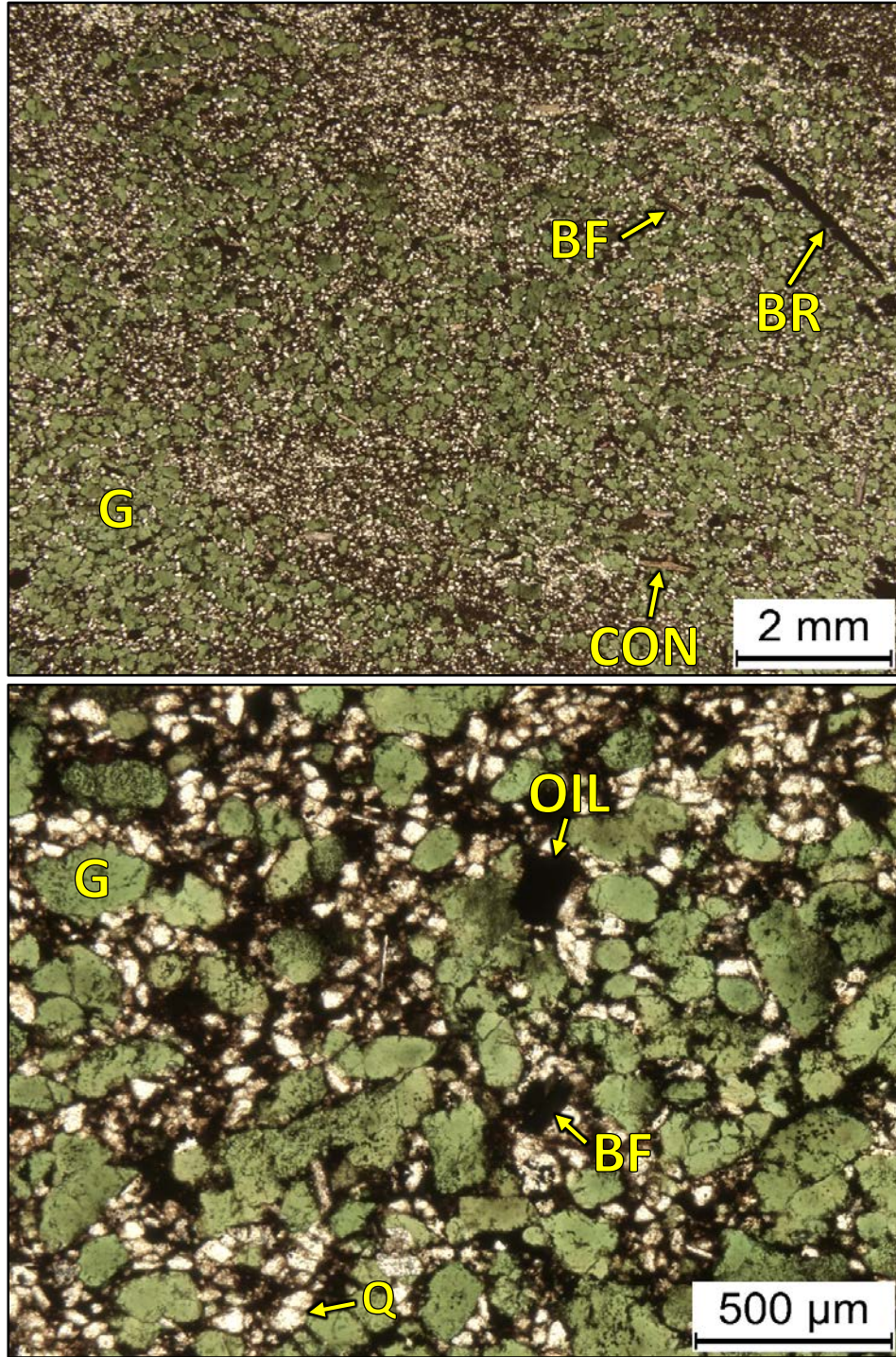
2WN – 5309.60' = Bioturbated wackestone-packstone. Sample is alizarin red stained. Porosity (NCS): 3.1%. Permeability (Klinkenberg): 0.0009 mD. TOC: 0.43%. XRD: 2% clays (1% illite and 1% mixed layer illite/smectite), 70% carbonates (55% calcite and 15% dolomite), and 28% other minerals (23% quartz, 1% potassium feldspar, 2% plagioclase feldspar, 1% pyrite, and 1% apatite). Sample contains silt-sized quartz grains (23%), crinoid fragments (15%), brachiopod fragments (5%), and sponge spicules (10%). Dominantly oil-filled vug porosity.



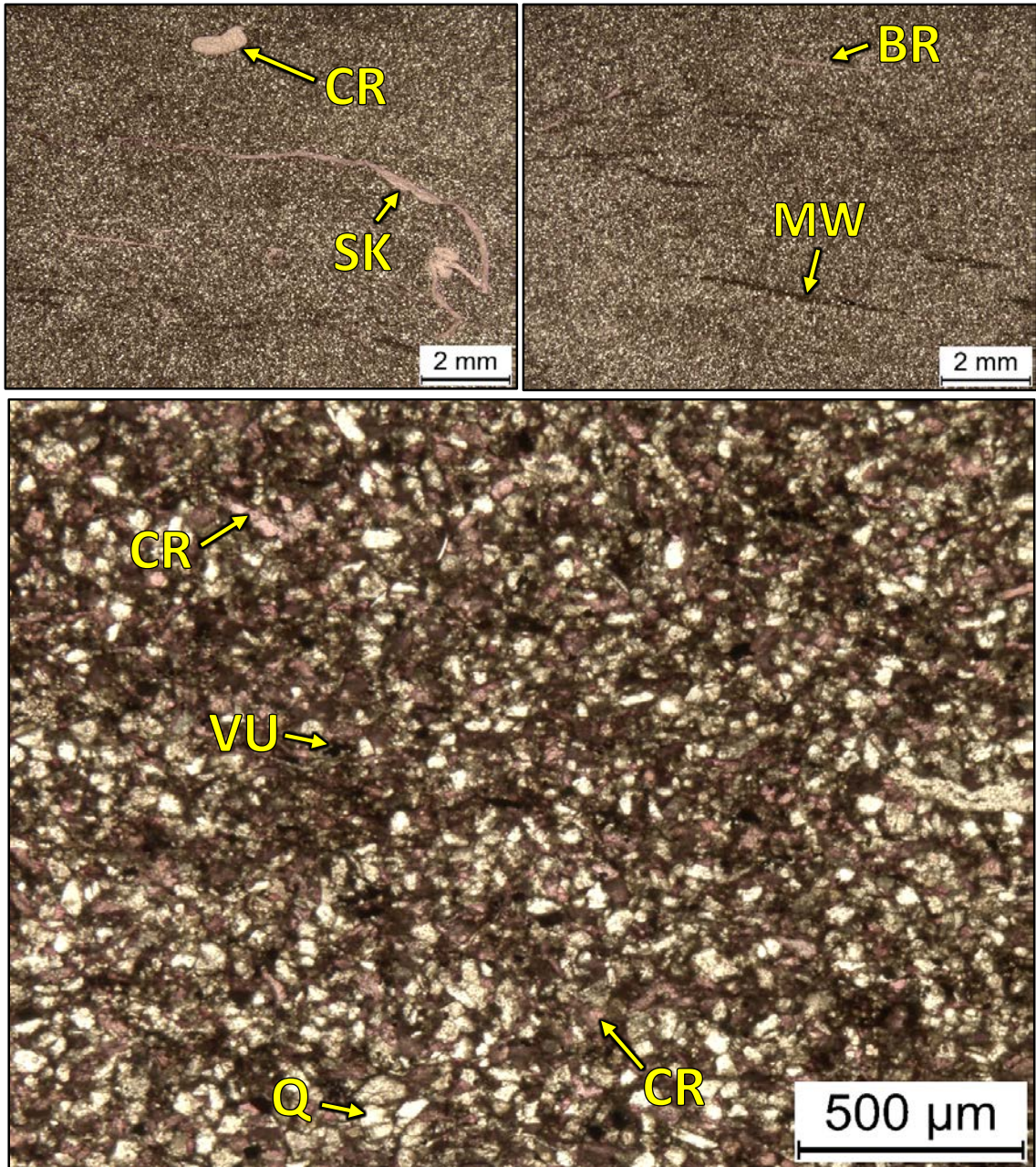
2WN – 5305.35' = Bioturbated crinoidal wackestone-packstone. Sample is alizarin red stained. Porosity (NCS): 0.4%. Permeability (Klinkenberg): <0.0001 mD. TOC: 0.08%. XRD: 1% clays (5% illite), 84% carbonates (83% calcite and 1% dolomite), and 15% other minerals (12% quartz, 1% potassium feldspar, 2% plagioclase feldspar, and trace amounts of pyrite and apatite). Sample contains abundant crinoid grains (40%), peloids (10%), and sponge spicules (15%). Oil-filled vug porosity observed.



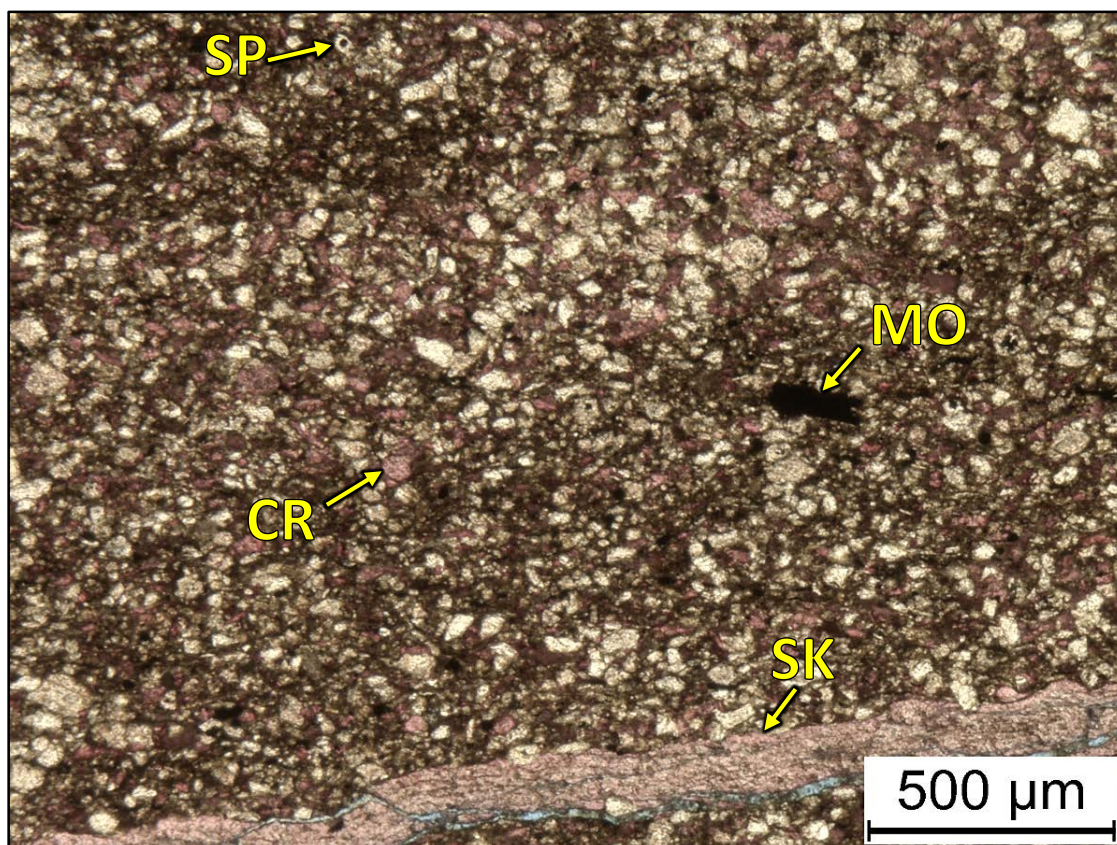
2WN – 5298.45' = Bioturbated mudstone-wackestone. Sample is alizarin red stained. Porosity (NCS): 0.7%. Permeability (Klinkenberg): <0.0001 mD. TOC: 0.18%. XRD: 4% clays (2% illite and 2% mixed layer illite/smectite), 68% carbonates (65% calcite and 3% dolomite), and 28% other minerals (25% quartz, 1% potassium feldspar, 2% plagioclase feldspar, and trace amounts of pyrite). Sample contains silt-sized quartz grains (25%) and crinoid (15%) and brachiopod (5%) fragments.



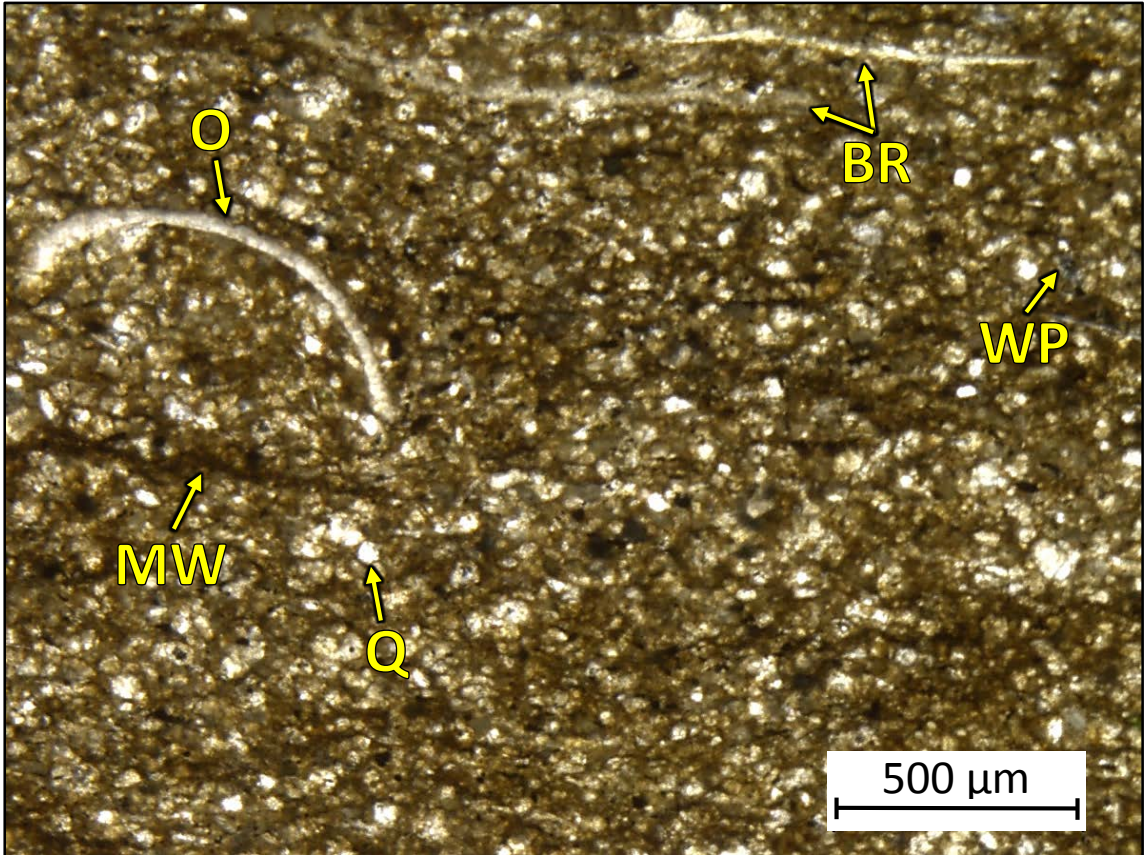
2WN – 5292.60' = Glauconitic sandstone. Sample is alizarin red stained. Porosity (NCS): 9.6%. Permeability (Klinkenberg): 0.710 mD. TOC: 1.30%. XRD: 26% clays (21% illite and 5% mixed layer illite/smectite), 13% carbonates (11% calcite and 2% dolomite), and 61% other minerals (47% quartz, 2% potassium feldspar, 5% plagioclase feldspar, 5% pyrite, and 2% apatite). Sample contains silt-sized quartz grains (47%), fine to medium sand-sized glauconite grains (35%), bone fragments (3%), brachiopod fragments (3%), and conodonts (1%). Significant amounts of oil observed throughout sample.



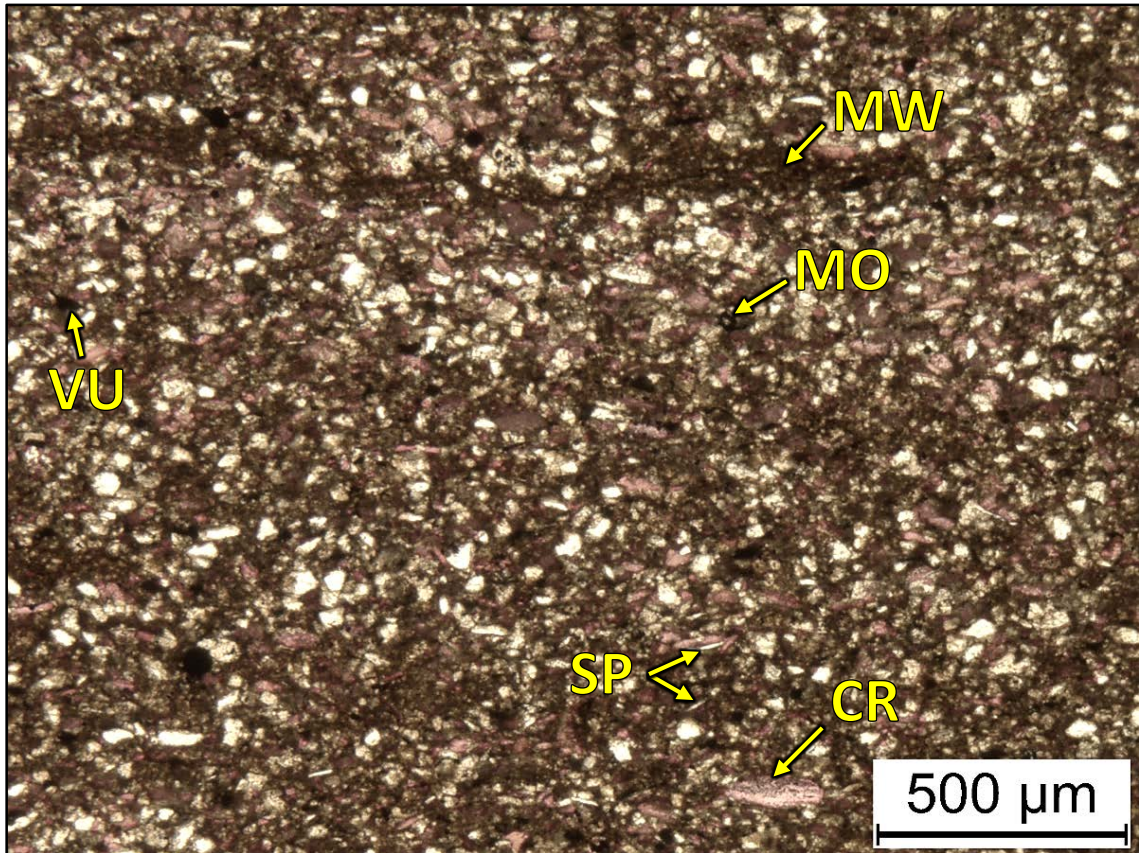
2WN – 5289.55' = Bioturbated wackestone-packstone. Sample is alizarin red stained. Porosity (NCS): 3.7%. Permeability (Klinkenberg): 0.369 mD. TOC: 0.64%. XRD: 14% clays (1% chlorite, 9% illite, and 4% mixed layer illite/smectite), 34% carbonates (25% calcite and 9% dolomite), and 52% other minerals (41% quartz, 3% potassium feldspar, 5% plagioclase feldspar, 3% pyrite and trace amounts of apatite). Sample contains silt-sized quartz grains (40%) and crinoid fragments (30%). Oil-filled moldic and vug porosity observed.



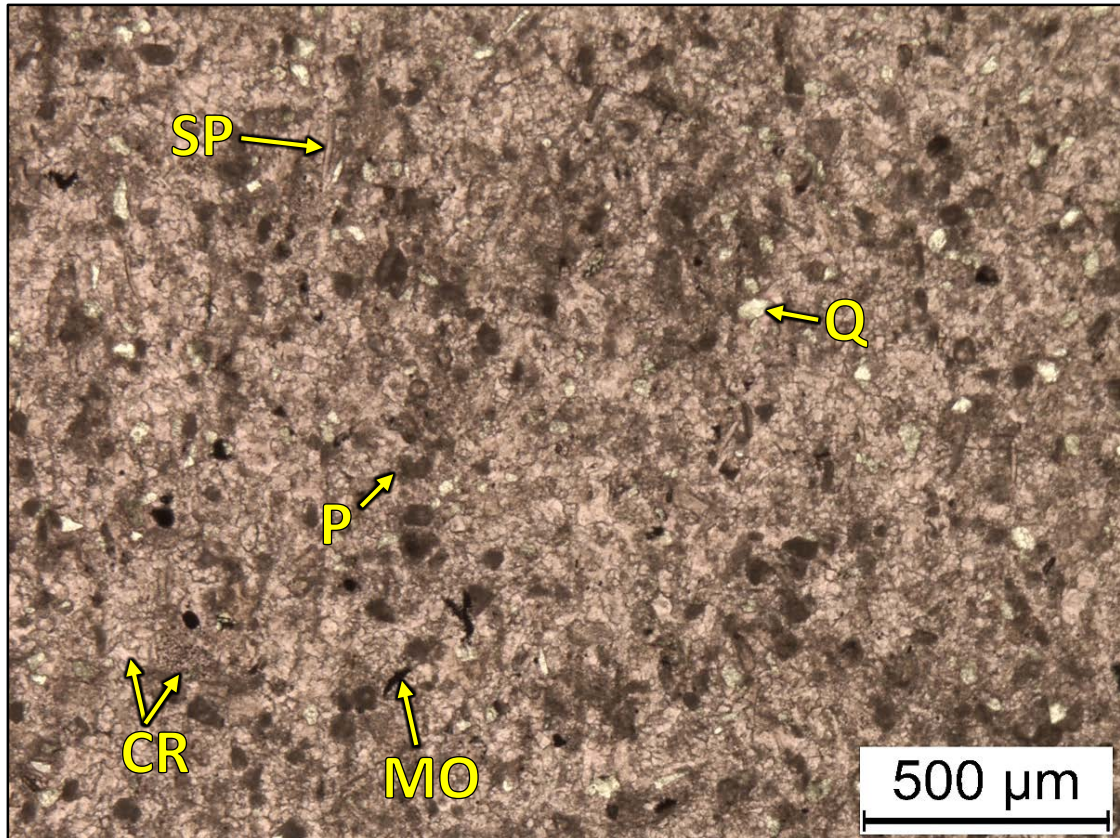
2WN – 5285.55' = Bioturbated wackestone. Sample is alizarin red stained and blue epoxy impregnated. Porosity (ambient): 3.5%. Permeability (Klinkenberg): Sample was unsuitable for this type of measurement. TOC: 0.75%. XRD: 15% clays (10% illite and 5% mixed layer illite/smectite), 38% carbonates (28% calcite and 10% dolomite), and 47% other minerals (37% quartz, 1% potassium feldspar, 5% plagioclase feldspar, 3% pyrite, and 1% apatite). Sample contains silt-sized quartz grains (37%), crinoid fragments (10%), scattered sponge spicules, and undifferentiated microbioclastic debris. Oil-filled moldic porosity from the dissolution of crinoid grains observed.



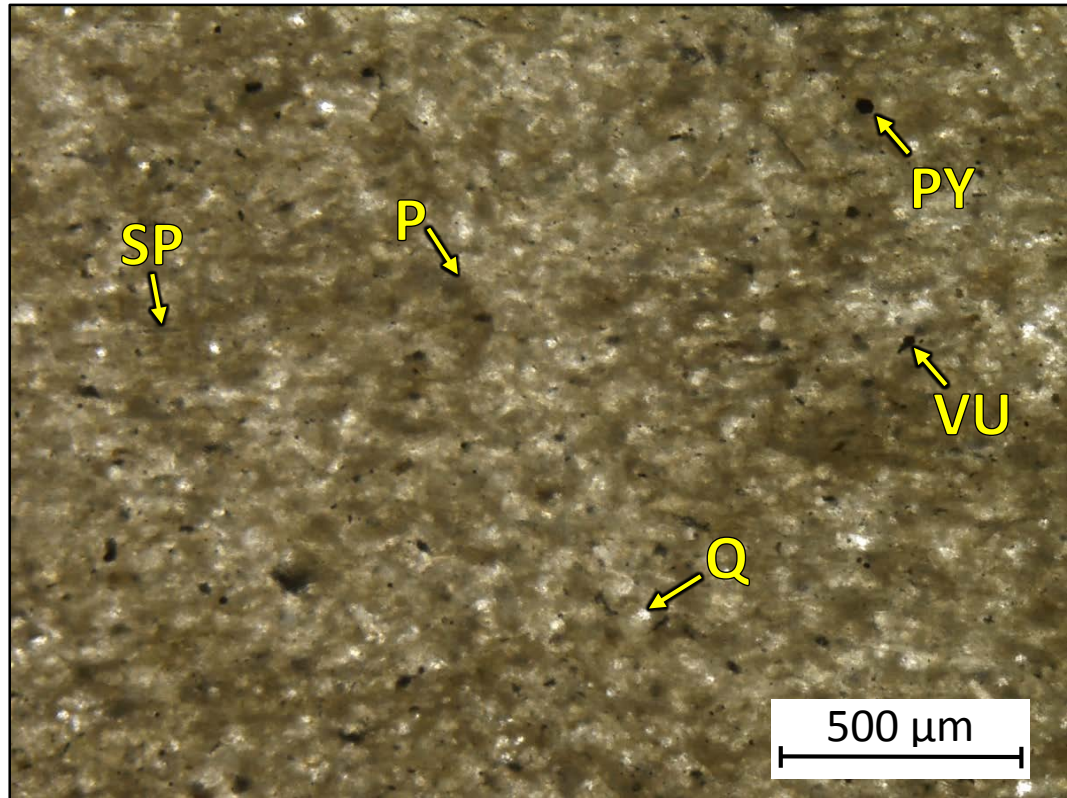
2WN – 5282.80' = Bioturbated wackestone. Porosity (visual estimation): 2.5%. Visual estimation: 15% clays, 35% carbonates, and 50% other minerals. Sample contains silt-sized quartz grains, ostracodes (3%), brachiopod fragments (5%), and undifferentiated microbioclastic debris. Moldic, vug, and intracrystalline porosity observed.



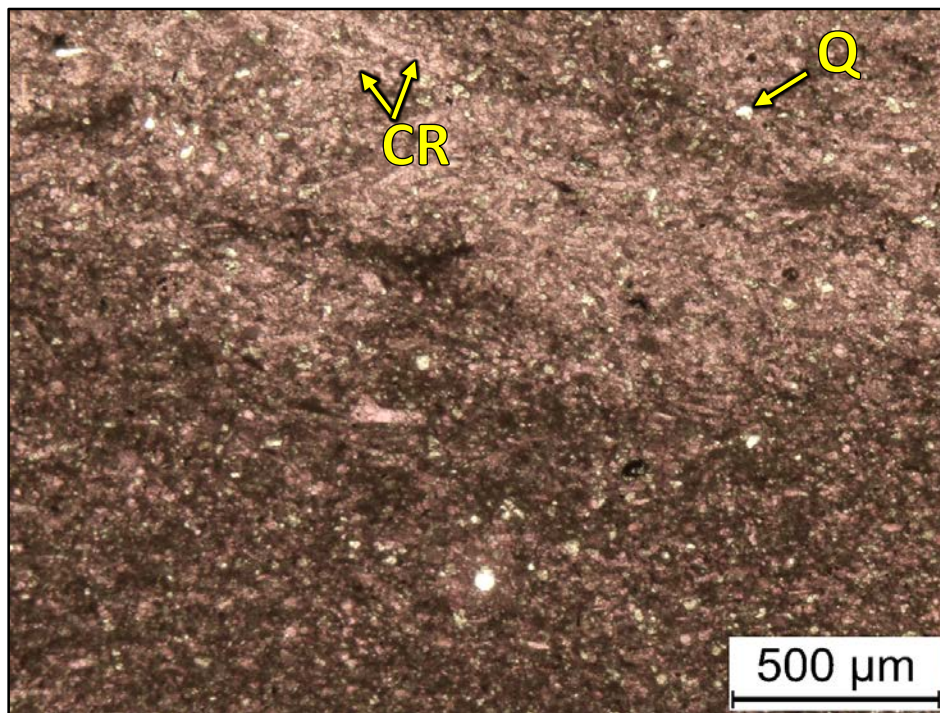
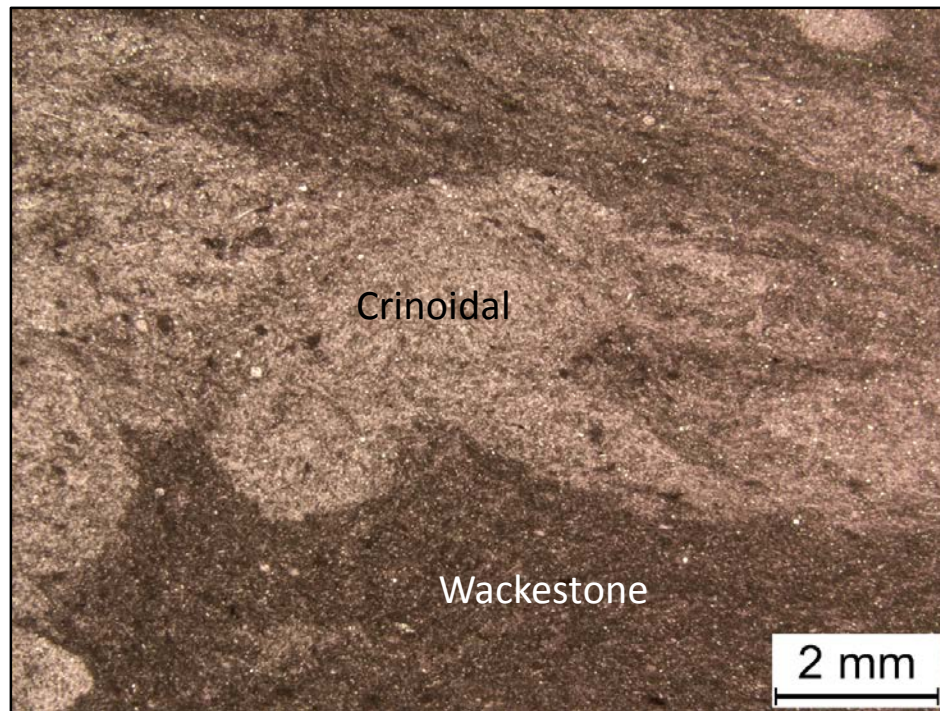
2WN – 5279.85' = Bioturbated wackestone. Sample is alizarin red stained. Porosity (NCS): 2.4%. Permeability (Klinkenberg): 0.039 mD. TOC: 0.85%. XRD: 12% clays (8% illite and 4% mixed layer illite/smectite), 36% carbonates (26% calcite and 10% dolomite), and 52% other minerals (45% quartz, 1% potassium feldspar, 4% plagioclase feldspar, and 2% pyrite). Sample contains silt-sized quartz grains (40%), crinoid fragments (10%), sponge spicule fragments (5%), and undifferentiated microbioclastic debris. Oil-filled moldic and vug porosity observed.



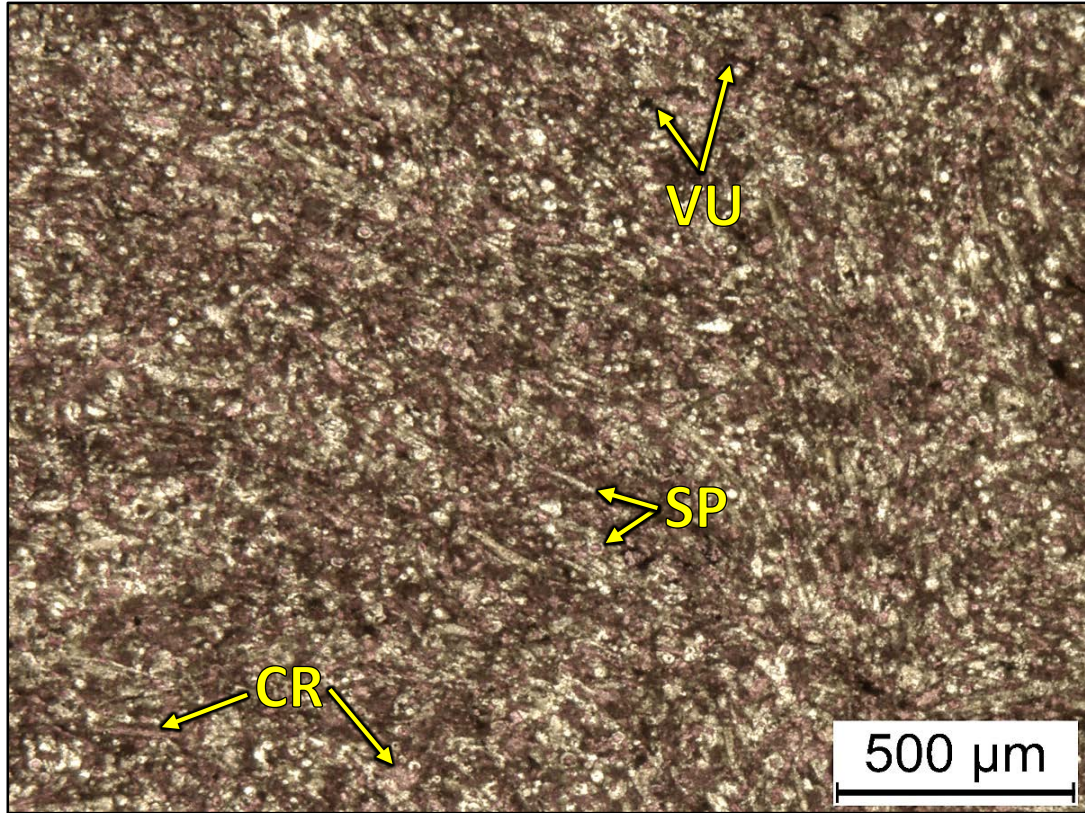
2WN – 5274.60' = Peloidal grainstone. Sample is alizarin red stained. Porosity (NCS): 0.7%. Permeability (Klinkenberg): <0.0001 mD. TOC: 0.05%. XRD: Trace amounts of clays, 83% carbonates (83% calcite), and 17% other minerals (13% quartz, trace amounts of potassium feldspar, 3% plagioclase feldspar, trace amounts of pyrite, and 1% apatite). Sample contains crinoid fragments (40%), peloids (25%), silt-sized quartz grains (13%), and sponge spicules (5%). Oil filled moldic porosity observed.



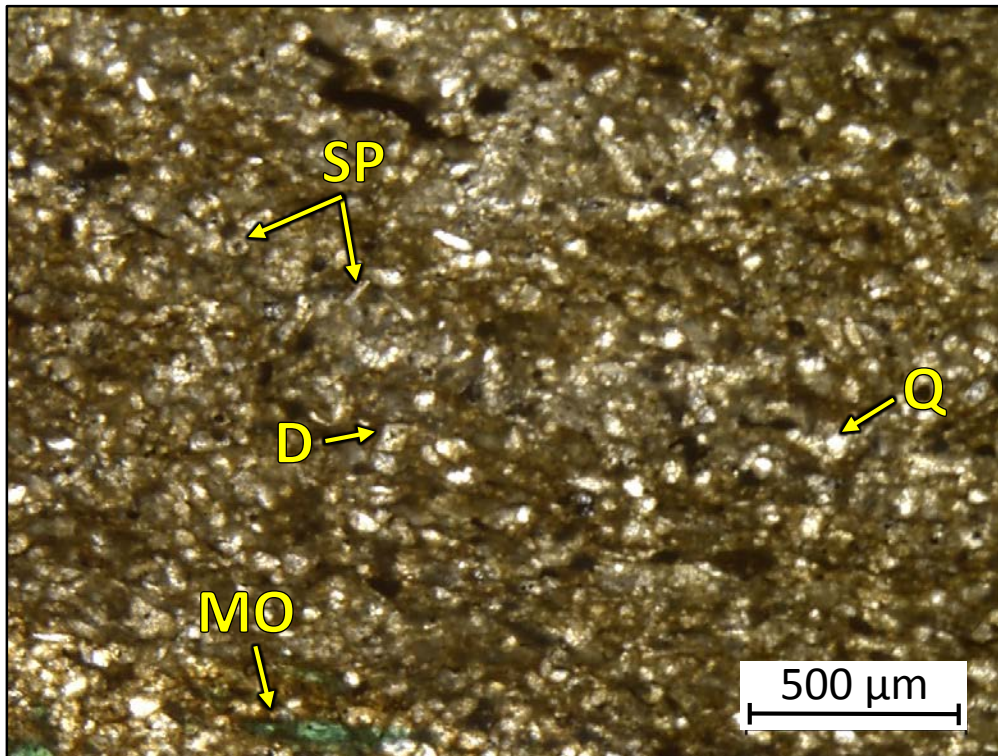
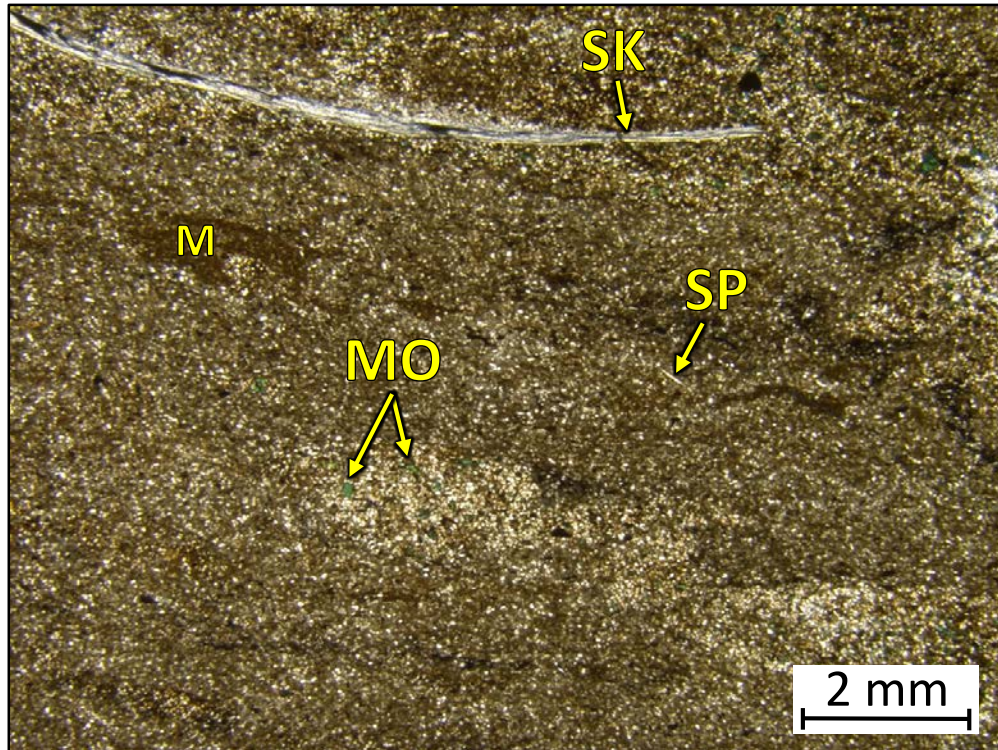
2WN – 5270.50' = Bioturbated wackestone. Porosity (visual estimation): 1.5%. Visual estimation: 10% clays, 40% carbonates, and 50% other minerals. Sample contains silt-sized quartz grains (30%), peloids (20%), sponge spicules (7%), and undifferentiated microbioclastic debris. Oil-filled vug and moldic porosity observed.



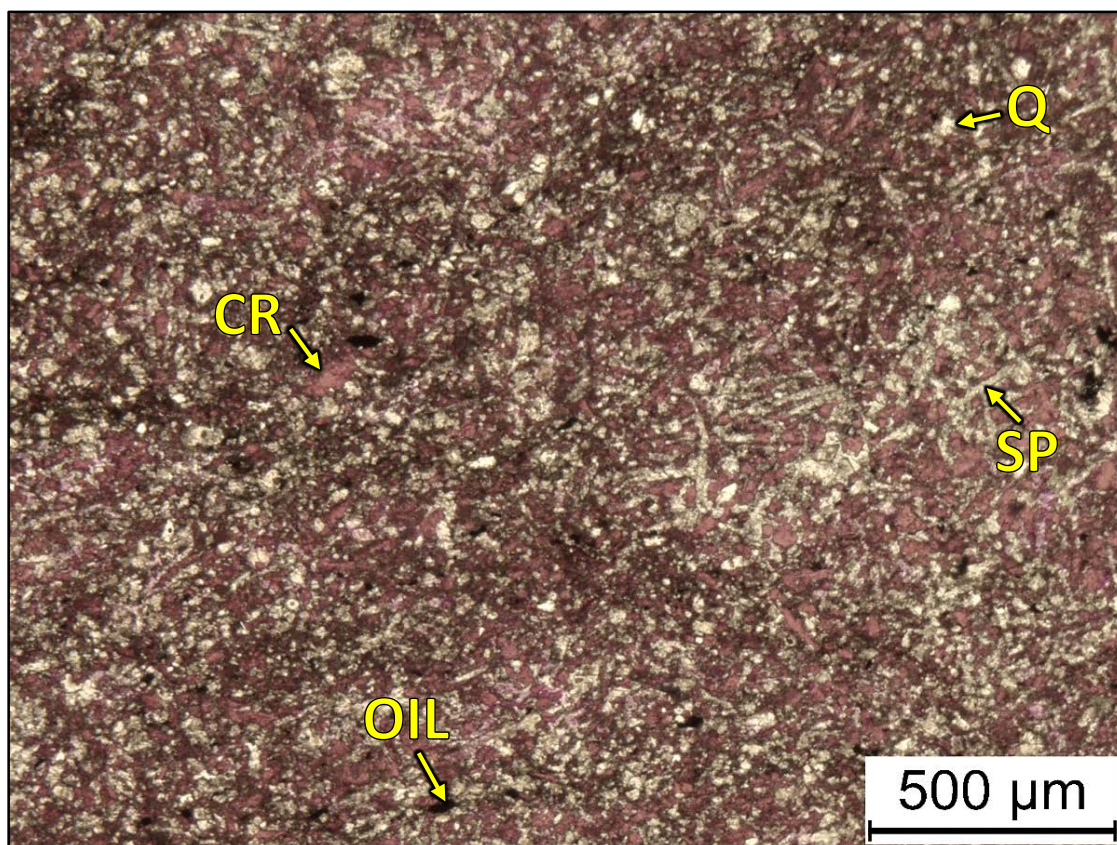
2WN – 5268.60' = Bioturbated wackestone to skeletal packstone. Sample is alizarin red stained. Porosity (NCS): 1.0%. Permeability (Klinkenberg): <0.0001 mD. TOC: 0.13%. XRD: 2% clays (2% illite), 77% carbonates (74% calcite and 3% dolomite), and 21% other minerals (17% quartz, 1% potassium feldspar, 3% plagioclase feldspar, and trace amounts of pyrite and apatite). Sample contains crinoid fragments and undifferentiated microbioclastic debris.



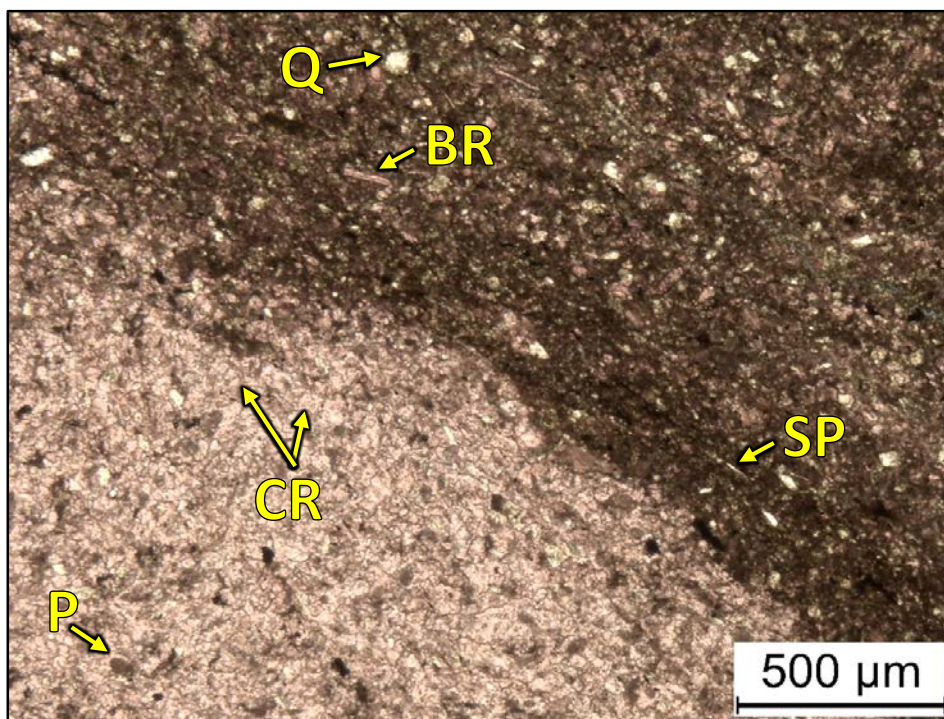
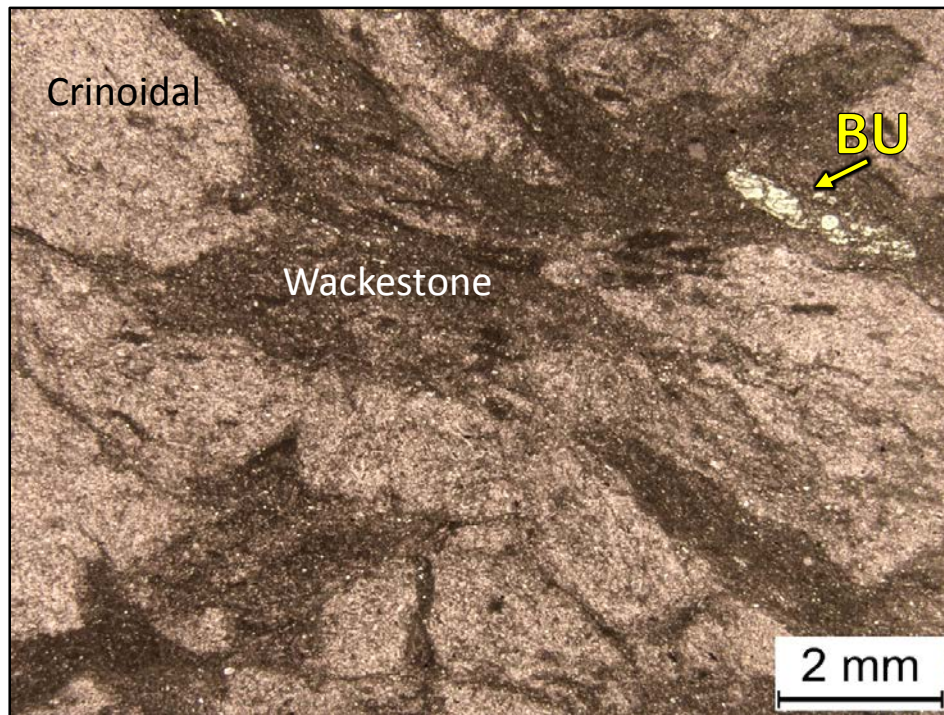
2WN – 5263.90' = Skeletal packstone. Sample is alizarin red stained. Porosity (NCS): 2.9%. Permeability (Klinkenberg): 0.0003 mD. TOC: 0.23%. XRD: 3% clays (2% illite and 1% mixed layer illite/smectite), 43% carbonates (39% calcite and 4% dolomite), and 54% other minerals (51% quartz, 1% potassium feldspar, 1% plagioclase feldspar, 1% pyrite, and trace amounts of apatite). Sample contains abundant sponge spicules (35%), silt-sized quartz grains (10%), crinoid fragments, and undifferentiated microbioclastic debris. Oil-filled vug porosity observed.



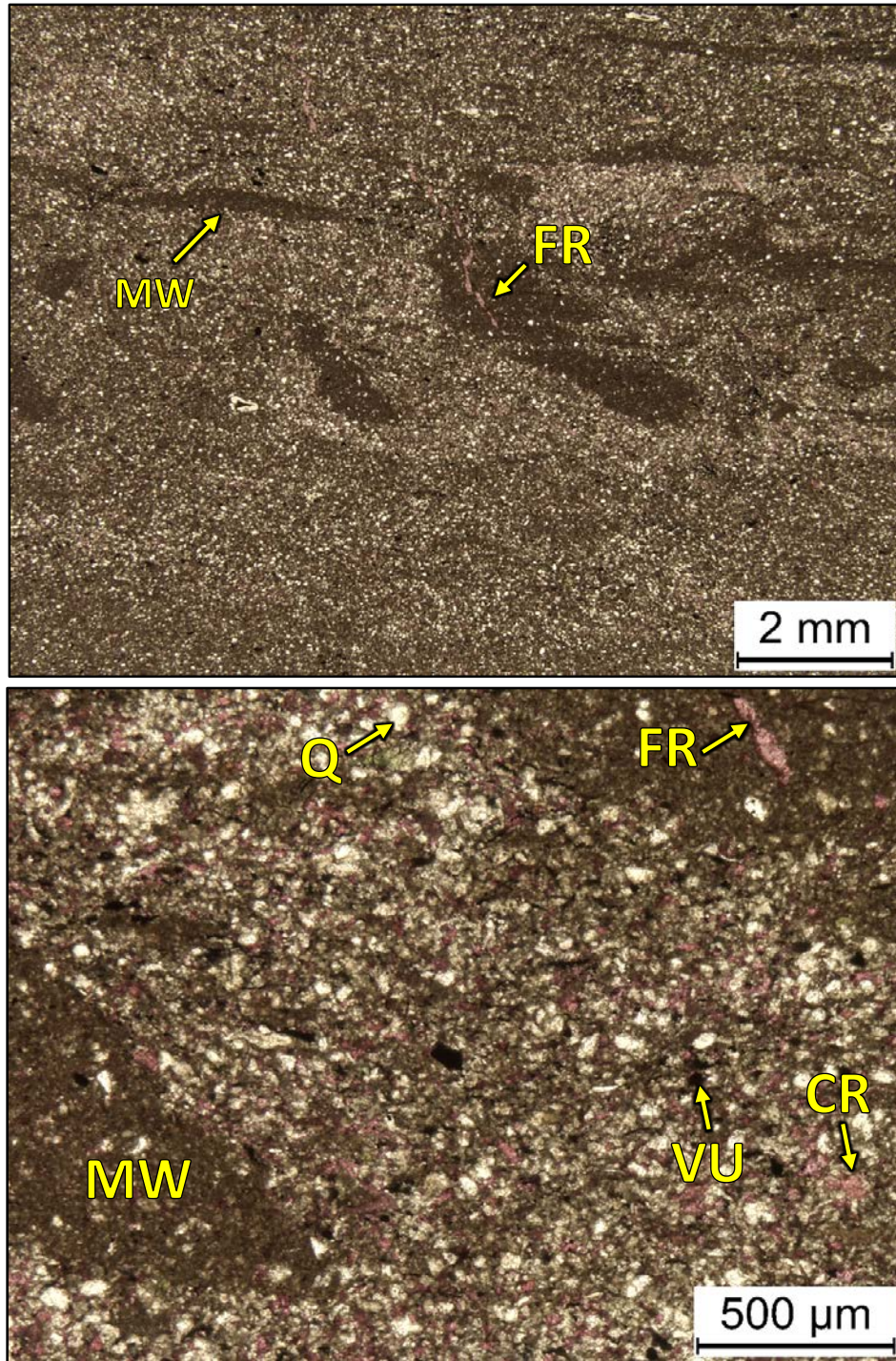
2WN – 5262.30' = Bioturbated wackestone. Sample is blue epoxy impregnated. Porosity (visual estimation): 2.0%. Visual estimation: 15% clays, 35% carbonates, and 50% other minerals. Sample contains silt-sized quartz grains (20%), sponge spicules (10%), and undifferentiated microbioclastic debris. Open and oil-filled moldic porosity observed.



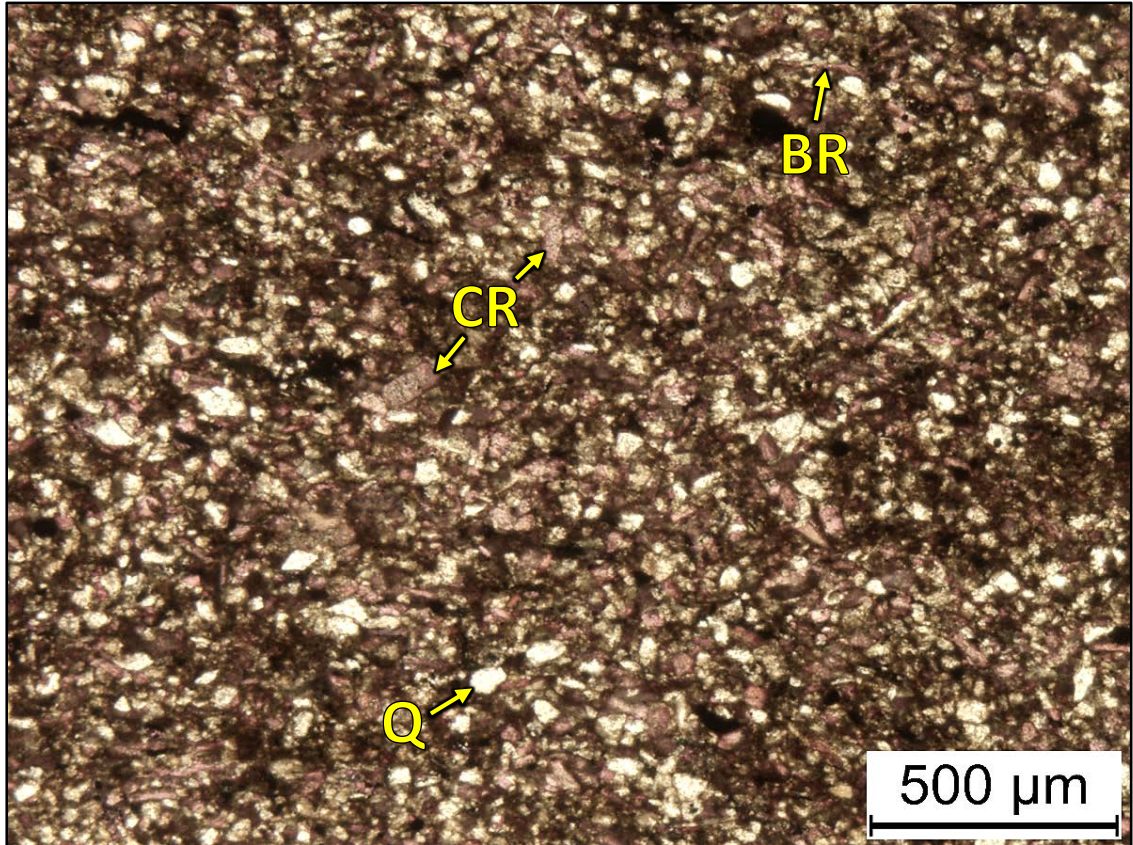
2WN – 5260.10' = Skeletal packstone-grainstone. Sample is alizarin red stained. Porosity (NCS): 5.4%. Permeability (Klinkenberg): 0.001 mD. TOC: 0.57%. XRD: 3% clays (2% illite and 1% mixed layer illite/smectite), 71% carbonates (61% calcite and 10% dolomite), and 26% other minerals (22% quartz, 1% potassium feldspar, 3% plagioclase feldspar, and trace amounts of pyrite and apatite). Sample contains abundant sponge spicules (20%), crinoid fragments (15%), silt-sized quartz grains (12%), and undifferentiated skeletal debris. Oil-filled moldic and vug porosity observed.



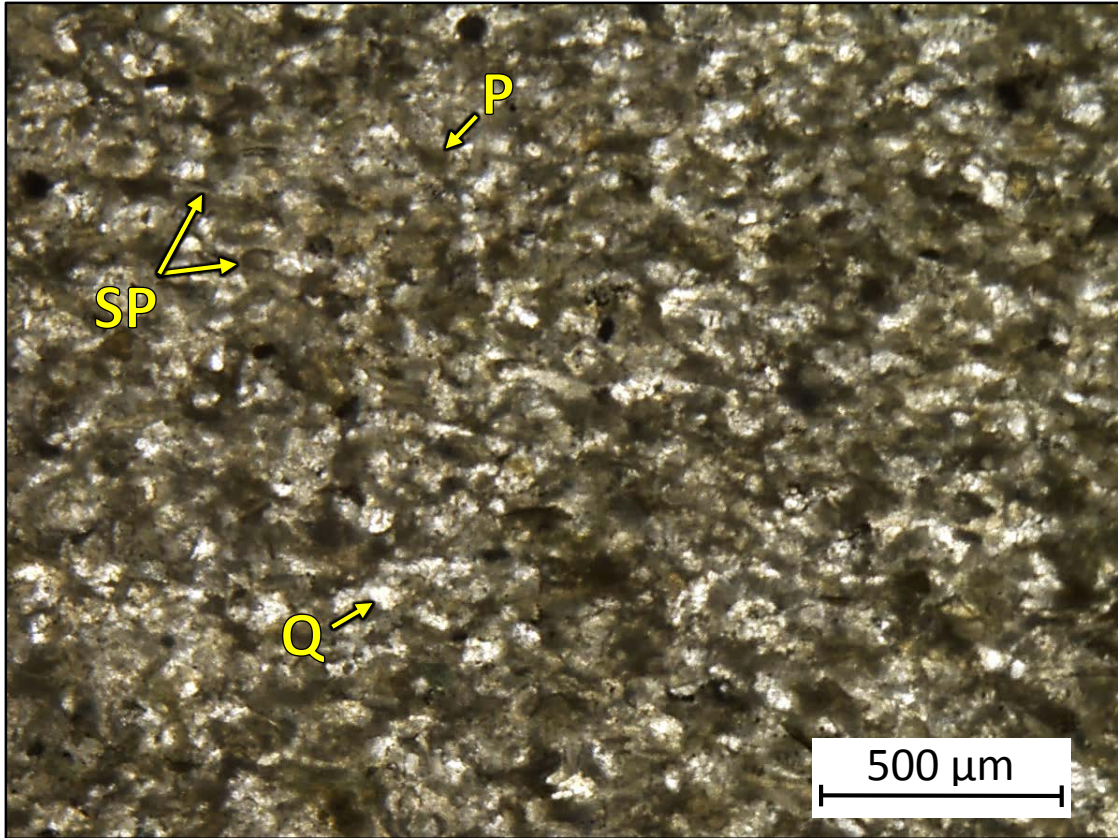
2WN – 5258.50' = Bioturbated wackestone to peloidal grainstone. Sample is alizarin red stained. Porosity (NCS): 2.2%. Permeability (Klinkenberg): 0.0004 mD. TOC: 0.15%. XRD: 1% clays (1% illite), 84% carbonates (80% calcite and 4% dolomite), and 15% other minerals (12% quartz, trace amounts of potassium feldspar, 3% plagioclase feldspar, and trace amounts of pyrite and apatite). Sample contains peloids (5%), silt-sized quartz grains (10%), brachiopod fragments (5%), and sponge spicules (2%). Oil-filled vug porosity observed.



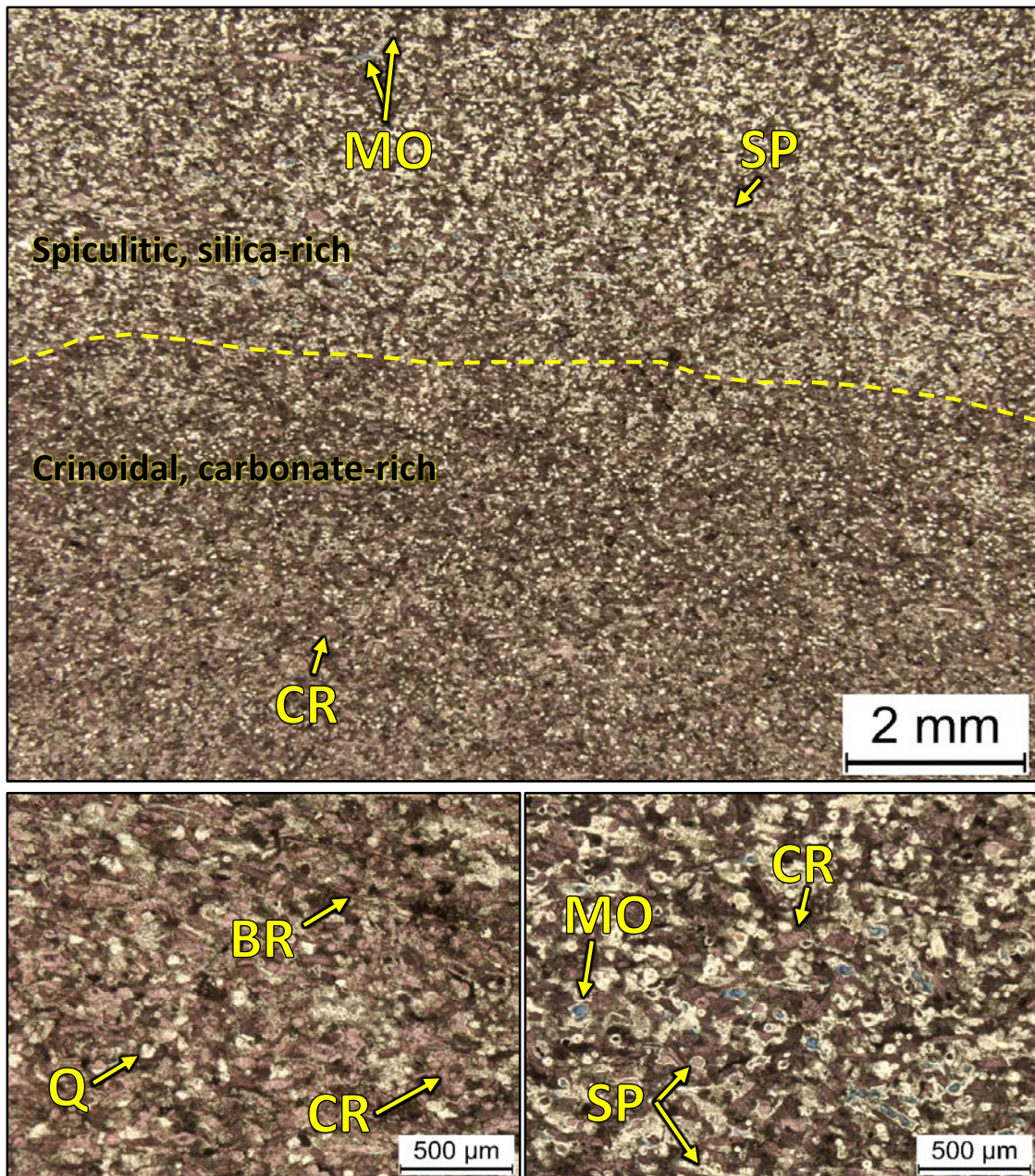
2WN – 5253.80-5254.00' = Bioturbated mudstone-wackestone. Sample is alizarin red stained. TOC: 0.39%. XRD: 17% clays (12% illite and 5% mixed layer illite/smectite), 30% carbonates (22% calcite and 8% dolomite), and 53% other minerals (43% quartz, 1% potassium feldspar, 5% plagioclase feldspar, 3% pyrite, and 1% marcasite). Sample contains silt-sized quartz grains (40%) and undifferentiated microbioclastic debris. Oil-filled moldic and vug porosity observed.



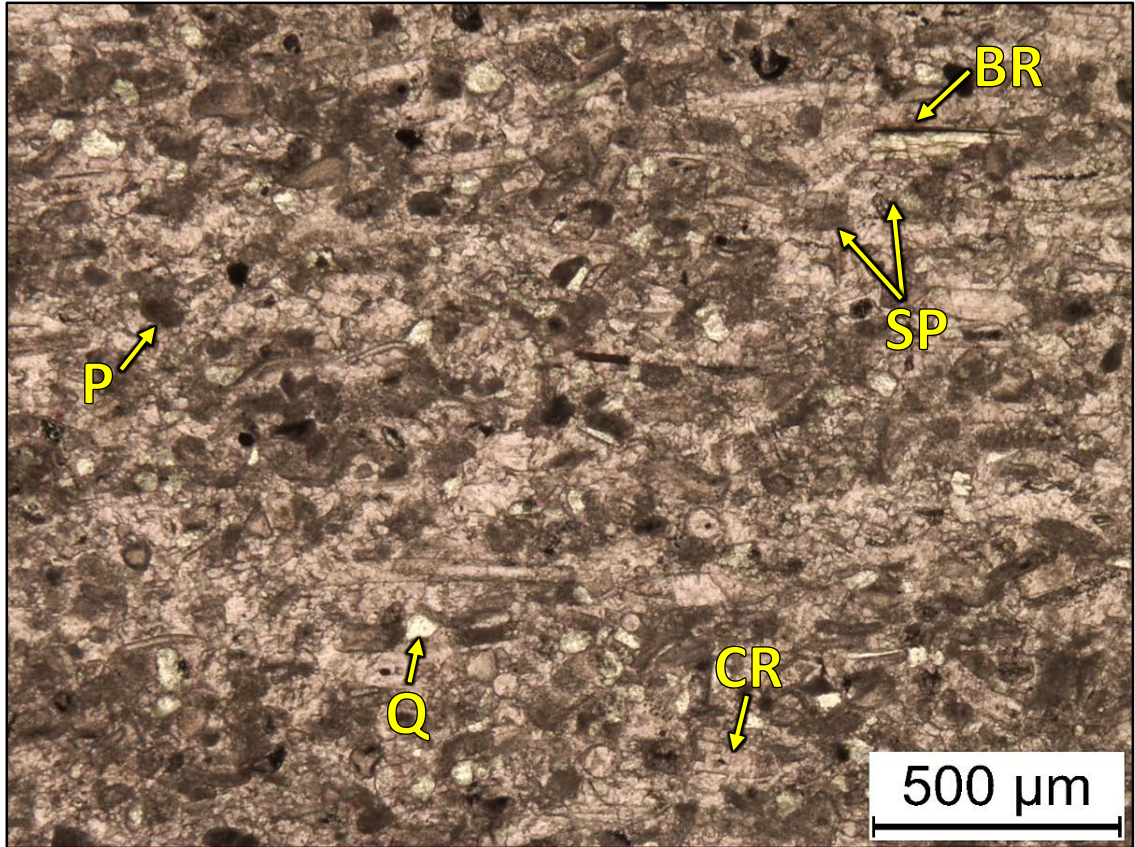
2WN – 5249.75' = Bioturbated wackestone. Sample is alizarin red stained. Porosity (NCS): 1.6%. Permeability (Klinkenberg): <0.0001 mD. TOC: 0.63%. XRD: 9% clays (1% chlorite, 5% illite, and 3% mixed layer illite/smectite), 32% carbonates (30% calcite and 2% dolomite), and 59% other minerals (20% quartz, 2% potassium feldspar, 5% plagioclase feldspar, 2% pyrite, and trace amounts of apatite). Sample contains silt-sized quartz grains (20%), crinoid fragments (15%), brachiopod fragments (5%), and undifferentiated microbioclastic debris. Oil-filled moldic and vug porosity observed.



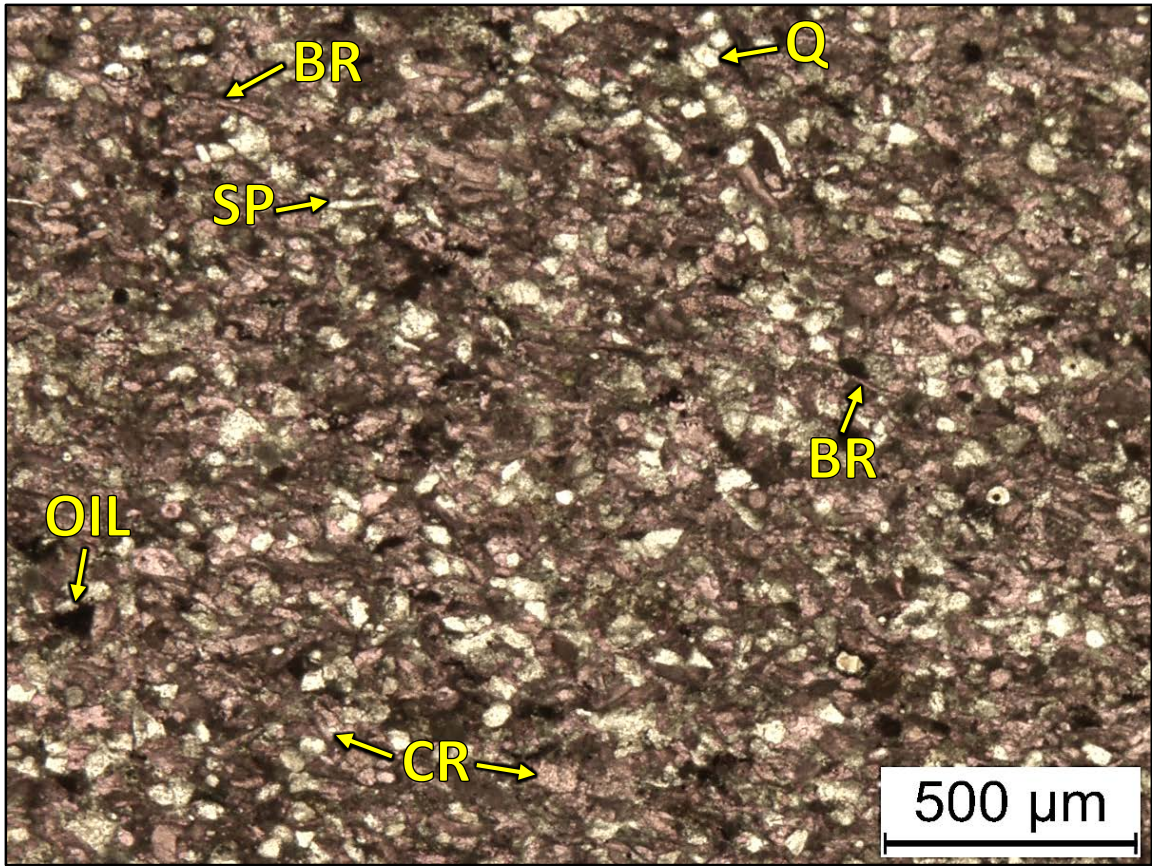
2WN – 5243.00' = Peloidal packstone. Sample is blue epoxy impregnated. Porosity (visual estimation): 1.0%. Visual estimation: 2% clays, 73% carbonates (70% calcite and 3% dolomite), and 25% other minerals. Sample contains peloids, silt-sized quartz grains, and sponge spicules. Oil-filled vug and intracrystalline porosity observed.



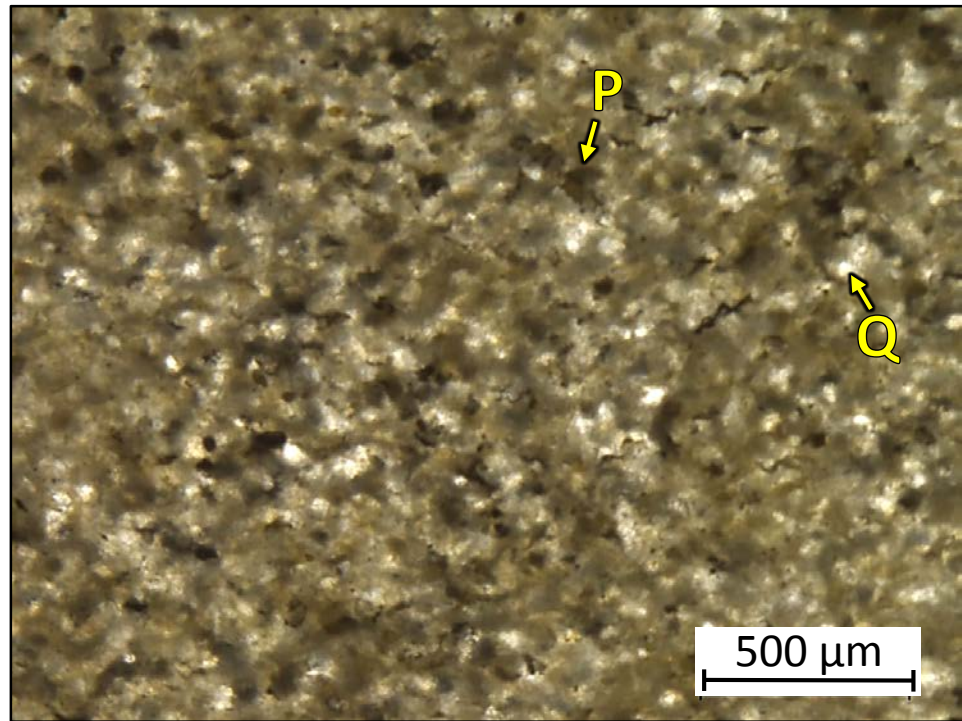
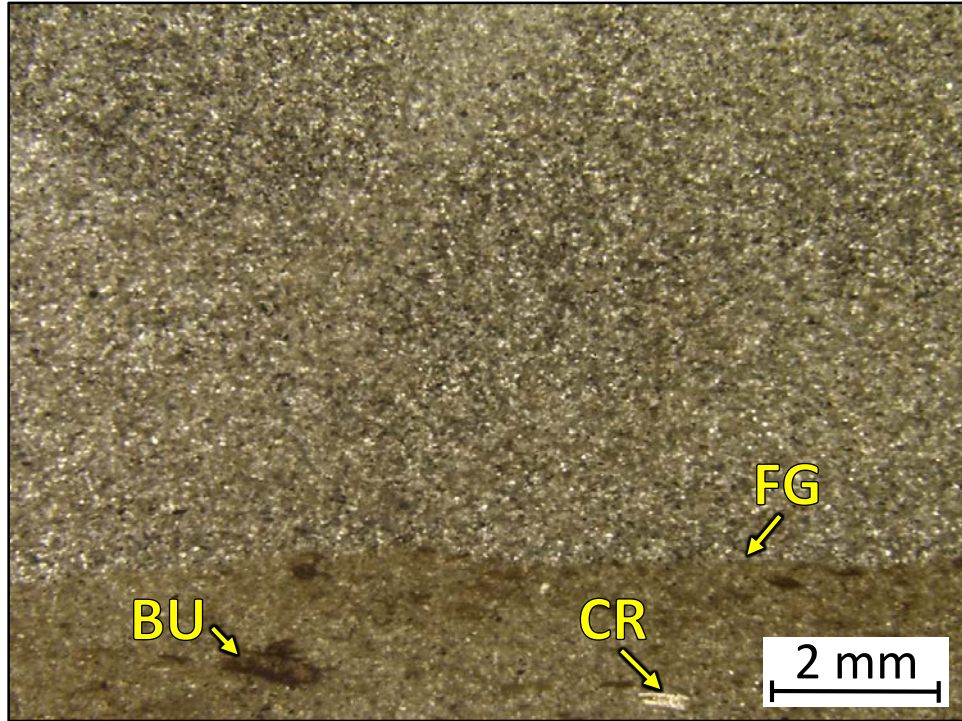
2WN – 5239.30' = Skeletal grainstone. Sample is alizarin red stained and blue epoxy impregnated. Porosity (NCS): 1.6%. Permeability (Klinkenberg): <0.0001 mD. TOC: 0.18%. XRD: 1% clays (1% illite), 45% carbonates (42% calcite and 3% dolomite), and 54% other minerals (50% quartz, 1% potassium feldspar, 1% plagioclase feldspar, 1% pyrite, and 1% apatite). Sample is characterized by varying mineralogies and varying amounts of crinoid (10-40%), spicule (10-40%), and brachiopod (1-5%) fragments depending on location.



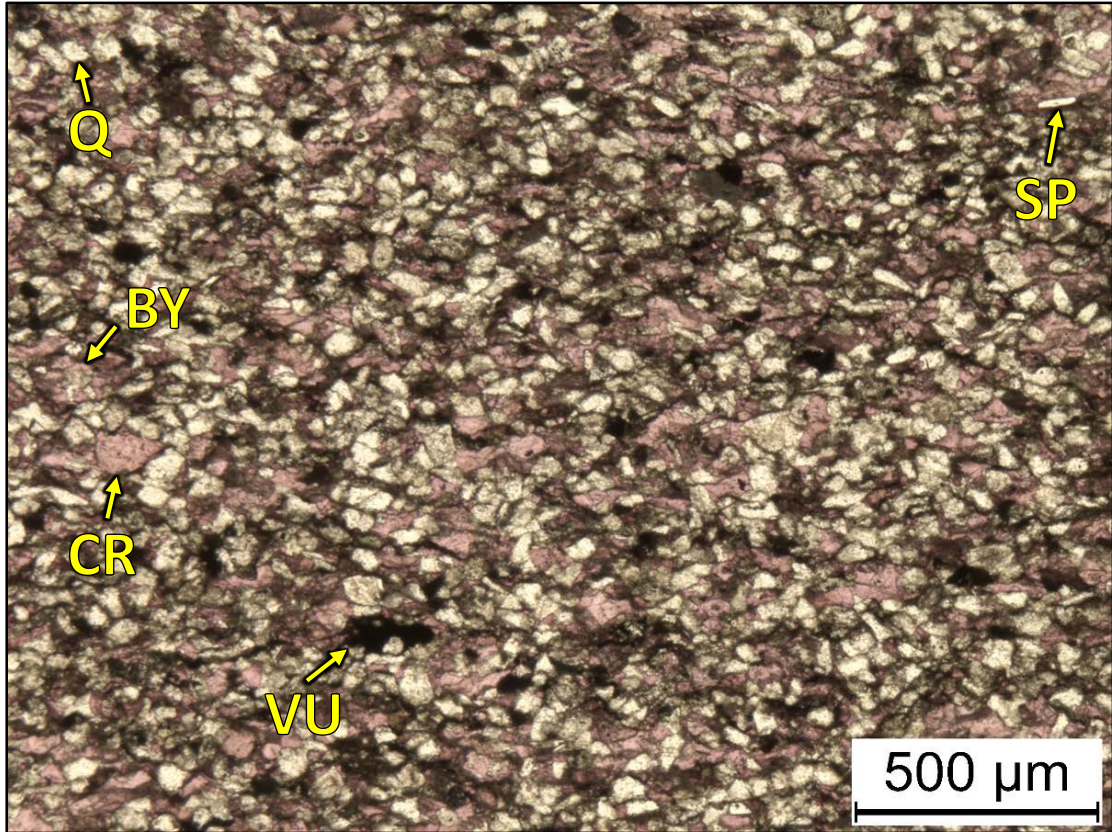
2WN – 5238.65' = Peloidal grainstone. Sample is alizarin red stained. Porosity (NCS): 0.8%. Permeability (Klinkenberg): <0.0001 mD. TOC: 0.05%. XRD: 1% clays (1% illite), 73% carbonates (73% calcite), and 26% other minerals (22% quartz, 1% potassium feldspar, 3% plagioclase feldspar, and trace amounts of pyrite and apatite). Sample contains peloids (20%), sponge spicules (20%), crinoid fragments (15%), silt-sized quartz fragments (10%), and brachiopod fragments (3%).



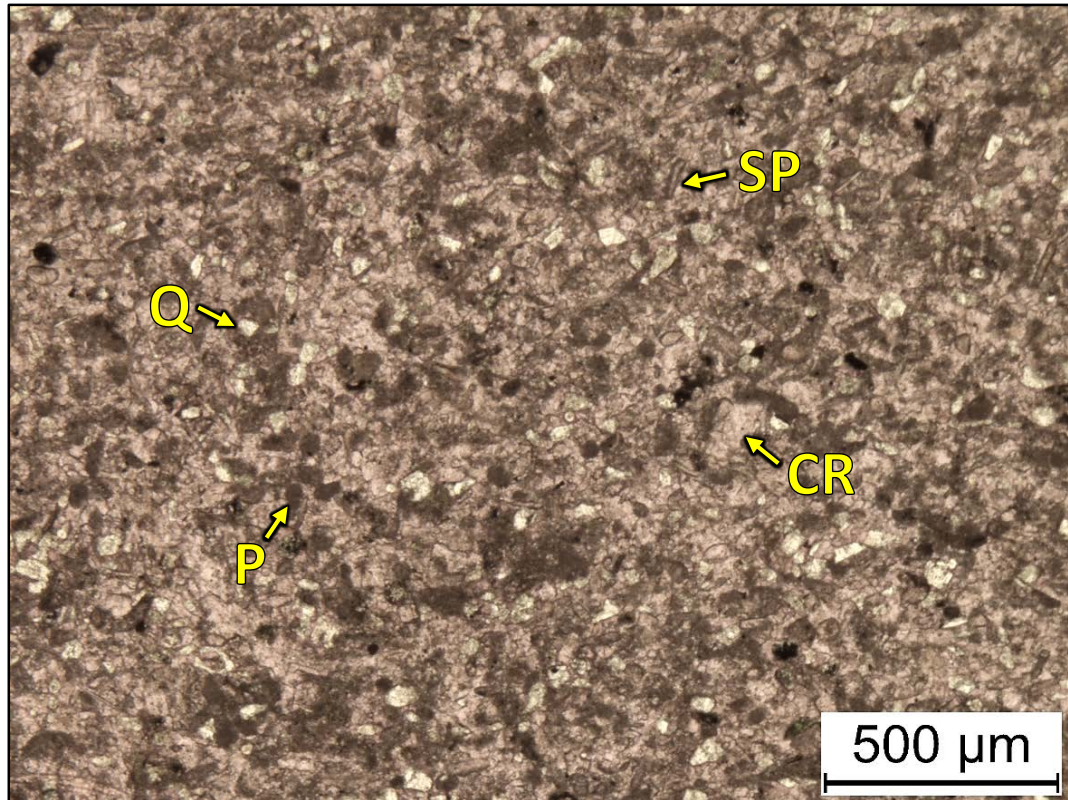
2WN – 5234.60' = Bioturbated wackestone-packstone. Sample is alizarin red stained. Porosity (NCS): 3.3%. Permeability (Klinkenberg): <0.0001 mD. TOC: 0.19%. XRD: 3% clays (2% illite and 1% mixed layer illite/smectite), 48% carbonates (46% calcite and 2% dolomite), and 49% other minerals (43% quartz, 1% potassium feldspar, 3% plagioclase feldspar, 1% pyrite, and 1% apatite). Sample contains silt-sized quartz grains (25%), crinoid fragments (20%), brachiopod fragments (5%), sponge spicule fragments, and undifferentiated microbioclastic debris. Oil-filled moldic and vug porosity observed.



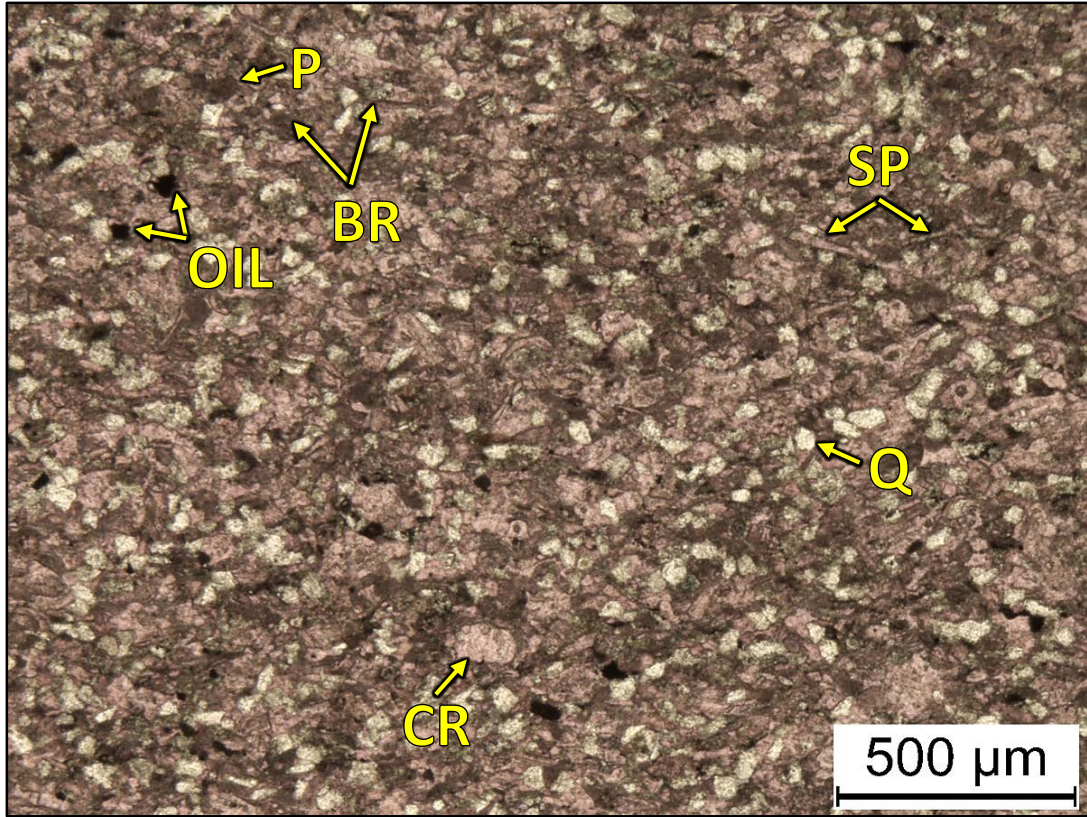
2WN – 5233.90' = Peloidal grainstone. Sample is blue epoxy impregnated. Porosity (visual estimation): 0.5%. Visual estimation: Trace amounts of clays, 85% carbonates, and 15% other minerals. Sample contains peloids (30%), silt-sized quartz grains (15%), and undifferentiated microbioclastic debris.



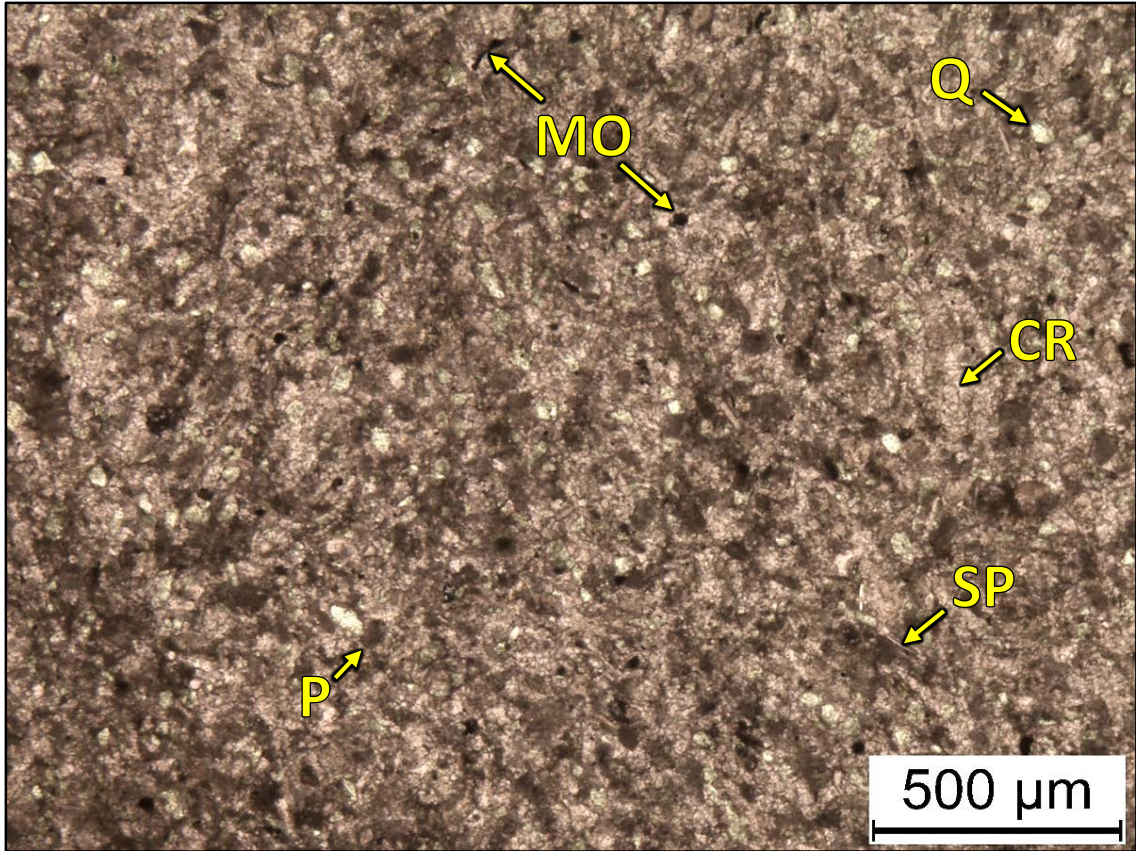
2WN – 5232.90' = Crinoidal packstone. Sample is alizarin red stained. Porosity (NCS): 2.6%. Permeability (Klinkenberg): <0.0001 mD. TOC: 0.18%. XRD: 3% clays (2% illite and 1% mixed layer illite/smectite), 38% carbonates (35% calcite and 3% dolomite), and 59% other minerals (51% quartz, 2% potassium feldspar, 4% plagioclase feldspar, 1% pyrite, and 1% apatite). Sample contains silt-sized quartz grains (40%), crinoid fragments (25%), sponge spicule fragments (10%), and bryozoans (3%). Oil-filled vug porosity observed.



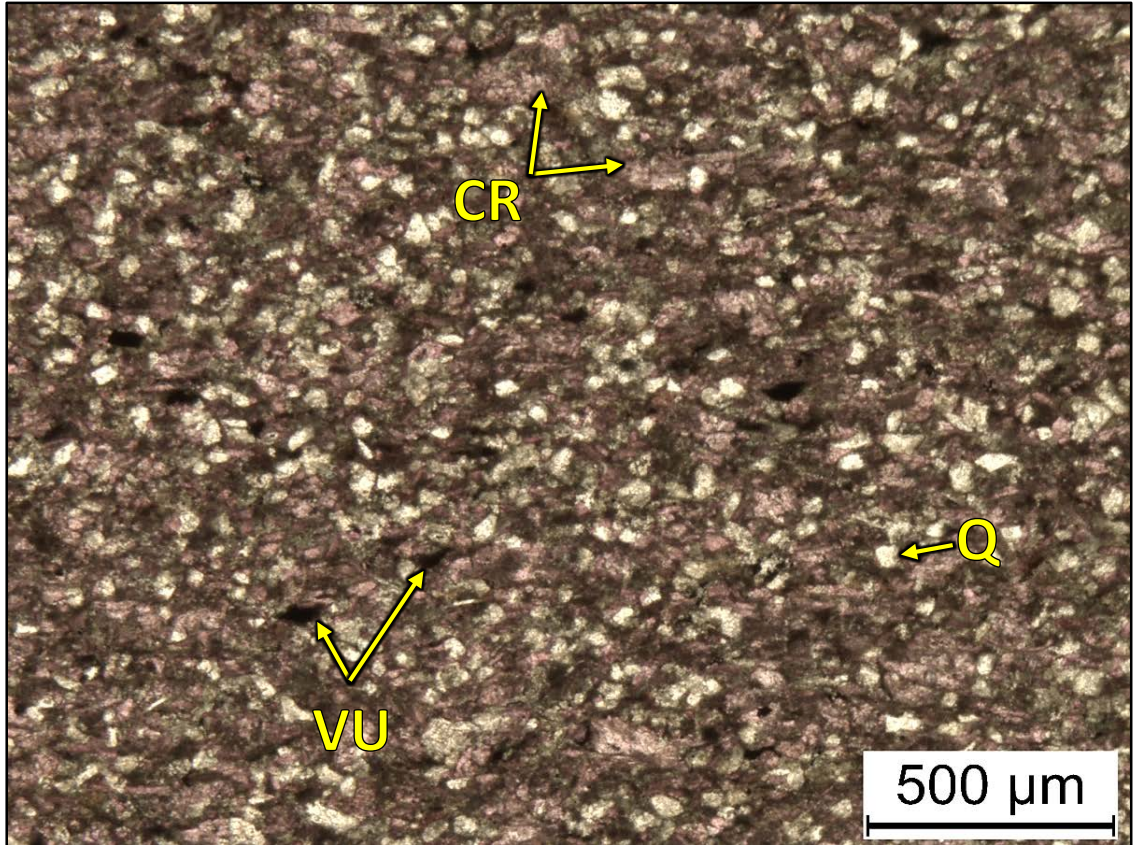
2WN – 5229.75' = Peloidal grainstone. Sample is alizarin red stained. Porosity (NCS): 0.9%. Permeability (Klinkenberg): <0.0001 mD. TOC: 0.03%. XRD: 1% clays (1% illite), 79% carbonates (77% calcite and 2% dolomite), and 20% other minerals (17% quartz, 1% potassium feldspar, 2% plagioclase feldspar, and trace amounts of pyrite and apatite). Sample contains peloids (30%), crinoid fragments (30%), sponge spicules (15%), and silt-sized quartz grains (15%). Minor amounts of oil-filled vug porosity observed.



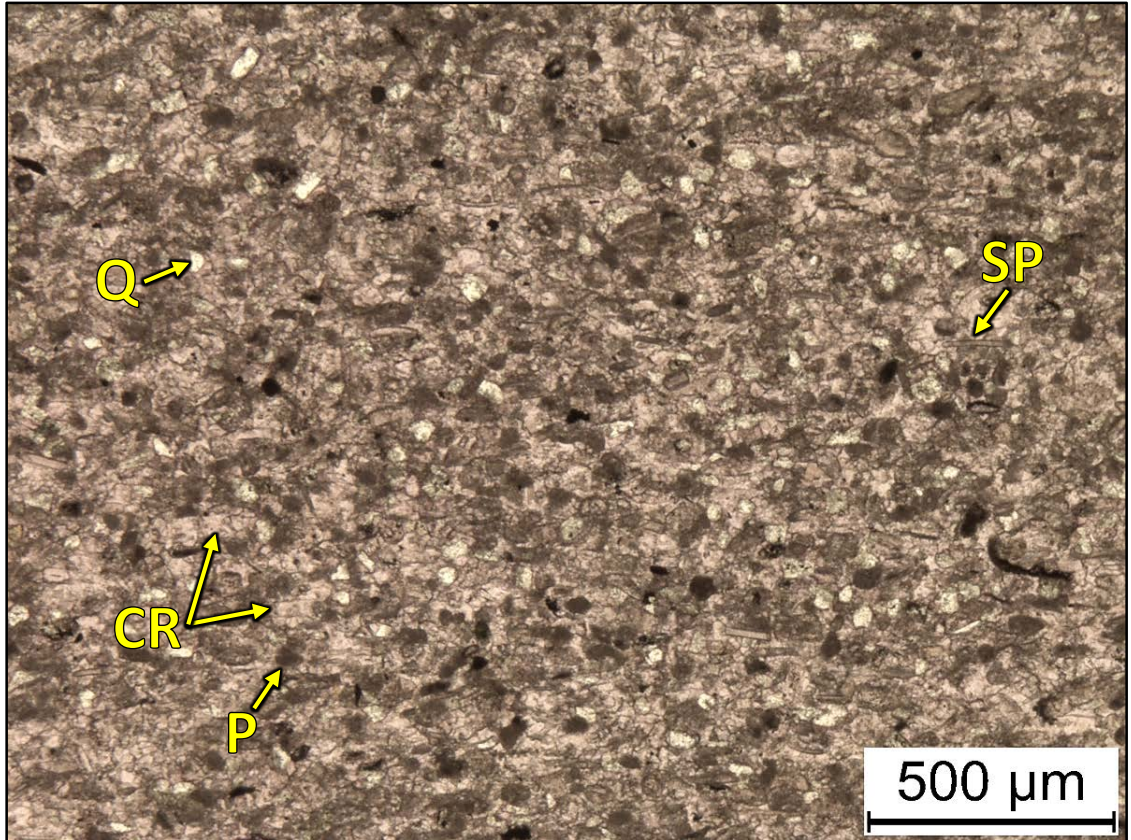
2WN – 5229.35' = Crinoidal grainstone. Sample is alizarin red stained. Porosity (NCS): 2.2%. Permeability (Klinkenberg): <0.0001 mD. TOC: 0.13%. XRD: 2% clays (2% illite), 55% carbonates (52% calcite and 3% dolomite), and 43% other minerals (40% quartz, 1% potassium feldspar, 2% plagioclase feldspar, and trace amounts of pyrite and apatite). Sample contains silt-sized quartz grains (40%), crinoid fragments (20%), peloids (20%), spicule fragments (15%), and brachiopod fragments (5%). Oil-filled moldic and vug porosity observed.



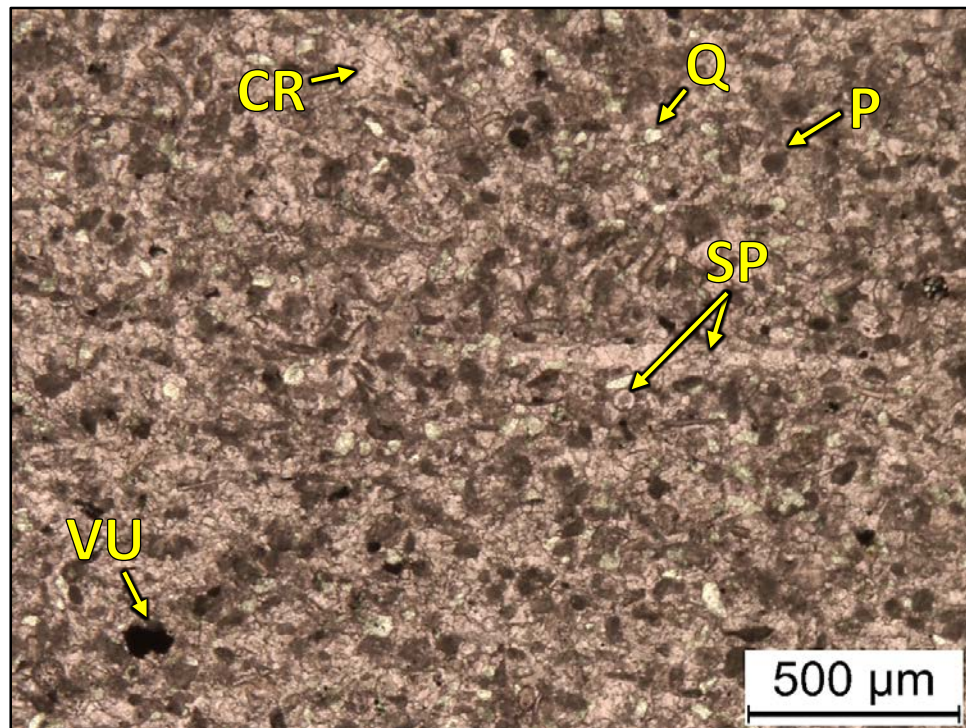
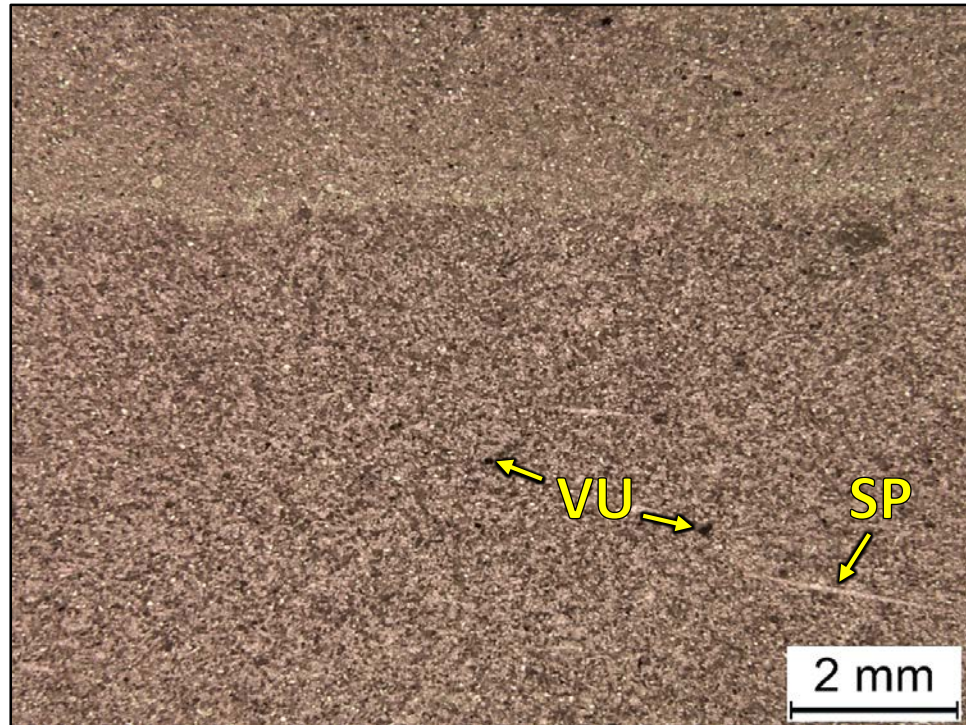
2WN – 5225.50' = Peloidal grainstone. Sample is alizarin red stained. Porosity (ambient): 1.7%. Permeability (Klinkenberg): Sample was unsuitable for this type of measurement. TOC: 0.07%. XRD: 1% clays (1% illite), 78% carbonates (76% calcite and 2% dolomite), and 21% other minerals (17% quartz, 1% potassium feldspar, 3% plagioclase feldspar, and trace amounts of pyrite and apatite). Sample contains crinoid fragments (40%), peloids (15%), sponge spicule fragments (10%), silt-sized quartz grains (15%), and undifferentiated microbioclastic debris. Oil-filled moldic porosity observed.



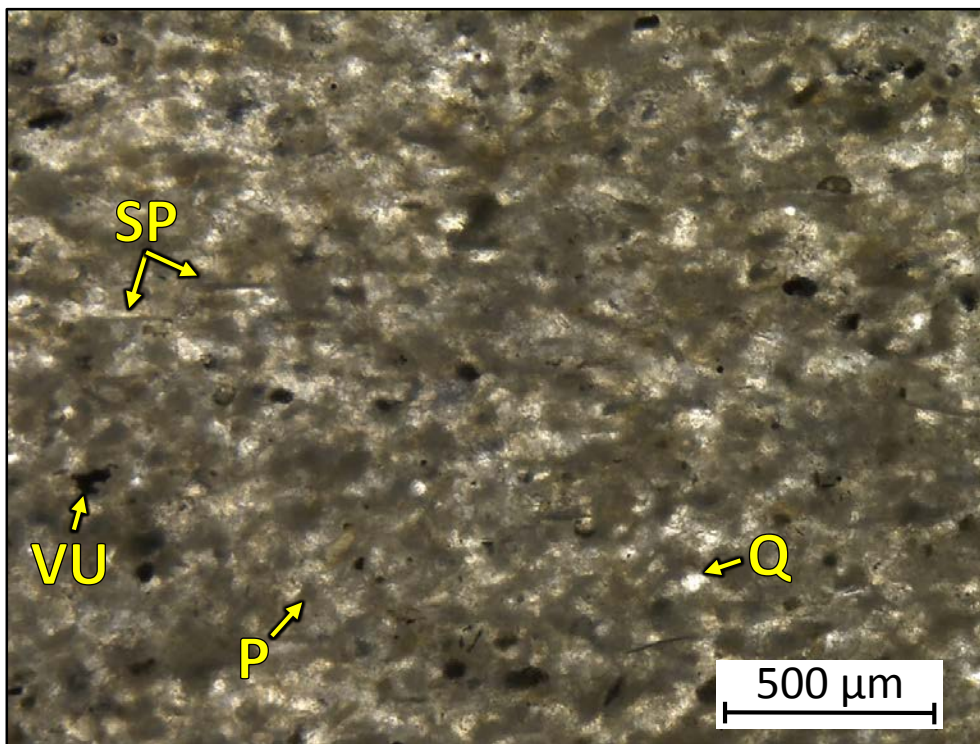
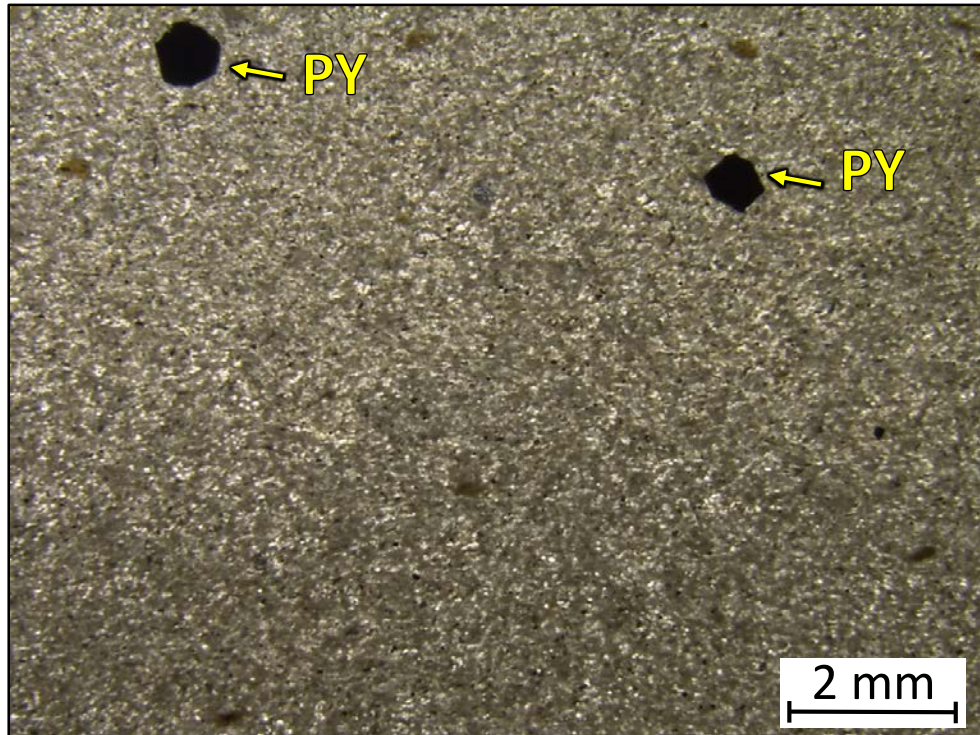
2WN – 5222.85' = Bioturbated crinoidal packstone. Sample is alizarin red stained. Porosity (NCS): 2.6%. Permeability (Klinkenberg): 0.0005 mD. TOC: 0.11%. XRD: 2% clays (2% illite), 40% carbonates (37% calcite and 3% dolomite), and 58% other minerals (53% quartz, 1% potassium feldspar, 3% plagioclase feldspar, and 1% pyrite). Sample contains silt-sized quartz grains (50%) and crinoidal debris (30%). Oil-filled moldic and vug porosity observed.



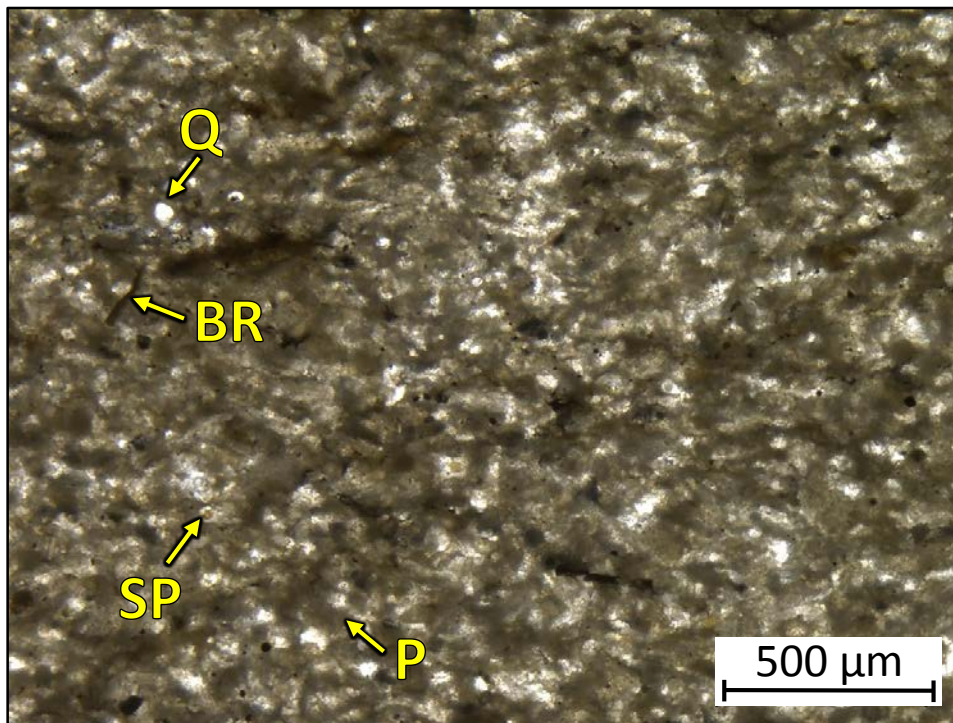
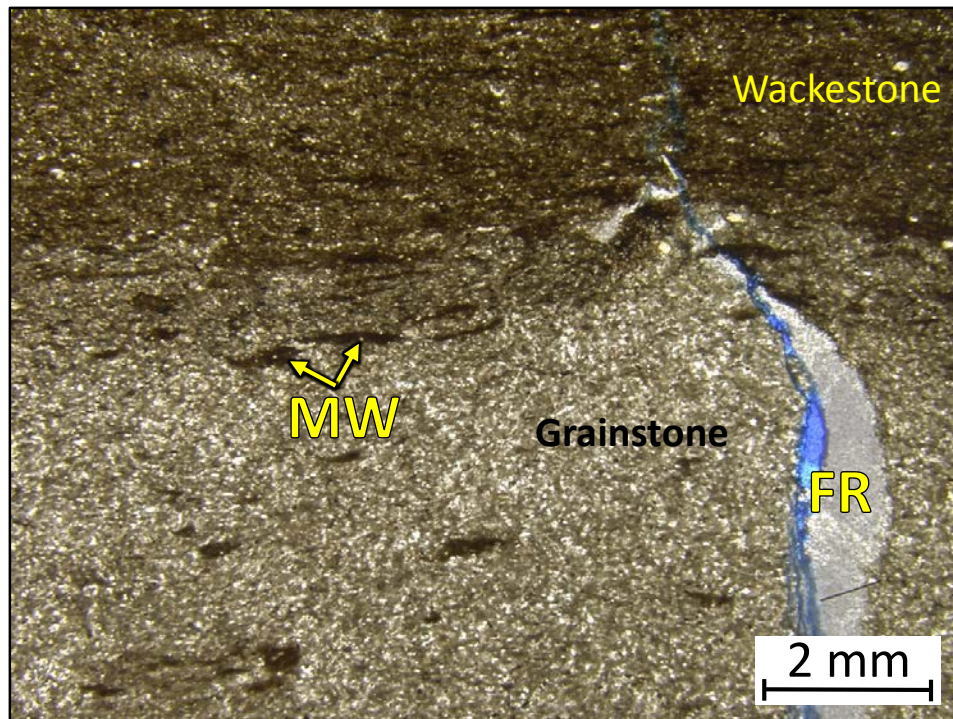
2WN – 5219.75' = Peloidal grainstone. Sample is alizarin red stained. Porosity (NCS): 0.7%. Permeability (Klinkenberg): <0.0001 mD. TOC: 0.07%. XRD: 1% clays (1% illite), 75% carbonates (74% calcite and 1% dolomite), and 24% other minerals (21% quartz, 1% potassium feldspar, 2% plagioclase feldspar, and trace amounts of pyrite and apatite). Sample contains crinoidal debris (40%), peloids (30%), silt-sized quartz grains (20%), and sponge spicules (15%).



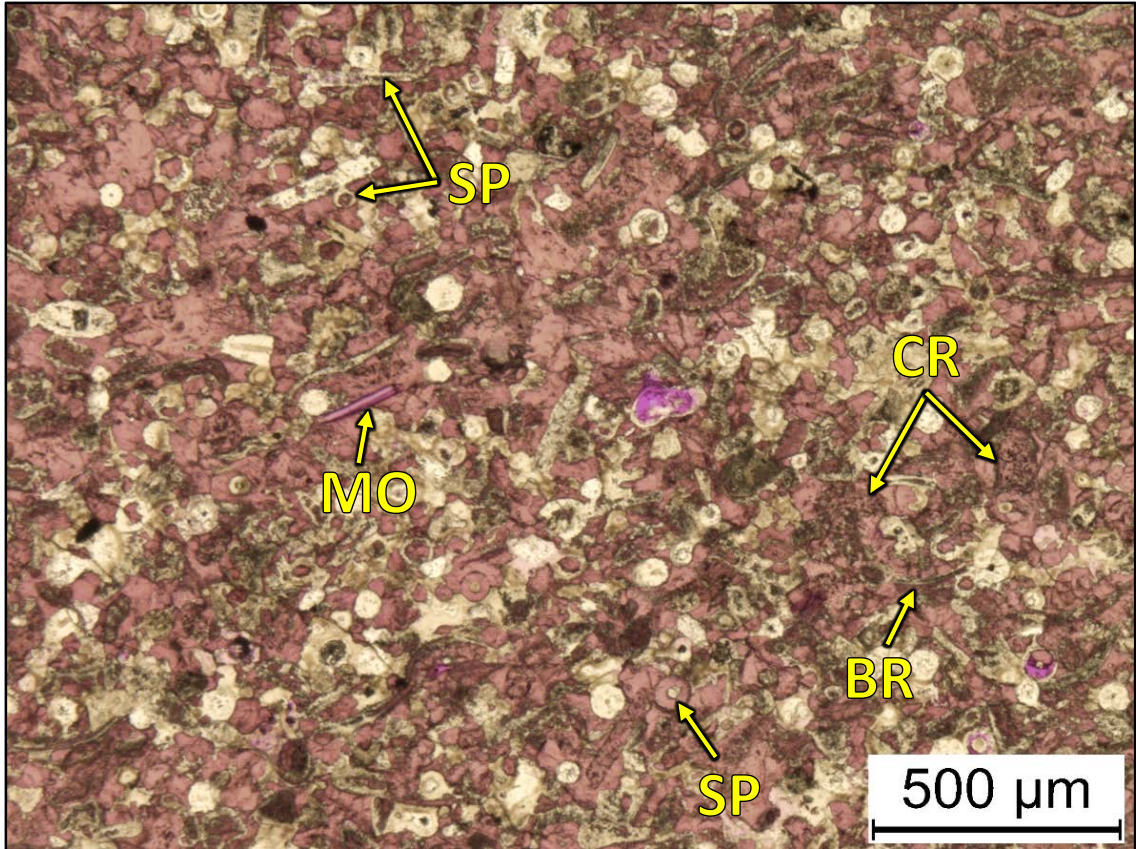
2WN – 5212.55-5215.75' = Peloidal grainstone. Sample is alizarin red stained. Porosity (visual estimations): 0.5%. TOC: 0.09%. XRD: Trace amounts of clays, 74% carbonates (63% calcite and 1% dolomite), and 26% other minerals (22% quartz, 1% potassium feldspar, 3% plagioclase feldspar, and trace amounts of pyrite and apatite). Sample contains peloids (20%), crinoidal debris (30%), silt-sized quartz grains (22%), sponge spicules (10%), and undifferentiated microbioclastic debris. Minor amounts of oil-filled vug porosity observed.



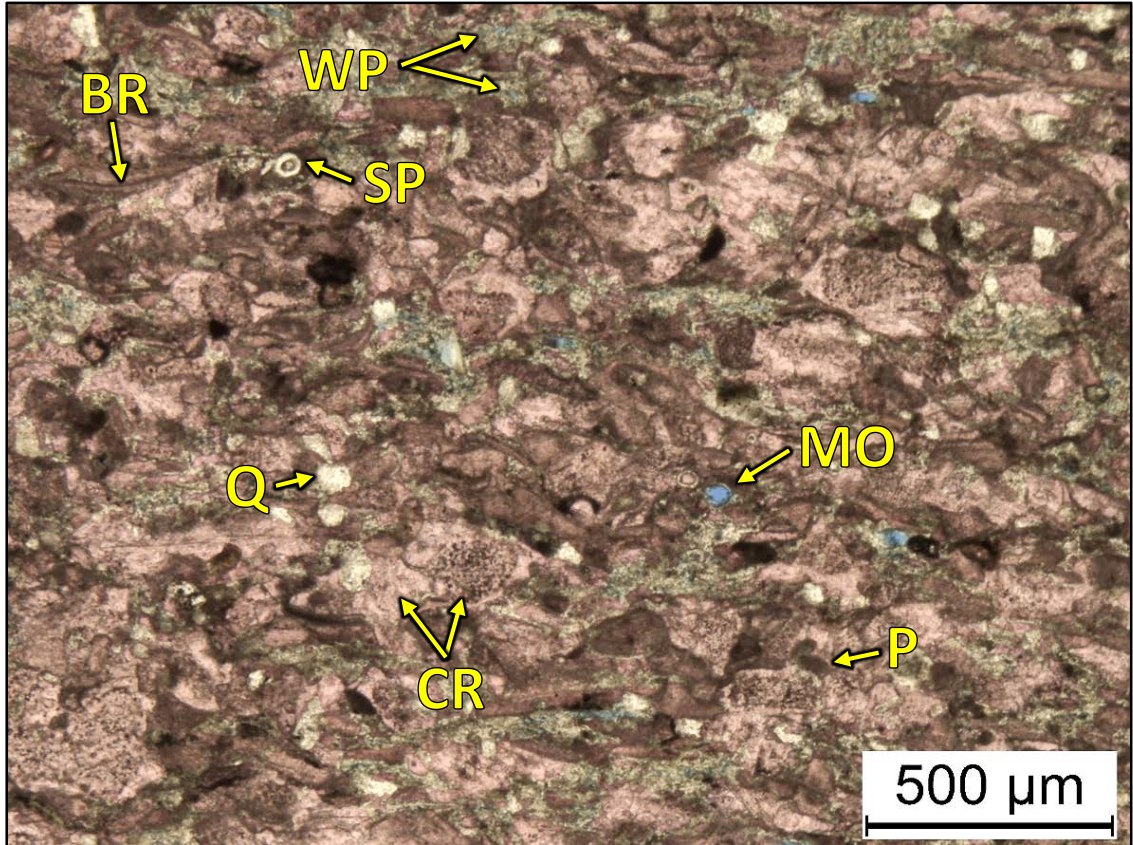
2WN – 5207.50' = Peloidal-skeletal grainstone. Sample is blue epoxy impregnated. Porosity (visual estimation): 1.5%. Visual estimation: 2% clays, 70% carbonates, 28% other minerals. Sample contains peloids (15%), sponge spicules (10%), very coarse sand-sized pyrite grains (2%), and undifferentiated microbioclastic debris. Minor amounts of oil-filled vug porosity is observed.



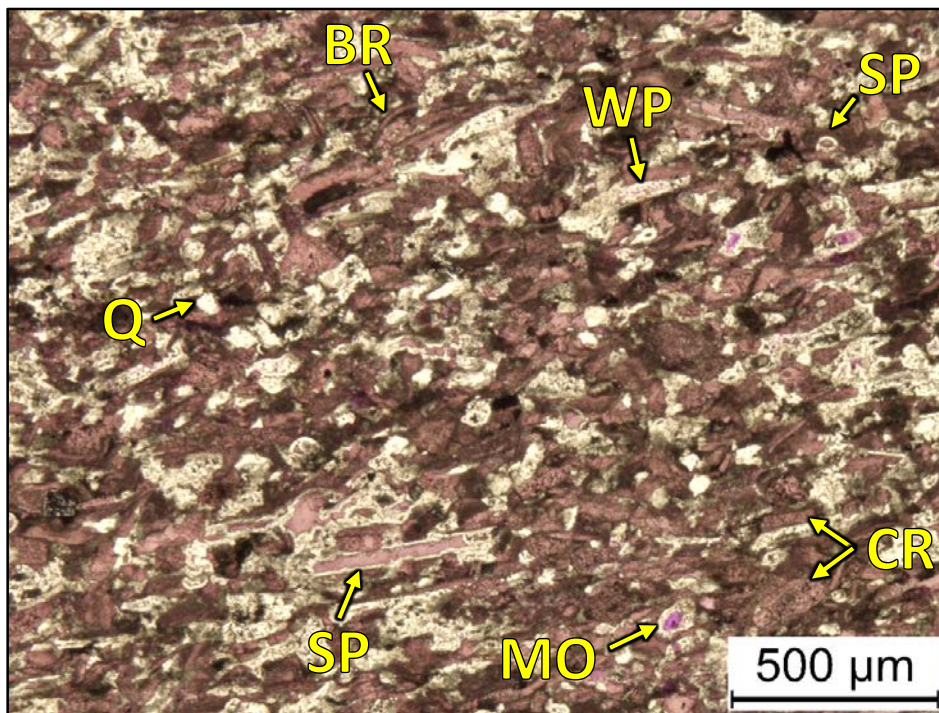
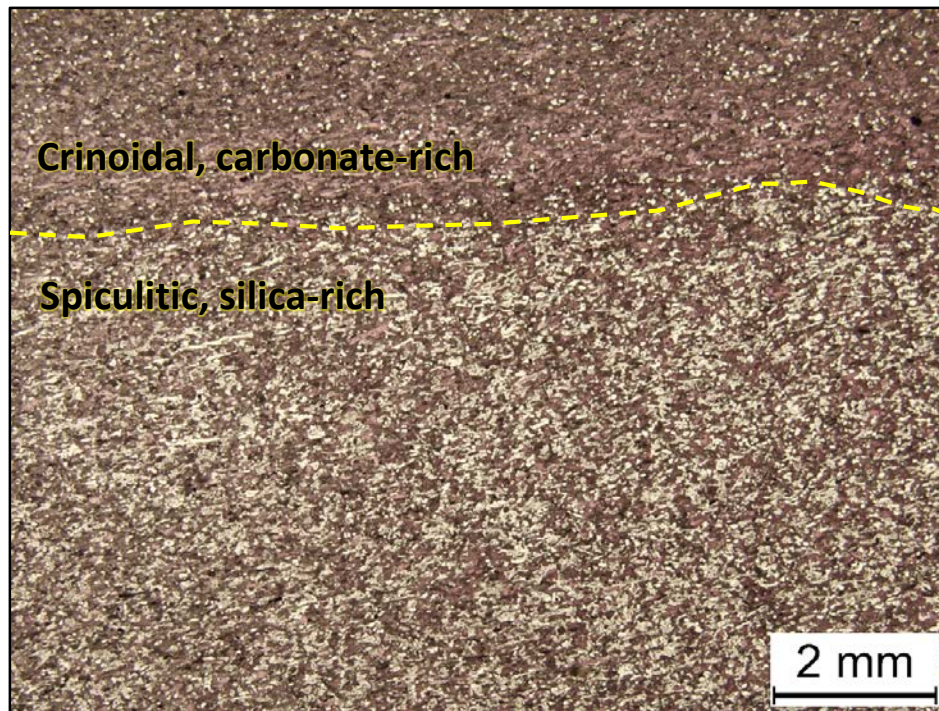
2WN – 5205.30' = Peloidal-skeletal grainstone. Sample is blue epoxy impregnated. Porosity (visual estimation): 0.5%. Visual estimation: 5% clays, 60% carbonates, 35% other minerals. Sample contains silt-sized quartz grains (10%), sponge spicules (10%), peloids (5%), brachiopod fragments (3%), and undifferentiated microbioclastic debris. Fracture in sample shows good porosity and permeability and terminates into mud-rich, bioturbated interval.



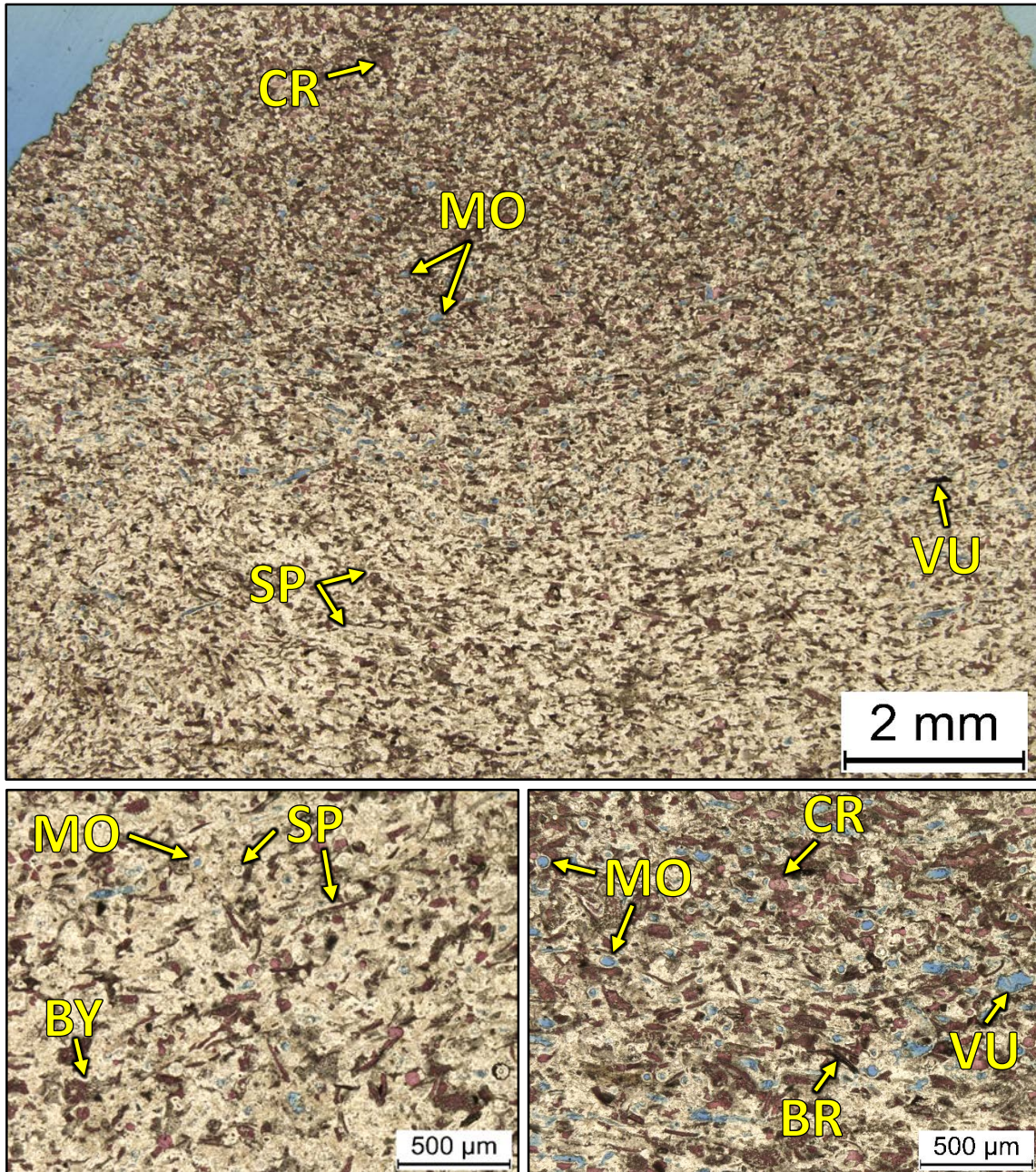
2WN – 5199.80' = Skeletal grainstone. Sample is alizarin red stained and porosity is shown in bright fuchsia. Porosity (NCS): 1.7%. Permeability (Klinkenberg): 0.0001 mD. TOC: 0.03%. XRD: 1% clays (1% illite), 51% carbonates (51% calcite), and 48% other minerals (47% quartz, 1% potassium feldspar, and trace amounts plagioclase feldspar, pyrite, and apatite). Sample contains abundant sponge spicules (40%), crinoid fragments (15%), and brachiopod fragments (5%). Some sponge spicules have been replaced with calcite. Moldic porosity from the dissolution of skeletal grains observed.



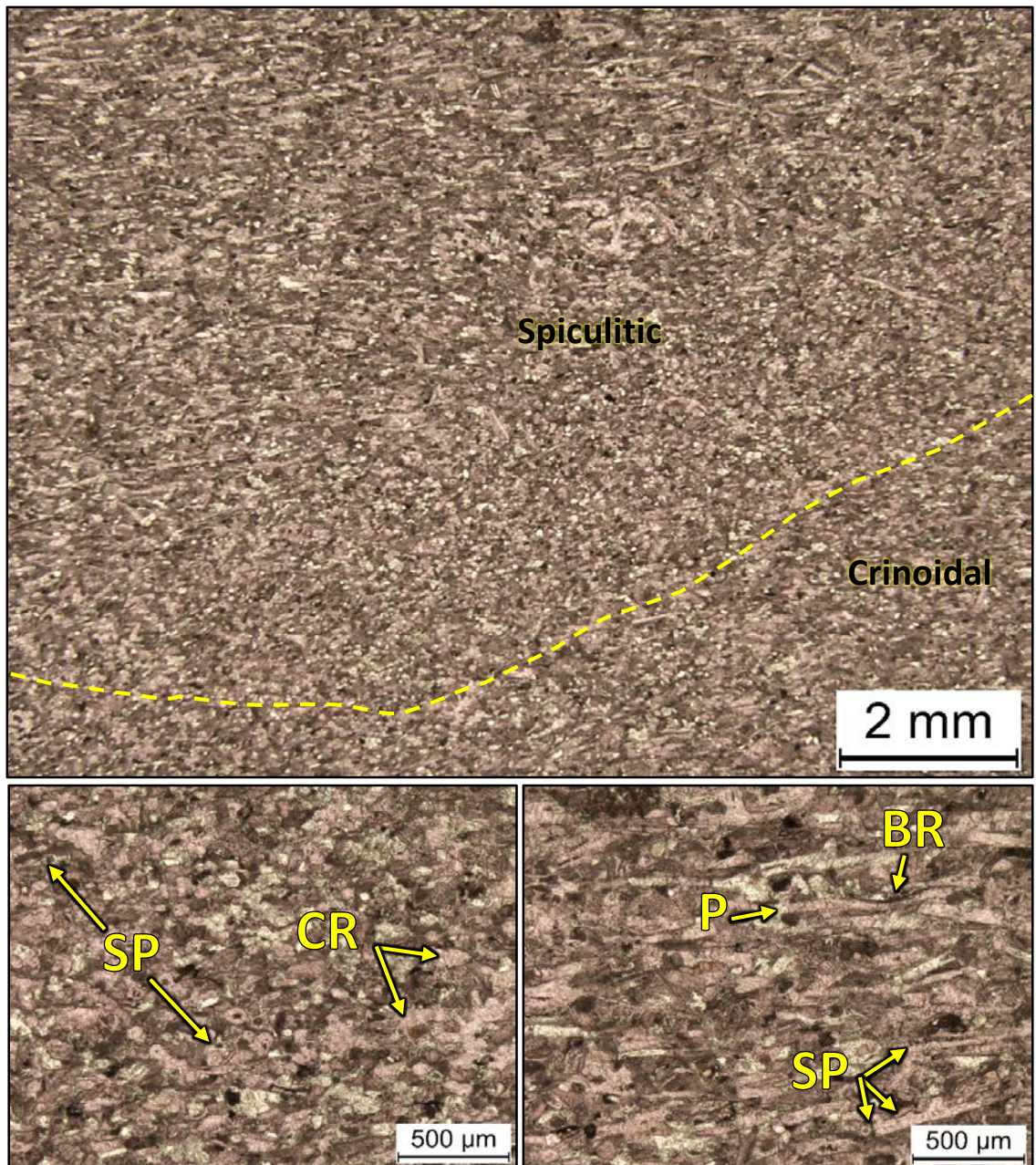
2WN – 5198.75' = Skeletal grainstone. Sample is alizarin red stained and blue epoxy impregnated. Porosity (NCS): 1.7%. Permeability (Klinkenberg): <0.0001 mD. TOC: 0.13%. XRD: Trace amounts of clays, 70% carbonates (69% calcite and 1% dolomite), and 30% other minerals (27% quartz, 1% potassium feldspar, 1% plagioclase feldspar, trace amounts of pyrite, and 1% apatite). Sample contains abundant crinoid fragments (30%), brachiopod fragments (10%), sponge spicules (5%), and peloids (5%). Moldic porosity from the dissolution of sponge spicules observed. Intraparticle porosity observed within silicified portions.



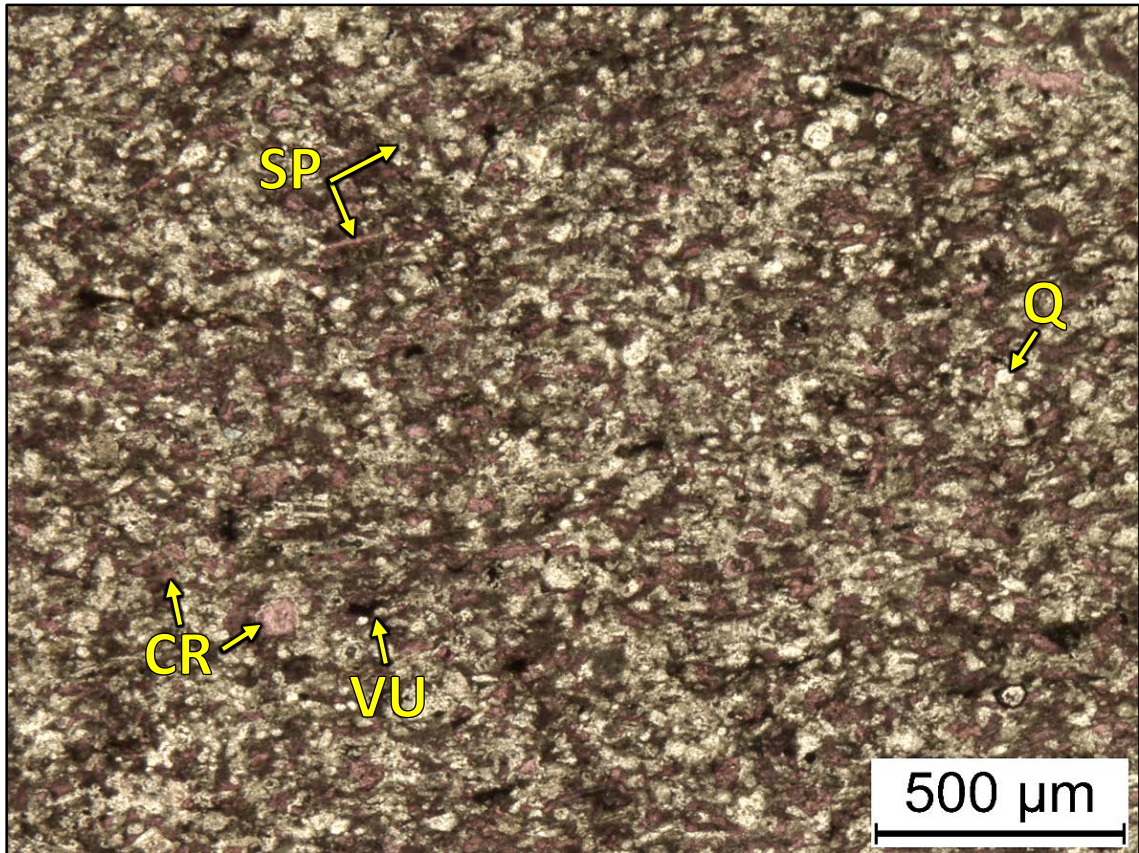
2WN – 5190.10' = Skeletal grainstone. Sample is alizarin red stained and porosity is shown in bright fuchsia. Porosity (NCS): 1.0%. Permeability (Klinkenberg): <0.0001 mD. TOC: 0.07%. XRD: 1% clays (1% illite), 51% carbonates (51% calcite), and 48% other minerals (42% quartz, 2% potassium feldspar, 3% plagioclase feldspar, 1% pyrite, and trace amounts of apatite). Sample contains abundant sponge spicules (35%), crinoid fragments (15%), and brachiopod fragments (5%). Moldic porosity and intraparticle porosity observed.



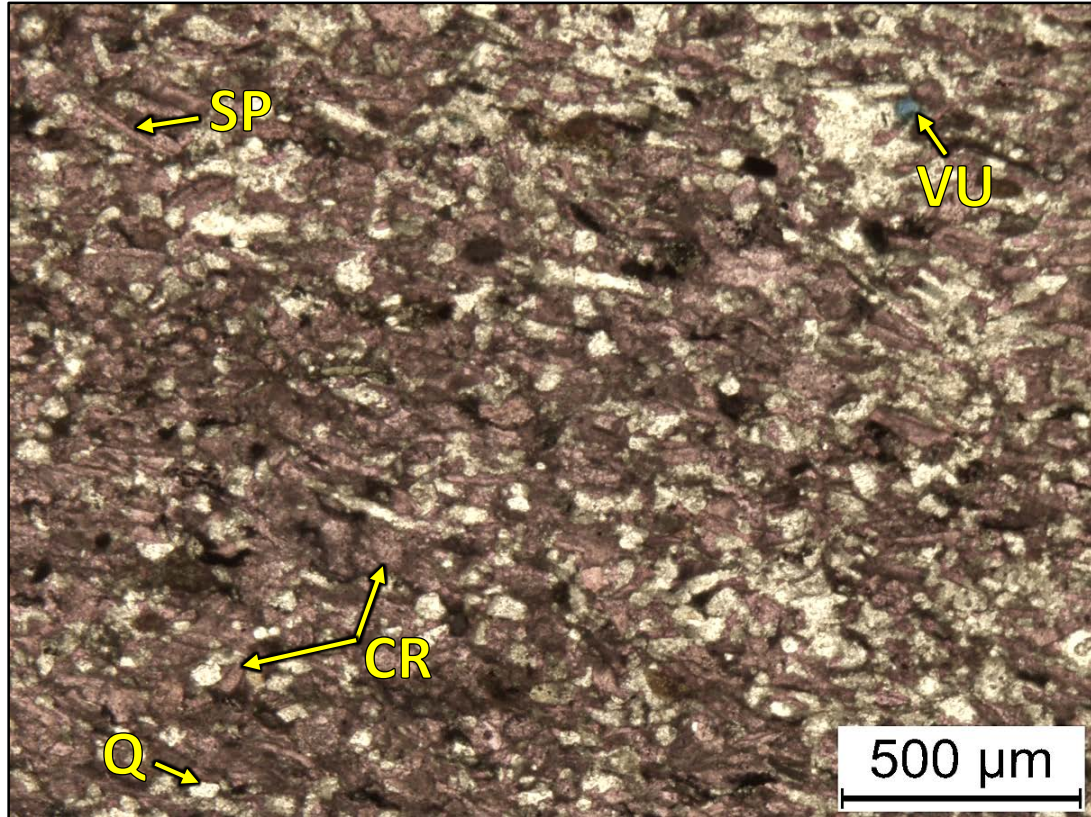
2WN – 5187.90' = Silicified skeletal grainstone. Sample is alizarin red stained and blue epoxy impregnated. Porosity (ambient): 1.5%. Permeability (Klinkenberg): Sample was unsuitable for this type of measurement. TOC: 0.22%. XRD: 1% clays (1% illite), 27% carbonates (26% calcite and 1% dolomite), and 72% other minerals (68% quartz, 1% potassium feldspar, trace amounts of plagioclase feldspar, 3% pyrite, and trace amounts of apatite). Sample contains abundant sponge spicules (50%), crinoid fragments (15%), brachiopod fragments (3%), and bryozoan fragments (3%). Moldic and vug porosity observed.



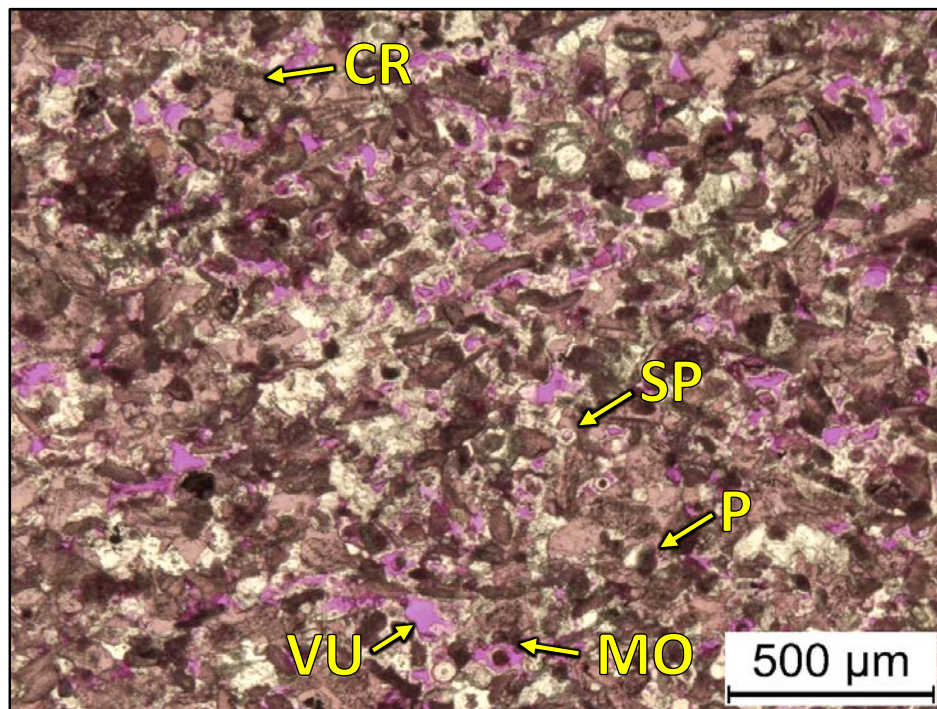
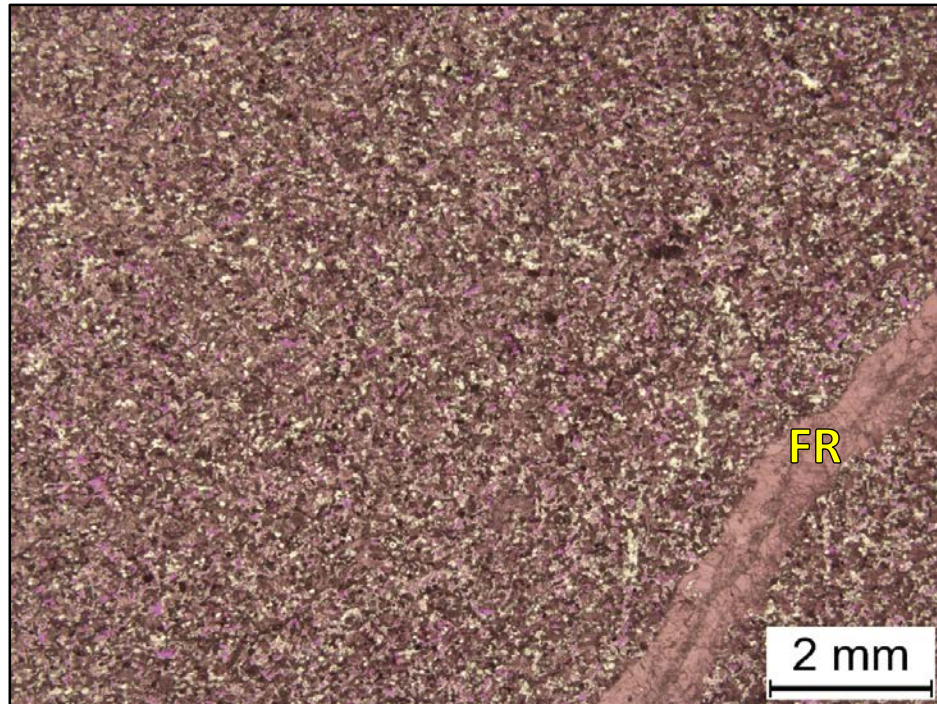
2WN – 5186.65' = Skeletal grainstone. Sample is alizarin red stained. Porosity (NCS): 0.1%. Permeability (Klinkenberg): <0.0001 mD. TOC: 0.04%. XRD: 1% clays (1% illite), 47% carbonates (41% calcite and 6% dolomite), and 52% other minerals (50% quartz, 1% potassium feldspar, 1% plagioclase feldspar, and trace amounts of pyrite and apatite). Sample contains crinoid fragments (15%), brachiopod fragments (10%), sponge spicules (10%), peloids (10%), and silt-sized quartz grains (20%).



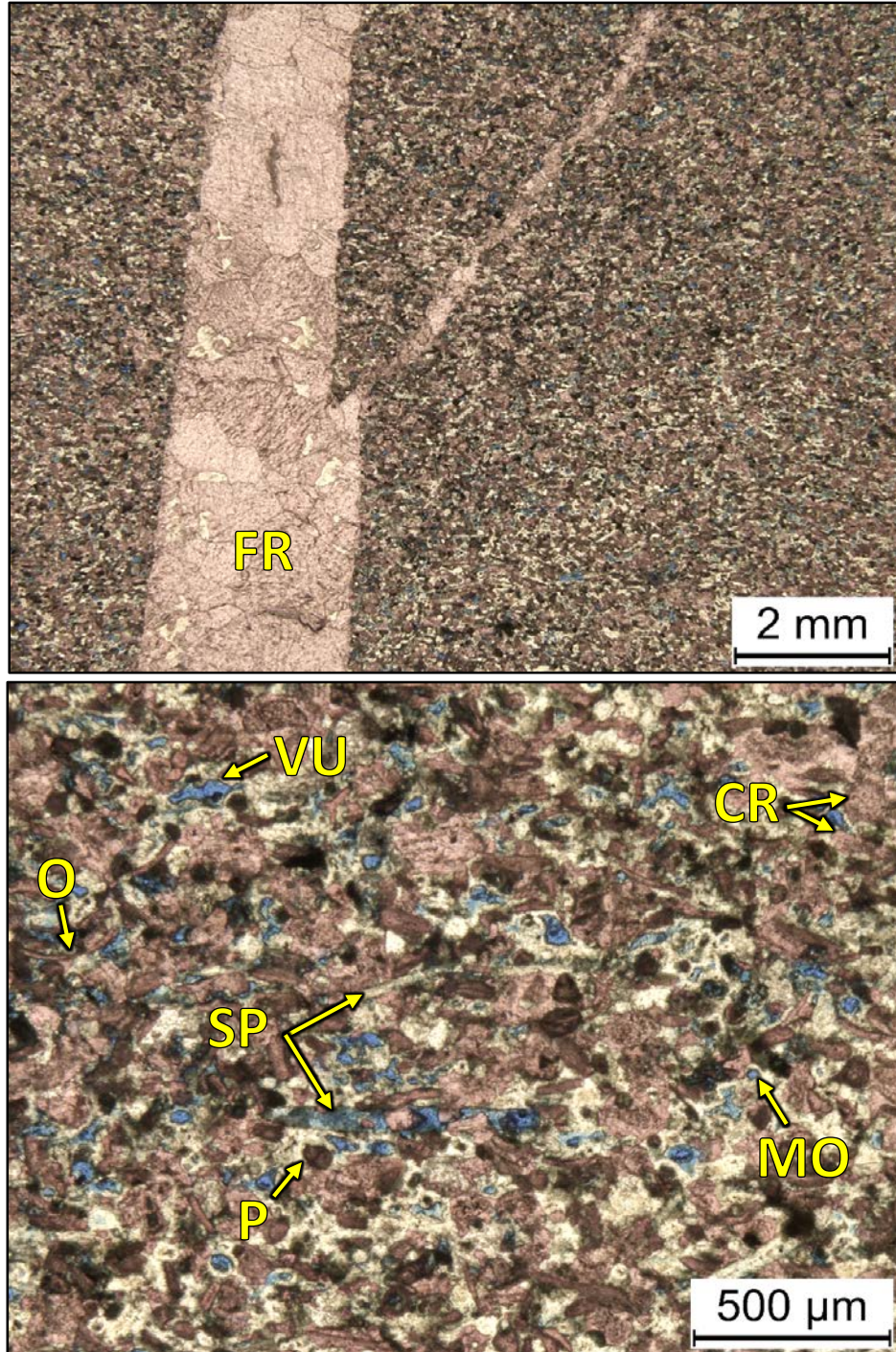
2WN – 5184.15' = Skeletal packstone. Sample is alizarin red stained. Porosity (NCS): 3.2%. Permeability (Klinkenberg): <0.0001 mD. TOC: 0.23%. XRD: 3% clays (2% illite and 1% mixed layer illite/smectite), 28% carbonates (26% calcite and 2% dolomite), and 69% other minerals (66% quartz, 1% potassium feldspar, 2% plagioclase feldspar, and trace amounts of pyrite and apatite). Sample contains silt-sized quartz grains (40%), sponge spicules (20%), crinoid fragments (10%), and undifferentiated microbioclastic debris. Oil-filled vug porosity is observed.



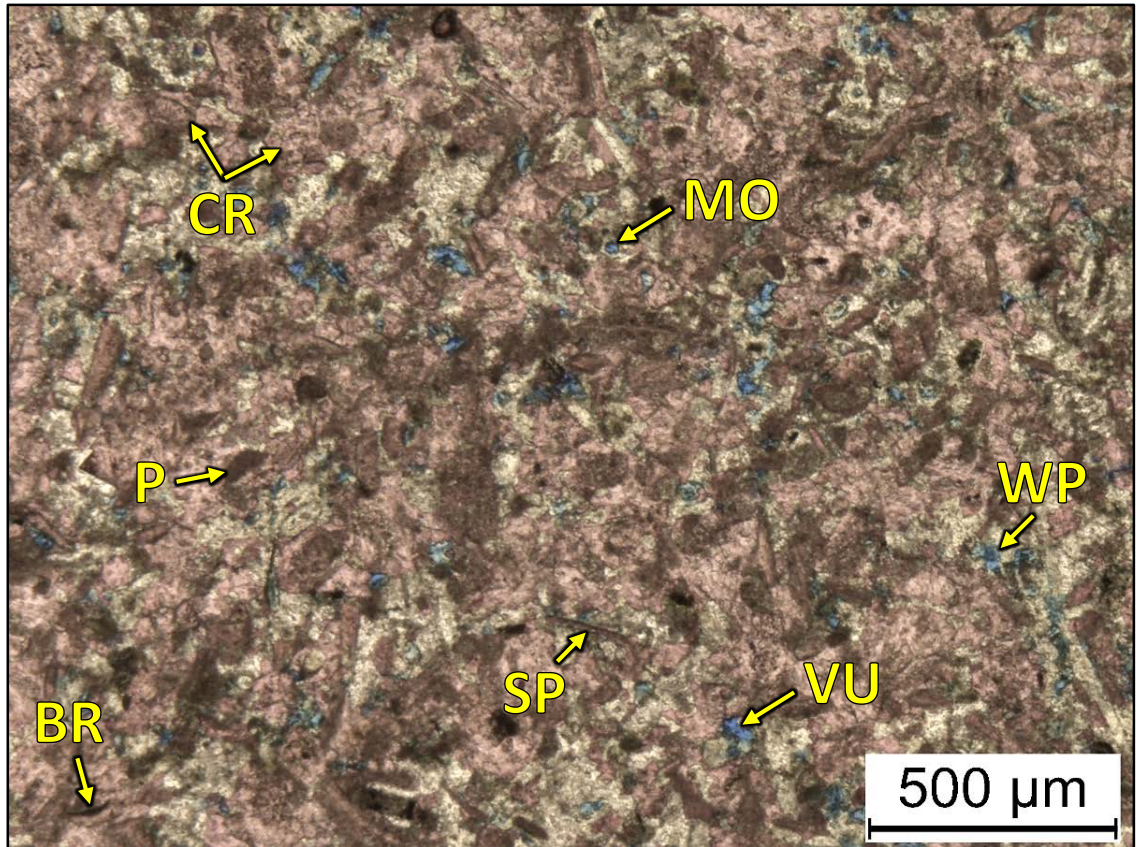
2WN – 5182.25' = Skeletal packstone. Sample is alizarin red stained and blue epoxy impregnated. Porosity (NCS): 1.5%. Permeability (Klinkenberg): <0.0001 mD. TOC: 0.08%. XRD: 2% clays (1% illite and 1% mixed layer illite/smectite), 63% carbonates (62% calcite and 1% dolomite), and 35% other minerals (31% quartz, 1% potassium feldspar, 3% plagioclase feldspar, and trace amounts of pyrite and apatite). Sample contains sponge spicules (20%), crinoid fragments (15%), silt-sized quartz grains (10%), and undifferentiated microbioclastic debris. Some spicules have been replaced by calcite. Open and oil-filled vug porosity observed.



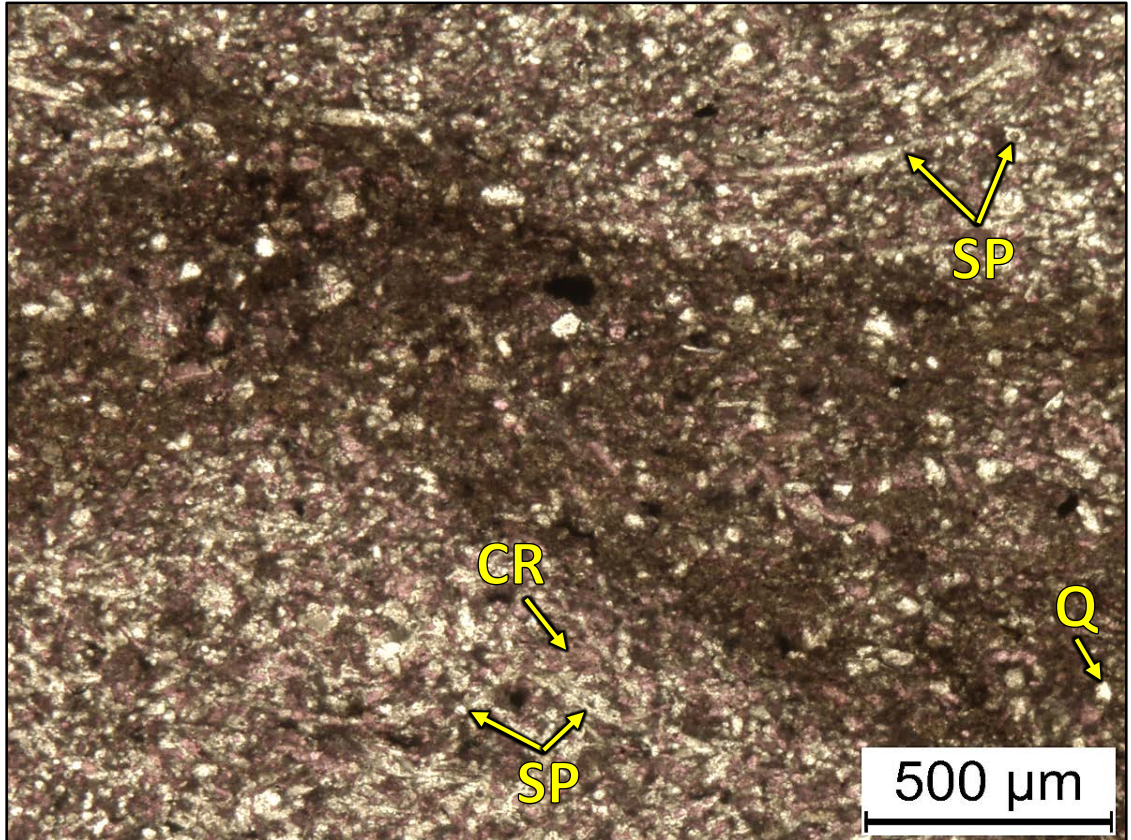
2WN – 5179.80' = Skeletal grainstone. Sample is alizarin red stained. Porosity (NCS): 9.3%. Permeability (Klinkenberg): 0.083 mD. TOC: 0.46%. XRD: 1% clays (1% illite), 71% carbonates (62% calcite and 9% dolomite), and 28% other minerals (25% quartz, 1% potassium feldspar, 2% plagioclase feldspar, and trace amounts of pyrite and apatite). Sample contains crinoid fragments (20%), sponge spicules (10%), and peloids (7%). Calcite-filled fracture present. Abundant moldic and vug porosity observed.



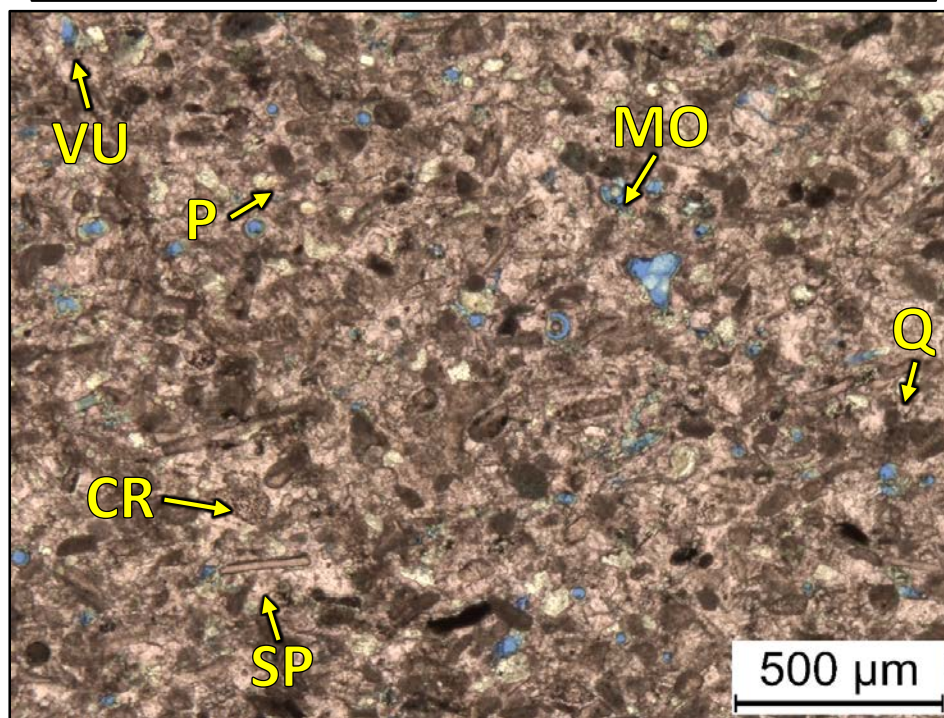
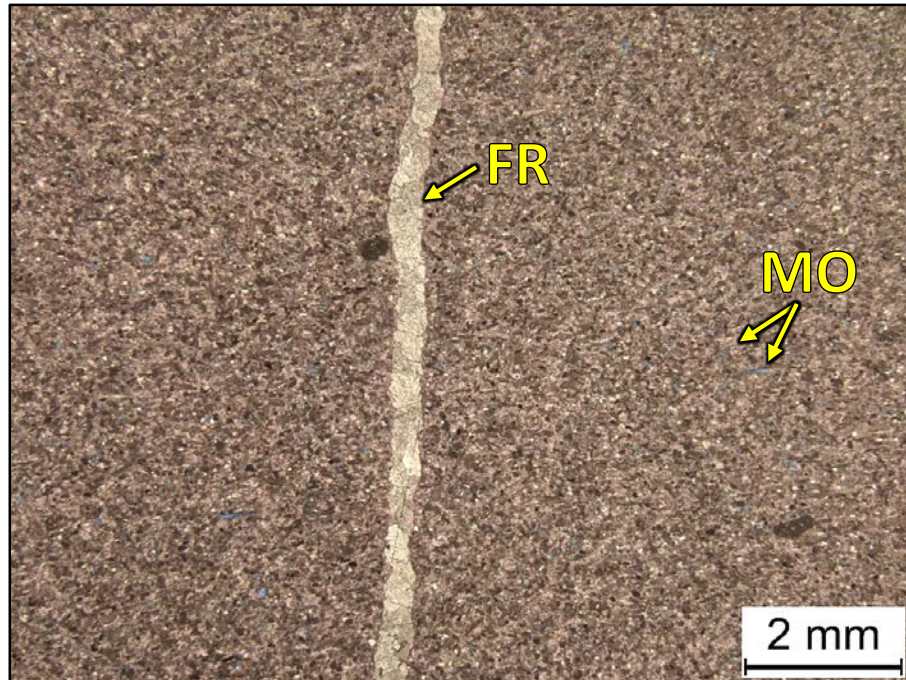
2WN – 5179.15' = Skeletal grainstone. Sample is alizarin red stained and blue epoxy impregnated. Porosity (NCS): 9.1%. Permeability (Klinkenberg): 0.075 mD. TOC: 0.43%. XRD: 1% clays (1% illite), 67% carbonates (57% calcite and 10% dolomite), and 32% other minerals (30% quartz, 1% potassium feldspar, 1% plagioclase feldspar, and trace amounts of pyrite and apatite). Sample contains crinoid fragments (15%), sponge spicules (15%), peloids (15%), silt-sized quartz grains (10%), and ostracodes (3%). Moldic and vug porosity observed.



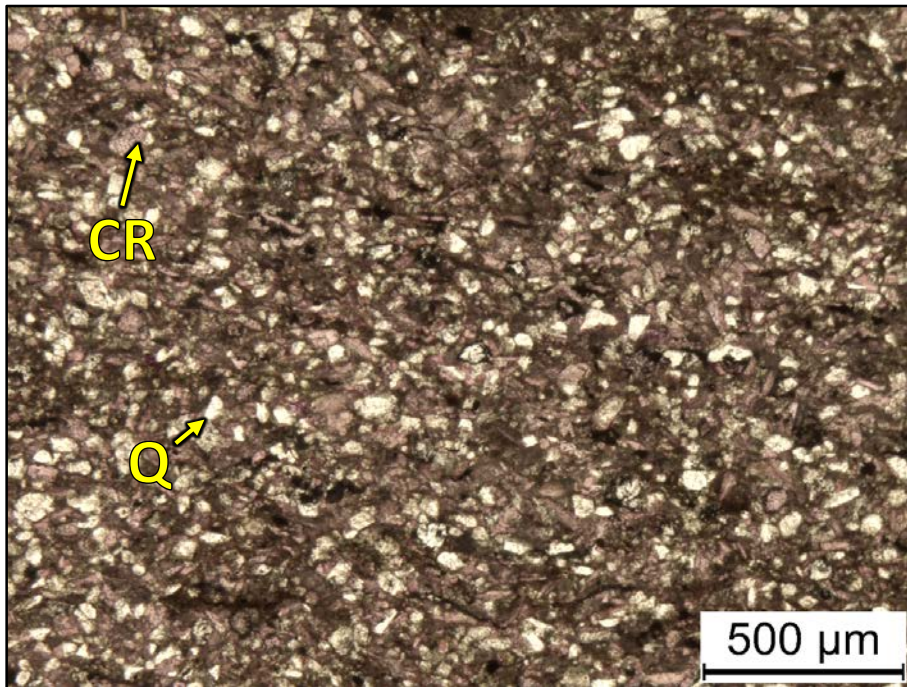
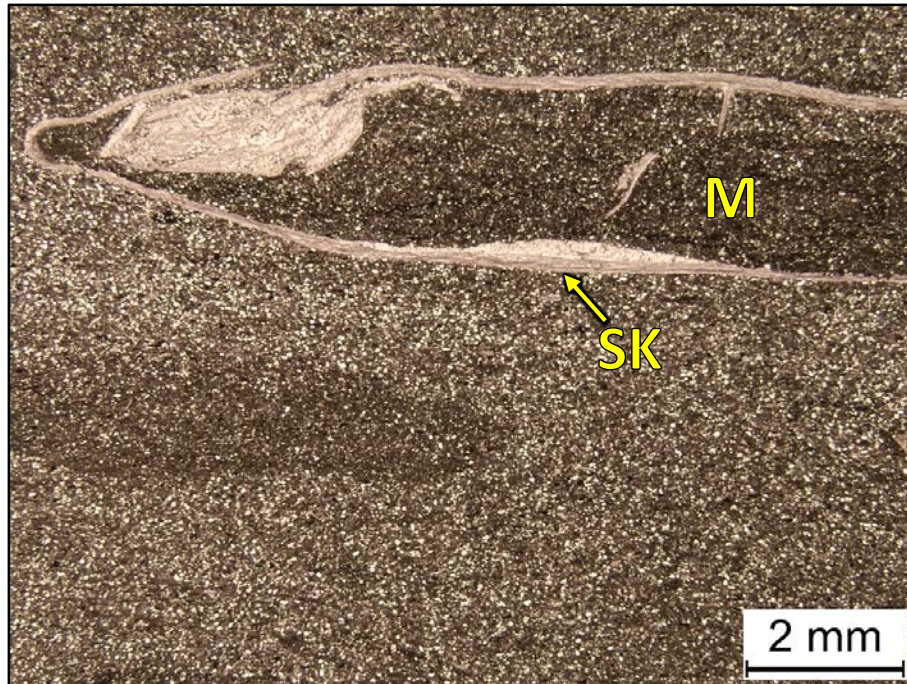
2WN – 5177.95' = Skeletal grainstone. Sample is alizarin red stained. Porosity (NCS): 2.9%. Permeability (Klinkenberg): 0.0001 mD. TOC: 0.08%. XRD: 1% clays (1% illite), 61% carbonates (54% calcite and 7% dolomite), and 38% other minerals (36% quartz, 1% potassium feldspar, 1% plagioclase feldspar, and trace amounts of pyrite and apatite). Sample contains crinoid grains (30%), sponge spicules (15%), peloids (10%), and brachiopod fragments (3%). Some spicules have been replaced by calcite. Moldic, vug, intracrystalline, and intraparticle porosity are observed.



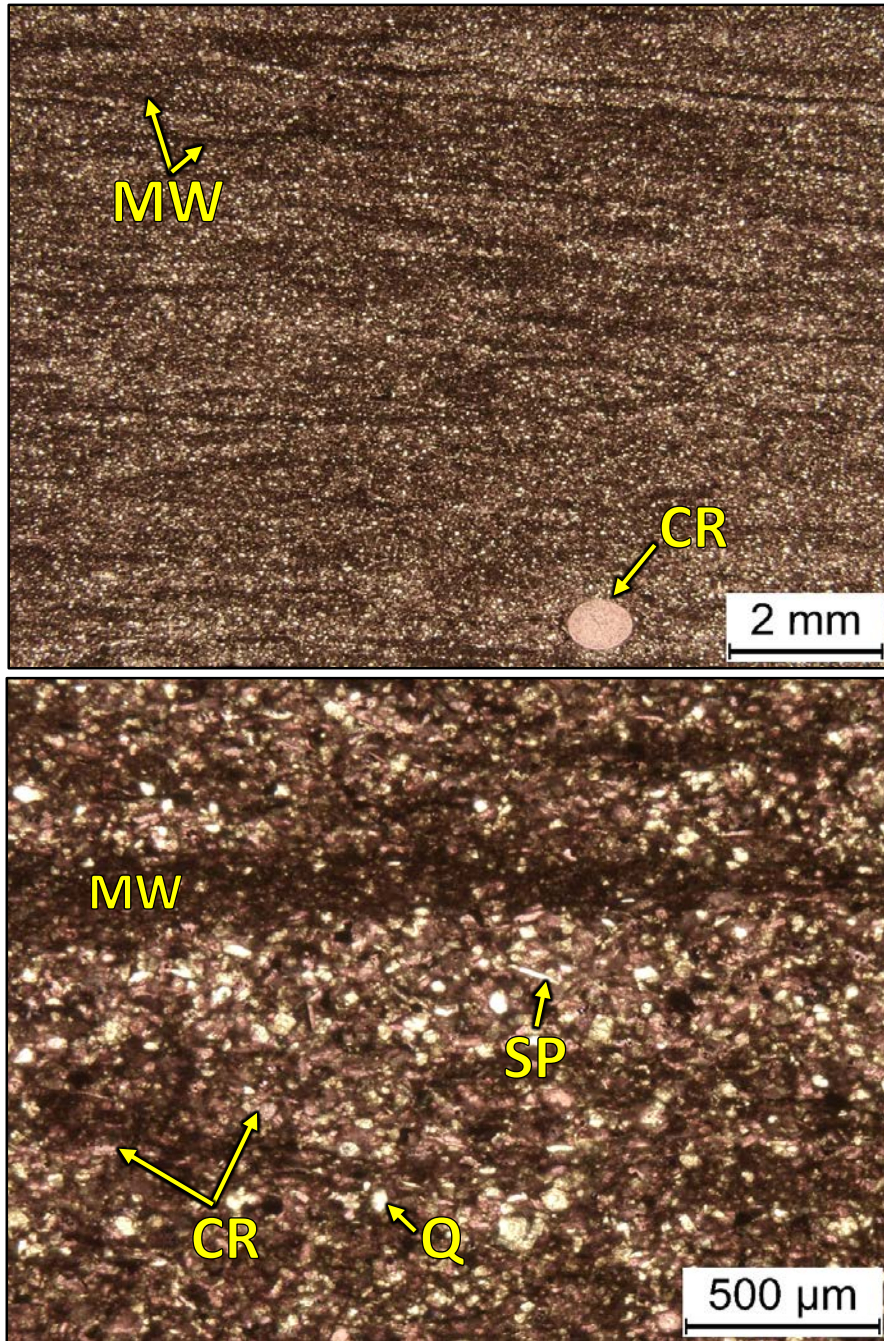
2WN – 5177.90' = Bioturbated wackestone-skeletal packstone. Sample is alizarin red stained. XRD: 4% clays (3% illite and 1% mixed layer illite/smectite), 40% carbonates (33% calcite and 7% dolomite), and 56% other minerals (50% quartz, 1% potassium feldspar, 3% plagioclase feldspar, 1% pyrite, and 1% apatite). Sample contains sponge spicules (15%), crinoid fragments (15%), and undifferentiated microbioclastic debris.



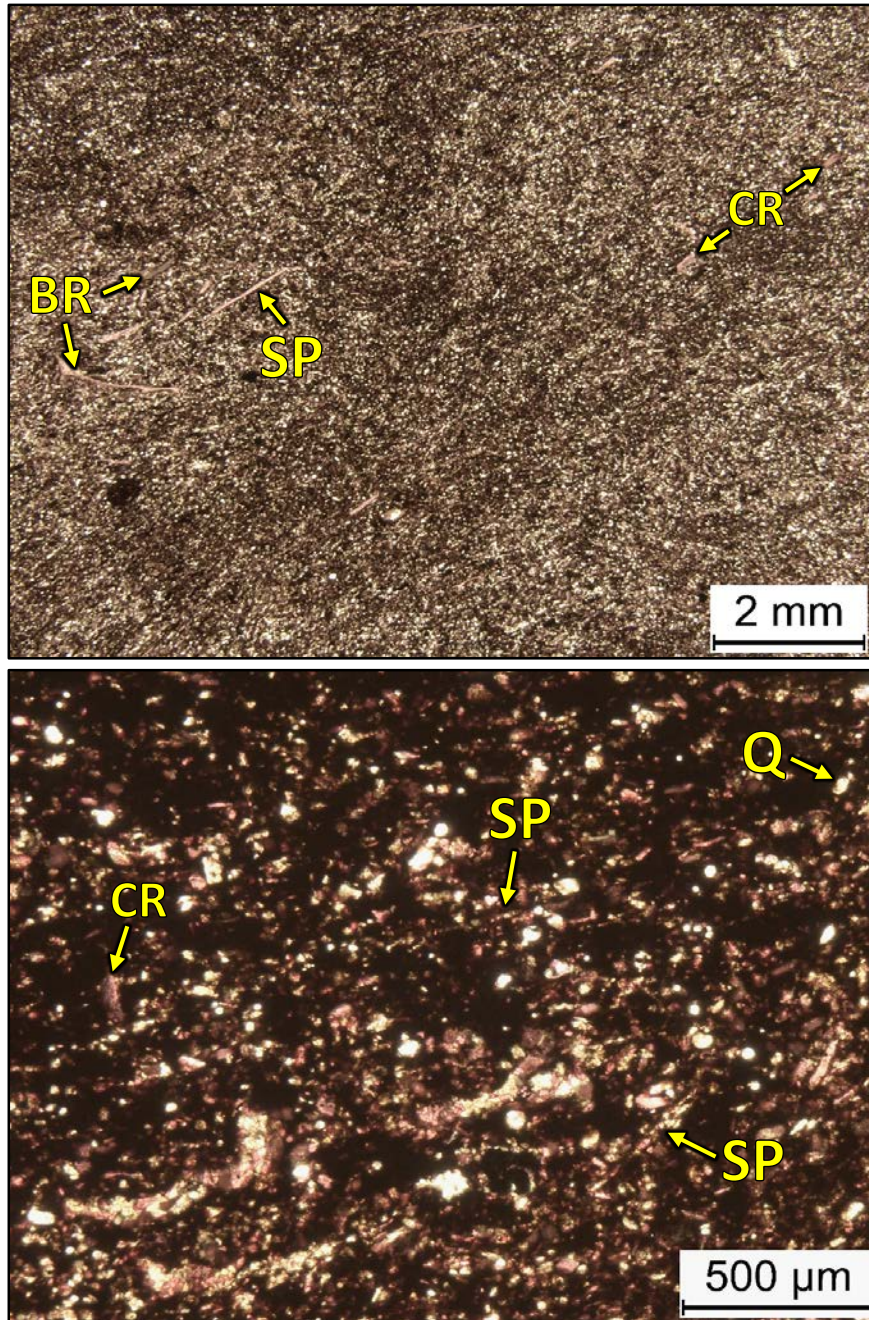
2WN – 5176.35' = Peloidal-skeletal grainstone. Sample is alizarin red stained and blue epoxy impregnated. Porosity (NCS): 2.3%. Permeability (Klinkenberg): 0.0001 mD. TOC: 0.07%. XRD: 1% clays (1% illite), 82% carbonates (81% calcite and 1% dolomite), and 17% other minerals (13% quartz, 1% potassium feldspar, 3% plagioclase feldspar, and trace amounts of pyrite and apatite). Sample contains crinoid fragments (20%), peloids (15%), sponge spicules (12%), and silt-sized quartz grains. Mineralized vertical fracture is present within sample. Open and oil-filled moldic and intracrystalline porosity is observed.



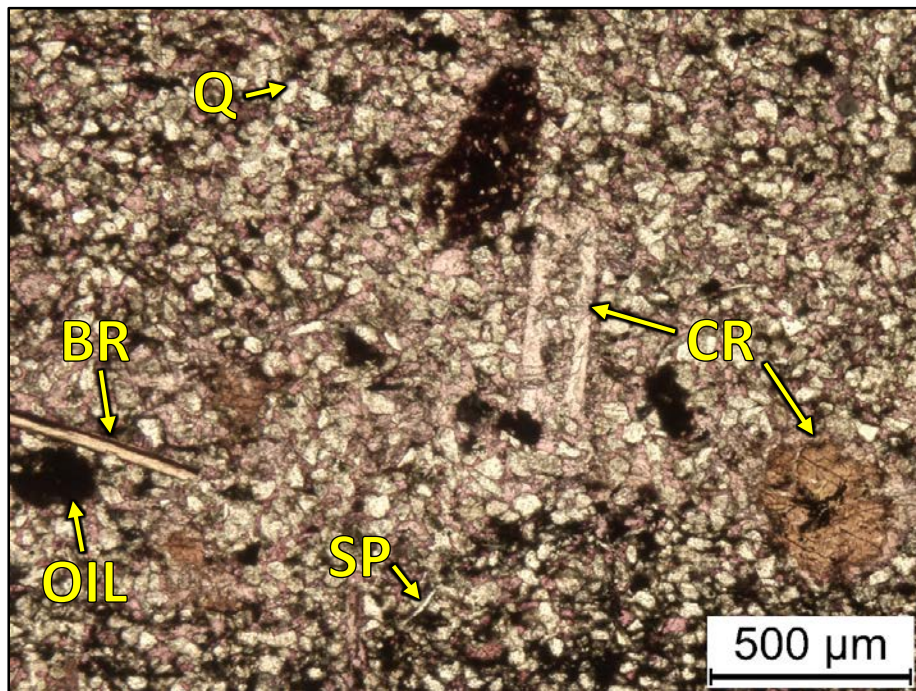
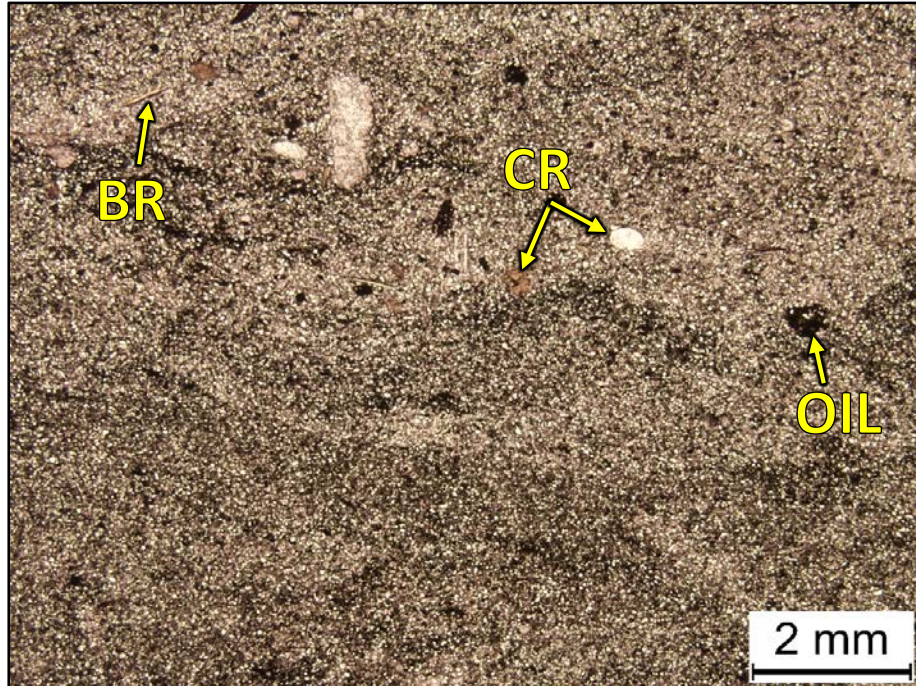
2WN – 5170.15' = Bioturbated packstone. Sample is alizarin red stained. Porosity (NCS): 2.8%. Permeability (Klinkenberg): 0.0001 mD. TOC: 0.26%. XRD: 2% clays (1% illite and 1% mixed layer illite/smectite), 43% carbonates (38% calcite and 5% dolomite), and 55% other minerals (47% quartz, 2% potassium feldspar, 5% plagioclase feldspar, 1% pyrite, and trace amounts of apatite). Sample contains silt-sized quartz grains (47%), crinoid fragments (15%), and undifferentiated microbioclastic debris. A large skeletal fragment (possibly a large ostracode or a brachiopod) is observed in this sample. Oil-filled porosity observed throughout sample.



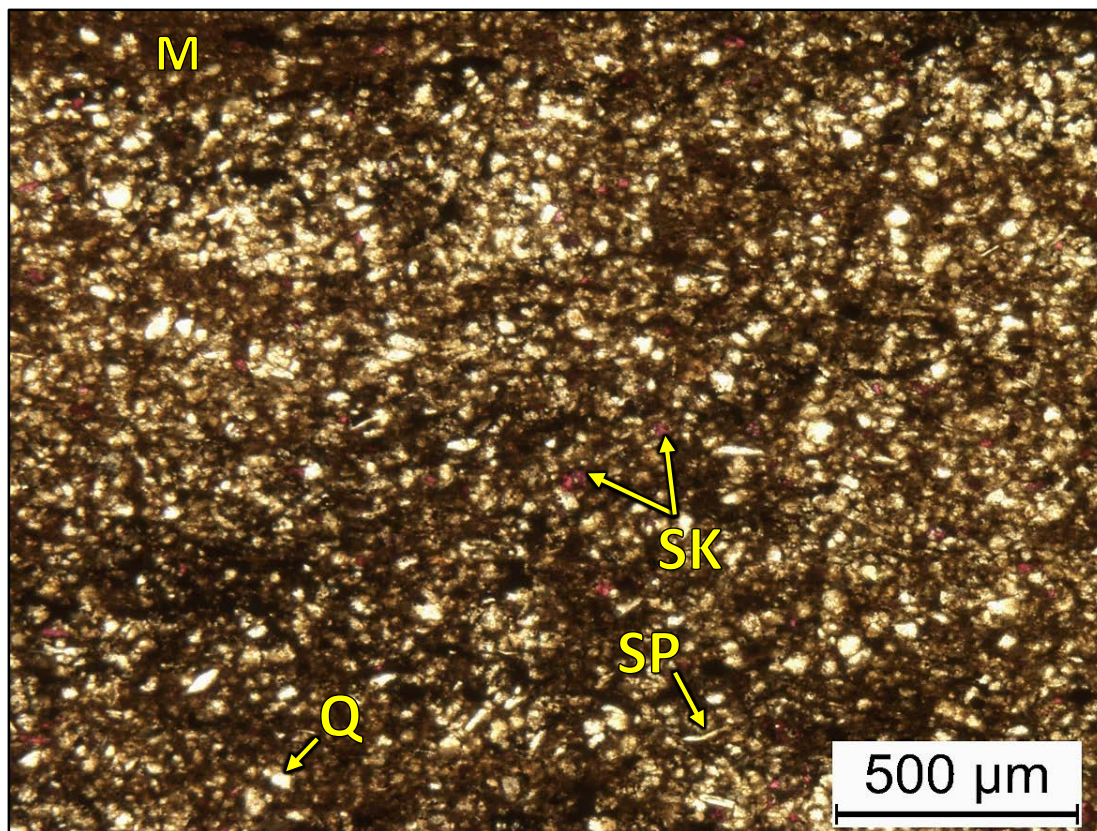
2WN – 5166.35-5166.55' = Bioturbated mudstone-wackestone. Sample is alizarin red stained. TOC: 3.13%. XRD: 11% clays (7% illite and 4% mixed layer illite/smectite), 50% carbonates (45% calcite and 5% dolomite), and 39% other minerals (31% quartz, 1% potassium feldspar, 3% plagioclase feldspar, 3% pyrite, and 1% apatite). Sample contains silt-sized quartz grains (30%), crinoid fragments (15%), sponge spicules (5%), and undifferentiated microbioclastic debris.



2WN – 5161.70' = Bioturbated mudstone-wackestone. Sample is alizarin red stained. Porosity (ambient): 2.5%. Permeability (Klinkenberg): Sample was unsuitable for this type of measurement. TOC: 1.29%. XRD: 9% clays (6% illite and 3% mixed layer illite/smectite), 54% carbonates (45% calcite and 9% dolomite), and 37% other minerals (32% quartz, 1% potassium feldspar, 2% plagioclase feldspar, 1% pyrite, and 1% apatite). Sample contains silt-sized quartz grains (30%), sponge spicules (5%), crinoid fragments (5%), and undifferentiated microbioclastic debris. Some spicules are replaced with calcite.

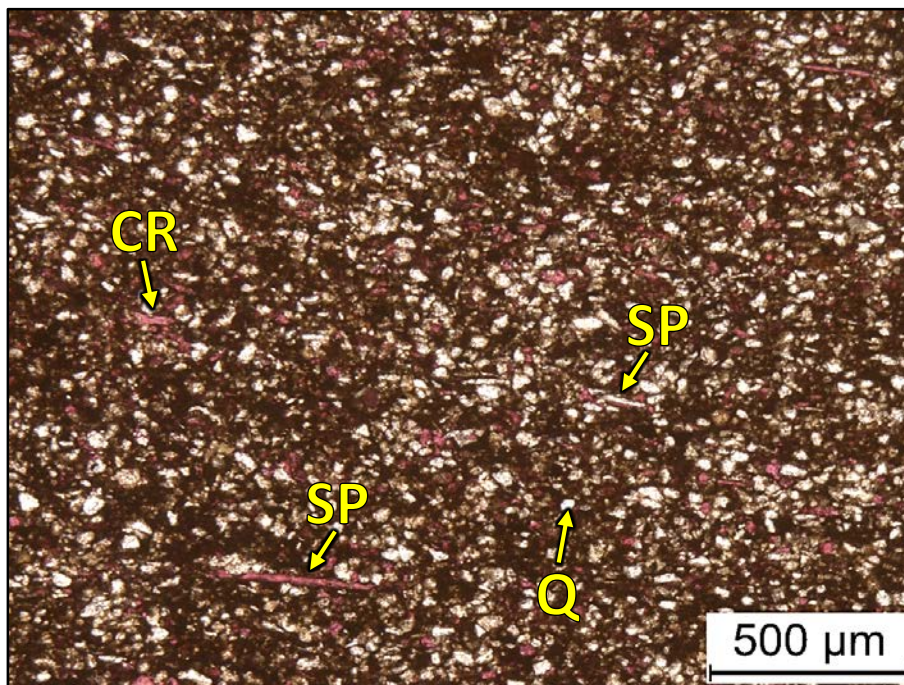
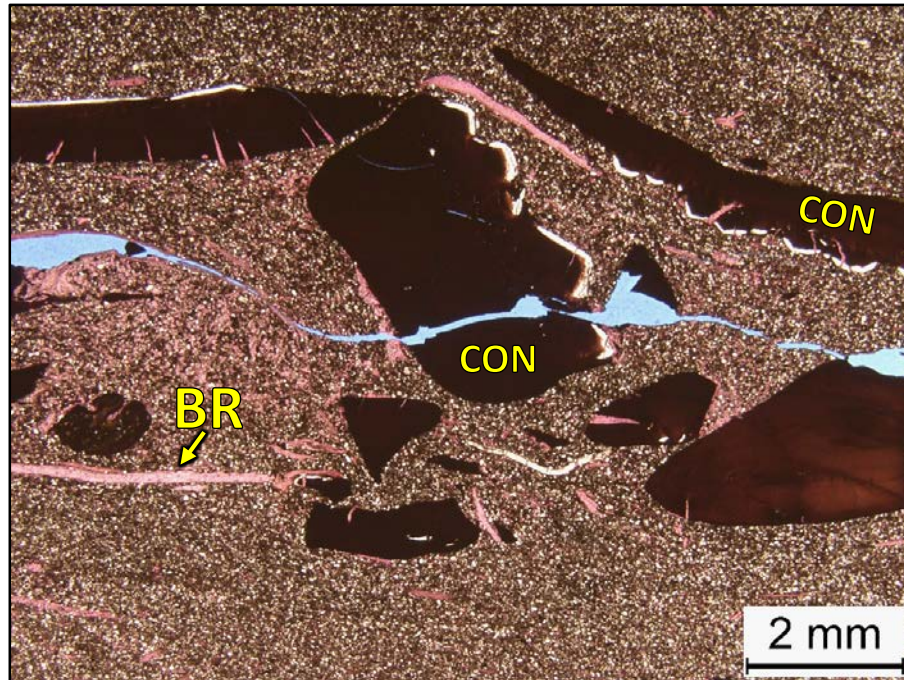


2WN – 5159.85' = Bioturbated wackestone-skeletal packstone. Sample is alizarin red stained. Porosity (NCS): 3.0%. Permeability (Klinkenberg): 0.0006 mD. TOC: 0.57%. XRD: 9% clays (1% chlorite, 6% illite, and 2% mixed layer illite/smectite), 21% carbonates (19% calcite and 2% dolomite), and 70% other minerals (48% quartz, 1% potassium feldspar, 7% plagioclase feldspar, 1% pyrite, and 13% apatite). Sample contains crinoid grains (20%), brachiopod fragments (5%), sponge spicule fragments (2%), and undifferentiated microbioclastic debris. Oil-filled vug porosity observed.

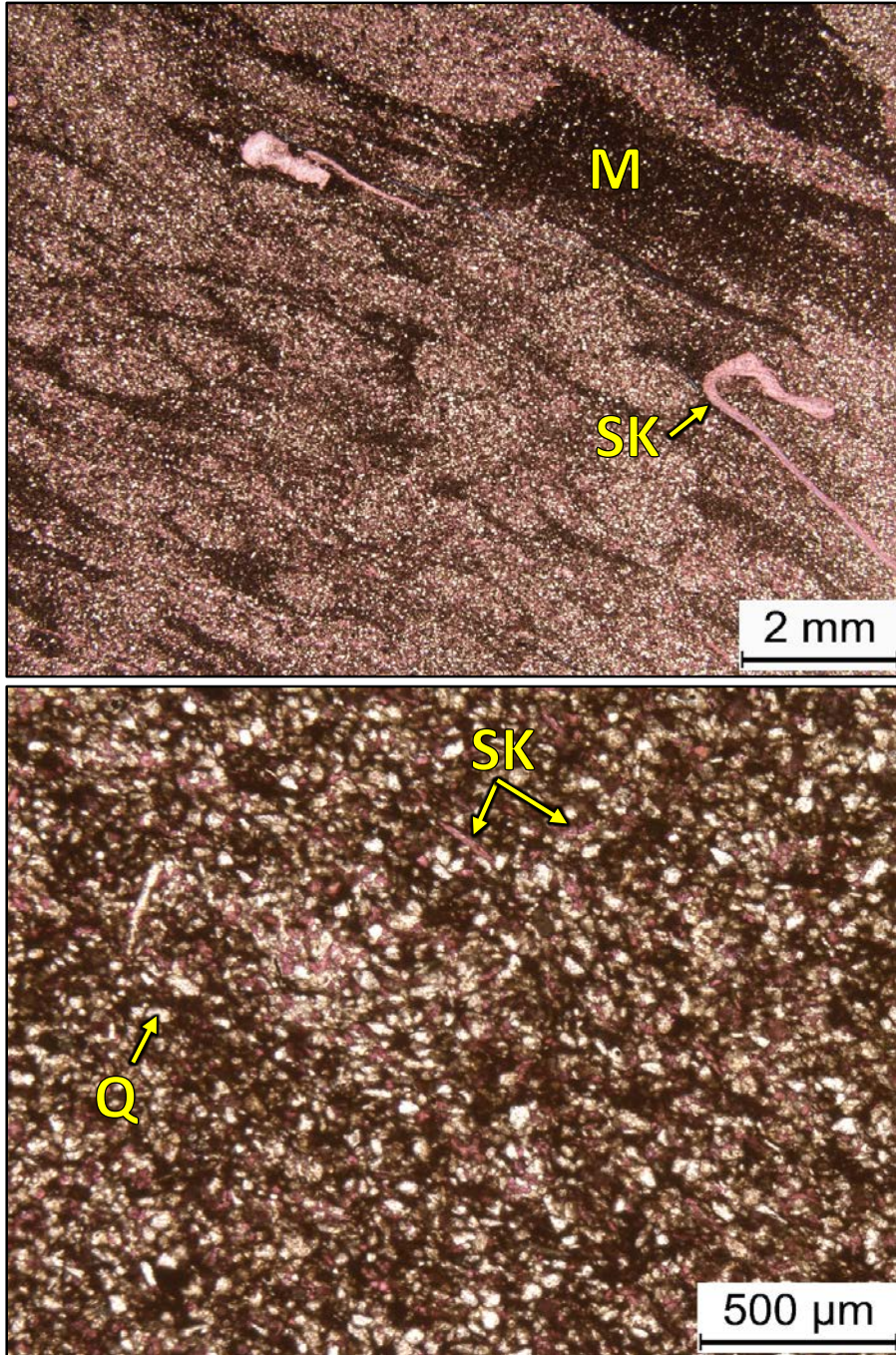


2WN – 5158.70-5158.90' = Weakly calcareous bioturbated mudstone-wackestone.

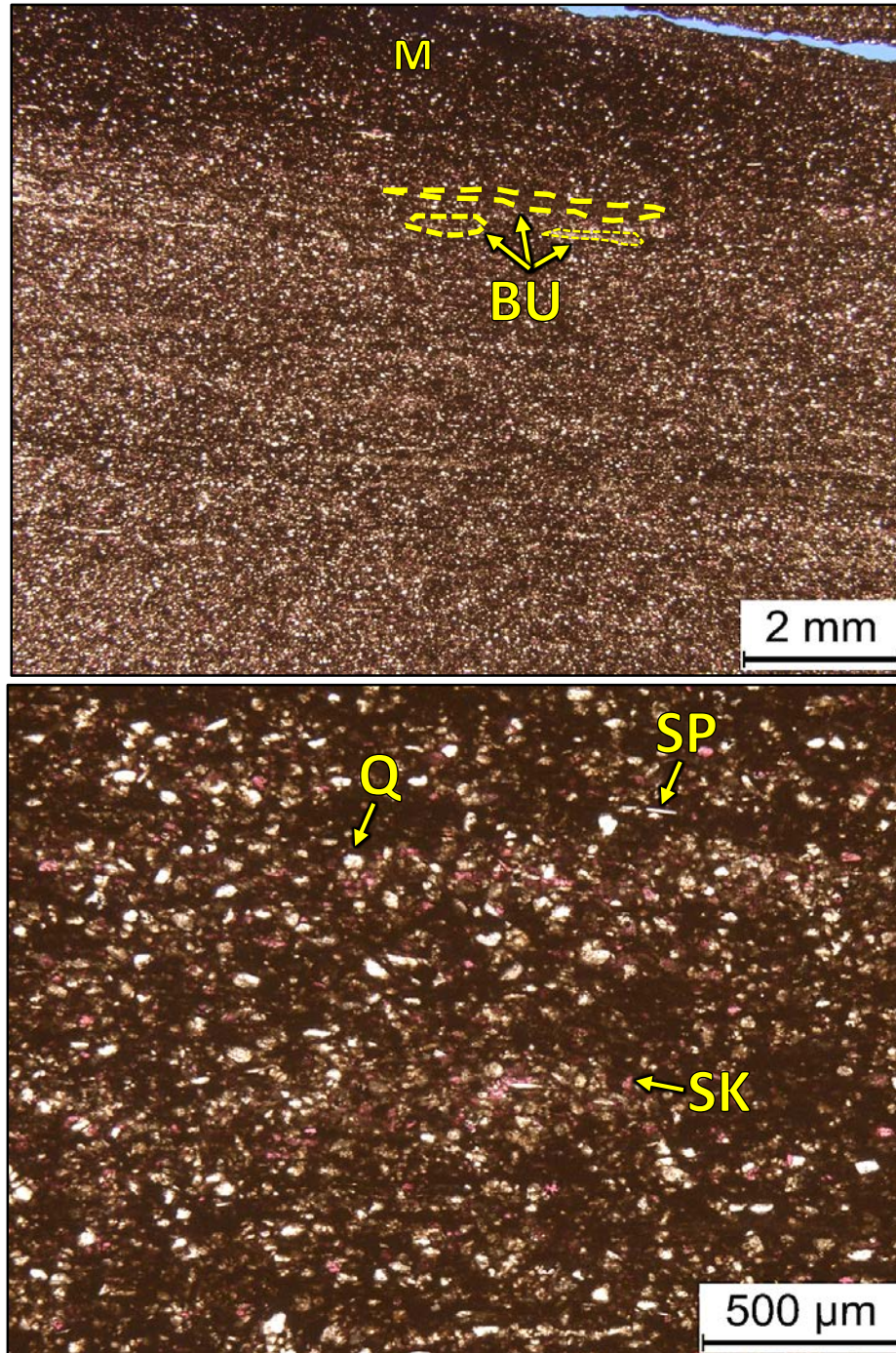
Sample is alizarin red stained. TOC: 0.79%. XRD: 33% clays (24% illite and 9% mixed layer illite/smectite), 11% carbonates (10% calcite and 1% dolomite), and 56% other minerals (45% quartz, 2% potassium feldspar, 5% plagioclase feldspar, 4% pyrite, and trace amounts of apatite). Sample contains silt-sized quartz grains (45%), sponge spicules (5%), and undifferentiated microbioclastic debris.



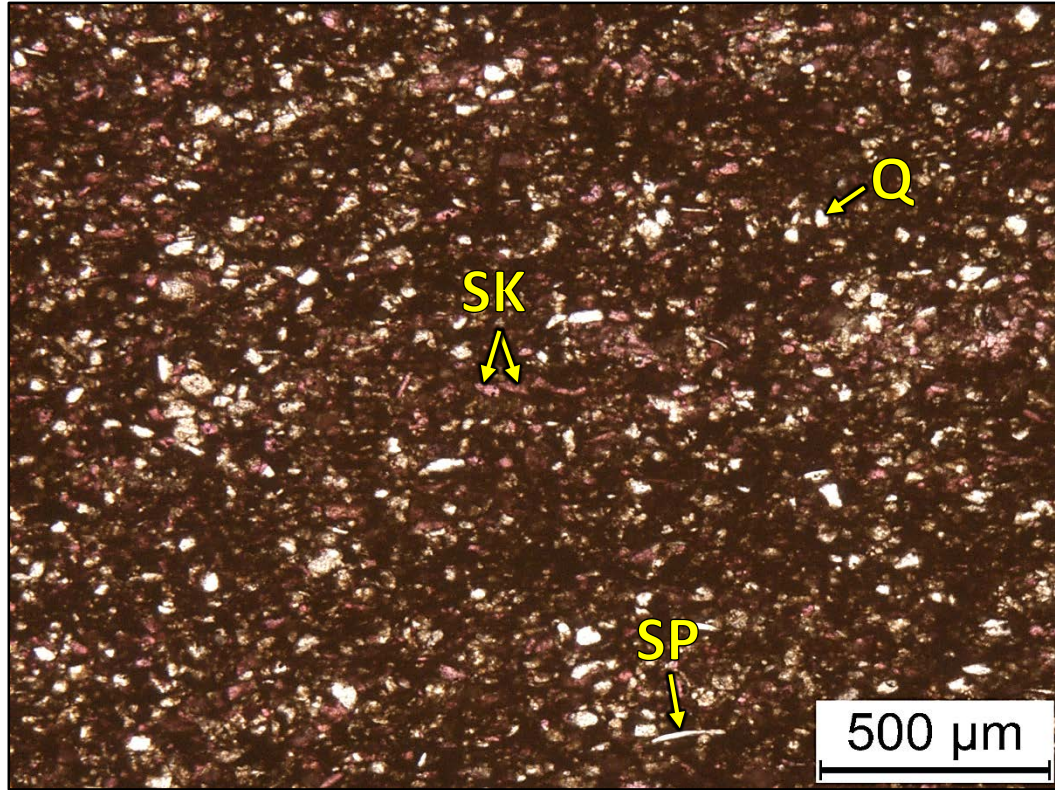
2WN – 5157.25' = Bioturbated wackestone. Sample is alizarin red stained. Porosity (ambient): 4.6%. Permeability (Klinkenberg): Sample was unsuitable for this type of measurement. TOC: 1.91%. XRD: 17% clays (11% illite and 6% mixed layer illite/smectite), 36% carbonates (31% calcite and 5% dolomite), and 47% other minerals (36% quartz, 1% potassium feldspar, 5% plagioclase feldspar, 2% pyrite, and 3% apatite). Sample contains conodont fragments (15%), brachiopod fragments (10%), sponge spicules (5%), and undifferentiated microbioclastic debris.



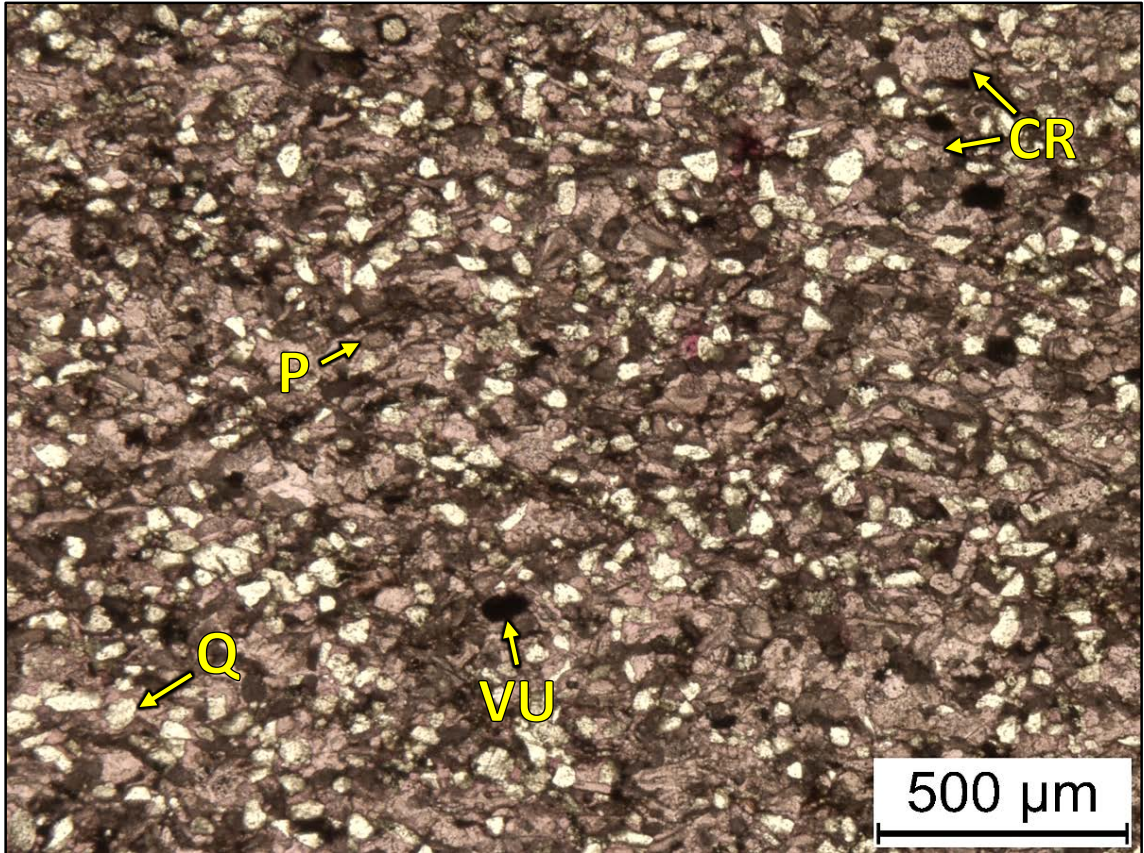
2WN – 5155.65' = Bioturbated wackestone. Sample is alizarin red stained. Porosity (ambient): 2.2%. Permeability (Klinkenberg): Sample was not suitable for this type of analysis. TOC: 2.49%. XRD: 12% clays (8% illite and 4% mixed layer illite/smectite), 42% carbonates (38% calcite and 4% dolomite), and 46% other minerals (30% quartz, 1% potassium feldspar, 6% plagioclase feldspar, 3% pyrite, and 6% apatite). Sample contains large skeletal fragments (3%), silt-sized quartz grains (30%), and undifferentiated microbioclastic debris.



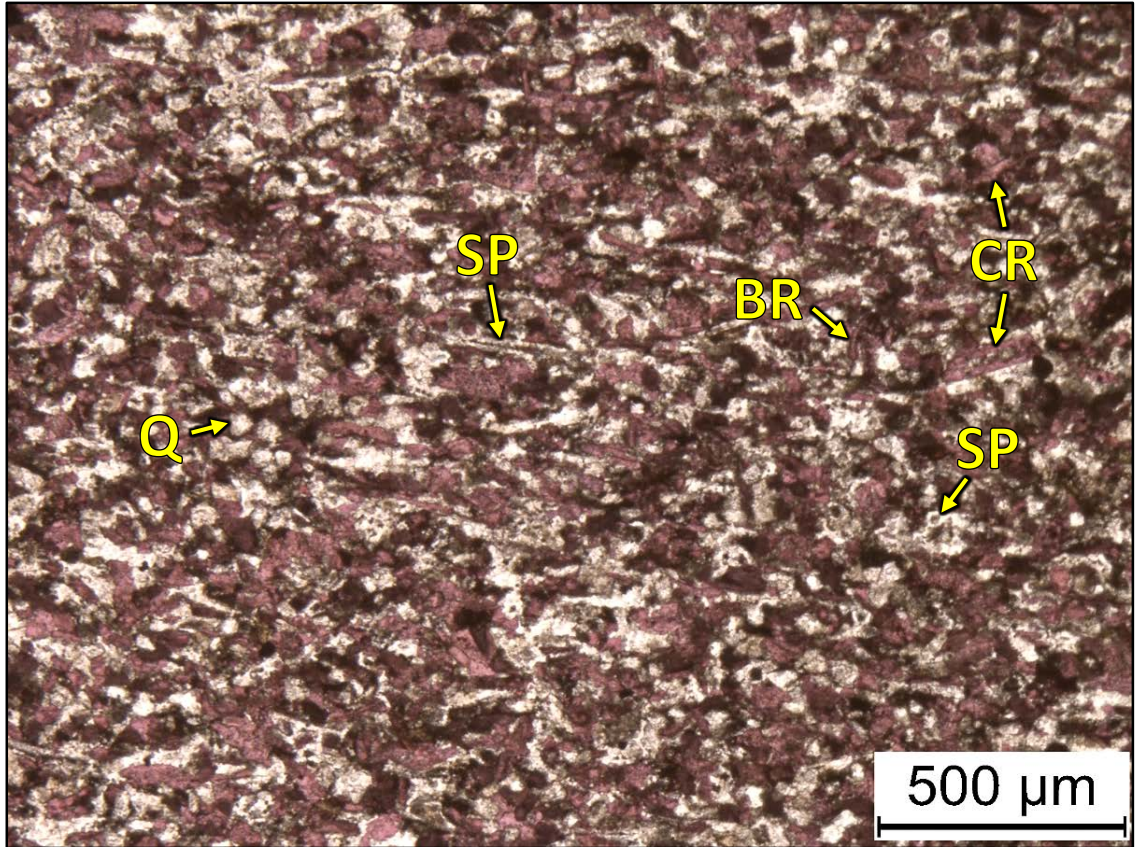
2WN – 5153.80-5154.00' = Laminated mudstone-wackestone. Sample is alizarin red stained. TOC: 1.82%. XRD: 20% clays (1% chlorite, 15% illite, and 4% mixed layer illite/smectite), 27% carbonates (25% calcite and 2% dolomite), and 53% other minerals (45% quartz, 1% potassium feldspar, 4% plagioclase feldspar, 2% pyrite, trace amounts of apatite, and 1% marcasite). Sample contains silt-sized quartz grains and undifferentiated microbioclastic debris.



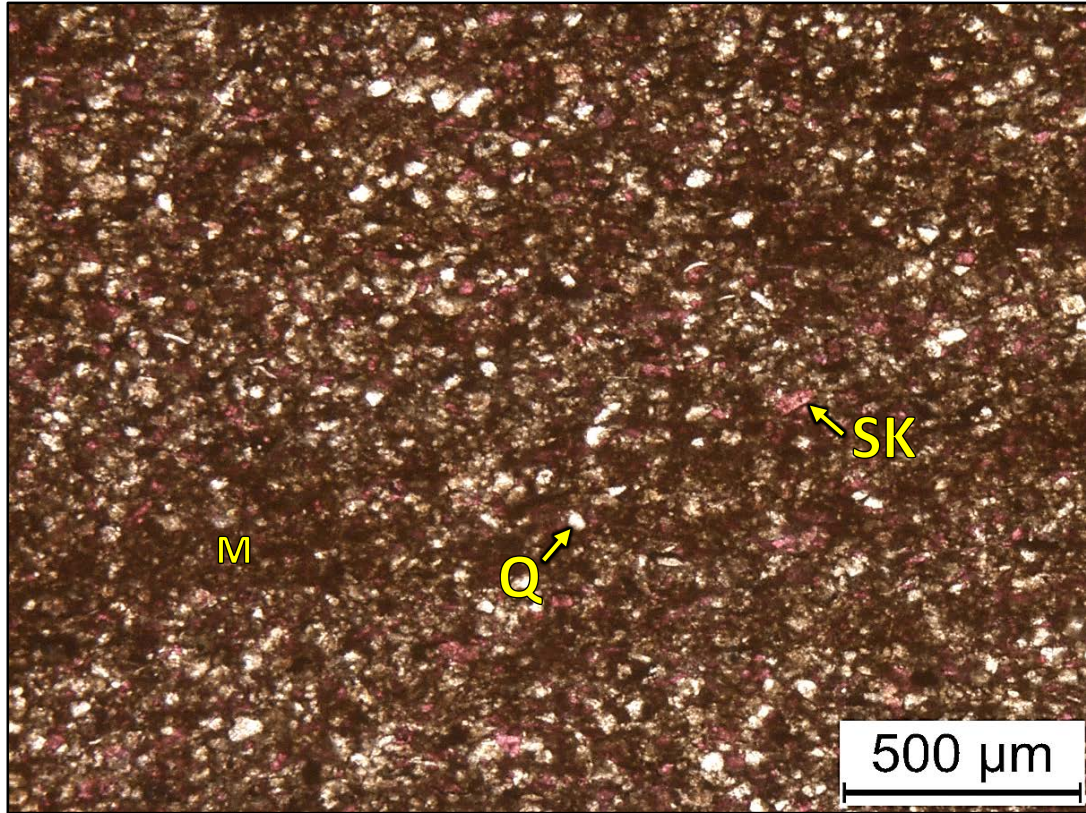
2WN – 5152.90' = Calcareous mudstone-wackestone. Sample is alizarin red stained. Porosity (NCS): 1.8%. Permeability (Klinkenberg): 0.191 mD. TOC: 1.61%. XRD: 13% clays (10% illite and 3% mixed layer illite/smectite), 43% carbonates (41% calcite and 2% dolomite), and 44% other minerals (34% quartz, trace amounts of potassium feldspar, 5% plagioclase feldspar, 2% pyrite, and 3% apatite). Sample contains silt-sized quartz grains and undifferentiated microbioclastic debris.



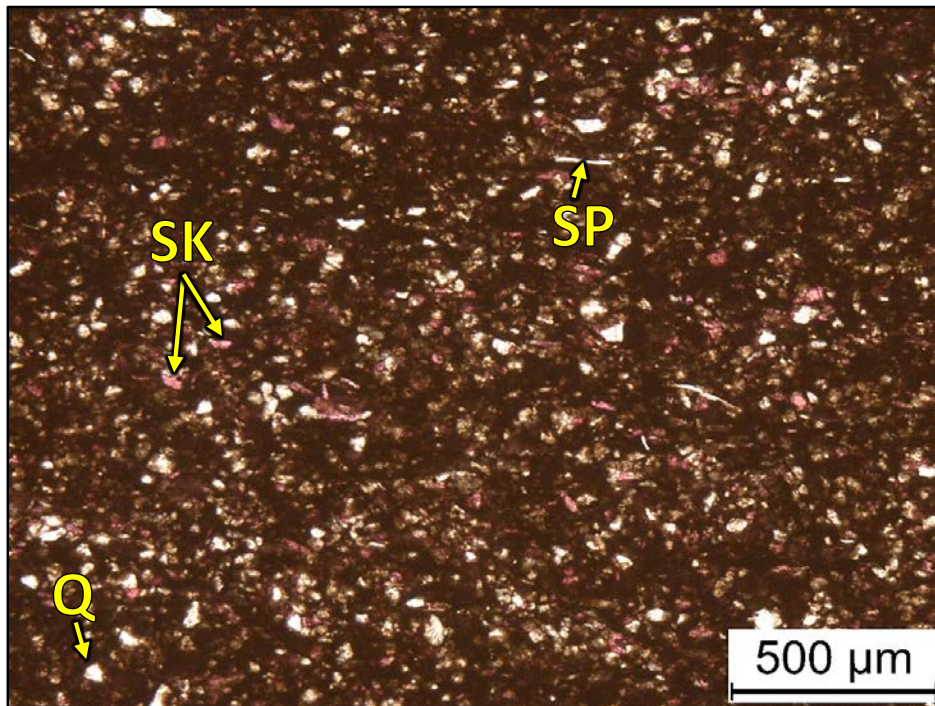
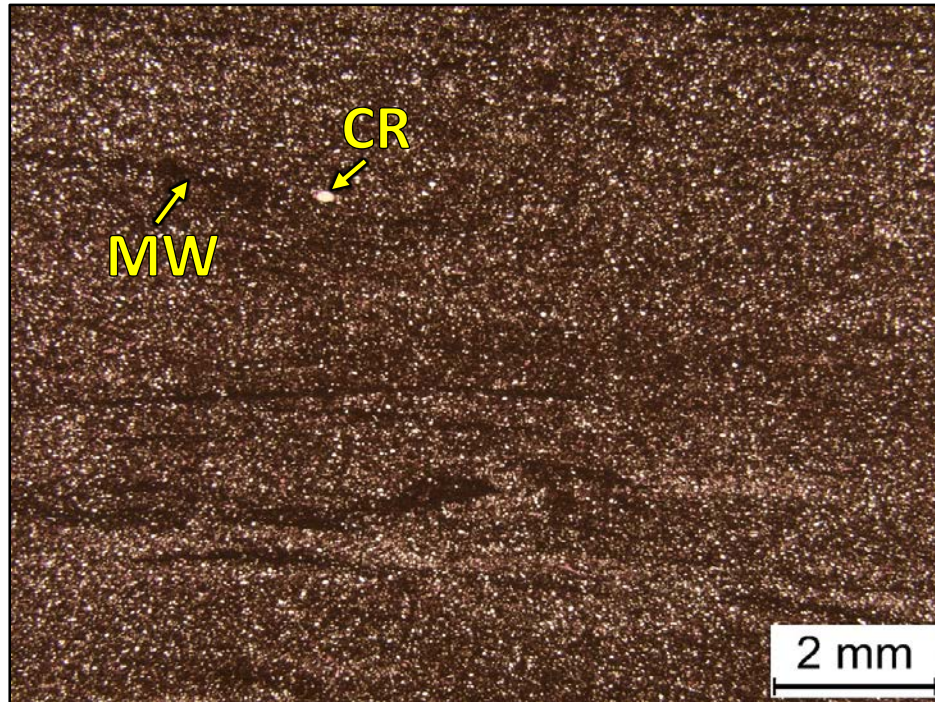
2WN – 5149.80' = Peloidal packstone. Sample is alizarin red stained. Porosity (NCS): 2.1%. Permeability (Klinkenberg): <0.0001 mD. TOC: 0.38%. XRD: 2% clays (1% illite and 1% mixed layer illite/smectite), 62% carbonates (59% calcite and 3% dolomite), and 36% other minerals (26% quartz, 2% potassium feldspar, 6% plagioclase feldspar, 1% pyrite, and 1% apatite). Sample contains crinoid fragments (30%), silt-sized quartz grains (26%), peloids (20%), and undifferentiated microbioclastic debris. Vug porosity observed.



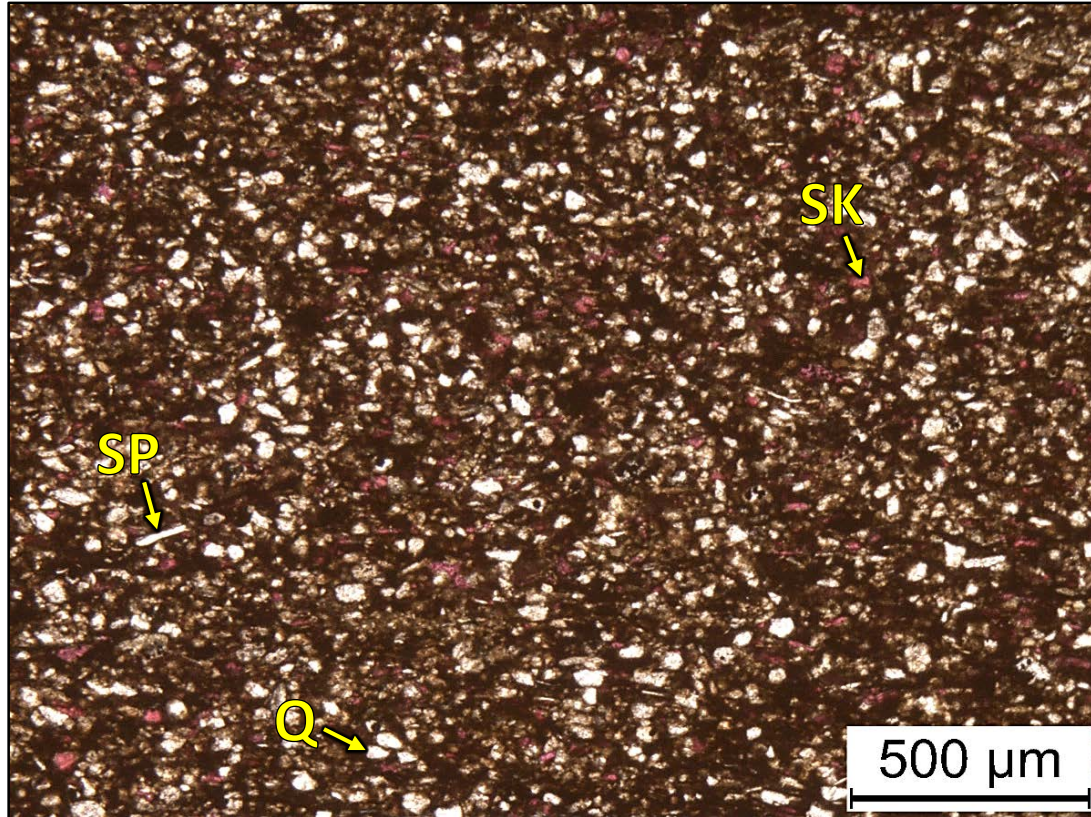
2WN – 5148.40' = Skeletal grainstone. Sample is alizarin red stained. Porosity (NCS): 2.6%. Permeability (Klinkenberg): 0.0001 mD. TOC: 0.15%. XRD: 10% clays (8% illite and 2% mixed layer illite/smectite), 35% carbonates (26% calcite and 9% dolomite), and 55% other minerals (46% quartz, 1% potassium feldspar, 5% plagioclase feldspar, 2% pyrite, and trace amounts of apatite). Sample contains crinoid fragments (23%), sponge spicules (15%), and brachiopod fragments (3%).



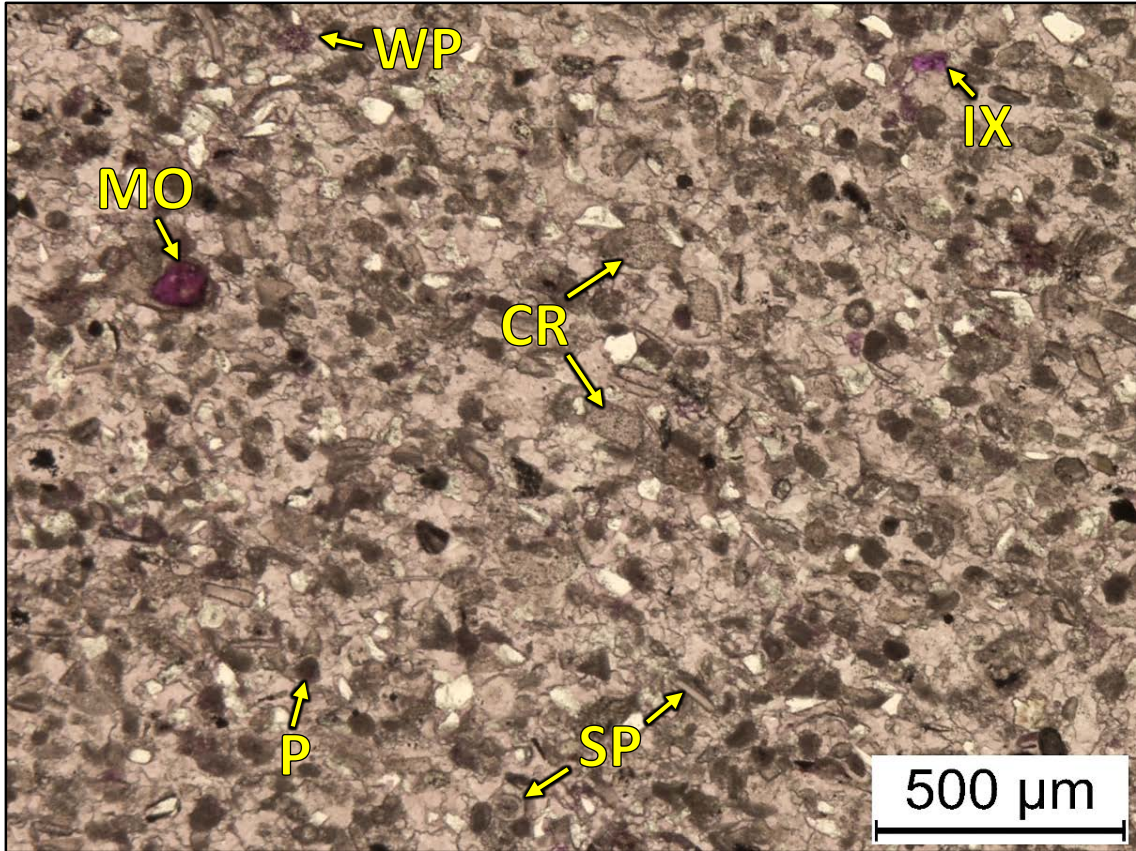
2WN – 5145.90' = Bioturbated mudstone-wackestone. Sample is alizarin red stained. Porosity (NCS): 1.8%. Permeability (Klinkenberg): <0.0001 mD. TOC: 0.57%. XRD: 12% clays (9% illite and 3% mixed layer illite/smectite), 40% carbonates (23% calcite and 17% dolomite), and 48% other minerals (42% quartz, 1% potassium feldspar, 2% plagioclase feldspar, 2% pyrite, and 1% apatite). Sample contains silt-sized quartz grains, sponge spicules (2%), and undifferentiated microbioclastic debris.



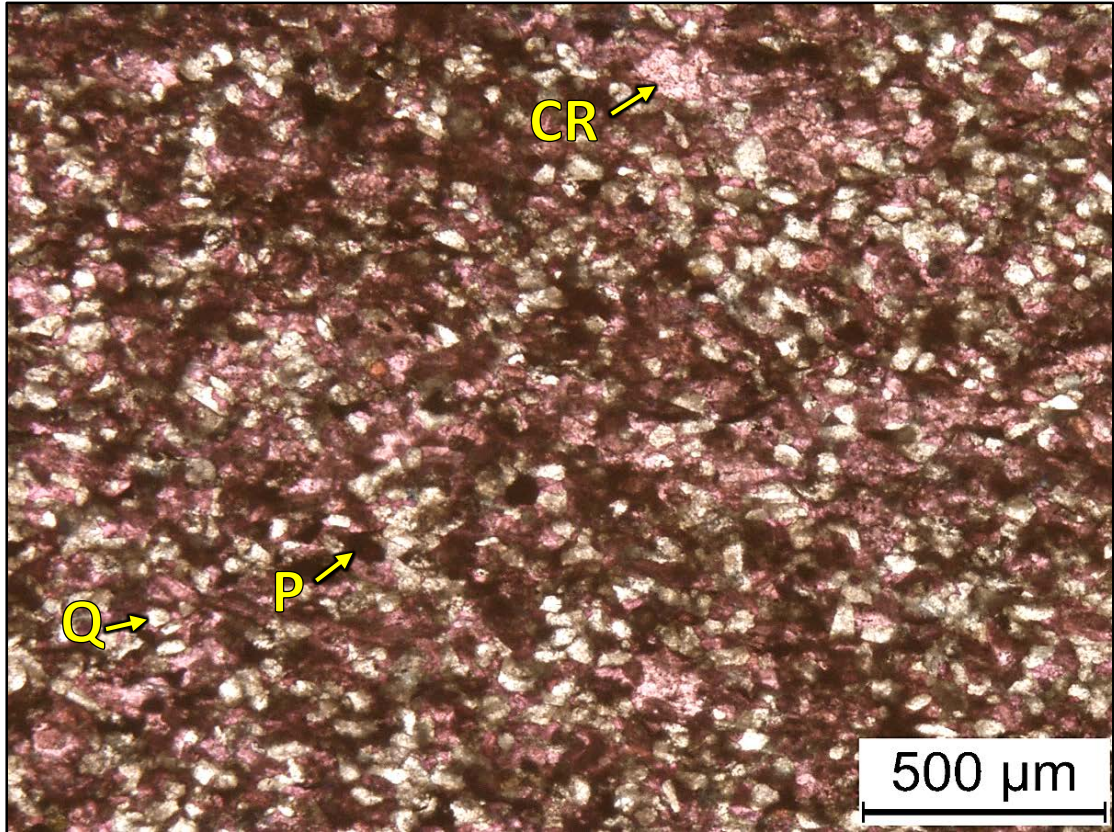
2WN – 5144.75-5145.00' = Calcareous mudstone-wackestone. Sample is alizarin red stained. TOC: 1.91%. XRD: 15% clays (1% chlorite, 11% illite, and 3% mixed layer illite/smectite), 31% carbonates (29% calcite and 2% dolomite), and 54% other minerals (44% quartz, 1% potassium feldspar, 4% plagioclase feldspar, 4% pyrite, and 1% apatite). Sample contains silt-sized quartz grains, sponge spicules (2%), crinoid fragments, and undifferentiated microbioclastic debris.



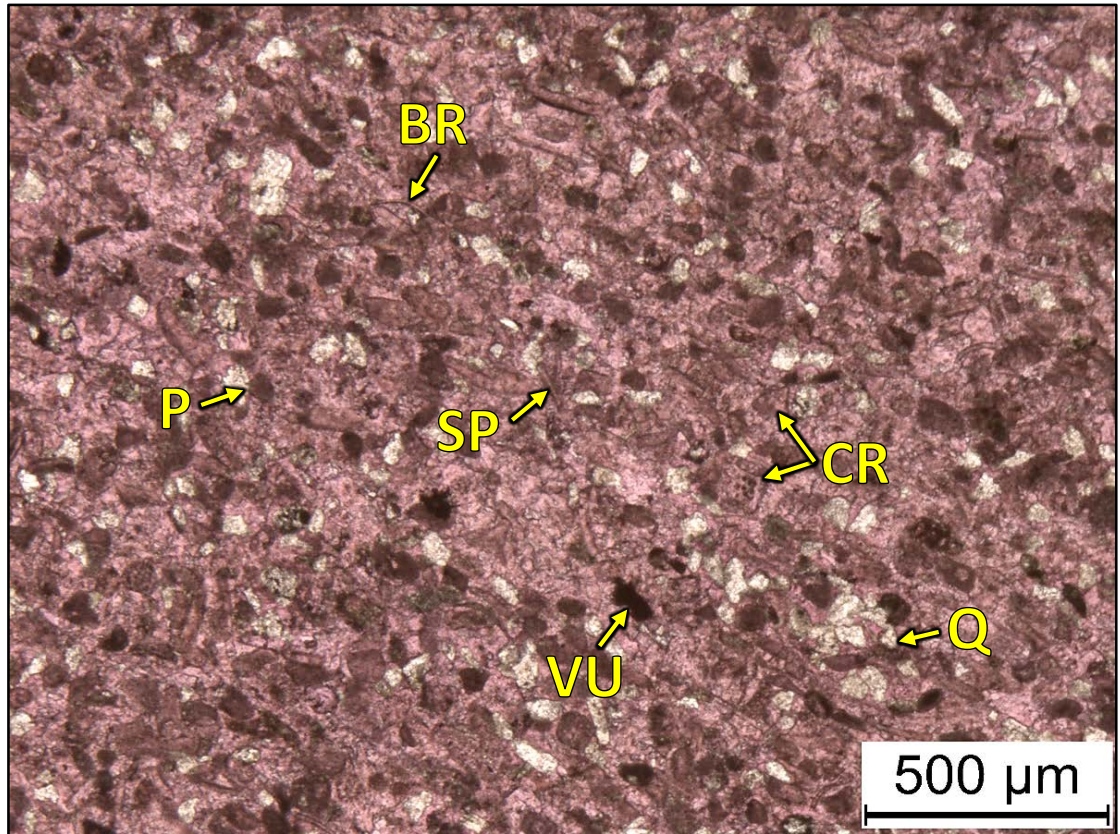
2WN – 5144.00-5144.20' = Calcareous wackestone. Sample is alizarin red stained. TOC: 1.98%. XRD: 23% clays (1% chlorite, 17% illite/mica and 5% mixed layer illite/smectite), 18% carbonates (17% calcite and 1% dolomite), and 59% other minerals (47% quartz, 2% potassium feldspar, 5% plagioclase feldspar, 4% pyrite, and 1% apatite). Sample contains silt-sized quartz grains, sponge spicules (2%), and undifferentiated microbioclastic debris.



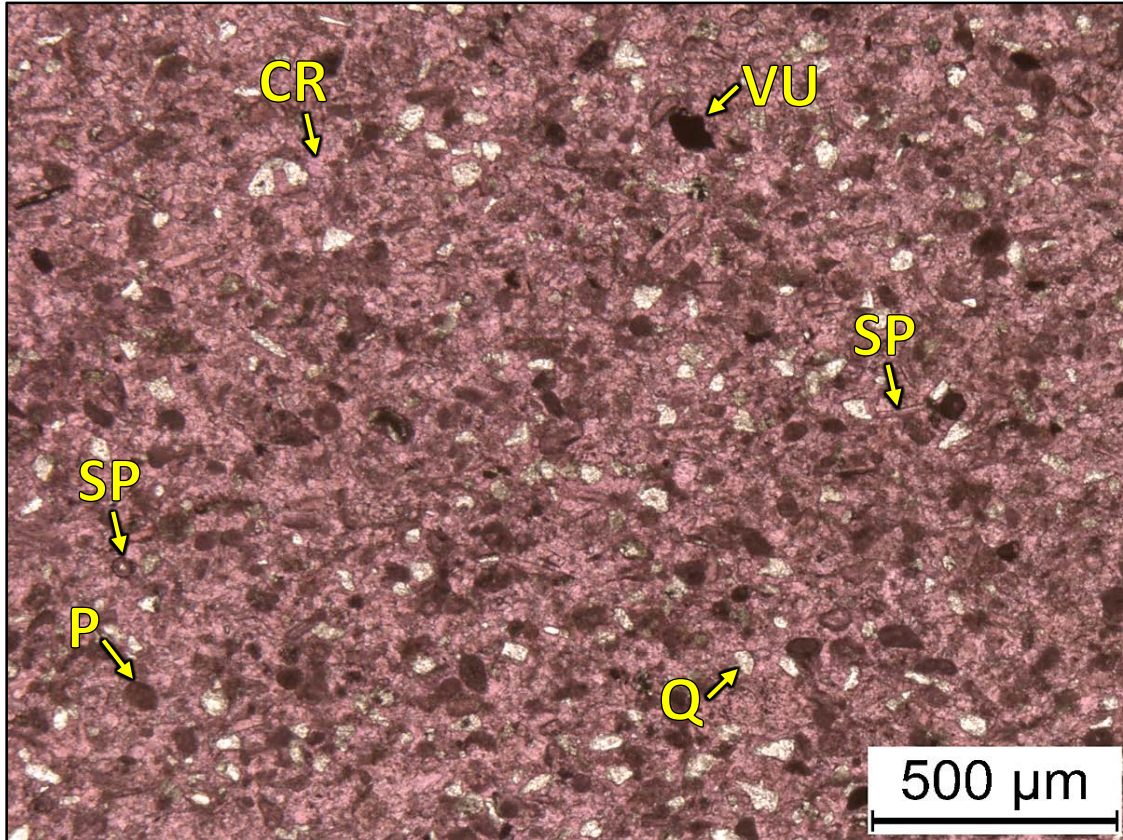
2WN – 5140.25' = Peloidal grainstone. Sample is alizarin red stained. Porosity (NCS): 1.6%. Permeability (Klinkenberg): 0.0001 mD. TOC: 0.08%. XRD: 2% clays (1% illite and 1% mixed layer illite/smectite), 80% carbonates (78% calcite and 2% dolomite), and 18% other minerals (14% quartz, 1% potassium feldspar, 3% plagioclase feldspar, and trace amounts of pyrite and apatite). Sample contains crinoid fragments (15%), peloids (15%), sponge spicules (10%), and silt-sized quartz grains. Intraparticle, moldic, and minor amounts in intercrystalline porosity observed.



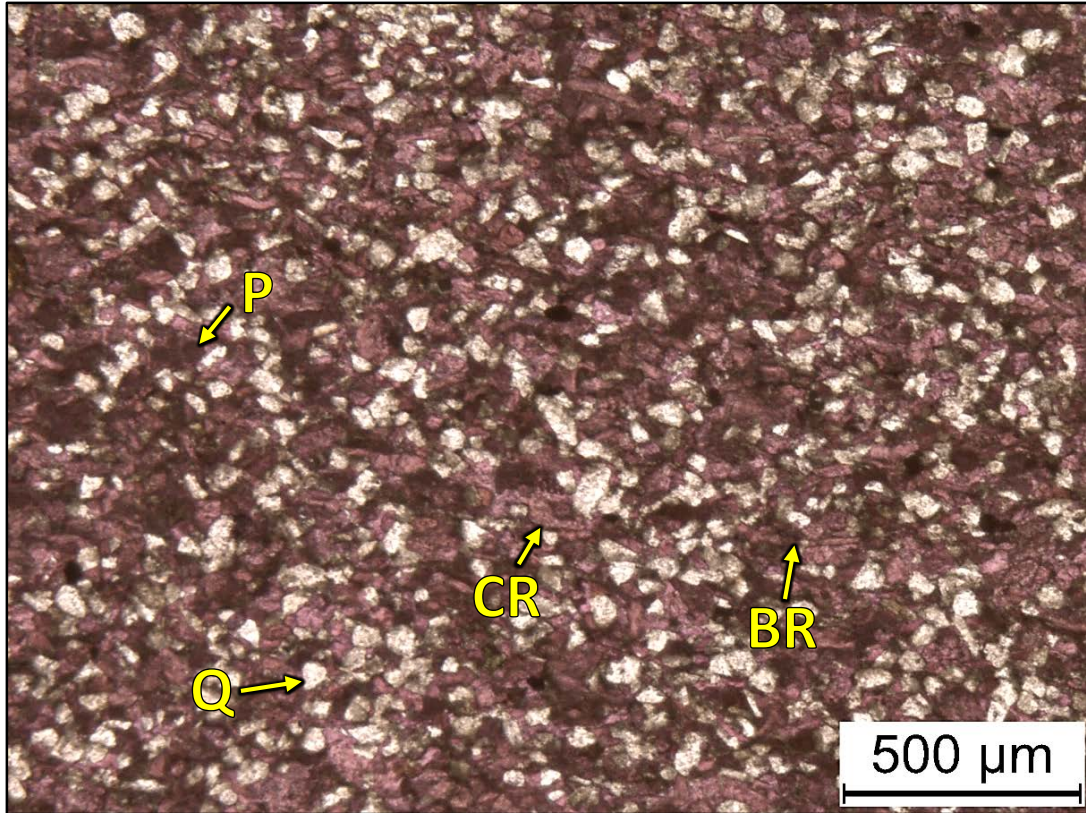
2WN – 5139.15' = Skeletal-peloidal packstone. Sample is alizarin red stained. Porosity (ambient): 4.4%. Permeability (Klinkenberg): Sample was unsuitable for this type of measurement. TOC: 0.25%. XRD: 1% clays (1% mixed layer illite/smectite), 58% carbonates (55% calcite and 3% dolomite), and 41% other minerals (35% quartz, 1% potassium feldspar, 3% plagioclase feldspar, 1% pyrite, and 1% apatite). Sample contains silt-sized quartz grains (35%), crinoid fragments (20%), and undifferentiated microbioclastic debris. Oil-filled moldic and vug porosity observed.



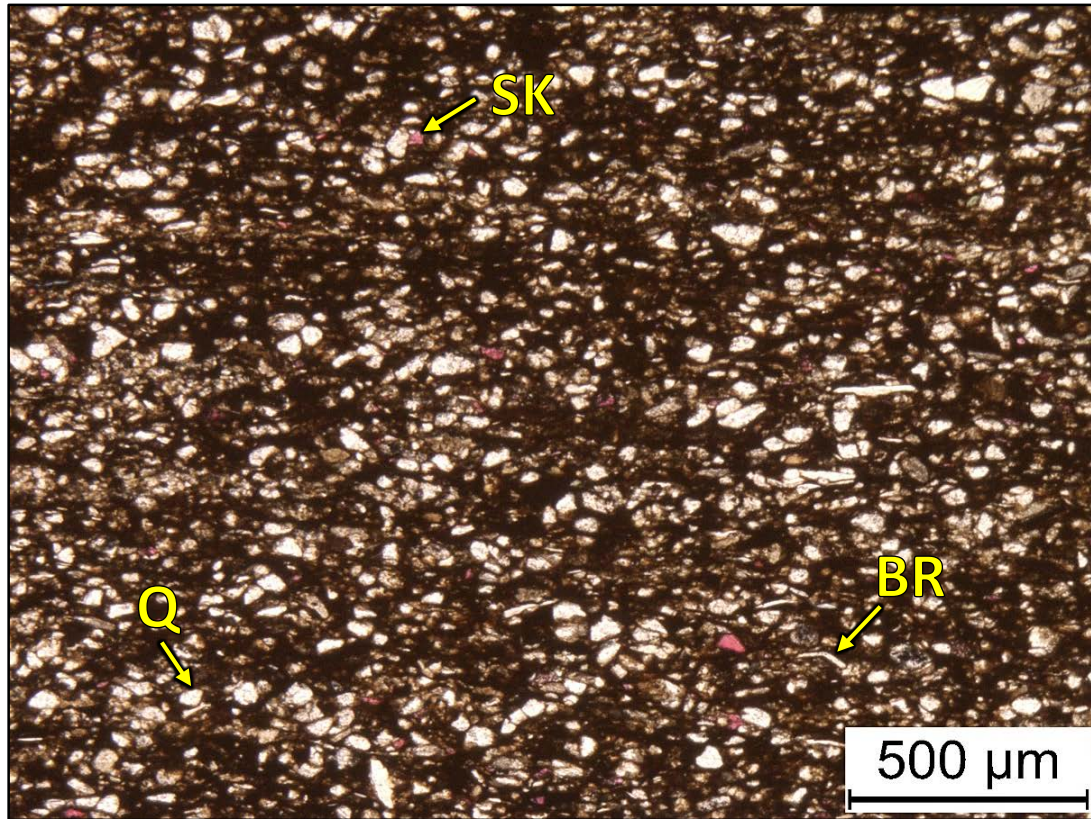
2WN – 5138.35' = Peloidal grainstone. Sample is alizarin red stained. Porosity (NCS): 1.7%. Permeability (Klinkenberg): <0.0001 mD. TOC: 0.05%. XRD: Trace amounts of clays, 79% carbonates (78% calcite and 1% dolomite), and 21% other minerals (17% quartz, 1% potassium feldspar, 3% plagioclase feldspar, and trace amounts of pyrite and apatite). Sample contains silt-sized quartz grains (15%), peloids (15%), sponge spicules (10%), crinoid fragments (10%), brachiopod fragments (1%), and undifferentiated microbioclastic debris.



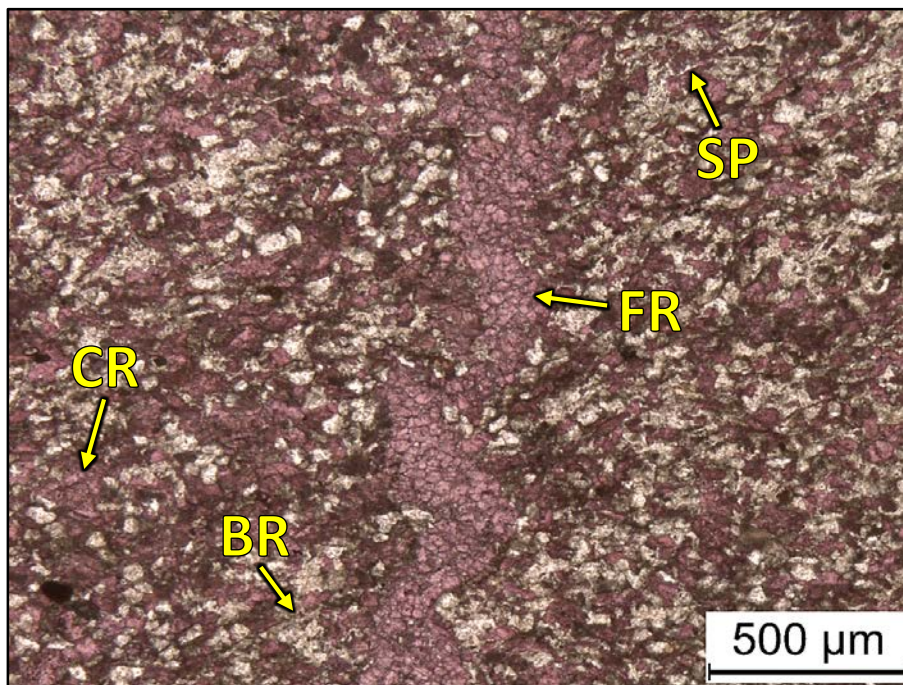
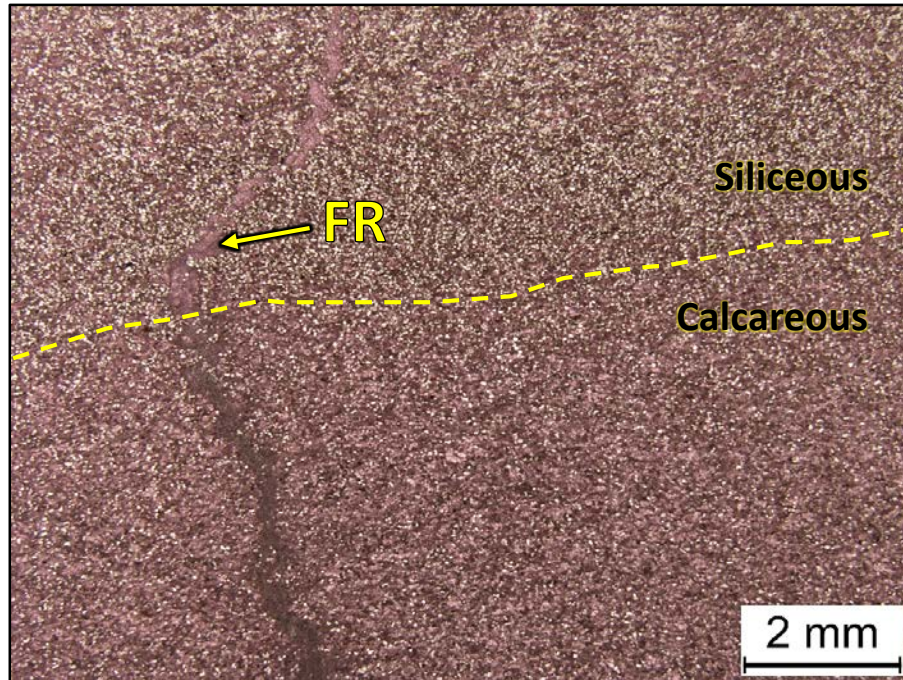
2WN – 5136.60' = Peloidal grainstone. Sample is alizarin red stained. Porosity (NCS): 0.7%. Permeability (Klinkenberg): <0.0001 mD. TOC: 0.05%. XRD: 1% clays (1% illite), 81% carbonates (81% calcite), and 18% other minerals (14% quartz, 1% potassium feldspar, 3% plagioclase feldspar, and trace amounts of pyrite and apatite). Sample contains silt-sized quartz grains (15%), peloids (15%), sponge spicules (10%), crinoid fragments (10%), and undifferentiated microbioclastic debris.



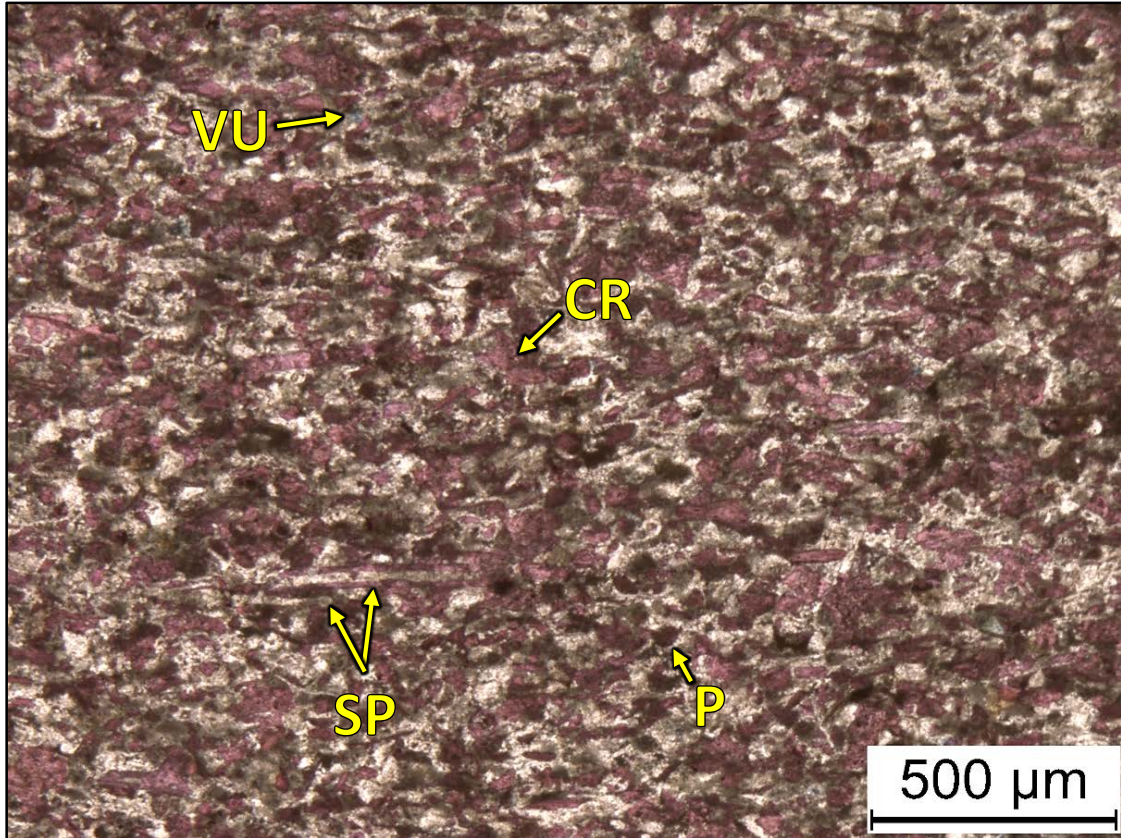
2WN – 5134.25' = Peloidal-skeletal packstone. Sample is alizarin red stained. Porosity (NCS): 1.2%. Permeability (Klinkenberg): <0.0001 mD. TOC: 0.09%. XRD: 2% clays (1% illite and 1% mixed layer illite/smectite), 58% carbonates (58% calcite), and 40% other minerals (34% quartz, 1% potassium feldspar, 4% plagioclase feldspar, trace amounts of pyrite, and 1% apatite). Sample contains silt-sized quartz grains (34%), crinoid fragments (15%), brachiopod fragments (10%), and undifferentiated microbioclastic debris.



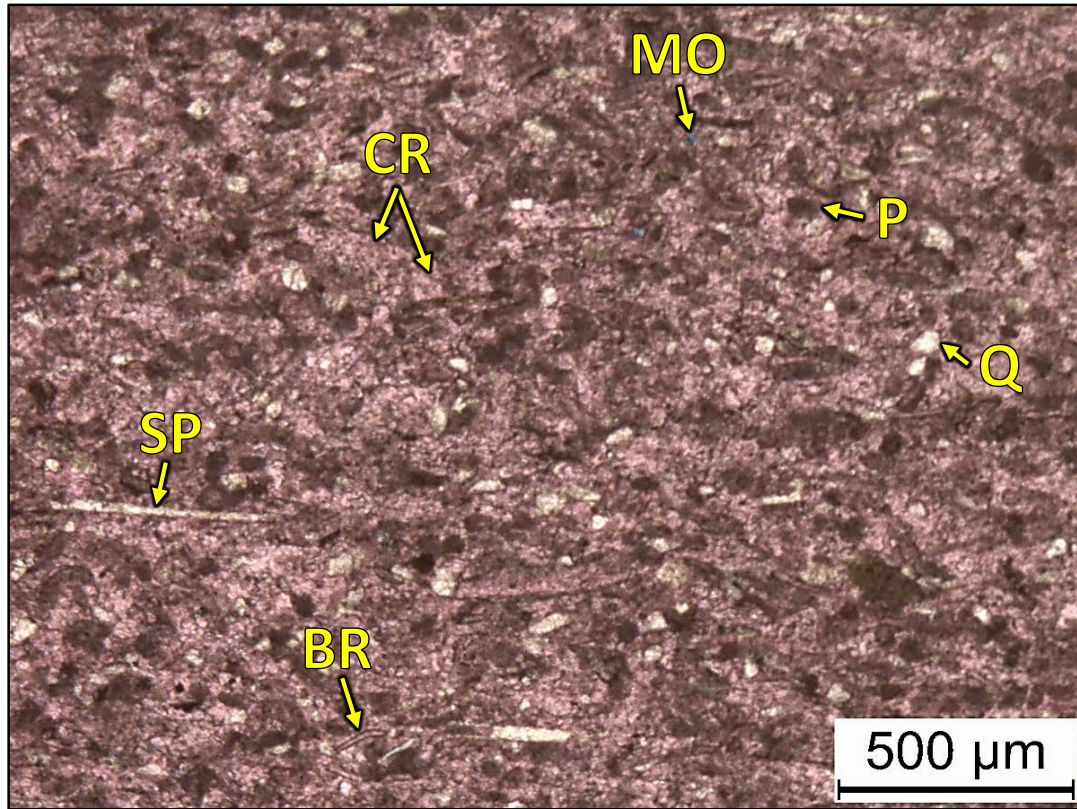
2WN – 5133.60-5133.80' = Calcareous wackestone. Sample is alizarin red stained. TOC: 2.05%. XRD: 34% clays (1% chlorite, 1% kaolinite, 27% illite, and 5% mixed layer illite/smectite), 7% carbonates (7% calcite), and 59% other minerals (48% quartz, 2% potassium feldspar, 3% plagioclase feldspar, 3% pyrite, 2% apatite, and 1% marcasite). Sample contains silt-sized quartz grains (40%), sponge spicules (5%), and undifferentiated microbioclastic debris.



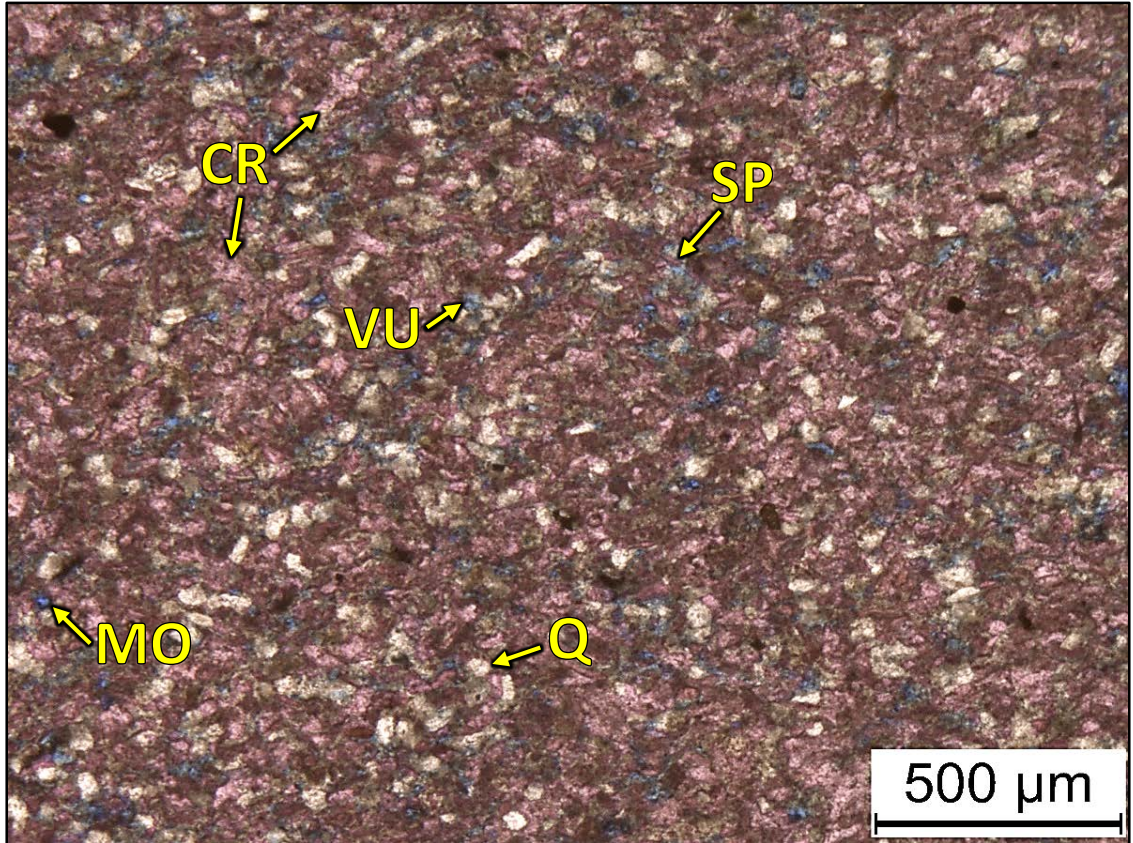
2WN – 5132.75' = Skeletal grainstone. Sample is alizarin red stained. Porosity (NCS): 2.8%. Permeability (Klinkenberg): <0.0001 mD. TOC: 0.06%. XRD: 8% clays (7% illite and 1% mixed layer illite/smectite), 30% carbonates (30% calcite), and 62% other minerals (53% quartz, 1% potassium feldspar, 5% plagioclase feldspar, trace amounts of pyrite, and 3% apatite). Sample contains silt-sized quartz grains (50%), crinoid fragments (35%), and lesser amounts of sponge spicules and brachiopod fragments. Ptygmatic fracture is filled with blocky calcite cement.



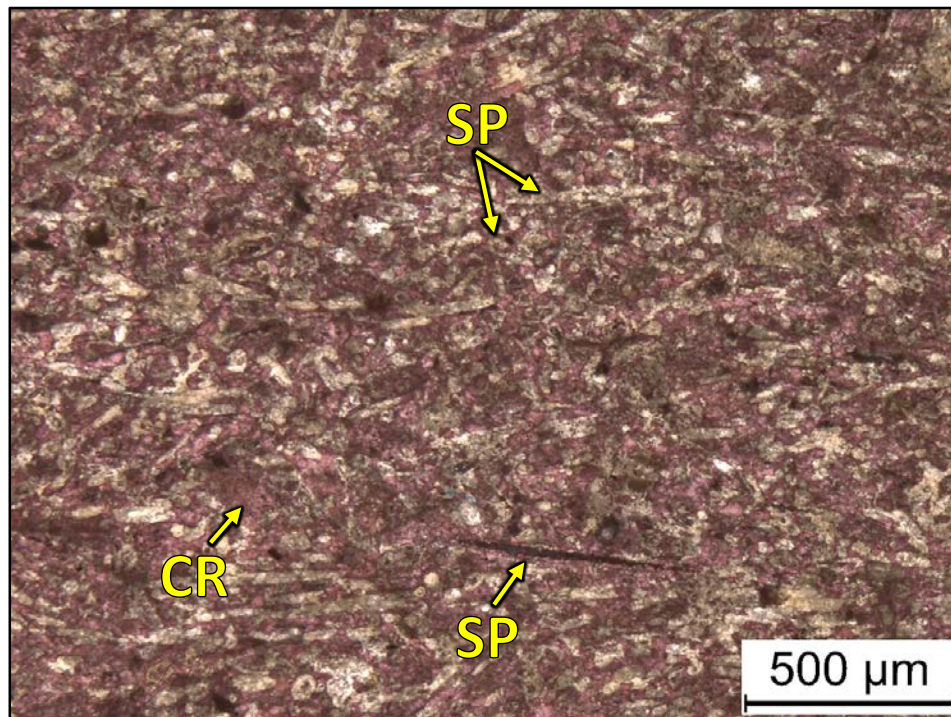
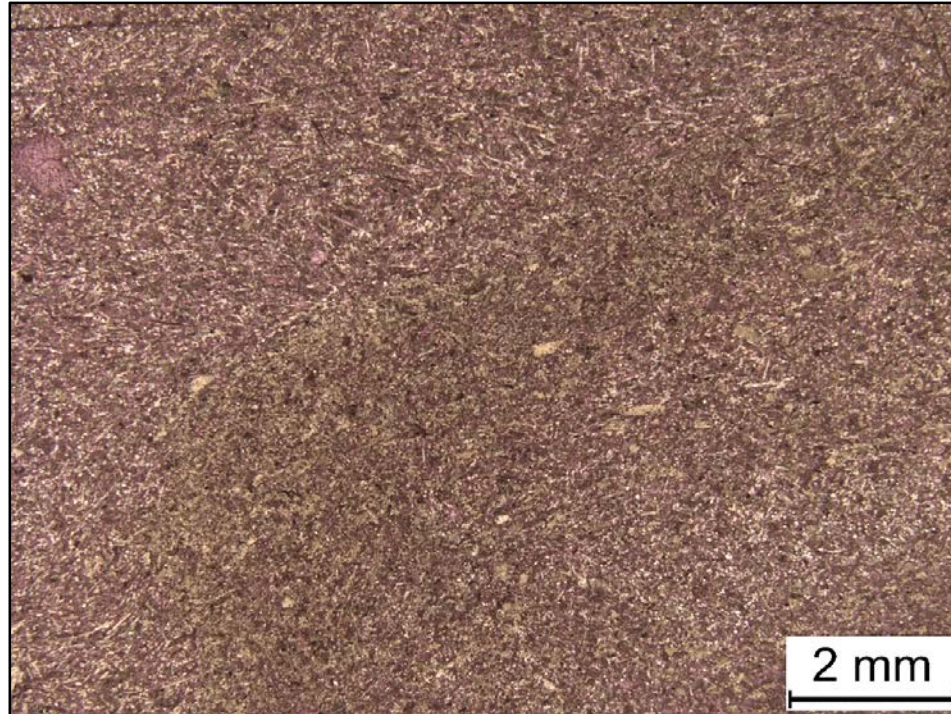
2WN – 5132.25' = Skeletal grainstone. Sample is alizarin red stained and blue epoxy impregnated. Porosity (NCS): 2.7%. Permeability (Klinkenberg): <0.0001 mD. TOC: 0.19%. XRD: 1% clays (1% illite), 39% carbonates (39% calcite), and 60% other minerals (58% quartz, 1% potassium feldspar, 1% plagioclase feldspar, and trace amounts of pyrite and apatite). Sample contains crinoid fragments (30%), sponge spicules (15%), and peloids (10%). Oil-filled vug porosity and intracrystalline porosity observed.



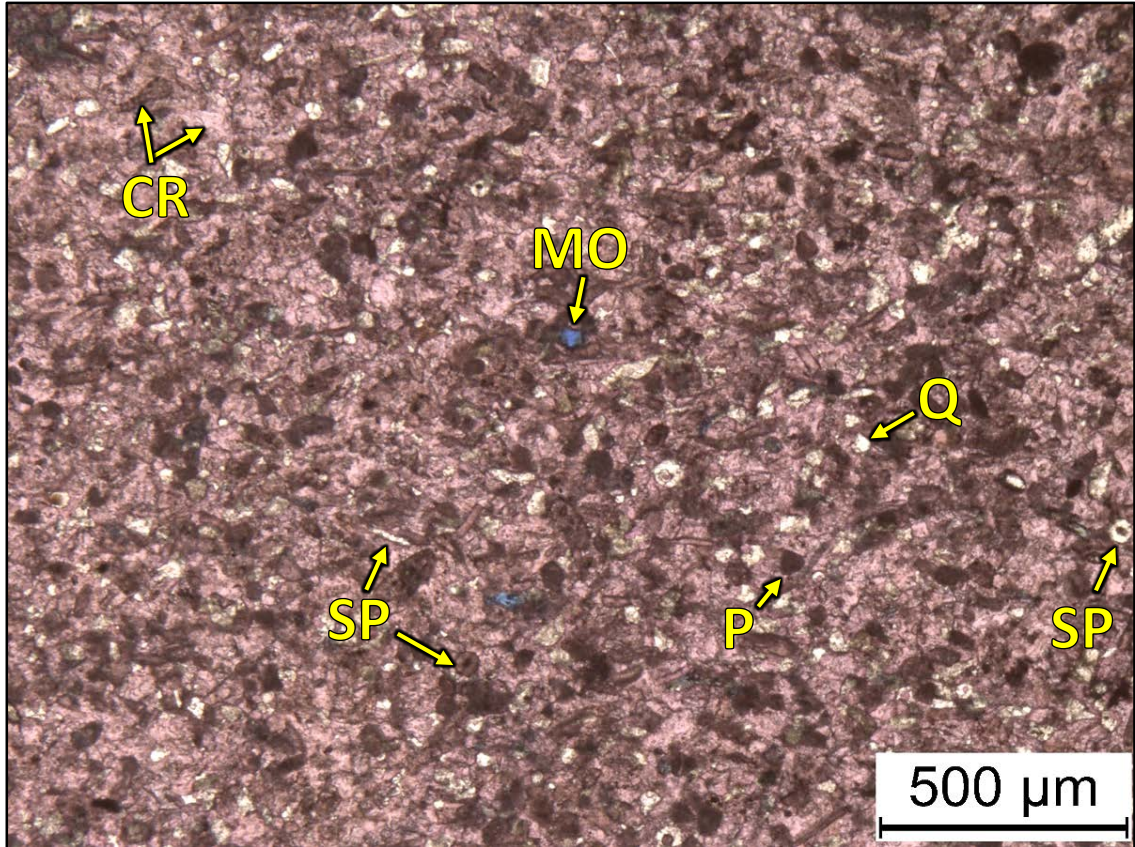
2WN – 5131.75' = Peloidal-skeletal grainstone. Sample is alizarin red stained. Porosity (NCS): 1.6%. Permeability (Klinkenberg): <0.0001 mD. TOC: 0.04%. XRD: 1% clays (1% illite), 78% carbonates (78% calcite), and 21% other minerals (17% quartz, 1% potassium feldspar, 2% plagioclase feldspar, 1% pyrite, and trace amounts of apatite). Sample contains crinoid fragments, sponge spicules (10-15%), peloids (15%), silt-sized quartz grains (10%), and brachiopod fragments (5%).



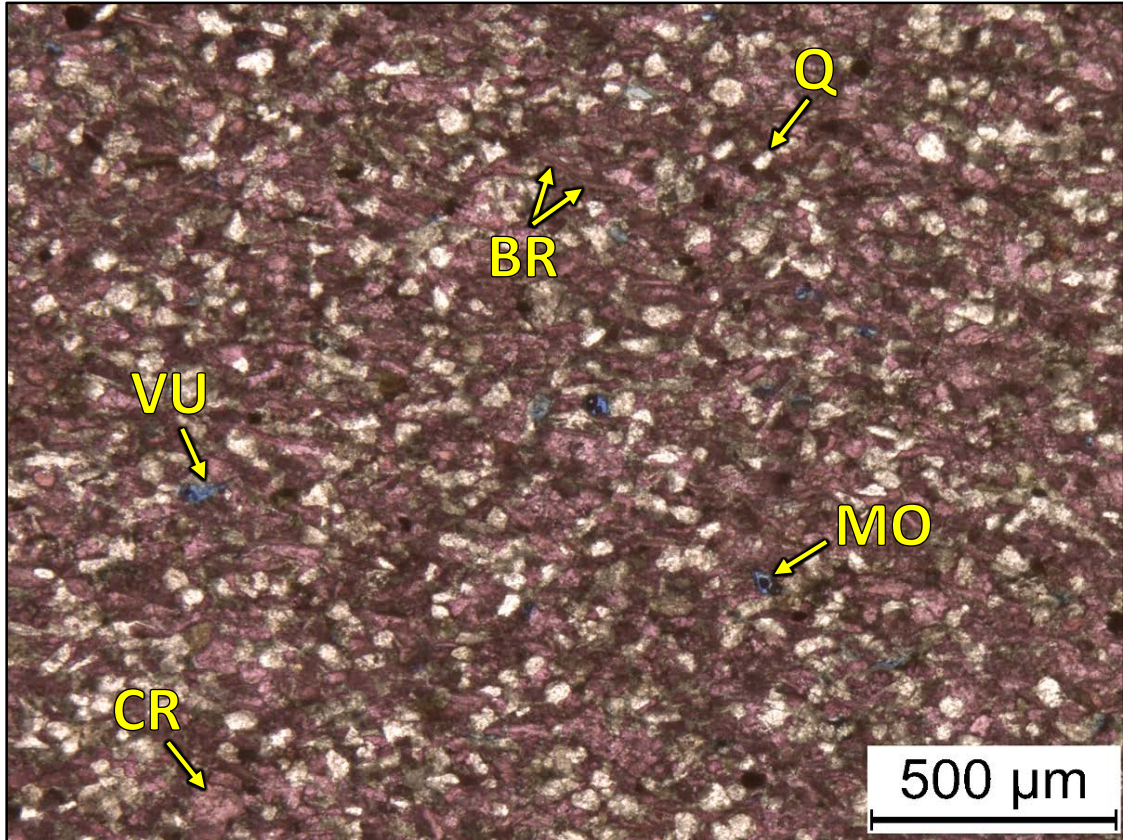
2WN – 5129.75' = Peloidal-skeletal grainstone. Sample is alizarin red stained and blue epoxy impregnated. Porosity (NCS): 6.5%. Permeability (Klinkenberg): 0.0082 mD. TOC: 0.23%. XRD: 2% clays (1% kaolinite and 1% illite), 52% carbonates (52% calcite), and 46% other minerals (43% quartz, 1% potassium feldspar, 2% plagioclase feldspar, and trace amounts of pyrite and apatite). Sample contains crinoid fragments (25%), silt-sized quartz grains (20%), and undifferentiated microbioclastic debris. Open and oil-filled moldic and vug porosity observed.



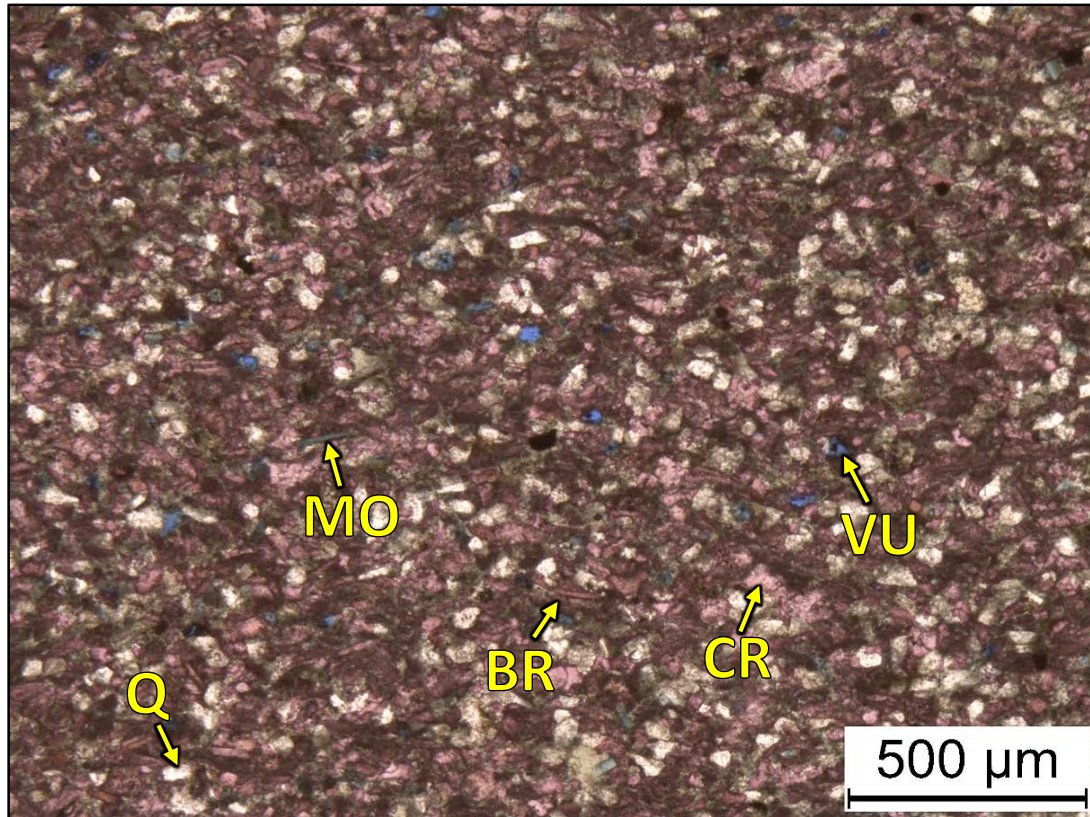
2WN – 5129.30' = Spiculitic grainstone. Sample is alizarin red stained. Porosity (NCS): 0.8%. Permeability (Klinkenberg): <0.0001 mD. TOC: 0.06%. XRD: Trace amounts of clays, 48% carbonates (48% calcite), and 52% other minerals (50% quartz, 1% potassium feldspar, 1% plagioclase feldspar, and trace amounts of pyrite). Sample contains sponge spicules (50%) and crinoid fragments (25%). Minor amounts of moldic porosity observed.



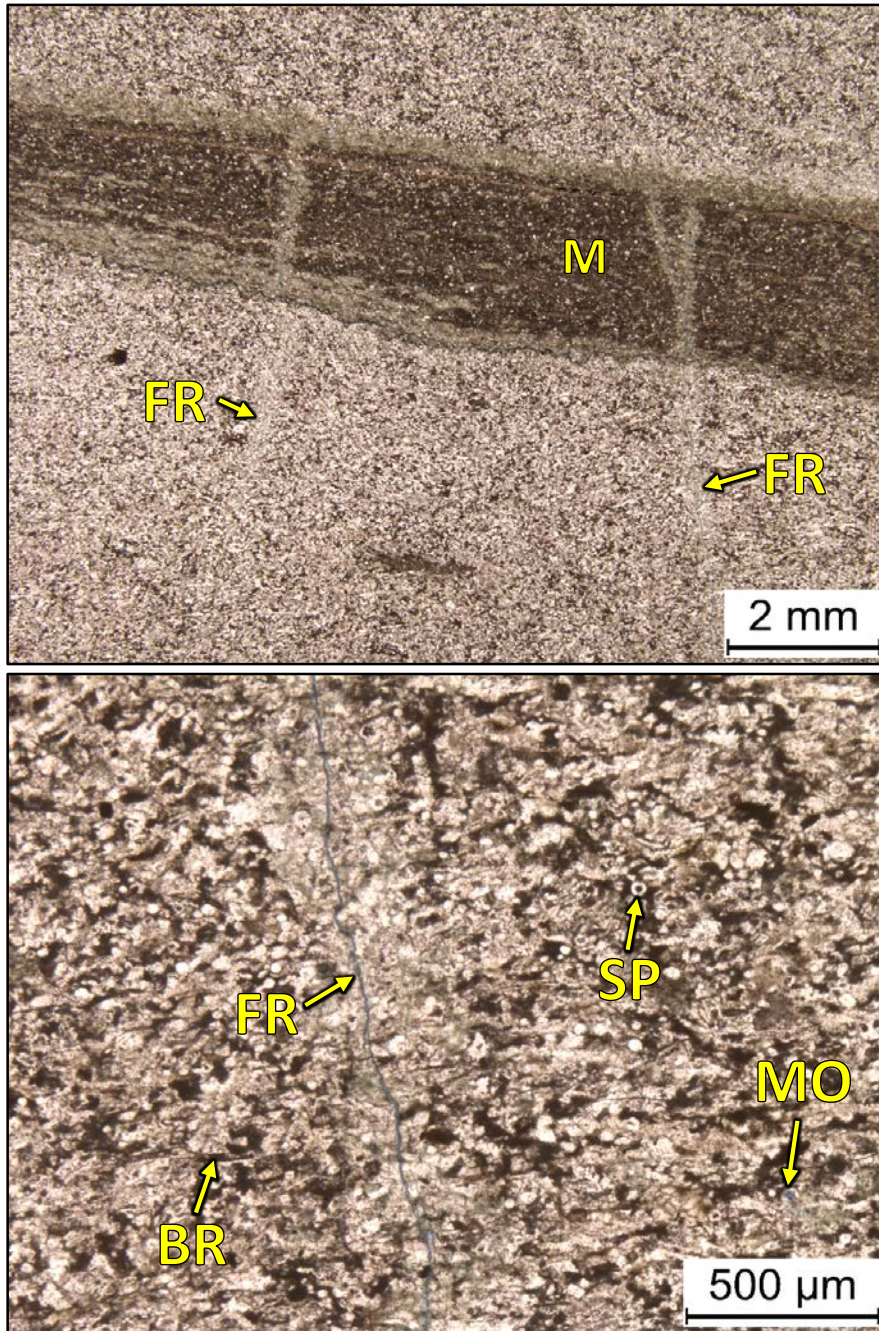
2WN – 5127.35' = Peloidal grainstone. Sample is alizarin red stained and blue epoxy impregnated. Porosity (ambient): 3.2%. Permeability (Klinkenberg): Sample was unsuitable for this type of measurement. TOC: 0.05%. XRD: 1% clays (1% illite), 79% carbonates (79% calcite), and 20% other minerals (17% quartz, 1% potassium feldspar, 1% plagioclase feldspar, trace amounts of pyrite, and 1% apatite). Sample contains crinoid fragments, peloids (20%), and sponge spicules (10%). Moldic and vug porosity observed.



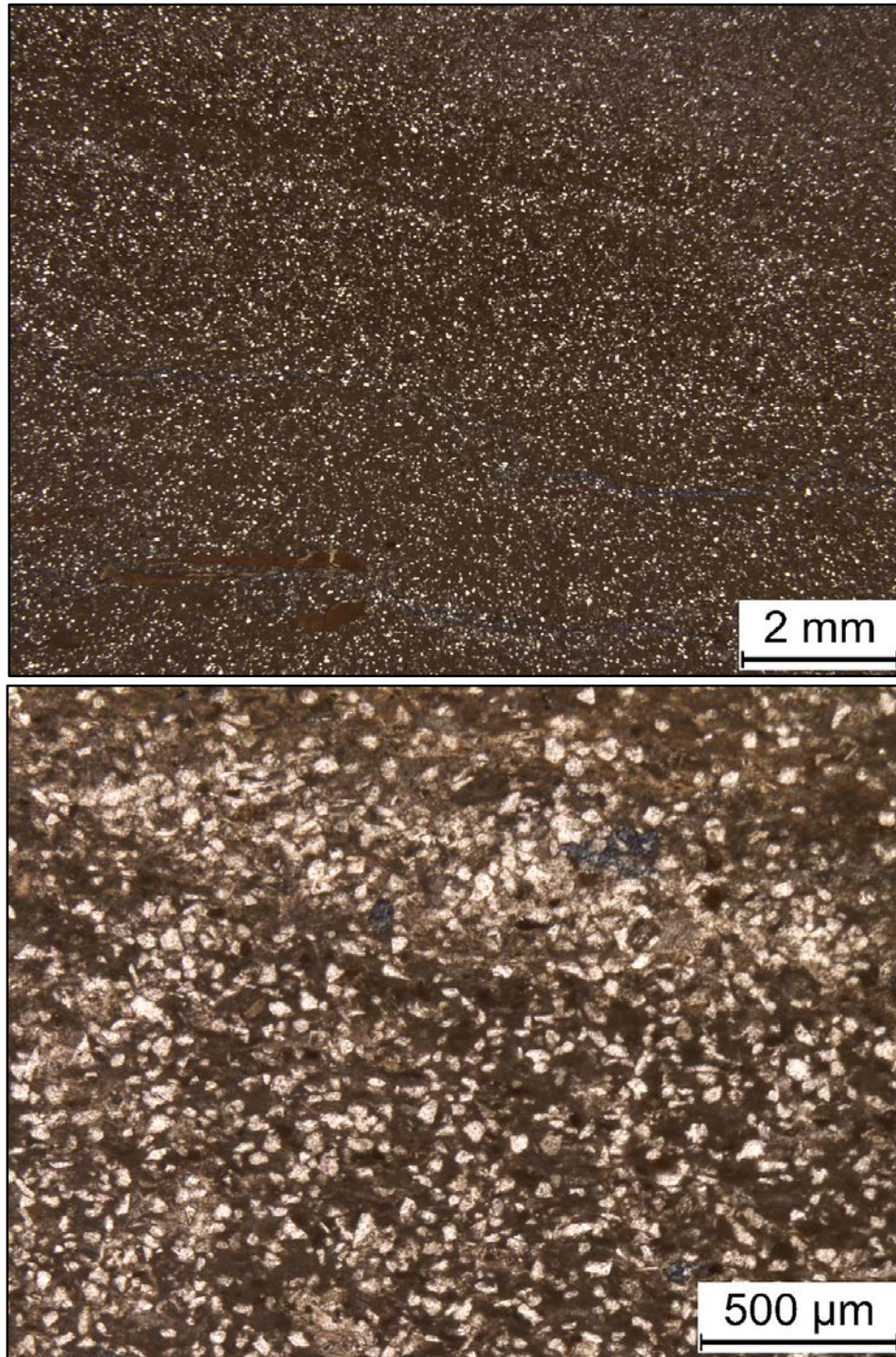
2WN – 5126.80' = Skeletal-peloidal grainstone. Sample is alizarin red stained and blue epoxy impregnated. Porosity (NCS): 4.6%. Permeability (Klinkenberg): 0.0002 mD. TOC: 0.16%. XRD: 3% clays (1% kaolinite and 2% illite), 54% carbonates (53% calcite and 1% siderite), and 43% other minerals (39% quartz, 1% potassium feldspar, 1% plagioclase feldspar, trace amounts of pyrite, and 2% apatite). Sample contains silt-sized quartz grains (39%), crinoid fragments (20%), and brachiopod fragments (15%). Moldic and vug porosity observed.



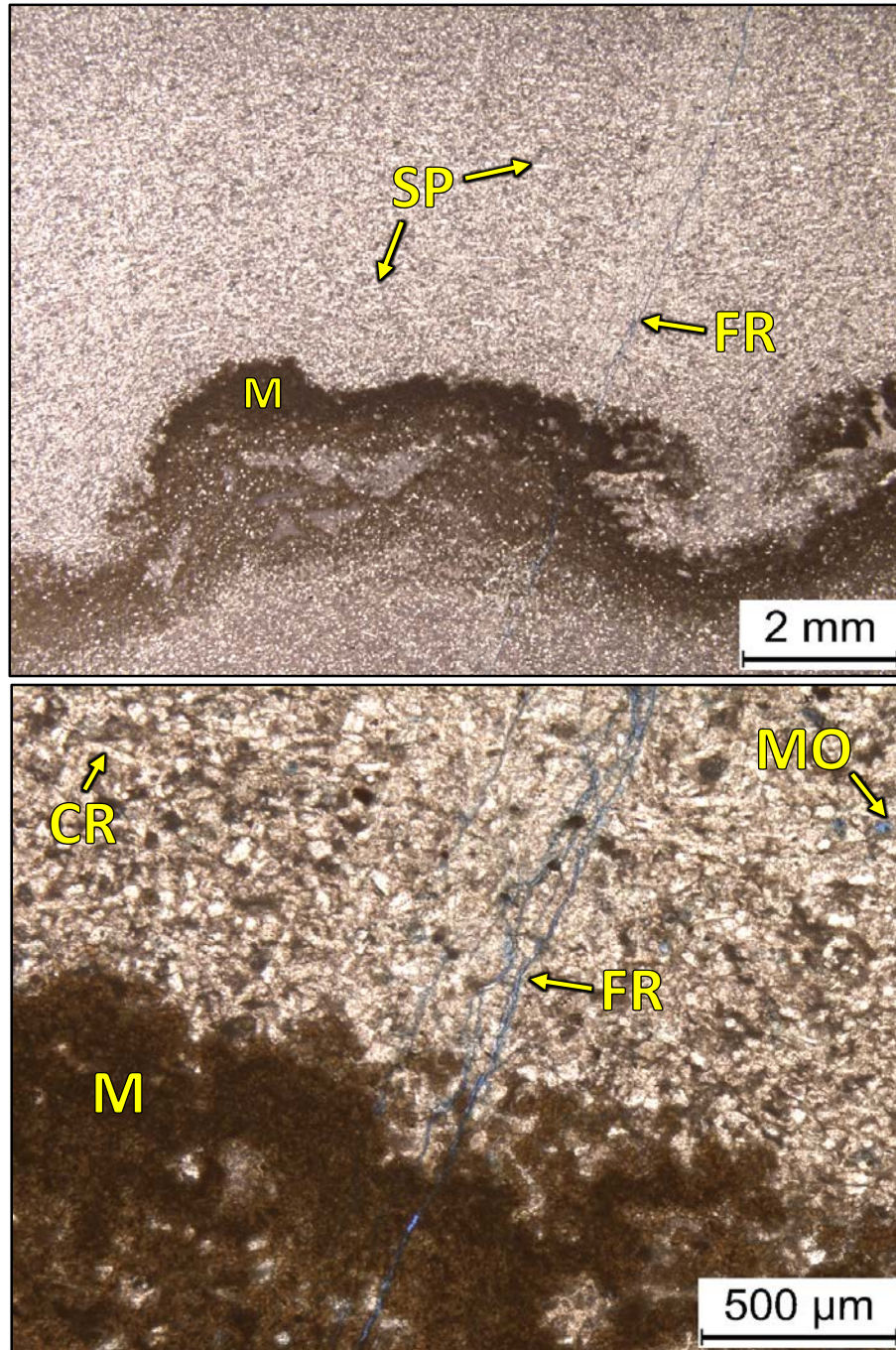
2WN – 5126.40' = Skeletal-peloidal packstone. Sample is alizarin red stained and blue epoxy impregnated. Porosity (ambient): 5.9%. Permeability (Klinkenberg): Sample was unsuitable for this type of analysis. TOC: 0.27%. XRD: 4% clays (1% kaolinite and 3% illite), 42% carbonates (41% calcite and 1% dolomite), and 54% other minerals (48% quartz, 2% potassium feldspar, 2% plagioclase feldspar, trace amounts of pyrite, and 2% apatite). Sample contains silt-sized quartz grains (39%), crinoid fragments (20%), and brachiopod fragments (15%). Moldic and vug porosity observed.



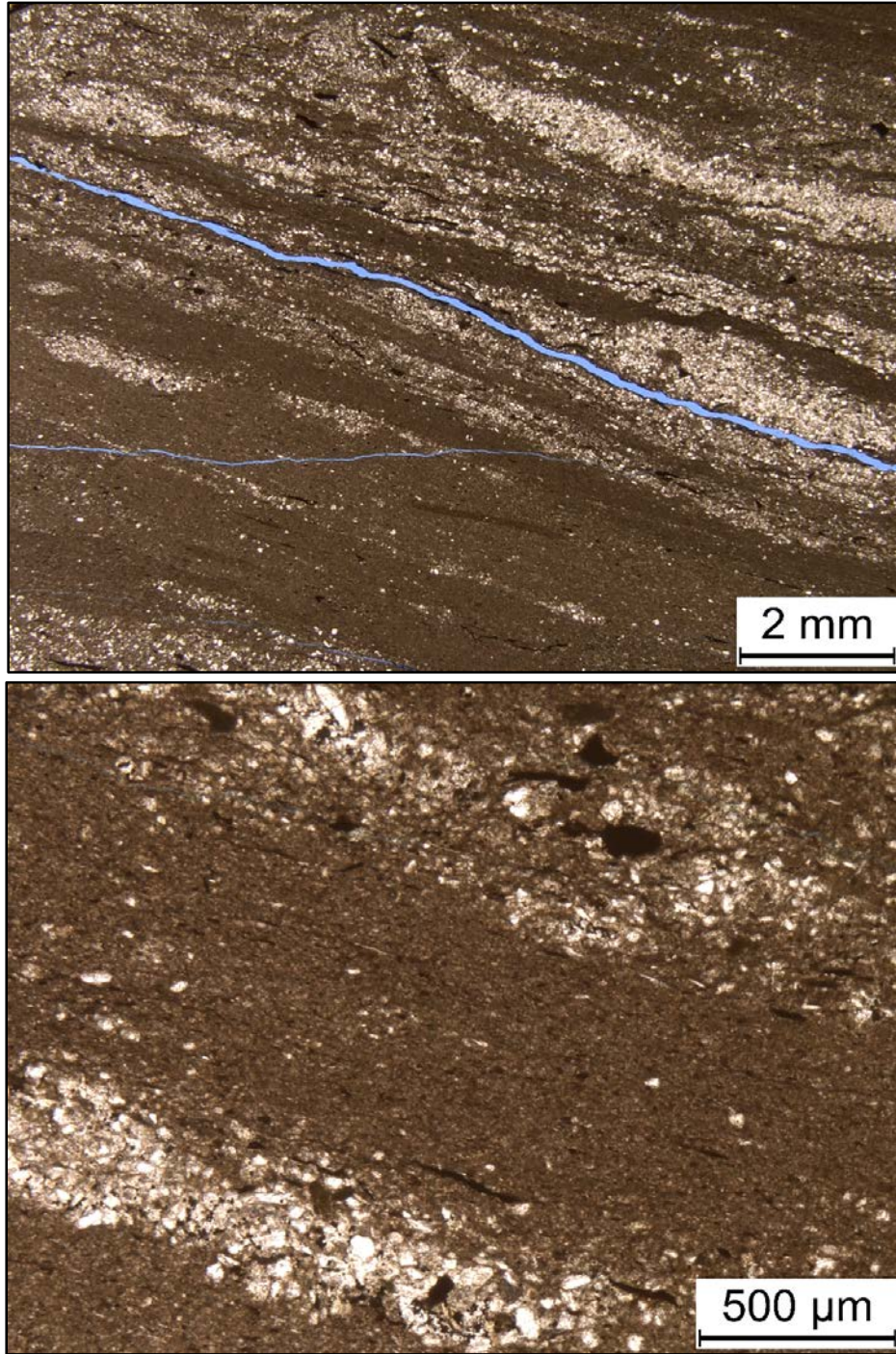
2WN – 5124.55' = Silicified skeletal grainstone. Sample is alizarin red stained and blue epoxy impregnated. Porosity (NCS): 4.6%. Permeability (Klinkenberg): <0.0001 mD. TOC: 0.06%. XRD: 3% clays (1% kaolinite and 2% illite), trace amounts of carbonates, and 97% other minerals (93% quartz, 2% potassium feldspar, 1% plagioclase feldspar, trace amounts of pyrite, and 1% apatite). Sample contains silicified crinoid grains, brachiopod fragments, and sponge spicules. Micro-fractures within sample show porosity and permeability, and terminate into thin, mud-rich interval. Fracture and moldic porosity is observed.



2WN – 5124.10' = Siltstone. Sample is alizarin red stained and blue epoxy impregnated. Porosity (NCS): 9.5%. Permeability (Klinkenberg): 0.0037 mD. TOC: 0.33%. XRD: 7% clays (1% kaolinite and 6% illite), 1% carbonates (trace amounts of calcite and 1% siderite), and 92% other minerals (85% quartz, 2% potassium feldspar, 2% plagioclase feldspar, 1% pyrite, and 2% of apatite). Sample contains abundant quartz and detrital minerals.



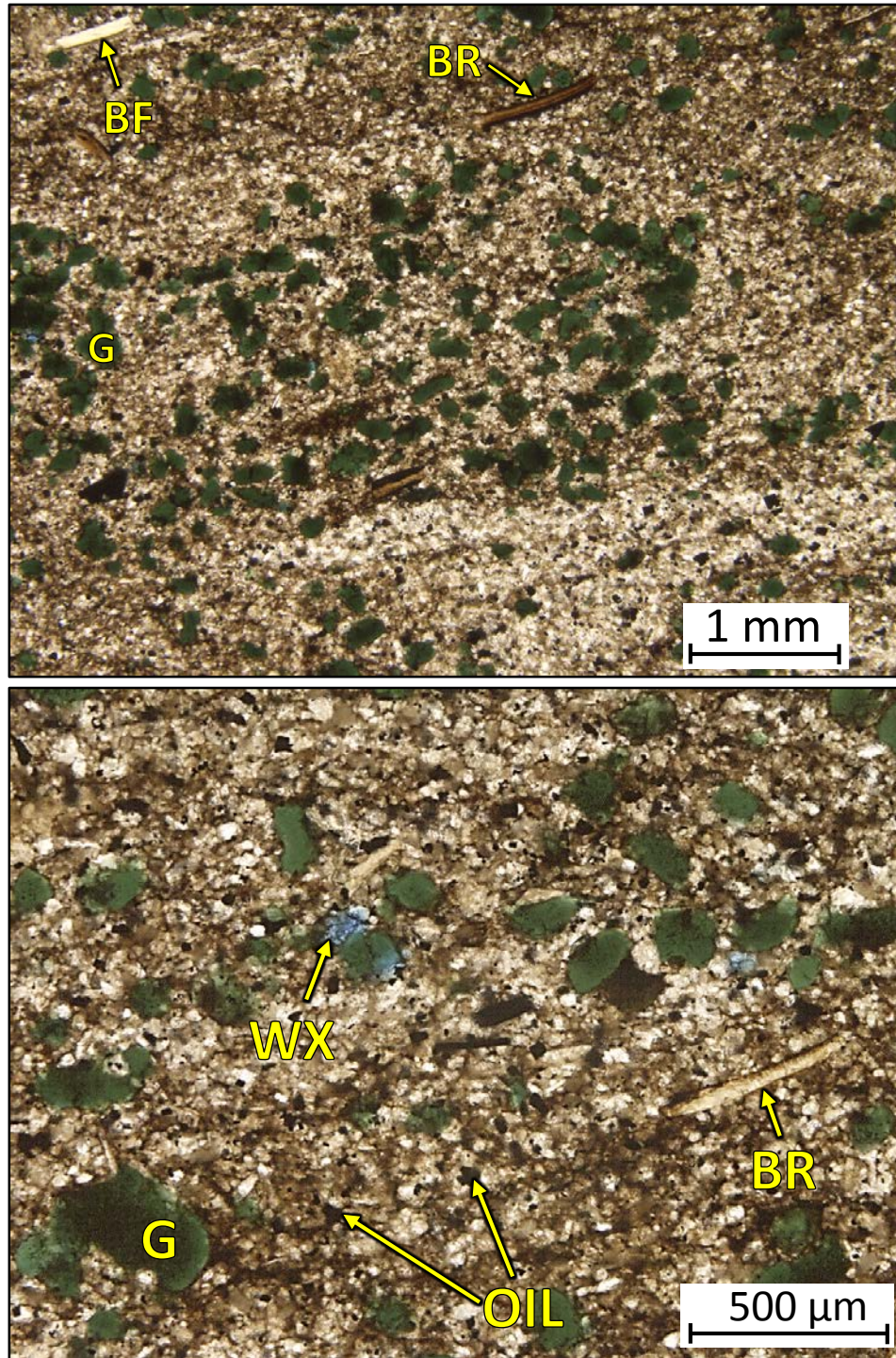
2WN – 5123.70' = Silicified skeletal grainstone. Sample is alizarin red stained and blue epoxy impregnated. Porosity (ambient): 3.0%. Permeability (Klinkenberg): Sample was unsuitable for this type of measurement. TOC: 0.18%. XRD: 4% clays (2% kaolinite and 2% illite), 6% carbonates (6% siderite), and 90% other minerals (87% quartz, 2% potassium feldspar, 1% plagioclase feldspar, and trace amounts of pyrite). Sample is composed of silicified skeletal fragments, dominantly sponge spicules (15%). Micro-fractures within sample show porosity and permeability. Moldic porosity is also observed within the sample.



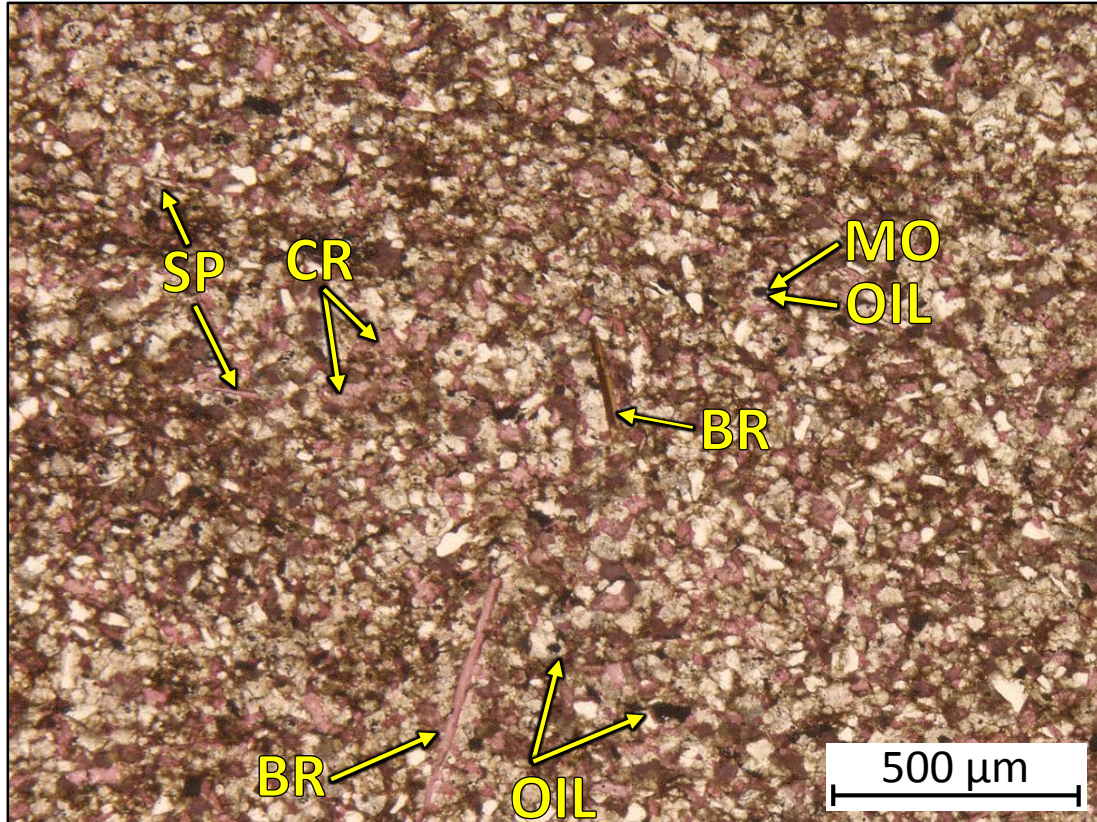
2WN – 5123.20' = Pennsylvanian shale-siltstone. Sample is alizarin red stained and blue epoxy impregnated. Porosity (ambient): 6.0%. Permeability (Klinkenberg): Sample was unsuitable for this type of measurement. TOC: 0.64%. XRD: 48% clays (13% chlorite, 7% kaolinite, 26% illite, and 2% mixed layer illite/smectite), 1% carbonates (trace amounts of calcite and 1% siderite), and 51% other minerals (35% quartz, 2% potassium feldspar, 14% plagioclase feldspar, trace amounts of pyrite and apatite). Sample contains thin, grainy, quartz-rich intervals.

Core #3

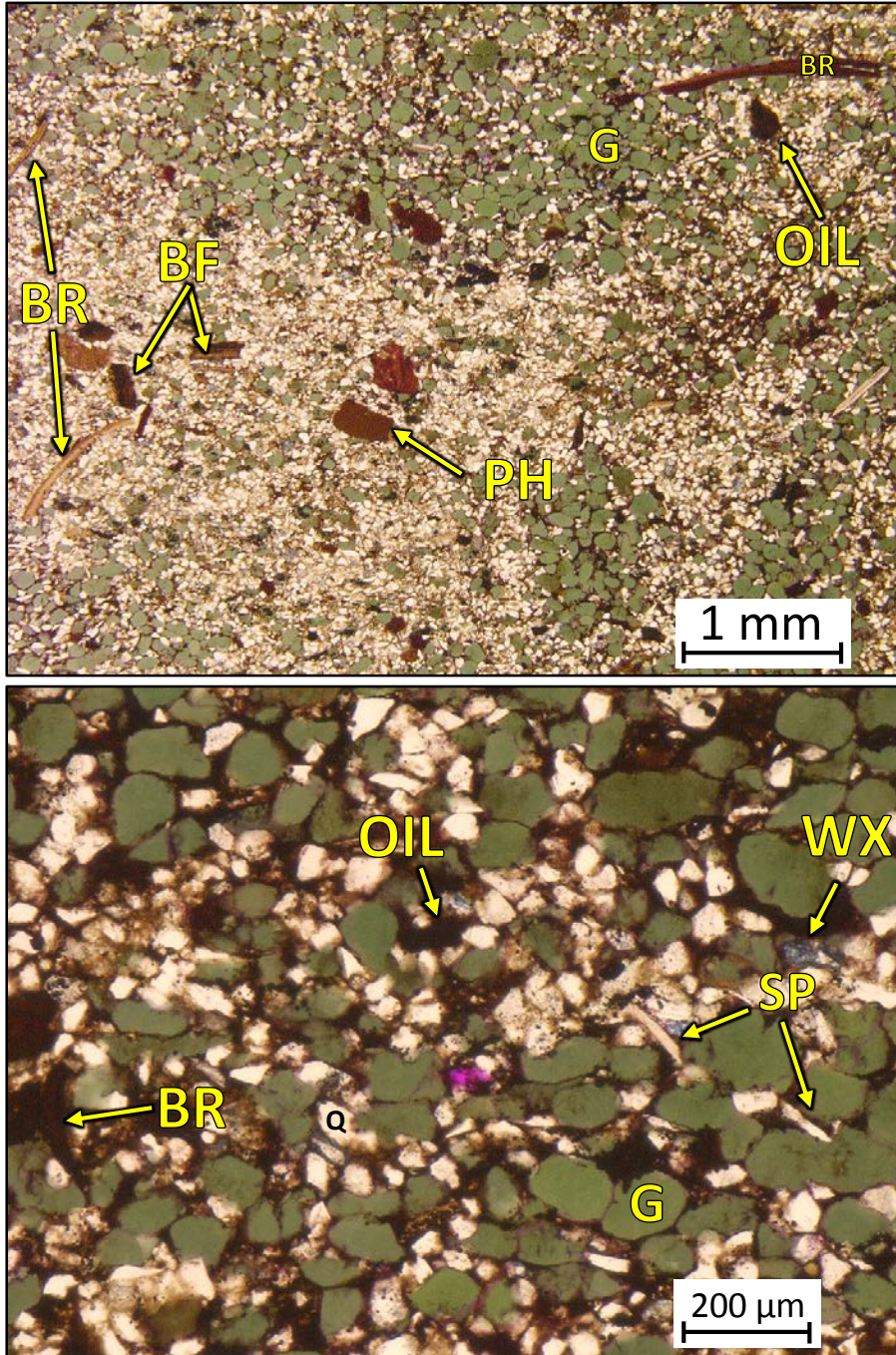
Elinore #1-18 SWD



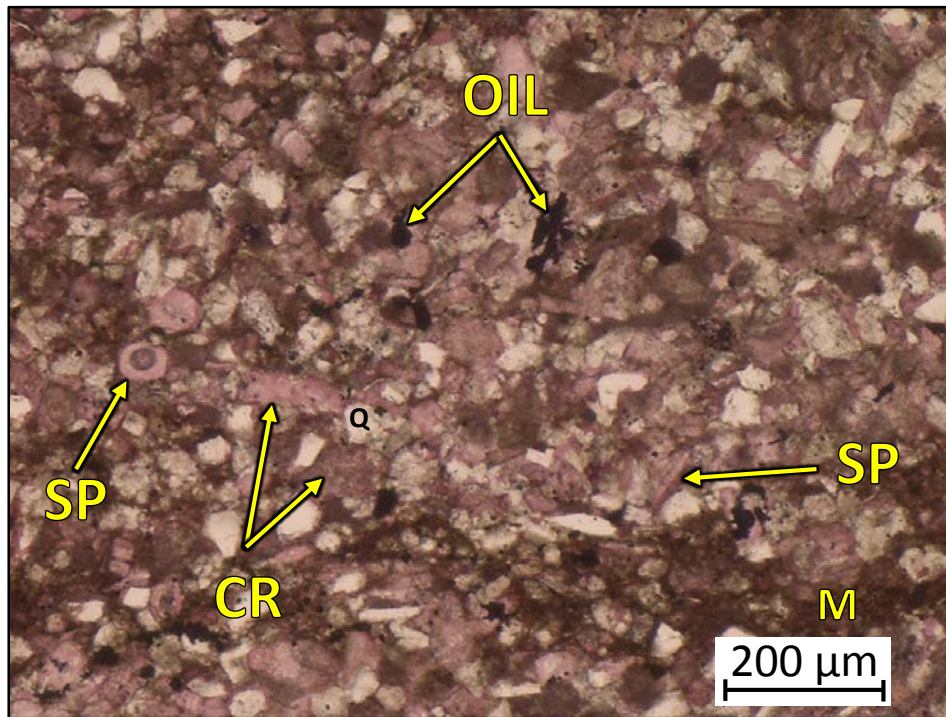
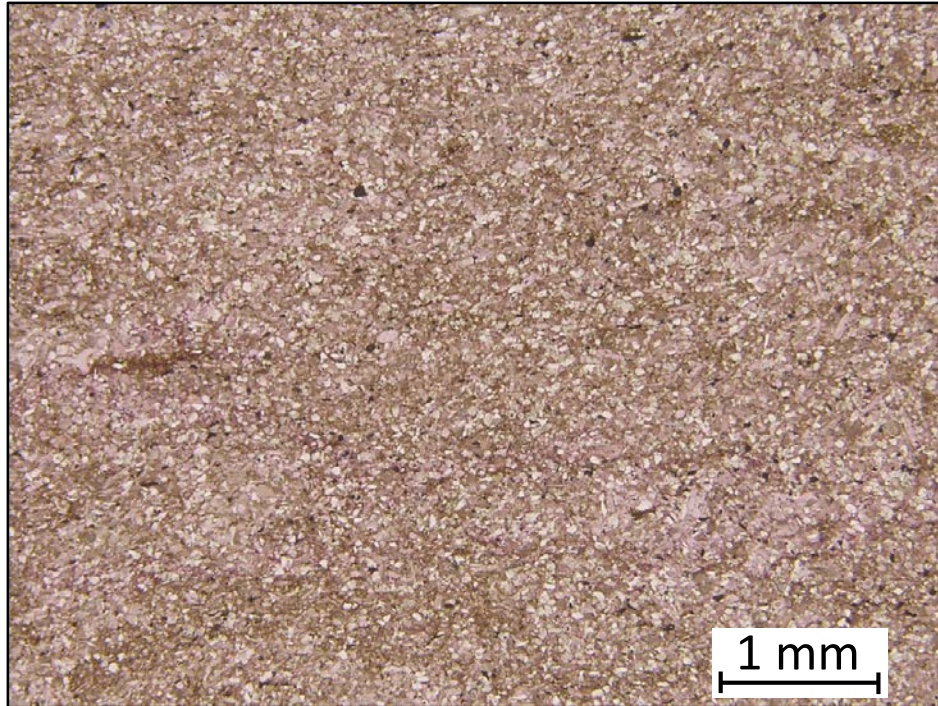
3EL – 4481.50' = Glauconitic packstone. Sample is blue epoxy impregnated. Porosity (NCS): 3.7%. Permeability (Klinkenberg): 0.947 mD. TOC: 0.81%. XRD: 6% clays (4% illite and 2% mixed layer illite/smectite), 80% carbonates (80% calcite), and 14% other minerals (8% quartz, 1% potassium feldspar, 3% plagioclase feldspar, and 2% pyrite). Sample contains fine to very fine sand-sized glauconite grains (15%), silt-sized quartz grains (8%), and scattered brachiopod (3%) and bone fragments (3%). Intracrystalline porosity observed. Oil present throughout sample.



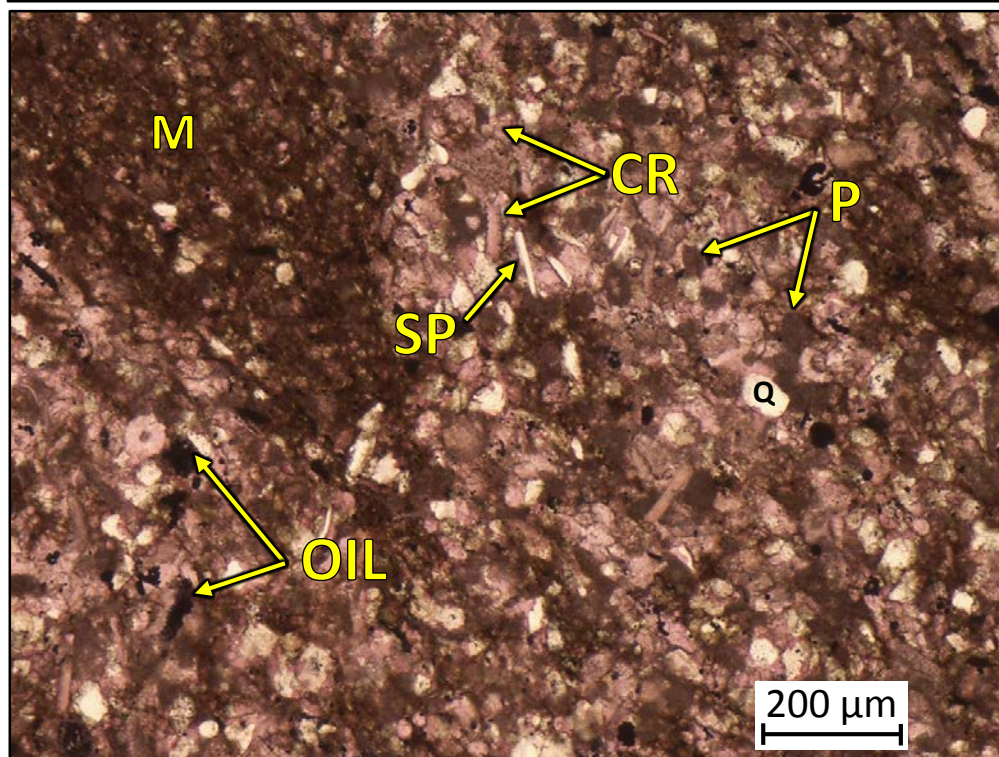
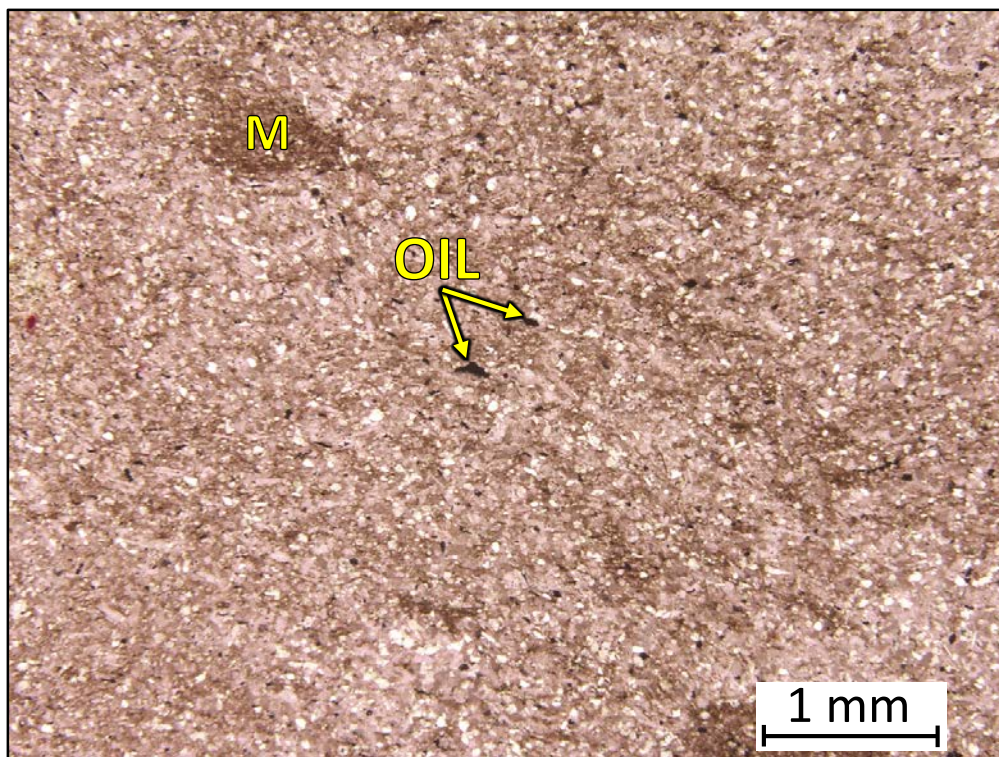
3EL – 4480.50' = Bioturbated wackestone to packstone. Sample is alizarin red stained. Porosity (NCS): 2.8%. Permeability (Klinkenberg): <0.0001 mD. XRD: 8% clays (5% illite and 3% mixed layer illite/smectite), 47% carbonates (28% calcite and 19% dolomite), and 45% other minerals (36% quartz, 2% potassium feldspar, 5% plagioclase feldspar, and 2% pyrite). Sample is composed of silt-sized quartz grains (36%), crinoid fragments (10%), brachiopod fragments (5%), spicule fragments (5%), and undifferentiated microbioclastic debris. Dominantly moldic and vug porosity filled with oil.



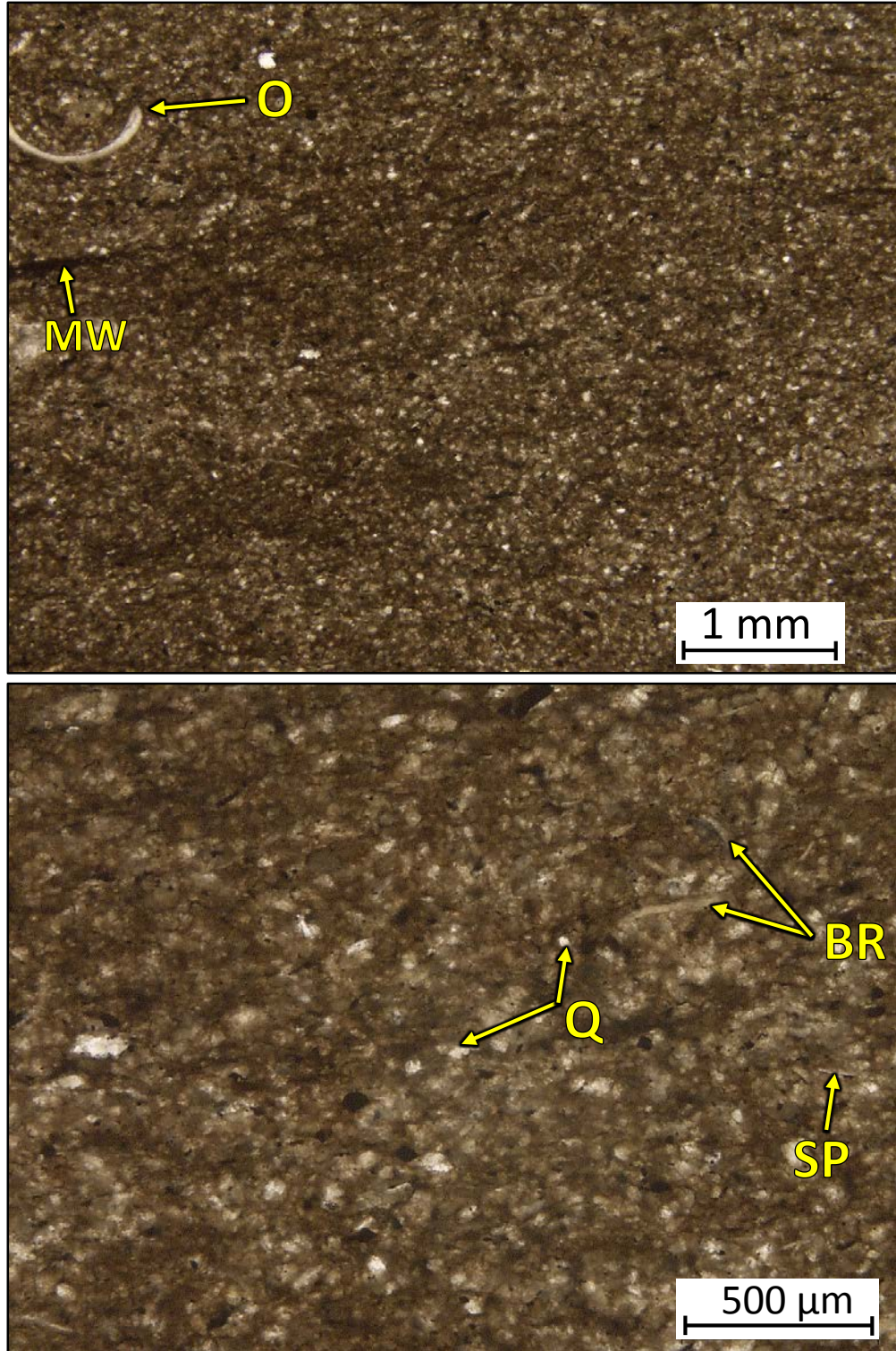
3EL – 4479.40' = Glauconitic sandstone. Sample is alizarin red stained and blue epoxy impregnated. Porosity (NCS): 9.3%. Permeability (Klinkenberg): 0.0062 mD. XRD: 20% clays (11% illite and 9% mixed layer illite/smectite), 22% carbonates (13% calcite and 9% dolomite), and 58% other minerals (49% quartz, 2% potassium feldspar, 3% plagioclase feldspar, 3% pyrite, and 1% apatite). Sample contains slit-sized quartz grains (49%), fine sand-sized glauconite grains (40%), coarse sand-sized phosphate nodules (5%), brachiopod fragments (3%), bone fragments (1%), and some spicule fragments. Intracrystalline porosity observed within dolomite crystals and lesser amounts of interparticle porosity observed between grains. Oil present throughout sample.



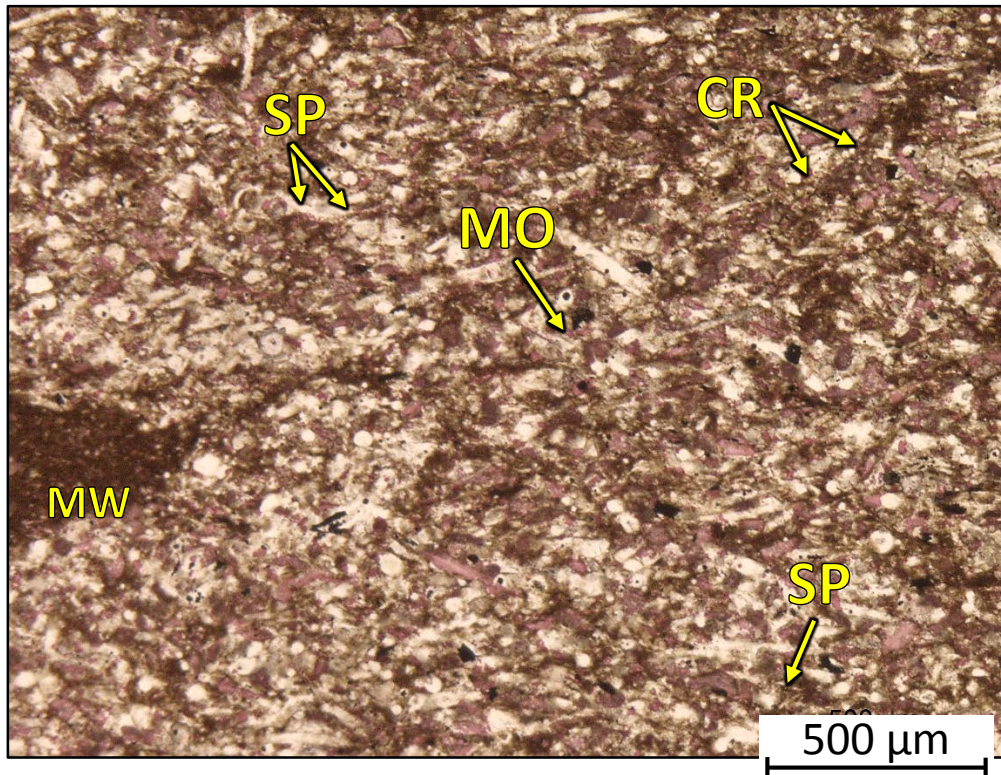
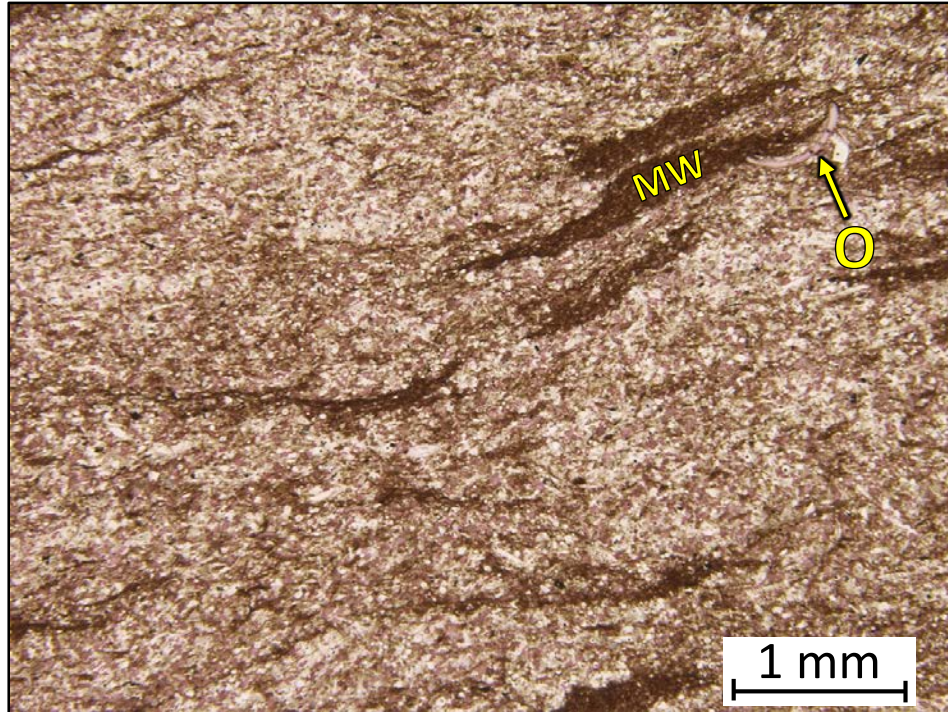
3EL – 4476.40' = Bioturbated packstone. Sample is alizarin red stained. Porosity (NCS): 4.0%. Permeability (Klinkenberg): 0.0009 mD. XRD: 8% clays (5% illite and 3% mixed layer illite/smectite), 54% carbonates (42% calcite and 12% dolomite), and 38% other minerals (29% quartz, 3% potassium feldspar, 4% plagioclase feldspar, 1% pyrite, and 1% apatite). Sample is composed of silt-sized quartz grains (29%), silt to fine sand-sized crinoid fragments (30%), and calcite replaced spicules (20%). Dominantly vug porosity with oil observed in pore spaces.



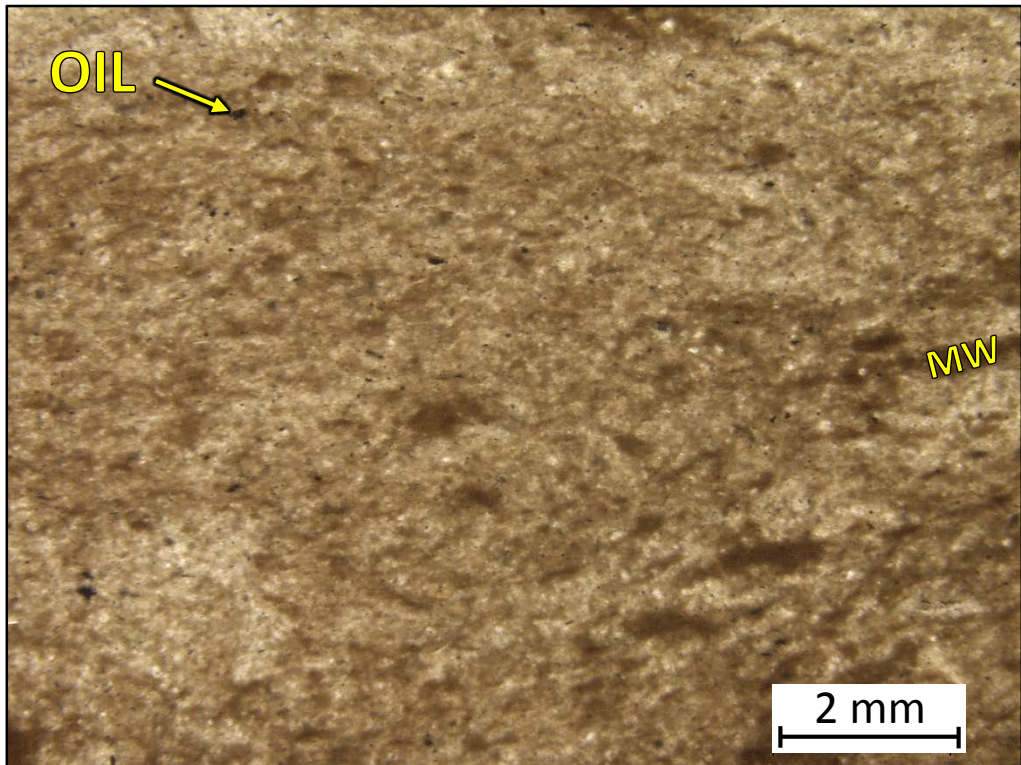
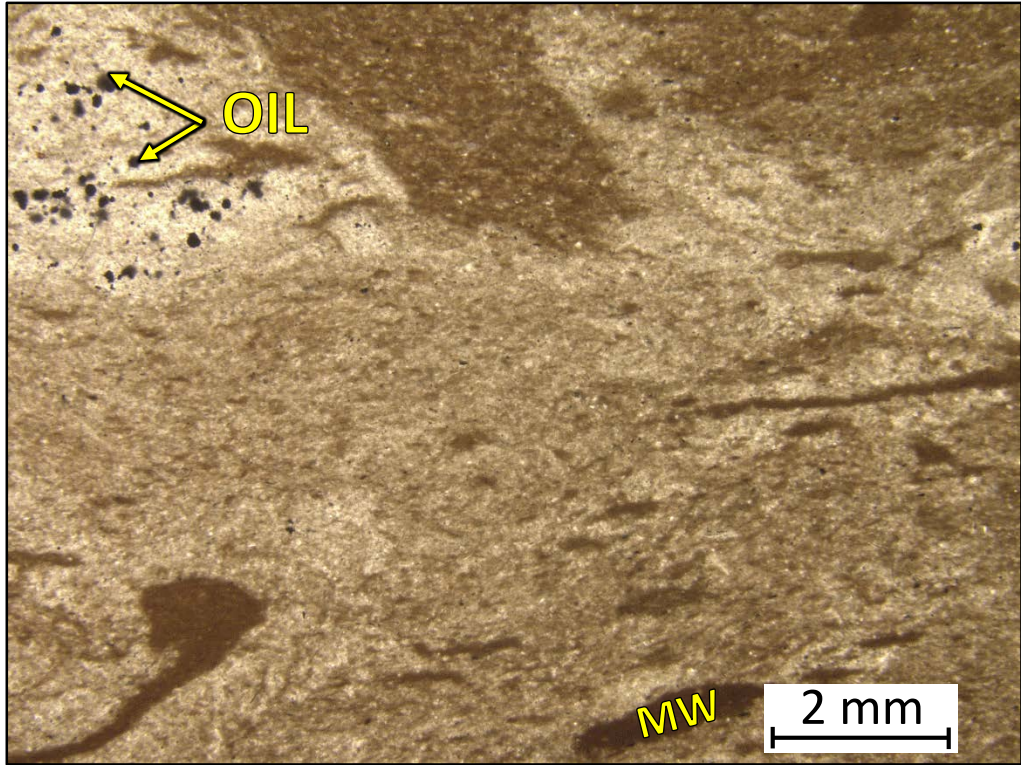
3EL – 4471.30' = Bioturbated wackestone to packstone. Sample is alizarin red stained. Porosity (NCS): 2.3%. Permeability (Klinkenberg): <0.0001 mD. XRD: 5% clays, 65% carbonates, and 30% other minerals. Sample contains silt-sized quartz grains (15%), peloids (20%), siliceous and calcareous spicules (10%), and crinoid fragments (20%). Dominantly vug porosity with oil observed in pore spaces.



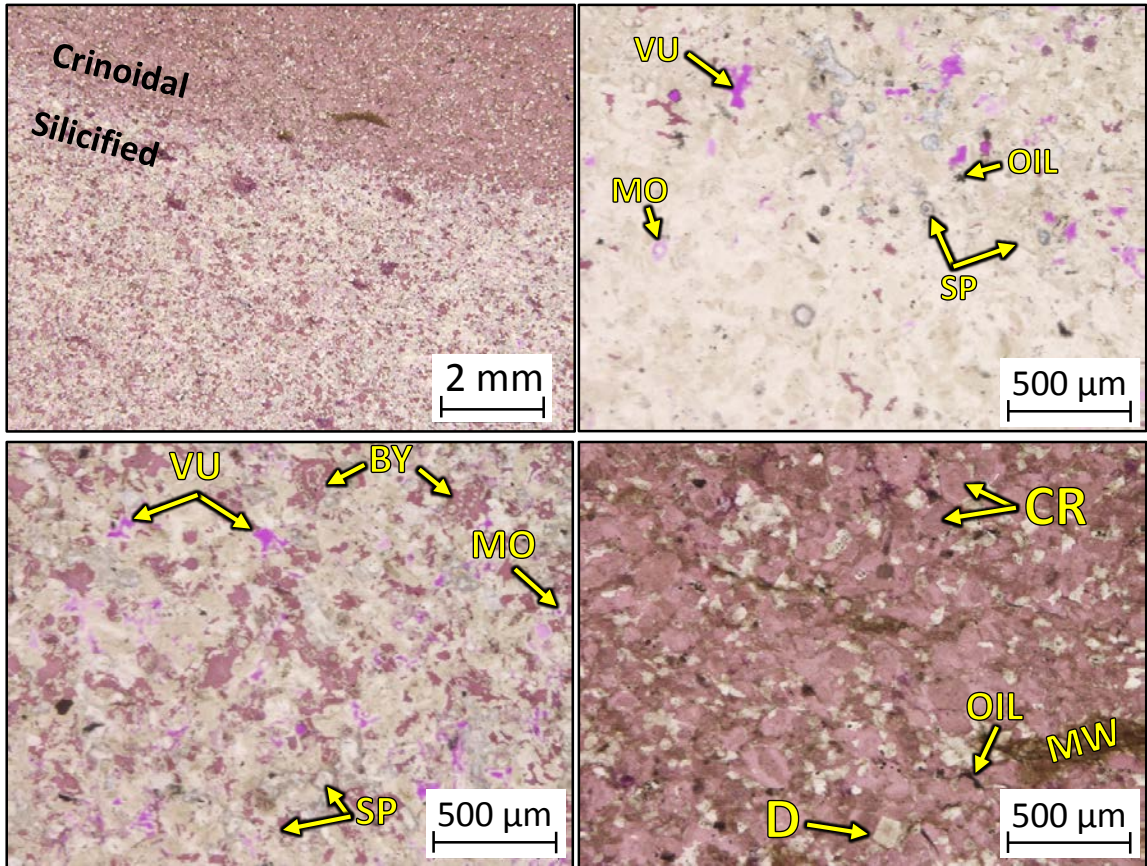
3EL – 4470.50' = Bioturbated wackestone to packstone. Sample is blue epoxy impregnated. Visual estimation: 15% clays, 40% carbonates, and 45% other minerals. Sample contains ostracode (5%), brachiopod (5%), spicule fragments (5%), and undifferentiated microbioclastic debris. Dominantly oil-filled porosity.



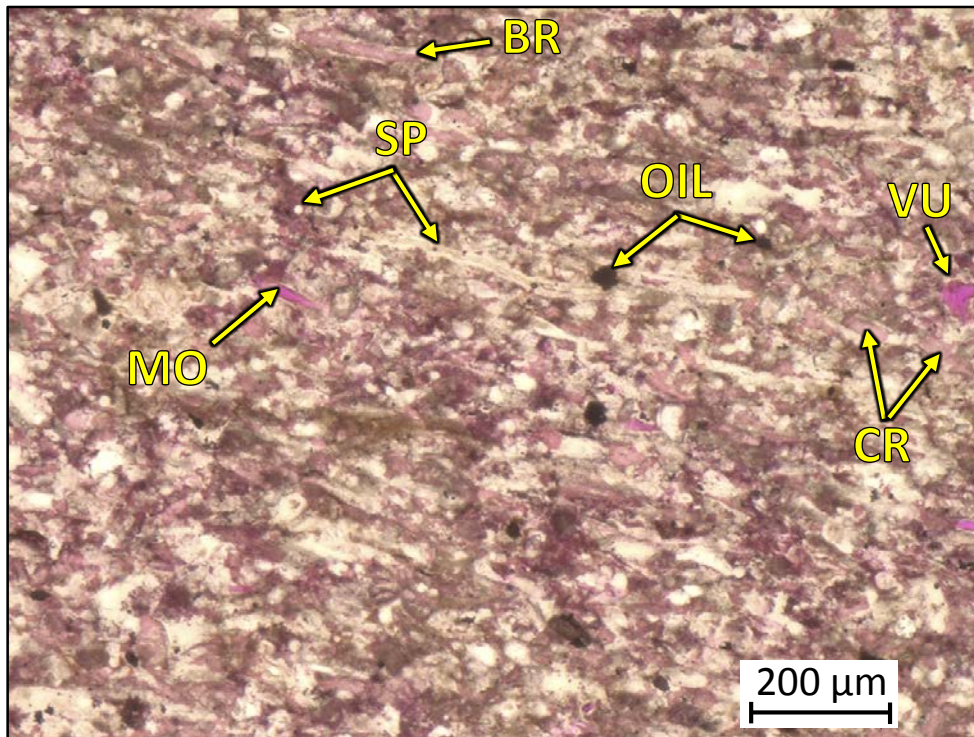
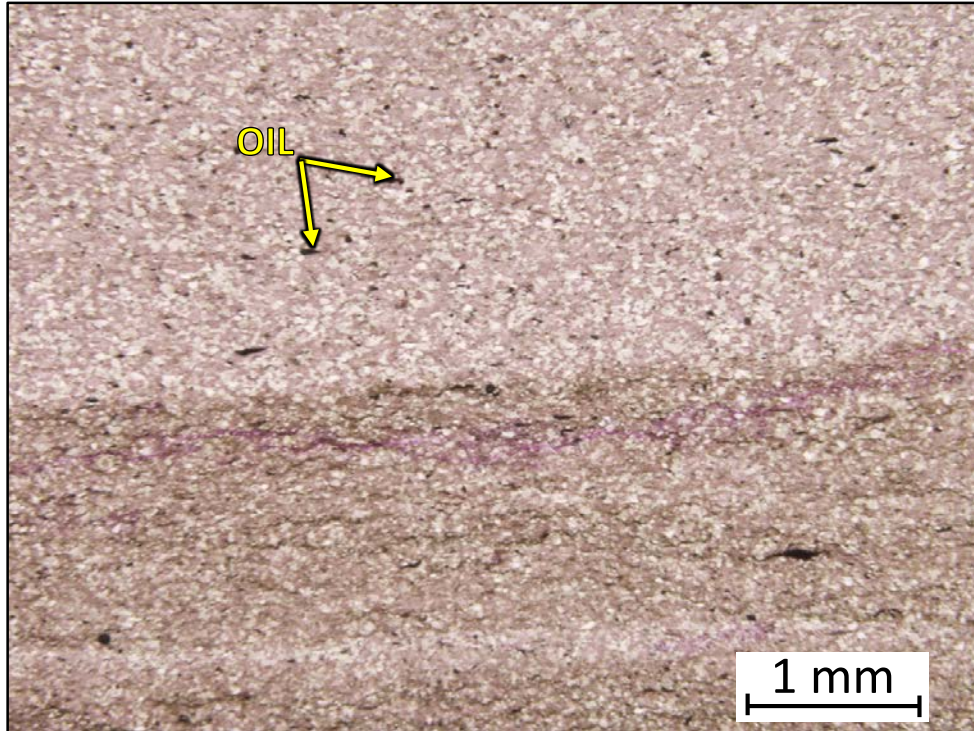
3EL – 4466.85' = Partially silicified bioturbated packstone-grainstone. Sample is alizarin red stained. Porosity (NCS): 1.6%. Permeability (Klinkenberg): 0.0001 mD. Visual estimation: 5% clays, 30% carbonates, and 65% other minerals. Sample contains abundant sponge spicules (30%) and crinoid (15%) and ostracode (3%) fragments. Dominantly oil-filled moldic porosity from dissolution of sponge spicules and some interparticle porosity.



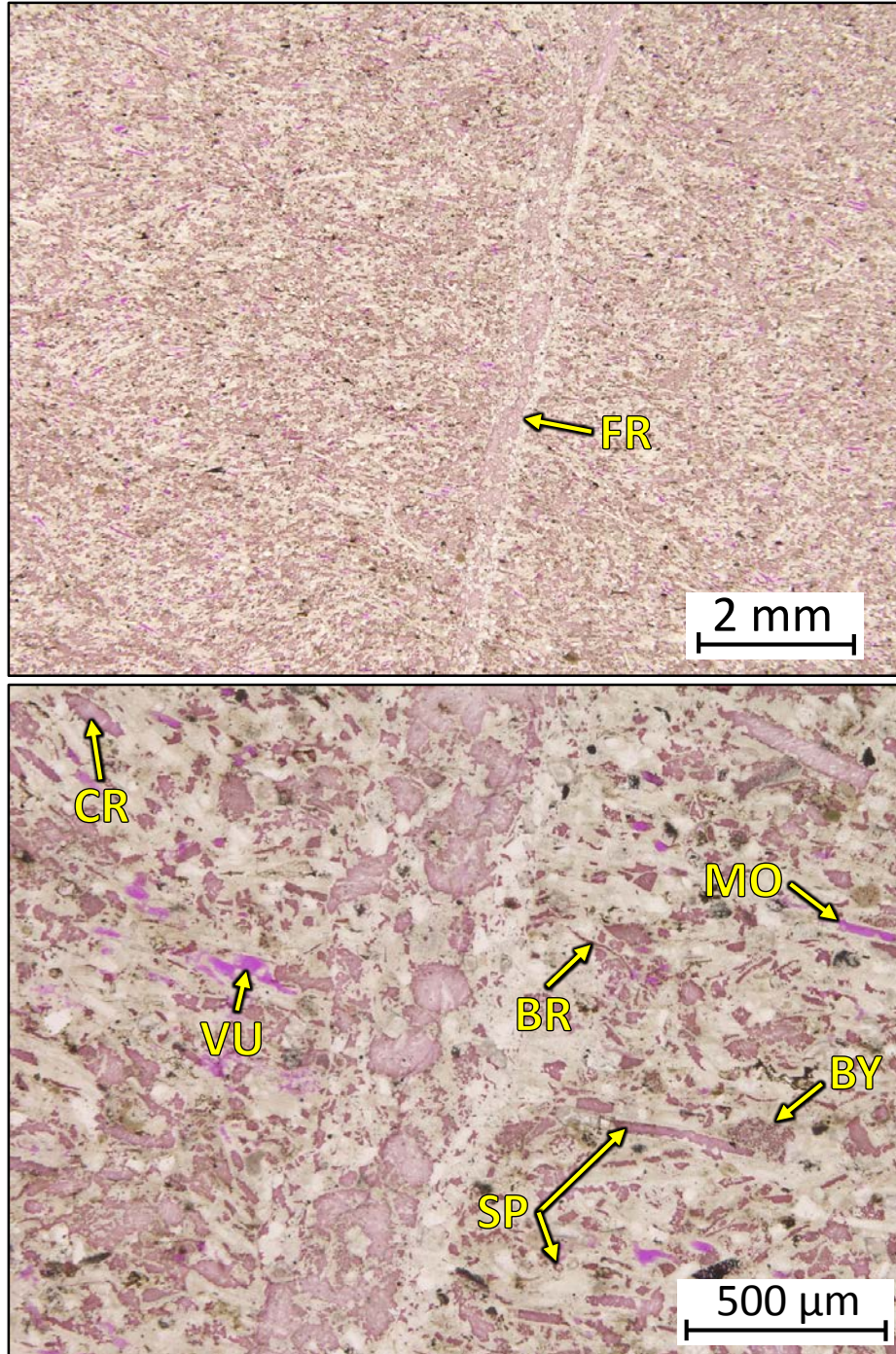
3EL – 4459.00' = Bioturbated wackestone. Sample is blue epoxy impregnated. Porosity (visual estimation): 0.5%. Visual estimation: 15% clays, 35% carbonates, and 50% other minerals. Sample contains silt-sized quartz grains and undifferentiated microbioclastic debris. Dominantly oil-filled interparticle porosity.



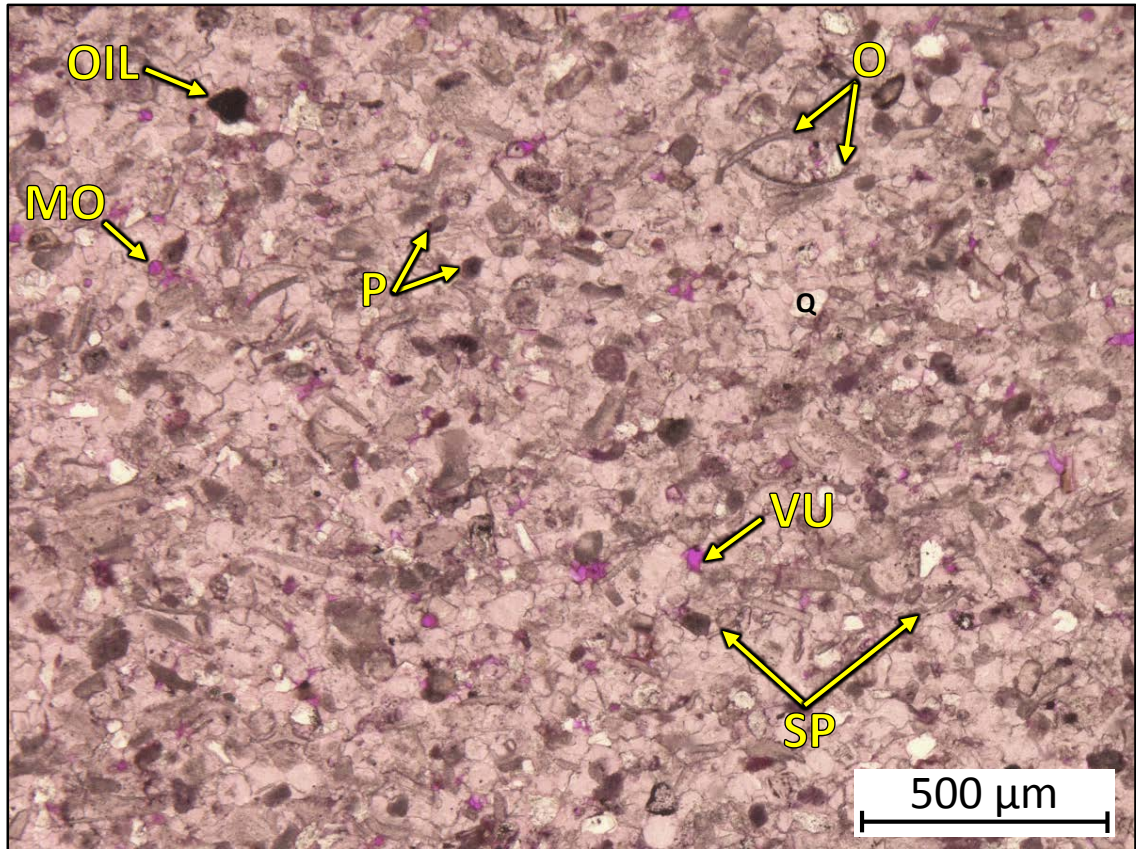
3EL – 4446.55' = Partially to completely silicified skeletal grainstone. Sample is alizarin red stained and porosity is shown in bright fuchsia. Porosity (NCS): 3.2%. Permeability (Klinkenberg): 0.023 mD. XRD: 1% clays (1% illite), 58% carbonates (54% calcite and 4% dolomite), and 41% other minerals (40% quartz and 1% plagioclase feldspar). Sample is characterized by varying mineralogies and varying amounts of crinoid, spicule, and bryozoan fragments depending on location. Dominantly moldic and vug porosity, with some oil-filled pores.



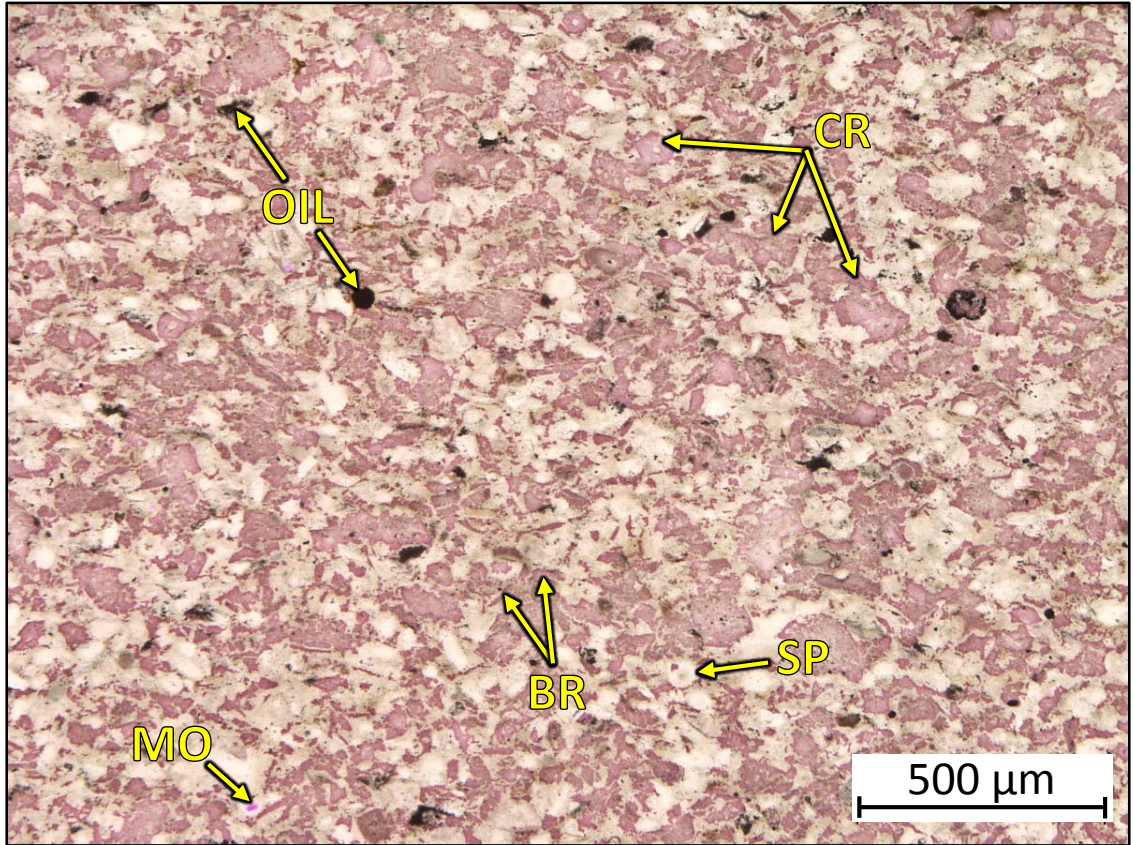
3EL – 4441.25' = Skeletal packstone-grainstone. Sample is alizarin red stained and porosity is shown in bright fuchsia. Porosity (NCS): 4.6%. Permeability (Klinkenberg): 0.013 mD. Visual estimation: 1% clays, 35% carbonates, 64% other minerals. Sample contains silt-sized quartz grains, brachiopod fragments (5%), spicules (20%), and crinoid fragments (10%). Dominantly moldic and vug porosity, with some oil-filled pores.



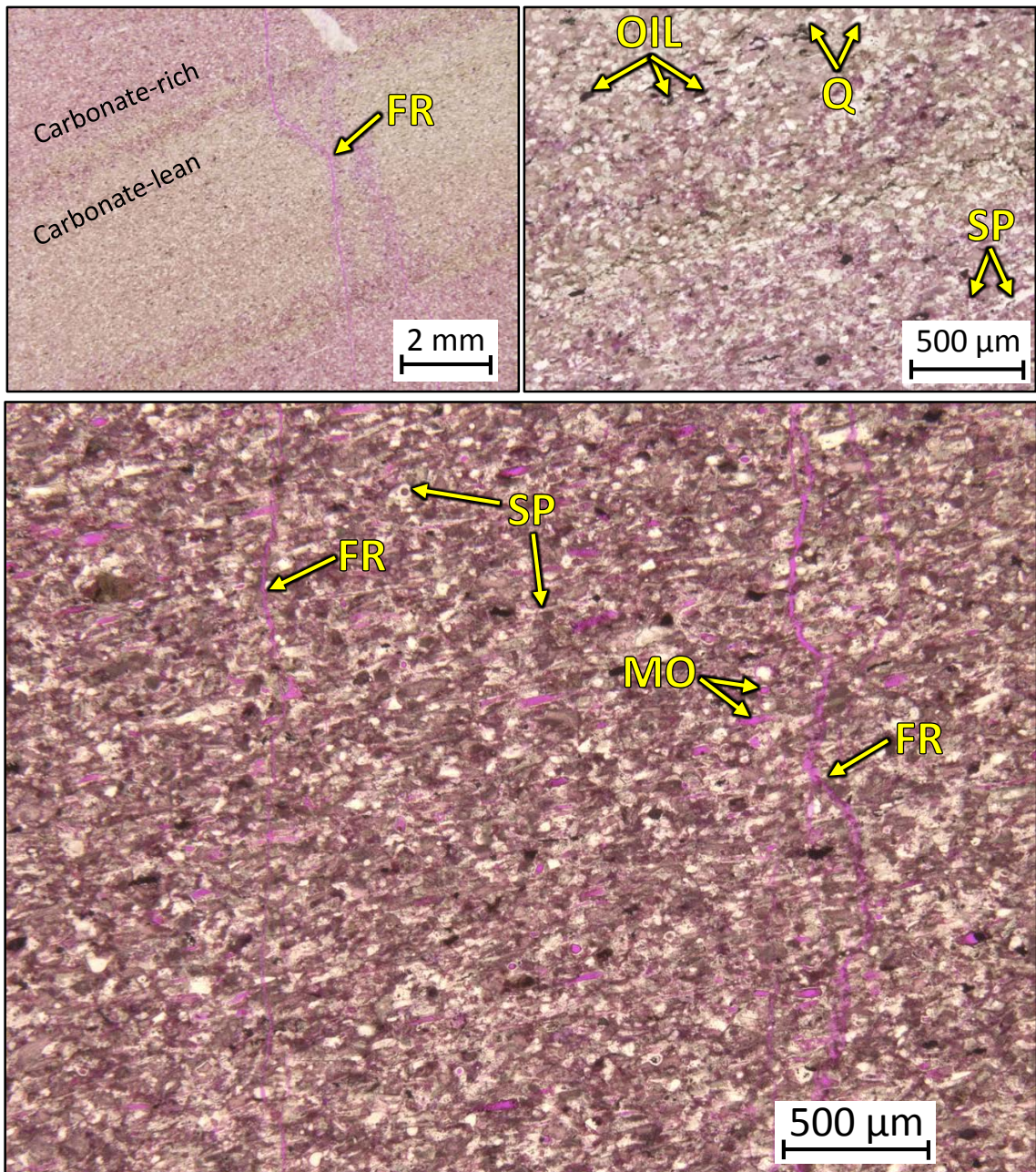
3EL – 4438.75' = Silicified skeletal grainstone. Sample is alizarin red stained and porosity is shown in bright fuchsia. Porosity (NCS): 1.4%. Permeability (Klinkenberg): <0.0001 mD. XRD: Trace amounts of clays, 29% carbonates (27% calcite and 2% dolomite), and 71% other minerals (66% quartz, 2% potassium feldspar, and 3% plagioclase feldspar). Sample contains abundant sponge spicules (40%) and lesser amounts of brachiopod (3%), bryozoan (5%), and crinoid (10%) fragments. A calcite-filled fracture is shown passing through the middle of the sample. Dominantly moldic and vug porosity.



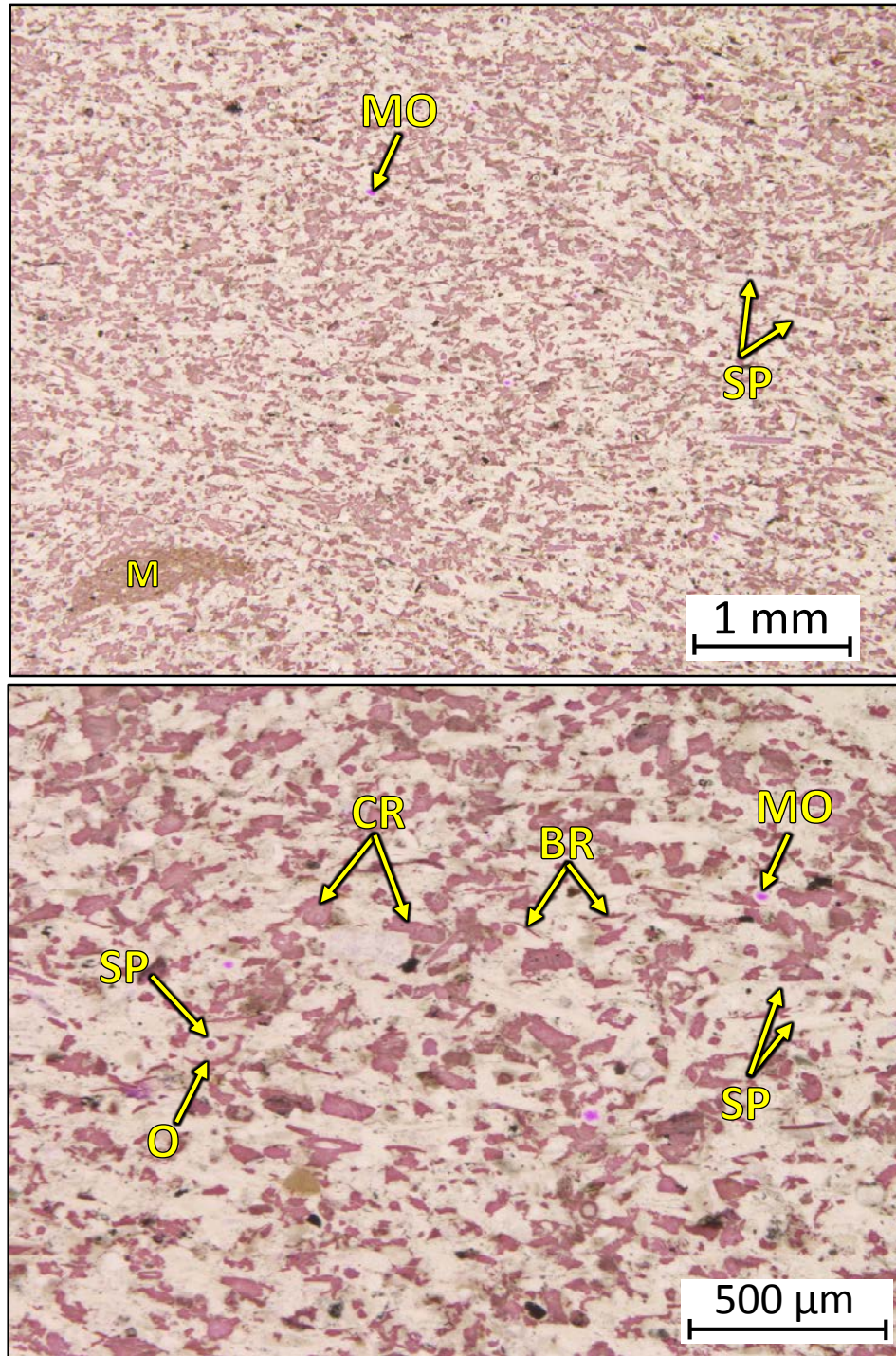
3EL – 4429.10' = Peloidal grainstone. Sample is alizarin red stained and porosity is shown in bright fuchsia. Porosity (NCS): 3.1%. Permeability (Klinkenberg): 0.001 mD. XRD: 1% clays (1% illite), 85% carbonates (84% calcite and 1% dolomite), and 14% other minerals (11% quartz, 1% potassium feldspar, and 2% plagioclase feldspar). Sample is composed of silt-sized quartz grains (11%), abundant peloids (20%), spicules (15%), and ostracodes (5%). Dominantly moldic porosity from dissolution of sponge spicules and vug and intercrystalline porosity.



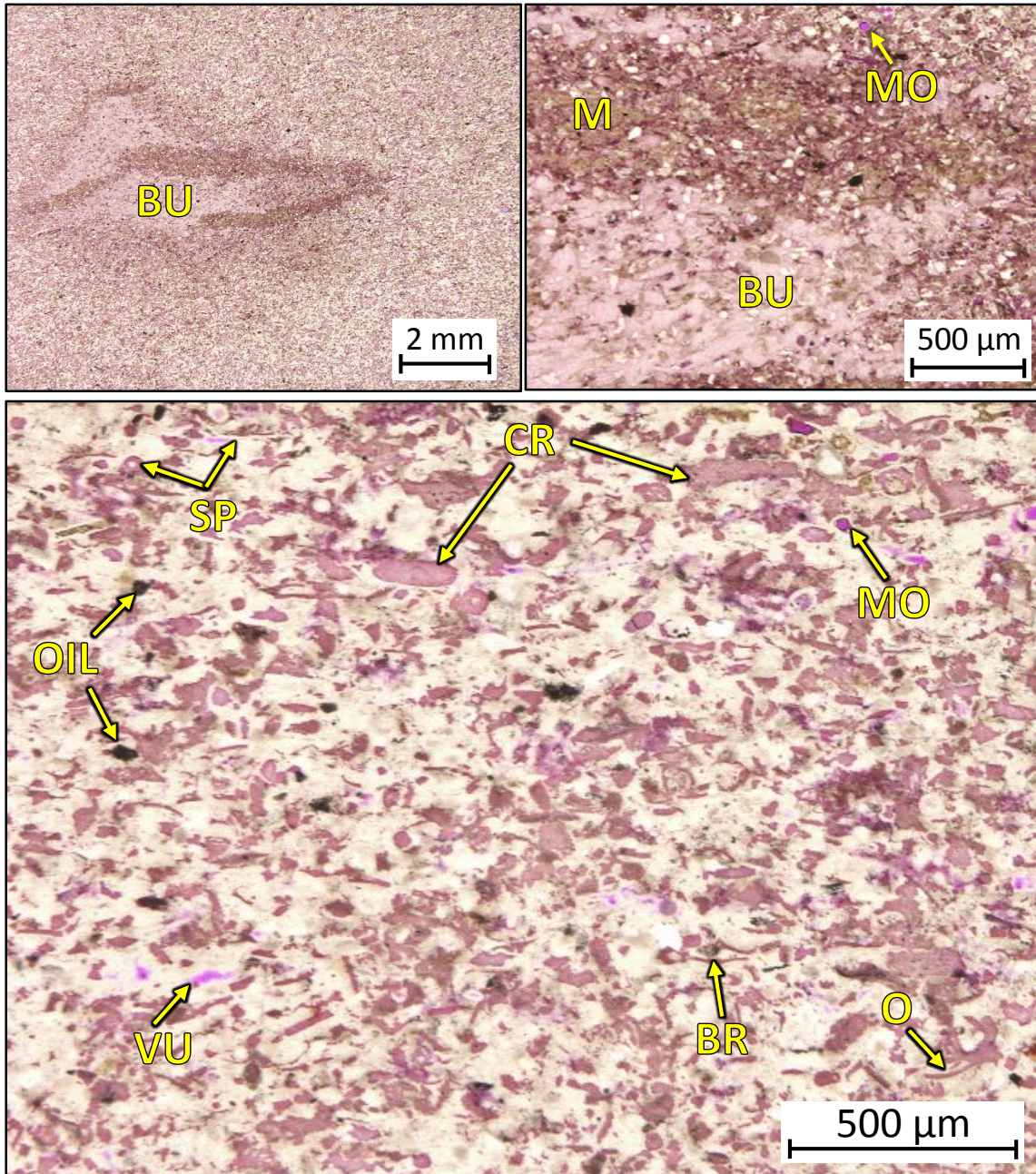
3EL – 4426.20' = Partially silicified skeletal grainstone. Sample is alizarin red stained and porosity is shown in bright fuchsia. Porosity (NCS): 1.0%. Permeability (Klinkenberg): <0.0001 mD. XRD: Trace amounts of clays, 49% carbonates (47% calcite and 2% dolomite), and 51% other minerals (48% quartz, 1% potassium feldspar, and 2% plagioclase feldspar). Sample contains crinoid (30%) and brachiopod (10%) fragments and sponge spicules (5%). Minor amounts of moldic porosity from the dissolution of sponge spicules.



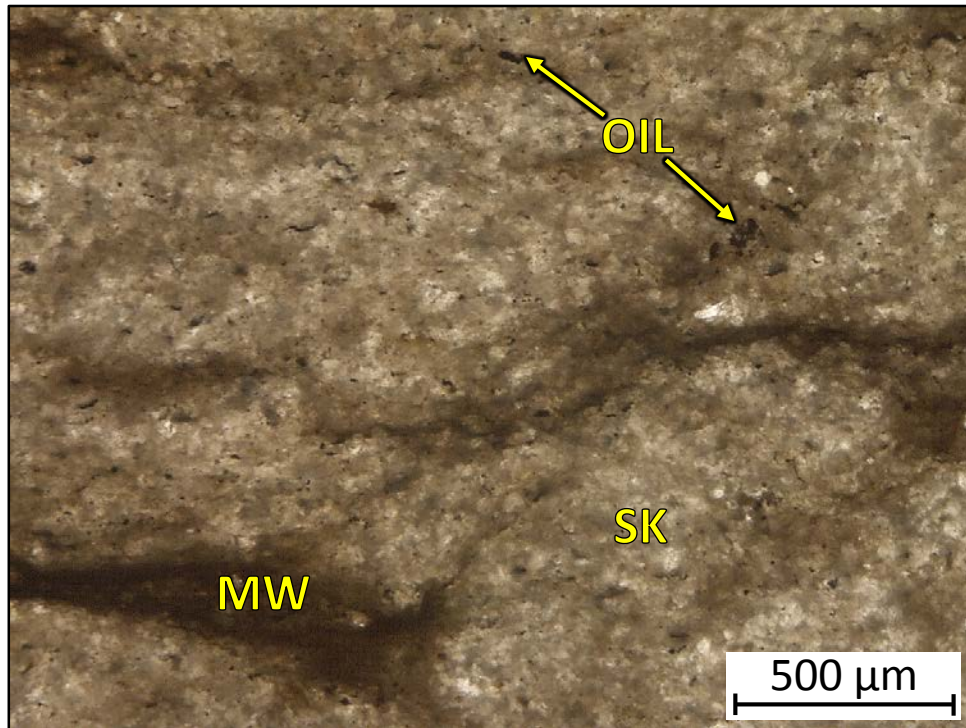
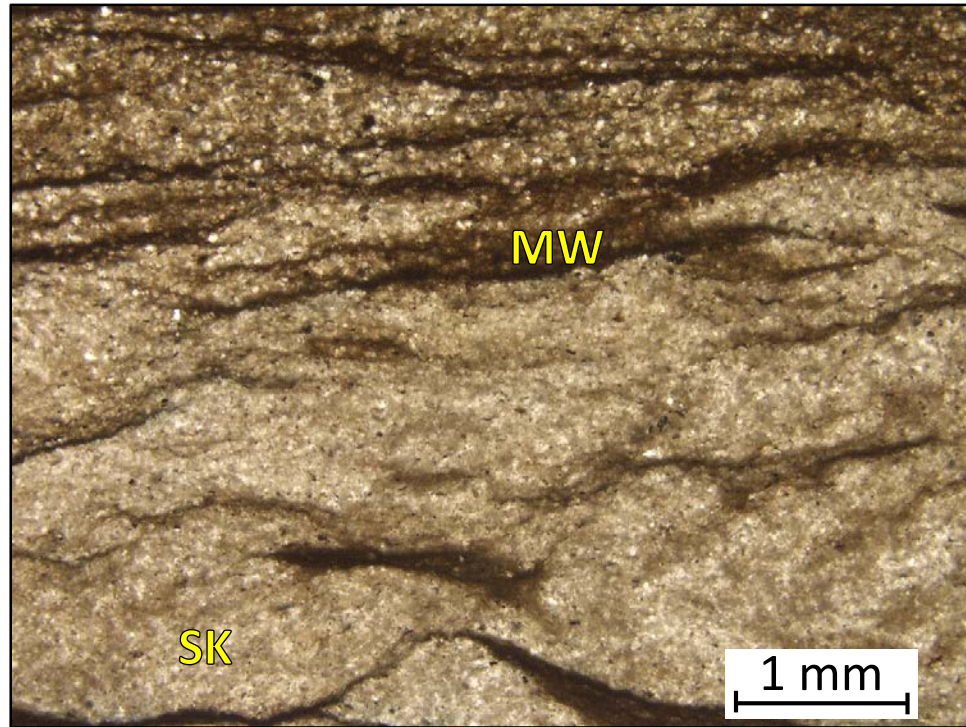
3EL – 4410.55' = Skeletal packstone-grainstone. Sample is alizarin red stained. Porosity (NCS): 5.3%. Permeability (Klinkenberg): 0.238 mD. XRD: 1% clays (1% illite), 55% carbonates (53% calcite and 2% dolomite), and 44% other minerals (41% quartz, 1% potassium feldspar, and 2% plagioclase feldspar). Sample contains abundant sponge spicules and increased skeletal content in carbonate-rich intervals. Carbonate-lean intervals are dominated by silt-sized quartz grains. Thin, open ptigmatic fractures in this sample show good porosity and permeability. Dominantly moldic porosity from the dissolution of sponge spicules and fracture porosity.



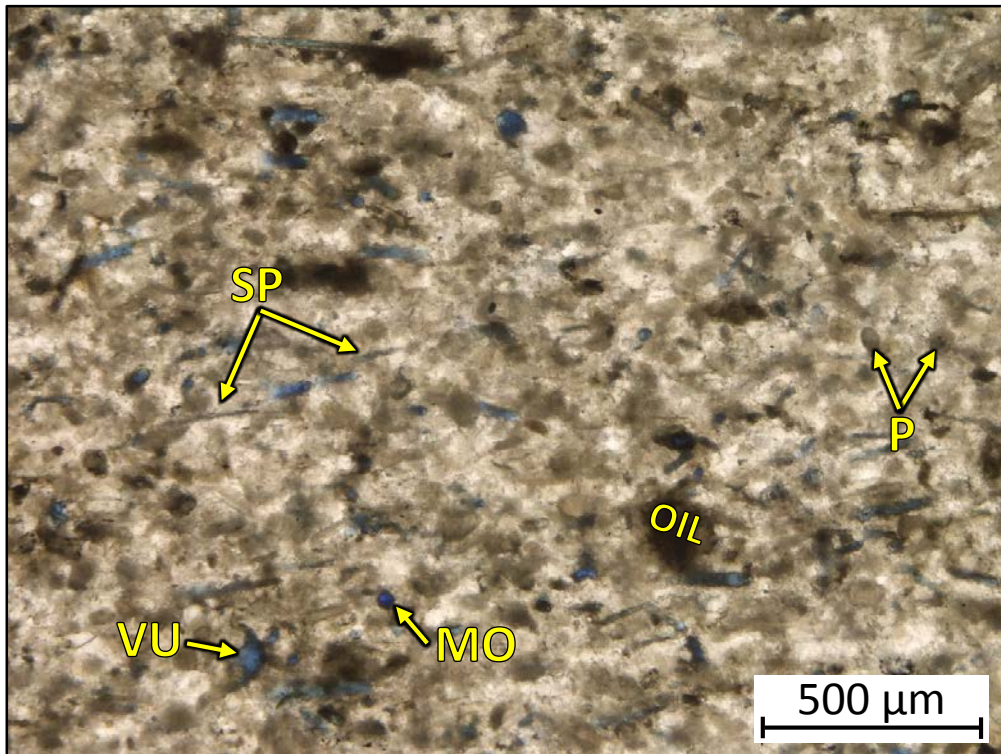
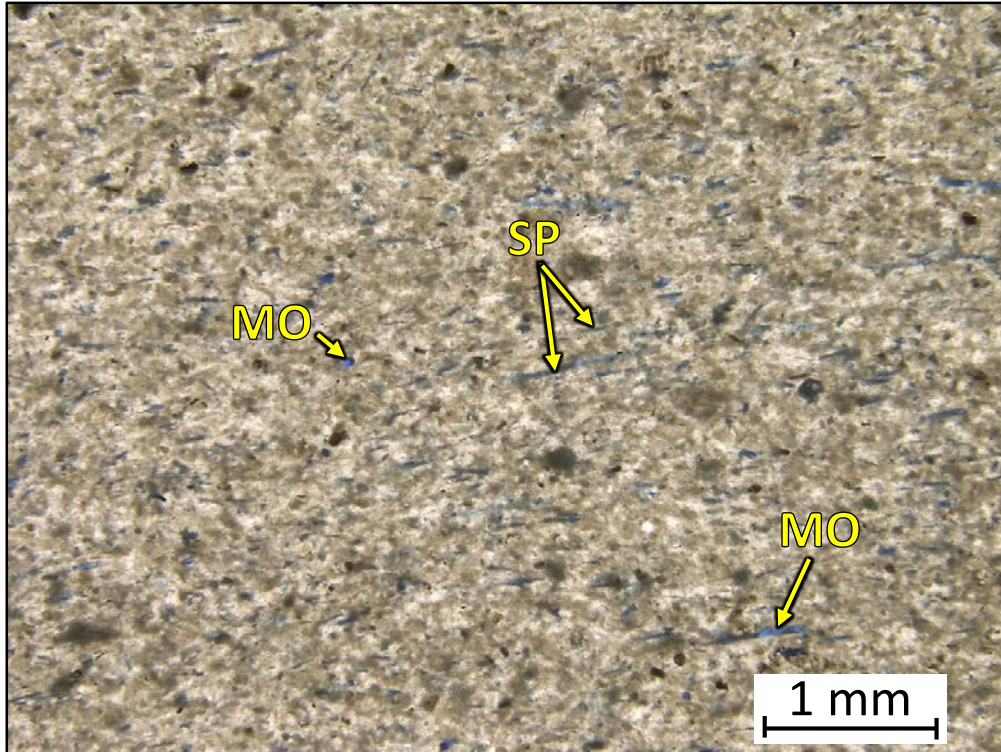
3EL – 4407.10' = Silicified spiculitic grainstone Sample is alizarin red stained. Porosity (NCS): 2.9%. Permeability (Klinkenberg): <0.0001 mD. XRD: 1% clays (1% illite), 33% carbonates (33% calcite), and 66% other minerals (61% quartz, 2% potassium feldspar, 3% plagioclase feldspar, and trace amounts of pyrite). Sample is composed of abundant sponge spicules (30%), crinoid fragments (15%), and minor occurrences of ostracode (3%) and brachiopod fragments (3%). Dominantly moldic porosity from the dissolution of sponge spicules.



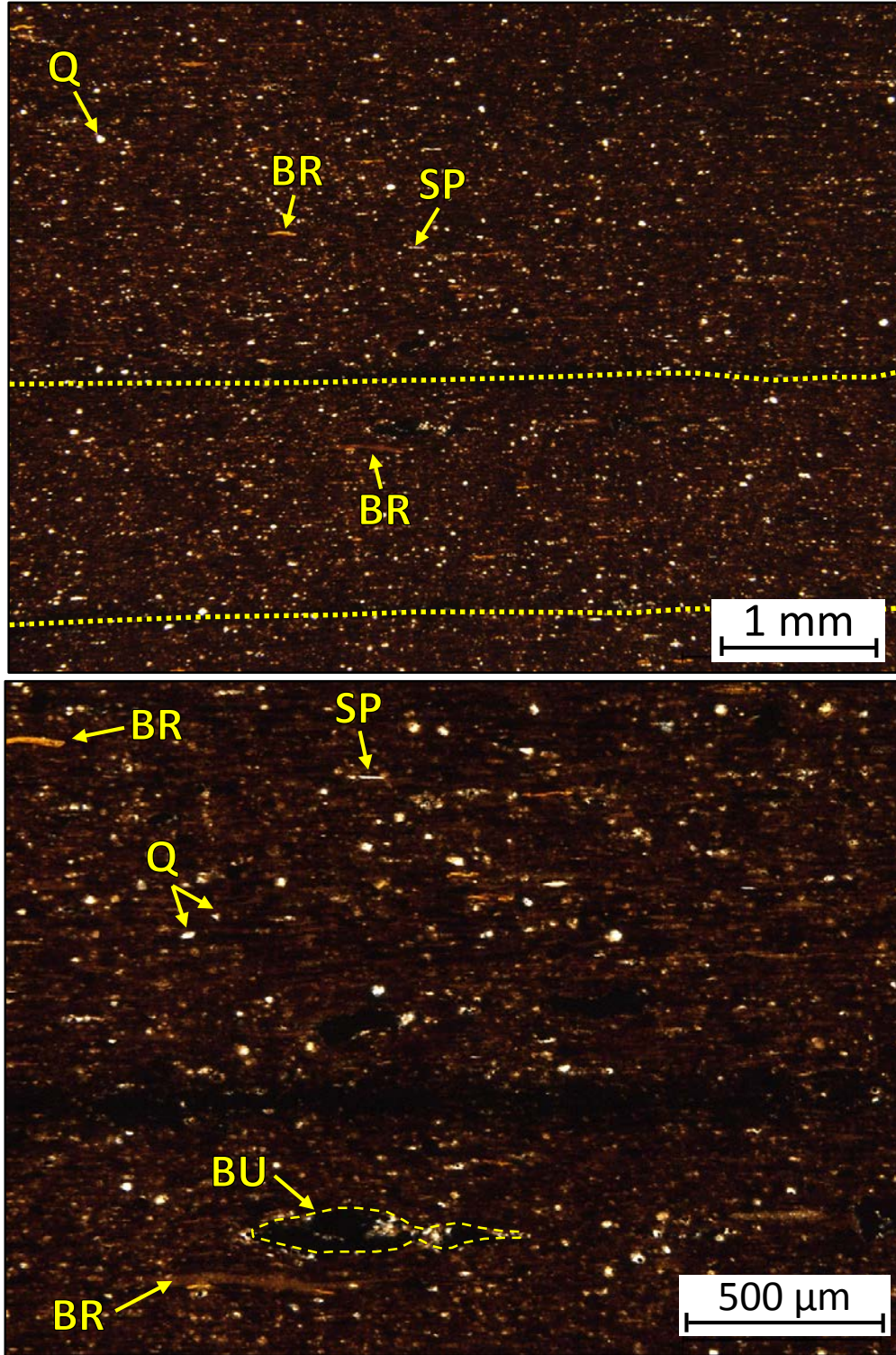
3EL – 4406.65' = Silicified spiculitic grainstone. Sample is alizarin red stained. Porosity (NCS): 3.0%. Permeability (Klinkenberg): 0.0001 mD. XRD: 1% clays (1% illite), 38% carbonates (37% calcite and 1% dolomite), and 61% other minerals (56% quartz, 2% potassium feldspar, 3% plagioclase feldspar, and trace amounts of pyrite and apatite). Sample is composed of abundant sponge spicules (40%), crinoid fragments (15%), ostracode fragments (7%), and minor occurrences of brachiopod fragments (3%). A calcite-filled burrow with silt-sized quartz grains is observed within the sample. Dominantly moldic and vug porosity observed within silicified portions of the sample.



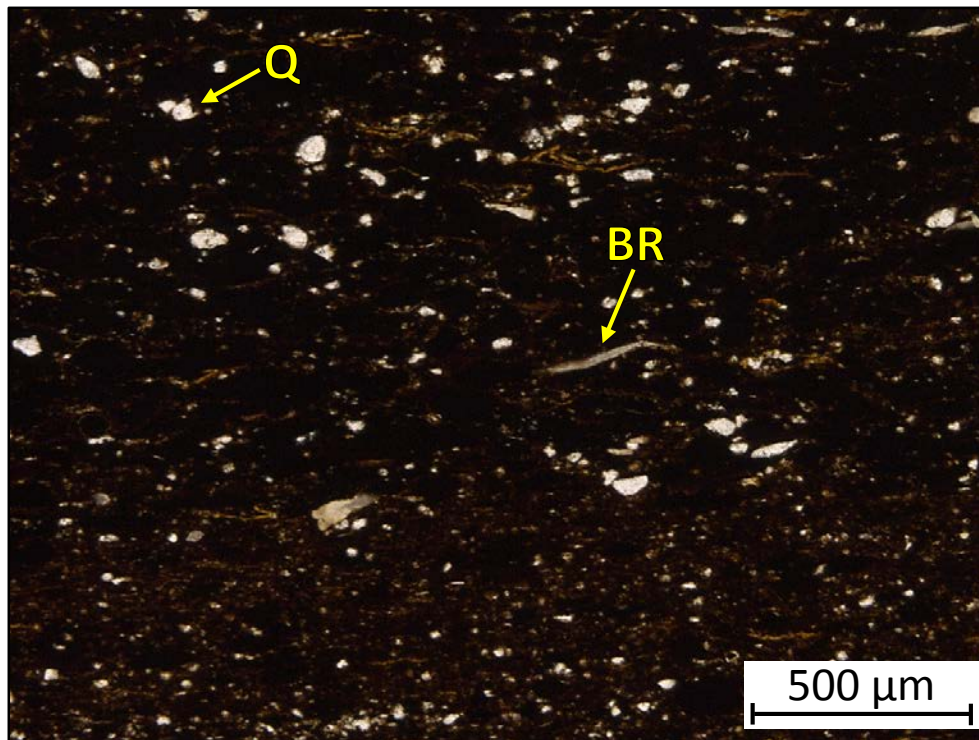
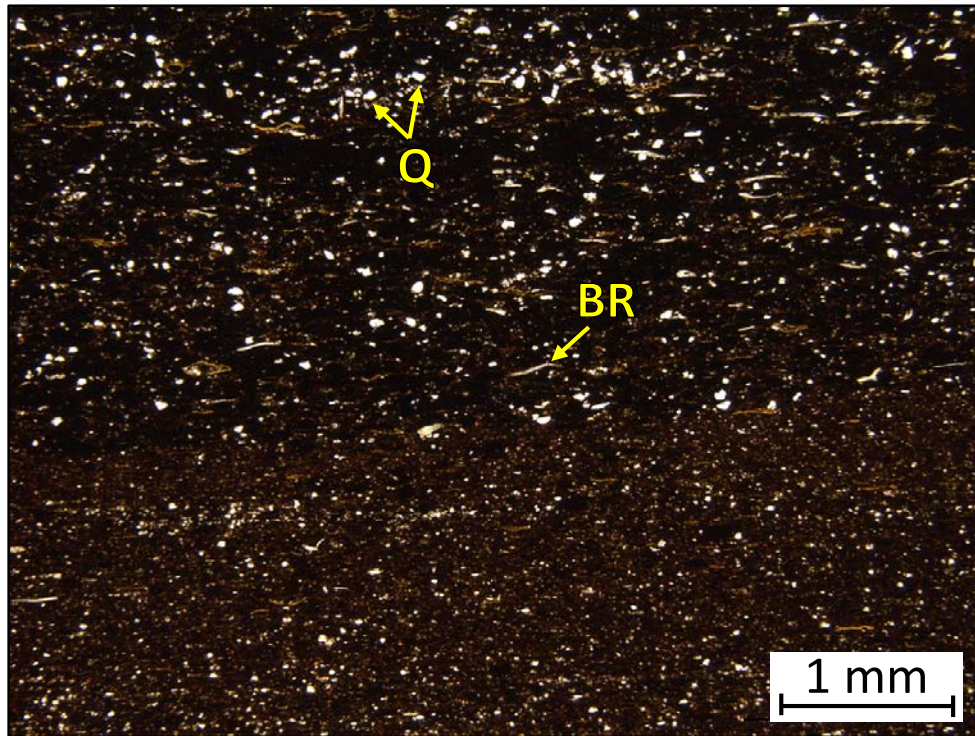
3EL – 4403.00' = Bioturbated mudstone to wackestone. Porosity (visual estimation): 1.0%. Visual estimation: 5% clays, 55% carbonates, and 40% other minerals. Sample contains silt-sized quartz grains and undifferentiated microbioclastic debris. Dominantly oil-filled porosity.



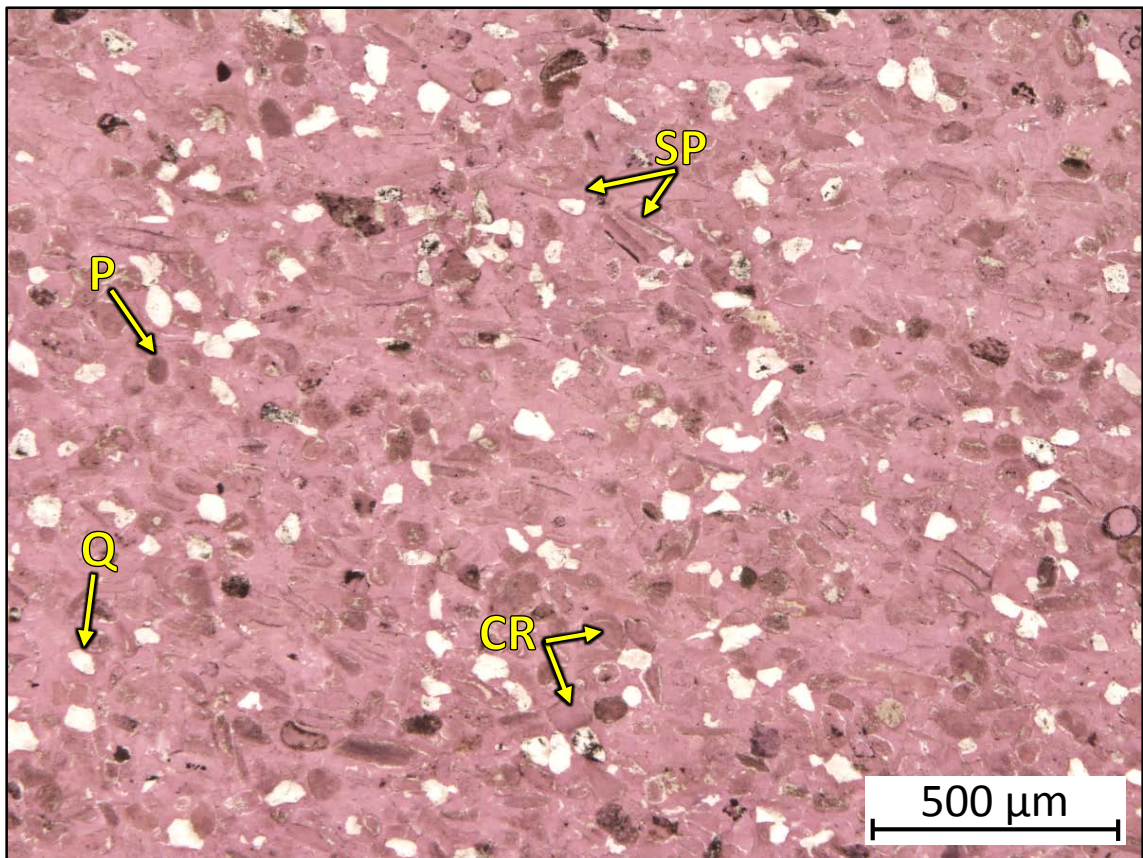
3EL – 4395.00' = **Silicified skeletal grainstone**. Sample is blue epoxy impregnated. Porosity (visual estimation): 6.0%. Visual estimation: 1% clays, 35% carbonates, 64% other minerals. Sample contains silt-sized quartz grains, peloids (10%), spicules (15%), and undifferentiated microbioclastic debris. Dominantly moldic porosity from the dissolution of sponge spicules and lesser amounts of vug porosity.



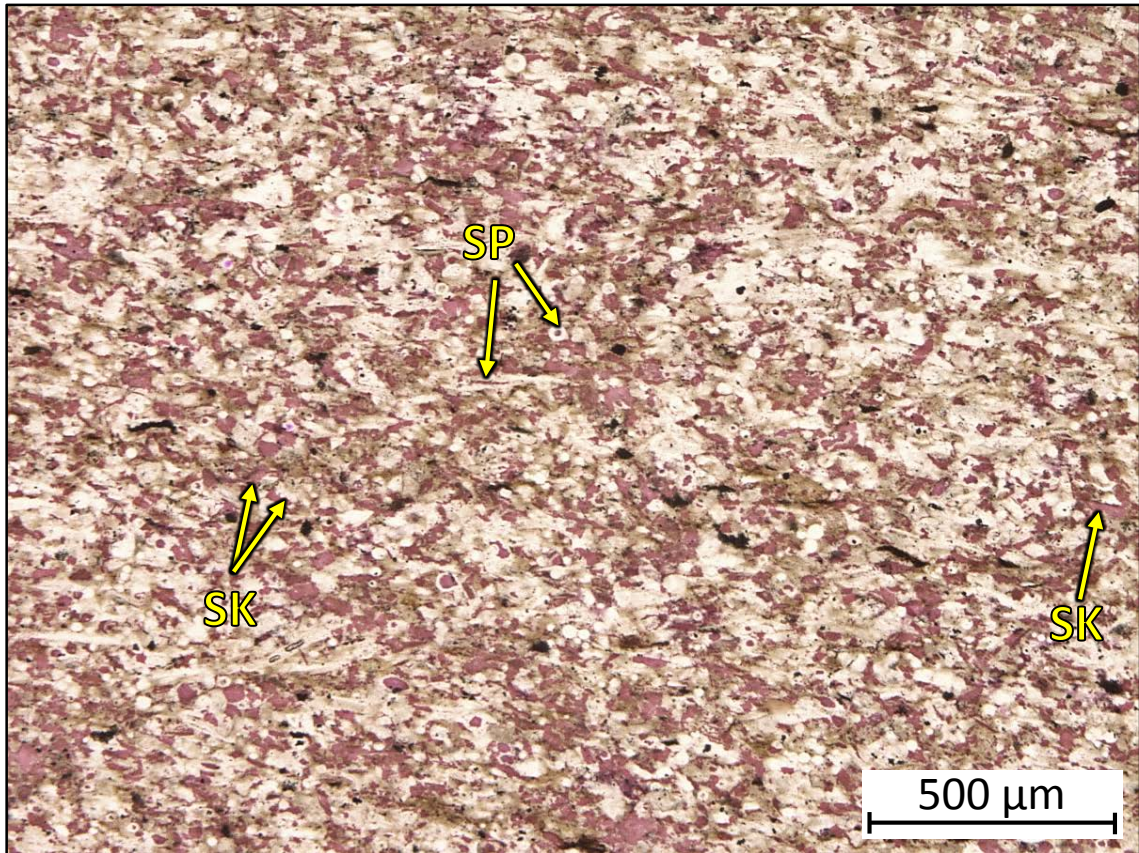
3EL – 4393.50' = Laminated mudstone-wackestone. Sample is blue epoxy impregnated. Visual estimations: 10% clays, 55% carbonates, and 35% other minerals. Sample contains silt-sized quartz grains (7%), mm-scale burrows (outlined in dashed yellow line), and brachiopod fragments (10%). Laminations are highlighted in yellow in top photomicrograph.



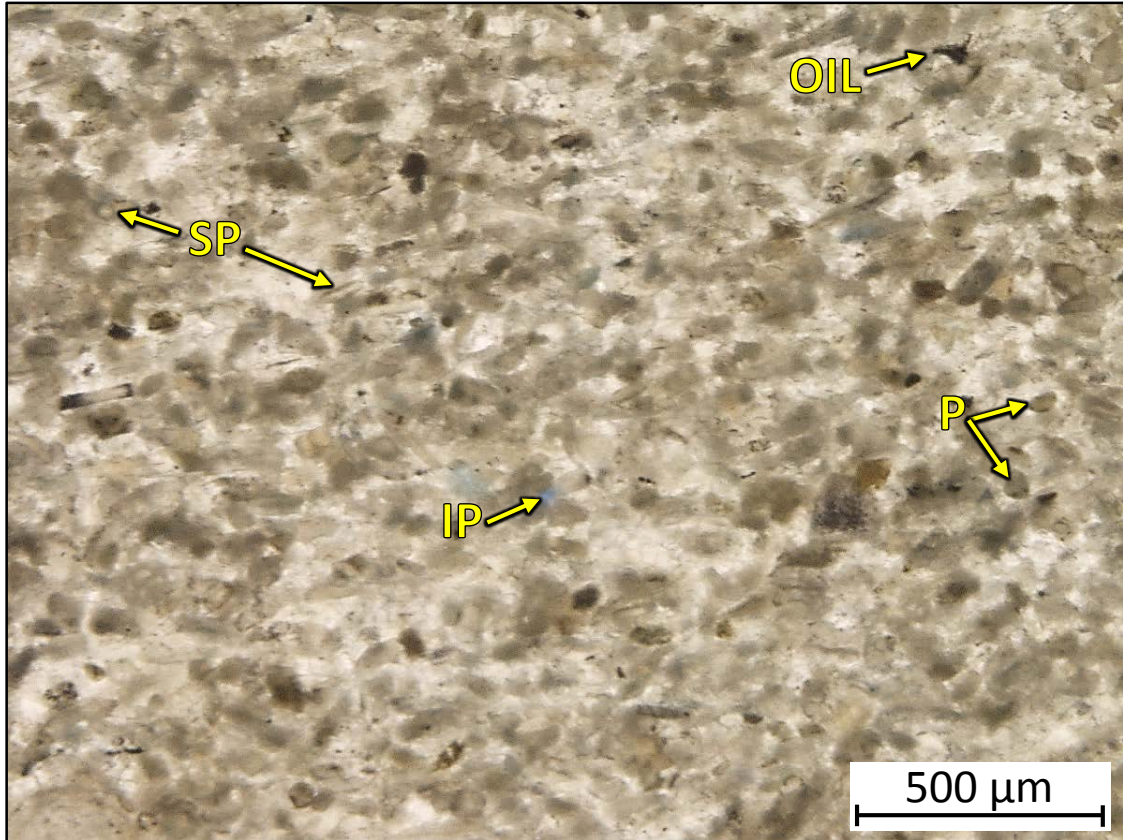
3EL – 4389.80' = Laminated mudstone-wackestone. Sample is blue epoxy impregnated. Visual estimations: 10% clays, 55% carbonates, and 35% other minerals. Sample contains silt-sized quartz grains (10%) and brachiopod fragments (15%).



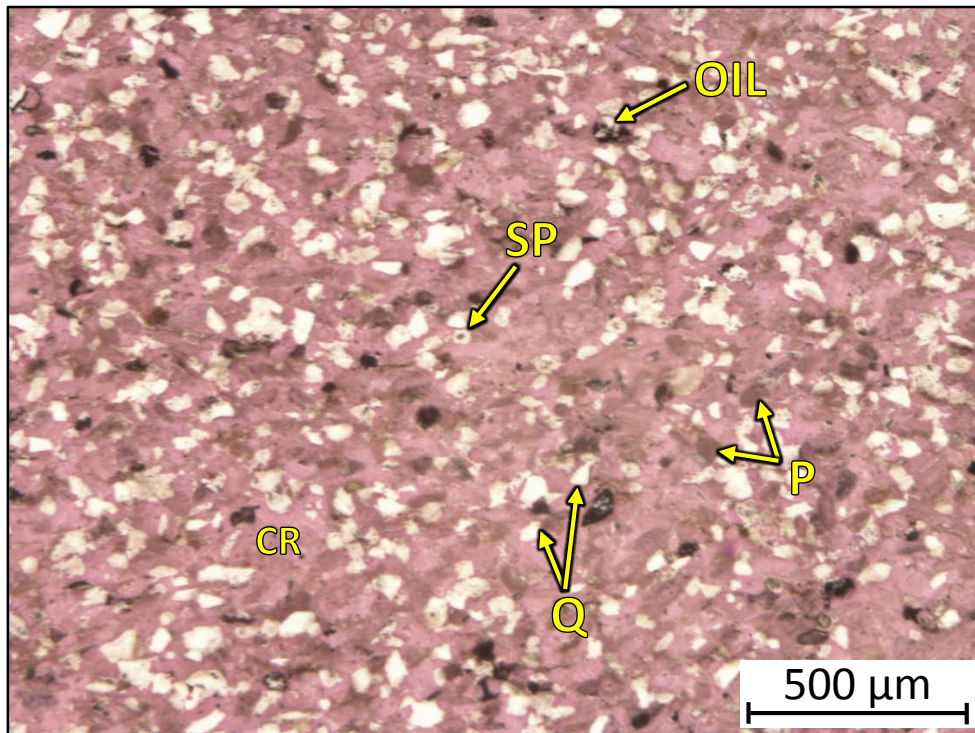
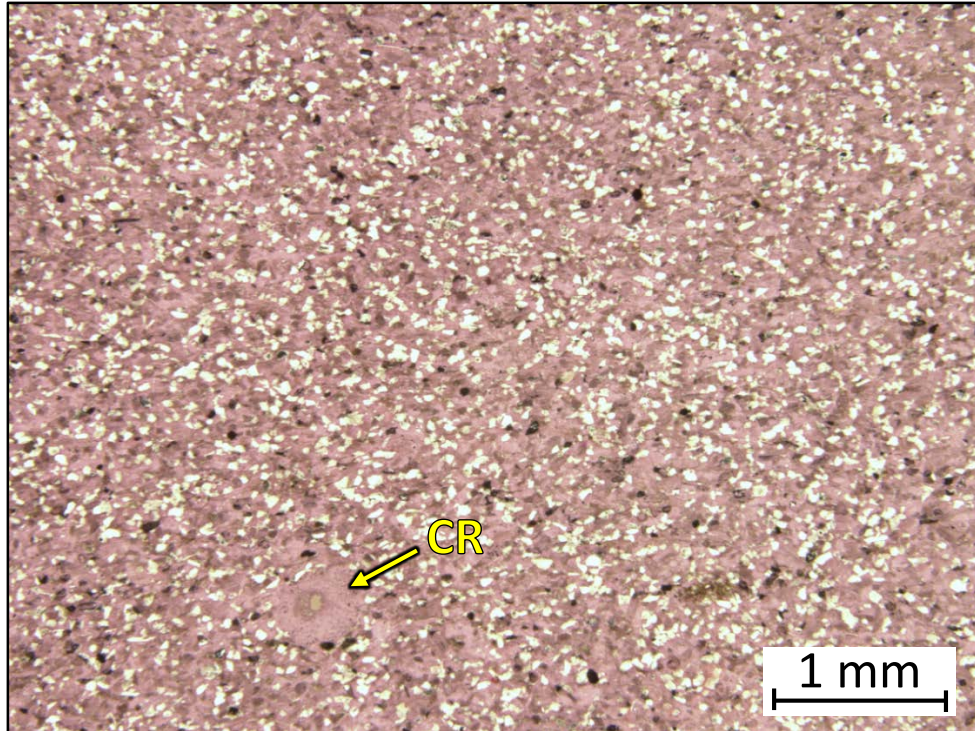
3EL – 4384.70' = Peloidal grainstone. Sample is alizarin red stained. Porosity (NCS): 1.7%. Permeability (Klinkenberg): <0.0001 mD. Visual estimations: Trace amounts of clays, 70% carbonates, and 30% other minerals. Sample contains peloids (25%), silt-sized quartz grains (30%), calcareous spicules (15%), and crinoid fragments (15%).



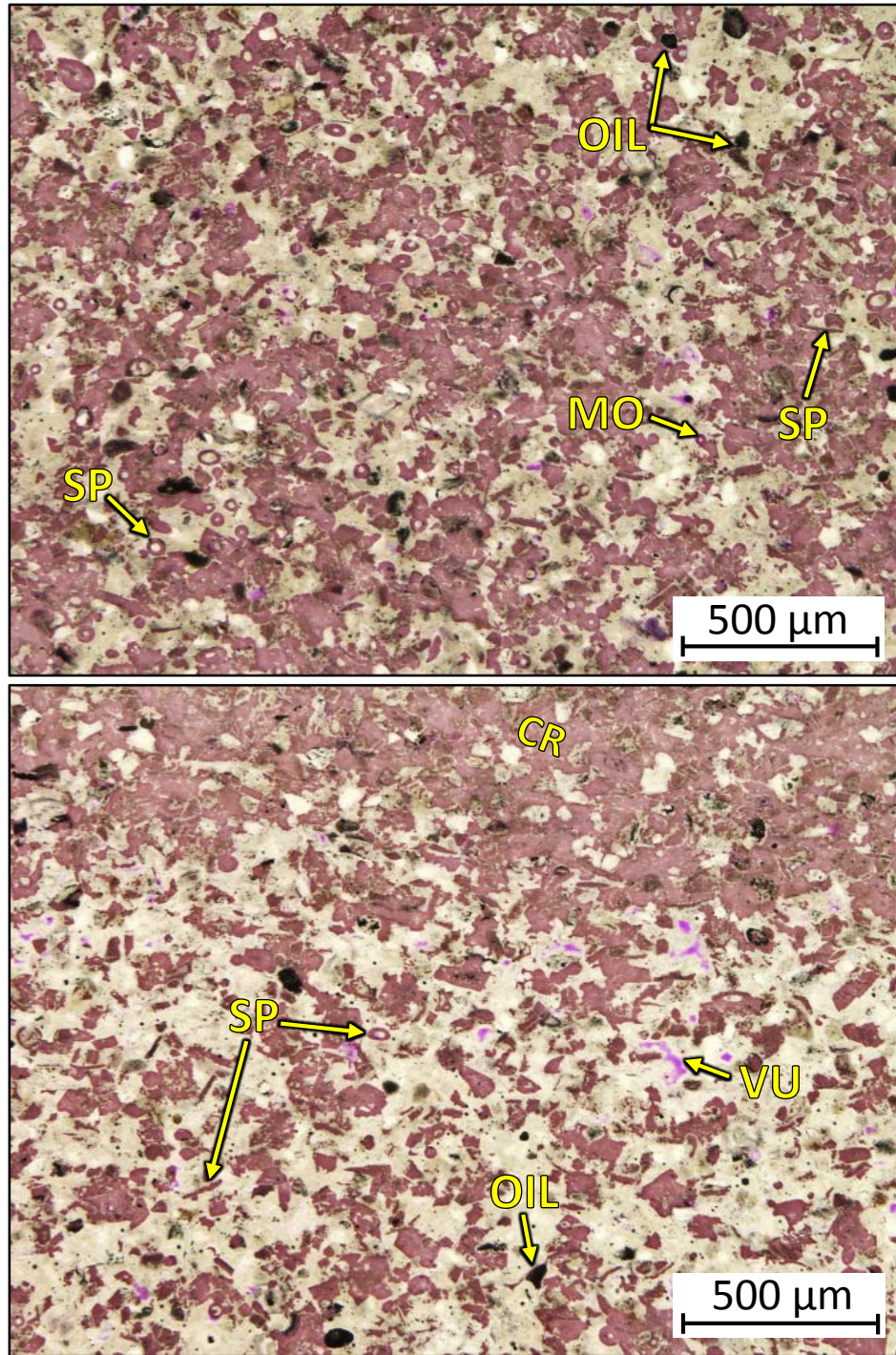
3EL – 4380.95' = Silicified skeletal grainstone. Sample is alizarin red stained. Porosity (NCS): 3.7%. Visual estimation: 5% clays, 25% carbonates, and 70% other minerals. Sample contains abundant sponge spicules (40%) and undifferentiated microbioclastic debris likely composed of abundant crinoid fragments. Dominantly oil-filled moldic and vug porosity.



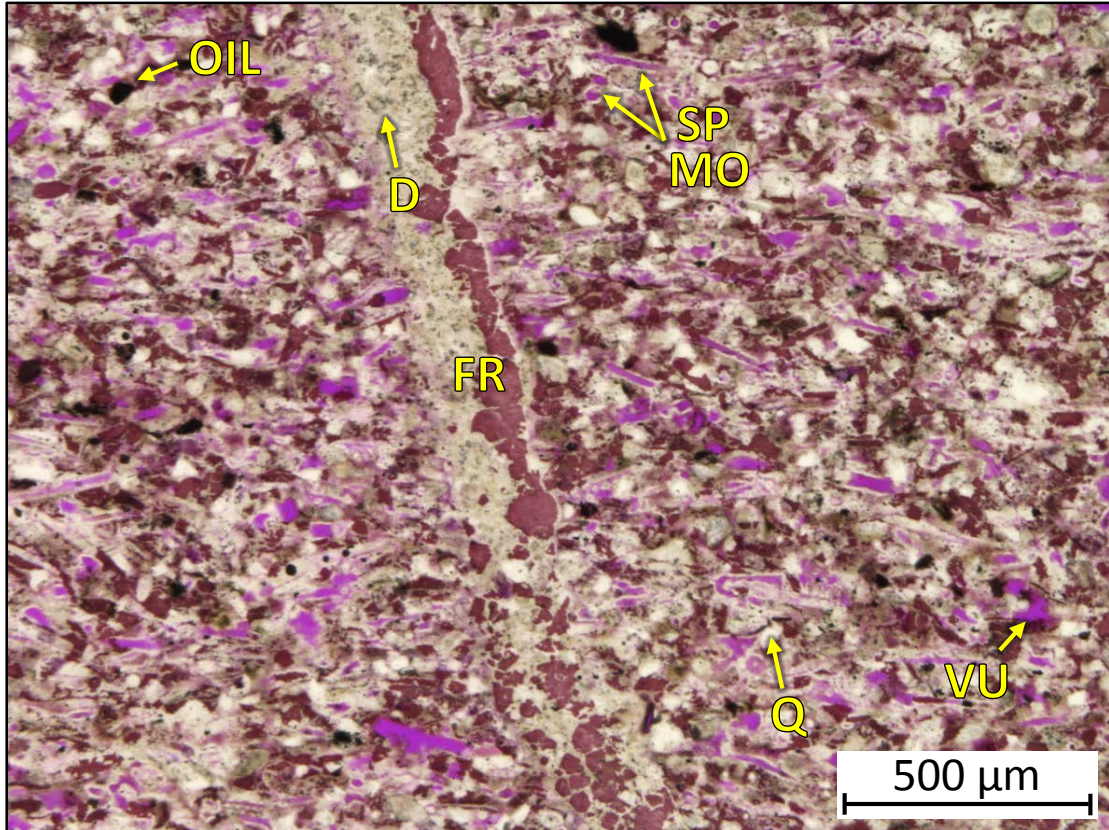
3EL – 4376.50' = Peloidal grainstone. Sample is blue epoxy impregnated. Porosity: 2.0% (visual estimation). Visual estimation: 1% clays, 85% carbonates, and 14% other minerals. Sample is composed of silt-sized quartz grains (14%), abundant peloids (35%), and sponge spicules (5%). Dominantly moldic porosity from dissolution of sponge spicules and vug and interparticle porosity.



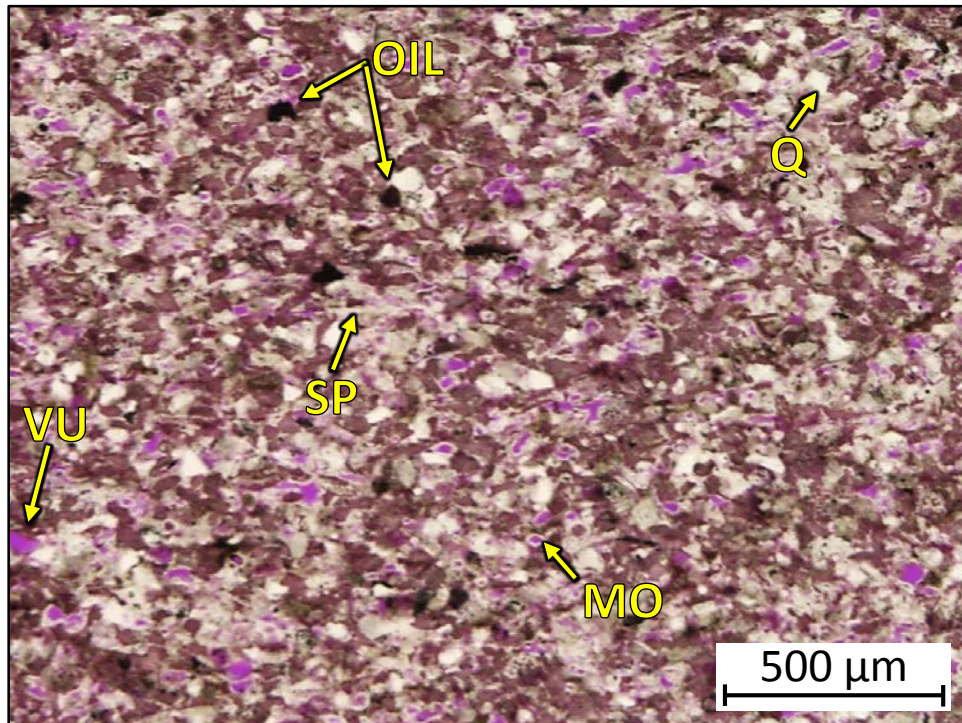
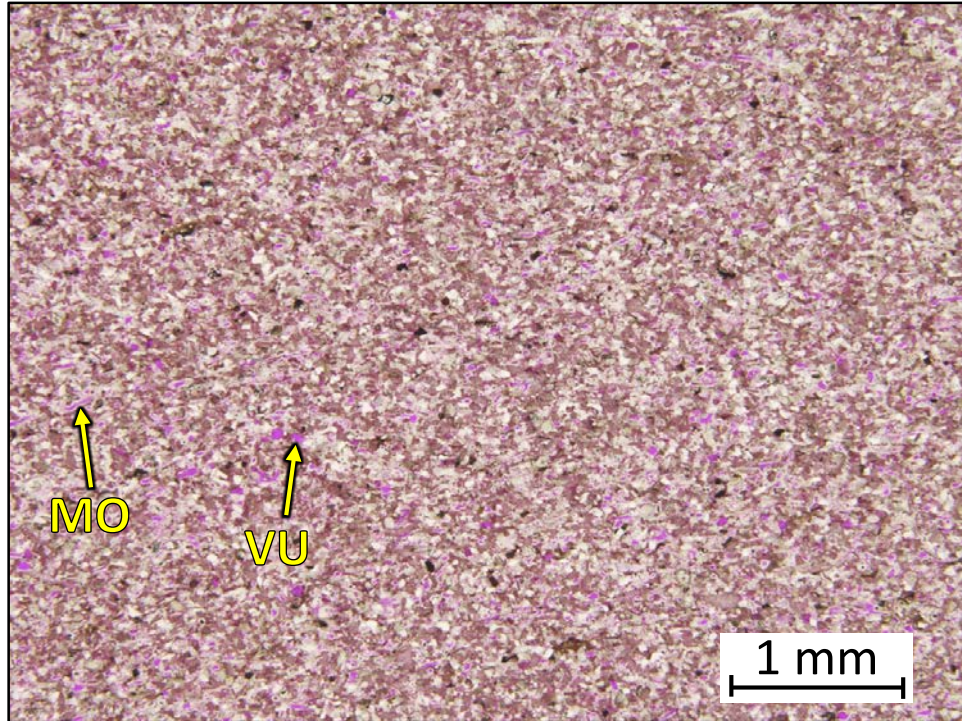
3EL – 4362.35' = Peloidal grainstone. Sample is alizarin red stained. Porosity (NCS): 1.3%. Permeability (Klinkenberg): <0.0001 mD. XRD: 1% clays (1% illite), 67% carbonates (66% calcite and 1% dolomite), and 32% other minerals (26% quartz, 1% potassium feldspar, 4% plagioclase feldspar, 1% pyrite, and trace amounts of apatite). Sample is composed of silt-sized quartz grains (26%), crinoid fragments (25%), peloids (10%), and sponge spicules (5%). Dominantly oil-filled moldic and vug porosity.



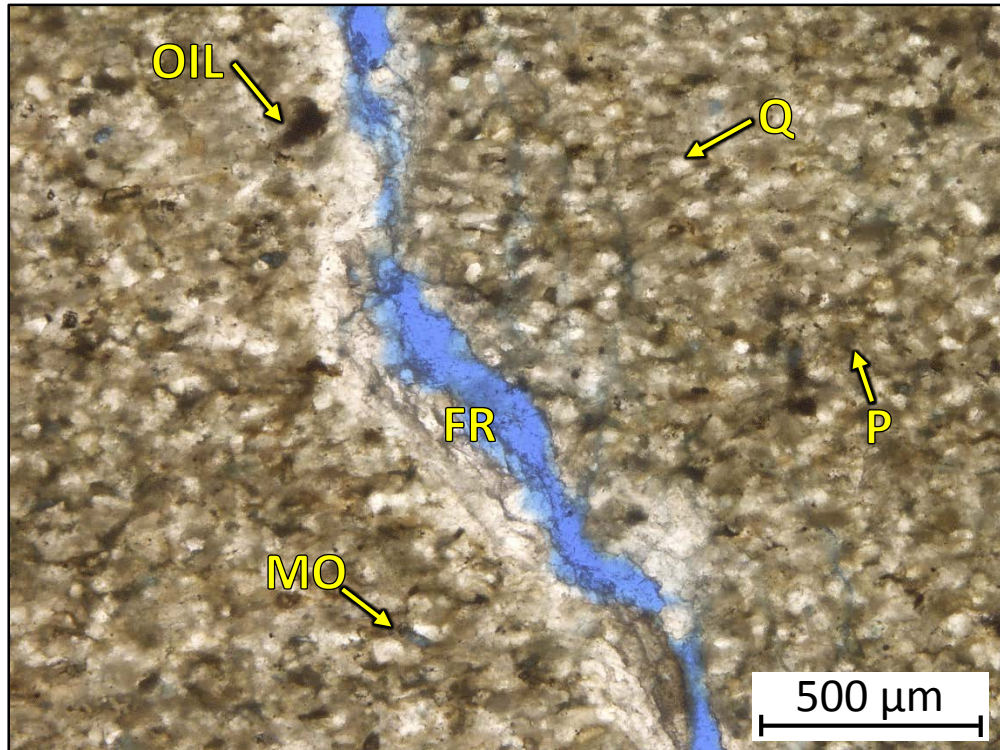
3EL – 4354.30' = Partially silicified skeletal grainstone. Sample is alizarin red stained. Porosity (NCS): 1.8%. Permeability (Klinkenberg): <0.0001 mD. XRD: 1% clays (1% illite), 76% carbonates (75% calcite and 1% dolomite), and 23% other minerals (19% quartz, 1% potassium feldspar, 3% plagioclase feldspar, and trace amounts of pyrite). Sample is characterized by varying mineralogies and varying amounts of crinoid (10-70%) and sponge spicules (15-40%) depending on location. Dominantly moldic and vug porosity, with some oil-filled pores.



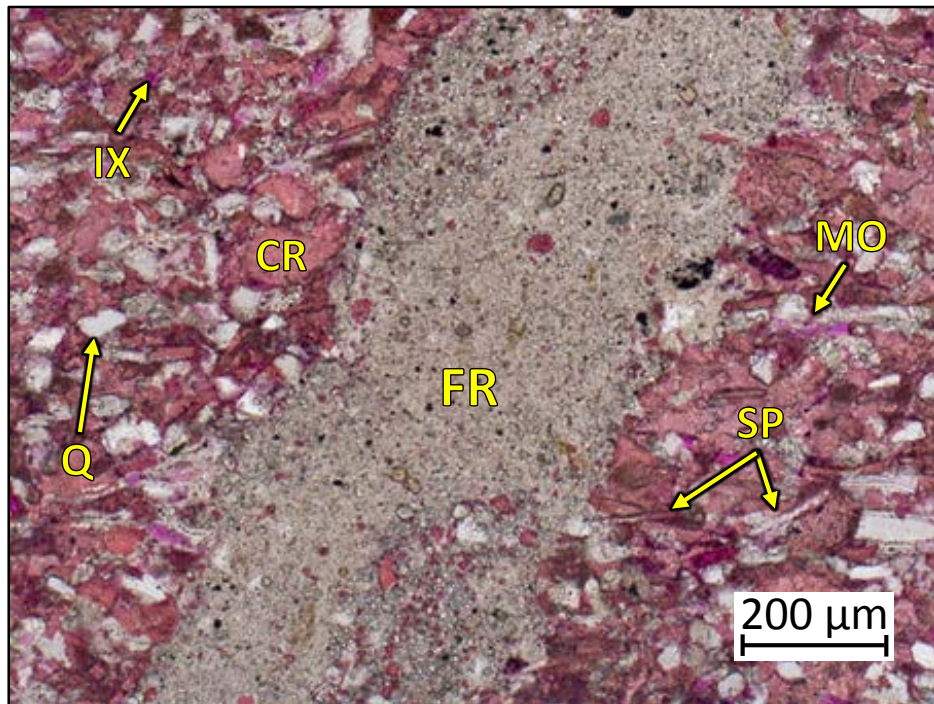
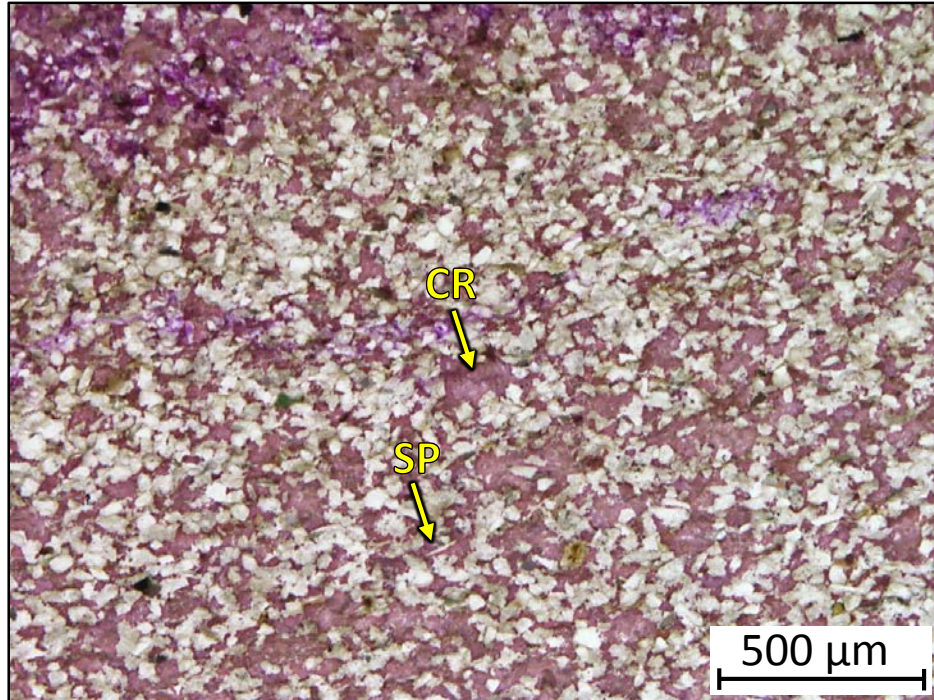
3EL – 4353.90' = Skeletal grainstone. Sample is alizarin red stained. Porosity (NCS): 8.9%. Permeability (Klinkenberg): 0.0074 mD. XRD: 1% clays (1% illite), 33% carbonates (31% calcite and 2% dolomite), and 66% other minerals (61% quartz, 2% potassium feldspar, 2% plagioclase feldspar, and 1% pyrite). Sample contains abundant sponge spicules (40%), silt-sized quartz grains, and undifferentiated microbioclastic debris. Dominantly moldic porosity from the dissolution of sponge spicules and vug porosity, with lesser amounts of intercrystalline porosity within the fracture filling cements.



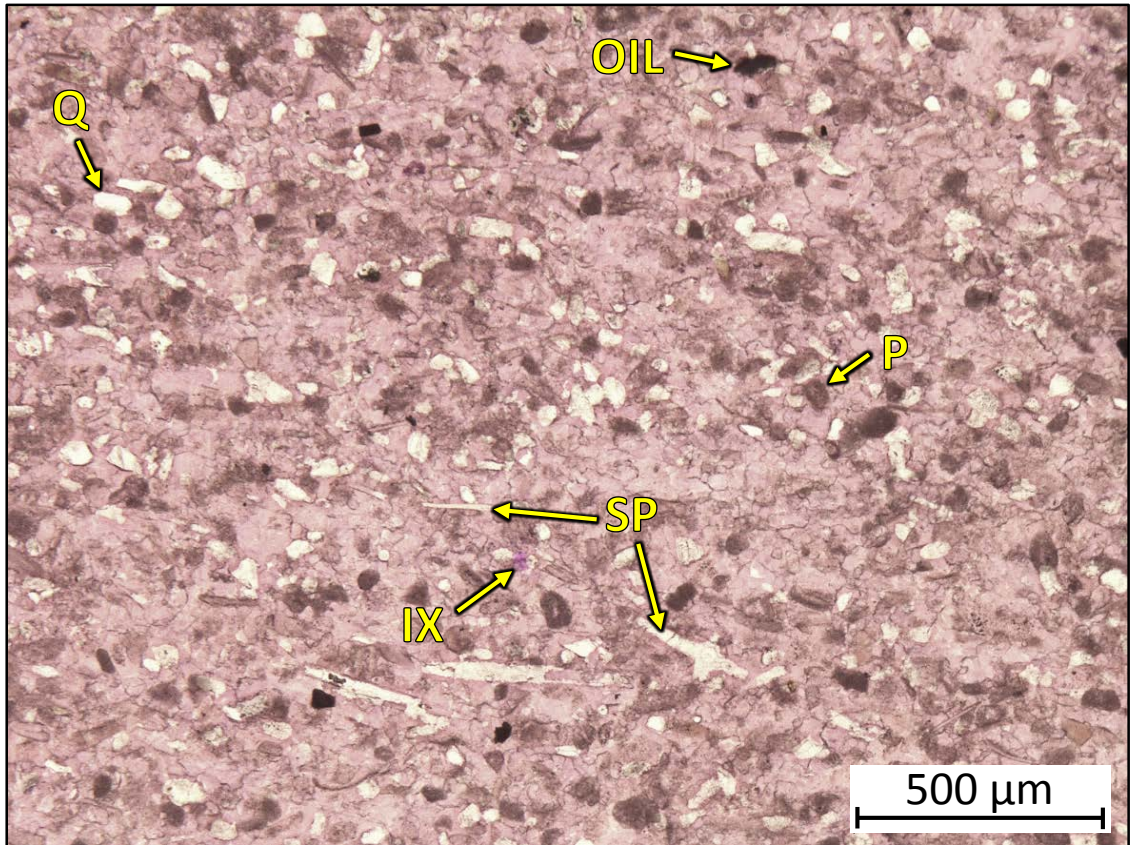
3EL – 4349.90' = Skeletal grainstone. Sample is alizarin red stained. Porosity (NCS): 11.4%. Permeability (Klinkenberg): 0.023 mD. XRD: 1% clays (1% illite), 29% carbonates (26% calcite and 3% dolomite), and 70% other minerals (65% quartz, 2% potassium feldspar, 3% plagioclase feldspar, and trace amounts of pyrite and apatite). Sample contains abundant spicules (40%) and silt-sized quartz grains (50%) as well as undifferentiated microbioclastic debris. Dominantly moldic and vug porosity.



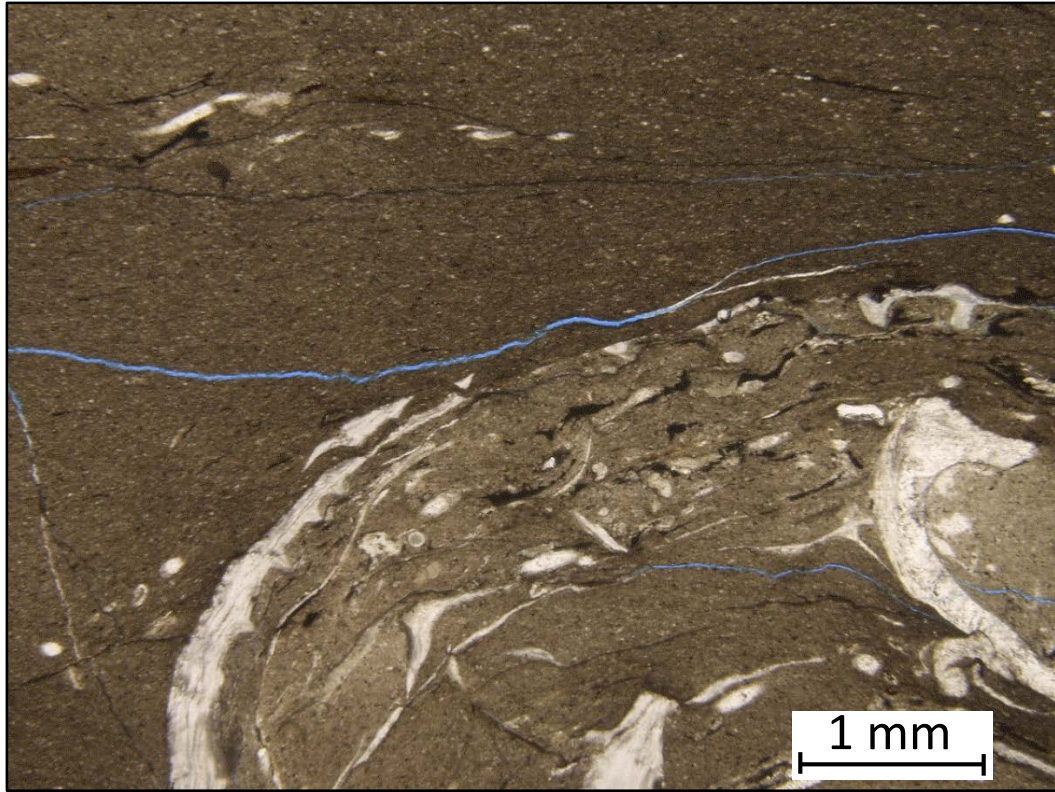
3EL – 4345.50' = Peloidal packstone-grainstone. Sample is blue epoxy impregnated. Porosity (visual estimation): 0.5% Visual estimation: 1% clays, 85% carbonates, and 14% other minerals. Sample is composed of silt-sized quartz grains (14%), abundant peloids (45%), and undifferentiated microbioclastic debris. Sample shows an example of good fracture porosity and permeability. Moldic porosity from the dissolution of skeletal grains is also observed.



3EL – 4341.90' = Silicified peloidal-skeletal grainstone. Sample is alizarin red stained. Porosity (NCS): 5.8%. Permeability (Klinkenberg): 0.0004 mD. XRD: 1% clays (1% illite), 45% carbonates (45% calcite and trace amounts of dolomite), and 54% other minerals (51% quartz, 1% potassium feldspar, 2% plagioclase feldspar, and trace amounts of pyrite and apatite). Sample is composed of abundant silt- to sand-sized quartz grains (45%), spicules (7%), and undifferentiated microbioclastic debris. Dominantly moldic porosity from the dissolution of sponge spicules and minor amounts of intercrystalline porosity.



3EL – 4340.25' = Peloidal grainstone. Sample is alizarin red stained and porosity is shown in bright fuchsia. Porosity: 2.2%. XRD: 1% clays (1% illite), 85% carbonates (85% calcite), and 14% other minerals (10% quartz, 1% potassium feldspar, 3% plagioclase feldspar, and trace amounts of pyrite). Sample is composed of sand- and silt-sized quartz grains (5%), peloids (15%), spicules (10%), and minor amounts of ostracode fragments and undifferentiated microbioclastic debris. Minor amounts of intracrystalline porosity observed.



3EL – 4338.50' = Pennsylvanian wackestone. Sample is blue epoxy impregnated.

VITA

Stephanie LeBlanc

Candidate for the Degree of

Master of Science

Thesis: HIGH RESOLUTION SEQUENCE STRATIGRAPHY AND RESERVOIR
CHARACTERIZATION OF THE "MISSISSIPPIAN LIMESTONE" IN NORTH-CENTRAL
OKLAHOMA

Major Field: Geology

Biographical:

Education:

Completed the requirements for the Master of Science in Geology at Oklahoma State University, Stillwater, Oklahoma in December, 2014.

Completed the requirements for the Bachelor of Science in Geology at Baylor University, Waco, TX/USA in 2012.

Experience:

Interned at ExxonMobil in Houston, TX in 2012.

Geological Specialist at Samson Resources in Tulsa, OK in 2012.

Interned at Occidental Oil and Gas in Houston, TX in 2013.

Began full-time job as a geologist at ExxonMobil in Houston, TX in 2014.

Professional Memberships:

American Association of Petroleum Geologists